Exploratory analysis to investigate the diseases of polymyalgia rheumatica, giant cell arteritis and rheumatoid arthritis

by

Julia Elizabeth Manning

A thesis submitted to the University of Birmingham for the degree of

DOCTOR OF PHILOSOPHY

Institute of Inflammation and Ageing

College of Medical and Dental Sciences

University of Birmingham

November 2022

Abstract

This thesis uses exploratory forms of analysis to investigate three inflammatory, autoimmune rheumatic diseases; polymyalgia rheumatica (PMR), giant cell arteritis (GCA) and rheumatoid arthritis (RA).

PMR and GCA are closely related diseases. Whilst glucocorticoids (GCs) effectively manage the inflammation and some related symptoms (i.e., pain and stiffness) in these diseases, they also cause adverse effects and subsets of patients still suffer from fatigue. In this thesis, we performed metabolomics on serum from patients with PMR and GCA to assess the effect of disease. In PMR, we went on to evaluate associations with GC treatment and patient symptoms. Compared to controls, this identified several metabolite alterations (e.g., glycerol and lactate) in PMR and GCA patients. Correspondingly, metabolite changes also correlated with inflammation, pain and stiffness (e.g., ketone bodies). Furthermore, PMR patients reporting high and low fatigue had different metabolomic signatures, both before and after treatment. Notably, low glutamine associated with high fatigue at both time points.

In RA, we investigated the role of stromal cells in disease. Firstly, we examined the changing role of the endothelium, investigating a curated list of functionally important molecules. From publicly available bulk RNA-sequencing, we observed a heterogeneous expression pattern, which varied depending on pathotype. Whilst multiplex imaging revealed the majority of these molecules increased with disease duration. We then used transcriptomic analysis to explore the role of fibroblasts (from non-inflamed, resolving arthritis, very early

RA and late-stage RA) on healthy endothelial cells and macrophages. Whilst we observed few transcriptomic changes in endothelial cells according to the diagnosis of fibroblast in co-culture, there were many transcriptomic changes in macrophages. These included alterations in IFN and TNF-α signalling. Notably, co-culture with either cell type induced transcriptional changes in the fibroblasts. Indeed, co-culture with macrophages revealed different differentially expressed genes in the fibroblasts, with changes in TGF-β signalling and genes associated with migratory phenotype.

Thus, within this thesis we have identified a number differentially regulated molecules in GCA, PMR and RA. However, due to the exploratory nature in all of these analyses, and limitations in samples sizes, validation of these findings is required.

Dedication

Dedicated, with lots of love,

to my Mum, Dad and Elliot.

Acknowledgments

Firstly, thank you to MRC and Novartis for funding the project and enabling this work to be carried out. Thank you to my supervisor Dr Helen McGettrick for your support thought-out the years, providing me with lots of opportunities and keeping me (somewhat) calm whenever I started to panic. Thank you also to Prof Andrew Filer for your expertise and putting up with my many patient information requests. Thank you to the multiple collaborators of this PhD. Particular thanks to Sarah Mackie, Anne Morgan, Louise Sorenson, Raashid Laqmani, and Steve Young for your help in analysing and putting together the metabolomics work. Thank you to Mark Coles and Dylan Windell for letting me use the CellDIVE imaging platform and helping immensely with this work. Thank you also to Yousra and Miriam in Switzerland, for running the RNA Seq - in spite of a pandemic. Thanks, must also go to the patients who volunteered for these studies. Likewise, to all of the clinicians, research nurses and midwives that recruited them. None of the work in this PhD would have been completed without them.

Thanks, must also go to the patients who volunteered for these studies. Likewise, to all of the clinicians, research nurses and midwives that recruited them. None of the work in this PhD would have been completed without them.

Many thanks go to all members of the RRG and LTG who have helped me along the way. Particular thanks must go to Jason Turner, for your help getting me started in the lab (and teaching me flow!) and all the bioinformatics help throughout the years. Thank you also to Holly, John, and many others who taught me the experimental techniques and gave me useful advice. Thank you also to Triin, Saba, David and Emily T. for providing me with tissue

sections and helping with all my staining needs, and to Chelsea and Kalvin for your metabolomics help. To all the techs thank you for keeping the lab running smoothly, especially to Holly (also for always getting me fibroblasts), and to Em (and for your music chats).

To all past and present members of the LTG and RRG groups, it has been a pleasure to work with you all. There are too many people to name everyone, but it has been an honour to work with such lovely people. You have made some of the most difficult years the most fun. I do, and will, sorely miss working with you all. To name just a few, thanks to Laurence, Kieran, Georgiana, Mel and Lucy for your stimulating lab chats. Particular thanks must go to Jonny for keeping me sane, having a laugh, and always listening to (/putting up with) my complaining. Also thank you (and your successors Kathryn and Imy) very much for the works of art left of my desk. Special thanks as well goes to Sophie, for always sharing a room with me at a conference and your assistance at Halloween parties.

Most of all, thank you to my parents. You are always there when I need to talk (rant) and your constant support has got me where I am today. I will be forever grateful. Last, but not least, thank you, of course, to Elliot, for providing me with the hugs and support which were, and still are, frequently required.

Contents

List of Figures

Appendix

List of Tables

Appendix

Abbreviations

ACPA	Anti citrullinated protein antibody
ACR	American college for Rheumatology
ADDRESS-PMR	Diagnostic Accuracy of Ultrasound in Suspected Polymyalgia Rheumatica
ADMECs	Adipose derived microvascular endothelial cells
AIA	Adjuvant induced arthritis
ANCA	Anti-neutrophil cytoplasmic antibody
ARD	Autoimmune rheumatic disease
BEACON	Birmingham early arthritis cohort
CCL	Chemokine (C-C motif) ligand
CCP	Cyclic citrullinated peptide
CD	Cluster of differentiation
cDNA	complementary DNA
CIA	Collagen induced arthritis
CLEC14A	C-Type Lectin Domain Containing 14A
CRP	C-reactive protein
CV-ANOVA	Cross validated - Analysis of variance
CXCL	C-X-C motif ligand
DAMP	Damage associated molecular pattern molecules
DARC	Duffy Receptor for Chemokines
DAS	Disease activity score
DCs	Dendritic cells
DEG	Differentially expressed genes
DLL4	Delta-like canonical notch signalling 4
DMARD	Disease modifying anti-rheumatic drugs
DNA	Deoxyribonucleic acid
ECM	Extracellular matrix
ECs	Endothelial cells
EDTA	Ethylenediaminetetraacetic acid
ELS	Ectopic lymphoid-like structures
EMA	European Medicines Agency
ESR	Erythrocyte sedimentation rate
EULAR	European Alliance of Associations for Rheumatology
FACIT-F	Functional Assessment of Chronic Illness Therapy – Fatigue
FAP-α	Fibroblast activation protein alpha
FDR	False discovery rate
FFPE	Formalin-fixed paraffin-embedded
GC	Glucocorticoid
GCA	Giant cell arteritis
GM-CSF	Granulocyte macrophage colony-stimulating factor
GSEA	Gene set enrichment analysis
HBEGF	Heparin binding EGF-like growth factor

HEVs	High endothelial venules
HLA	Human leukocyte antigens
HUVECs	Human umbilical vein endothelial cells
ICAM	Intracellular adhesion protein
IF	Immunofluorescence
IFN-γ	Interferon gamma
IHC	Immunohistochemistry
IL	Interleukin
iNOS	Inducible nitric oxide synthase
IPA	Ingenuity pathway analysis
ISGs	Interferon stimulated genes
JAK	Janus kinase
JRep	Rheumatoid arthritis patients undergoing joint replacement
KO	Knock-out
LC-MS	Liquid chromatography - Mass spectrometry
LPS	Lipopolysaccharide
LVV	Large vessel vasculitis
M-CSF	Macrophage colony-stimulating factor
MDMs	Monocyte derived macrophages
MerTK	Mer tyrosine kinase
MHC	Major histocompatibility complex
MHC	Major histocompatibility complex
MMPs	Matrix metalloproteinase
MMRN2	Multimerin 2
mRNA	messenger RNA
MS	Mass Spectrometry
MTX	Methotrexate
Mϕ	Macrophages
ncRNA	Non-coding RNA
NF-κB	Nuclear factor kappa light chain enhancer of activated B cells
NGS	Next generation sequencing
NI/Norm	Non-inflamed
NLPR3	NLR Family Pyrin Domain Containing 3
NMR	Nuclear magnetic resonance
NOESY	1D-1H-Nuclear Overhauser Effect spectroscopy
NRES	National Research Ethics Service
NSAID	Non-steroidal anti-inflammatory drugs
OA	Osteoarthritis
OPG	Osteprotegrin
OPLS-DA	Orthogonal partial least squares discriminant analysis
PAMP	Pathogen associated molecular pattern molecules
PBS	Phosphate-buffered saline

PCA	Principal components analysis
PCR	Polymerase chain reaction
PDPN	Podoplanin
PEAC	Pathobiology of Early Arthritis
PLS-R	Partial least squares regression
PMR	Polymyalgia rheumatica
PNAd	Peripheral node addressin
PsA	Psoriatic arthritis
QC	Quality control
RA	Rheumatoid arthritis
RDS	Relative standard deviation
REC	Research Ethics Committee
Res	Resolving
RF	Rheumatoid Factor
RIN	RNA integrity number
RNA-Seq	RNA - Sequencing
ROS	Reactive oxygen species
RT	Room temperature
SA	Septic arthritis
SCID	Severe combined immunodeficiency
scRNA-seq	Single cell RNA sequencing
SF	Synovial fibroblasts
SJC	Swollen joint count
SMECs	Synovial microvascular endothelial cells
STAT	Signal transducer and activator of transcription
STIA	Serum transfers induced arthritis
TABUL	The Temporal Artery Biopsy -v- Ultrasound in diagnosis of Giant Cell Arteritis
TAK	Takayasu's arteritis
TGF-β	Transforming growth factor beta
TJC	Tender joint count
TLR	Toll-like receptor
TLS	Tertiary lymphoid structures
TNF-α	Tumour necrosis factor alpha
TRMs	Tissue resident macrophages
UHPMC-MS	Ultra-High Performance: Liquid Chromatography
VAP1	Vascular adhesion protein 1
VAS	Visual analogue score
VCAM-1	Vascular adhesion protein
VE-cadherin	Vascular endothelial cadherin
VEGFA	Vascular endothelial growth factor A
VeRA	Very early rheumatoid arthritis

VIP	Variable importance for prediction score
VSMCs	Vascular smooth muscle cells

Contributions

Multiple people have contributed to the work described in this thesis. Dr Steve Young processed the NMR samples in chapter 3. Dr Helen McGettrick processed the fibroblast: endothelial cell co-cultures used for Mass Spectrometry in chapter 5 and Professor Warwick Dunn performed the analysis of these samples. Dr Jason Turner prepared all the macrophage: fibroblast co-cultures in chapter 6. All other analysis, and any sample preparation was performed by myself.

1 Introduction

1.1 Overview

Autoimmune rheumatic diseases (ARDs) effect up to 5% of the population (1), and cases are rising (2). This thesis broadly covers three, inflammatory, ARDs; polymyalgia rheumatica (PMR), giant cell arteritis (GCA) and rheumatoid arthritis (RA). Characteristic symptoms of these diseases include pain, stiffness and swelling of the affected area due uncontrolled leukocyte recruitment, alongside systemic symptoms such as fatigue, fever and weight loss (3-5). There are effective treatments for these diseases (e.g. glucocorticoids, and in the case of RA, biologics), but they often cause significant side effects or do not improve all symptoms (e.g. fatigue), and crucially cannot cure the disease (4, 6). Thus, there is an urgent clinical need to fully elucidate the pathogenic mechanisms of these diseases and to find potential biomarkers and novel therapeutic targets. Regarding PMR and GCA, analysis of the circulating metabolome is utilised to understand how disease and treatment affect metabolism, in order to find novel targets for diagnosis and assessing responses to therapy. Whilst in RA, the thesis focuses on underpinning pathogenic mechanisms, in particular the role that endothelial and stromal cells (i.e. macrophages and fibroblasts) play in the initiation and propagation of inflammation (7-10).

1.2 Acute inflammation

Inflammation is initiated when tissue-resident sentinel cells (e.g. fibroblasts, dendritic cells or macrophages) respond to signs of infection or damage (pathogen/damage - associated molecular pattern molecules; PAMPs/DAMPs) by producing pro-inflammatory signals, such as tumour necrosis factor α (TNF-α), interferon γ (IFNγ), histamine and interleukin-6 (IL-6)

(11). These molecules activate the endothelium to express leukocyte trafficking molecules (e.g. selectins, integrin ligands, chemokines and chemoattractants) that interact with and hence capture circulating leukocytes (12, 13). Leukocytes are then able to extravasate in the multi-step leukocyte adhesion cascade (14) as summarised in Figure 1.1.

Prompt and efficient resolution of inflammation is crucial to heal tissue and return it to homeostasis (15). It is an active process, closely linked to the initiation of inflammation (16). It involves multiple mechanisms including: (i) limiting or ceasing leukocyte extravasation; (ii) preventing oedema formation; (iii) switching off pathways that propagate leukocyte survival; (iv) inducing leukocyte apoptosis/netosis and subsequent efferocytosis to remove them; (v) returning non-apoptotic cells to the blood or lymph vasculature; (vi) the phenotypic switch of M1 to M2 macrophages; and (vii) the initiation of healing (17). Insufficient resolution coupled with uncontrolled recruitment, results in the chronic inflammation observed in inflammatory diseases, for example GCA, PMR and RA.

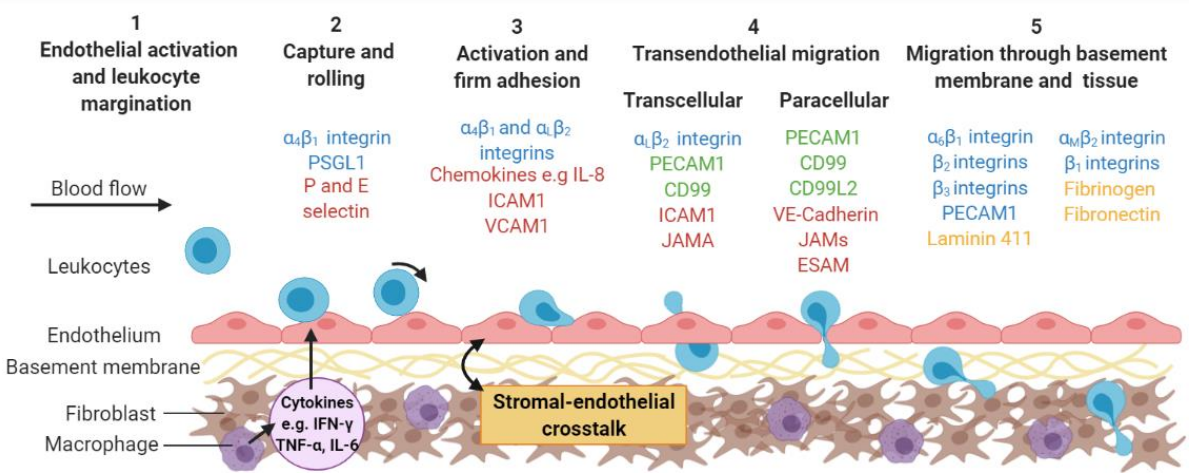

Figure 1.1: The leukocyte adhesion cascade. Infection or tissue damage causes the localised release of danger signals, including cytokines, which (1) activate the endothelium causing the expression of capture receptors (P- or E-selectins), adhesion molecules (IgSF members - ICAM-1; VCAM-1) and presentation of chemokines or lipids on their surface. (2) Marginated leukocytes are captured, roll along the endothelial surface until (3) they receive an activation signal (typically chemokine mediated) resulting in inside-out signalling and integrin activation ($\alpha_L\beta_2$-integrin; $\alpha_4\beta_1$-integrin). This allows for stabilisation of the adhesive interactions ($\alpha_L\beta_2$-ICAM-1 and $\alpha_4\beta_1$-VCAM-1 interactions) and cytoskeletal rearrangement in the leukocyte allowing (4) them to crawl over the endothelium, migrate across the endothelium ($\alpha_L\beta_2$-integrin; ICAM-1; JAMs; CD31; VE-cadherin; CD99; ESAM) and into the sub endothelial space, (5) where they encounter the basement membrane and stromal compartment. This process is tightly regulated by the haemodynamic forces of the flowing blood and the stromal derived signals experienced by the endothelium. Some of the major molecules involved in this process are represented in the schematic, with molecules coloured according to cell type expressing them; leukocytes, blue; endothelial cells (ECs), red and expressed by both leukocytes and ECs, green. ESAM, endothelial cell-selective adhesion molecule; ICAM-1, Intracellular adhesion protein 1; IL-8, interleukin-8; JAM, junctional adhesion molecule; PECAM-1, platelet endothelial cell adhesion molecule 1; PSGL1, P-selectin glycoprotein ligand-1; VE-cadherin, vascular endothelial cadherin; VCAM-1, vascular adhesion protein 1. Created with BioRender.com. Figure adapted from (18).

1.3 Autoimmune rheumatic diseases

Autoimmune diseases are triggered when the immune system becomes dysfunctional and begins attacking self-molecules (19). Those that principally affect the joints and muscles are classified under the umbrella term of autoimmune rheumatic diseases (ARDs) (20). These include RA, PMR, the systemic vasculitides (e.g. GCA), Lupus, Sjogren's syndrome and other forms of arthritis (Spondyloarthropathies, infectious and juvenile idiopathic arthritis) (20). ARDs share a number of the same symptoms and clinical presentation, particularly in the earliest stages of disease; e.g. fatigue, fever, weight loss, polyarthralgia and headaches (20). This overlap, combined with the large amount of heterogeneity within each disease makes diagnosis difficult (20). In fact, at 12 months follow up, up to 50% of patients suffering "connective tissue disorders" did not have a definitive diagnosis (20, 21). ARDs also have comparable causes, i.e., genetics (e.g. mutations in the HLA allele (22, 23)) or environmental factors (e.g. smoking (24-27) or infections (28-30)). Likewise, the systemic nature of these diseases often results in the same co-morbidities. These include cardiovascular disease (50% more common in RA patients than the general population (31)), kidney, lung and gastrointestinal diseases, depression, infections, and cancer (32).

Despite the known similarities and overlap of these diseases there are large disparities in our current knowledge and understanding of ARDs. This may be in part due to patient/clinical need (i.e., the more common or debilitating a disease, that cannot be well treated, the more it is investigated), combined with accessibility to clinical samples or availability of appropriate animal models. For example, RA is one of the most common autoimmune diseases (33), and whilst there are a number of treatments available they are not always

efficacious (RA is reportedly inadequately controlled in > 25% of patients (34)). Therefore, there is an urgent critical need to find new treatment targets and strategies. Fortunately, multiple animal models (e.g. K/BxN, Adjuvant-induced arthritis and TNF-transgenic models) are available to help investigate this multifaceted disease (35). On the other hand, for rarer diseases such as PMR and GCA, where glucocorticoids (GCs) can effectively manage the inflammation, there is a less demanding clinical need to investigate underlying pathological causes. Furthermore, whilst there are some animal models for GCA (36), there are none of PMR making it challenging to underpin the mechanisms of disease. Therefore, despite the complexity of RA, a relatively large amount is known regarding its pathogenesis, particularly when compared to other ARDs such as GCA and PMR. Similarly to how research into inflammatory diseases often follows that of the cancer field, research into the less common and harder to investigate ARDs often follows that of RA or lupus.

Due to these factors, the key unanswered questions for these diseases are different. In PMR and GCA a broader approach is required, which also assesses the consequences of effective, but non-ideal, GC treatment. Therefore, in this study the serum of PMR and GCA was assessed via metabolomics to get the first overview of the metabolomic changes that occur with disease and GC treatment. Whilst in RA, a lot more is known already of the systemic metabolomic changes (37, 38). Indeed, the changes previously observed in RA suggest there are likely systemic changes in all ARDs. It would be advantageous to find which of those are similar across, or specific to, particular ARDs. This would allow a better understanding of what properties are shared amongst ARDs, and/or better initial diagnosis (i.e. disease specific biomarkers). In the more advanced field of RA research, the underpinning cellular

mechanism of disease is arguably a more pressing question. Thus, due to the well-known role of stromal cells in RA (10, 39), but the current limited therapeutic options targeting these (particularly fibroblasts), there is an urgent need to investigate the role of the stroma further. Consequently, this study focuses on stromal cells and their crosstalk in RA during the course of disease.

1.4 Polymyalgia rheumatica and giant cell arteritis

1.4.1 Overview of the diseases

Polymyalgia rheumatica (PMR) is the most common disease in people over 50 with a lifetime risk of 2% (33, 40, and 41). It is characterised by musculoskeletal extracapsular inflammation (42, 43), which results in pain and stiffness of the neck, shoulders and pelvic girdles (44, 45) alongside systemic symptoms such as fatigue (46). It is closely related to GCA, a rarer (effects 1 in 100,000 individuals), but more severe disease, that occurs in around 20% of PMR patients and would likely develop in all PMR patients if they were left untreated (44, 47). GCA is the most common form of large vessel vasculitis (LVV) (48), caused by inflammation of the medium to large blood vessels, with a prediction to the temporal artery (49, 50). The inflammation leads to occlusion of the artery lumens and potential ischemic damage of the surrounding organs (49). This causes the characteristic GCA symptoms; scalp tenderness, head pain, jaw pain, fever, fatigue, and, in 25% of patients, vision loss or stroke (51, 52).

Glucocorticoids (GCs) remain the gold-standard treatment for both diseases (53) and are highly effective at treating the inflammation within these diseases. Due to the severity of GCA, current European Alliance of Associations for Rheumatology (EULAR) recommendation

is to immediately prescribe high dose (40-60mg/day) GCs (Figure 1.2A) (54). Once controlled, (within 2-3 months) the dose should be lowered to 15-30mg/day and after a year lowered again to ≤5mg/day for GCA (54) (Figure 1.2A). For PMR, the combined recommendation of EULAR and the American college for Rheumatology (ACR) is to prescribe a comparatively low dose of GCs (12.5-25mg/day), and monitor patient response at 2-4 weeks, then taper or increase steroid treatment as required (Figure 1.2B) (55).

While low dose GC use can be a safe and effective treatment strategy (56), higher doses and long term use may have severe effects (53, 57). This is highlighted in GCA, where 86% of patients have reported having at least one adverse effect, and 58% had 2 or more (53, 57). These adverse-effects include: hypercortisolism (aka Cushing syndrome; puffy cheeks and easy bruising), bone fractures, diabetes mellitus, gastrointestinal bleeding, hypertension, infection and posterior subcapsular cataracts (57). In order to prevent or minimise these effects, GC use should be limited and tapering is recommend as soon as remission is achieved (54). Due of the lower dose of GC use in PMR, side effects are seen in fewer, but still in a substantial number (50%), of patients (53). Due to the severe GC-related effects experienced by the vast number of patients, further understanding of these diseases, and identification of biomarkers or more specific drug targets is required.

Most significantly, in both diseases, patients suffer from pain, stiffness and fatigue. Whilst the pain and stiffness are likely caused by the inflammation and can be effectively managed by GC treatment (53, 58, 59), fatigue persists in a subset of patients which significantly impacts their quality of life (58, 60). Furthermore, fatigue scores have been proposed to

correlate with different imaging phenotypes (42), suggesting an underlying biological cause of the symptom. However, the mechanism behind this, remains poorly understood. Accordingly, there is an urgent clinical to need to further understand the molecular signatures underpinning these diseases; how and whether these are altered following GC treatment, and which of these are driving fatigue.

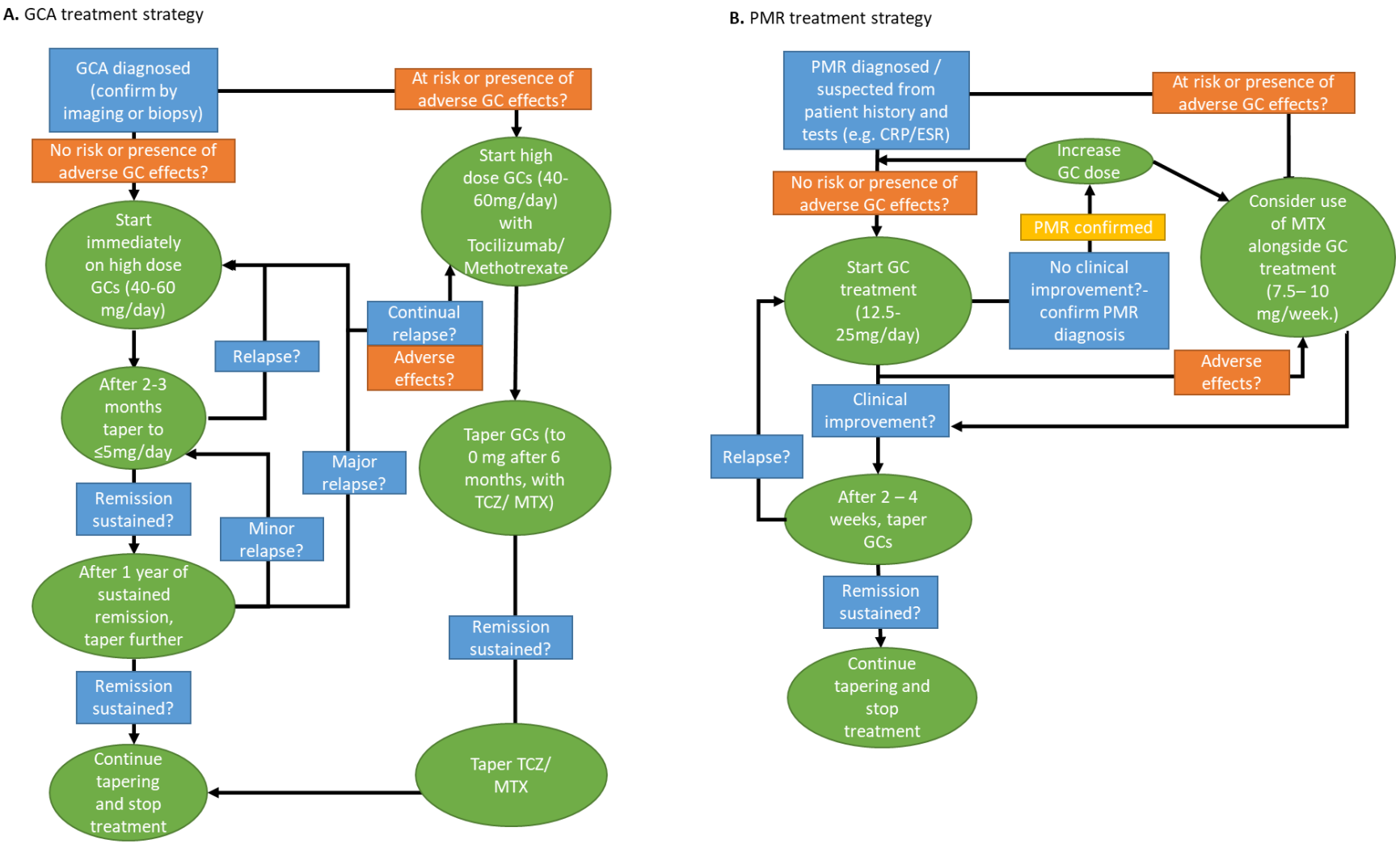

Figure 1.2: Schematic of the EULAR recommendation for the treatment of giant cell arteritis (GCA) and polymyalgia rheumatica (PMR)). Schematics adapted from **(A)** 2018 EULAR recommended algorithm for the treatment of GCA (54) and **(B)** 2015 EULAR/ACR recommendation for treatment of PMR (55). GC, glucocorticoids; MTX, Methotrexate; TCZ, tocilizumab.

1.4.2 Aetiology and mechanisms of diseases

The aetiology and immunopathology of GCA and PMR is not well understood (61, 62), however, they are known to share common risk factors. The greatest risk factor is being elderly; indeed diagnosis criteria includes being over 50 (63, 64). Incidence also with age, peaking in those aged 71-80 (63, 64). This suggests that age-related changes to the immune system, tissues, and neurohumoral regulation may be involved (65, 66). Both diseases are ~2-3 times more likely to affect women than men and occur more frequently in Northern European descended populations, due to both genetic and environmental factors (24, 67-69). Genetic risk factors include polymorphisms in the genes encoding cytokines (e.g. IL-6, TNF-α) and adhesion molecules (e.g. ICAM1) (67) which are associated with both diseases. The most significant mutation is the *HLA-DRB1*04* allele, but this appears to be specific to GCA (68, 69). Regarding environmental factors, a low BMI prior to onset of disease, and smoking (in women) may be a predictor (24). Infection might also contribute, with known links to mycoplasma pneumoniae, parvovirus B19, and the parainfluenza virus infections (28, 29). However, so far these are purely correlative and any definite cause-effect relationship is yet to be determined (28, 29). Due to the similarities in these disease and definite overlap (50% GCA patients have PMR (70)), they are frequently considered subsets, or a spectrum, of the same disease (67).

GCA is an inflammatory disease of the large to medium arteries, although the exact mechanisms of pathogenesis are yet to be fully elucidated. As shown in Figure 1.3, large and medium arteries consist of 3 layers; the intima (containing endothelial cells), the media (containing vascular smooth muscle cells; VSMCs) and the adventitia (containing dendritic

cells and a network of blood vessels (vasa vasorum)). In GCA, an unknown trigger activates the dendritic cells of the adventitia which results in chemokine production and recruitment of T cells and macrophages (71). In particular, $CD4^+$ are the most common T cells that infiltrate the arterial wall layers and then intermingle with the highly activated macrophages (aka histiocytes), which often gives rise to multinucleated giant cells (hence the disease name) (71). The VSMCs, endothelial cells (ECs) and fibroblasts within the artery then poorly repair it, causing medial thinning and a hyperplastic intima that occludes the lumen (71).

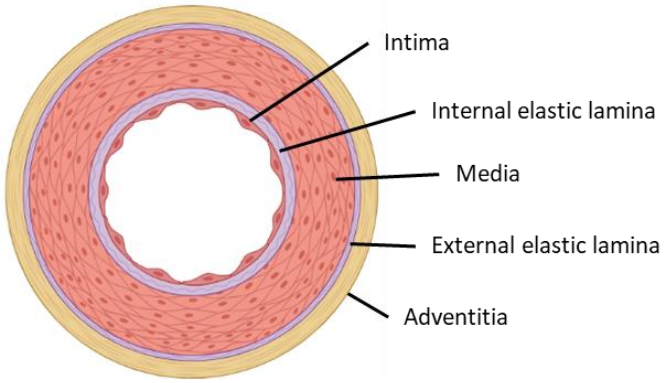

Figure 1.3: Structure of medium and large artery walls. The human artery is multi-layered, consisting of the intima, media and adventitia, each separated by elastic lamina. In health, the intima is formed of endothelial cells, the media consists primarily of smooth muscle cells, and the adventitia is formed from dendritic cells, fibroblasts and a network of blood vessels (the vasa vasorum) (49). Image created in BioRender.com.

Building on the findings in other ARDs (72), such as RA, it is becoming apparent that immunostromal interactions are likely to play a pivotal role in GCA pathogenesis (49). This is highly plausible due to the preference of GCA for particular arteries (49). Wall-embedded vascular dendritic cell (DCs) are present in multiple arteries, but some are untouched by GCA, whilst others are evidently targets (i.e. predilection to the temporal artery) (49). This points towards the involvement of other tissue specific cell types (49). Moreover, notch-

notch ligand interaction is important in GCA pathogenesis and connects T cells, VSMCs and ECs within GCA (49). $CD4^+$ T cells in GCA patients are known to up-regulate expression of the Notch1 receptor by 20-fold, alongside increasing expression of the notch ligand, Jagged 2 (49, 73). VSMCs and ECs also express notch ligands, and in the case of VSMCs notch receptors (49). In health, these are needed for the development of organ systems and vascular structures (49). However, regarding disease, their presence suggests VSMCs can both send and receive signals, which may allow them to communicate with T cells and hence play a role in orchestrating GCA (49). Most importantly, blockade of notch-notch signalling in a humanised mouse model of GCA had immunosuppressive effects, decreasing the number of infiltrated T cells (73). This suggests a crucial role of VSMCs signalling via Notch to allow T cell survival (49, 73).

Due to a lack of appropriate animal models and accessible clinical material even less is known regarding PMR pathology. Even though the disease is characterised by musculoskeletal extracapsular inflammation (42, 43), a lot of the same cell types and molecules of GCA pathogenesis are likely to be involved. Early immunohistochemistry (IHC) staining of PMR synovial biopsies revealed the presence of DCs and macrophages, alongside a large number of infiltrated T cells (58). This suggests DCs and tissue-resident macrophages, respond to an unknown stimuli and recruit T cells and monocytes from the blood (74). Interestingly, and further supporting the link between GCA-PMR, it has been shown that adventitial DCs from PMR patients are activated (express CCL19 and CCL21) and implanting PMR arteries with GCA arteries in severe combined immunodeficiency (SCID) mice caused

the PMR arteries to retain and activate T cells from GCA lesions (75). This indicates that activation of DCs initiates GCA, and highlights a link between the diseases (75).

The current limited understating of these diseases, combined with the adverse effects of the current mainstay treatment (GCs) highlights the need to identify new biomarkers, treatment targets and improve current understating. Furthermore, considering both diseases occur predominately in the elderly, prevalence is likely to increase with our ageing population (76) thus making research into this even more imperative.

1.4.3 Searching for biomarkers and the use of metabolomics

Omics approaches allow the unbiased analysis of samples to identify novel markers of disease development; progression; response to treatment; or that may underpin specific symptoms. Whilst large studies have been carried out to assess any genetic associations in PMR and GCA patients (77, 78), very few have looked at the effects on the metabolome. Moreover, none have examined the combined effects of PMR or GCA and GC treatment.

1.4.3.1 Metabolomics and disease

The systemic symptoms (e.g. fatigue) observed in both PMR and GCA, are likely to be caused by global changes in metabolism and so may be discerned by measuring circulating metabolite levels (79). For example, lactate and lipids (80) and histidine and guanidoacetic acid (81) correlated with increased inflammation (C-reactive protein (CRP) or Disease activity score-28-Erythrocyte sedimentation rate (DAS28-ESR) scores) and disease activity in patients with rheumatoid arthritis (RA) (80, 81). Furthermore, fatigue scores also correlated with a decrease in specific metabolites linked to in the urea cycle and fatty acid metabolism in

treatment naïve RA patients (82). Regarding vasculitis, nuclear magnetic resonance (NMR) revealed increased serum glutamate and N-acetyl glycoprotein in Takayasu's arteritis (TAK) and increased urine myo-inositol: citrate ratio in anti-neutrophil cytoplasmic antibody (ANCA) vasculitis were associated with increased disease activity (83-85). Collectively these data strongly indicate the utility of metabolites as biomarkers of disease activity, patient symptoms and response to therapy. However, upon searching the current literature, only one study (published as an abstract) has so far examined the effect of PMR on the circulating metabolome (86) and none are currently published in the field of GCA. Interestingly, PMR and RA patients display a similar circulating metabolome, as a result Cedola *et al* combined the two patient populations prior to analysis. Lower choline, histidine and sarcosine and higher lactate, glucose, glutamine, formate and acetate levels were found in the PMR+RA group when compared to age and sex matched controls, and these correlated with baseline clinical scores (86). Clearly there is an urgent need to consolidate these data in PMR and GCA to better understand the molecular mechanisms underpinning pathology, particularly regarding fatigue, and whether these are altered in response to therapy.

1.4.3.2 Metabolomics and glucocorticoids

Whilst glucocorticoids (GCs) are the gold standard treatment for PMR and GCA (41, 53), they do not always modulate fatigue (58, 87). Furthermore, they can have severe side effects (57, 88, 89), which can be linked to their systemic effects on the metabolome (53, 86, 90, 91). Perturbations of gluconeogenesis and catabolism observed in rats treated with GC corresponded to their weight loss and abnormal bone metabolism (91). Indeed, GC treatment significantly increased lysophospholipids (a known risk factor for cardiovascular

disease) in female RA patients compared to patients given non-GC treatments. Long term (>6 months) GC treatment may also have beneficial effects with reduced asymmetric dimethyl arginine (ADMA), and metabolite associated with endothelial dysfunction in RA (92). In the mixed population of PMR and RA patients, one-month of treatment (91% on GCs, 51% GCs + 1 disease modifying anti-rheumatic drug (DMARD)) reduced hydroxyacetone and 3-hydroxybutyrate levels (both ketones) (86). This suggests treatment (and likely GCs) can alter the metabolome of PMR and RA patients, and in particular ketone body synthesis (86). Collectively these studies indicate that metabolomics can assess a patient's response to GC treatment. However, it remains unclear: (i) how the metabolic profile is altered specifically in patients PMR and GCA; (ii) how these correspond to patient symptoms; and (iii) whether these profiles can be used to identify an individual patient's response to therapy early in their clinical management.

1.4.3.3 Metabolomics and the use of nuclear magnetic resonance

Metabolomics is the comprehensive analysis of all metabolites in a system (the metabolome). Metabolites are a group of low molecular weight molecules used in metabolism and include amino acids, lipids and nucleic acids (93, 94). As these are downstream of the genome and proteome, they closely reflect the state of an organism at any point in time (95). By studying the metabolome of a system we can identify changes that underlie disease; identify new therapeutic targets; and find novel biomarkers for diagnosing or assessing responses to therapy (79, 96). One classic example of using metabolites for the diagnosis of disease is the glucose test for diabetes (97).

Nuclear magnetic resonance (NMR) and mass spectrometry (MS) are the primary methods used in metabolomics (94). NMR analyses the molecular structure of a material by observing and measuring the interaction of nuclear spins when the material is placed into a magnetic field (98). It is typically used to detect hydrogen atoms (^{1}H-NMR), therefore all molecules containing an H atom will produce a spectrum, i.e. nearly all metabolites (99, 100). Although NMR is inherently less sensitive than MS, it is highly reproducible, involves relatively easy sample preparation and doesn't require sample separation, thus allowing the re-analysis of samples (99, 101). Most significantly, unlike an untargeted MS approach (100, 102), NMR determines the absolute concentrations of a wide range of metabolites simultaneously making the technique ideal for an initial untargeted analysis approach (99). Therefore, for the work in this thesis, NMR was utilised to measure serum metabolite concentrations in order to get an overview of changes with disease and glucocorticoid treatment and how these correlated with patient reported outcomes.

1.5 Rheumatoid arthritis

1.5.1 Overview and treatment

Rheumatoid arthritis (RA) is an inflammatory autoimmune disease of the synovial joints, affecting around 1% of the worldwide population (33). Similar to other inflammatory diseases (e.g., GCA and PMR), RA is more common in women than men (~2-3 fold). While it can develop at any stage of life, incidence increases with age, reaching a prevalence of 2% in people over 60 (103, 104).

In healthy conditions, the synovial membrane provides fluid which lubricates and nourishes the joint and is comprised primarily of two cell types (fibroblasts and macrophages), alongside the vascular network and nerve supply (105, 106). However, during RA, a breach in self-tolerance causes immune cells to attack self-molecules (e.g., citrullinated proteins) (107). This stimulates an immune response and the synovium is consequently invaded by T and B cells, which accumulate within the synovial membrane (105). As the disease progresses, the synoviocytes (fibroblasts and macrophages) proliferate and pannus forms (105). The hyperplastic tissue then begins destroying articular cartilage and eroding bone (105), as summarised in Figure 1.4. These processes cause the characteristic symptoms of RA: pain, swelling, warmth and stiffness of the joint, as well as systemic symptoms; fatigue, fever and weight loss.

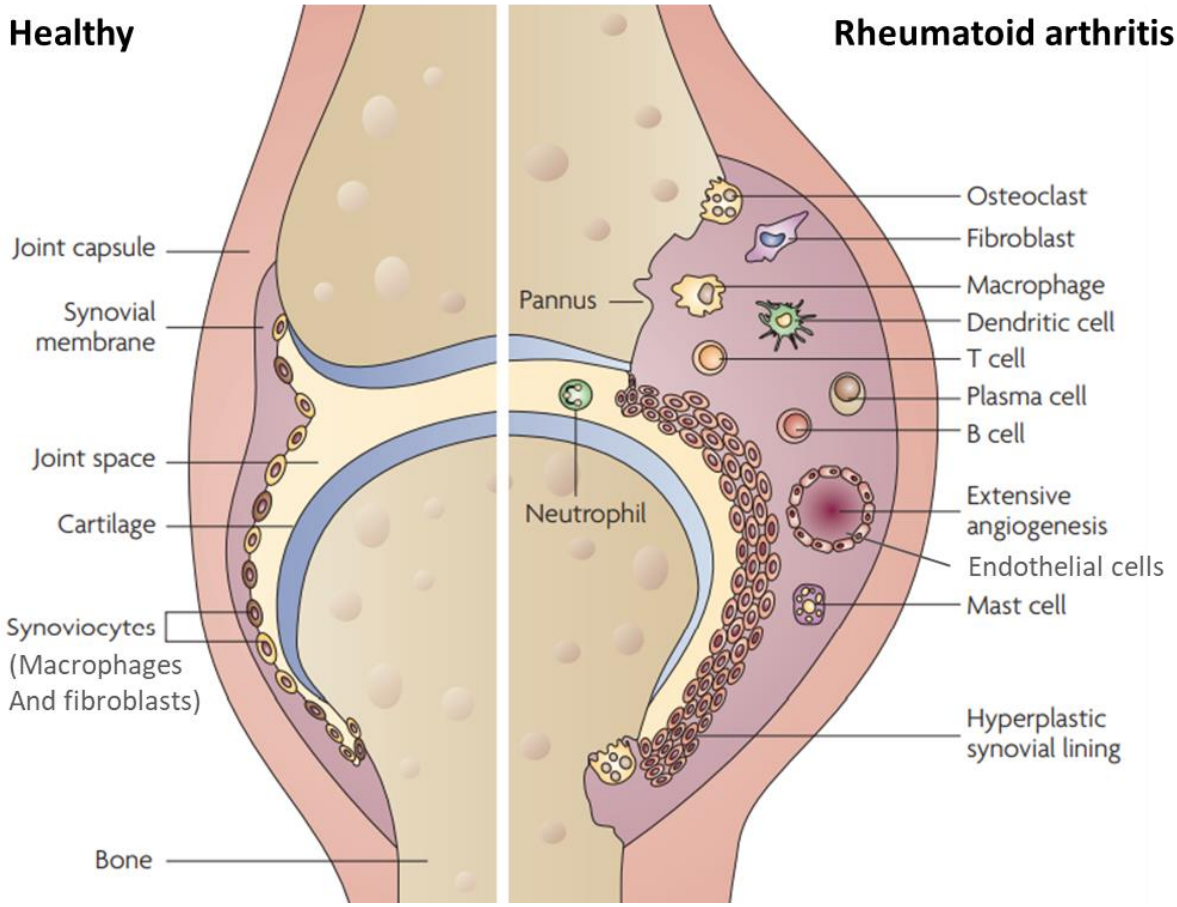

Figure 1.4: Diagram of the healthy joint compared to an inflamed joint in a patient with rheumatoid arthritis. In health, the joint consists of a thin synovial membrane with few synoviocytes. In rheumatoid arthritis, multiple immune cell types infiltrate and accumulate in the synovial membrane. The synoviocytes proliferate forming a hyperplastic synovial lining. A pannus forms and begins eroding the neighbouring bone. Diagram taken and adapted from (105).

Left untreated, RA can lead to progressive joint destruction causing disability, poor life quality and increased mortality (108). Fortunately, there are a number of effective treatments, ranging from nonsteroidal anti-inflammatory drugs (NSAIDs) to specific biological therapies (105). However, the complex nature and heterogeneity of the disease, combined with ensuring safety and cost-efficacy makes finding the appropriate treatment strategy difficult (109). The current treatment recommendation from EULAR (109) (Figure 1.5) is to initially prescribe patients glucocorticoids (GCs) which immediately reduce inflammation. However, due to the known side effects of GCs (discussed in 1.4.1) they should be limited to short term and low dose use. Therefore, these are combined with a conventional synthetic disease-modifying anti rheumatic drug (csDMARD) of which methotrexate is the most common (108, 109). Patients must then to be monitored closely (every 1-3 months) and other csDMARDs, biological DMARDs [i.e., anti-TNF-α (e.g. adalimumab) and IL-6R inhibitors] or Janus kinase (JAK) inhibitors are then added to or switched into the patients treatment strategy until improvement is seen at 3 months, or target achieved in 6 months [assessed according to the ACR-EULAR definition] (109). This "trial and error" approach to treatment is far from ideal, both with respect to patient care and cost of treatment. For example, in clinical trials, only 50-70% of patients responded to anti-TNF-α therapy (110), but anti-TNF-α treatment costs the NHS ~£10,000 per person, per year (111). Thus, there is an urgent clinical need to find (i) novel biomarkers that identify patient subsets to enable precision medicine and the treatment of processes underpinning the disease, and (ii) to fully elucidate the disease mechanism to identify new, and more effective, treatment targets.

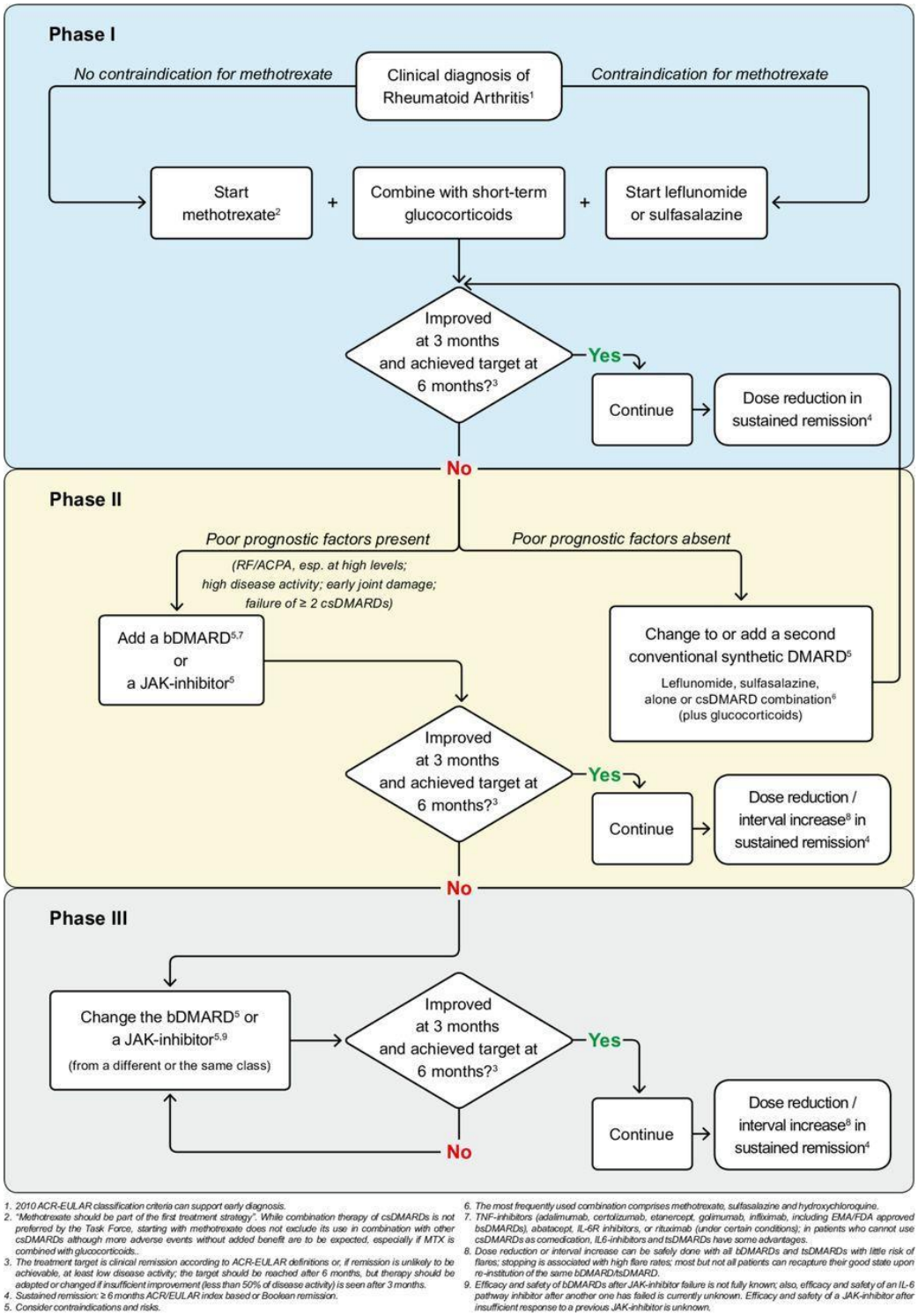

Figure 1.5: EULAR recommend RA management algorithm. ACPA, anti-citrullinated protein antibody; ACR, American College of Rheumatology; bDMARDs, biological DMARDs; bsDMARD, biosimilar DMARDs; csDMARDs, conventional synthetic DMARDs; DMARDs, disease-modifying antirheumatic drugs; EMA, European Medicines Agency; EULAR, European League Against Rheumatism; FDA, Food and Drug Administration; IL-6R, interleukin 6 receptor; JAK, Janus kinase; MTX, methotrexate; RA, rheumatoid arthritis; RF, rheumatoid factor; TNF, tumour necrosis factor; tsDMARDs, targeted synthetic DMARDs. Taken from (109).

1.5.2 Aetiology and heterogeneity

The aetiology of RA is not fully understood, but genetics, environmental factors and the microbiome are known to play a role (26). For example, RA is more common in women than men, due to genetic (X-linked) and hormonal factors (104). The most significant genetic risk factor is the expression of the HLA-DRB1*04 epitope (carried by 80% of patients), alongside other mutations in the HLA genes and across the major histocompatibility complex (MHC) (26). It is well known that environmental factors, such as smoking and infection [e.g. *Porphyromonas gingivalis* (30)], also contribute to disease development, severity and progression. For example, rheumatoid factor (RF) positive men who smoked were twice as likely to develop RA, than those who did not (25-27). Increasing evidence also suggests the microbiome plays a crucial role in RA pathogenesis (112, 113). RA patients have around 40% less lung microbiome diversity compared to healthy controls (10, 114) and specific changes to gut and oral mucosa correlate with a higher autoantibody titre (low *Haemophilus* spp. levels) and more active disease (increased *Lactobacillus salivarius)* (10, 115). It is clear that the aetiology of RA is complex and multifaceted; and consequently, contributes to large heterogeneity (described below) observed in RA patients and the differences seen in their response to treatment (109, 116-118).

Whilst RA primarily affects the synovium, the presence of autoantibodies in the patient sera and synovial fluid suggests it is a systemic autoimmune disease (119). Many forms of auto-antibody have been found in RA patients, but the clinical and pathological significance is only known for two major types; rheumatoid factor (RF) and anti-citrullinated protein antibodies (ACPAs) (119). These circulating antibodies can be found up to 10 years prior to clinical

disease onset, and the presence of both antibodies is a useful predictor for the likelihood of developing the disease (120, 121). RF autoantibodies target the Fc region of IgG antibodies (122). Interestingly, only around 40% of RA patients are RF^+ at clinical onset, but up to 80% will eventually become positive (122). The other common antibody is against citrullinated proteins. Citrullination occurs via enzymatic conversion of peptidylarginine to peptidylcitrulline by peptidylarginine deiminase (PAD) in post-translational modification (123, 124) to a range of proteins (fibrin, vimentin, fibronectin etc.) found throughout the body (123), and is required for terminal differentiation of the epidermis, and apoptosis (125). RA patients with antibodies against these citrullinated proteins (67%) exhibit a much more aggressive phenotype (increased bone and joint destruction) than their ACPA-negative counterparts and have different genetic associations, particularly within the HLA region (123, 126, and 127). The presence of either of these antibodies is associated with higher disease severity and can dictate patient's response to therapy (128). For example, methotrexate and rituximab are less effective in ACPA- patients, but rituximab treatment may even be used as a preventative measure for ACPA+ individuals with no signs of synovitis (127). It is therefore essential to bear this in mind when unpicking the mechanisms of disease and in deciding the best treatment strategies.

Immunohistochemistry of RA tissue, combined with transcriptional data, has also revealed subtypes of synovitis according to type and degree of lymphocyte infiltration, described as: lympho-myeloid, diffuse myeloid and pauci-immune fibroid (10, 129-131). Myeloid-lymphoid (also known as follicular) phenotypes are dominated primarily by B cells and ectopic/tertiary lymphoid-like structures (ELS/TLSs) (10, 129-131). In the diffuse myeloid pathotype, the

infiltrate is scattered and consists primarily of myeloid cells, with few B-cells or plasma cells and undetectable ELSs/TLSs (129). Importantly, these two are not mutually exclusive and can occur at varying degrees across the tissue of individuals (129). On the other hand, the pauci-immune fibroid phenotype has very few infiltrating cells (130). Notably, this pathotype disease and early (<12 months symptom duration) untreated arthritis, hence it is not simply the result of a "burned-out" or successfully treated synovium (129). Significantly, these pathotypes have also been found useful in predicting patient response to treatment. For example, only 29% of patients with a pauci-immune pathotype achieved clinical response to the TNF-α inhibitor certolizumab-pegol compared to 83% of patients with leukocyte infiltration (both follicular and diffuse) (117). These tissue pathotypes are likely driven by differences in leukocyte recruitment, a process highly controlled by the endothelium, which turn is influenced by its microenvironment. Thus, alterations in endothelial or stromal cell phenotype may be driving these distinct pathotypes. One clear example of this is the high level of peripheral node addressin (PNAd) expression [commonly associated with the high endothelial vessels (HEVs) of lymphoid organs] observed in and around large TLSs in the RA synovium (132). The idea of pathogenic changes to the endothelial and stromal cell phenotype and how this contributes to disease is discussed in the following section, 1.5.3.

In summary, the multiple risk factors of RA, combined with the clear patient's subsets defined by differences in tissue and blood (circulating antibodies), highlight RA as an incredibly complicated and heterogeneous disease. Considering this is crucial when unpicking the mechanisms of disease, and determining appropriate treatment strategies (130).

1.5.3 Cellular basis of disease

RA pathogenesis is complex and associated with the abnormal behaviour of multiple cell types which interact in a multitude of ways. For the purposes of this thesis, the focus will be on the role played by endothelial cells, macrophages and fibroblasts, and their interactions. In health, these cells are responsible for the production connective tissue, vessels, nerves and extracellular matrix, which together supports the parenchyma of the organ (39). However, in RA they undergo changes which aid the initiation and propagation of disease (10, 39). Furthermore, subtypes of these cell types have been found to have different functions and consequently different interactions. In this thesis the focus will be on ECs and fibroblast: EC and fibroblast: macrophage interactions. The major known pathogenic interactions of these cells and their subtypes is described in more detail below and summarised in Figure 1.6.

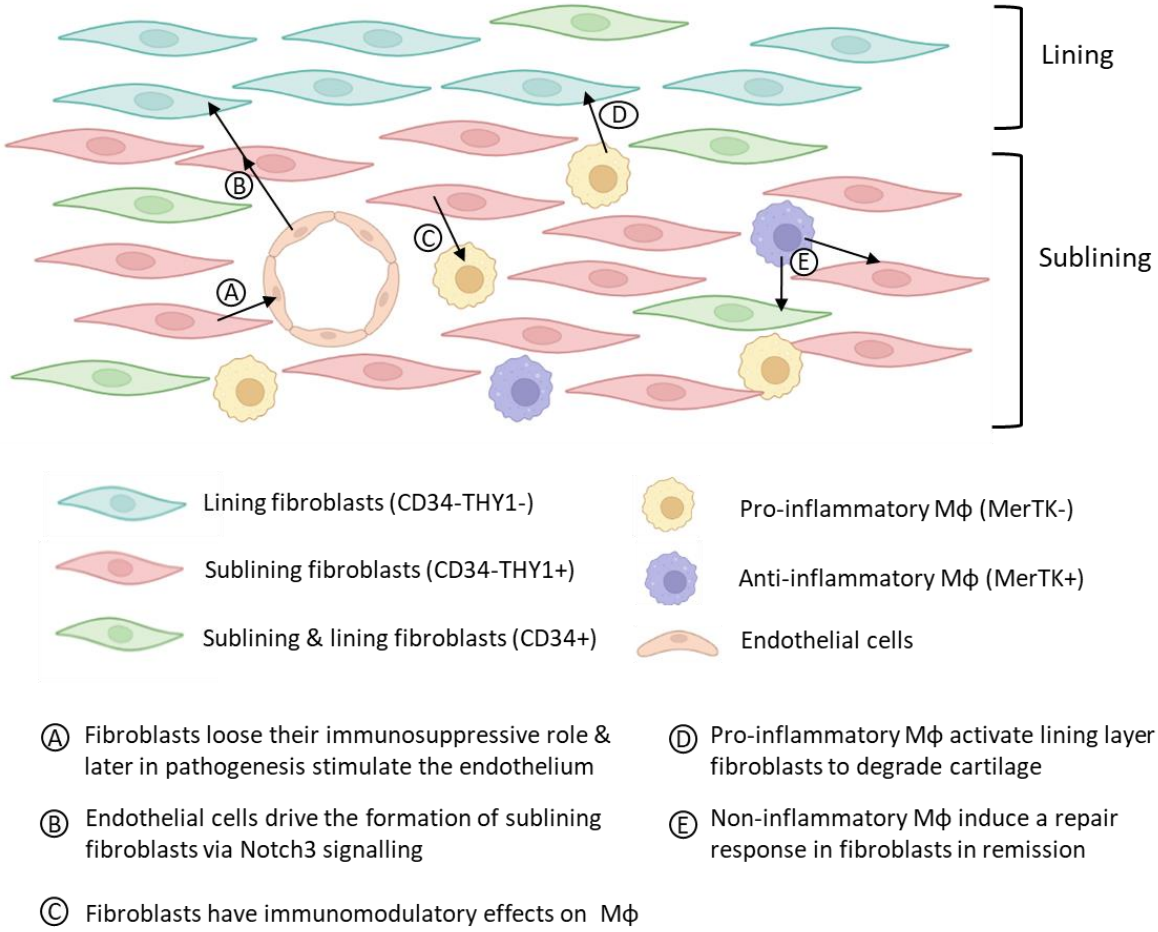

Figure 1.6: Schematic summary of key stromal cell subtypes and their interactions in the rheumatoid arthritis synovium. The synovium consists of three stromal cells types; fibroblasts, macrophage (Mϕ) and endothelial cells. In rheumatoid arthritis (RA), these cells types consist of subsets with differing functions. Fibroblasts can be classed as: CD34-THY1- (blue), CD34-THY1+ (red) or CD34+ (green). CD34-THY1- are found in the lining layer, produce MMP1 and MMP13 and are involved in cartilage destruction. CD34-THY1+, found in the sublining and exhibit inflammation "memory". CD34+, found in lining and sublining, are immunoregulatory and cause fibroblast accumulation and invasion. Mϕ can be broadly categorised as having pro-inflammatory (MerTK-, purple), and anti-inflammatory (MerTK+ orange) phenotypes (133, 134). Endothelial cells (although not depicted here) also exist in subpopulations via differential expression of adhesion molecules (135-140). These three cell types are known to interact, and in some cases, the specific subtype: subtype interaction is known. **(A)** In health, fibroblasts exhibit an immunosuppressive effect limiting endothelial recruitment of leukocytes, however, in very early RA this is lost. Later in disease, they gain a stimulatory phenotype; activating endothelial cells to recruit lymphocytes (9). Whilst it not known which subtypes cause this, this is likely not to be lining layer fibroblasts (8). **(B)** Endothelial cells drive the formation of sublining fibroblasts via Notch3 signalling (141). **(C)** Fibroblasts exhibit immunomodulatory effects on Mϕ, contributing to their pro-inflammatory phenotype (133, 134, 142, and 143). **(D)** Pro-inflammatory Mϕ increase fibroblast invasiveness (133, 134, and 144). **(E)** Anti-inflammatory Mϕ induce a repair response in fibroblasts (e.g., increasing expression of collagen type 1A and transforming Growth Factor Beta Induced) (133). Created with BioRender.com, adapted from (39).

1.5.3.1 Fibroblasts

Fibroblasts in health

Fibroblasts are the most abundant cell of the joint and their primary role is to maintain cartilage integrity and lubricate the joint (39, 145). Increasing evidence suggests synovial fibroblasts are also involved with, and in fact orchestrate, processes of inflammation (39, 146). They can be described as immune sentinel cells due to their expression of toll-like receptors (TLRs) 2, 3 and 4 and PAMP recognition receptors (e.g., non-obese diabetic (NOD)-like receptor) (147). Furthermore, they have been demonstrated to exhibit memory which can be maintained in culture (148). Fibroblasts isolated from the non-inflamed joint, but not those isolated from the dermis, were able to mount an augmented response (producing IL-6, and NF-κB signalling molecules) when re-stimulated with either TNF-α or IL-1α (stimulated for 24 hours, rested for 24 hours, and re-stimulated) (148). This suggests joint fibroblasts are primed to respond to inflammatory stimuli (148), at least partially explaining their pathogenic role in RA.

Fibroblasts in RA

In RA, synovial fibroblasts (SF) drive disease via two mechanisms. Firstly, they become activated and adopt a pro-inflammatory phenotype which actively drives persistent inflammation (39, 149). Furthermore, via production of matrix metalloproteinases (MMPs), they also contribute to the damage and destruction of the joint; degrading cartilage and bone (150, 151).

The idea of the pathogenic switch in RA has been around for many years and, as early as 1966, abnormalities in rheumatoid synovial cells were reported (152). Furthermore, this

pathogenic phenotype is maintained in culture (39, 153). Isolated and cultured RA fibroblasts express multiples markers of activation including; THY1 (CD90), podoplanin (PDPN), VCAM1, CD44 and fibroblast activation protein α (FAPα) (39, 153). Notably, a number of epigenetic changes in SF have also been identified, the most prevalent of which is DNA methylation (154, 155). Indeed, alterations in the DNA methylation state was able to separate non-inflamed, resolving arthritis, established RA (7-50 yrs. symptom duration, on DMARDs) and very early RA (< 12-week symptom duration) patients (154). This showed for the first changes occur in methylation at the very stages of disease (154).

This phenotypic switch may be caused, at least in part, by priming of fibroblasts from the inflammatory milieu of the inflamed joint (e.g. TNF-α) (156). For instance, the aforementioned augmented response observed in both inflamed and non-inflamed synovial fibroblasts (148). Likewise, fibroblasts isolated from RA patients undergoing joint replacement which were chronically stimulated with TNF-α for 3 days, then with IFNγ or IFNβ for 3 hours, acquired a series of genetic and epigenetic changes, compared to those not chronically stimulated with TNF-α (156). This included chromatin priming, nuclear factor kappa light chain enhancer of activated B cells (NF-κB) activation, and increased mRNA and protein levels of signal transducer and activation of transcription 1 (STAT1) and its downstream effectors (156). Furthermore, up to 3 days after the removal of TNF-α stimuli this heightened response was maintained (156). This indicates that, due to the inflammatory milieu within the joint (in particular TNF-α), fibroblasts can be primed and this imprint is maintained even in the absence of any stimuli.

Due to this priming effect, fibroblasts may be regarded as “passive responders” to their inflammatory microenvironment (157). However, during the course of disease this genetic and epigenetic imprinting causes them to become active drivers of inflammation, i.e. “imprinted aggressors” (157). This change in phenotype is highlighted by fibroblasts role in the progression of disease multiple joints (158). *In vivo* experiments have demonstrated that RA fibroblasts implanted into SCID mice migrated to the cartilage via the vasculature (independent of where they were applied) and resulted in destruction of the target cartilage (158). Likewise, when exploring fibroblast: EC interactions (more in section 1.5.3.2), it was demonstrated that fibroblasts undergo 2 pathogenic switches; (1) a loss of the immunosuppressive function, and (2) acquisition of a stimulatory phenotype (9). Thus, whilst fibroblasts might initially only be responding to a pro-inflammatory environment, they become key drivers in the pathogenesis and progression of RA.

SF are known to exist as subsets (8, 141, 159) and are often classified according to their location in the lining or sublining layer of the synovium (39, 160, 161). Some of the first single-cell RNA-seq (scRNA-seq) data (combined with bulk RNA-seq and immunofluorescent staining) of RA and osteoarthritis (OA) patients defined three major fibroblast subsets; $CD34^{-}THY^{-}$, $CD34^{+}$ and $CD34^{-}THY1^{+}$ (160). The $CD34^{-}THY1^{-}$ fibroblasts were specific to the lining layer and expressed high gene and protein levels of matrix metalloproteinases 1 and 3 (MMP1 and 3), known to mediate tissue damage in the joint (39, 160). The $CD34^{+}$ population were located in both the lining and sublining had high expression of IL-6, CXCL12 and CCL2, and secreted large amounts of these when stimulated with TNF-α *in vitro* (39, 160). Correspondingly, these fibroblasts also recruited a larger number of monocytes in the

transwell assay compared to the other fibroblast subsets (39, 160). The $CD34^{-}THY1^{+}$ fibroblasts were found in the sublining, close to blood vessels (39, 160). In RA, these were located in large perivascular zone close to accumulated leukocytes, but in OA appeared as a thin layer with few cells (39, 160). These $CD34^{-}THY1^{+}$ were described as pathogenic, as they expressed high levels of FAP, PDPN and VCAM1 (known markers of fibroblast activation) (39, 160). Further supporting this, swollen joints had fewer $CD34^{-}THY1^{-}$ and more $CD34^{-}THY1^{+}$ and $CD34^{+}$ fibroblasts (160). Moreover, the $CD34^{-}THY1^{+}$ fibroblasts, also positive for PDPN and CDH11, were expanded threefold in patients with RA compared to OA (160). Thus, it is evident that there are subsets of fibroblasts responsible for driving RA, and furthermore different subsets drive different aspects of disease. This is further supported by recent *in vivo* studies where adoptive transfer of $FAP\alpha^{+}THY1^{+}$ (sub-lining) fibroblasts into serum transfer induced arthritic (STIA) mice caused a significant increase in leukocyte infiltration with minimal bone erosion, whilst the opposite was observed with the adoptive transfer of $FAP\alpha^{+}THY1^{-}$ (lining) fibroblasts (8). This demonstrates that sub-lining fibroblasts drive inflammation, whilst lining layer fibroblasts are responsible for tissue damage (8).

A recent study has demonstrated that different pathotypes of RA (i.e., lymphoid, myeloid and fibroid) are associated with different fibroblast subsets (162). Deconvolution of bulk-RNA seq data from 87 treatment-naïve patients with early RA (<1 year symptom duration) was performed using publicly available scRNA-seq data and identified 4 fibroblast clusters associated with the lining (Proteoglycan 4; $PRG4^{+}$) and sublining ($CXCL12^{+}$, Periostin ($POSTN^{+}$ and $CXCL14^{+}$) (162). Of these, $PRG4^{+}$ SF were highest in myeloid, whilst $CXCL12^{+}$ and $POSTN^{+}$ were increased in the fibroid phenotype and no significant differences was observed

in CXCL14+ SF across the pathotypes (162). These SF subtypes were then correlated with a variety of clinical parameters (e.g. CRP, DAS, swollen and tender joint count (SJC and TJC)) to assess associations with disease activity (162). $PRG4^+$ SF correlated positively with disease in fibroid, but negatively for myeloid, whilst $POSTN^+$ SF correlated positively in lymphoid (162). $CXCL14^+$ SF had a negative association with disease severity across all pathotypes (162). Taken together, these results suggest that fibroblast subsets drive different aspects of disease. This may result in different forms of "communication" with neighbouring cells (macrophages and endothelial cells), and indeed might play a role in driving the subsets observed in these cell types.

1.5.3.2 Endothelial cells

Endothelial cells in health

The blood vascular network performs many crucial roles; including, but not limited to; maintaining and regulating blood flow, controlling vessel permeability and the quiescence of circulating leukocytes. Most significantly in the context of this work they act as a gatekeeper to control leukocyte recruitment and infiltration into tissue (163). In order to perform these wide variety of functions, endothelial cells (ECs) are very heterogeneous with differences largely dependent on function, anatomical location and vessel type (i.e., artery, vein or capillary) (164). Indeed, hierarchical clustering of transcriptional data from 53 cultured ECs found they clustered based on site of origin and split into 2 main branches; large vessels vs microvascular (165). More recently, single cell transcriptome analysis of murine healthy tissue showed that whilst ECs had similar transcriptomes dependent on vessel type (arteries, capillaries, veins and lymphatics), tissue was the cause of EC heterogeneity (166). This demonstrates that ECs act as reporters for their local microenvironment.

Building on this idea, fibroblasts and other stromal cells are able to define tissue specific "address codes", via their interactions with ECs (10, 167). The effect of stromal cells on the EC phenotype has been demonstrated multiple times via *in vitro* co-culture assays (9, 168). For example, microarray analysis of human vein umbilical ECs (HUVECs) cultured with dermal or synovial fibroblasts, revealed ECs clustered strongly dependent to the fibroblasts site of origin (168). Crucially, in health, stromal cells exert a pro-resolving effect on ECs and help maintain homeostasis. For example, in a flow based adhesion assay, fibroblasts isolated from the skin, non-inflamed (NI) or resolving arthritis (Res), down-regulated EC responses to cytokines such that less lymphocyte recruitment was observed (9, 168). Similar observations have been seen with other stromal cells from healthy donors, for instance podocytes from the kidney and adipocytes in stem cell or mature state, limited lymphocyte recruitment (169). Likewise, mesenchymal stem cells from bone marrow, umbilical cord or trabecular bone of healthy donors restricted neutrophil recruitment in an IL-6 dependent manner (169). These immunoprotective functions of stromal cells highlights the importance of stromal-endothelial crosstalk and via this, the ability of stromal cells to regulate leukocyte recruitment. Significantly, however, pathogenic changes in stromal cells (e.g., fibroblasts in RA) results in pathogenic interactions with the ECs and can have severe consequences.

Endothelial cells in RA

The endothelium is known to play an active role in perpetuating inflammation within all chronic inflammatory diseases (170). In RA, they do this principally via (i) increased adhesion molecule expression leading to increased leukocyte recruitment; (ii) angiogenesis to allow

the growing pannus to form; and (ii) increased permeability leading to oedema formation and swelling of the joint (170, 171). Of particular interest within this thesis is the role they play regarding leukocyte recruitment to the joint, as well as their interactions with surrounding fibroblasts.

Whilst the precise mechanism remains unclear, at some point in the initial stages of disease, the endothelium is activated to express high levels of adhesion molecules (135, 136). IHC of the chronically inflamed established RA synovium, revealed that ICAM-1 and Clever-1 (a.k.a. Stabilin-1) are ubiquitously expressed, but selectins and VCAM-1 and ICAM-3 appeared only on a subset of ECs, suggesting the presence of endothelial subpopulations (136-138). Likewise, in patients with untreated inflammatory arthritis (disease duration ~16 months; 9 RA, 3 PsA and 1 ankylosing spondylitis), expression of E-selectin and ICAM1 (both soluble and membrane-bound) were inversely correlated, indicating that these molecules play differing roles in leukocyte trafficking and disease pathogenesis (182). Further supporting the idea of subpopulations, PNAd, typically seen on the HEVs of lymphoid organs (139), was also found on subsets of ECs in both RA and psoriatic arthritis (PsA) sections (136, 140), and as mentioned in 1.5.2 is associated with the formation of TLSs (132). This may, at least partially, account for the different pathotypes observed, in particular follicular vs diffuses (129). Surprisingly, vascular adhesion protein (VAP1), typically found on mucosal EC, was also highly expressed across the RA endothelium (136). Furthermore, using a Stamper-Woodruff assay (which measures lymphocyte binding to tissue sections) it was demonstrated that VAP-1 was crucial for the binding of gut-derived lymphocytes and immunoblasts to RA synovial sections (136). This suggests that the synovial endothelium acquires the ability to traffic gut-

homing T cells by “hijacking” the stromal address codes of other tissues, supporting the idea of mucosal microbiome involvement in RA pathogenesis (10, 18, 112, 113, 136). Interestingly, studies in CIA (collagen induced arthritis) mice have shown that trafficking of gut-derived T cells, in particular Tregs, suppressed disease and production of the gut-derived neuropeptide, cortistatin, suppressed synovial expression of IL-17 (10, 172, 173). Furthermore, preventing trafficking of T_{FH} and T_H17 back to the gut (via blockade of β7 integrin) in K/BxN mice lead to exacerbated arthritis (10, 174). Taken together, this suggests gut-derived T cells play a regulatory role during joint inflammation which is altered in the pathogenesis of RA.

Crucially, isolation of joint replacement RA synovial microvascular ECs (SMECs) has revealed that ECs are imprinted with a disease-specific phenotype that is maintained in culture (175). In response to 24-hour TNF-α stimulation, SMECs expressed less VCAM-1, similar levels of ICAM-1, and 30% more E-selectin compared to human umbilical vein endothelial cells (HUVECs) or adipose-derived microvascular EC (ADMECs) (175). Most importantly, TNF-α stimulated SMECs captured significantly more T cells and neutrophils than HUVECs in flow-based adhesion assays (175). This demonstrates that at the late stages of RA the microvasculature is imprinted with a pathogenic phenotype that is highly sensitive to TNF-α stimulation (175). This pathogenic endothelium enables the selective recruitment of leukocytes and suggests they play a crucial role in maintaining chronic inflammation within the joint (175)

In addition, decreasing expression of EC adhesion molecules also highlights their pathogenic role (171, 176-180). For example, preliminary data from phase I/II trials showed that blocking of ICAM-1 was able to prevent T cell trafficking and reduced disease activity in some patients (171, 177, and 178). Similarly, TNF-α inhibitors, commonly used to treat RA, have been shown to decrease serum levels of ICAM-1 and E-selectin (176), suggesting these decrease endothelial activation and hence reduce leukocyte migration (171). Furthermore, anti-TNF treatment has been associated with improved endothelial function (the ability to dilate and restrict in response to stimuli) (180). In animal models, blocking of E-selectin, but not P-selectin, in rat adjuvant-induced arthritis (AIA) inhibited T cell migration (179). Whilst blocking of VCAM-1 in CIA mice reduced disease severity, most likely by preventing B cell recruitment [as the population of immature B cells in peripheral blood increased the most (3.8 fold) compared to other leukocyte populations following blockade treatment] (181). Thus, decreasing endothelial adhesion molecules (either via blockade or decreasing expression), in both animal models and humans, results in reduced disease activity and underscores the importance of the endothelium in RA pathogenesis.

Interestingly, differences in expression of EC adhesion molecules within the early stages of RA have also been observed. For example, expression of the Duffy antigen was significantly higher in seen in early (< 1-year symptom duration) RA patients compared to non-RA (183). However, this subsequently decreased with disease duration, and patients with longstanding (18 years) RA had significantly lower expression of the Duffy antigen than the non-RA controls (183). This differential expression across disease duration may be due to effects of

treatment, however, the increased expression of Duffy antigen early in RA indicates a role in the initial events of pathogenesis (183).

In summary, the endothelial phenotype is altered with disease and thus contributes to the perpetuation of inflammation within RA. Most significantly, these changes can occur very early in disease pathogenesis. Understanding precisely what, how, and why these changes occur is crucial for unpicking the mechanisms of disease. Moreover, part of the puzzle may lie in endothelial communication with neighbouring fibroblasts, a topic discussed in more depth below.

Endothelial-fibroblast crosstalk in RA

As mentioned in 1.5.3.1, in RA, fibroblasts undergo two distinct phenotypic changes; the loss of their immunosuppressive function and later acquisition of a stimulatory phenotype (9). This was demonstrated analysing fibroblast communication with ECs in an *in vitro* flow based adhesion assay (9). Under TNF-α-IFNγ stimulated conditions, ECs cultured with fibroblasts from patients with very early RA (<12 weeks symptom duration; VeRA), recruited significantly more lymphocytes than when in co-culture with NI or Res fibroblasts; comparable to no fibroblasts being present (9). Importantly, both the immunosuppressive function of Res SF and loss of immunosuppressive function in VeRA SF was dependent on IL-6 and TGF-β (9). This was supported by transcriptional changes; qPCR revealed expression of Suppressor of Cytokine Signalling 3 (SOCS3; a negative regulator of IL-6) was significantly lower in ECs cultured with VeRA or JRep, compared to Res fibroblasts (9).

On the other hand, fibroblasts from patients with RA undergoing joint replacement (JRep) were able to stimulate the endothelium in the absence of any exogenous cytokines and consequently increased recruitment of both lymphocytes and neutrophils (9, 168, 184-186). That JRep fibroblasts alter the EC phenotype is further supported by a range of transcriptional and functional data (168, 184). For instance, hierarchal clustering of microarray data, demonstrated that ECs cultured with JRep synovial fibroblasts were distinct from ECs in mono-culture or cultured with dermal fibroblasts (from the same RA patients) (168). Similarly, qPCR of ECs co-cultured with JRep fibroblasts showed expression of Duffy Antigen Receptor for Chemokines (DARC) and CXCL5 is upregulated in ECs co-cultured with JRep fibroblasts, compared to mono-cultures or culture with patient matched dermal fibroblasts (184). Further functional experiments demonstrated that DARC is essential for the recruitment of neutrophils in a CXCL5 dependent manner, which combined with the high expression of Duffy antigen observed in early RA (183), suggests DARC mediated neutrophil recruitment is elevated in early RA (183, 184). This pro-inflammatory action was caused primarily via trafficking of the fibroblast derived chemokines, CXCL5 and CXCL12, to the surface of the endothelium where they can support leukocyte binding via P-selectin (neutrophils) (184, 185) or $\alpha_4\beta_1$-VCAM-1 interactions (lymphocytes) (18, 168).

Taken together, these results demonstrate there is a changing role of fibroblasts during the course of RA. Moreover, fibroblasts are able to exert their pathogenic effects by altering the endothelial phenotype. Further investigations into how and why this occurs are required in order to unpick the mechanisms of disease, and find potential therapeutic interventions.

In relation to the fibroblast subsets (described in 1.5.3.1), the adoptive transfer of $FAP\alpha^{+}THY1^{+}$ (sub-lining), but not the $FAP\alpha^{+}THY1^{-}$ (lining), layer fibroblasts was able to increase leukocyte recruitment (8). This suggests only the $FAP\alpha^{+}THY1^{+}$ subset of fibroblasts would be able to "talk" to the endothelium and thus fuel the recruitment of leukocytes (8). However, if this is truly case, or whether these fibroblasts are stimulating macrophages which in turn stimulate the endothelium is yet to be elucidated.

Crucially, fibroblast: EC crosstalk is also bidirectional. Building on the above knowledge of fibroblast subsets driving different aspects of disease, single cell analysis of RA patient tissue revealed a transcriptional gradient emanating from the endothelium outwards (141). Creation of fibroblast organoids with and without ECs then demonstrated that ECs were required for the formation of sublining fibroblasts; driven by Notch3 signalling (141). Moreover, absence of NOTCH3 (either knock out mice or antagonist antibody treatment) significantly reduced disease activity and paw swelling in STIA mice compared to control animals (141). This suggests both EC to fibroblast and fibroblast to EC cross-talk is required in the pathogenesis of RA. Further investigation into these two cell types and their interactions is urgently needed.

1.5.3.3 Macrophages

Macrophages in health

Macrophages are innate immune cells of myeloid lineage, responsible for maintaining tissue homeostasis; crucial in both the initiation and resolution of inflammation (187). They are known to have at least two origins; (1) tissue-resident macrophages (TRMs), derived from the yolk sac and persist in tissue via self-renewal (188, 189) and (2) monocyte derived

macrophages (MDMs) that are present due to monocytes infiltrating the tissue and differentiating into macrophages (188, 189). During homeostasis, the TRMs remove or respond to pathogens and toxins, clear any apoptotic cells, proteins or phospholipids and via crosstalk with other stromal cells maintain tissue homeostasis (188). In response to infection or damage, monocytes in the circulation are recruited to the tissue (188-190), and differentiate into macrophages (MDMs). These MDMs have an overtly pro-inflammatory phenotype expressing cytokines such as IL-1β and TNF-α, whilst TRMs are anti-inflammatory, expressing cytokines such as IL-4 and IL-10 (189, 190). During acute inflammation the proportion of TRMs to MDMs changes as MDMs are recruited and proliferate, whilst TRMs decrease due to cell death and suppression of proliferation (191). In resolution, the populations revert back to those seen in homeostasis as TRMs self-renew and MDMs undergo apoptosis or conversion into tissue-resident macrophages (191).

Macrophages are also commonly described as having an M1 (classically) or M2 (alternatively) activated phenotype, summarised in Figure 1.7 (192-194). M1-like (classically activated) macrophages are induced by exposure to IFN-γ combined with either lipopolysaccharide (LPS) or TNF-α resulting in a Th1 response (i.e. type 1 inflammation, killing intracellular pathogens and tumour resistance) (194). On the other hand, M2 macrophages have a Th2 response with more immunoregulatory and pro-tumoral properties (194). These can be further separated into; M2a, induced by IL-4 and IL-13; M2b, induced by immune complexes and TLR or IL-1R ligands, and M2c, induced by IL-10, each with slightly differing immunoregulatory functions ((194)).

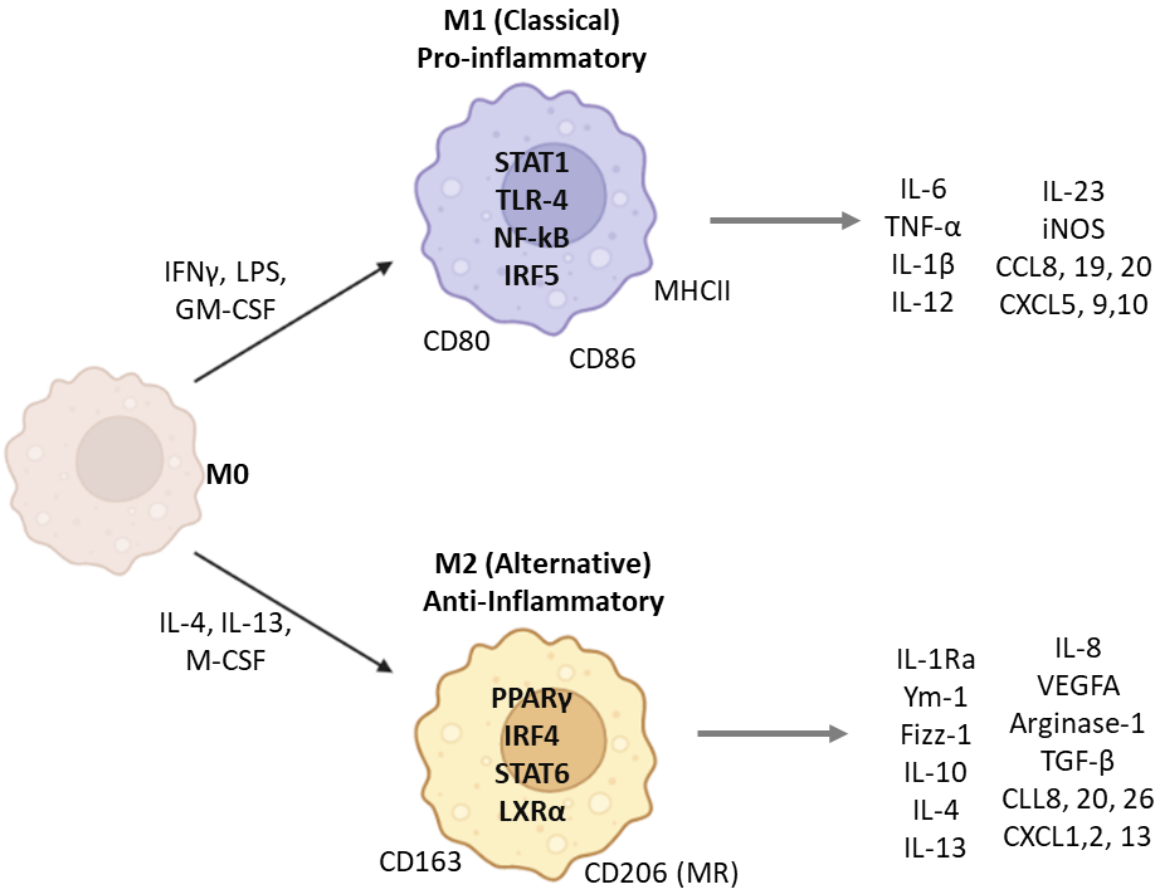

Figure 1.7: Polarisation of M1 and M2 like macrophages. Polarisation of macrophages from M0 (brown) into an M1 (blue/purple) or M2 (orange) like phenotype. Examples of characteristic stimuli, transcription factors, cell surface markers and mediators each type produce is also shown. (G)M-CSF = (Granulocyte-) Macrophage-Colony stimulating factor; IFNγ = Interferon gamma; IL = Interleukin; iNOS = Inducible nitric oxide synthase; IRF = Interferon regulatory factor; LPS = Lipopolysaccharide; LXRα = Liver X receptor alpha; MHCII = Major histocompatibility complex II; MR = mannose receptor; NF-κB = Nuclear factor kappa B; PPARγ = Peroxisome proliferator-activated receptor gamma; STAT = Signal transducer and activator of transcription; TGF-β = Transforming growth factor beta; TLR = Toll-like receptor ; TNF-α = Tumour necrosis factor alpha; VEGFA = Vascular endothelial growth factor A. Figure created with BioRender.com and adapted from multiple sources (194-199).

Macrophages in RA

Macrophages, and moreover an altered macrophages phenotype or change in the proportion of subsets, plays a major role in the pathogenesis of RA (200). In fact, during RA disease progression, macrophages become one of the most abundant cells (30-40%) of the joint due to a major influx of monocytes, evasion of apoptosis and increased proliferation (200-202). Accordingly, changes in the $CD68^+$ cell population of the sublining directly correlate with the DAS28 score and can be used to predict the efficacy of treatment in patients (203). Likewise, macrophage count has been demonstrated to correlate with articular destruction in RA patients (182).

As highlighted in the previous section, macrophages are an incredibly heterogeneous (204) and multiple subsets of macrophages have been described (205, 206). Early studies looking at septic arthritis (SA), RA, OA and healthy joints identified three populations of macrophage; 25F9+, CD163+ and the S100A8/9 alarmin+, which changed in distribution according to the state of inflammation (205, 206). $25F9^+$ macrophages were associated with non-inflamed sections of synovium in OA and SA patients (205, 206), and due to their high expression of IL-1Ra (the IL-1R antagonist) were thought to have anti-inflammatory role (206, 207). CD163+ macrophages were found primarily in healthy joints and deemed to have protective phenotype against inflammation due to the presence of phagosomes and expression of MHC-II, IL-1R antagonist and osteprotegerin (OPG; an inhibitor of bone degradation) (207). On the other hand, the S100A8/9+ macrophages were observed in RA and the inflamed areas of SA joints, but much less in OA (205, 207, and 208). Notably S100A8/9 alarmins (aka MRP8 and MRP14), are known biomarkers of inflammation (174),

suggesting these are a distinctly pro-inflammatory subset (205, 208, 209). They may also be described as having M1-like phenotype, as they produce pro-inflammatory cytokines and chemokines including; TNF, IL-1β, IL-6, IL-15, granulocyte macrophage colony-stimulating factor (GM-CSF), TGF-β and, particularly in early stages of disease, CXCL4 and CXCL7 (for the recruitment of neutrophils and monocytes) (207). Furthermore, these macrophages are susceptible to anti-TNF treatment (208), which removes them via rapid efflux (210). On the other hand, the RM3/1^{+} macrophages were unaffected by TNF treatment, supporting the idea that these are anti- or at non-inflammatory macrophages.

The growing field of scRNA-Seq further supports the idea of macrophage subsets. Recent data has shown Macrophages from the RA and OA synovium clustered into 4 groups, and subsequent bulk RNA-Seq assessed whether genes associated with each cluster were higher in RA or OA (134). From this, a heparin binding EGF-like growth factor (HBEGF)$^{+}$ cluster and an "IFN/STAT" cluster, positive for IFN-stimulated genes (e.g., IFI6 and IFI44L) had genes enriched more in RA than OA (134). On the other hand, a MerTK^{+} cluster was identified, and these cells expressed genes more associated with OA than RA (134). This is consistent with other single cell data of Macrophages where the MerTK^{+}CD206^{+} population appeared in lower numbers in treatment naïve or resistant RA patients, with a lower population associated with a higher risk of flare (133). Furthermore, in response to lipopolysaccharides (LPS) this MerTK^{+}CD206^{+} population produced resolvin D1 (an inflammatory-resolving lipid mediator), whilst the MerTK^{-}CD206^{-} population produced pro-inflammatory cytokines (133). This again highlights macrophages populations in RA are primarily pro-inflammatory, but

with treatment and/or resolution of disease the populations shift back to a more anti-/non-inflammatory phenotype.

Similarly, murine models have indicated altered macrophage proportions in disease and furthermore that these drive disease in different ways (207, 211). Macrophages can originate from either the bone marrow (MDMs; F4/80^{-}CD11b^{+}) or embryo (TRMs; F4/80^{+}CD11b^{-}), and are regarded as having pro or anti-inflammatory properties, respectively (189). In CIA mice, the population of the pro-inflammatory MDMs increased at the peak of inflammation then decreased in resolution, whilst the anti-inflammatory TRMs did the opposite (189, 190). Furthermore, they demonstrated that the RA synovium had a lower percentage of EMR1^{+} (equivalent to F4/80^{+}) macrophages when compared to OA (190). Additionally, the EMR1^{high}CD11b^{low} macrophages population from RA patients had increased expression of CD163, suggesting an M2-like phenotype. Conversely, the EMR1^{low}CD11b^{high} population had increased expression of CD80 indicative of an M1 phenotype (190). Regarding subtypes driving different forms of pathogenesis, macrophage derived from Ly6C^{+} or Ly6C^{-} monocytes have different roles in RA mouse models (207). Via depletion and selective rescue, it was demonstrated that Ly6C^{-} cause inflammation in the STIA (212). On the other hand, AIA in CCR2 deficient mice (which is crucial for Ly6C^{+} monocyte trafficking) almost completely abolished the number of macrophages, suggesting Ly6C^{+} macrophages are crucial for AIA (211). In patients, radioisotope labelling of CD14^{+} (similar to Ly6C^{+}) monocytes found these were trafficked to the synovium during inflammation (213), however, trafficking of CD14^{-} monocytes remains to be confirmed (207).

Taken together, these findings demonstrate that RA pathogenesis is associated not only with an increase in absolute number of macrophages, but also changes in the proportion of macrophage subsets. Due to the very distinct functions of these macrophage populations, it is essential to differentiate between them when discussing the effect of macrophages, as opposed to regarding them as one, pathogenic, cell type.

Macrophage-fibroblast crosstalk in RA

As the two predominant cells of the synovium, fibroblast-macrophage crosstalk has been studied for many years within the context of RA (133, 134, 142-144, 214). Early *in vitro* studies examined the effect of macrophages on fibroblast induced cartilage destruction (144). This revealed that macrophages (U937 cell-line), via their release of TNF-α and IL-1β, were required for OA or RA fibroblasts to degrade cartilage (144). Later studies assessed the inflammatory effects of co-culture conditions (142, 143). Using macrophage and fibroblast murine cell lines (RAW264.7 and CL.7 respectively), it was demonstrated that ICAM-1 and oxygen radicals from fibroblasts stimulated macrophages to produce macrophage inflammatory protein 1 α (MIP-1α) (142). Furthermore, experiments by Donlin *et al* examined the effect of RA fibroblasts (from patients undergoing joint replacement) co-cultured with M-CSF differentiated monocytes (143). In response to TNF-α, the synovial fibroblasts suppressed the IFN-β response in macrophages, including chemokines involved in classical macrophage activation (CXCL9 and CXCL10) (143). Incubation of the macrophages with fibroblast supernatants alone indicated the effect was driven by soluble factor(s) (143). Furthermore, these factor(s) decreased IFN-β and TNF-α induced production and phosphorylation of STAT1 and 2 (143). Transcriptional analysis revealed the fibroblasts

regulated around one third of the TNF-α stimulated genes in macrophages, including genes required for macrophage survival and differentiation to an activated phenotype (e.g. M-CSF, IL-4, IL-13) (143). Taken together these co-culture experiments suggest there is bidirectional crosstalk between macrophages and fibroblasts; macrophages are required for fibroblasts to degrade cartilage, whilst fibroblasts have immunomodulatory effects on the macrophages.

Combining the knowledge from these co-cultures, and the macrophage subsets identified from single cell RNA-sequencing, the crosstalk of macrophage subsets and fibroblasts has also been examined (133, 143). Co-culture of fibroblasts with monocyte derived macrophages, in TNF-α stimulated conditions, indicated that fibroblasts drove the formation of the $HBEGF^+$ inflammatory macrophage subset (134). On the other hand, co-culture of the $HBEGF^+$ macrophages subset with fibroblasts, increased fibroblast expression of multiple genes, including granulocyte colony-stimulating factor (G-CSF) and IL-33 (134). Subsequent pathway analysis and functional inhibition identified epidermal growth factor receptor (EGFR) as an upstream regulator in these co-cultures (134). Furthermore in a Matrigel invasion assay, incubation with $HBEGF^+$ macrophages caused increased invasiveness of fibroblasts which was diminished upon EGFR inhibition (134). This demonstrates (similarly to the earlier studies described in the above paragraph), a bidirectional crosstalk; the $HBEGF^+$ macrophages are shaped by the presence of fibroblasts in the joint, whilst at same time these macrophages promote the invasiveness of the fibroblasts in an EGFR dependent manner (134). Another single cell study investigated how macrophage subsets can alter the fibroblast subsets they are cultured with (133). Mono-cultured RA SF clustered into 4 subsets according to the expression of: (1) ECM proteins, (2) cell adhesion molecules, (3) receptors

of TGF-β and resolvin, or (4) glycolytic enzyme and proliferation markers (133). However, when co-cultured with MerTK^{-}CD206^{-} macrophage populations, a fifth fibroblast population emerged characterised by high expression of mediators for cartilage and bone destruction (e.g., MMP1/3 and RANKL), pro-inflammatory cytokines (e.g. IL-6) and chemokines (e.g. CXCL8) (133). On the other hand, co-culture with MerTK^{+}CD206^{+} macrophages (particularly those from sustained RA remission) induced the repair response of the fibroblasts by increasing expression of collagen and TGF-β response genes (133). This again demonstrates that pro-inflammatory (MerTK^{-}CD206^{-}) macrophages induce a destructive phenotype in fibroblasts (133). Moreover, non-inflammatory (MerTK^{+}CD206^{+}) macrophages do not, and instead communicate with fibroblasts to aid the remission of disease (133).

Taken together, these results suggest pro-inflammatory macrophage: SF crosstalk contributes to pathogenesis of RA. However, there is still little known about how, or even if, this crosstalk changes during the course of disease. Consequently, this aspect of macrophage: fibroblast crosstalk was investigated in the thesis of Dr Jason Turner (214). Initial quantitative real-time polymerase chain reaction (qRT-PCR) experiments performed on unstimulated macrophages (M-CSF differentiated blood monocytes) co-cultured with fibroblast from resolving arthritis, very early RA (VeRA) and joint replacement RA (JRep) showed no significant difference in TNF-α, IL-10 or STAT1 gene expression (214). However, following the work of Donlin *et al* (discussed above) further co-cultures experiments were performed, assessing gene expression upon 16 hours of TNF-α stimulation (214). Consistent with these previous findings, upon culture with fibroblasts, there was decreased macrophage expression of CXCL9, CXCL10, IFIT1 (Interferon Induced Protein with

Tetratricopeptide Repeats 1) and MX1 (Interferon-induced GTP-binding protein) (143, 214). However, contrary to Donlin *et al*, a decrease was also observed in IL-1β and NKG7 (Natural Killer Cell Granule Protein 7), and no modulation was seen in the interferon genes (143, 214). Despite the variability of these results, these data, combined with that of others, suggests there is a change in macrophage and fibroblast gene expression upon co-culture. Whether and how this is interaction is altered during disease remains to be determined.

1.5.4 Technologies used to investigate stromal cells in RA

1.5.4.1 Staining of tissue sections

As highlighted in the sections on RA and PMR pathogenesis, staining of tissue sections is an incredibly useful tool for analysing the protein expression on cells and consequently aids in understanding the mechanisms of disease. For example, within RA this led to the identification of the different tissue pathotypes, and revealed the patterns of adhesion molecule expression on the chronically inflamed (e.g., RA) compared to normal synovial endothelium (1.5.3.2). Furthermore, imaging can be used to identify novel biomarkers or distinguish patient subsets for targeted treatments. This is already commonly used in the cancer field (215), and will most likely become routine in RA [e.g., stratifying patients treatment according to tissue pathotypes (117)].

IHC and immunofluorescence (IF) staining are most commonly used to analyse tissue sections and can be performed on paraffin-embedded or frozen sections. IHC is perfect for giving an overview of tissue architecture and morphology and can image multiple antigens (multiplexing) to identify different cell populations. However, IHC cannot easily distinguish antigens that co-localise within a cell and so for this (and often other forms of multiplexing),

IF is preferred. Standard IF staining allows the visualisation of up to 5 fluorescent markers per section due to limits in the excitation/emission spectra (216). The CellDIVE multiplex imaging platform overcomes this limitation by bleaching the slide in between rounds of staining with 4 fluorescent dyes (one of which is always DAPI) (217). The stain, bleach, re-stain process can be repeated multiple times and enables the imaging of up to 60 markers per section (217). This is useful, as it enables the assessment of markers simultaneously across the tissue and also uses the minimal amount of tissue. Notably, however, there are drawbacks to this technique. In particular, continuously coverslipping and decoverslipping of the sections can lead to considerable loss of tissue sections (discussed more in 4.1.1.1), especially when using sensitive tissues such as synovial biopsies. Here, this relatively novel technique is used to assess the expression of endothelial cell markers in very early RA, resolving and RA patients undergoing joint replacement to assess if there are changes in expression of these, between RA and resolving patients and across the course of disease.

1.5.4.2 RNA sequencing

RNA sequencing (RNA-Seq) provides an in-depth, untargeted analysis of cells transcriptome. The transcriptome consists of two types of RNA; protein coding and non-coding. Historically, the protein coding mRNAs were of more interest as they were thought to provide an indirect measurement of protein expression within the cell. However, there are also many types of non-coding RNAs (ncRNAs), including micro RNAs, piwi-interacting RNAs, and long-noncoding RNAs, which are able to regulate gene expression and interest in these classes of RNA is quickly gaining traction (218). Compared to previous techniques, such as Sanger sequencing and microarray-based methods, RNA-Seq offers wider coverage and greater resolution (218, 219). Even in relation to more recent technologies (e.g. single cell-

sequencing and spatial transcriptomics) which provide higher sequencing precision (i.e. looking at very few or single cells), these techniques do not yet match the depth (i.e. ability to detect lowly expressed genes) obtained in RNA-Seq analysis (219).

Generally, an RNA-Seq experiment consists of RNA isolation and selection of species of interest (e.g. via ribosomal depletion, poly-A selection); conversion to complementary DNA (cDNA); preparation of the cDNA library; and finally sequencing on a next generation sequencing (NGS) platform (218). There are primarily two forms of NGS; ensemble-based, which sequences multiple copies of one DNA fragment, or single molecule, which sequences one DNA molecule. By far the most commonly used, is Illumina's ensemble-based, sequencing-by-synthesis approach (218). For this, the DNA molecules are immobilised then clonally amplified with fluorescently labelled reversible-terminator nucleotides (218). This has very low (<1%) sequencing error, however due to the use of PCR may introduce amplification biases that needs correcting in downstream analysis (218). On the other hand, single-molecule sequencing platforms, such as PacBio, lack this PCR step so have no amplification bias, but it also have a relatively high (~5%) error rate (218). The resulting reads are then aligned to the genome and quantified.

In this study, RNA sequencing has been used to assess the cross-talk of endothelial cells: fibroblasts, and macrophages: fibroblasts. This method was chosen due to the high sequencing depth (compared to scRNA-seq), unbiased approach and large number of transcripts quantified (compared to qPCR/microarrays) which allows the broad assessment of transcriptomic changes. There are issues with using only this technique, as it only

quantifies the mRNA levels, but protein levels or epigenetic changes (e.g., phosphorylation) cannot be determined. However, it is ideal as an initial screening tool to determine if there are any large or small transcriptomic differences that warrant further investigation.

2 Materials and methods

2.1 Ethics

All human samples were obtained with written, informed consent and in compliance with the Declaration of Helsinki.

Serum for NMR analysis were provided by Dr Sarah Mackie, Professor Ann Morgan and Dr Louise Sorensen from the University of Leeds, under the UK GCA Consortium 05/Q1108/28, Leeds West Research Ethics Committee (REC), Clinical trial identifier: NCT04102930; ADDRESS-PMR 13/LO/1094, National Research Ethics Service (NRES) Committee London – Camberwell St Giles, Characterisation of genes/proteins in autoimmune/inflammatory diseases 04/Q1206/107 Leeds East Research Ethics Committee; TABUL 09/H0505/132., Berkshire Research Ethics Committee; Clinical trial identifier NCT00974883.

Biopsy and joint replacement samples were used during this study. Outgrowth fibroblasts were kindly provided by Professor Andrew Filer and Holly Adams (University of Birmingham), whilst tissue sections were kindly provided by Professor Andrew Filer, Dr Saba Nayar and Dr Triin Major (University of Birmingham). Synovial tissue biopsy samples were obtained from treatment-naïve patients with inflammatory arthritis of ≤12-week symptom duration, who at follow up had resolving arthritis (Res) or fulfilled RA classification criteria (very early RA, VeRA). Biopsies were also obtained from patients with arthralgia, but signs of inflammation (Norm) and treatment naïve RA patients with >12 week symptom duration (EstRA). The biopsy samples were collected with approval from the NRES Committee West Midlands – The Black Country (REC 12/WM/0258). Additionally, synovial tissue samples were collected

from patients with established, treated RA undergoing joint replacement at the Royal Orthopaedics Hospital (REC 07/H1204/191).

Sections of tonsil tissue were kindly provided by Saba Nayar (University of Birmingham), REC 10-018.

Human vein endothelial cells (HUVECs) were isolated from umbilical cords donated by participants undergoing an elective caesarean section obtained from Sandwell and West Birmingham Hospitals NHS Foundation Trust and approved by NRES Committee North East – Tyne and Wear South (REC 15/NE/0285).

Monocytes were isolated from the blood of a healthy donor, REC 12/EE/0122.

2.2 Nuclear magnetic resonance sample collection, preparation and analysis

2.2.1 Participants

Samples were provided, and work done in collaboration with Dr Sarah Mackie, Professor Anne Morgan, Dr Louise Sorensen, Emma Harris and Hannah Mathieson from the University of Leeds and Professor Raashid Luqmani at the University of Oxford.

Forty patients with untreated PMR were recruited into the ADDRESS-PMR (The Diagnostic Accuracy of Ultrasound in Suspected PMR) study. They completed visual analogue scores (VAS) for pain and stiffness and FACIT-F (Functional Assessment of Chronic Illness Therapy – Fatigue) scores for fatigue (220) and measurement of inflammatory markers, including CRP,

in the NHS routine diagnostic laboratory. For fatigue analysis to align with the pain and stiffness VAS, FACIT-F scores were reversed (i.e., 52 minus the FACIT-F score) so that those with high fatigue had higher scores, and those with lower levels of fatigue had lower scores. Patients were treated with prednisolone according to clinical guidelines for PMR and attended follow-up at 4- and 26-weeks following treatment (visits 2 and 3) at which time points PMR was confirmed clinically. At each of these time points sera was stored for later analysis.

One hundred and thirty seven patients with suspected GCA recruited into the multi-centre TABUL (The Temporal Artery Biopsy -v- Ultrasound in diagnosis of Giant Cell Arteritis) study (221) were included in the current study if biological samples had been collected within 7 days of high dose prednisolone treatment. It was later confirmed that 84 had GCA (confirmed GCA) and 53 had alternative diagnoses (confirmed non-GCA).

Thirty-nine age-matched controls with no intercurrent illness or underlying autoimmune or inflammatory disease were recruited from members of staff at the University of Leeds or at a cataract pre-assessment clinic.

All participant characteristics are given in results 3.2, Table 3.1.

2.2.2 Sample collection and preparation

Samples were collected and processed as previously described (80, 222). Blood was collected from participants in vacutainer tubes containing clotting accelerator. It was left at room

temperature (RT) for 30 minutes and centrifuged at 2500g for 15 minutes. The serum was extracted and stored at -80°C, until being shipped on dry ice to the University of Birmingham for sample preparation by Dr Stephen Young.

The serum samples were thawed at 4°C then centrifuged at 15,000g at 4°C for 5 minutes. To remove proteins, 200µl from the middle of the sample was added to a washed nanosep filter (washed 6 times as described by Tiziani *et al* (222)) and centrifuged at 10,000g at 4°C for 15 minutes. The filtrate was diluted in a 3:4 ratio with NMR buffer consisting of 1.6mM Difluorotrimethylsilylmethylphosphonic acid, 400mM phosphate, 40% D_2O, 0.4% azide and 2mM 3-(Trimethylsilyl)-1-propanesulfonic acid-d6 (dds-d6)sodium salt and adjusted to pH 7 using hydrogen chloride and then frozen at -80^{o}C until analysis.

2.2.3 Nuclear magnetic resonance spectroscopy

Samples were run by Dr Stephen Young at the University of Birmingham biomolecular NMR facility. Samples were defrosted and transferred to 1.7mm NMR tubes (Bruker Biospin, Coventry, UK) using an Anachem Autosampler. One-dimensional ^{1}H spectra were acquired at 300K using a standard 1D-1H-Nuclear Overhauser Effect Spectroscopy (NOESY) pulse sequence with water saturation using pre-sat in a Bruker AVANCE II 600 MHz NMR spectrometer (Bruker Corp., USA) equipped with a 1.7 mm cryoprobe. Spectral width was set to 12 ppm (parts per million) and the scans were repeated 128 times. Samples series were loaded into 96-tube racks and held at 6^{o}C in the SampleJet sample handing device until processed.

2.2.4 Nuclear magnetic resonance spectroscopy analysis

Spectra were read and processed with Metabolab software (Version 2018.x; Birmingham, UK) (223), and phased, aligned and binned as previously described (80, 224, 225). Each spectrum was phased according to the DSS-d6 peak, then aligned and corrected for baseline offset (80, 224). The spectra were truncated to a range of 0.6 - 8.6 ppm and the water peak removed (80). Spectra were divided into chemical shift "bins" of 0.005 ppm and the spectral area of each bin integrated, then scaled with probabilistic quotient normalization (PQN) to account for differences in sample dilutions (225) and normalised with a generalised log transform ($\lambda = 4e^{-07}$) to equalize the weightings of smaller and larger peaks. Data were then compiled into a matrix where each row represented an individual sample before statistical analysis (80). Metabolites were identified by matching the spectra of known metabolites in serum to the spectrum of the sample using Chenomx (Version 8.1; Chenomx Inc., Edmonton, Canada) (226). The concentration of each metabolite was determined according to the concentration of the reference signal, in this case 0.5mM of DSS-d6, using Chenomx (226).

Data were initially subject to principal component analysis (PCA) to assess the variability and identify any outliers. Supervised analyses were then performed to assess variation in the data with regards to a Y variable (e.g. case vs control or CRP) using orthogonal partial least squares discriminant analysis (OPLS-DA) or partial least squares regression analysis (PLS-R).

OPLS-DA was used to compare between groups of interest (i.e. case vs control, or PMR patients at different treatment points). This assessed the fold change between the groups of interest and gave each metabolite a variable importance for prediction (VIP) score, which

indicated how much that metabolite contributes to the model (higher number = higher contribution), a cut-off of 0.9 was used those metabolites taken forward in the models.

PLS-R, is a form of regression analysis that identifies which metabolites predict a given variable. Here, we used measured levels of C-reactive protein (CRP), pain, stiffness and fatigue. Similarly to the OPLS-DA models, the metabolites were given a VIP score to indicate their contribution to the model, and 0.9 was used as a cut-off again.

In both the OPLS-DA and PLS-R model, qualities were assessed using R^2 (goodness of fit), Q^2 (goodness of prediction) and cross-validated analysis of variance (CV-ANOVA) to determine significance levels. An $R^2 > 0.25$, with the difference between R^2 and $Q^2 < 0.2$, and $P < 0.05$ was deemed to be a well modelled and significant, the higher the R^2 the better the fit. All statistical analysis was performed in SIMCA-P, version 16 (227) (Umetrics, Sweden); with the exception of metabolites of interest, where Kruskal-wallis with Dunn's post-test was performed on the metabolite concentrations in GraphPad version 8.0.

2.2.5 Pathway analysis

Metabolites with a variable importance score (VIP) score of >0.9 in the PLS-R for CRP, pain, stiffness and fatigue were selected for pathway analysis in MetaboAnalyst (228, 229). Importance and relevance of pathways were indicated by the impact factor (X axis) and –log (P value) (Y axis).

2.3 Immunofluorescence staining

To explore the expression of endothelial cell molecules of interest across Res, VeRA and JRep patients, multiplex imaging of markers was run using the CellDIVE imaging platform. The markers of interest were first validated using conventional immunofluorescence (2.3.1) before performing the multiplex stain at the University of Oxford (2.3.2). Reasoning for use of the CellDIVE is given in 1.5.4.1 and the markers chosen and validation of antibodies discussed in 4.2.1.

All tissues were kindly provided and prepared by Professor Andrew Filer, Dr Saba Nayar and Dr Triin Major, and sectioned by Dr Triin Mayor, the human biomaterials resource centre (HBRC) or myself.

2.3.1 Conventional immunofluorescent staining

To initially validate antibodies, conventional staining was carried out as previously described (141). Formalin-fixed paraffin-embedded (FFPE) sections were deparaffinised by washing 3 times for 5 minutes in Histoclear (National diagnostics, Nottingham, UK), and rehydrated by washing in 100%, 90%, 80% and 70% ethanol for 3 minutes each followed by 3, 3-minute washes in distilled water. Antigen retrieval was performed in 10mM sodium citrate (Merck, Dorset), 0.05% Tween®20 (Fisher Scientific, Loughborough) buffer at pH6 for VAP-1, PNAd, P selectin, p53 and Multimerin2 (MMRN2) or 10mM Tris, 1mM EDTA (Ethylenediaminetetraacetic acid) (both Merck) 0.05% Tween®20 buffer pH9 for VCAM-1, CD31, Delta-like canonical notch signalling 4 (DLL4), Lyve1, E selectin and C-Type Lectin Domain Containing 14A (CLEC14A). For all expect P and E selectin, slides were placed in retrieval buffer and put at 96°C for 1 hour. For P and E selectin, slides were placed in the

buffer and were microwaved twice on high (setting 10/10) for 3 minutes and cooled for 5 minutes, then microwaved on medium-low (setting 4/10) for 1 minute and left to cool till at RT. Slides were then rehydrated in phosphate-buffered saline (PBS) for 5 minutes and blocked in 10% normal horse serum (Vector Laboratories, Cambridge, UK) for 10 minutes at RT.

Primary antibodies were added for 1 hour at RT. Sections were washed for 5 minutes in PBS and when unconjugated antibodies used, an appropriate secondary against the primary antibody was added. Secondary antibodies included streptavidin Alexa Flour 647, goat anti-rabbit Alexa Flour 546, goat anti-rat Alexa Flour 555, goat anti-mouse IgG1 Alexa Flour 546 (all used at 1:400), goat anti-rabbit 488 (1:200) (all from Thermofisher, Massachusetts, USA). Slides were mounted with ProLong Diamond with DAPI (ThermoFisher) and dried overnight at RT. Slides were then imaged immediately or stored at -20°C before imaging. Imaging was carried out in the University of Birmingham Medical School Imaging Suite and images obtained on the Zeiss LSM 780, Zeiss LSM 880 or Leica DM6000.

Multiple antibodies were initially tested (Table 2.1) and the final antibodies chosen for use on Cell DIVE are shown in black, and unused in grey. Expect for PNAd and CLEC14A, all were conjugated to an appropriate fluorophore with biotium Mix-n-Stain antibody labelling kits (San Francisco, USA) and labelled according to the manufacturer's instructions prior to confirmation of positive staining before being used in the CellDIVE staining. Positive staining was verified by determining if expression was similar to that described in the literature or by others (i.e. staining around the blood vessels, and/or lining layer dependent on the marker).

In order to potentially do single cell segmentation, vimentin (clone EPR3776, abcam), which is expressed in mesenchymal cells (including ECs, macrophages, fibroblasts and leukocytes (230)), was added to the panel. Full panel details are given in Table 2.2.

Table 2.1: Antibodies tested for validation

Target	Species	Isotype	Conjugate	Clone	Catalogue number	Manufacturer	pH	Concentration (ug/ml)
Lectin from	Ulex Europaeus	NA	Streptavidin	NA	L8262	Merck	6 and 9	20
Ulex	Rabbit /Ulex Europaeus	IgG	AF555	NA	bs-10025R-A555	Bioss	6 and 9	20
VE-Cadherin	Mouse	IgG_{2a}	AF647	BV9	348514	BioLegend	6 and 9	10
CD31	Mouse	IgG1	AF488	WM58	303110	BioLegend	6 and 9	10
	Mouse	IgG	Unconjugated	C31.3	NBP2-15202	Novus	9	2
Lyve1	Rabbit	IgG	Unconjugated	EPR21857	ab219556	Abcam	9	1.6
P selectin	Mouse	IgG1	AF488	Psel.KO.2.7	NB100-65392AF488	Novus	6	10
	Mouse	IgG1	Unconjugated	Psel.KO2.5	ab118522	Abcam	6	10
	Mouse	IgG1	Unconjugated	AK-6	MA5-16567	Thermofisher	6	10
	Mouse	IgG1	Unconjugated	CTB201	sc-8419	Santa Cruz	6	4
	Mouse	IgG_{2a}	Unconjugated	1 E 3	sc-19672	Santa Cruz	6	4
	Rabbit	IgG	Unconjugated	EPR2146(2)	ab182135	Abcam	6	0.25
E selectin	Mouse	IgG_1	Unconjugated	BIGG-E4	BBA16	R & D	9	10
	Mouse	IgG2a	Unconjugated	D-7	sc-137054	Santa Cruz	9	4
	Rabbit	IgG	Unconjugated	Polyclonal	ab185698	Abcam	9	12.3
VCAM1	Mouse	IgG_1	AF488	6G9	NBP1-47491AF488	Novus	9	10
	Rabbit	IgG	Unconjugated	EPR5047	ab134047	Abcam	9	8
	Goat	IgG	Unconjugated	Polyclonal	BBA19	R & D	9	10
VAP1	Goat	IgG	Unconjugated	Polyclonal	EB07582	Everest	6	6.6
PNAd	Rat	IgM	AF647	MECA-79	120808	BioLegend		10
p53	Rabbit	IgG	Unconjugated	E26	ab32389	Abcam	9	3.97
DLL4	Rat	IgG_{2a}	Unconjugated	# 207822	MAB1389	R & D	9	5
MMRN2	Rabbit	IgG	Unconjugated	Polyclonal	ab121639	Abcam	6	1
CLEC14A	Sheep	IgG	Unconjugated	Polyclonal	AF4968	R & D	9	2

DLL4, Delta-like protein 4; CLEC14A, C-type lectin domain containing 14A; Lyve1, Lymphatic vessel endothelial hyaluronic acid receptor 1; MMRN2, Multimerin 2; VAP-1, Vascular adhesion protein 1; VCAM1, Vascular cell adhesion protein 1

Table 2.2: Antibodies used in the CellDIVE panel

Stain round	Target	Species	Isotype	Clone	Catalogue number	Manufacturer	Conjugate or secondary used	Concentration used (ug/ml)
1	VAP1	Goat	IgG	Polyclonal	EB07582	Everest	Donkey anti-goat AF488 (abcam)	6.7
	P selectin	Rabbit	IgG	EPR2146(2)	ab182135	Abcam	Donkey anti-rabbit AF555 (Invitrogen)	0.254
	PNAd	Rat	IgM	MECA-79	120808	BioLegend	AF647	10
2	Lyve1	Rabbit	IgG	EPR21857	ab219556	Abcam	CF450	3.81
	Mmrn2	Rabbit	IgG	Polyclonal	ab121639	Abcam	CF555	2
	VCAM1	Rabbit	IgG	EPR5047	ab134047	Abcam	AF647	8
3	CD31	Mouse	IgG	C31.3	NBP2-15202	Novus	Donkey anti-mouse AF488 (Invitrogen)	2
	E selectin	Rabbit	IgG	Polyclonal	ab185698	Abcam	CF555	13.46
	p53	Rabbit	IgG	E26	ab32389	Abcam	CF647	10.2
4	Vimentin	Rabbit	IgG	EPR3776	ab185030	Abcam	AF488	10
	Clec14A	Sheep	IgG	Polyclonal	AF4968	R & D	Donkey anti-sheep AF555 (abcam)	2
	DLL4	Rat	IgG2a	# 207822	MAB1389	R & D	CF647	8.26

DLL4, Delta-like protein 4; CLEC14A, C-type lectin domain containing 14A; Lyve1, Lymphatic vessel endothelial hyaluronic acid receptor 1; MMRN2, Multimerin 2; VAP-1, Vascular adhesion protein 1; VCAM1, Vascular cell adhesion protein 1

Table 2.3: Isotype controls used in CellDIVE panel

Target	Manufacturer	Clone	Catalogue number
Goat IgG	Bioss	Polyclonal	bs-0294P
Rabbit IgG	Bioss	Polyclonal	bs-0295P
Mouse IgG	Bioss	Polyclonal	bs-0296P
Rat IgG2a	Invitrogen	eBR2a	16-4321-82
Rat IgM	BioLegend	RTK2118	400801
Rabbit – AF488	Bioss	Polyclonal	bs-0295P-A488
Rabbit –AF555	Bioss	Polyclonal	bs-0295P-A555
Rabbit – AF647	Bioss	Polyclonal	bs-0295P-A647

2.3.2 CellDIVE multiplex staining

Multiplex imaging was performed as previously described (231) using the CellDIVE™ (previously GE Research, now Leica Microsystems, Cambridge, UK) platform at The Kennedy, University of Oxford. It involved rounds of staining with 3 markers of interest, plus DAPI, to allow the imaging and quantification of multiple markers. To do this, sections were initially stained only with DAPI, and the background fluorescence imaged. Slides were then stained with the first round of antibodies and imaged, then bleached and imaged (as a background round), before being stained with the next round of markers. The process was repeated until the final round of staining. At each imaging round, sections were aligned to the previous round according to the DAPI stain.

2.3.2.1 Slide clearing, rehydration and antigen retrieval

Firstly, slide clearing and rehydration was performed in the Sakura Tissue-Tek DRS 2000 autostainer. This consisted of two, 5-minute washes in xylene, followed by 5 minute washes in decreasing concentrations of ethanol (100%, 95%, 70% and 50%), then in PBS. Tissues were then permeabilized for 10 minutes in 0.3% Triton X100 – PBS and washed in PBS for 5 minutes.

Antigen retrieval was then performed in the NxGen Decloacker (Biocare, Pacheco CA, USA). Slides were first placed in citrate-antigen retrieval buffer (ARS1, Vector Laboratories) inside the decloaker and once the temperature reached 70°C, timed for 20 minutes. During this time, pressure and temperature continued to rise until reaching 110°C where it was held for 4 minutes, before decreasing. Following the 20-minute incubation slides were transferred to the Tris-Antigen retrieval buffer (ARS2, Vector Laboratories) and incubated in the decloaker

for a further 20 minutes. The Tris-Antigen retrieval buffer containing the slides was then removed from the decloaker and slides left for a further 10 minutes at RT. Slides were then washed 3 times for 5 minutes with gentle agitation in PBS, before blocking overnight at 4°C in with 10% donkey serum (Biorad, Watford, UK), 3% Bovine Serum Albumin (BSA; Sigma-Aldrich, Poole, UK) in PBS.

2.3.2.2 Background imaging

Following the overnight block, slides were washed 3 times for 5 minutes in PBS with gentle agitation. Slides were coverslipped (Leica, Milton Keynes, UK) with mounting media (10% PBS, 4% w/v propyl gallate (Sigma) and 1% w/v DABCO in glycerol (Sigma)) and imaged on the IN Cell 2500HS at The Kennedy Institute, University of Oxford. Scanplans of the sections were then obtained by selecting the regions of interest (ROI) in RHEDeye using DAPI. Following this, background imaging was run, with DAPI set at an appropriate exposure and FITC, Cy3 and Cy5 channels at the default exposures of 100ms, 200ms and 500ms respectively. Sections were then decoverslipped by placing in PBS and Fc blocked (1:200 in PBS; Miltenyi, Woking, UK) for 1 hour at RT before proceeding to the staining.

2.3.2.3 Staining and imaging of sections

Sections were stained with the antibodies at the concentrations and in the rounds shown in Table 2.2. Isotypes were used at the same concentration as the antibody, details given in Table 2.3.

When primary-secondary staining was required, samples were incubated overnight with the primary antibody at 4°C. Secondary staining or conjugated antibodies were incubated for 1

hour at RT. Between primary-secondary and following staining, slides were washed 3 times for 5 minutes in PBS with gentle agitation.

Prior to next round of staining, sections were bleached by placing the slides in dye inactivation solution (0.5M $NaHCO_3$, 30% H_2O_2 in H_2O) for 15 minutes, 3 times, placing slides in PBS for a minute between each round. Slides were then washed 3 times for 5 minutes in PBS before cover slipping and imaging with default exposures (FITC 100ms, Cy3 200ms, and Cy5 500ms).

2.3.2.4 Analysis of imaged sections

Images were analysed in QuPath (232), as depicted in Figure 2.1. Vessels were detected by training the classifier to identify CD31 expression. Quantification of all other markers was then assessed via simple thresholding. Whilst a different threshold was set for each marker and image (thresholds given in), this was always based on the histogram of the marker within that image. Vessel expression of each marker, and marker co-expression then determined by applying all the classifiers, to give % of vessel cells expressing the markers.

Table 2.4: Threshold values used for each marker of interest in QuPath analysis of CellDIVE imaged sections

	CLEC14A	DDL4	MMRN2	P53	PSEL	VAP1	VCAM1
BX115	4000	1700	800	4000	1000	600	600
BX178	11000	3000	800	1800	1000	5000	2400
BX194	5000	2000	800	2500	200	2700	4000
BX202	5000	2000	1000	2500	300	1000	1000
BX248	8000	2700	60	2000	300	500	4000
BX290	8000	2100	900	1000	500	3500	2500
BX064	9800	2100	800	4000	500	1800	2000
JRP099	4000	1200	800	1000	500	2500	600
JRP118	7000	900	1000	2200	300	1800	1500
JRP122	7000	2000	800	1200	300	2500	2000
JRP132	7000	2000	800	1200	300	3500	1800
JRP139a	5000	2500	1200	1400	300	1800	3000
JRP130	7000	2000	1500	600	300	1800	800
JRP136	7000	3000	800	2000	150	1800	1600

DLL4, Delta-like protein 4; CLEC14A, C-type lectin domain containing 14A; MMRN2, Multimerin 2; VAP-1, Vascular adhesion protein 1; VCAM1, Vascular cell adhesion protein 1

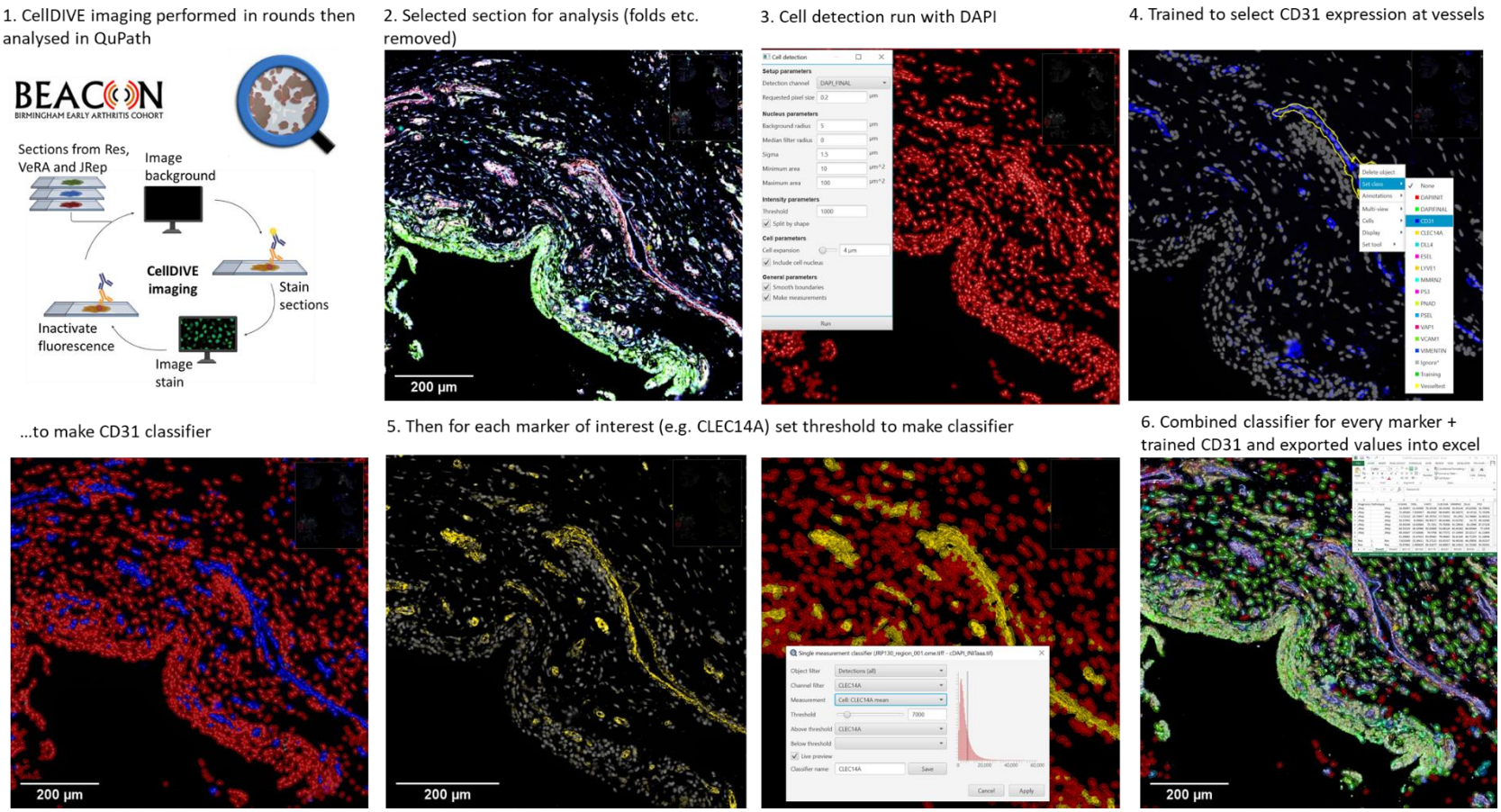

Figure 2.1: Schematic of image analysis performed in QuPath. Formalin fixed paraffin embedded (FFPE) sections of synovial sections were deparaffinised, rehydrated and antigen retrieval was performed. Sections were blocked with donkey serum and bovine serum albumin prior to addition of antibody against: CD31, vimentin, delta-like 4 (DLL4), Multimerin 2 (MMRN2), C-type lectin domain containing 14A (CLEC14A), p53, vascular cell adhesion protein 1 (VCAM1), P selectin, vascular adhesion protein 1 (VAP1), E-selectin (ESEL), lymphatic vessel endothelial hyaluronan receptor 1 (Lyve1) and peripheral node addressin (PNAd). Image analysis was performed in QuPath (232). Firstly, the section was drawn around, then cell detection performed. For the CD31 stain at vessels was trained, in order to not pick up any CD31+ staining on leukocytes. All other makers were then classified using a threshold. The classifiers markers were combined and the final values for number of positive cells for each marker exported into excel. Scale bar at 200µm.

2.4 Culture of patient derived human fibroblasts

2.4.1 Culture media

Fibroblasts were grown in Complete Fibroblast Media (CFM): Roswell Park Memorial Institute (RPMI) 1640 medium (Sigma) supplemented with 10% foetal calf serum (Biosera, Nuaillé, France), 1% sodium orthopyruvate, 1% minimal essential medium non-essential amino acids, 2mM L-glutamine, 100U/ml penicillin and 100µg/ml streptomycin (all from Sigma).

2.4.2 Recovery of fibroblasts from liquid nitrogen and cell culture

Culture of fibroblasts used in endothelial: fibroblast cultures was performed by myself, and for the macrophage: fibroblast cultures by Dr Jason Turner. Cryopreserved vials of human synovial fibroblasts (HSF) at passage 3 or 4 were kindly supplied by Professor Andrew Filer and Holly Adams (Rheumatology Research Group, University of Birmingham, UK). Patient details of fibroblasts used are outlined in results chapters 5.2 and 6.2 in Table 5.1 and Table 6.1. The HSF were quickly defrosted by placing them directly into a 37°C water bath and resuspended in pre-warmed CFM, then centrifuged at 250g for 6 minutes. The pellet was resuspended in CFM and fibroblasts incubated at 37°C and 5% CO_2 in a T75 flask until nearly confluent. To feed the cells, two thirds of the medium was replaced with fresh CFM once a week (to make 33% conditioned media), until reaching 80-90% confluency.

2.4.3 Detachment of fibroblasts from tissue culture flasks

Once cells reached 80-90% confluency, they were passaged to expand the population or used in the co-culture assay. When passaging, fibroblasts were usually 1:3, but faster

growing cells split 1:4 and slower growing cells split 1:2. Between 4 and 6, fibroblasts were used in the co-cultures.

Firstly, the old media was removed. When splitting this media was retained to make 33% conditioned media for use after splitting. The cells were then washed with PBS (Oxoid, Thermo Scientific, Basingstoke, UK) to remove any remaining media. Cells were then trypsinised by adding enough trypsin-EDTA (Sigma; 10X diluted to 2X in PBS) to cover the flask, 5ml for a T75, and incubating at 37°C for 5 minutes. Detachment was confirmed with phase contrast microscopy and CFM, at a ratio of 8:5 with trypsin, added to stop the reaction. Cells were centrifuged for 6 minutes at 300g and supernatant discarded. For passaging, the pellet was resuspended in 33% conditioned CFM (1:3 ratio of conditioned and fresh media) and plated into T75 flasks then incubated 37°C and 5% CO_2 until 80-90% confluent. For seeding, please refer to section 2.6.1.

2.5 Isolation and culture of human umbilical vein endothelial cells

2.5.1 Culture media

Human umbilical cord vein endothelial cells (HUVECs) were grown in HUVEC medium: Medium 199 (ThermoFisher, Loughborough, UK) supplemented with 20% foetal calf serum , 100U/ml penicillin and 100µg/ml streptomycin, 10 ng/ml human epidermal growth factor, 1 µg/ml hydrocortisone, (all from Sigma) and 2.5 µg /ml amphotericin B (Life Technologies, Paisley, UK).

2.5.2 Isolation and culture of HUVECs

Umbilical cords were collected by research midwives from the Birmingham Women's Health Care NHS Trust and Sandwell and West Birmingham NHS Trust. HUVECs were isolated from the cords as previously described (233-235). Firstly, the cord was inspected and any clamp marks or sites of injection cut off and the vein cannulated at one end. To clear the vein of blood, PBS (Sigma) perfused through until it ran clear, then a syringe full of air passed through to remove any remaining PBS. The other end of the cord cannulated and the vein filled with 1mg/ml collagenase type 1a from *Clostridium histolyticum* (Sigma; diluted in PBS), and incubated at 37°C and 5% CO_2 for 15 minutes. Whilst incubating, T25 flasks (Corning, Amsterdam, The Netherlands) were gelatin coated; 2% gelatin in water (Sigma), diluted to 1% in PBS (Sigma), was added to the flask for ~10 minutes and removed before adding HUVECs. Size of the cord determined how many T25 flasks were obtained, 4-6 inches of cord was required per flask. Following the 15-minute incubation, the cord was gently massaged for 1 minute to ensure HUVEC detachment. The collagenase cell suspension was flushed through with PBS and collected into a falcon, then centrifuged at 250g for 5 minutes. The supernatant was removed and pellet resuspended in 4ml of HUVEC media per flask, then plated into the gelatin coated T25 flask and cultured at 37°C, at 5% CO_2. The medium was changed the following day and then every two days until HUVEC were fully confluent. Cells were confluent 4-6 days after isolation and always used at passage 1.

2.6 Co-culture of fibroblasts and endothelial cells

2.6.1 Seeding fibroblasts on transwell filters

Fibroblasts and HUVECs were co-cultured either side of the porous transwell filer as previously described (9, 233) and shown in results section 5.2.1, Figure 5.1. Fibroblasts were

detached from tissue culture flasks as described in section 2.4.3. They were then seeded on the outer surface of a 6-well 0.4µm-pore transwell filter (BD Pharmingen, Cowley, UK) at a density of $0.5x10^5$ cells/filter. Cells were then incubated at 37°C, 5% CO_2 for 45 minutes to allow them to adhere to the filter. The filters were then inverted and placed into a 6-well tissue culture plate (VWR) and cultured in 5ml CFM (3ml below and 2ml above the filter) per well for 24 hours at 37°C and 5% CO_2.

2.6.2 Seeding endothelial cells on transwell filters

After 24 hours, media in all wells containing fibroblasts was changed. For each donor one filter was kept as mono-culture, and one as co-culture (shown in section 5.2.1, Figure 5.1). Those that were co-cultured with ECs, had HUVECs seeded on inner side of the filter at a density of $0.5x10^5$. For seeding, the HUVECs were detached from the tissue culture flask as described below. To chelate any Ca and Mg on the cell surface, cells were bathed for 30 seconds in enough EDTA (0.02%; Sigma) to the cover the cells. Cells were then trypsinised by adding pre-warmed (37°C) trypsin (2.5mg/ml; Sigma): EDTA at a ratio of 2:1, with sufficient volume to cover the cells. Cells were then incubated at 37°C and 5% CO_2 until rounding was observed via bright field microscopy. The flask was tapped to dislodge the cells and the reaction stopped by adding CFM at a ratio of 8:3 (CFM: trypsin-EDTA). The cell suspension was centrifuged at 250g for 5 minutes, supernatant removed and the pellet resuspended in CFM at a concentration of $0.25x10^5$ cells/ml and 2ml added to the top of each filter (3 wells for co-cultured with fibroblasts, and 1 well mono-cultured).

2.6.3 Treating fibroblast: endothelial cell co-cultures

Twenty-four hours after seeding the HUVEC, the cells were cytokine stimulated by replacing all media in the well with CFM supplemented with 100units/ml TNF-α (R&D Systems) and 10ng/ml IFN-γ (PeproTech, London, UK). Cells were cultured in cytokine supplemented media for another 24 hours at 37°C and 5% CO_2.

2.6.4 Sample collection for RNA isolation of fibroblast: endothelial cell co-cultures

Following 24-hour stimulation, cells were trypsinised and cell pellets collected, similar to the methods described in 2.6.2. Firstly, cells were bathed in EDTA for 30 seconds, with enough to cover the filter (2ml beneath and 1ml above the filter). Then trypsin: EDTA was added (enough to cover the filter) and HUVECs left to trypsinise for 1 minute at 37°C at 5% CO_2. The reaction was stopped with CFM and HUVECs collected from the upper side of the filter and wells. The upper side of the well was washed with EDTA, Trypsin: EDTA was then added back to the top of the wells and fibroblasts left to trypsinised for a further 4 minutes. CFM then added to the bottom of the wells and the lower side of the filters washed with CFM to collect the fibroblasts. Cell suspensions were then centrifuged at 250g for 5 minutes, then resuspended in PBS and centrifuged at 300g for 5 minutes. The supernatant was carefully aspirated of and cell pellets snap-frozen in liquid nitrogen then stored at -80°C until use.

2.6.5 RNA isolation of fibroblast: endothelial cell co-cultures

The snap-frozen cells pellets were thawed on ice and RNA isolated according to the manufacturer's instructions using RNeasy mini kit with QIAshredder's to homogenise the sample and DNase treatment to remove DNA contamination (all QIAGEN, Manchester, UK).

A brief summary of the protocol is given below and unless stated all regents were supplied in the aforementioned kits. Pellets were resuspended in 350µl RLT lysis buffer with β-Mercaptoethanol (Sigma) then transferred to a QIAshreder and centrifuged at 17,000g for 2 minutes. An equal volume (350µl) of 70% ethanol (not supplied in the kit) was added to the lysed sample. The full volume was transferred to an RNeasy spin column, and samples centrifuged at 13,000g for 30 seconds. The flow-through was discarded, 350µl of RW1 added to the column and spun at 13,000g for 30 seconds. The flow-through was discarded then 80µl of the DNase solution (1:8 DNase 1 to RRD buffer) was added directly to column membrane and incubated at RT for 15 minutes before adding 350µl of RW1 and centrifuging at 13,000g for 30 seconds. The flow-through was discarded and 500µl of buffer RPE added, then centrifuged at 13,000g for 30 seconds. The flow-through was discarded, 500µl of buffer RPE added again and centrifuged at 13,000g for 2 minutes. The RNeasy spin column was then transferred to a new 2ml collection tube and the column spun at 17,000g for 1 minute to prevent any carryover of RPE or previous flow-through. The RNeasy spin column was then transferred to a 1.5ml collection tube and 15µl of RNAse-free water added to the column membrane, then incubated for 2 minutes at RT before spinning at 13,000g for 1 minute to elute the RNA.

Following isolation, samples were placed on ice and the concentrations, and purity ratios (260/280nm and 260/230nm) were measured with the Nanodrop 2000 (ThermoFisher Scientific, UK) and are given in results Appendix Table 3. A 260nm to 280nm ratio of ~2.0 suggests pure RNA and the 260nm to 230nm ratio indicates the presence of organic compounds, with a ratio of ~2.0-2.2 considered acceptable (236).

2.6.6 Culture media collection for Ultra High-Performance Liquid Chromatograph-Mass-Spectrometry

Conditioned culture media was collected following 24 hours co-culture (unstimulated supernatants) and following 24 hours TNF-α-IFNγ stimulation (stimulated supernatants). The supernatants were centrifuged at 10,000g for 10 minutes at 3°C to pellet any cell debris, the supernatants were aliquoted in to separate and new 1.5mL Eppendorf tube and then stored at -80°C until extraction.

2.7 Isolation of monocytes

Monocytes were isolated for the use in fibroblast: macrophage co-cultures (2.8), prepared by Dr Jason Turner (214). Peripheral blood from a healthy donor was collected in K_2EDTA coated tubes (Sarstedt, Nümbrecht, Germany). The experiment was carried out in 3 batches and the same donor used each time in order to minimise variability. The blood was diluted 1:1 in Hanks balanced Salt solution (HBSS, without Ca or Mg, Life Technologies) and 20ml blood/HBSS mix layered onto 20ml Ficoll-Paque PLUS (GE Healthcare) then centrifuged for 20 minutes at 500g with no brake or acceleration to sediment at the plasma: Ficoll interface. The PBMC buffy coat layer was carefully pipetted off and cells washed 3 times in HBSS by centrifuging at 250g for 5 minutes.

Monocytes were then isolated from PBMCs via negative magnetic bead selection using a pan-human monocyte labelling magnetic kit, according to the manufacturer's instructions (MilltenyiBiotec). Firstly, PBMCs were labelled with the kit, which involved resuspending 10^7

cells in 30µl MACs buffer (0.5% BSA and 2mM EDTA in PBS). Subsequently, per 10^7 cells, 10µl FcR blocking reagent was added followed by 10µl Biotin-Antibody cocktail. This was mixed and incubated for 5 minutes at 4°C. Then 30µl of MACs buffer and 20µl anti-biotin Microbeads were added per 10^7 cells and incubated for 10 minutes at 4°C. An LS column (MiltenyiBiotec) was washed 3 times with MACs buffer before passing through the labelled cell suspension. The flow through of unlabelled enriched monocytes was collected and passed through a second, washed LS column. Purity and subset bias checks were performed using flow cytometry to assess CD14 (-PE) and CD16 (-FITC) (BD Biosciences, clones MϕP9 and 3G8, respectively) cell-surface expression with the Dako Cyan-ADP. Data provided in Dr Turner's thesis ((214); section 3.3.2).

2.8 Co-culture of fibroblasts and M-CSF stimulated monocytes

Samples were prepared by Dr Jason Turner (214) and closely following the protocol of Donlin *et al* (143), described in section 3.2.8 of Dr Turners thesis and briefly here. Monocytes were isolated as described in section 2.7 and seeded into a 24 well plate at a density of $0.5x10^5$ monocytes/well. Cells were then cultured at 37°C, 5% CO_2, for 2 days in complete fibroblast media (described in 2.4.1) supplemented with 10ng/ml macrophage colony stimulating factor (M-CSF) to induce macrophage differentiation as described by Donlin *et al* (143). Notably, this is a shorter induction of monocyte to macrophage differentiation then described by others (237), therefore these may not be regarded as fully differentiated macrophages, but for simplicity will be referred to as macrophages hereon in.

2.8.1 Seeding fibroblasts

Fibroblasts were seeded similarly to that described in 2.6.1, onto the upper chamber of 24-well, 0.4µm pore transwell filters. Cells were seeded at a density of $0.2x10^5$ cells per filter, with 200µl complete fibroblast media above and 600µl below the filter. Cells were then incubated and cultured at 37°C and 5% CO_2 for 2 days.

2.8.2 Treating fibroblast: M-CSF stimulated monocyte co-cultures

Following 2 days of culture, both cell types were washed twice with PBS and the transwells containing fibroblasts were added to the 24 well plate containing the M-CSF (PeproTech) stimulated monocytes. CFM supplemented with 20ng/ml TNF-α (PeproTech) was then added to each well, 200µl above and 600µl below each filter. The cells were then incubated at 37°C and 5% CO_2 for 16 hours.

2.8.3 Sample collection and RNA isolation

After 16 hours stimulation the cell types were separated and washed with PBS. Fibroblasts were detached from the filters using 600µl trypsin-EDTA for 15 minutes, before inhibiting the reaction with an equal volume of CFM. The macrophages were detached from the plates by adding fresh PBS to the wells, putting the plate on ice and using a cell scraper to scrap off the cells. Cells were the then pelleted by centrifuging at 250g for 5 minutes.

RNA was then isolated from the cell pellets using the PicoPure® isolation kit (ThermoFisher) according to manufacturer's guidelines and described briefly here. The cells were washed twice by resuspending in 500µl MACs buffer and centrifuging in at 3,000g for 5 minutes. The supernatant was aspirated off and the pellet resuspended in 100µl extraction buffer then incubated at 42°C for 30 minutes. Cells were then centrifuged at 3,000g for 2 minutes and

the supernatant, containing the extracted RNA, was carefully transferred to new microfuge tube. Purification columns were then prepared by adding 250µl of conditioning buffer to each column and incubating for 5 minutes at RT, before centrifuging at 16,000g for 1 minute. Ethanol (70%) was added to the extracted RNA at 1:1 ratio and transferred to the column then spun at 100g for 2 minutes, followed by 16,000g for 30 seconds. The flow-through was discarded and columns left open to air-dry for 5 minutes, before adding 100µl wash buffer 1 and centrifuging at 8000g for 1minute. Then 40µl of DNase treatment (20µl RRD buffer + 10µl DNase) was added to each column and left to incubate for 15 minutes, followed by 40µl of wash buffer, and column centrifuged at 8000g for 15seconds. Then 100µl of wash buffer 2 was added to column and centrifuged at 8000g 1 minute. Another 100µl added again and spun at 16,000g for 2 minutes. Flow through was discarded then centrifuged at 16,000g for 1 minute to dry the membrane. Columns were transferred to the picopure micotubes and 11µl elution buffer added to the membrane then incubated for 1 minute before spinning at 16,000g for 1 minute. RNA was stored at -80°C until use.

2.9 RNA sequencing and statistical analysis

2.9.1 Quality control

Prior to sequencing, the RNA integrity number (RIN) of the samples was measured either in house with RNA 6000 Pico Bioanalyzer according to manufacturer's instructions or processed by the Genomics Birmingham (University of Birmingham, UK) using the High Sensitivity RNA ScreenTape® (both Agilent Technologies, Stockport, UK). These scores range from 1-10, with 10 having the highest integrity (238) and a RIN of 6.4-7.9 generally considered as a cut-off (239). For the fibroblast: EC co-cultures, all RINs were >9, Appendix Table 3. For the

fibroblast: macrophage co-cultures, RINs ranged from 1.8 to 9.6, with an average score of 9, and 10 samples <6.4. Values shown in Appendix Table 8. Despite the low RIN of some samples, all were sequenced, but RIN scores were considered in the analysis (i.e., for outliers) (239).

2.9.2 Sequencing

RNA isolated from both cell types of the fibroblast: EC co-cultures (2.6) was sent to Novartis (Basel, Switzerland) and the total RNA was sequenced by Fasteris (Plan-les-Ouates, Switzerland) with the NovaSeq6000 (Illumina, Cambridge, UK).

RNA isolated from all cells of the fibroblast-macrophage samples (2.8) were processed by University of Birmingham Genomics Service (Birmingham, UK) using the QuantSeq 3' mRNA-Seq Library Prep Kit FWD for Illumina and included Spike-In RNA Variants (SIRVs) set 3 / External RNA Controls Consortium (ERCC) RNA spike-in (all from Lexogen, Vienna, Austria) with the NextSeq500 (Illumina).

2.9.3 RNA sequencing analysis

All sequence data was provided in. fastq format. Figure 2.2 gives an overview of the analysis pipelines involving: trimming of sequences; aligning them the genome; and generating a counts table of the aligned genes. This was then used to identify the differentially expressed genes and carry out subsequent pathway analysis. The pipelines differ slightly between experiments due to the different types of sequencing performed. Pre-processing up to generating a counts table was performed in Unix command line and all latter analysis in R studio (240), with tidyverse (241). Scripts used for analysis can be found here

https://github.com/JuliaManning/Endothelial-fibroblast_co-cultures for the endothelial: fibroblast data at and https://github.com/JuliaManning/Macrophage-fibroblast_co-cultures for the macrophage: fibroblast co-cultures. Initial quality of all samples was assessed with FASTQC (242) and this, as well as results from the alignment and FeatureCounts, were summarised and visualized with MultiQC (243).

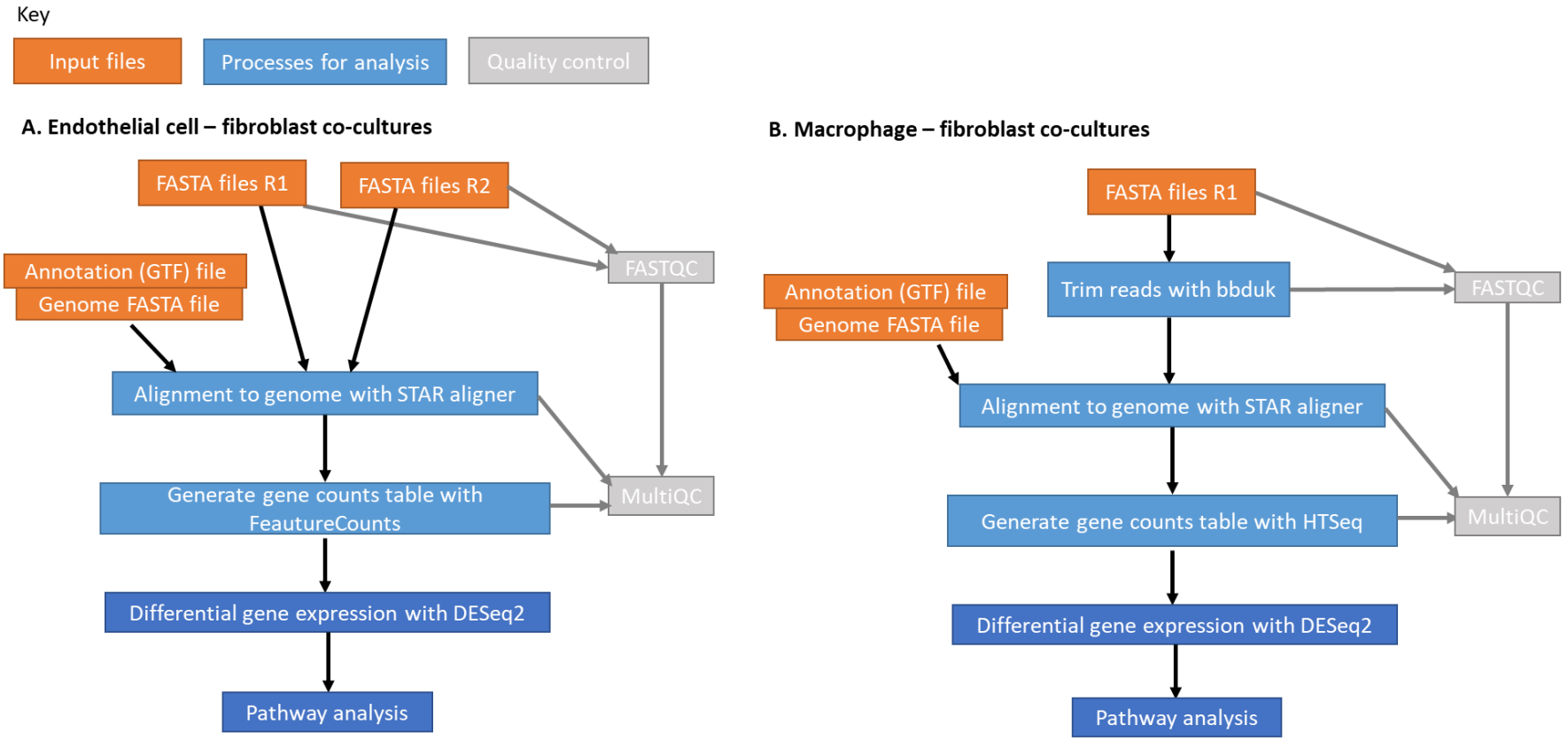

Figure 2.2: Schematic workflow of the RNA-sequencing analysis. Sequencing data in fasta files was aligned to the human genome with STAR aligner using the genome fasta file, and annotation (GTF) file downloaded from ensembl website. In the case of the **(A)** endothelial-fibroblast co-cultures, the sequencing was paired-end reads (hence R2 fasta files). The **(B)** macrophage-fibroblast data required trimming to remove adapters and poorer quality ends of reads, however, endothelial cell-fibroblast data was of relatively high quality and had little to no adapter contamination so did not require trimming. Following alignment, a counts table was generated with FeatureCounts, and HTSeq for the macrophage data. This table was then used for differential gene expression analysis with DESeq2.

2.9.3.1 Trimming

Macrophage-fibroblast samples files were supplied as runs per lane, with 4 fastq files per sample. These were first merged and FASTQC performed. Sequences were then trimmed to remove adapter contamination, polyA read through and low-quality ends using bbduk (244). The fibroblast-endothelial samples were not trimmed as the FASTQC reports showed no overrepresented sequences; therefore no trimming was required.

2.9.3.2 Alignment to the genome

Sequences were aligned to the genome with STAR aligner (245). To do this, firstly genome indexes were generated from the 'Homo_sapiens.GRCh38.dna Subread.primary_assembly' human genome file and the corresponding gene transfer format (GTF) annotation file, 'Homo_sapiens.GRCh38.101', downloaded from ensembl website (246), release 102. The genome indexes were then used to align sequences to the genome. The macrophage-fibroblast data were aligned with standard settings, whilst the pair-end reads for the fibroblast-endothelial data were aligned as the forward and reverse reads. MultiQC was run on outputs from the alignment (i.e. the percentage of mapped reads). Uniquely mapped alignments of >80% indicate good library preparation and data processing (247). FeatureCounts from the Subread package (248) was then used to generate a counts table of genes for the fibroblast: endothelial cell samples. Due to poor sequence quality in the fibroblast: macrophage samples, Mohammed Elasrag from the University of Birmingham Genomics Services (Birmingham, UK) assisted in pre-processing. He utilised HTSeq generate a counts table of genes for these samples (249).

2.9.3.3 Analysis of gene expression and pathways

Initial principal component analysis plots, boxplots are histograms were generated with built in R tools (250). Subsequent transformations, normalisation and differential gene expression were performed with DESeq2 (251). For visualisation (e.g., PCA and heatmaps), counts were transformed with variance stabilising transformation (VST) (252-254). To visualise the p value histograms, genes where there are less than 3 samples with normalized counts greater than or equal to 10 were filtered out, otherwise no genes were filtered as DESeq2 performs independent filtering based on the normalised gene counts (251). PCAs, pairsplots and biplots were generated with PCAtools (255). Heatmaps of the top variably expressed genes or genes of interest were produced with ComplexHeatmap (256). For the volcano plots, the log2Fold changes were shrunk with the 'ashr' (257) and volcano plots generated with EnhancedVolcano (258). For the endothelial cell data, batch correction was performed in limma (14) and ComBat-Seq (15) from the sva package (16, 17).

2.9.3.4 Pathway analysis

ClusterProfiler (16, 17) was used to identify significantly enriched Kyoto encyclopaedia of genes and genomes (KEGG) pathways (18). Pathview (19) was then used to visualise up and down regulated genes in the pathways of interest. G Profiler (20) was used for functional gene ontology of differential expressed genes. Gene set enrichment analysis (GSEA) was performed with the broad institute GSEA software and Molecular signature database (MSigDB) (21, 22) using the hallmark gene sets (23). Ingenuity pathway analysis (IPA; QIAGEN Inc., https://digitalinsights.qiagen.com/IPA (259)) was performed on the macrophage: fibroblast co-cultures.

2.10 Ultra-High Performance Liquid Chromatograph-Mass-Spectrometry of fibroblast: endothelial co-culture supernatants

Ultra-High Performance Liquid Chromatography – Mass Spectrometry (UHPLC-MS) was performed by Professor Warwick Dunn at the University of Birmingham Phenome Centre, on supernatants collected from fibroblast: endothelial cell co-cultures prepared by Dr Helen McGettrick (described in 2.6.6). Methods, as described by Professor Warwick Dunn, are as follows.

2.10.1 Sample preparation

100µL of each sample was transferred to a 1.5mL Eppendorf tube and was dried applying a vacuum centrifugal evaporator (Thermo Scientific Savant SPD111V speedvac concentrator coupled to a Savant RVT5105 vapour trap). A pooled QC sample was prepared by combining 100 µL of each sample in a 15mL Falcon tube. Multiple 100µL aliquots of the pooled QC sample were prepared for analysis in an identical process as described for the biological samples. All dried samples were stored at -80°C prior to analysis. A solvent blank sample was prepared on the day of analysis (80/20 methanol/water).

2.10.2 Ultra-High Performance Liquid Chromatograph-Mass-Spectrometry

Samples were analysed applying Ultra Performance Liquid Chromatography (Ultimate3000RS; Thermo Scientific, Hemel Hempstead, UK) interfaced to an electrospray mass spectrometry (Q Exactive, Thermo Scientific, Hemel Hempstead, UK). Samples were reconstituted in 100µL 80/20 methanol/water and analysed. QC samples were analysed ten times at the start of the batch (for system equilibration and MS/MS data acquisition), followed by injection after every 5th sample and finally two QC samples were analysed at

the end of the analytical batch. Biological samples were analysed in a random order (using Microsoft Excel RAND function). The mass spectrometer was tuned and calibrated applying standard procedures and solutions as defined by Thermo Scientific. UHPLC separations were performed applying a Hypersil Gold C18 reversed phase column (100 x 2.1 mm, 1.9 mm) at a flow rate of 400 mL.min-1, temperature of 40°C and with two solvents: solvent A (HPLC grade water +0.1% formic acid) and solvent B (HPLC grade methanol +0.1% formic acid). A gradient elution was performed as follows: hold 100% A 0–1.5 min, 100% A–100% B 1.5–6 min curve 3, hold 100% B 6–12 min, 100% B–100% A 12–13 min curve 3, hold 100% A 13–15 min. Injection volume was 5µL. UHPLC eluent was introduced directly in to the electrospray mass spectrometer with source conditions as follows: spray voltage -4.0 kV (ESI-) and +4.5 kV (ESI+), sheath gas 30 arbitrary units, aux gas 15 arbitrary units, capillary voltage 35 V, tube lens voltage -100 V (ESI-) and +90 V (ESI+), capillary temperature 280°C, ESI heater temperature 300°C. Data were acquired in ion mode switching in the m/z range 100–1000 at a mass resolution of 35 000 (FWHM defined at m/z 200), with a scan speed of 0.4 s and an AGC setting of 1 x 106.

2.10.3 Raw data processing and metabolite annotation

LC-MS raw data profiles were first converted into an mzML centroid format within ProteoWizard MSConvert software. Each mzML based three-dimensional data matrix (intensity × m/z × time – one per sample) was then converted (or deconvolved) into a vector of peak responses, where a peak response is defined as the sum of intensities over a window of specified mass and time range (e.g., m/z = 102.1 ± 0.01 and time = 130 ± 10 s). MzML files were processed applying XCMS as described previously (260). All metabolites reporting a

relative standard deviation (RSD) > 30% and which were detected in <70% of QC samples from injection nine onwards were removed. Metabolites were annotated applying the in-house software BEAMS (https://more.bham.ac.uk/beams/) and where feasible by comparison of HCD MS/MS mass spectra acquired for QC samples to the mass spectral library mzCloud (https://www.mzcloud.org/). All metabolites were annotated according to level 2 or 3 as defined by the Metabolomics Standards Initiative (261).

2.10.4 Univariate and multivariate data analysis

All data analyses were performed in MetaboAnalyst (229). For univariate analysis all data were normalised to total peak area for each sample and log transformed. The resulting data matrix was analysed by applying one-way ANOVA without correction for multiple testing. For multivariate analysis all data were normalised to total peak area for each sample and was log transformed and Pareto scaled. Principal Components Analysis, Partial Least Squares-Discriminant Analysis and Random Forest. Metabolites defined as important following univariate and multivariate analysis were grouped in to classes related to chemical structure or metabolic function similarity.

3 Metabolomic profiling of serum from patients with polymyalgia rheumatica and giant cell arteritis

3.1 Introduction

Polymyalgia rheumatica (PMR) and giant cell arteritis (GCA) are closely-related, poorly understood diseases characterised by inflammation of extracapsular musculoskeletal sites (42, 43), and the arterial wall (41), respectively. Glucocorticoids (GCs) effectively manage inflammation and remain the gold standard treatment for both diseases, in spite of their adverse effects (4). Whilst GCs often treat the pain and stiffness associated with the diseases, some patients continue to experience fatigue which significantly impacts their quality of life (5, 6). This likely due to the complex, interacting impact of inflammatory disease and GC therapy, however, the mechanisms for this are unknown.

Metabolomics is an emerging technology to detect the physiological changes of diseases and treatments (79). This technology has identified various alterations in metabolites correlating with disease activity in rheumatoid arthritis (RA) (80, 81), Takayasu's arteritis (TAK) (83) and anti-neutrophil cytoplasmic antibody (ANCA)-associated vasculitis (85). Furthermore, metabolomics has been suggested as a possible tool for the early detection of adverse GC-related effects (262), and has detected GC associated changes in a preliminary study of combined RA and PMR patients (86).

This chapter aims to identify metabolite signatures from patient serum, in order to explore changes that occur in PMR and GCA patients with disease. Furthermore, in PMR, examine the effect of GCs and any metabolomic correlates with patient symptoms.

3.2 Results

3.2.1 Experiment design and patient groups

The patient characteristics of all study participants are given in Table 3.1, and schematic of recruited patients shown in Figure 3.1A and B. As part of the ADDRESS-PMR study, 40 PMR patients were recruited and serum samples collected at 3 time points; baseline, 4 weeks and 26 weeks following GC treatment. Thirty-nine non-inflammatory, age-matched and sex-matched controls were also recruited. As part of the TABUL study, anyone with suspected GCA was immediately prescribed high dose GCs, and a serum sample taken within 7 days of GC use. Later 84 were confirmed to have GCA and 53 non-GCA.

In order to explore the metabolic profile of PMR and GCA patients, nuclear magnetic resonance (NMR) spectra were obtained from the serum of these patients. The data were then analysed in two ways: (1) using binned NMR spectra which gives a highly sensitive form of analysis, and (2) on only the identified metabolite concentrations, which gives more functionally useful outputs (Figure 3.1C).

Table 3.1: Characteristics of study participants

	Non-inflammatory controls (n=39)	PMR (n=40)	Confirmed GCA (n=84)	Confirmed non-GCA (n=53)
Age, median (IQR) years	71 (60-80)	75 (68-80)	73 (67-77)	67 (59-74)
Female, n (%)	27 (69)	24 (60)	59 (70)	38 (72)
Diabetes, n (%)	4 (10)	6 (15)	12 (14)	5 (9)
Current smoker (%)	6 (15)	1 (3)	10 (12)	8 (15)
Previous smoker (%)	19 (49)	17 (43)	42 (50)	22 (42)
CRP, median (IQR), mg/L	-	33.5 (22-45)	46.6 (26.2-104.8)	18.6 (7.9-42.1)
TAB positive, n (%)	-	-	31 (36)	-

CRP = C-reactive protein; IQR = Interquartile range; GCA = Giant cell arteritis; PMR = Polymyalgia rheumatica; TAB = Temporal artery biopsy; VAS = Visual analogue score

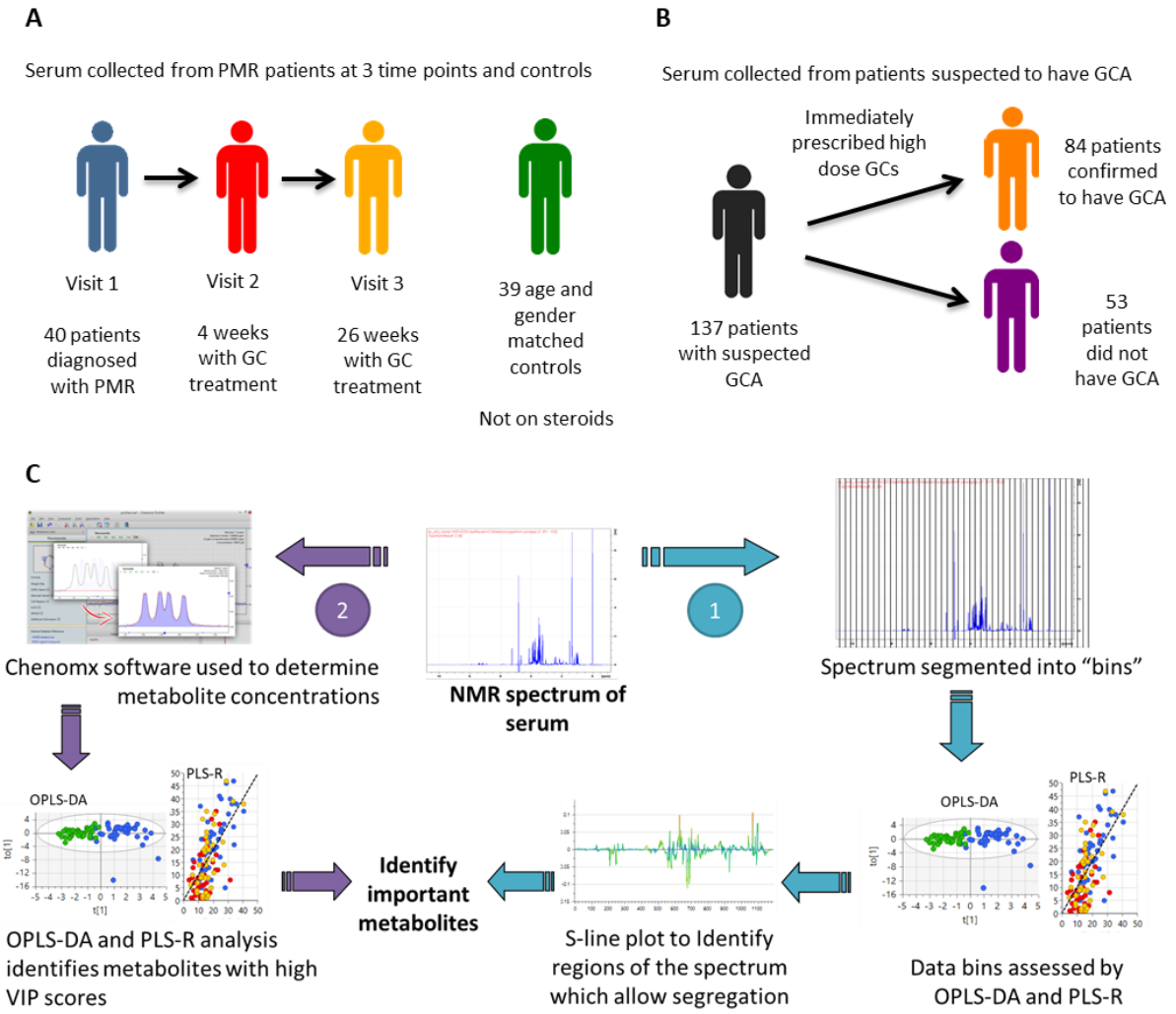

Figure 3.1: Schematic of the patients recruited and the process for nuclear magnetic resonance spectra analysis. (A) Serum was collected from 40 PMR patients at three time points; baseline (blue), 4 weeks with GC (glucocorticoid) treatment (red), and 26 weeks with GC treatment (yellow), as part of the ADDRESS-PMR study. Serum was also collected from 39 age and gender matched controls not on steroids (green). **(B)** 137 with suspected GCA who were immediately prescribed high dose GCs and serum collected within 7 days on steroids. It was later confirmed that 84 patients had GCA and 53 did not. **(C)** The ^{1}H nuclear magnetic resonance (NMR) spectra were obtained from these serum samples and analysed via two methods. (1) The NMR spectra was segmented into "bins" and the data bins assessed via orthogonal partial least squares discriminant analysis (OPLS-DA) and partial least squares regression (PLS-R) and the S-line plots generated to identify differences in the spectra between the groups. (2) Metabolite concentrations were identified from the spectra using Chenomx software and these concentrations used in OPLS-DA and PLS-R models to identify which metabolites contributed to differences between groups or associated with known variables (e.g. CRP), according the variable importance for prediction (VIP) score.

3.2.2 Circulating metabolome changes with polymyalgia rheumatica and is sensitive to glucocorticoid treatment

Firstly, the baseline metabolome of treatment-naïve PMR patients was compared to the matched controls using OPLS-DA of NMR spectra (Figure 3.2A) and metabolite concentrations (Figure 3.3A), which gave a clear separation (R^2 = 0.93 and 0.74 respectively). Subsequently, OPLS-DA was used to compare PMR patient serum spectra (Figure 3.2C-H) and metabolite concentrations (Figure 3.3B) at 3 time points: (i) baseline prior to steroid therapy, and at (ii) 4 weeks and (iii) 26 weeks of GC treatment. We observed a significant difference between the 3 groups (Figure 3.2C-H and Figure 3.3B) where, using metabolite concentrations (Figure 3.3B), separation between treatment-naïve and treated patients was largely dependent on latent variable t [1], whilst latent variable t[2] revealed further separation between the GC treatment duration (4 or 26 weeks). Finally, there was a persistent separation between PMR at 26 weeks and controls (Figure 3.2 I and J, and Figure 3.3C).

Metabolites that contributed to separation of groups in the OPLS-DAs (Figure 3.3) were identified. The fold changes and variable importance of prediction (VIP) scores of these are given in Table 3.2, and concentrations of selected metabolite were plotted (Figure 3.4). VIP scores indicate how important the metabolite is for the model, the higher the VIP the better, here we use a VIP 1 as a cut-off. Of these, the concentration of glycerol (Figure 3.4A) was higher, and methanol (Figure 3.4B) was lower in PMR patients compared to controls. Pyruvate, lactate and ornithine concentrations were slightly (but not significantly) higher in PMR patients compared to controls, but then was significantly increased once treated with GCs (Figure 3.4C and D). On the other hand, acetone was increased in PMR patients

following 4 weeks GC treatment, but decreased after longer (26 weeks) use (Figure 3.4E). Taken together, these results demonstrate the serum metabolome is altered by disease (PMR), then further altered by GC treatment, but does not return to the same state as in health despite 26 weeks of GC treatment.

3.2.3 Separation of metabolome in patients with suspected GCA according to final diagnosis

The NMR spectra and metabolite concentrations from the sera of patients with a confirmed diagnosis of GCA in the TABUL study, were then compared to two other groups: Firstly, the age-matched controls without infections, autoimmune and inflammatory disease, which was also used in the PMR comparison, above (Figure 3.5A, B and E). Secondly, compared to TABUL patients with suspected, but subsequently confirmed non-GCA (Figure 3.5C, D and F). OPLS-DA revealed a separation between patients with GCA and age-matched controls (R^2= 0.94 (spectra) or 0.78 (concentrations); Figure 3.5A and E). Within the TABUL study, however, there was a much smaller separation between the confirmed patients with GCA and the confirmed non-GCA patients (R^2=0.28 (spectra) or 0.15 (concentrations); Figure 3.5C and F). Many of the non-GCA patients had an elevated CRP due to other inflammatory conditions (Table 3.1) and we speculated that metabolites might be correlating with inflammation rather than mechanisms specific to GCA. Removing the inflammation-associated metabolites according to their variable importance for prediction (VIP) scores marginally increased the separation between the confirmed GCA and confirmed non-GCA cases (Figure 3.5G).

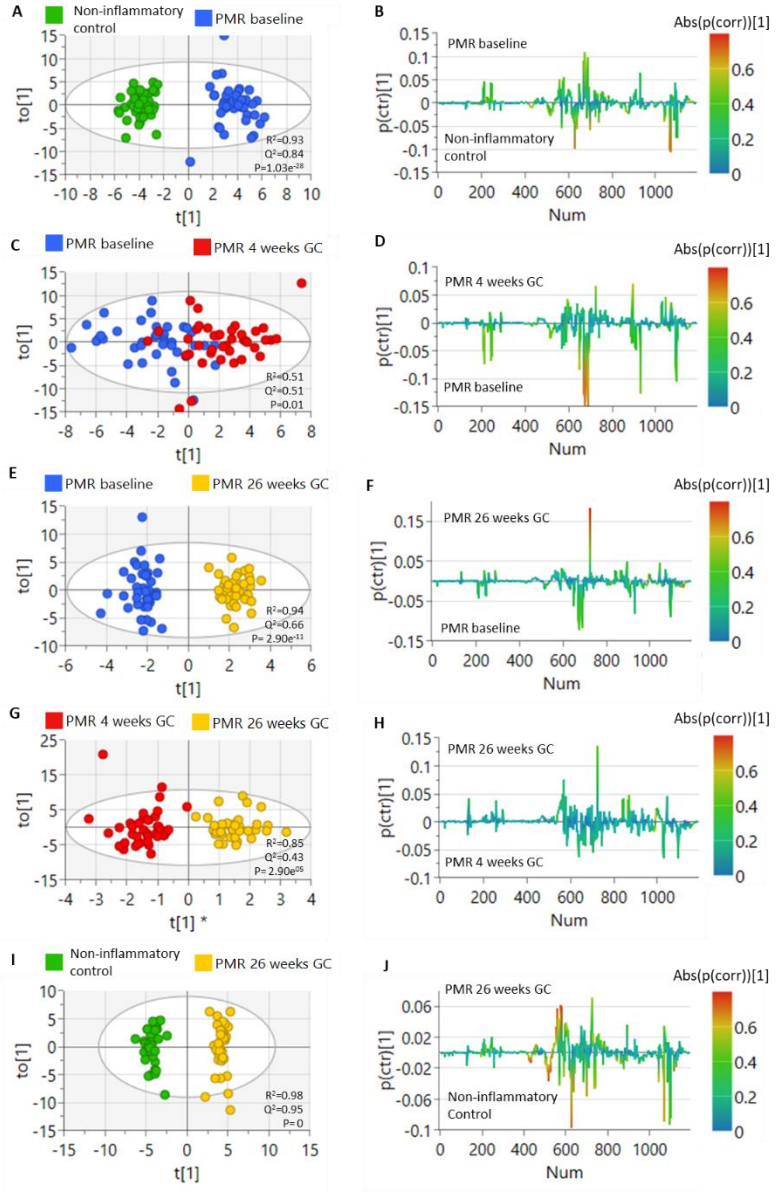

Figure 3.2: NMR spectra reveal distinct metabolite profiles in polymyalgia rheumatica patients and are sensitive to glucocorticoid treatment. One-dimensional ^{1}H-nuclear magnetic resonance (NMR) spectra were obtained from the serum of 39 age and sex-matched controls with no inflammation (green) and 40 patients with polymyalgia rheumatica (PMR) at 3 visits: (i) baseline pre-steroids with active inflammation (blue), at (ii) 4 weeks (red) and (iii) 26 weeks (yellow) of glucocorticoid (GC) treatment. Spectra were subjected to orthogonal partial least squares discriminant analysis (OPLS-DA) and from this obtained an OPLS-DA **(A,C,E,G,I)** and S-line plot **(B,D,F,H, J)** The metabolomic profile was assessed by comparing PMR baselines with **(A, B)** healthy controls, R^2=0.93, Q^2=0.84, P=1.03e^{-28}, **(C,D)** 4 week GC treatment, R^2=0.51, Q^2=0.51, P=0.0 or **(E,F)** 26 week GC treatment, R^2=0.94, Q^2=0.66, P=2.90e^{-11}. Spectra from patients with 26 weeks of GC treatment were also compared to **(G, H)** 4 week GC treatment R^2=0.85, Q^2=0.43, P= 2.90e^{05} or **(I, J)** healthy controls, R^2=0.98, Q^2=0.95, P= 0. **(A, C, E, G, I)**. Axis values indicate the proportion of variance captured by the latent variables. **(B, D, F, H, J)** Red colour indicates the highest value of the correlation coefficient and the strongly discriminatory variables have a high intensity and reliability. P values were determined using cross-validated ANOVA.

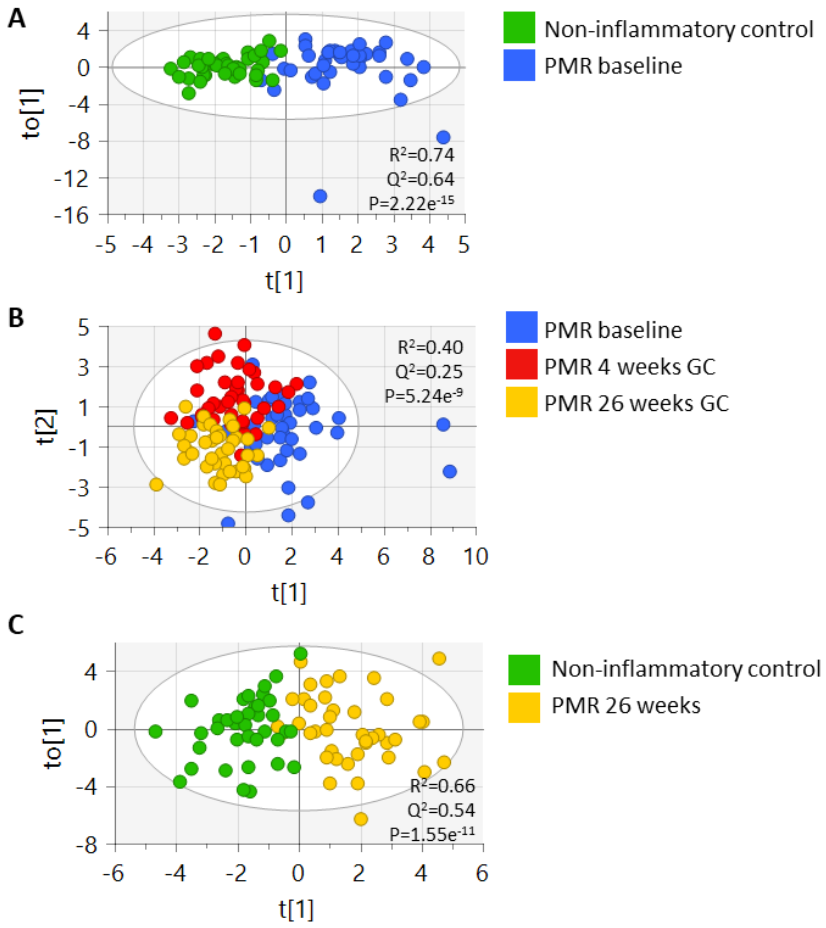

Figure 3.3: Metabolite concentrations reveal distinct metabolite profiles exist in polymyalgia rheumatica patients and are sensitive to glucocorticoid treatment. One-dimensional 1H-nuclear magnetic resonance (NMR) spectra were obtained from the serum of 39 age and sex-matched controls with no infection or underlying autoimmune and inflammatory disease (non-inflammatory control; green) and 40 patients with polymyalgia rheumatica (PMR) at 3 visits: (i) baseline pre-steroids with active inflammation (blue), at (ii) 4 weeks (red) and (iii) 26 weeks (yellow) of glucocorticoid (GC) treatment. Metabolite concentrations were determined from the spectra with Chenomx and analysed in SIMCA. Samples were subjected to orthogonal partial least squares discriminant analysis (OPLS-DA), then metabolites with a variable importance score of >1 were taken forward and subjected to OPLS-DA. **(A)** Comparison of metabolite profile in PMR vs controls, R^2=0.74, Q^2=0.64, P=2.22e^{-15}. **(B)** Effect of GC treatment on the metabolomic profile of PMR patients, R^2=0.40, Q^2=0.25, P=5.24e^{-9}. **(C)** Comparison of metabolite profile in GC treated PMR patients to non-inflammatory controls, R^2=0.66, Q^2=0.54, P=1.55e^{-11}. Axis expressed as the proportion of variance captured by the latent variables (t and to). P values were determined using cross-validated ANOVA.

Table 3.2 Metabolites contributing to the difference between groups as determined with orthogonal partial least squares – discriminant analysis

Metabolite	PMR baseline/ control		PMR baseline/ 4 weeks		PMR baseline/ 26 weeks		PMR 4 weeks/ 26 weeks		Control/ PMR 26 weeks		GCA/ control		GCA/ suspected GCA	
	FC	VIP	FC	VIP	FC	VIP	FC	VIP	FC	VIP	FC	VIP	FC	VIP
1,3-Dimethylurate	5.183	1.005	0.353	0.717	0.474	0.821	-	-	-	-	-	-	-	-
2-Hydroxybutyrate	-	-	1.273	0.608	-	-	0.878	0.939	-	-	2.004	1.506	-	-
2-Hydroxyisobutyrate	-	-	-	-	-	-	2.258	1.939	1.413	1.188	-	-	-	-
2-Oxoisocaproate	-	-	-	-	-	-	0.991	0.418	1.058	0.886	1.29	1.132	-	-
3-Hydroxybutyrate	2.07	0.961	-	-	-	-	-	-	-	-	-	-	1.353	1.036
4-Pyridoxate	-	-	-	-	-	-	1.596	0.988	-	-	-	-		
Acetaminophen	4.436	1.37	-	-	-	-	-	-	3.896	1.098	4.295		1.502	0.496
Acetoin	0.397	1.248	-	-	-	-	4.651	2.092	-	-	-	-	-	-
Acetone			1.283	0.833	0.747	1.04	0.582	1.663	-	-	1.99	0.879	1.231	0.941
Alanine	0.882	0.719	1.223	1.234	1.233	1.233	1.008	0.358	1.087	1.002	1.127	1.023	0.937	1.393
Anserine	-	-	-	-	-	-	-	-	1.963	-	-	-	1.381	0.501
Asparagine	0.713	0.939	-	-	-	-	-	-		-	-	-	-	-
Aspartate	2.471	1.155	-	-	-	-	-	-	1.981	0.982	2.401	0.915	-	-
Choline	-	-	-	-	-	-	-	-	-	-	1.455	0.85	-	-
Citrate	-	-	1.364	1.072	1.327	0.93	-	-	-	-	-	-	-	-
Creatine	1.124	0.813	0.778	0.974	-	-	-	-	-	-	0.67	0.927	0.771	0.945
Creatine phosphate	-	-	-	-	-	-	-	-	-	-	0.624	0.89	-	-
Ethanol	-	-	-	-	-	-	-	-	0.217	1.437	2.366	0.723	-	-
Ethylene glycol	-	-	0.335	1.05					0.49	0.756	2.395	1	-	-
Formate	-	-	-	-	-	-	0.868	1.105	0.852	0.987	0.669	1.029	1.243	0.448
Fucose	-	-	-	-	-	-	-	-	-	-	4.58	0.932	-	-
Glucose	-	-	-	-	-	-	-	-	1.132	0.885	1.263	0.983	-	-
Glutamate	1.776	1.385	-	-	-	-	-	-	2.428	1.206	1.883	0.964	-	-
Glutamine	-	-	1.073	0.788	-	-	0.856	0.861	0.937	0.748	1.16	0.846	0.967	1.145
Glycerol	2.758	1.469	0.582	1.231	0.605	1.07			1.669	0.838	3.325	1.301		
Guanidoacetate	-	-	0.503	0.987	-	-	1.895	1.567	-	-	-	-	0.933	0.553
Histidine	0.809	0.936	-	-	-	-	1.111	0.228	-	-	-	-	-	-
Hydroxyacetone	2.713	0.658	-	-	-	-	-	-	3.005	0.879	2.132	1.391	-	-
Inosine	-	-	-	-	-	-	-	-	0.661	0.81	-	-	-	-
Lactate	1.136	0.924	1.236	1.049	1.157	1.136	0.936	0.264	1.314	1.359	1.592	1.569		
Leucine	1.081	0.814	1.024	1.05	1.025	0.944	1.001	0.045	1.108	1	1.058	0.931	0.885	1.473
Lysine	-	-	1.029	0.929	1.119	0.848	1.088	0.442	1.279	1.21	1.077	0.956	0.999	1.146
Methanol	0.689	1.818	2.173	1.827	3.896	0.888	1.793	0.797	-	-	1.493	0.886	-	-
Methionine	-	-	1.125	0.773	1.249	0.808	1.111	0.235	1.235	0.865	1.391	1.049	0.933	1.552
Methylmalonate	-	-	1.274	1.025	1.121	0.882	-	-	1.248	0.971	1.582	1.365	-	-
Methylsuccinate	0.661	1.158	1.528	0.968	1.785	1.189	1.169	0.554	1.181	0.812	1.293	0.859	0.893	0.905
myo-Inositol	-	-	1.527	0.768	1.513	1.095	-	-	1.185	0.756	1.236	0.795	-	-
N6-Acetyllysine	-	-	-	-	-	-	4.575	0.907	-	-	-	-	-	-
N-Acetylglutamate	-	-	-	-	-	-	-	-	2.063	0.901	-	-	1.725	0.792
O-Acetylcarnitine	2.882	1.023	-	-	-	-	1.369	0.844	3.726	1.583	1.68	0.746	-	-
Ornithine	1.157	0.714	1.207	1.199	1.113	0.664	-	-	1.288	0.941	-	-	-	-
Pantothenate	-	-					1.213	0.383	1.16	0.9	1.185	0.769	1.123	0.361
Phenylalanine	1.179	1.251	1.067	0.765	0.909	0.98	0.852	0.625	1.071	0.865	1.216	0.999	0.986	0.899
Pyroglutamate	0.515	0.914	-	-	-	-	1.509	1.502	-	-	0.704	0.727	-	-
Pyruvate	-	-	1.426	1.386	1.295	1.398	-	-	1.471	1.24	1.959	1.453	-	-
Sarcosine			1.873	0.823	1.845	1.465	-	-	-	-	-	-	-	-
sn-Glycero-3-phosphocholine	-	-	-	-	-	-	-	-	3.986	0.924	-	-	-	-
Succinylacetone	1.949	0.86	-	-	-	-	-	-	-	-	-	-	-	-
Threonine	-	-	-	-	-	-	-	-	-	-	1.291	0.738	1.017	0.817
Trimethylamine N-oxide	-	-	-	-	-	-	-	-	1.437	0.828	-	-	-	-
Tryptophan	-	-	-	-	-	-	-	-	-	-	11.85	0.715	-	-
Tyrosine	0.911	0.911	1.187	0.849	1.183	0.904	-	-	-	-	-	-	1.047	0.938
Valine	1.061	0.693	1.027	1.021	0.942	0.892	0.917	0.569	0.999	1.019	0.997	0.974	0.893	1.516
π-Methylhistidine	-	-	1.46	0.939	-	-	-	-	-	-	-	-	0.884	0.823

FC = fold change; VIP = Variable importance for prediction. Significant fold changes (P>0.05) in black, non-significant in grey. Metabolites not significant for any group change are not shown. FC refers to average concentration in the first group divided by average concentration in the second. Only metabolites with a VIP > 1 were used in each analysis, therefore not all metabolites appeared in all comparisons, missing metabolites are indicated with a dash (-).

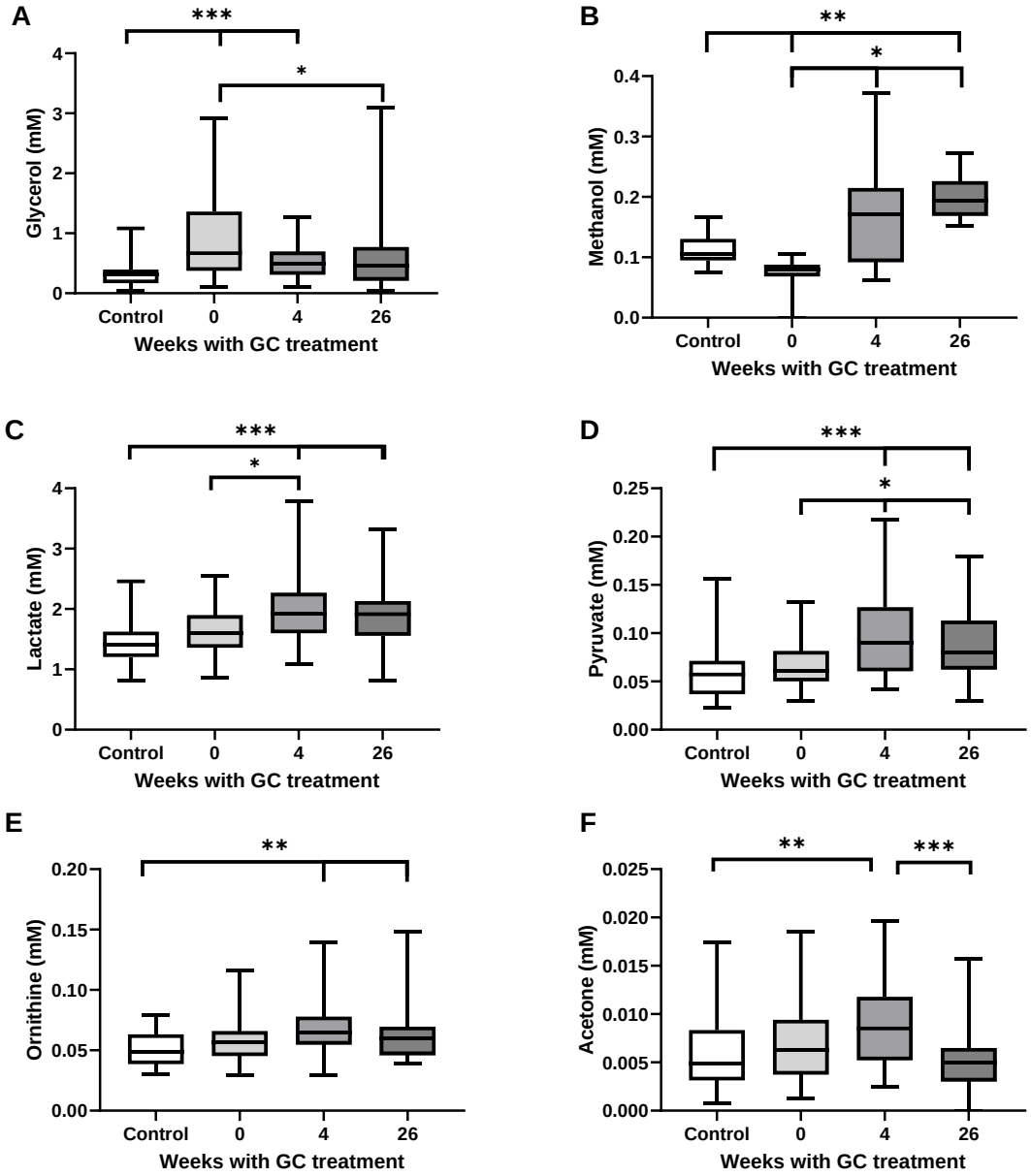

Figure 3.4: Metabolites show significant change in polymyalgia rheumatica patients compared to age and sex-matched controls and with glucocorticoid treatment. One-dimensional 1H-nuclear magnetic resonance (NMR) spectra were obtained from the serum of 39 age and sex-matched controls with no infection or underlying autoimmune and inflammatory disease (control; white) and 40 patients with polymyalgia rheumatica (PMR) at 3 visits: (i) baseline pre-steroids with active inflammation (light grey), at (ii) 4 weeks (mid grey) and (iii) 26 weeks of glucocorticoid (GC) treatment (dark grey). Metabolite concentrations were determined from the spectra using Chenomx. The concentration of metabolites with a significant difference in three or more comparisons between controls and PMR patients at each visit (described in Table 3.2) were plotted for **(A)** Glycerol, **(B**) Methanol, **(C)** Lactate, **(D)** Pyruvate, **(E)** Ornithine, and **(F)** Acetone. Box and whisker of median, error bars show interquartile range, max and min. Kruskal-wallis showed significant difference between groups for all metabolites and *P<0.05, **p<0.01 ***P<0.001 with Dunn's post-test.

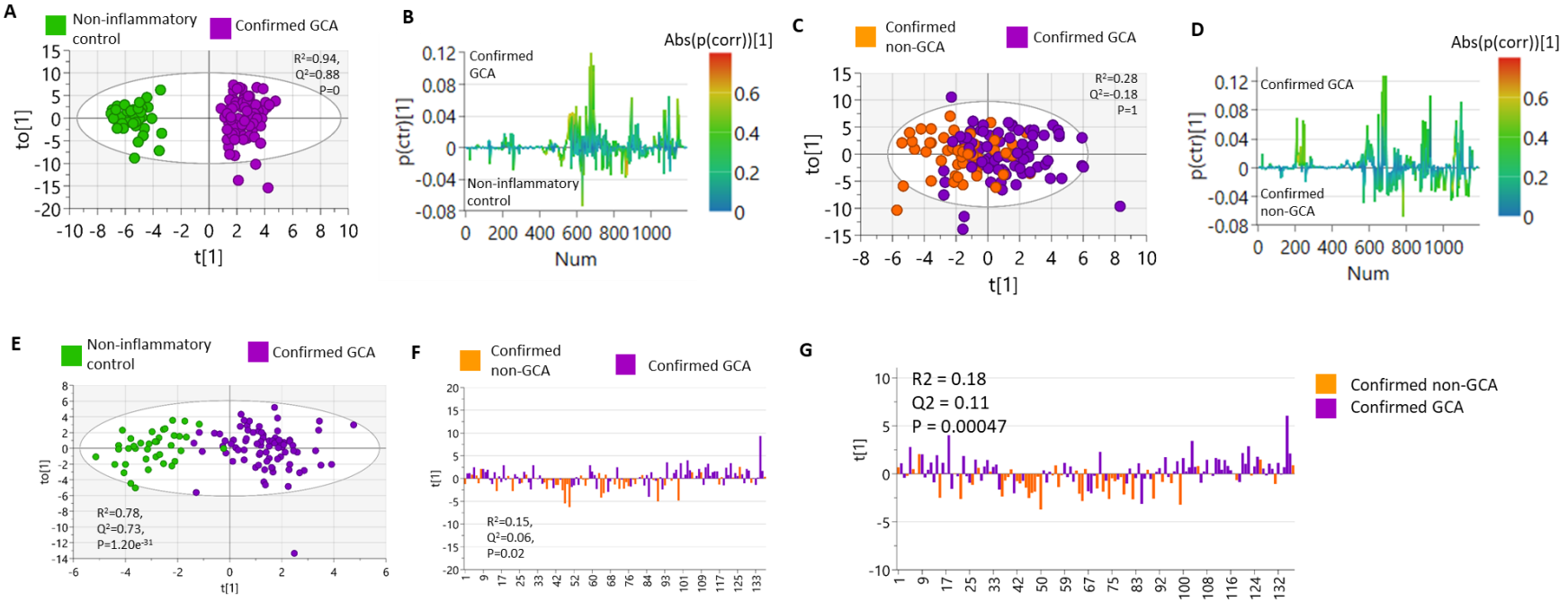

Figure 3.5: NMR spectra and metabolite concentrations in sera distinguishes giant cell arteritis patients from non-inflammatory controls and suspected giant cell arteritis. One-dimensional 1H-nuclear magnetic resonance (NMR) spectra were obtained from the serum of 84 giant cell arteritis (confirmed GCA) patients (purple), 39 age and sex-matched controls with no inflammation, control (non-inflammatory control, green) and 53 patients with suspected, but not confirmed giant cell arteritis (confirmed non-GCA) and analysed in SIMCA). In SIMCA, spectra samples were subjected to orthogonal partial least squares discriminant analysis (OPLS-DA to obtain OPLS-DA **(A and B)** or S-line plots **(C and D)**. **(A)** Control and GCA, R^2=0.94, Q^2=0.86, P=0 and **(B)** Suspected GCA and GCA, R^2=0.27, Q^2=0.17, P=1. **(A and B)** Axis values indicate the proportion of variance captured by the latent variables. **(C and D)** Red colour indicates the highest value of the correlation coefficient and the strongly discriminatory variables have a high intensity and reliability. **(E and F)** Identified metabolites were also subjected to OPLS-DA, and metabolites with a variable importance score of >1 were re-subjected OPLS-DA and analysed. Comparison of GCA with **(E)** non-inflammatory control R2=0.78, Q2=0.73, P=1.20e-31 and **(F)** confirmed non-GCA R2=0.15, Q2=0.06, P=0.02. Axis values indicate the proportion of variance captured by the latent variables. **(G)** To identify, and subsequently remove, metabolites predictive of the inflammatory marker CRP, samples were first subjected to partial least squares regression analysis (PLS-R). Metabolites with variable importance score of prediction (VIP) >1 for CRP were removed and remaining metabolites subjected to orthogonal partial least squares discriminant analysis (OPLS-DA). Metabolites with a VIP of >1 were then re-subjected OPLS-DA and analysed. Comparison of confirmed GCA and non-GCA; R^2=0.183, Q^2=0.11, P=0.00047. P values determined with cross-validated ANOVA.

3.2.4 Inflammation and patient reported outcomes are associated with metabolomic profile

Metabolomic studies in RA have demonstrated an association between metabolomic profile and CRP (80, 263). To assess this in the PMR and GCA patients, PLS-R was performed using the metabolite concentrations (Figure 3.6A and B) and NMR spectral bins (Figure 3.8A and B). This gave moderate R^2 and Q^2 values indicating an association between the metabolite concentrations and systemic inflammation. Pathway analysis of metabolites (Figure 3.6C and D) revealed that that the "synthesis and degradation of ketone bodies" pathway, in particular 3-hydroxybutyrate and acetoacetate, significantly contributed to the PLS-R model of CRP in patients with both PMR and GCA. Taken together, this suggests that concentrations of multiple metabolites, especially ketone bodies, correlate with systemic inflammation as reflected by CRP.

Using PLS-R, we then examined whether metabolite concentrations associated pain, stiffness, and fatigue in PMR patients. Baseline median scores were 8 (IQR 7-9) for both pain and stiffness VAS, and 25 (IQR 17-32) for fatigue (52 - FACIT-F score). A significant association was found between metabolites and pain, stiffness, or fatigue with moderate goodness of fit and prediction (Figure 3.7). Using colour to visualise the samples according to the date of patient visit (0, 4 or 26 week's treatment) shows that pain and stiffness decreased with treatment (Figure 3.7A and B, and Figure 3.8C and D), whereas some patients had persistent fatigue after 26 weeks of GC treatment (Figure 3.7C and Figure 3.8E). Importantly, these patterns were by the metabolites (Figure 3.7A-C), with $R^2 \geq 0.39$ for pain, stiffness and fatigue. Similar to CRP, pathway analysis of revealed that the "synthesis and degradation of ketone bodies" pathway significantly contributed to the pain and stiffness

(Figure 3.7D-E). However, no relationship was seen with fatigue (Figure 3.7F). To ensure no correlations were observed simply due to samples being from the patients at different time points, the CRP and PROs analyses were repeated on PMR patients at baseline, 4 weeks and 26 weeks on GC treatment separately (Figure 3.9). These models all had high R^2, suggesting appropriate modelling and gave similar metabolites to the grouped analyses. These data indicate that pain and stiffness, but not fatigue, are associated with inflammation in PMR.

To investigate this further the metabolites associated with CRP (VIP>1) were removed, and the remaining metabolites used in PLS-R analysis of fatigue, Figure 3.10A. These remaining metabolites significantly correlated with fatigue, suggesting an inflammation-independent distinct metabolite profile underpinning fatigue. Using all metabolites, patients were divided into those with “high” and “low” fatigue scores at baseline and after 26 weeks GC treatment to identify metabolites associated with fatigue. Groups were determined by selecting the patients still suffering from fatigue (FACIT-F < 20 (264)) after 26 weeks GC treatment, of which there were 9, then selecting the 9 patients with lowest levels of fatigue at 26 weeks, and the 9 patients with highest and lowest fatigue at baseline (encircled in Figure 3.10B and C). OPLS-DA revealed a separation between the “high” and “low” fatigue groups at both time points, Figure 3.10D and E, with the metabolites that drive the separation in low and high fatigue scores described in Table 3.3. Of particular interest was the significantly lower glutamine concentration and higher histidine and 2-hydroxyisobutyrate concentrations at both time points. This suggests that circulating metabolite concentrations correlate with level of fatigue in patients with PMR.

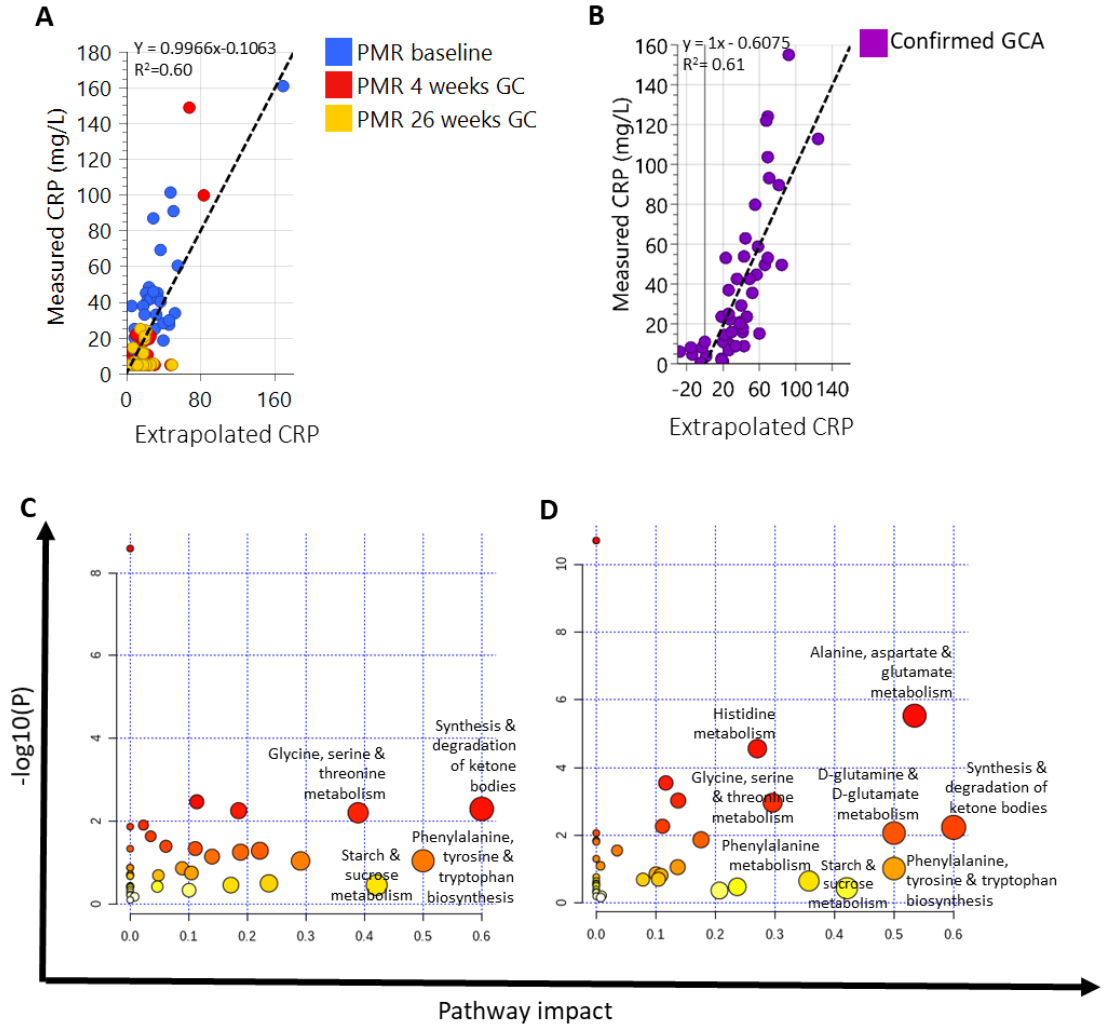

Figure 3.6: Metabolite concentrations in sera correlate with C-reactive protein. One-dimensional ^{1}H-nuclear magnetic resonance (NMR) spectra were obtained from the serum of patients and metabolite concentrations were determined from the spectra with Chenomx. Predicted values of patient reported outcomes were determined from the metabolites using partial least squares regression analysis (PLS-R). Metabolites with variable importance for prediction (VIP) >1 were taken forward and predicted values from these metabolites were compared to the CRP measured on the day the samples were taken, for **(A)** PMR patients before (blue) and after glucocorticoid treatment at 4 (red) and 26 weeks (yellow), P= $2.65e^{-13}$, R^2=0.60, Q^2=0.42 and **(B)** GCA patients, P= $2.55e^{-05}$ R^2=0.61, Q^2=0.38. **(C-D)** VIP >0.9 for individual metabolites were subsequently assessed for importance in metabolic pathways using Metaboanalyst for **(C)** PMR, **(D)** GCA patients, axis show the –log P values and the impact of metabolites on each pathway (0-1). Statistical analysis was determined using cross validated ANOVA.

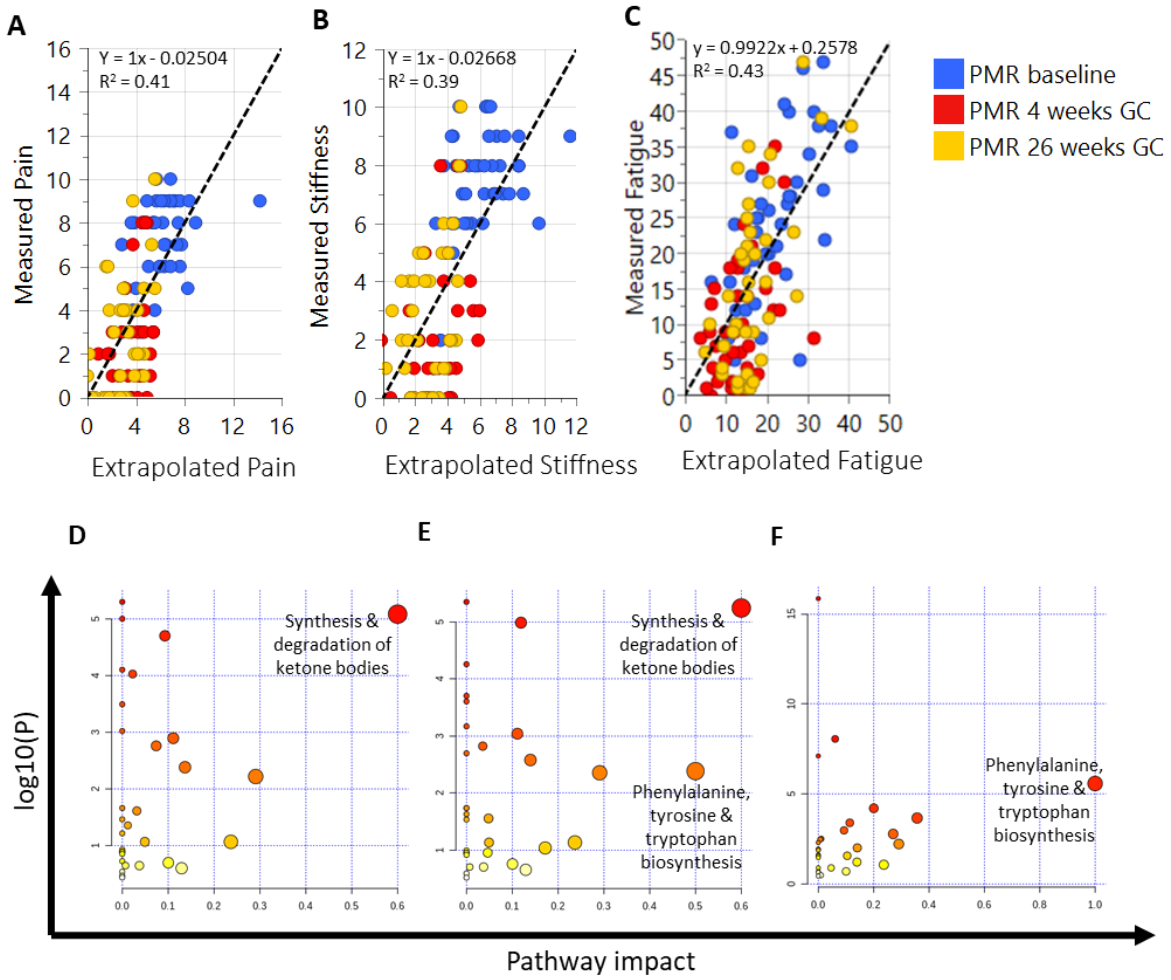

Figure 3.7 Metabolite concentrations in sera correlate with patient reported outcome measures. One-dimensional 1H-nuclear magnetic resonance (NMR) spectra were obtained from the serum of 40 patients with polymyalgia rheumatica at baseline (blue) and following glucocorticoid (GC) treatment for 4 (red) and 26 weeks (yellow). Metabolite concentrations were determined from the spectra with Chenomx and analysed in SIMCA. Predicted values of patient reported outcomes were determined from the metabolites using partial least squares regression analysis (PLS-R). Metabolites with variable importance for prediction (VIP >1) were taken forward and predicted values from these metabolites were compared to patient reported outcome measures for **(A)** pain, P=5.05e-10, R2=0.41, Q2=0.31, **(B)** stiffness P=4.36^{-05}, R2=0.39, Q2=0.25 and **(C)** fatigue, P=8.10e^{-05}, R2=0.41, Q2=0.19, where P values determined with cross-validated ANOVA. **(D-F)** VIP >0.9 for individual metabolites were subsequently assessed for importance in metabolic pathways using Metaboanalyst for **(D)** pain, **(E)** stiffness and **(F)** fatigue, axis show the –log P values and the impact of metabolites on each pathway (0-1).

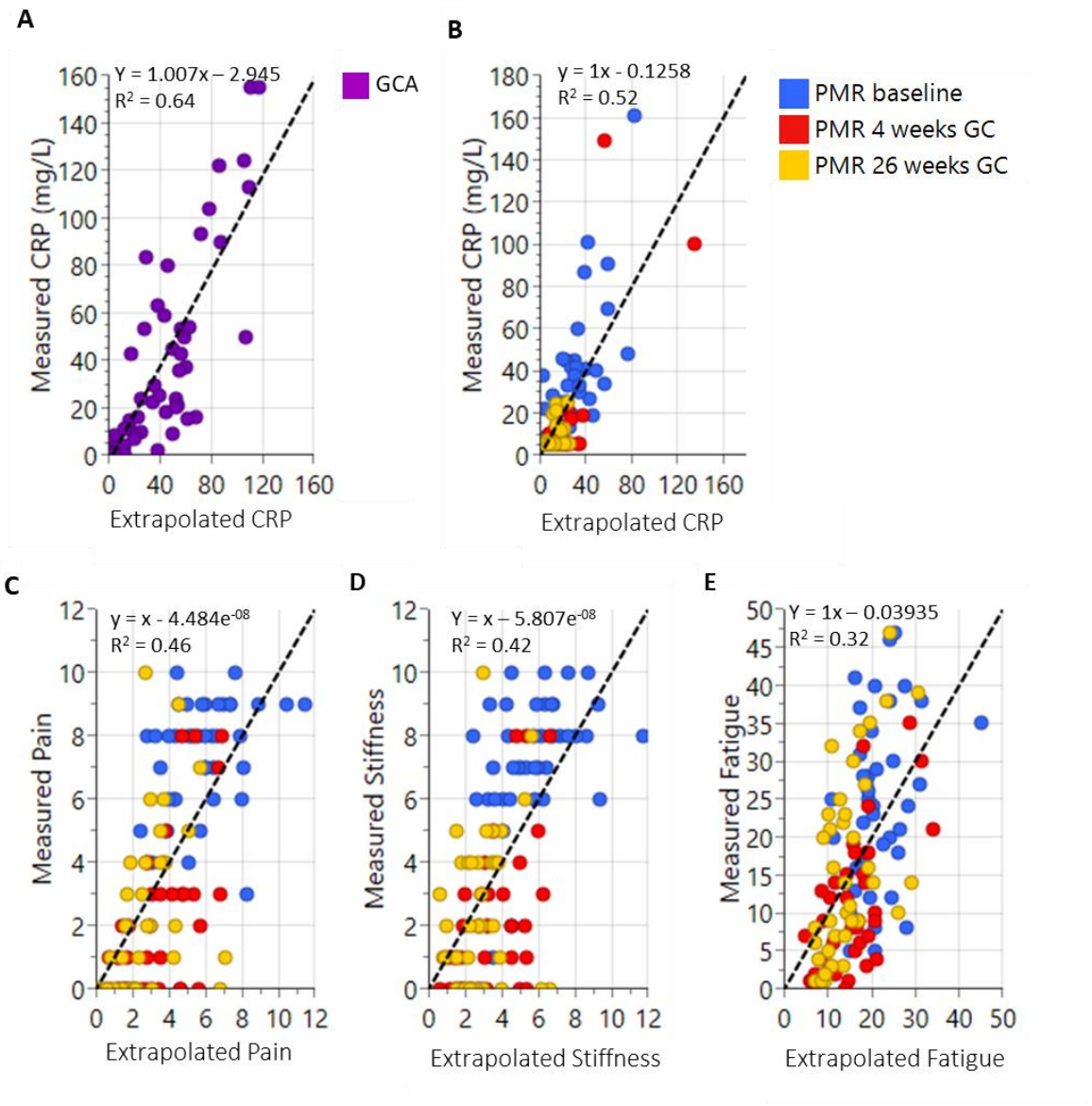

Figure 3.8: Metabolic profiles of sera correlate with C-reactive protein, pain, stiffness and fatigue. One-dimensional 1H-nuclear magnetic resonance (NMR) spectra were obtained from the serum of giant cell arteritis (GCA) and polymyalgia rheumatica (PMR) patients and used to predict the measured C-reactive protein levels (CRP) and for PMR patients of pain, stiffness and fatigue scores using partial least squares regression analysis (PLS-R). **(A)** CRP levels of GCA patients, P= $2.65e^{-13}$, R^2=0.64, Q^2=0.29. **(B-E)** PMR patients before (blue) and after glucocorticoid treatment at 4 (red) and 26 weeks (yellow). **(B)** CRP, P= $2.99e^{-4}$, R2=0.52, Q2=0.34. **(C)** Pain, P= $1.87e^{-08}$, R2=0.46, Q2=0.26. **(D)** Stiffness, P= $2.40e^{-06}$, R2=0.42, Q2=0.2. **(E)** Fatigue, P= 0.017, R2=0.32, Q2=0.07. Statistical analysis was determined using cross validated ANOVA.

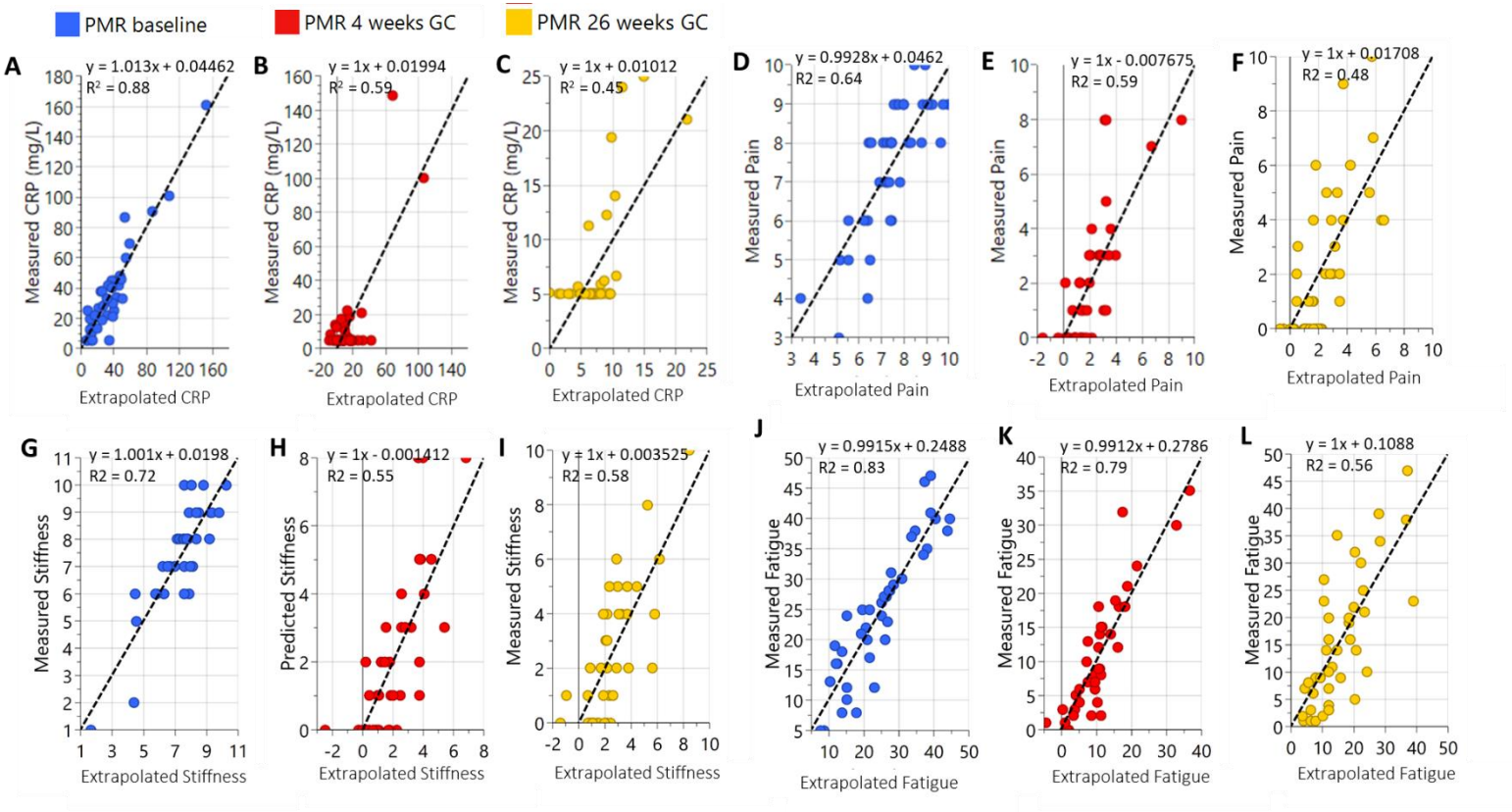

Figure 3.9 Metabolic profiles of sera correlate with C-reactive protein, pain, stiffness and fatigue. One-dimensional 1H-nuclear magnetic resonance (NMR) spectra were obtained from the serum of polymyalgia rheumatica (PMR) patients, metabolites concentrations identified and these used to predict the measured C-reactive protein levels (CRP) and for PMR patients of pain, stiffness and fatigue scores using partial least squares regression analysis (PLS-R). The analysis was performed separately on the patients at 3 time points; pre-steroids (blue) and after 4 weeks (red) or 26 weeks (yellow) glucocorticoid (GC) treatment. **(A)** Baseline CRP, $P=5.25e^{-4}$, $Q^2=0.57$, $R^2=0.86$, **(B)** 4 weeks GC, CRP, $P=6.44e^{-3}$, $Q^2=0.24$, $R^2=0.58$, **(C)** 26 weeks GC, CRP, $P=8.67e^{-3}$, $Q^2=0.23$, $R^2=0.43$, **(D)** Baseline pain, $P=2.47e^{-4}$,$Q^2=0.46$, $R^2=0.64$, **(E)** 4 weeks GC pain, $P=5.95e^{-3}$, $Q^2=0.24$, $R^2=0.59$, **(F)** 26 weeks GC pain, $P=2.16e^{-3}$, $Q^2=0.28$, $R^2=0.49$, **(G)** Baseline stiffness, $P=3.67e^{-3}$, $Q^2=0.34$, $R^2=0.72$, **(H)** 4 weeks GC stiffness, $P=0.023$, $Q^2=0.18$, $R^2=0.55$, **(I)** 26 weeks GC stiffness, $P=0.0011$, $Q^2=0.31$, $R^2=0.58$, **(J)** Baseline fatigue, $P=6.26e^{-5}$, $Q^2=0.57$, $R^2=0.83$, **(K)** 4 weeks GC fatigue, $P=1.11e^{-5}$, $Q^2=0.57$, $R^2=0.79$, **(L)** 26 weeks GC fatigue, $P=0.0042$, $Q^2=0.26$, $R^2=0.60$.

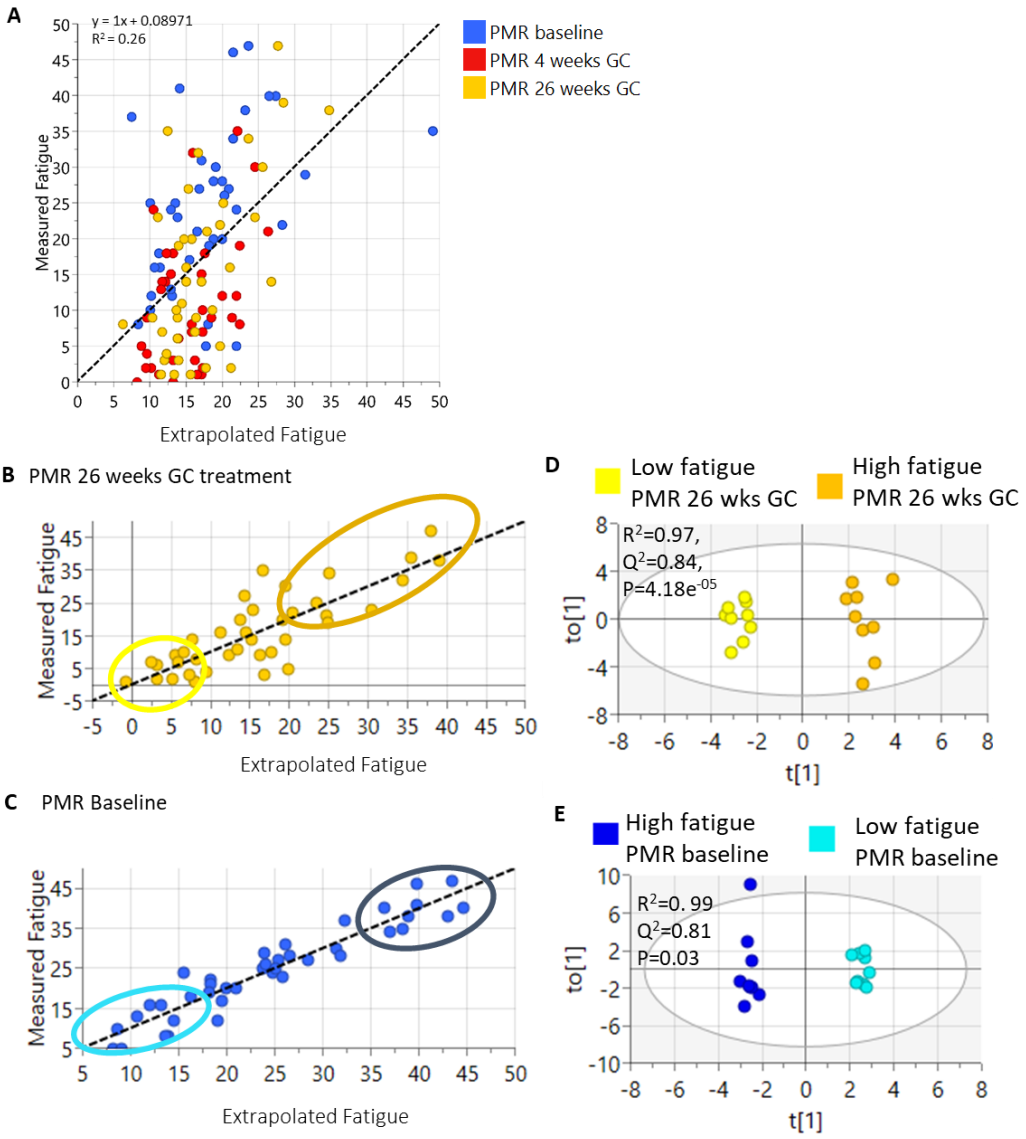

Figure 3.10: Non-inflammatory metabolites correlate with fatigue and metabolites can distinguish between patients with high and low fatigue in polymyalgia rheumatica patients. One-dimensional 1H-nuclear magnetic resonance (NMR) spectra were obtained from the serum of 40 patients with polymyalgia rheumatica (PMR) at 3 visits; baseline (blue) and following glucocorticoid (GC treatment for 4 (red) and 26 weeks (yellow). Metabolite concentrations were determined from the spectra with Chenomx then analysed in SIMCA. **(A)** Firstly, partial least squares regression (PLS-R) identified metabolites predictive of CRP (with a variable importance of prediction, VIP>1). These were removed and PLS-R of fatigue performed on the remaining metabolites. Metabolites with a VIP > 1 were re-subjected to PLS-R and predicted vs measured fatigue, P = 0, R^2 = 0.26, Q^2=0.14. P value determined with cross-validated ANOVA. **(B-E)** Using all metabolites, predicted values of fatigue were determined with PLS-R separately on patients at **(B)** 26 weeks and **(C)** baseline. The 9 highest and lowest scoring patients (circled) for the predicted and measured fatigue were separated into groups and subjected to orthogonal partial least squares – discriminant analysis (OPLS-DA), for **(D)** PMR patients 26 weeks into GC treatment, P = $4.18e^{-05}$, R^2 = 0.97, Q^2=0.84 and **(E)** Baseline PMR patients, P = 0.03, R^2 = 0.99, Q^2=0.81.

Table 3.3: Fold change and variable importance of prediction scores of metabolites in polymyalgia rheumatica patients reporting high compared to low fatigue

Metabolite	Baseline		26 weeks	
	FC	VIP	FC	VIP
2-Hydroxyisobutyrate	4.065	1.178	1.558	1.102
3-Hydroxyisovalerate	2.564	1.164	-	-
Acetoin	0	1.215	0.696	0.84
Carnitine	2.433	1.271	-	-
Choline	-	-	1.736	1.17
cis-Aconitate	-	-	0	1.436
Creatinine	1.418	0.961	1.514	1.131
Dimethyl sulfone	1.969	1.19	1.611	1.009
Ethylene glycol	-	-	0	1.197
Galactarate	0.424	0.985	0.332	1.174
Galactitol	-	--	2.385	1.465
Glutamine	0.79	1.144	0.791	1.155
Histidine	1.618	1.051	1.248	1.149
Methanol	0.879	0.976	-	-
Methylsuccinate	1.859	0.923	1.432	1.095
myo-Inositol	2.381	1.022	-	-
N-Methylhydantoin	1.965	1.038	1.49	1.091
O-Phosphocholine	0.096	0.975	-	-
Pantothenate	-	-	1.359	1.229
Sarcosine	-	-	0.628	1.255

FC = fold change (high fatigue/low fatigue); VIP = variable importance for prediction. Metabolites with statistically significant (P>0.05) fold changes are black and non-significant in grey. Metabolites that don't significantly change for either group change are not shown. FC refers to the average concentration of "high" fatigued patients divided by "low" fatigued patients. Only metabolites with a VIP > 1 were used in each analysis, therefore not all metabolites appeared in all comparisons, missing metabolites are indicated with a dash (-).

3.3 Discussion

The molecular mechanisms underpinning PMR and GCA, and the effect of GC treatment in these, remains poorly understood. Moreover, it is currently unclear why a subset of PMR patients continue to suffer fatigue despite the control of the pain and stiffness with GC treatment. Here, we have demonstrated that the circulating metabolomic profile of patients with PMR and GCA is distinct from age and sex-matched controls, as seen in other chronic inflammatory diseases (80, 83). In PMR, this disease-specific profile is altered following initiation of GC treatment, but does not become similar to that seen in age-matched controls; these alterations are akin to those observed in other GC-treated inflammatory diseases (265). Pain and stiffness, but not fatigue, appeared to be coupled with inflammation and shared similar associated metabolites (acetoacetate, 3-hydroxybutyrate and methanol). Furthermore, metabolite profiles, particularly a low glutamine concentration, distinguished patients reporting high and low fatigue, and associated with fatigue both before and after treatment. We have shown for the first time that disease, GC treatment, and importantly fatigue, correlate with significant changes in the circulating metabolic profile of PMR and GCA patients. Our data highlights the possibility of using glutamine as a biomarker to predict and monitor fatigue in these patient groups. Furthermore, investigations into the role of glutamine in fatigue may pave the way to develop novel therapeutics to significantly reduce fatigue across a range of inflammatory diseases.

3.3.1 Inflammation-associated metabolite signatures

Elevated levels of ketone bodies, glycerol, lactate, and pyruvate are often reported in patients with inflammatory diseases (80, 86); we observed similar increases in these metabolites in PMR and GCA. Collectively these data strongly indicate these metabolites are

a hallmark of inflammation, rather than being a disease-specific metabolic response, and that inflammation is associated with aberrations in the main energy pathways (80). Indeed, the elevated ketone bodies (3-hydroxybutyrate and acetoacetate) and glycerol levels observed here and in studies using samples with RA patients (80, 86) point toward pro-inflammatory cytokines (e.g. TNF) driving lipolysis (266). This is further supported by the fact PMR and GCA patients often present with weight loss alongside raised laboratory markers of inflammation (267). Nevertheless, the metabolite 3-hydroxybutyrate is also known to block the NLR Family Pyrin Domain Containing 3 (NLPR3)-inflammasome exerting an anti-inflammatory effect (268). Mutations in the *NPLPR1* inflammasome locus and NLPR3-inflammasome involvement have been attributed to pathogenesis of GCA (269) and RA (270) respectively, suggesting that pathologically elevated levels of 3-hydroxybutyrate might contribute to disease onset and chronicity of inflammation. Both acetoacetate and 3-hydroxybutyrate were also associated with pain and stiffness levels in our PMR cohort. Given several reports highlighting the close relationship between pain, stiffness and inflammation in PMR [e.g. (271)], it is unsurprising that some of these inflammation-associated metabolites also associated with pain and stiffness. It must be noted, however, that at baseline, patients with PMR had fasted, whilst at 4 and 26 weeks they had not. This may have contributed to the observed association as ketosis and the generation of ketone bodies is related to fasting (272). Furthermore, loss of appetite and reduced food intake are common in inflammatory states and could also have affected metabolite levels. If this were to be repeated, and in future studies, serum would be taken in a fasted state to limit the effects of this confounder.

By contrast, lactate and pyruvate increased with inflammation, but did not associated with pain, stiffness, or fatigue, most likely due to GC-associated changes (described below (3.3.2)). Despite this, there was an inflammation-associated elevation of these metabolites (lactate and pyruvate), suggestive of abnormal energy metabolism. This may be explained by an inflammation-induced hypoxic environment, combined with increased energy demands of proliferating immune cells and proteolysis, resulting in a switch to aerobic glycolysis and gluconeogenesis and leading to lactate accumulation and pyruvate synthesis (80). Indeed, other studies have also found elevated lactate levels in PMR (273). Lactate derivatives can inhibit the motility of T-cells resulting in their accumulation in tissue, as well as inducing Th17 formation and reducing the cytolytic function of $CD8^+$ T-cells (274), raising the question of whether lactate is involved in PMR and GCA pathogenesis via these mechanisms. Therefore, the changes observed in lactate and 3-hydroxybutyrate could indicate not only alterations in energy metabolism, but also in T-cell signalling. Thus, further investigation is required to fully dissect the role of these metabolites in the pathogenesis of PMR and GCA.

3.3.2 Metabolite signatures following glucocorticoid treatment

Due to ethical reasons, we were unable to have a control of untreated patients where metabolites were measured alongside treated patients. Therefore, we cannot assume that changes observed following GC treatment would occur with time and disease progression. Notably as well, we do not know if these are a GC specific change, or signs of reduced inflammation. In these cohorts of PMR and GCA patients, following treatment with GCs, we observed divergent effects on the inflammation-associated metabolites. Some metabolites were reduced following therapy (ketone bodies and glycerol), whilst others were increased

(lactate and pyruvate). The decreased ketone body (3-hydroxybutyrate and acetoacetate) levels suggest a reduction in lipolysis, similar to that observed in healthy males following continuous treatment with 7.5mg or 30mg prednisolone over 2 weeks (275). In contrast, increased lipolysis was reported in healthy males following a single low dose (4mg) of dexamethasone (262). Thus, acute and prolonged GC treatment appears to exert differential effects on systemic metabolism (262, 276), which may account for reduced levels of ketone bodies seen in PMR following 4 and 26 weeks of GC therapy. The elevated levels of lactate and pyruvate we report here are a typical response following short-term GC treatment (262), as they are known to cause increased hepatic gluconeogenesis and protein catabolism, in conjunction with reduced glucose uptake (262). Furthermore, elevated lactate levels are a feature of insulin resistance (277) and may potentially be an early biomarker of patients at risk of steroid-induced hyperglycaemia, as elevated lactate predicts incident diabetes in the general population (278). Similarly, pyruvate levels are well-known to increase with adiposity and obesity (279, 280). GCs can inhibit pyruvic acid conversion to acetyl-CoA (281) and enhance amino acid conversion to pyruvate, further contributing to pyruvate and/or lactate accumulation in tissues – e.g. in the lymphocytes of rat lymph nodes (282). In PMR, a previous study showed that elevated lactate and pyruvate in interstitial muscle, rose even further with GC treatment (283). The GC-induced lactate/pyruvate elevation suggests that lactate has not only the pro-inflammatory effects described earlier, but also anti-inflammatory properties, perhaps dependent on concentration and location. Indeed, LPS-induced production of IL-1β, IL-6, TNF and IL-10 in peripheral blood mononuclear cells was decreased by lactate *in vitro*; however, *in vivo* infusion had limited effects on cytokine production suggesting rapid adaptations of the immune system to lactate concentrations

(284). Taken together, the evidence suggests a complex role for lactate in inflammation, with further investigations required to determine its precise function.

Surprisingly, methanol sharply increased in patients after GC treatment indicative of alterations to its synthesis or degradation. Methanol and its oxidised product, formaldehyde, are often present in blood due to exogenous sources (fruit, vegetables, alcoholic beverages, or the artificial sweetener aspartame), but can also be formed endogenously via gut bacteria fermentation or metabolic processes involving S-adenosyl methionine (285). Unfortunately, no data was collected on whether patients with PMR altered their diet following GC therapy. Whatever its source, in healthy individuals, methanol concentration is tightly controlled to keep it at low concentrations (285), with high levels being linked neurological diseases, such as Alzheimer's (285, 286). The substantial GC induced increase in methanol we observe here suggests GCs cause a loss of the tight methanol regulations and as high levels have been linked to other diseases is indicative of a possible negative role. Replication of this data is required, but if it holds true then this may link to the observed adverse effects of GC treatment.

3.3.3 Fatigue-associated metabolite signatures

Fatigue is a common symptom experienced by patients with chronic inflammatory diseases, especially those treated with GC, but as yet the underlying mechanisms responsible for fatigue have remained elusive. Studies have postulated that fatigue is due to reduced cellular energy availability (287) or oxidative stress leading to pain and depression (288), with some individuals more severely affected than others due to their genetic background

(289). We have identified a fatigue-specific metabolic signature that distinguishes between patients with PMR who have high or low fatigue levels, independent of disease duration or GC treatment timeline.

Of particular interest is the possibility that the metabolite glutamine may act as a biomarker for fatigue, with markedly reduced levels of glutamine observed in highly fatigued patients both before and after treatment. However, it must be noted that glutamine levels were not prominently perturbed in a metabolomic study of fatigue in rheumatoid arthritis (82) and our findings in PMR require replication. As a conditionally essential amino acid, glutamine is a key fuel source for rapidly dividing leukocytes, playing a pivotal role in the immune response (290). Consequently, low serum glutamine concentrations have been associated with a range of diseases including cancer (291), inflammatory bowel disease (292), and chronic fatigue syndrome (293). Glutamine is also required as a fuel for muscles during intense exercise (290). It is normally produced by skeletal muscle; therefore low glutamine concentrations occur in catabolic states, such as high altitude-associated muscle wasting (294). It is possible that as a consequence of the symptoms of PMR, patients are less mobile, leading to a degree of sarcopenia (295). Alternatively, some patients may experience GC treatment-induced proteolysis and muscle atrophy (296); however, it remains unclear why only a subgroup of patients would respond this way. Further investigations to monitor the muscle mass in fatigued vs non-fatigued PMR patients is required to determine if cachexia may be the cause. From our data there was no correlation between those who reported weight loss at baseline and those who were categorised as having “high” fatigue levels. An alternative explanation may be that modifications to the citric acid cycle (choline, glutamine,

and methylsuccinate dysregulation) alter ATP availability, supporting the notion that reduced cellular energy caused by inflammation (287) underpins fatigue. Thus, further investigation is required to determine if glutamine plays an important role in driving fatigue or is a by-product of an underlying metabolic change.

Recently, low glutamine levels were described in association with human obesity and insulin resistance, with animal studies indicating a possible beneficial effect of glutamine supplementation (297). Similarly, glutamine supplementation improved exercise-induced fatigue markers in human studies, albeit with limited effects on physical performance (298). However, these studies suggest that glutamine supplementation may a therapeutic avenue for patients with high fatigue levels. Further work is required to understand the importance of changes in glutamine metabolism in the symptoms of fatigue, and to identify patients with PMR who are at risk of prolonged fatigue and who might benefit from additional intervention to manage their fatigue. Low glutamine levels in treated PMR patients might reflect ongoing immune activation, PMR- or GC-related muscle changes, or a combination of both factors. Regardless, glutamine might be an additional biomarker of poor prognosis in patients with PMR.

3.3.4 Limitations

Whilst this exploratory study provides a first look at the metabolite changes within PMR and GCA patients, there are limitations. Most significantly, the sample size is relatively small, especially once exploring patient subsets (i.e., those with fatigue following GC treatment), and validation of these findings would be required in separate cohorts. The data comparing

GCA and non-GCA patients are hard to interpret since many of the non-GCA patients had elevated CRP and/or were treated with similar doses of glucocorticoids to the GCA patient. This may have contributed to the non-significant result observed between the two patient groups and makes it difficult to identify disease-specific alterations. Furthermore, patient reported outcome data was not available for the GCA cohort. Therefore, these could not be correlated to see if the same metabolites associated with pain and inflammation, as seen in the PMR cohort. It would also have been interesting to determine how many PMR and GCA patients had overlapping disease and if there were any differences in these patients. However, these data were not readily available and analysis of subsets would have reduced the sample sizes further. Furthermore, because PMR and GCA are often regarded as spectrums of the same disease (67), even if a patient was not diagnosed with the other disease, there may still have been overlap. Likewise, as the diseases are not mutually exclusive, no direct comparisons between the PMR and GCA groups were carried out.

3.3.5 Conclusions

Taken together the data suggest that metabolomic perturbations can be detected in PMR and GCA, and that GC therapy for these diseases is associated with further metabolomic changes. The most significant changes indicate alterations in energy metabolism, associated with both the diseases themselves and following GC treatment. Furthermore, both 3-hydroxybutyrate and lactate are known to participate in cell signalling. Metabolites also associated with inflammation and symptoms, however, only pain and stiffness (and not fatigue) appeared to be associated with inflammation. The fact that fatigue was associated with a different time course and different metabolomic fingerprint than pain and stiffness,

suggests a multifactorial aetiology of this symptom. Most notably, patients reporting high and low fatigue could be distinguished by their metabolomic profile, with glutamine identified as a new biomarker or treatment target for fatigue in PMR. These results are promising; however, further investigations to validate these metabolites in a separate cohort and functional experiments to determine the cellular basis of these changes are required. If these preliminary results can be validated in a separate cohort, they might enable definition of subsets of PMR at greater risk of fatigue or of GC-related adverse effects that might warrant early intervention to optimise long-term outcome.

4 Endothelial phenotypes in rheumatoid arthritis

4.1 Introduction

The endothelium is known to play a major in the pathogenesis of RA. It does this via a variety of process including angiogenesis and increased permeability leading to oedema formation. Arguably one it's most pivotal roles, is that it becomes activated and expresses multiple adhesion molecules and cytokines (135, 136, 171), which allow leukocytes to extravasate into the joint. This increase in adhesion molecules expression has been demonstrated in multiple studies via synovial tissue staining (136-138, 140), and measuring adhesion molecule expression of isolated RA ECs (175). Interestingly, studies have also shown that whilst some adhesion molecules (e.g., ICAM1 and VAP1) are ubiquitously expressed throughout the synovium, some (e.g. VCAM1 and PNAd) can only found on subsets of endothelial cells (136-138, 140). These subsets may potentially account for the range of pathotypes observed in RA (i.e. fibroid, myeloid and pauci-immune) (129). However, whether this is the case is yet to be fully explored. Furthermore, how or if the expression of these are different in patients with arthritis that resolves compared to RA, or whether expression patterns change during the course of disease is currently unknown. Therefore, in this chapter, the aim was to examine if endothelial markers of interest (e.g., adhesion molecules) are altered dependent on disease or pathotypes. This was determined using CellDIVE multiplex imaging of tissue sections from the Birmingham Early Arthritis cohort (BEACON), as well as the publicly available bulk RNA-sequencing dataset from the pathobiology in early rheumatoid arthritis cohort (PEAC).

4.2 Results

4.2.1 Target selection and panel design

As described in 1.5.4.1 and 2.3.2, by repeated rounds of staining and bleaching, CellDIVE multiplex imaging allows the visualisation of up to 60 markers in one tissue section (217). To investigate alterations in the endothelial phenotype, a panel of endothelial markers of interest was compiled based on literature searches and current in-house research, which suggested the markers had interesting or selective expression within the inflamed synovium. This included adhesion molecules, senescence markers, and notch3 signalling and angiogenesis molecules. The markers chosen, and the reasoning for their selection is given in Table 4.1. Figure 4.1 also shows, where possible, previous staining (carried out by Salmi *et* al (136), Vincent Gauthier and Triin Major) of these markers within the synovium of patients with chronic arthritis (rheumatoid, psoriatic, spondyloarthropathies).

Table 4.1: Plan for endothelial marker panel

Target	Function	Reason(s) for inclusion
Markers of the endothelium		
CD31, PECAM-1	A transmembrane glycoprotein (299, 300).	Marker of endothelial cells (ECs), although it is also expressed on some leukocytes (299, 300).
Lyve1	A transmembrane glycoprotein (2).	Marker of lymphatic ECs, although it is also expressed on liver sinuses, and to lesser extent Kupffer cells, Langerhans islands, cortical neurons, and renal epithelium (300, 301).
Adhesion molecules		
VAP1, AOC3	An endothelial surface glycoprotein. It functions both as an ectoenzyme (catalysing the deamination of primary amines to produce hydrogen peroxide, ammonium and aldehydes) and adhesion molecule to facilitate leukocyte binding to the endothelium (302, 303). It is highly expressed in the tonsil and lymph nodes, particularly the high endothelial venules (HEVs) as well as a subset of venules of the skin, brain, kidney, liver and heart (304). Under inflammatory conditions, it's also been found in the synovium, skin, gut and liver (136, 304-306).	Immunohistochemistry demonstrated prominent expression in chronic arthritis (rheumatoid arthritis, spondylarthropathies, and psoriatic arthritis) (136). Stamper-Woodruff (S-W) assays have shown it can mediate the binding of mucosal effector cells to the synovium (136).
VCAM1; CD106	A glycoprotein. Expression is in increased by pro-inflammatory mediators such as TNF-α (307). Supports T and B cell adhesion (308).	Immunohistochemistry showed it is more highly expressed in the RA compared to the OA synovium (309). Expression of VCAM-1 under TNF-α stimulated conditions was significantly lower in ECs isolated from the RA synovium, compared to ECs from adipose tissue or HUVECs (175).
P selectin; CD62P	A single chain glycoprotein. It is expressed by endothelial cells and platelets. In ECs, it is stored in the Weibel-palade bodies, where, in response to pro-inflammatory mediators it is transported to the surface of the endothelium and aids in capture and rolling of leukocytes (308).	Immunohistochemistry showed P selectin expression was restricted to subpopulations of ECs in patients with chronic arthritis (136). S-W assays demonstrated that binding of gut-derived macrophages to the synovium was almost entirely P-selectin dependent (136).

E selectin; CD62E	A single chain glycoprotein. It is expressed only by endothelial cells and required for the capture and rolling of leukocytes (308).	Immunohistochemistry showed E selectin expression was restricted to subpopulations of ECs in patients with chronic arthritis (136). Expression of E-selectin under TNF-α stimulated conditions was significantly higher in ECs isolated from the RA synovium, compared to ECs from adipose tissue or HUVECs (175).
PNAd	A sulphated and fucosylated glycoprotein. It is most commonly expressed by high endothelial venules (HEVs). It is crucial in the recruitment of lymphocytes into the lymphoid organs of non-mucosal tissues (310).	Immunohistochemistry showed PNAd expression was seen in certain venules, of some, but not all, patients with chronic arthritis (136). PNAd positive vessels have been associated with increased bone damage (311).
Senescence		
p53	Tumour suppressor protein, often altered in cancers. It responds to stress (e.g., hypoxia) and can activate various responses such as cell cycle arrest and apoptosis (312).	Overexpressed in early and longstanding rheumatoid arthritis patients compared to patients with reactive arthritis or OA (313). Expression appears localised to the endothelium and lining layer fibroblasts [unpublished, shown in Figure 4.1]
Notch signalling		
DLL4	A molecule involved in Notch signalling, including notch-3 signalling between Notch-3 on fibroblasts and DLL4 on endothelial cells in RA (141).	Endothelium derived Notch-3 signalling is thought to drive fibroblasts into either PRG4+ lining, or Thy+ sublining fibroblasts. Notch3 and its ligands are highly expressed in the RA synovium. Blockade of this signalling attenuated inflammation and prevented joint damage in mouse models of RA. (141)
Angiogenesis		
CLEC14A	Transmembrane protein. Expressed on endothelial cells and known to play a role in angiogenesis, mediation of cell-cell contact, endothelial cell migration and tube formation (314).	CLEC14A is the binding partner of CD248 via MMRN2 (315). CLEC14A and CD248 bind at distinct locations on MMRN2, allowing binding to occur simultaneously (315). CD248 is expressed by sublining layer fibroblasts of RA patients (159). It contributes to synovial hyperplasia and leukocyte accumulation in inflammatory arthritis (316).
MMRN2	An extracellular matrix protein. Ligand for CLEC14A and CD93 at the same region, and CD248 a separate, distinct region (315).	

AOC3, Amine Oxidase Copper Containing 3; CLEC14A; C-type lectin domain containing 14A, DLL4, Delta-like protein 4; Lyve1, Lymphatic vessel endothelial hyaluronic acid receptor 1; MMRN2, Multimerin 2, PECAM1, platelet endothelial cell adhesion molecule 1; VAP1, Vascular adhesion protein 1; VCAM1, Vascular cell adhesion protein 1.

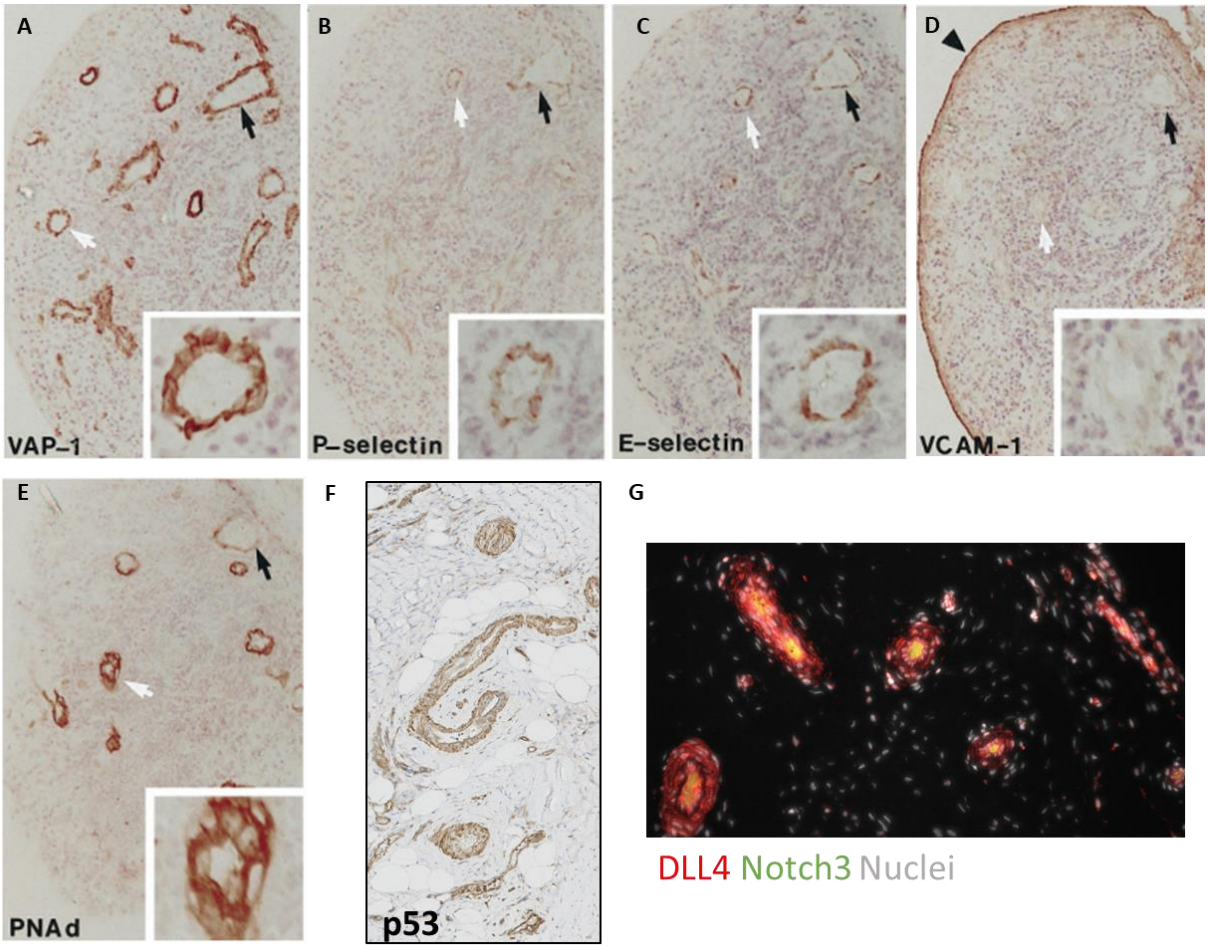

Figure 4.1: Expression of markers of interest within the inflamed synovium. (A-E) Images taken from (136) and show syonvium from patients with chronic arthritis (rheumatoid, psoriatic or spondyloarthropathies). Acetone-fixed frozen sections were stained with the appropriate antibody and second-stage peroxidase conjugated anti–mouse or anti–rat antibodies using diaminobenzidine as the chromogenic substrate for **(A)** VAP1; vascular adhesion protein 1, **(B)** P-selectin, **(C)** E-selectin, **(D)** VCAM-1; vascular cell adhesion molecule-1**,** and **(E)** PNAd; peripheral node addressin. **(F and G)** Images were kindly provided of formalin fixed paraffin embedded sections of rheumatoid arthritis patients undergoing joint replacement surgery. These were stained for **(F)** p53, by Vincent Gauthier and **(G)** DLL4 with Notch 3, by Triin Major.

4.2.2 Gene expression from bulk-RNA sequencing between the different pathotypes of RA

Before staining for the markers of interest, their gene expression was assessed using the publicly available bulk RNA-sequencing dataset from the Pathobiology of Early Arthritis Cohort (PEAC) (118, 131). This freely accessible website allows the comparison of gene expression in the synovium for patients classified as having; lymphoid (high number of infiltrated lymphoid and myeloid cells particularly CD20 B cell aggregate rich), myeloid (macrophage-rich and diffuse, low in B cells) and fibroid (pauci-immune) pathotypes (118, 131).

Of the adhesion molecules selected (Table 4.1), only VAP1 and E-selectin showed significant differences between pathotypes (Figure 4.2). VAP1 expression was significantly different between all three groups: highest in the fibroid and lowest in the lymphoid (Figure 4.2A). On the other hand, E-selectin only had a significant difference between the lymphoid and myeloid pathotypes, where of the three groups highest expression was in lymphoid, and lowest in the fibroid (Figure 4.2B). VCAM-1 had a similar pattern of gene expression E-selectin, albeit the changes were not statistically significant (Figure 4.2C). Surprisingly, P-selectin and PNAd expression was similar across the pathotypes with no significant differences observed (Figure 4.2E and F).

The senescence markers, p53 and p21, had similar patterns of expression; higher for lymphoid and myeloid pathotypes and lower for the fibroid pathotype, with a significant difference in expression detected between the lymphoid and fibroid pathotypes (Figure 4.3

A and B). However, the senescence marker p16 had no significant difference in expression pattern between the groups (Figure 4.3C).

Molecules involved in Notch signalling (Notch-3, DLL4 and Jag1) were all higher in the fibroid and myeloid pathotypes and lowest in lymphoid, Figure 4.4. Notch 3 only had a significant difference between lymphoid and fibroid, whilst DLL4 and JAG1 also showed a significant difference between the lymphoid and myeloid groups. No significant differences were observed between the myeloid and fibroid pathotypes, but Notch3 and DLL4 (Figure 4.4A and B) had the highest expression in fibroid, whilst for JAG1 (Figure 4.4C) highest expression was in the myeloid group.

Molecules involved in angiogenesis associated, CD248 signalling were generally higher in the fibroid compared to myeloid and lymphoid, and also slightly higher in myeloid compared to lymphoid pathotypes (Figure 4.5). Significant differences were observed for CLEC14A (Figure 4.5A) between lymphoid and myeloid, MMRN2 (Figure 4.5B) between lymphoid and both myeloid and fibroid pathotypes, and in ROBO4 (Figure 4.5E) between lymphoid and fibroid.

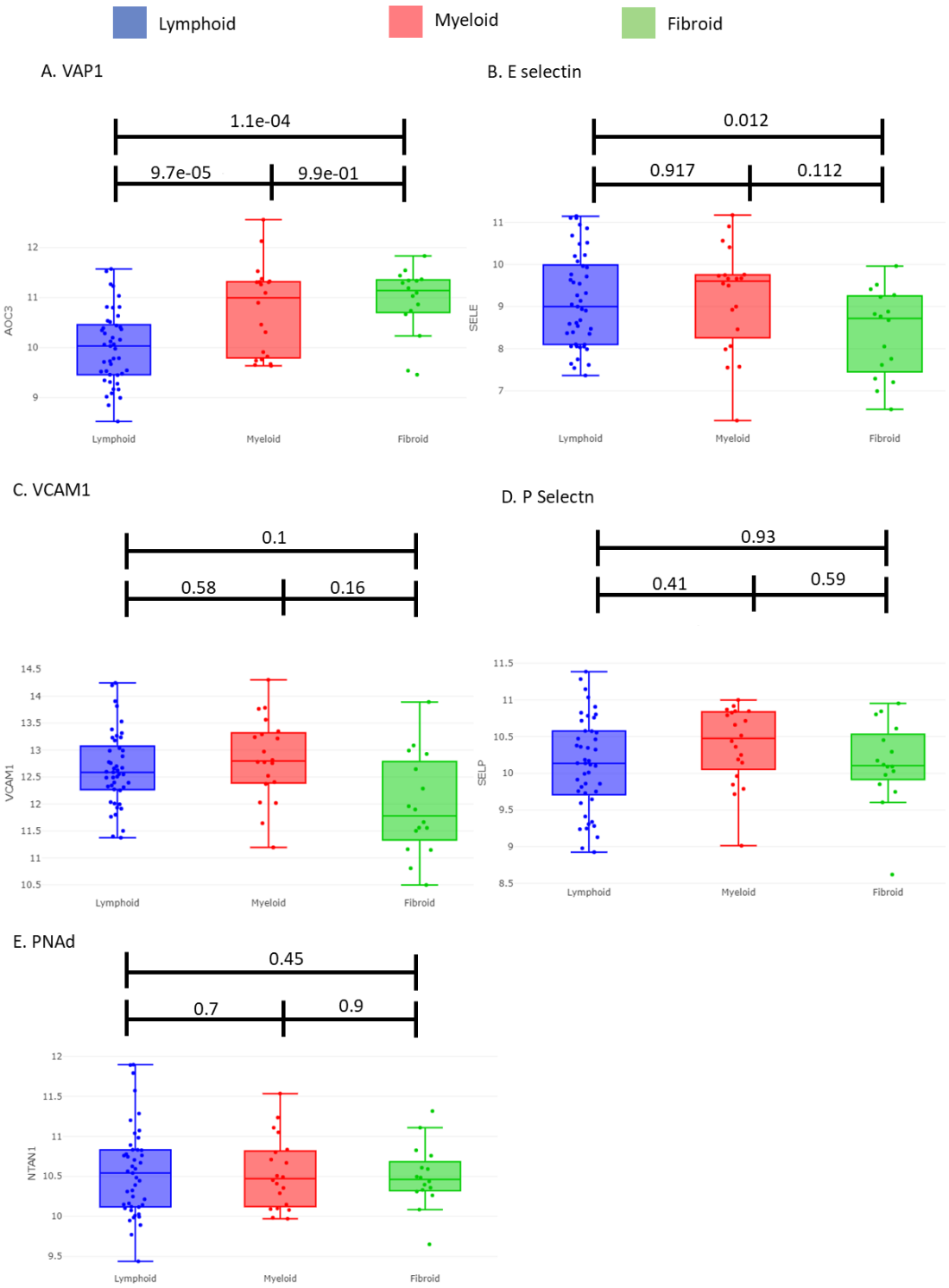

Figure 4.2: Expression of adhesion molecules in the pathotypes of rheumatoid arthritis. Bulk RNA-sequencing of Pathobiology of Early Arthritis Cohort (PEAC) of gene expression levels in myeloid, lymphoid and fibroid RA pathotypes were analysed by Myles *et al* (118, 131). Boxplots were obtained for adhesion molecules of interest; **(A)** VAP1, vascular adhesion protein 1 **(B)** E-selectin, **(C)** VCAM-1**,** vascular cell adhesion molecule 1, **(D)** P selectin**,** and **(E)** PNAd, peripheral node addressin**.** Y axis shows relative gene expression and X axis indicates RA pathotype. The FDR-adjusted P values are given above each plot.

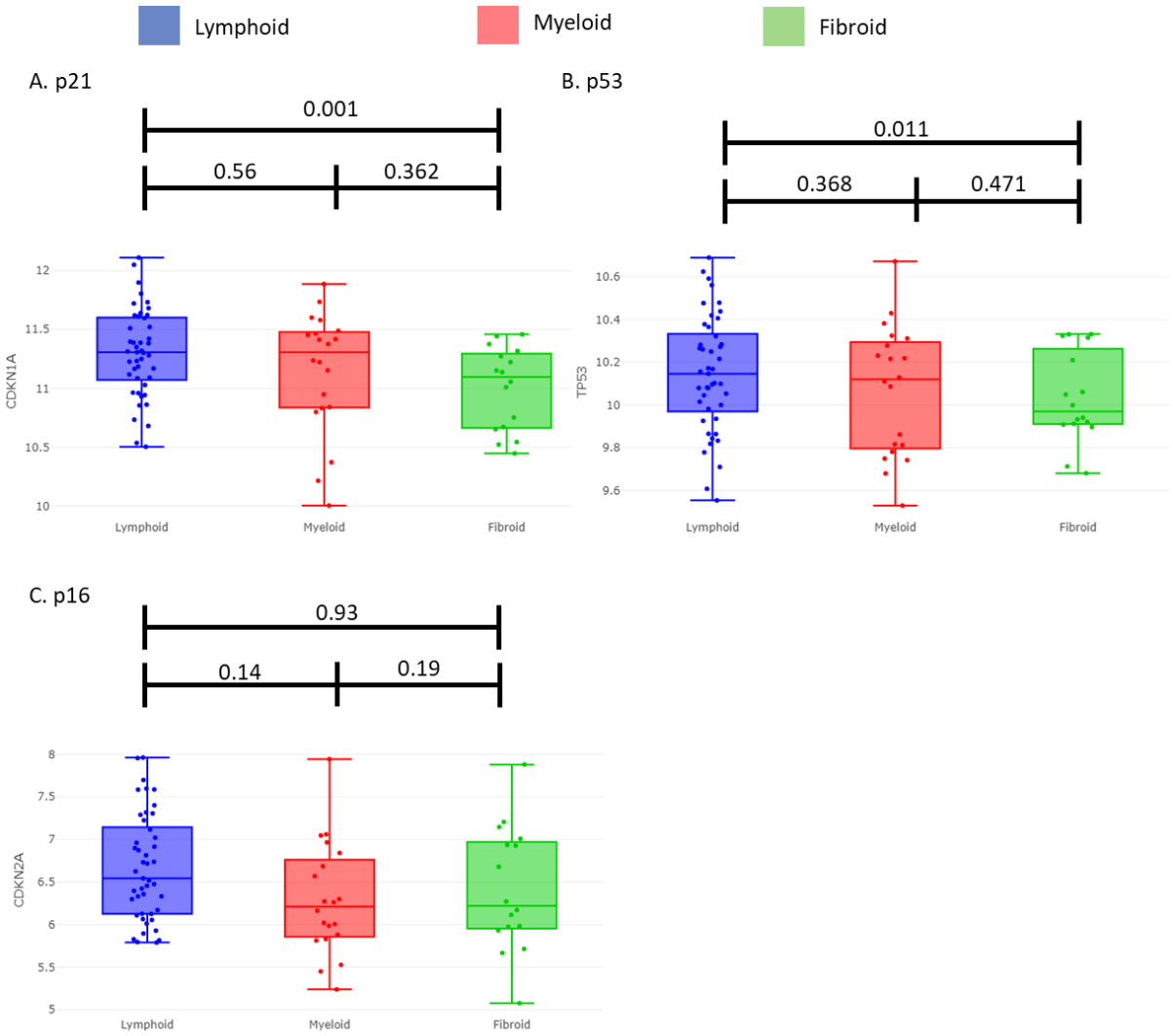

Figure 4.3: Senescence markers across disease pathotypes in rheumatoid arthritis. Bulk RNA-sequencing of Pathobiology of Early Arthritis Cohort (PEAC) of gene expression levels in myeloid, lymphoid and fibroid RA pathotypes were analysed by Myles *et al* (118, 131). Boxplots were obtained for senescence markers of interest; **(A)** p53 **(B)** p21, and **(C)** p16. Y axis shows relative gene expression and X axis indicates RA pathotype. The FDR-adjusted P values are given above each plot.

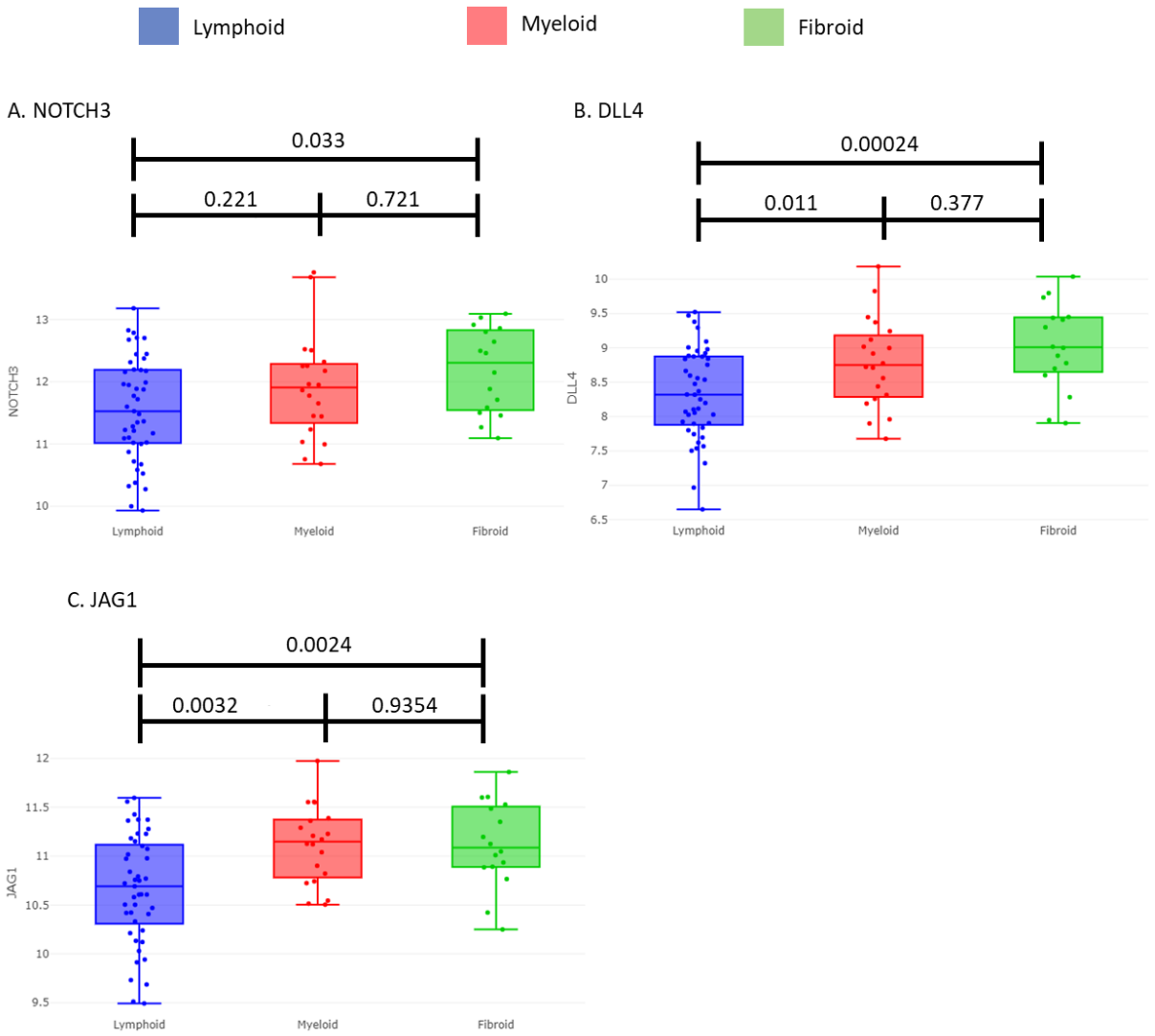

Figure 4.4: Notch3 signalling markers across disease pathotypes in rheumatoid arthritis. Bulk RNA-sequencing of Pathobiology of Early Arthritis Cohort (PEAC) of gene expression levels in myeloid, lymphoid and fibroid RA pathotypes were analysed by Myles *et al* (118, 131). Boxplots were obtained for notch signalling markers of interest; **(A)** Notch3 **(B)** DLL4, delta-like 4, and **(C)** Jag1, Jagged 1. Y axis shows relative gene expression and X axis indicates RA pathotype. The FDR-adjusted P values are given above each plot.

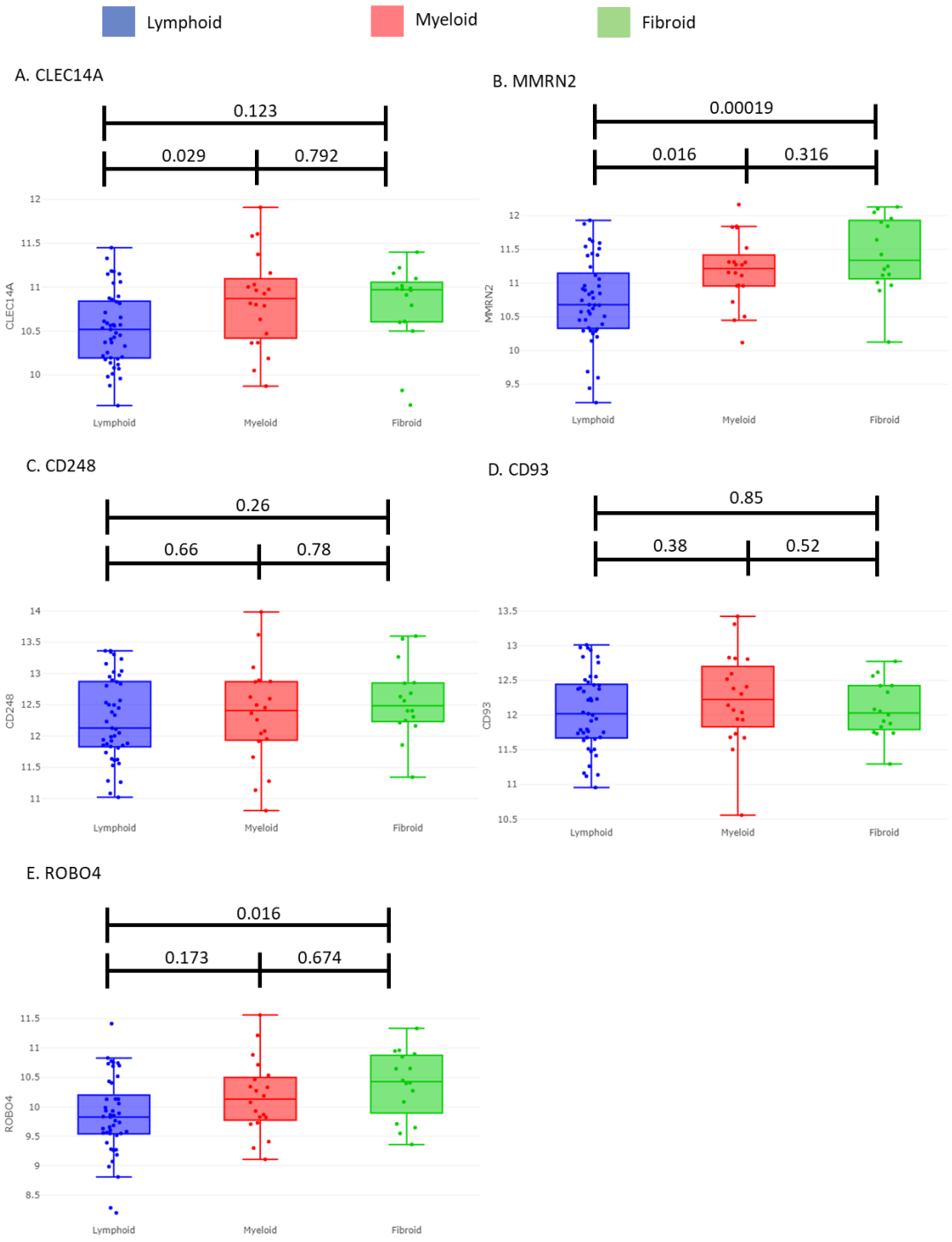

Figure 4.5: CD248 signalling molecules across pathotypes of rheumatoid arthritis. Bulk RNA-sequencing of Pathobiology of Early Arthritis Cohort (PEAC) of gene expression levels in myeloid, lymphoid and fibroid RA pathotypes were analysed by Myles *et al* (118, 131). Boxplots were obtained for notch signalling markers of interest; **(A)** CLEC14A, C-type lectin containing family 14A **(B)** MMRN2, Multimerin 2 **(C)** CD248 **(D)** CD93 and **(E)** ROBO4. Y axis shows relative gene expression and X axis indicates RA pathotype. The FDR-adjusted P values are given above each plot.

4.2.3 Validation of antibodies and panel design

In order to stain for the markers of interest (described in Table 4.1) we first need to validate the antibodies to ensure appropriate and specific staining. Due to use of multiple antibodies on one tissue, after the first stain with an antibody from one species, conjugated antibodies had to be used in order to prevent the species cross-reactivity which would occur with primary-secondary staining and antibodies from the same species. Where available, already conjugated antibodies were initially tested, however, most of these did not show the expected staining (described below). This is likely because the staining of these was too weak to be detected due to the lack of signal amplification that occurs using a two-step primary-secondary staining (317). For these markers, a validated unconjugated antibody was chosen then conjugated to the fluorophore of choice. Regarding the antibody concentration, either that recommended by the supplier or a standard concentration of 10µg/ml was used (as recommended by those running the CellDIVE in Oxford).

In order to mark the endothelium, Ulex was initially chosen and had stained the endothelium well previously (Appendix Figure 1A) however, this was out of stock for over a year, and another, conjugated, Ulex did not show staining of the endothelium (Appendix Figure 1B). Likewise, an AF647 conjugated VE-cadherin clone BV9 did not show any staining around the blood vessels (Appendix Figure 1C). Instead, CD31, another well-established marker of the endothelium (Table 4.1), was tested. Initial staining with the AF488 conjugated CD31 (clone WM59) did not show staining of the blood vessels (Appendix Figure 1D), but an unconjugated CD31 (clone C31.3), did show specific staining (Figure 4.6A). To mark

lymphatic vessels Lyve1 expression with clone EPR21857 work in tonsil and synovium, Figure 4.6C and E.

Similarly, for the adhesion markers, previously conjugated antibodies were initially tested. For P-selectin, the AF88 conjugated (clone P sel.K.O.2.7) as well as multiple unconjugated antibodies (Psel KO2.5, abcam, AK-6, Thermofisher, CTB201 and 1 E 3, Santa Cruz) were tested but did not show staining of any blood vessels. Likewise, initial analysis of E- selectin expression using antibody clones BBIG-E4 and D-7 showed non-specific or no staining of the endothelium, respectively. Eventually, after consulting with manufacturers, a microwave method of antigen retrieval was used and subsequently the P selectin clone EPR2146 (2) (Figure 4.7 A and C) and polyclonal E selectin (cat ab185698; Figure 4.7E and G) showed specific staining on the endothelium in both tonsil and synovial sections. For VCAM-1, the AF488 conjugated antibody clone 6G9 did not show the expected specific staining of the endothelium and synovial lining layer, but the unconjugated polyclonal antibody (cat BBA19) did (Figure 4.8A). Specific staining was also observed with the unconjugated polyclonal (cat# EB0758) anti-VAP1 antibody (Figure 4.8C). Of all the conjugated antibodies initially tested, only PNAd-AF647 (MECA-79) demonstrated specific staining around the endothelium in tonsil sections (Figure 4.8E) but had no staining in RA joint replacement tissue. This may be attributed to the selective expression of PNAd in RA patients (136, 311), therefore, the antibody was taken forward into the panel, alongside the use of tonsil sections as positive controls.

For staining of senescence and notch-3 signalling molecules, antibodies clones were selected according to previous staining by colleagues (Figure 4.1F and G). The unconjugated p53 clone, E26, showed staining around the endothelium and synovial lining layer (Figure 4.9A). The DLL4 clone # 207822 showed endothelial staining (Figure 4.9C), similar to that in Figure 4.1G.

Following validation, the unconjugated antibodies were conjugated and expression of the antigen confirmed again (Figure 4.11). All conjugated antibodies appeared to show good staining, except P-selectin (Figure 4.11D). One possible explanation for the absence of conjugated P-selectin staining may be due to the high BSA: antibody ratio, and low concentration of the antibody. Therefore, it was decided to use primary-secondary staining for this antibody. When designing the panel, markers of interest were put on the brighter markers, red (i.e. AF546) or far red (i.e. AF647) and markers of the endothelium/lymphatics, as well as VAP1 (which also showed strong staining), on green (i.e. AF488). The final panel design is given in Table 2.2

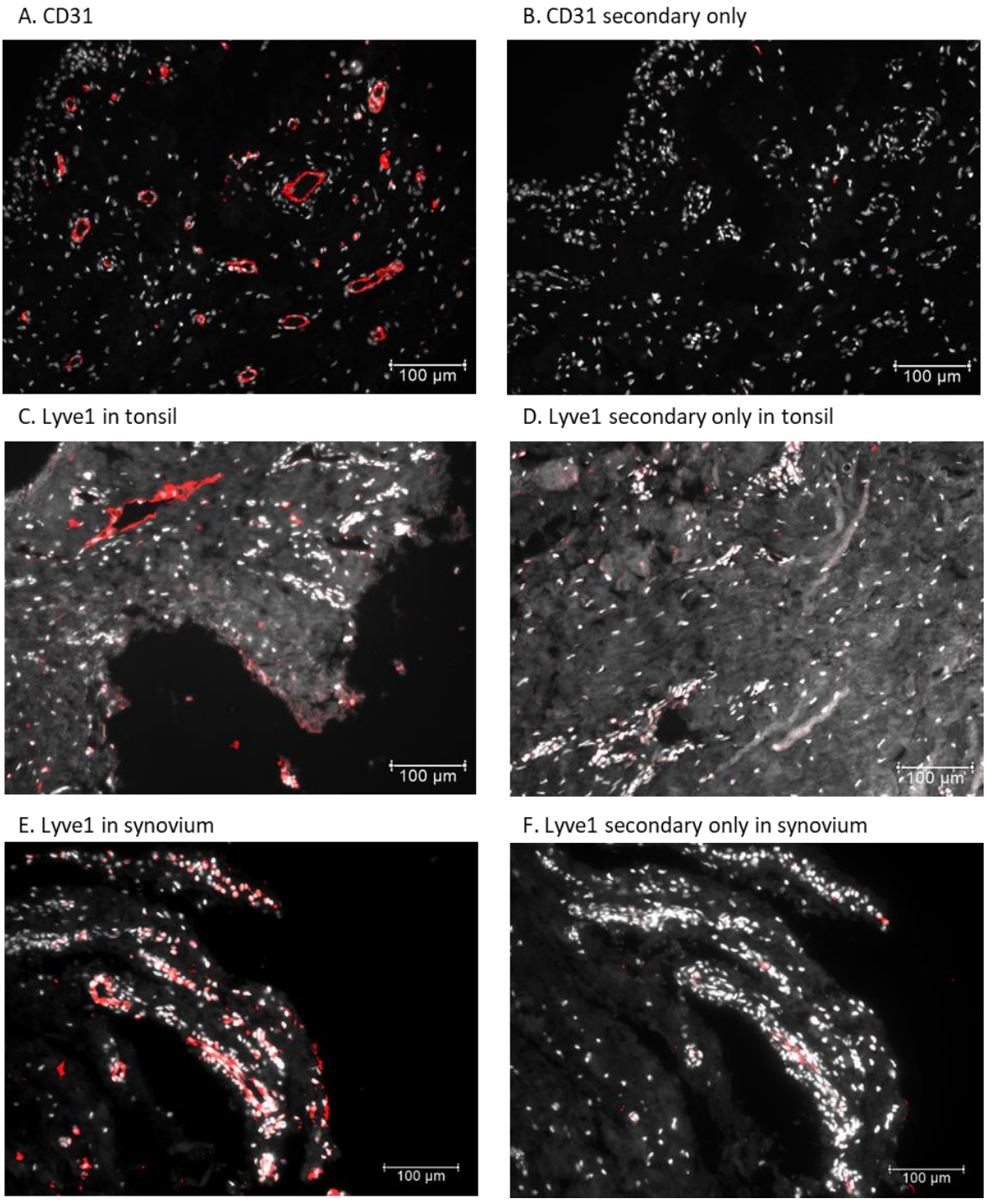

Figure 4.6: Markers of the endothelium antibody validation. Formalin fixed paraffin embedded (FFPE) sections were used from **(A, B, E & F)** RA joint replacement synovial tissue or **(C and D)** tonsil tissue. Sections were deparaffinised, rehydrated and antigen retrieval was performed at Ph9. Sections were blocked with normal horse serum prior to addition of primary antibodies against **(A)** CD31 or **(C & E)** Lyve1. Sections were washed and secondary added **(A & B)** anti-mouse IgG AF-546 or **(C – F)** anti-rabbit AF-546 IgG. Sections were counterstained with the nuclear dye 4', 6-diamidino-2-phenylindole (DAPI). DAPI is shown in grey and the antibody of interest in red. Scale bar at 100⌠m.

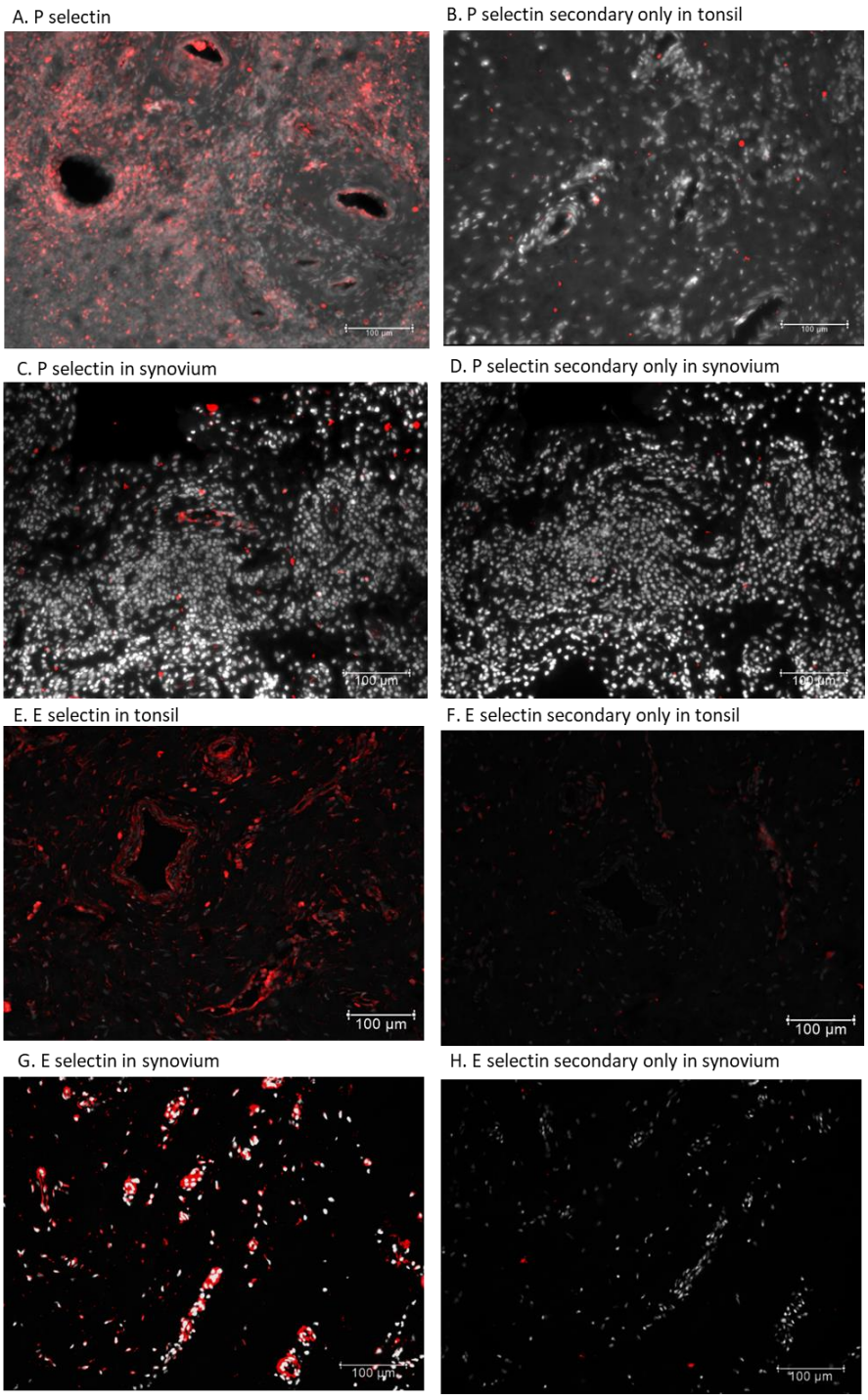

Figure 4.7: P and E selectin antibody validation. Formalin fixed paraffin embedded (FFPE) sections were used from **(A, B, E & F)** tonsil tissue or **(C, D, G & H)** RA joint replacement synovial tissue. Sections were deparaffinised, rehydrated and antigen retrieval was performed at **(A-D)** pH6 or **(E-H)** pH9. Sections were blocked with normal horse serum prior to addition of primary antibodies target **(A & C)** P selectin or **(E & G)** E selectin. Sections were washed, and anti-rabbit AF-546 IgG secondary added. Sections were counterstained with the nuclear dye 4', 6-diamidino-2-phenylindole (DAPI). DAPI is shown in grey and the antibody of interest in red. Scale bar at 100⌠m.

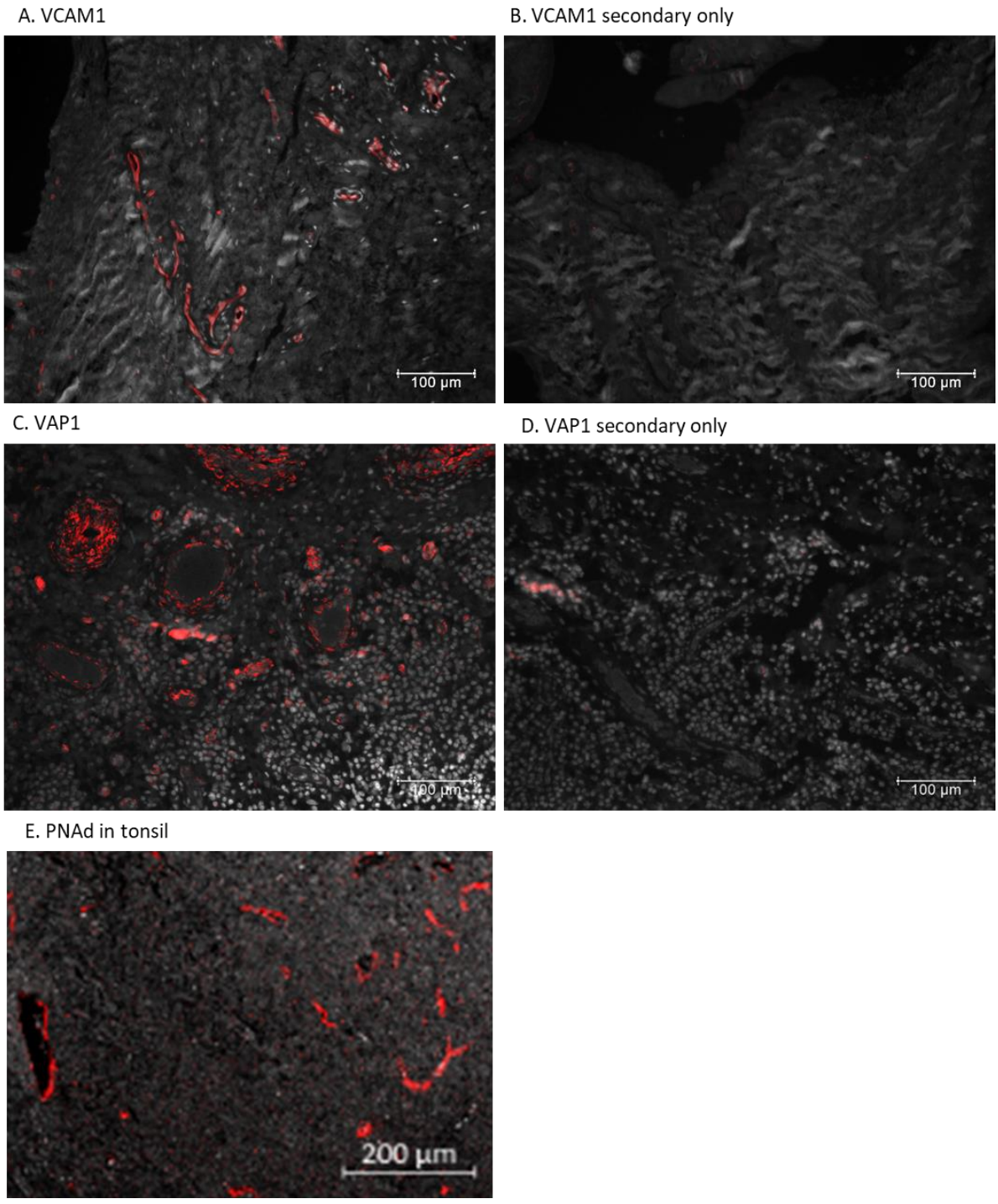

Figure 4.8: Adhesion molecule antibody validation. Formalin fixed paraffin embedded (FFPE) sections were used from were used from **(A-D)** RA joint replacement synovial tissue or **(E)** tonsil tissue. Sections were deparaffinised, rehydrated and antigen retrieval was performed at **(A & B)** pH9 or **(C-E)** pH6. Sections were blocked with normal horse serum prior to addition of primary antibodies target **(A)** VCAM1, **(C)** VAP1 or **(E)** conjugated PNAd. **(A-D)** Sections were washed, and anti-goat AF-546 IgG secondary added. Counterstained with the nuclear dye 4', 6-diamidino-2-phenylindole (DAPI). DAPI is shown in grey and the antibody of interest in red. Scale bar at **(A-D)** 100⌠m or **(E)** 200⌠m.

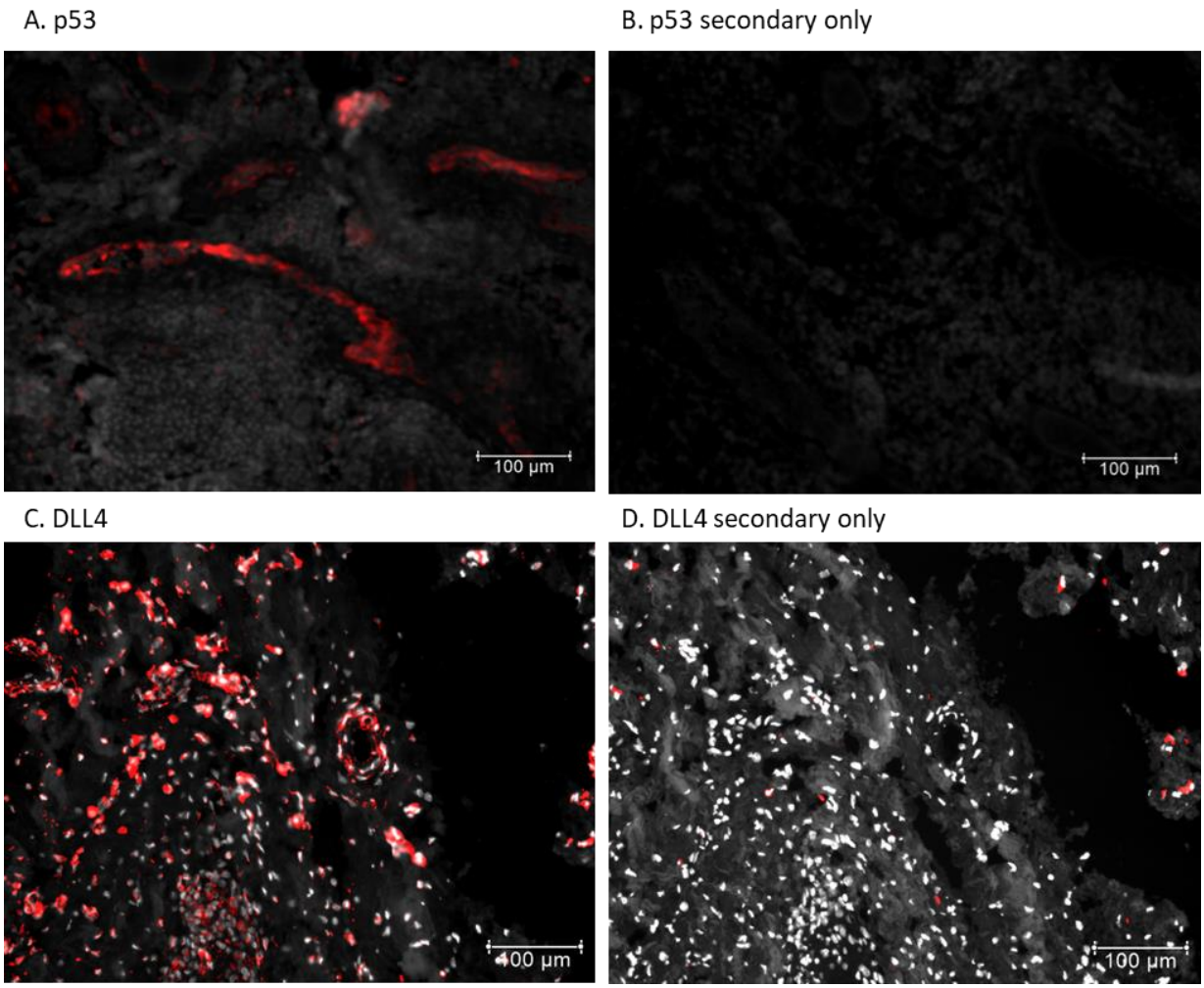

Figure 4.9: Senescence and Notch3 signalling antibody validation. Formalin fixed paraffin embedded (FFPE) sections were used from were used from RA joint replacement synovial tissue. Sections were deparaffinised, rehydrated and antigen retrieval was performed at **(A & B)** pH6 or **(C & D)** pH9. Sections were blocked with normal horse serum prior to addition of primary antibodies target**; A)** p53 or **(C)** DLL4. Sections were washed, and a secondary added **(A & B)** anti-rabbit IgG AF-546 or **(C & D)** anti-rat IgG AF-546. Counterstained with the nuclear dye 4', 6-diamidino-2-phenylindole (DAPI). DAPI is shown in grey and the antibody of interest in red. Scale bar at 100⌠m.

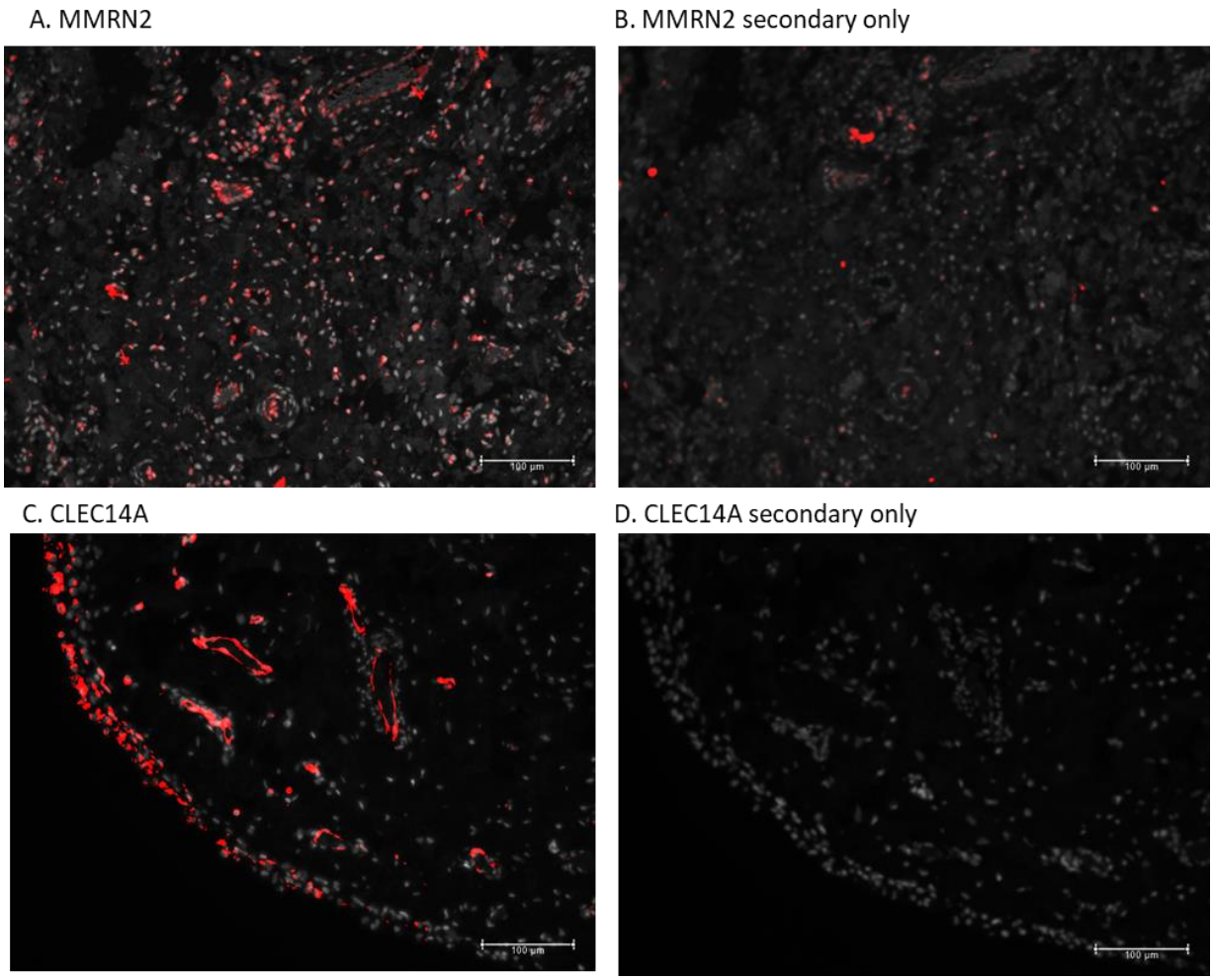

Figure 4.10: CLEC14A and MMRN2 antibody validation. Formalin fixed paraffin embedded (FFPE) sections were used from were used from RA joint replacement synovial tissue. Sections were deparaffinised, rehydrated and antigen retrieval was performed at **(A & B)** pH6 or **(C & D)** pH9. Sections were blocked with normal horse serum prior to addition of primary antibodies target; **(A)** MMRN2 or **(C)** CLEC14A. Sections were washed, and a secondary added **(A & B)** anti-rabbit IgG AF-546 or **(C & D)** anti-sheep IgG AF-546. Counterstained with the nuclear dye 4', 6-diamidino-2-phenylindole (DAPI). DAPI is shown in grey and the antibody of interest in red. Scale bar at 100⌠m.

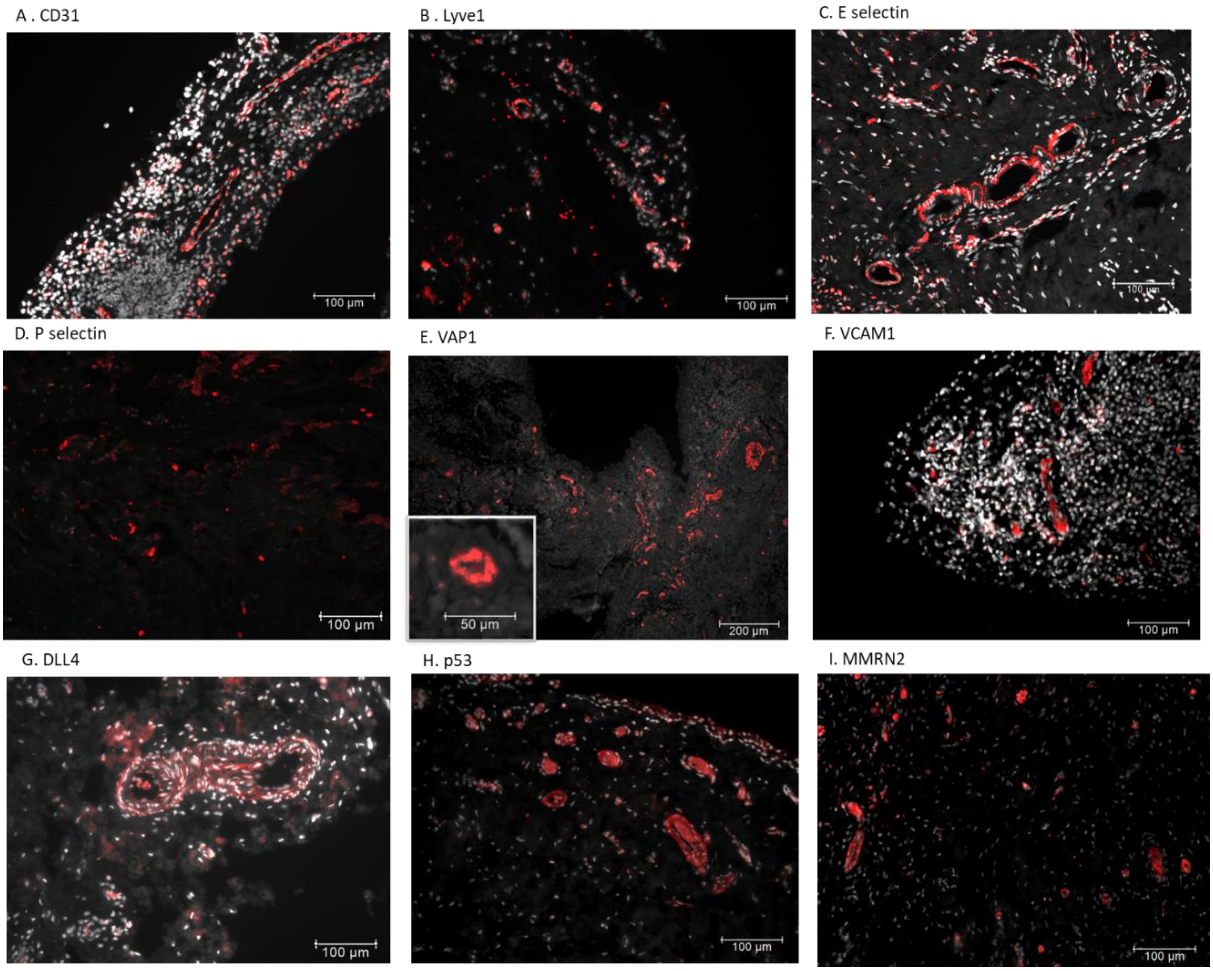

Figure 4.11: Antibody validation following conjugation. Formalin fixed paraffin embedded (FFPE) sections were used from were used from RA joint replacement synovial tissue. Sections were deparaffinised, rehydrated and antigen retrieval was performed at **(A-C, F & G)** pH9 or **(D, E, H)** pH6. Sections were blocked with normal horse serum prior to addition of primary antibodies target; **(A)** CD31, **(B)** Lyve1 **(C)** E selectin, **(D)** P selectin **(E)** VAP1 **(F)** VCAM1 **(G)** DLL4 **(H)** p53 **(I)** MMRN2. Counterstained with the nuclear dye 4', 6-diamidino-2-phenylindole (DAPI). DAPI is shown in grey and the antibody of interest in red. Scale bar at 100µm

4.2.4 Multiplex imaging with Cell DIVE imaging platform

Tissue sections from JRep, VeRA and Res patients were stained with the final CellDIVE panel (2.3.2; Table 2.2). A summary of the patient characteristics of patients used is given in Table 4.2 and full details in Appendix Table 1. Some patient sections were lost during processing (described in 4.2.4.2) therefore only the patient information those finally analysed is given.

4.2.4.1 Staining worked for most markers, but E selectin, Lyve1 and PNAd could not be quantified in the synovium

In the final CellDIVE stain, staining for most markers worked in the synovium (Figure 4.12), with limited background staining was observed in the isotype controls (Figure 4.113). However, specific staining was not observed for E selectin, Lyve1 and PNAd in synovium. E selectin had no clear staining (Figure 4.14A), whilst Lyve1 was not specific and did not appear co-localised with CD31 vessel expression (Figure 4.14B). Whilst the PNAd staining did not appear to stain any synovium (e.g., Figure 4.14C), positive staining was observed in the tonsil section (Figure 4.15). Therefore, either this specific antibody does not work in synovium, or there was no expression of PNAd in the synovial sections tested.

Table 4.2: Summary of patient characteristics stained in multiplex image analysis

	Resolving (n=4)	VeRA (n=3)	JRep (n= 7)
Age (years)	46(37-56)	59(55-68)	66(58-67) *
Female, n (%)	4 (57)	1 (25)	2 (67)
Symptom duration (weeks)	6 (1-11.5)	6 (4.5-7)	1066 (806-1443)
DAS28 ESR, mean (sd)	3 (±1.1)	6.3 (±1)	-
ESR (mm/hour)	18 (11-25.8)	39 (24.5-50)	14 (9-22) *
CRP, median (IQR), mg/L	13.5 9 (7.8-18.8)	39 (37.5-68)	4 (2-10) *
CCP positive, n (%)	1 (25)	1 (33)	2 (40) *
RF positive, n (%)	0 (0)	2 (66)	1 (50) *
SJC28	2 (0.8-3)	11 (10.5-15.5)	-
TJC28	1 (0.8-1.5)	12 (11.5-15.5)	-
VAS	26 (6.8-51)	50 (49.5-62.5)	-
US GS	0.5 (0-1)	3 (1.5-3)	-
US PD	1.5 (1-2)	2 (1.5-2.5)	-
NSAID, n (%)	0 (0)	1 (33)	2 (29)

Median (IQR) shown unless otherwise stated.

DAS28 = Disease Activity Score 28; CCP = cyclic citrullinated peptide, CRP = C-reactive protein; ESR = erythrocyte sedimentation rate; IQR = Interquartile range; JRep = joint replacement; NSAID = non-steroidal anti-inflammatory; RF = Rheumatoid factor; SJC28 = 28 swollen joint counts; TJC28 = 28 tender joint counts; US GS = ultrasound greyscale grade at the biopsied joint; US PD = ultrasound power Doppler grade at the biopsied joint; VAS = visual analogue score; VeRA = Very early rheumatoid arthritis.

*Of available data, missing information indicated in Appendix Table 1

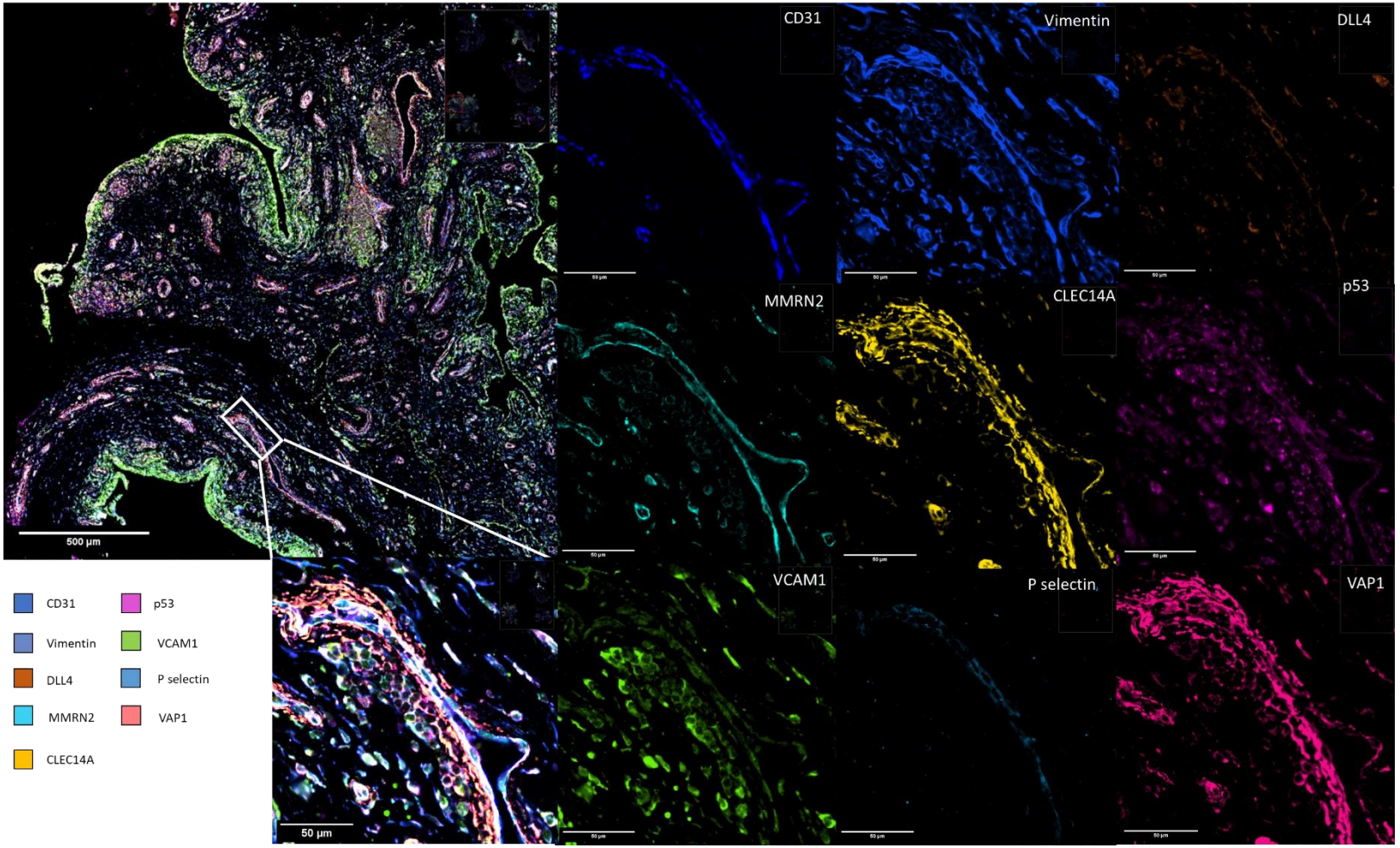

Figure 4.12: Representative image of CellDIVE stain. Formalin fixed paraffin embedded (FFPE) sections of synovial sections were deparaffinised, rehydrated and antigen retrieval was performed. Sections were blocked with donkey serum and bovine serum albumin prior to addition of antibody against: CD31, vimentin, delta-like 4 (DLL4), Multimerin 2 (MMRN2), C-type lectin domain containing 14A (CLEC14A), p53, vascular cell adhesion protein 1 (VCAM1), P selectin and vascular adhesion protein 1 (VAP1). Scale bar at 500µm in large image and 50µm for zoomed in image of vessel.

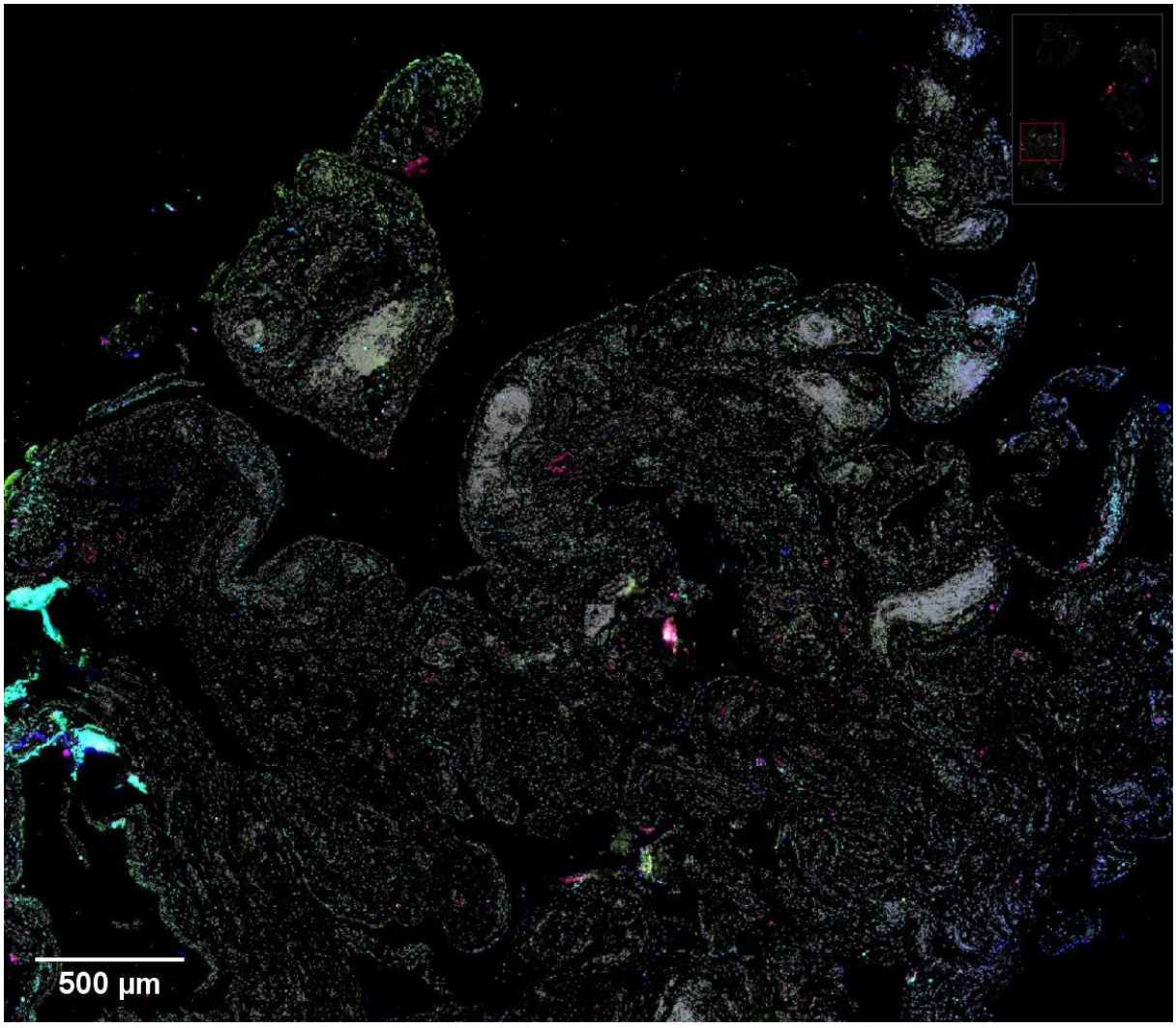

Figure 4.113: Minimal background staining observed in isotype controls of background stain. Formalin fixed paraffin embedded (FFPE) sections of synovial sections were deparaffinised, rehydrated and antigen retrieval was performed. Sections were blocked with donkey serum and bovine serum albumin prior to addition of isotype controls: Goat IgG, Rabbit IgG, Mouse IgG, Rat IgG2a, Rat IgM, Rabbit – AF488, Rabbit –AF555, Rabbit – AF647. Scale bar at 500µm.

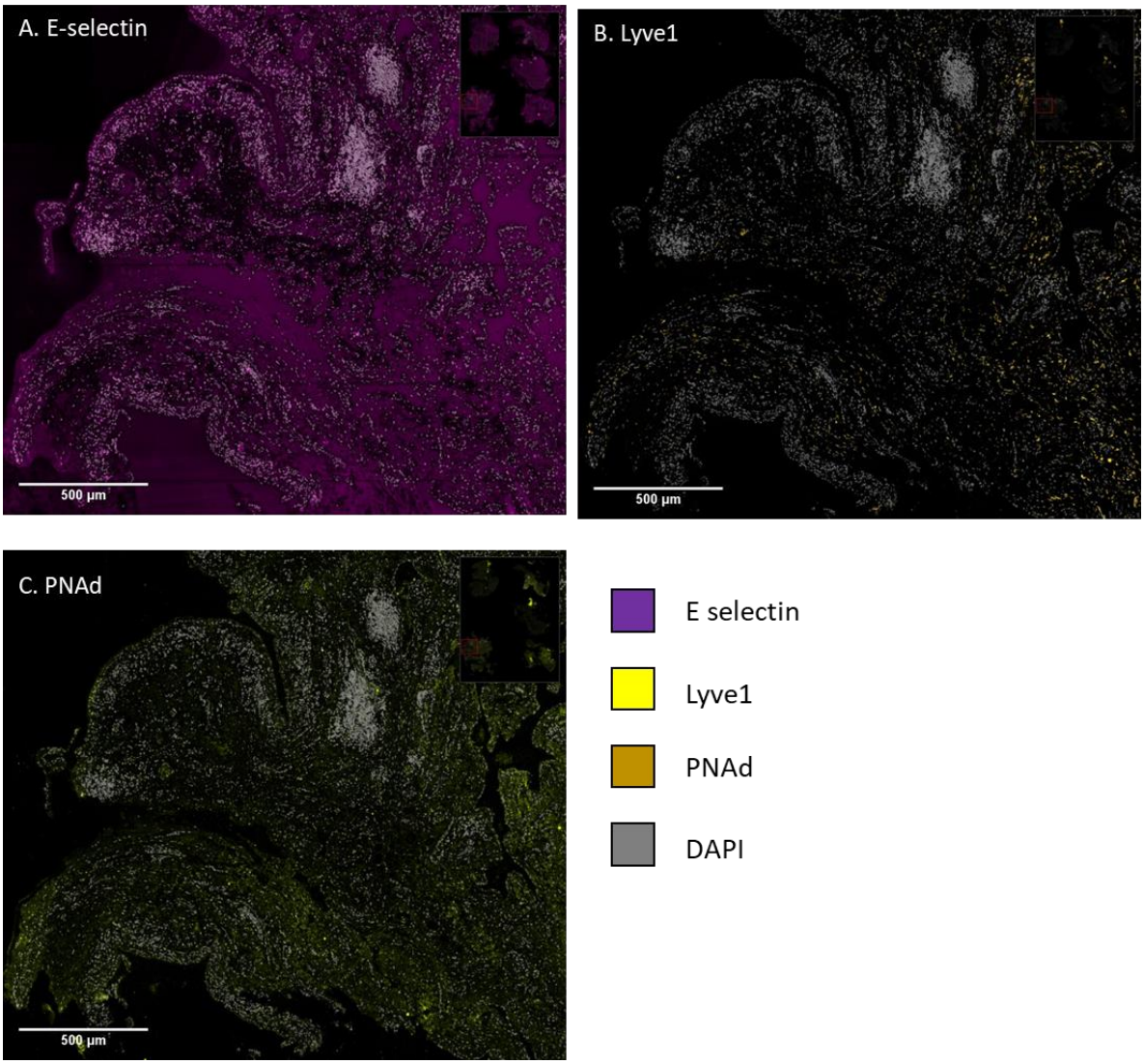

Figure 4.14: No specific staining observed in the synovium for PNAd, E selectin or Lyve1 with CellDIVE imaging. Formalin fixed paraffin embedded (FFPE) sections of synovial sections were deparaffinised, rehydrated and antigen retrieval was performed. Sections were blocked with donkey serum and bovine serum albumin prior to addition of antibody against: **(A)** E-selectin (ESEL), **(B)** lymphatic vessel endothelial hyaluronan receptor 1 (Lyve1) and **(C)** peripheral node addressin (PNAd). Scale bar at 500µm.

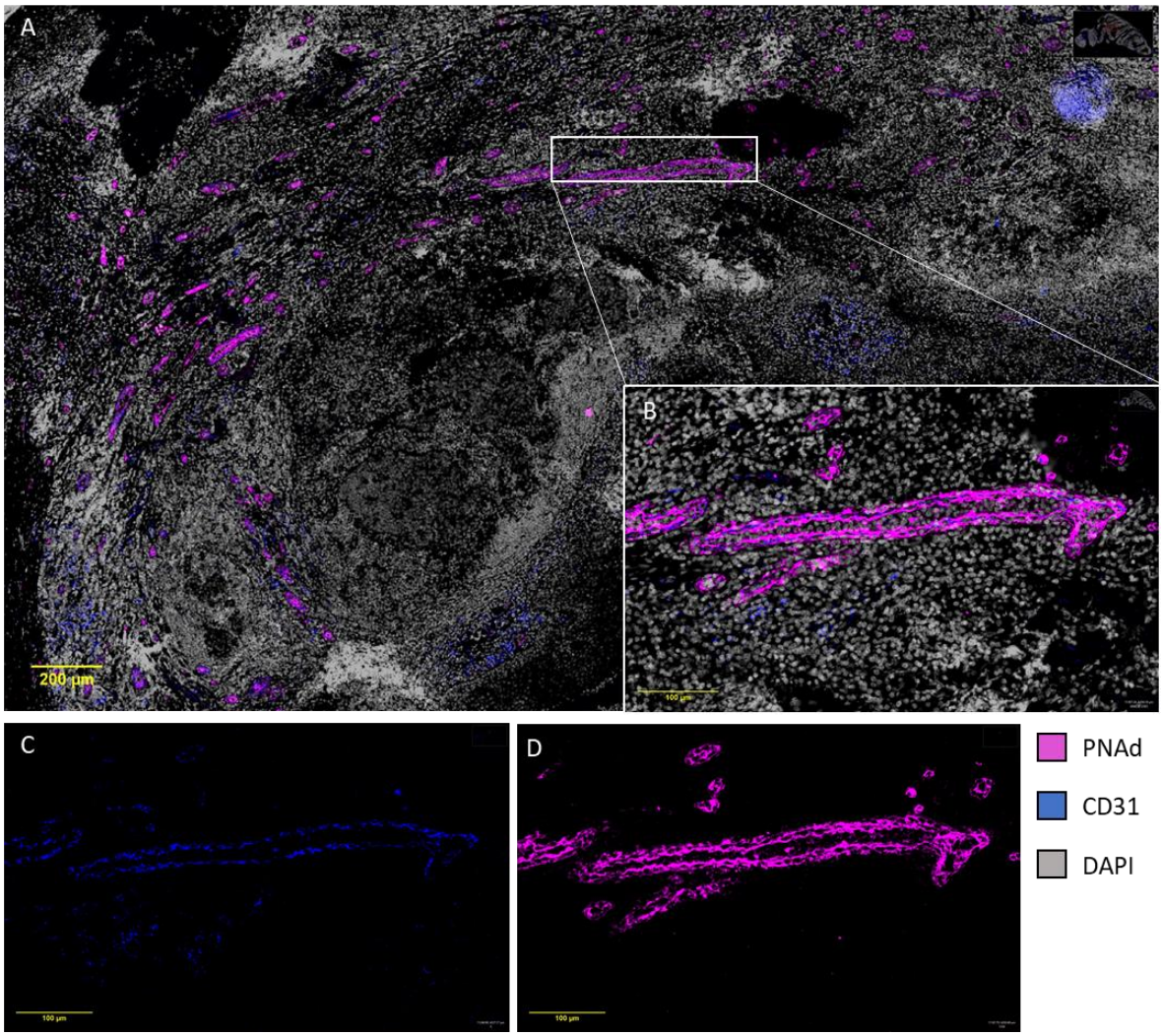

Figure 4.15: PNAd staining in the tonsil section with CellDIVE imaging staining. Formalin fixed paraffin embedded (FFPE) sections of tonsil tissue were deparaffinised, rehydrated and antigen retrieval was performed. Sections were blocked with donkey serum and bovine serum albumin prior to addition of antibody against CD31 (blue) antibody against PNAd (pink). Sections were counterstained with the nuclear dye 4', 6-diamidino-2-phenylindole (DAPI; grey). Scale bar at **(A)** 200µm for and **(B-D)** 100µm.

4.2.4.2 Tissue sections lost during processing, particularly pauci-immune pathotypes

At the time the CellDIVE staining was carried the technique was still relatively new. Whilst data had been generated, and the method optimised in the cancer field (231, 318), its uses in certain tissues (e.g., synovium) was still limited. One known disadvantage of the technique was that the multiple coverslipping and decoverslipping steps required could result in the tissue, or parts of the tissue coming off the slide. The severity of this often appeared to be dependent on the tissue type and this proved particularly problematic regarding synovial tissue sections and especially biopsy sections. This is highlighted in the virtual H&E's (Haematoxylin and Eosin) of the tissues from the first and last rounds of staining shown in Figure 4.16. An initial trial run was carried out using large sections from joint replacement (JRep) samples of patients, and whilst some tissue loss was observed, it was not too severe, and data could still be collected from the images (e.g., Figure 4.16A and B). However, when using tissue sections from synovial biopsies (for the VeRA and Res groups), which were often smaller sections to begin with, the tissue loss was considerable. Due to this, 3 of VeRA and 2 of the Res samples (from a total of 6) were lost completely (e.g., Figure 4.16C and D). Notably, this included all the pauci-immune samples and 1 lymphoid sample in VeRA. The remaining samples often had some tissue loss but were still useable (e.g., Figure 4.16E and F). Within the JRep samples, one patient was pauci-immune. To avoid any confounding effects of pathotype this was removed from the JRep samples.

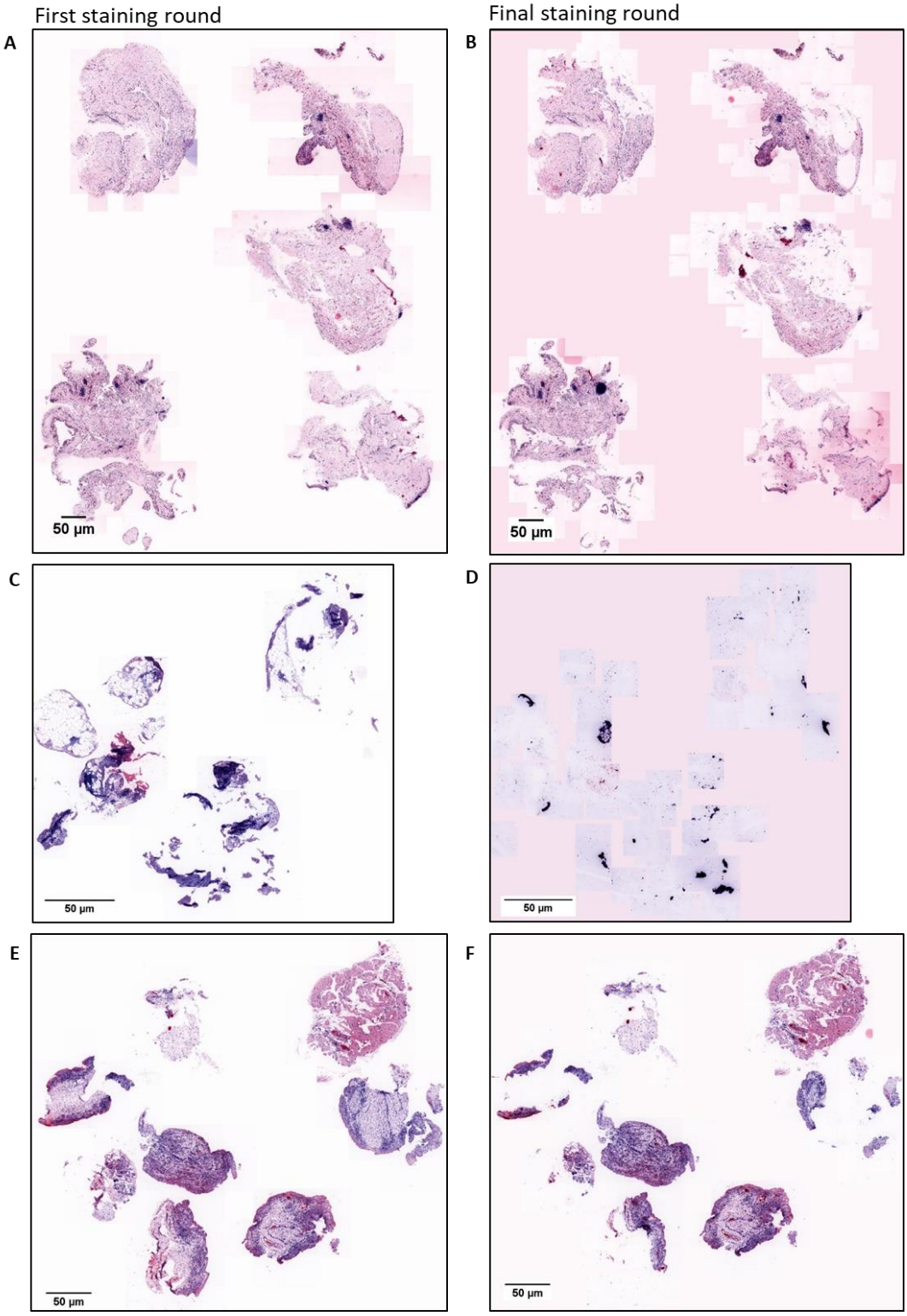

Figure 4.16: Representative images demonstrate the tissue loss that can occur with Cell DIVE imaging processing. Formalin fixed paraffin embedded (FFPE) synovial tissue sections from **(A & B)** rheumatoid arthritis (RA) undergoing joint replacement or **(C-F)** biopsies from arthritis patients with short term (<12 weeks) symptom duration were stained using and imaged with the CellDIVE platform. Virtual haematoxylin and eosin stains were captured at **(A, C, E)** before initial round of staining and **(B, D, F)** before the final round of staining. Scale bars at 50µm.

4.2.4.3 Expression levels of most molecules higher in the JRep compared to VeRA and Res groups, but differences were not significant

All the adhesion molecules (VCAM1, PSEL and VAP1; Figure 4.17A-C), had higher expression in the JRep compared to both VeRA and Res groups. VCAM1 had the lowest expression in Res, whilst P selectin and VAP1 were lowest in VeRA, although there was a large amount of variability within each group. Across all groups, expression was highest for VAP1 (60-80%) and lowest for P selectin (10-20%). Regarding co-expression of the adhesion molecules (Figure 4.18A), in all samples a large number co-expressed VAP1+VCAM1, then VAP1+PSEL, with very few cells co-expressing VCAM1 and PSEL, or all three (PSEL, VCAM1 + VAP1). Notably, MMRN2 and P53 (Figure 4.17E and G) had similar patterns of expression; both were highly expressed in the JRep (~50%) compared to VeRA or Res (~25%). On the other hand, CLEC14A and DLL4 (Figure 4.17D and F), were not particularly higher or lower in any group, with expression levels across all groups at around 80% and 40%, respectively. Interestingly, when assessing the co-expression of CLEC14A+MMRN2 (Figure 4.18B), the pattern was almost identical to that of MMRN2 alone, suggesting that nearly all MMRN2 expressing CD31+ cells were also expressed CLEC14A. Significance was assessed by a one-way ANOVA for all markers, but no differences were found to be significant

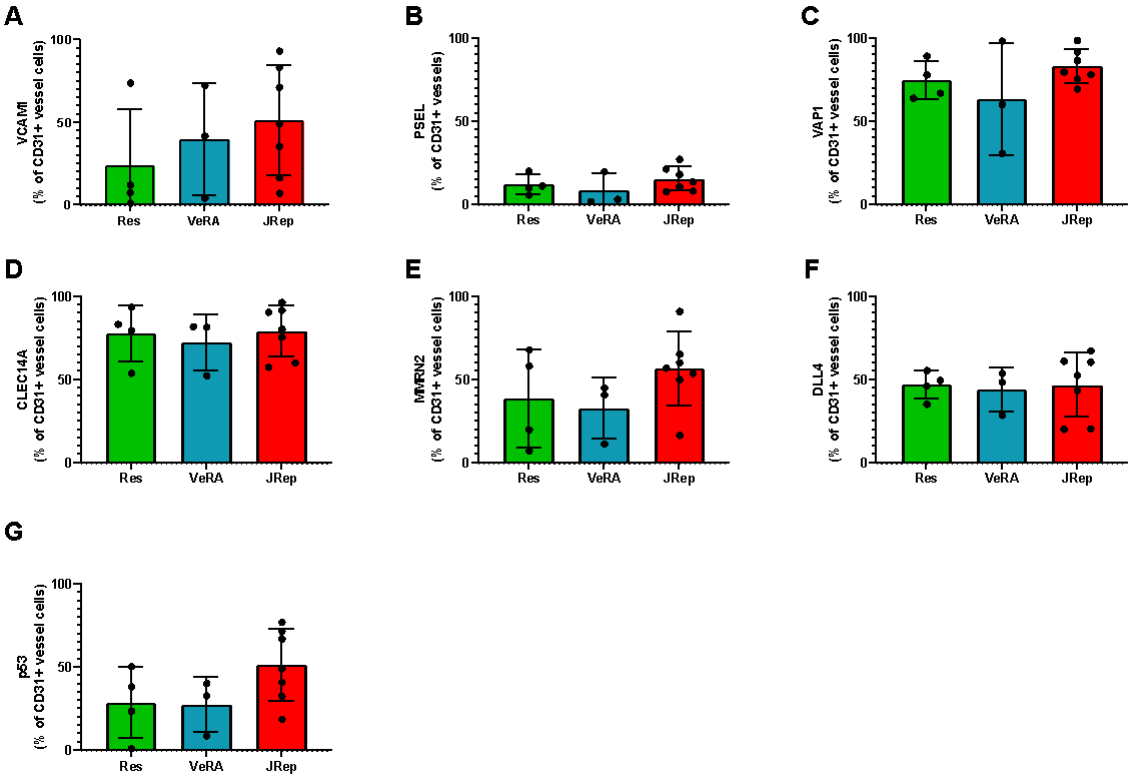

Figure 4.17: Expression level of most markers higher in the JRep compared to VeRA and Res samples, but no differences are significant. Tissue sections from patients with resolving arthritis (Res; green, n = 4), very early rheumatoid arthritis (VeRA; blue, n = 3) and patients undergoing joint replacement (JRep; red, n = 7), were stained with antibodies against **(A)** Vascular cell adhesion protein 1 (VCAM1), **(B)** P selectin (P sel), **(C)** vascular adhesion protein 1 (VAP1), **(D)** C-type lectin domain containing 14A (CLEC14A), **(E)** Multimerin 2 (MMRN2), **(F)** Delta-like 4 (DLL4) and **(G)** p53. Y axis is the expression of each marker as a percentage of all CD31+ vessel cells. Data are mean ± SD.

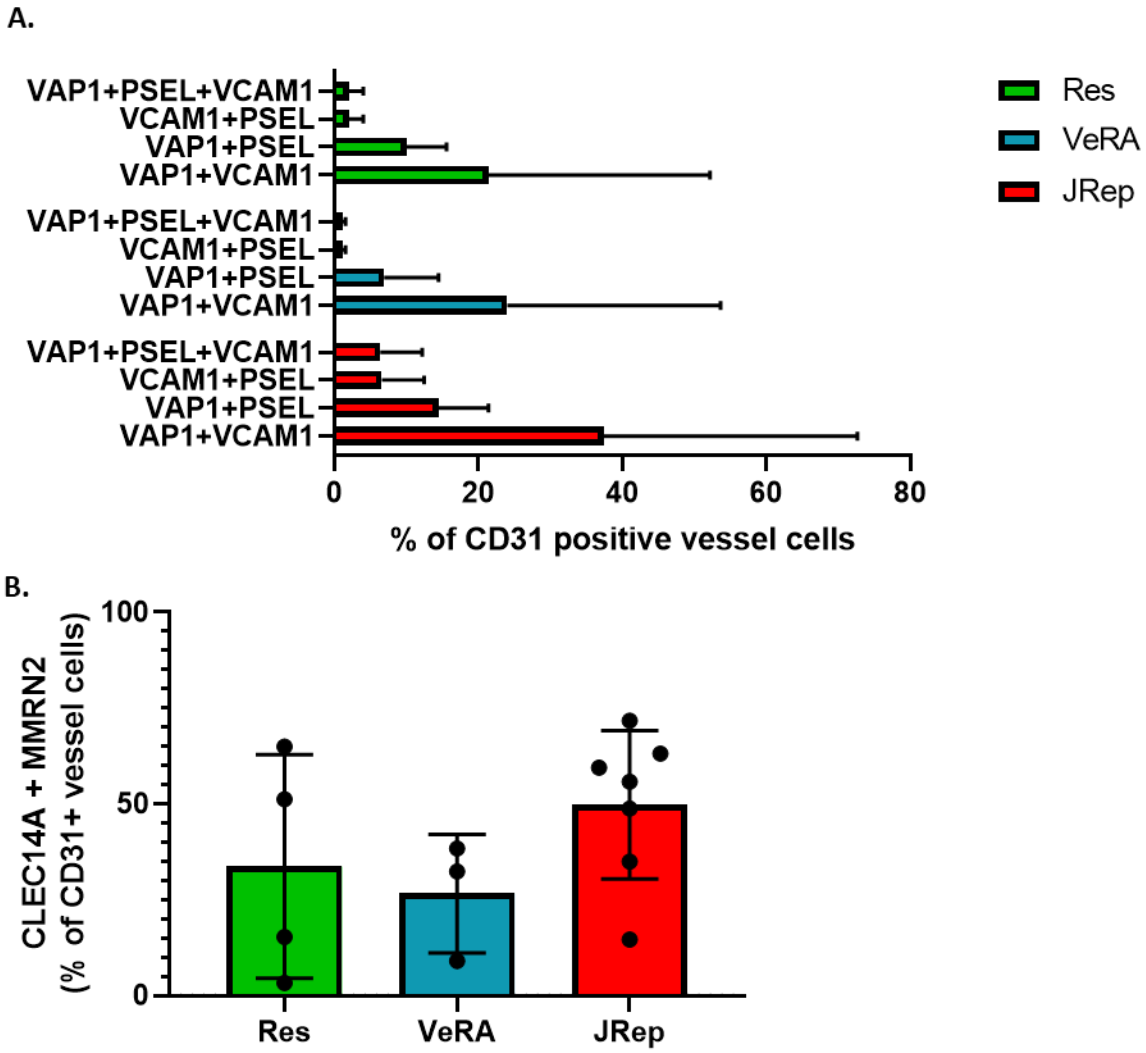

Figure 4.18: Co-expression of molecules. Tissue sections from patients with resolving arthritis (Res; green, n = 4), very early rheumatoid arthritis (VeRA; blue, n = 3) and patients undergoing joint replacement (JRep; red, n = 7) were stained with antibodies against vascular cell adhesion protein 1 (VCAM1), P selectin (PSEL) and vascular adhesion protein 1 (VAP1), C-type lectin domain type 14A (CLEC14A) and Multimerin 2 (MMRN2). The percentage of CD31 cells co-expressing these adhesion molecules was determined. The co-expression of the **(A)** adhesion molecules (VAP1, VCAM1 and P-selectin) and the **(B)** CD248 signalling molecules (CLEC14A and MMRN2) was quantified. For **(A)** X axis, and **(B)** Y axis is the co-expression of the markers as a percentage of all CD31+ vessel cells. Data are mean ± SD.

4.3 Discussion

The aim of this chapter was to identify expression pattern changes in endothelial cells in RA and changes with disease pathotype and duration. From the bulk-RNA sequencing of the PEAC dataset we found that levels of E selectin and senescence molecules was higher in the lymphoid and myeloid compared to the fibroid pathotype. However, the opposite was true for VAP1, CD248 and Notch signalling molecules. There were no significant differences in endothelial staining of molecules between the VeRA, JRep and Res groups. Interestingly the levels of protein staining were similar in the VeRA and resolving arthritis groups. However, expression of VAP-1, VCAM1-1, P-selectin, MMRN2 and p53 appeared higher in the JRep samples.

4.3.1 Adhesion molecules

Of the adhesion molecules in the PEAC dataset, only E selectin and VAP1 were significantly differentially expressed according to pathotype. As E selectin is selectively expressed by ECs (319) this equates to altered EC expression levels. E-selectin is known to mediate the capture and rolling of leukocytes prior to extravasation (308). The results shown here suggest that increased E selectin expression supports increased leukocyte recruitment, accounting for the higher levels of leukocyte infiltration observed in the myeloid and lymphoid, compared to fibroid pathotypes (118, 131). Unfortunately, in this analysis E selectin expression across the course of disease (Res, VeRA, and JRep) was not determined.

Somewhat surprisingly and in contrast to E-selectin, VAP1 was significantly differentially expressed between all pathotypes, but highest in fibroid and lowest in lymphoid. Previously, VAP1 has been demonstrated to play a role lymphocyte binding to EC. Indeed, under flow

conditions, blocking of VAP1 in TNF-α stimulated hepatic sinusoidal endothelial cells (HSEC) significantly reduced adherent leukocytes by 50% (320). Therefore, it was unexpected that the levels of VAP1 were significantly lower in the pathotype of RA associated with more leukocyte infiltration. Notably, VAP1 is not only expressed on ECs, but also on smooth muscle cells, adipocytes and pericytes (302, 321), which may have affected these results. It is possible that VAP1 has a function on these cells which causes a more fibroid-like phenotype. The CellDIVE analysis showed that, consistent with previous findings (136), VAP1 was expressed on the majority of vessels cells. There was a marginally higher expression in the JRep patients, suggesting expression may increase with disease duration. However, the change was relatively small, therefore limited conclusions can be drawn from this given the low n and high data variability.

Similarly to VAP1, P selectin and VCAM1 are also known to be expressed on other cell types; VCAM1 on lining layer fibroblasts ((181), shown in Figure 4.1D) and P-selectin on platelets (319). Therefore, high constitutive expression in other cell types may be masking any endothelial specific differences. In particular as we observed that P selectin, consistent with previous findings (136), is only expressed on a subset of endothelial cells. Similarly, VCAM1, is also expressed on fibroblasts (the major constituent of the joint (322)), therefore the VCAM1 expression measured will primarily be from the fibroblasts. Therefore, the lack of significant differences does not necessarily equate to there being no differences in EC phenotype between pathotypes. When assessing levels of co-expression, VCAM1 and P-selectin were often co-expressed with VAP1 and had similar levels of expression as each molecule on their own. Likewise, it appeared no cells co-expressed VCAM1 and P-selectin, without also

expressing VAP1. This suggests that few ECs express PSEL and/or VCAM1 without also expressing VAP1, most likely to the ubiquitous expression of VAP1 (136).

Notably, there was no difference in PNAd expression between pathotypes. As PNAd is only expressed on endothelial cells (136), this directly corresponds to there being no difference in EC expression of PNAd. This is surprising given that others have previously demonstrated its expression on subsets of ECs RA and PsA sections (136, 140), and considering PNAd is known to be associated with TLSs formation (132). Therefore, we would have predicted differences in pathotypes, particularly those with fewer or more TLSs. Interestingly, staining of the synovial sections was also negative. Previous data has indicated PNAd staining in the majority (80%) of patients (136), thus, we would have expected to have seen staining within the final 14 patients. In addition, when validating the antibody, sections were chosen that were known to have a large amount of immune cell infiltration and TLSs; where we were expecting to observe PNAd expression. As staining of PNAd was never observed in the synovium we cannot be sure that this was not an antibody specific problem, however, this is unlikely given its positive staining in the tonsil control.

4.3.2 Angiogenesis molecules

CLEC14A, MMRN2 and ROBO4, which are well known to play a role in tumour angiogenesis (315), were highest in fibroid>myeloid>lymphoid. This is consistent with previous microarray analysis that found angiogenesis-associated genes were more highly expressed in fibroid compared to other pathotypes (323). However, this is perhaps unexpected given that high levels of angiogenesis are often associated with severe disease and increased leukocyte

infiltration (324). On the other hand, considering that the fibroid pathotype is characterised by a large number of stromal cells, which are known to release pro-angiogenic molecules, it may be that increased angiogenesis is a consequence, rather than cause, of the fibroid pathotype (324).

Within the BEACON dataset, CLEC14A appeared to be consistently highly expressed. On the other hand, MMRN2, the endothelial matrix protein which binds CLEC14A, had a much lower expression, but was always co-expressed with CLEC14A. In cancer, blockade of MMRN2 has been shown to inhibit angiogenesis (315), therefore, it may be assumed that only cells co-expressing both molecules would be angiogenic. In contrast to CLEC14A, MRNN2 expression was increased in the JRep compared to VeRA or Res, suggesting higher levels of angiogenesis with increased disease duration. This is consistent with the idea that as the disease progresses more blood vessels are required for pannus formation and growth (171).

4.3.3 Notch3 signalling molecules

Similarly, to the CD248 signalling molecules, Notch3 signalling molecules were highest in the fibroid>myeloid>lymphoid. These similarities in expression pattern may be due to similar processes; Notch3 signalling is also known to play a role in tumour angiogenesis (325). Equally, as Notch3 is upregulated on fibroblasts, higher expression may be expected in fibroid pathotype (141). Notably, however, expression levels of DLL4 were very similar across the Res, VeRA and JRep samples. This suggests that although Notch3 signalling is important in driving the formation of the lining and sublining layers observed in RA synovium (141), this is not something that changes during the course of disease.

4.3.4 Senescence markers

Our results indicate that expression of p53 in ECs is higher in JRep compared VeRA and Res patients. Importantly, cellular senescence can be induced by multiple stimuli, including telomere shortening, ROS production and, most significantly, pro-inflammatory cytokines (326). Thus, it may be that the excessive prolonged exposure of ECs to TNF-α would result in higher amounts of senescence. Indeed, in vitro assays have demonstrated that prolonged TNF-α exposure (>6 days) induced senescence in HUVECs and cells also had increased production of NF-κB, ROS and cytokines (326, 327). Furthermore, TNF-α activated a positive feedback loop of JAK/STAT signalling which sustained cytokine production (327). Whilst these in vitro models were carried out relatively short term (up to 30 days) considering the duration of RA in JRep patients (many years), it does indicate that senescence increases with TNF-α exposure and via feedback loops within the cell. Likewise, it may be that chronic exposure to TNF-α during disease causes increased senescence. Moreover, as senescent ECs also increase cytokine production this may relate to, or explain why, other molecules of interest (e.g., P-selectin or VCAM1) are also higher in JRep compared to VeRA and Res samples.

All senescence markers were highest in lymphoid>myeloid>fibroid, with significant differences in p53 and p16 between lymphoid and myeloid. Thus, it may be that with senescence, there is an increase in pro-inflammatory cytokine production which results in increased leukocyte recruitment. However, in RA senescence also occurs in fibroblasts (328, 329), and, similarly to the ECs, causing increased production of pro-inflammatory mediators

(328). Therefore, from the bulk RNA data we cannot tell if this is caused by senescence in ECs, fibroblasts or both.

4.3.5 Limitations

4.3.5.1 PEAC bulk RNA-sequencing analysis

One of the major limitations when assessing marker expression using the PEAC dataset was that the data was from bulk RNA-sequencing. Whilst some markers are known to be expressed only, or primarily, by endothelial cells (e.g., E selectin (319)) others are expressed on other cells in the synovium. For example, lining layer fibroblasts are known to express VCAM-1 (181) (seen in Figure 4.1D) and senescence markers (329), whilst platelets strongly express P-selectin (319). Therefore, it is not known in any of the differences observed between pathotypes was due to altered endothelial phenotype or that in other cell types. Equally, if a marker has constitutively high expression in another cell type across all pathotypes, any altered expression in the ECs particularly may be masked. This could be overcome via deconvolution of the bulk RNA-sequencing data (e.g. (162)), but this was not performed due to time constraints.

4.3.5.2 Cell DIVE staining

One of the major limitations from the CellDIVE imaging data was the low number of samples for each patient group. This is especially problematic given the inherent heterogeneity of RA ((330), discussed in 1.5.2). Effects of the low n were further exacerbated by the tissue loss in the processing of sections required from CellDIVE. Furthermore, because sections of certain pathotypes (i.e. pauci-immune) were more prone to tissue loss than others, only the diffuse and lymphoid sections from the VeRA and Res group were analysed. Thus, any minor differences observed in pathotype could not be assessed. The small number of samples also

meant that whilst most molecules had a pattern of high expression in the JRep samples, no differences were statistically significant making it impossible to draw definitive conclusion. A minor limitation to consider as well, was that the sections for the VeRA and Res groups were much smaller than that of JRep. Consequently, the number of vessel cells assessed were higher per sample in the JRep than VeRA or Res.

Due to limitations in obtaining synovial biopsies from the non-inflamed joint we also lacked a non-inflamed control. Whilst the resolving arthritis patients do provide a form of control for inflammation, there would have been signs of inflammation at the time of biopsy. Therefore, we do not know the baseline levels of the markers in a non-inflamed synovium.

Limitations due time and money also meant we did not include markers of immune cells or vessel type (e.g., artery, vein etc.). Therefore, whilst we observed some markers (e.g. P selectin) were selectively expressed on particular vessels we cannot hypothesise why this is. Likewise, we could not stain all of the markers of interest, for instance only p53 of the senescence markers was stained. However, as mentioned before this was a preliminary experiment using a novel technique to explore the endothelial phenotype.

Another key limitation to the CellDIVE work was that the stains for Lyve1 and E-selectin did not work. The lack of Lyve1 stain made it impossible to know whether the CD31+ vessels identified were lymphatic or of the blood vasculature. This is problematic as, whilst both contribute to RA pathogenesis, they do so via different mechanisms (10) and when deciding which molecules to investigate it was changes primarily in the blood vasculature that was of

interest. The lack of E selectin stain was also limiting, particularly as alterations had been observed in the PEAC cohort, but why these stains did not work in this staining round is unknown. Unfortunately, the stains could not be repeated for quantification as the CellDIVE technique only bleaches the fluorescent part of the antibody, but otherwise the antigen will still be bound.

4.1.1.1 Overall limitations in examining the EC phenotype

Ideally, in order to get the best picture of the RA endothelial phenotype, endothelial cells from the joint would be isolated and RNA sequencing and functional analysis performed. This was attempted, however, due to the limited number of endothelial cells in the joint, and the amount of tissue available it was not possible to obtain enough RNA. Hopefully, as upcoming innovative techniques (e.g. single-cell sequencing or spatial transcriptomics) are utilised more frequently, the phenotype of the RA endothelium will be explored in more depth.

4.3.6 Conclusions

Taken together these data suggest that in rheumatoid arthritis, endothelial cells have a heterogeneous expression pattern of functionally important molecules. Some of these are dependent on pathotype and often increase in expression as disease progresses. Most notably E selectin and senescence molecule expression was associated with myeloid and lymphoid pathotypes, suggesting these may aid in increasing lymphocyte recruitment to the joint. On the other hand, VAP1, and CD248 or Notch signalling molecules, were increased in the fibroid pathotypes, suggesting that whilst these molecules may not be pivotal in

increasing leukocyte recruitment, they may play a role in the pathogenesis of RA via other mechanisms (e.g., angiogenesis).

5 The effect of synovial fibroblasts from different stages of rheumatoid arthritis on co-cultured endothelial cells

5.1 Introduction

As described in the previous chapter, the endothelium plays a role in the pathogenesis of rheumatoid arthritis (RA). However, the mechanism by which it does this are not fully understood. It is known to act as a reporter for its local microenvironment, with transcriptomic analysis of ECs showing clustering largely dependent on vessel type and anatomical location (164, 165). Indeed, microarray analysis has revealed that human umbilical vein endothelial cells (HUVECs) cluster according to whether they were co-cultured with skin or synovium fibroblasts from patients with RA undergoing joint replacement (168, 184).

Functional flow-based adhesion assays have demonstrated changes in EC phenotype according to the diagnosis of fibroblasts in culture (9). In TNF-α-IFNγ stimulated conditions, fibroblasts from non-inflamed and resolving patients were able to affect an immunosuppressive role, limiting the number of lymphocytes the ECs recruited (9). Furthermore, fibroblasts from very early RA (VeRA) and joint replacement (JRep) patients lost this immunosuppressive function (9). Moreover, in unstimulated conditions JRep fibroblasts appeared to activate the endothelium in order to recruit lymphocytes (9). Antibody blockade within the co-cultures suggested that changing roles in IL-6 and TGF-β (transforming growth factor-β) signalling, caused the differences observed between Res and VeRA (9). This is potentially mediated by differential SOCS3 expression (9). However, the mechanism for this and any soluble mediator(s) involved remains unknown. This aim of this

chapter was to identify any transcriptomic and metabolomic alterations that occur in the EC-fibroblast co-cultures and could explain this changing phenotype.

5.2 Results of transcriptomic analysis

5.2.1 The co-culture set-up

The objective was to explore any transcriptomic differences which may account for the functional differences observed by Filer *et al* (9). Therefore, cultures were set up similarly to that described in the paper. Briefly, human umbilical vein endothelial cells (HUVECs) were cultured on the apical side of a porous membrane, with patient derived fibroblasts on the basal side (Figure 5.1A) and cells were stimulated with 100U/ml TNF-α and 10ng/ml IFN-γ for 24 hours. In total, there were 8 HUVEC donors, each run as a separate experiment and at different times. Each HUVEC donor was cultured with fibroblasts derived from patients with; (1) resolving arthritis (Res), (2) very early rheumatoid arthritis (VeRA), (3) with RA undergoing joint replacement (JRep) or (4) with no fibroblasts and for each fibroblast donor, a mono-culture control was seeded. The experiment set-up is shown in Figure 5.1B. A summary of patient characteristics of the fibroblast donors is given in Table 5.1 and full details in Appendix Table 2. Notably, signs of inflammation (presence of CCP, RF and ESR, DAS and ESR) were highest in JRep > VeRA > Res.

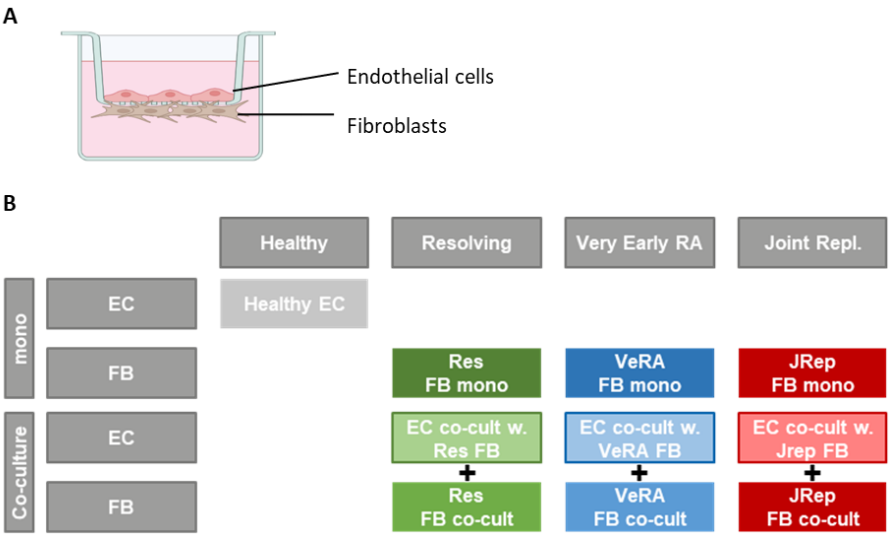

Figure 5.1: Schematic of the endothelial cell –fibroblast co-culture set-up. (A) Human umbilical cord endothelial cells (HUVECs) were cultured on the upper side of a porous membrane with fibroblasts on the lower side. **(B)** HUVECs were cultured with fibroblasts isolated from patients with resolving arthritis (Res), Very early arthritis (VeRA) and those undergoing joint replacement (JRep). This experimental set up was repeated for 8 HUVEC donors, each with different fibroblast donors; one from each patient group.

	Resolving (n=8)	VeRA (n=8)	JRep (n= 8)
Age (years)	38 (31 – 47)	52 (48 – 61)	59 (53 – 63)
Female, n (%)	3 (38)	4 (50)	5 (63)
Symptom duration (weeks)	5 (3 – 6)	7 (4 – 9)	1040 (923 – 1248)
DAS28 ESR, mean (sd)	3.4 (± 1.2)	4.6 (± 1.5)	5.5 (± 1.5)
ESR (mm/hour)	10 (3.5 – 22.8)	28 (23 – 38.5)	54 (21.5 – 60)
CRP, median (IQR), mg/L	8.5 (4.5 – 10)	29 (16.5 – 39.8)	46 (29 – 64)
RF positive, n (%)	0 (0)	4 (50)	7 (88)
CCP positive, n (%)	0 (0)	6 (75)	-
SJC28	3 (2 – 5)	4 (3 – 10)	9 (6 – 12)
TJC28	2 (1 – 3)	3 (3 – 9)	9 (3 – 11)
VAS	46 (9 – 85)	49 (24 – 64)	65 (54 – 80)
US GS	1.5 (1 – 2)	3 (2 – 3)	-
US PD	0.5 (0 – 1)	2 (1 – 2)	-
NSAID, n (%)	5 (63)	4 (50)	2 (25)

Table 5.1: Summary of patient characteristics of fibroblast donors from fibroblast-endothelial cell co-cultures used for RNA-sequencing

Median (IQR) shown unless otherwise stated.
DAS28 = Disease Activity Score 28; CCP = cyclic citrullinated peptide, CRP = C-reactive protein; ESR = erythrocyte sedimentation rate; IQR = Interquartile range; JRep = joint replacement; NSAID = non-steroidal anti-inflammatory; RF = Rheumatoid factor; SJC28 = 28 swollen joint counts; TJC28 = 28 tender joint counts; US GS = ultrasound greyscale grade at the biopsied joint; US PD = ultrasound power Doppler grade at the biopsied joint; VAS = visual analogue score; VeRA = Very early rheumatoid arthritis.

5.2.2 Sample quality control

Cells were collected from the co-cultures and RNA isolated; the 260/280 and 260/230 ratios and the RNA integrity numbers (RINs) are given in Appendix Table 3. The majority of the samples had 260/280 of above 1.8, suggesting primarily pure RNA. The 260/230 ratios were typically lower than the ideal 2-2.2 range, with an average at 1.14 indicating potential contaminants. All RINs were above 9, indicating a high level of integrity. Therefore, despite the low 260/230 ratios, samples were deemed acceptable to run for RNA sequencing. Once sequenced, samples were aligned with STAR aligner and gene counts table generated with FeatureCounts. The majority of reads (>80%) were uniquely mapped for all samples (Figure 5.2), indicative of good library preparation and data processing (247).

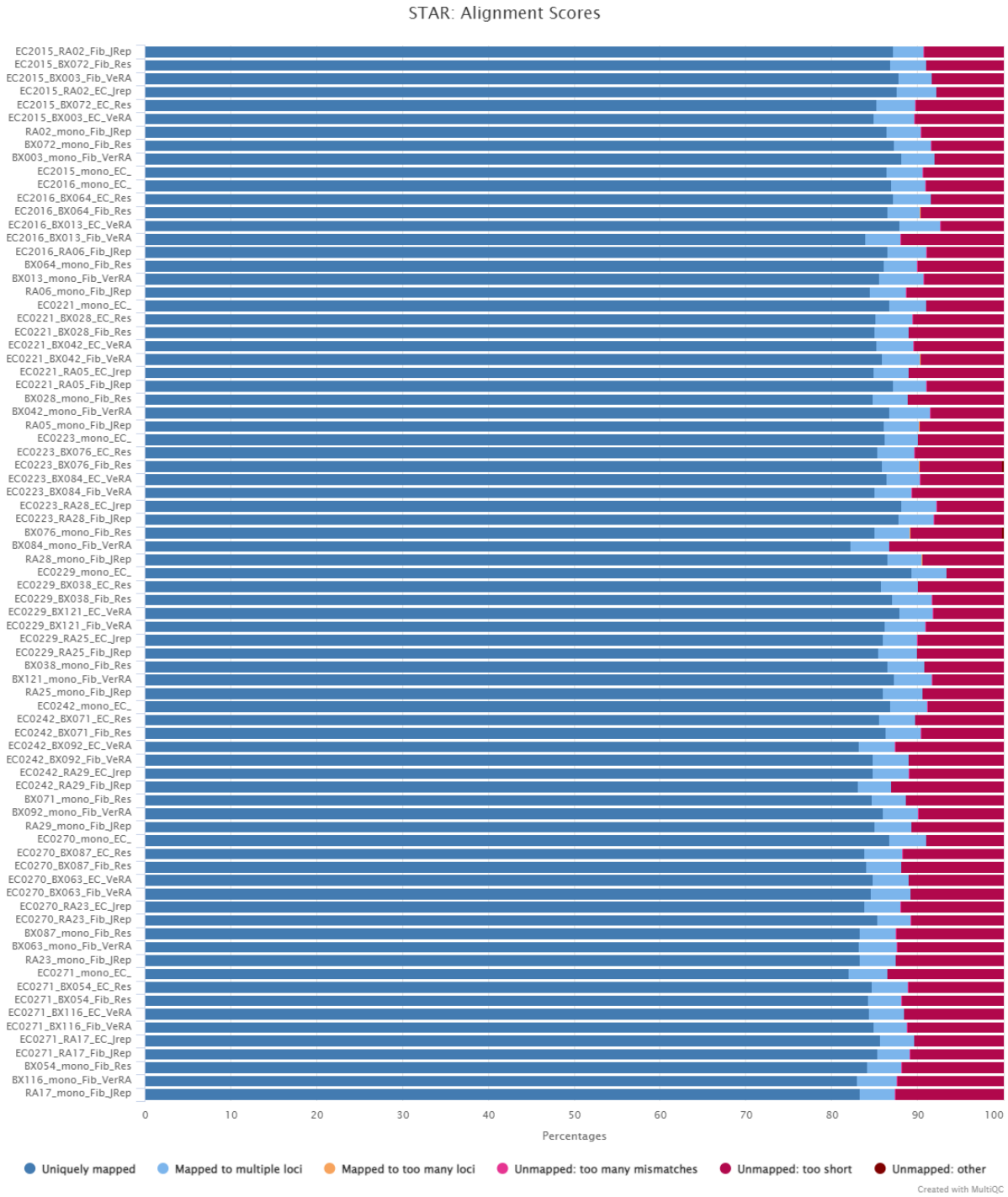

Figure 5.2: Alignment scores from STAR aligner. Endothelial cells and fibroblasts were co-cultured and treated with TNF-α+IFNγ for 24 hours. RNA was isolated, bulk RNA sequencing performed. Sequences were aligned to the GRCh38 human genome with STAR aligner. Plots of the percentage of reads aligned were generated in MultiQC. X axis indicates samples and y axis indicates the percentage of reads in each sample and how they are mapped. Uniquely mapped reads are dark blue, reads mapped to multiple loci in light blue and unmapped reads in red.

5.2.3 Pre-processing of data

To identify any outliers and give an overview of the data, an initial exploration of the top most variable genes was carried out. Principal component analysis (PCA) and boxplots (Figure 5.3) of all samples identified 3 outliers (EC2016_BX064_EC_Res, EC0223_BX076_Fib_Res and BX076_Fib_Res; in the red circle) which were removed for future analysis. As both the mono-cultured and co-cultured BX076 fibroblasts were outliers it indicated a potential issue with this donor. The corresponding endothelial cells (ECs) in co-culture did not appear to be an outlier so the sample was left in, but was monitored throughout the analysis. PCA also showed a strong clustering according to cell type, therefore for simplicity subsequent analysis was carried out on ECs and fibroblasts separately.

PCA of the ECs showed strong clustering according to EC donor and batch, Figure 5.4A. It must be highlighted that, due to the experimental design (each EC sample was collected at a separate time point) it is unknown how much of this was caused batch effect and how much by donor. A biplot showing the genes driving the principal component separation (Figure 5.4B), as well as a heatmap of the top 50 variably expressed genes (Figure 5.4C), demonstrated that the separation was driven, at least in part, by sex-associated genes (XIST and the Y-chromosome genes), highlighted with a red box in Figure 5.4C.

PCA of the fibroblasts showed some clustering according to the diagnosis of the patients, in principal components (PCs) 1 and 2, Figure 5.5A and B. The separation was driven by genes such as MMP1, CMKLR1, FDF10, CRTA1, HAPLN1, GOGN, SALL1, and EREG. However, similar

to the endothelial cells, the fibroblasts clustered primarily according to sex associated genes, in PC3 and PC5 (Figure 5.5C and D) and in a Heatmap of top 50 variably expressed genes (Figure 5.5E), with the sex genes highlighted in red.

In order to remove the effect of sex in both cell types, the female specific genes, XIST (X-inactive specific transcript) and TSIX (anti-sense RNA to XIST), and Y chromosome genes were removed from downstream analysis. To focus the research question on the differences between co-cultured conditions, the mono-cultured endothelial cells were removed from the analysis. It may be noted there were effects of monoculture observed, indicated by within donor clustering of the co-cultured cells separate from the mono-cultured (Figure 5.3A) and in differential gene expression analysis (Appendix Figure 2). Similarly, to remove the effects of potential confounder effect of co-culture conditions, only the co-cultured fibroblasts were initially analysed. Mono-cultured fibroblasts were later compared to see if there were any disease specific changes in fibroblasts upon co-culture.

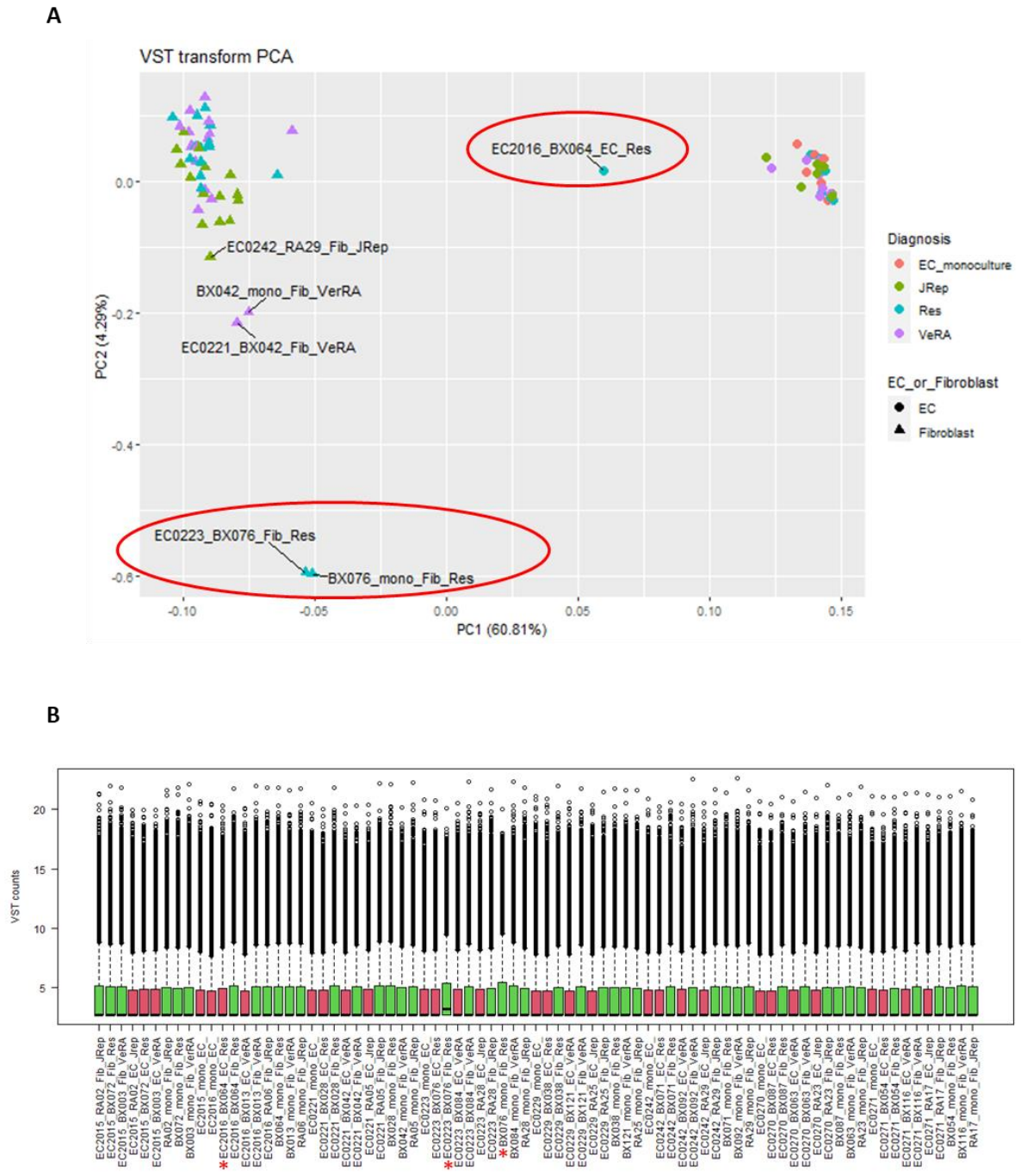

Figure 5.3: Principal component analysis of endothelial cell – fibroblast co-culture samples. RNA sequencing was performed on endothelial cells and fibroblasts co-cultures (and mono-culture controls) treated with TNF-α+IFNγ for 24 hours. Sequences were aligned to the genome STAR aligner and a gene counts table generated with Subread FeatureCounts. Data were subject to variance stabilising transformation (VST) and principal components identified in R. **(A)** Principal Components 1 and 2 were plotted, coloured by diagnosis of fibroblasts in culture, shape indicates cell type; endothelial cells as circle and fibroblasts as triangle. Outliers are circled in red. **(B)** Boxplot of the VST data, coloured according to cell type; fibroblasts in green and endothelial cells in pink. Red stars indicate the outlier samples.

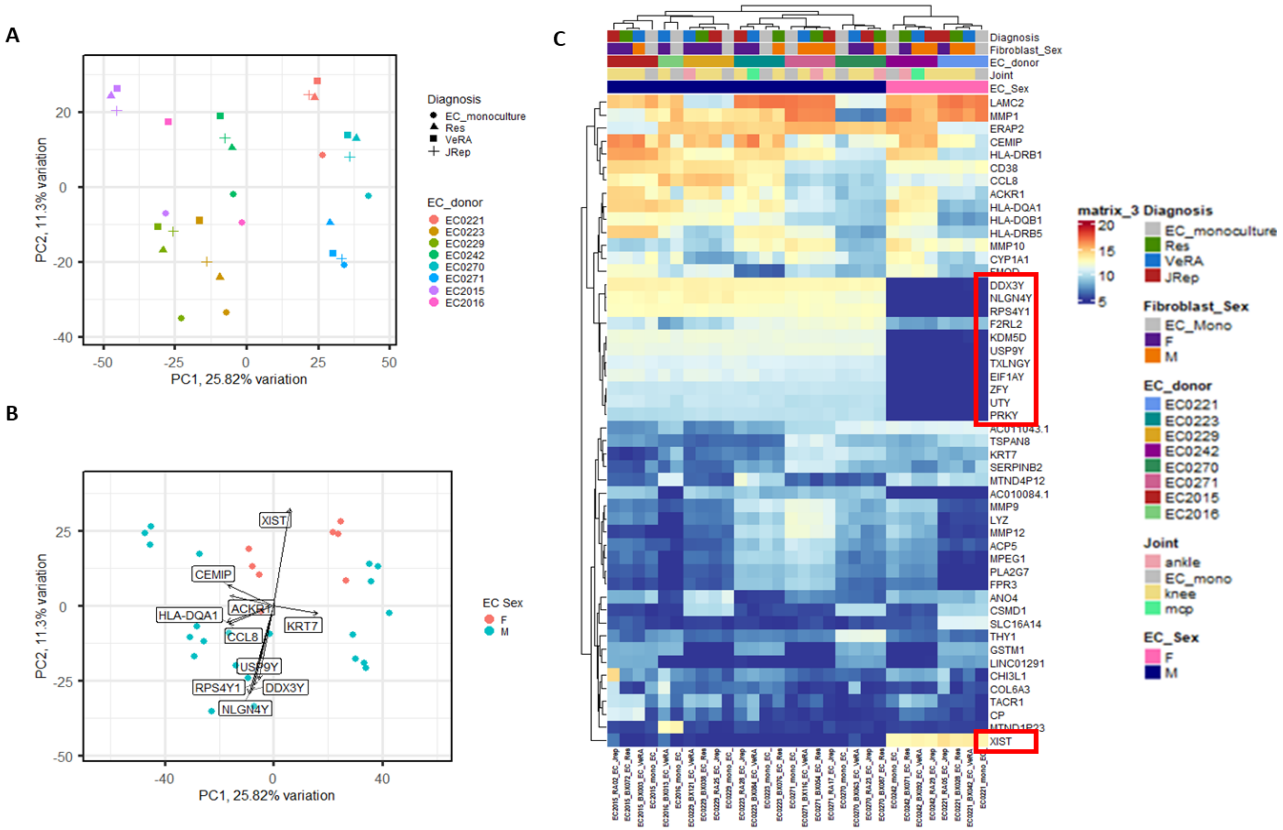

Figure 5.4: Endothelial cells cluster by donor and sex. Bulk RNA sequencing was performed on RNA isolated from endothelial cells (ECs) co-cultured with fibroblasts from resolving (Res), very early rheumatoid arthritis (VeRA) and RA patients undergoing joint replacement (JRep), or left as mono-cultures, and treated with TNF-α+IFNγ for 24 hours. Gene counts from the EC sequencing data were subject to variance stabilisation transformation (VST) and **(A-B)** principal component analysis (PCA) performed. **(A)** Colour indicates EC donor; shape indicates diagnosis of fibroblasts in co-culture. **(B)** Colour indicates sex of EC donor and gene contributing to PC loadings are shown with arrows. **(C)** The top 50 variably expressed genes of the VST data were plotted as a heatmap with hierarchical clustering on the columns and rows. Bars at the top show diagnosis and sex of the fibroblast donor and joint the fibroblasts were taken from, as well as EC donor and sex. Sex genes are highlighted in the red boxes. Res = resolving, VeRA = very early RA, JRep = joint replacement, F = female, M = male, MCP = metacarpophalangeal.

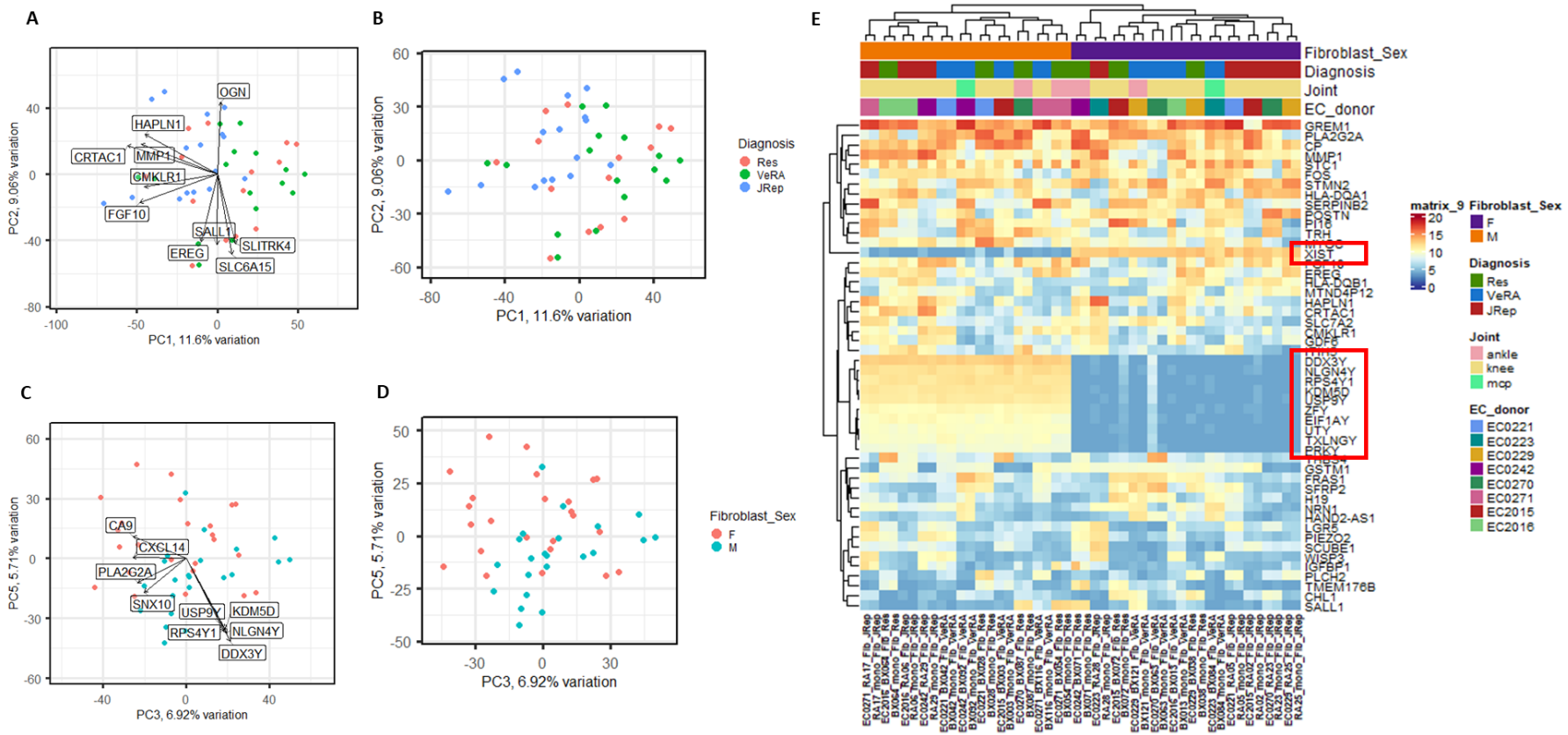

Figure 5.5: Fibroblasts cluster by diagnosis, sex and fibroblast donor. Bulk RNA sequencing was performed on RNA isolated from fibroblasts of resolving (Res), very early rheumatoid arthritis (VeRA) and RA patients undergoing joint replacement (JRep), in mono-culture and in co-culture with endothelial cells, treated with TNF-α+IFNγ for 24 hours. Fibroblast gene counts were subject to variance stabilisation transformation (VST) and **(A-D)** principal component analysis (PCA) performed. **(A-B)** PC1 and PC2 plotted, colour indicates diagnosis of donor, **(A)** with PC loadings. **(C-D)** PC3 and PC5 plotted, colour indicates sex of fibroblast donor, **(C)** with PC loadings. **(E)** The top 50 variably expressed genes of the VST data were plotted as a Heatmap, with hierarchical clustering on the columns and rows. Bars at the top show diagnosis and sex of the fibroblast donor and joint the fibroblasts were taken from, as well the endothelial cell donor batch. Sex genes are highlighted in the red boxes. Res = resolving, VeRA = very early RA, JRep = joint replacement, F = female, M = male, MCP = metacarpophalangeal.

5.2.4 Very few significantly differentially expressed genes were detected in endothelial cells according on the diagnosis of fibroblasts in culture

5.2.4.1 Exploration of the most variable genes in endothelial cells

To assess if there were any confounders that should be built into the model for differential expression, analysis of the top variable genes was carried out. Pairsplots of the top 5 PCs coloured by EC donor and sex showed that despite removal of the sex associated genes, the endothelial cells still clustered strongly according to donor (Figure 5.6A and B) and indeed, potentially still by sex in PC5 (Figure 5.6C-D). A heatmap of the top 50 variably expressed genes confirmed clustering by donor, but not sex of donor, Figure 5.7. To assess the impact of the fibroblasts in co-culture, pairsplots of the top 5PCs coloured by attributes from fibroblasts were constructed. No clustering was observed according to the diagnosis, sex or joint location of the fibroblasts in culture (Figure 5.8). Based on these observations, EC donor and diagnosis was built into the DESeq2 model, but not sex or joint of fibroblast donor.

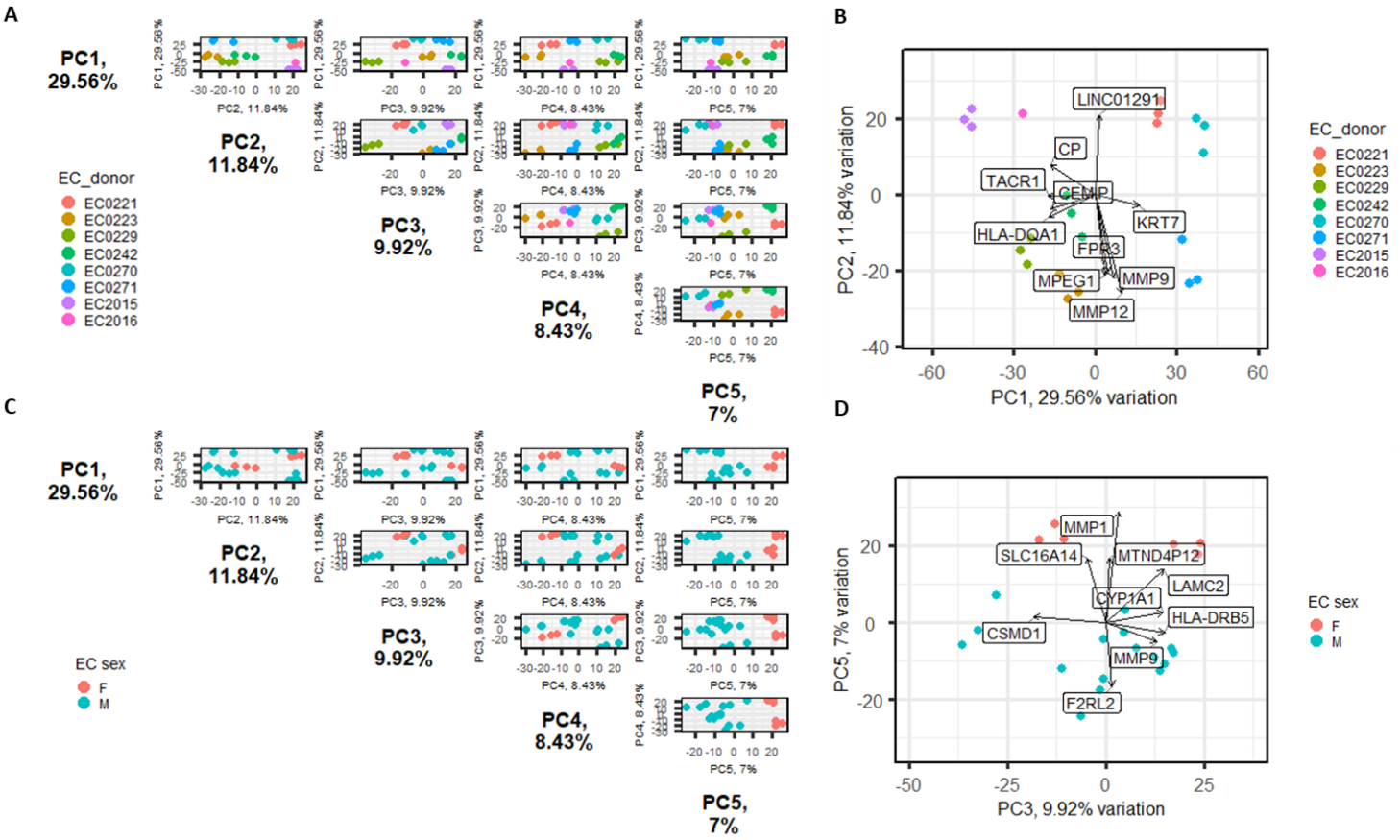

Figure 5.6: With sex genes removed, endothelial cells still cluster according to donor. Bulk RNA sequencing was performed on RNA isolated from endothelial cells (ECs) co-cultured with fibroblasts and treated with TNF-α+IFNγ for 24 hours. Sex associated genes were removed from the analysis. Gene counts from the endothelial cell (EC) sequencing data were subject to variance stabilising transformation (VST) and principal components (PCs) identified. **(A and C)** Pairsplots of the top 5 PCs and **(B and D)** biplots showing genes contributing to PCA loadings were generated. **(A-B)** Samples were coloured according to EC donor and **(C-D)** Samples coloured according to EC sex. F = female, M = male.

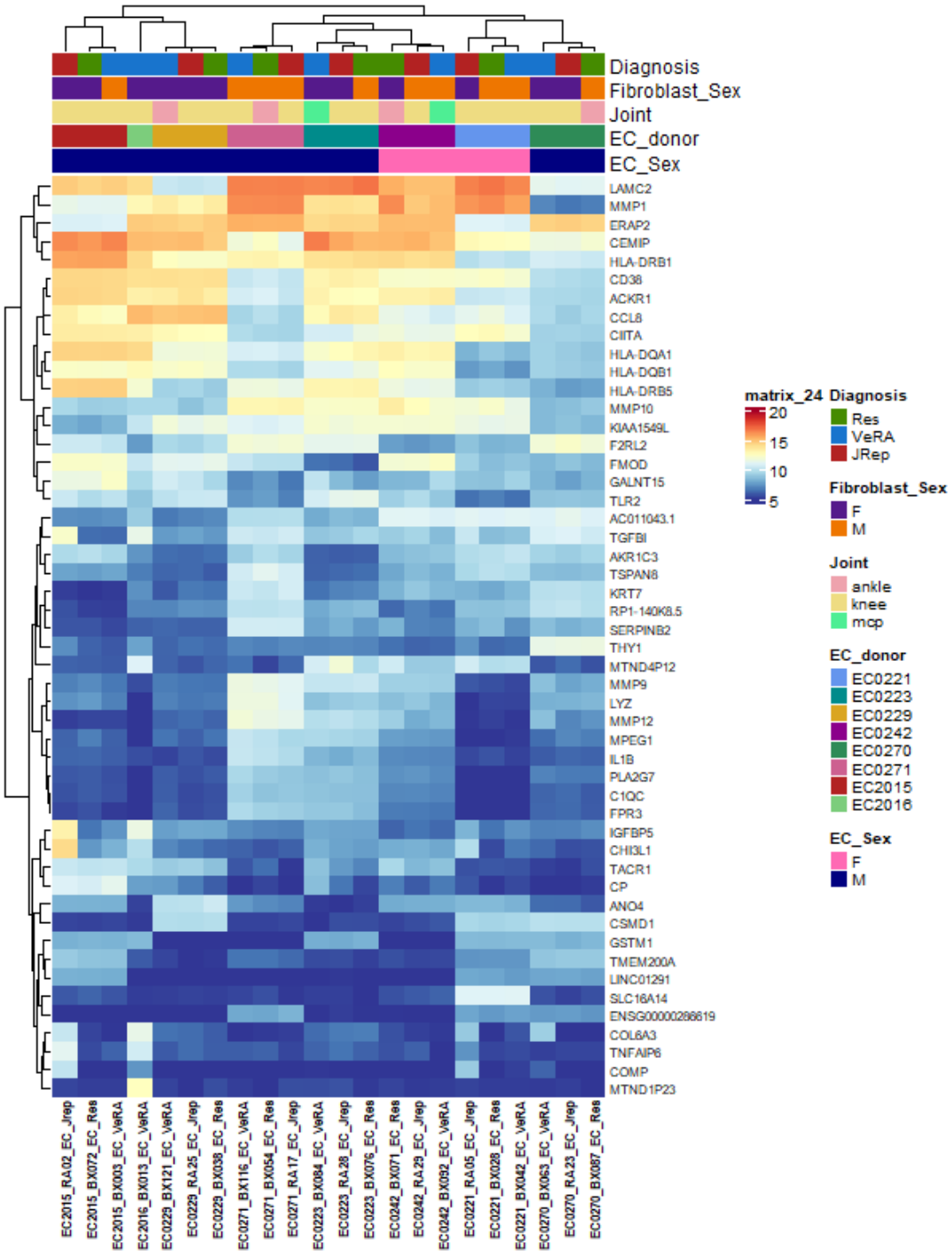

Figure 5.7: Endothelial cells cluster according to donor. Bulk RNA sequencing was performed on RNA isolated from endothelial cells (ECs) co-cultured with fibroblasts from patients with resolving arthritis (Res), very early rheumatoid arthritis (VeRA) and RA patients undergoing joint replacement (JRep), or left as mono-cultures, and treated with TNF-α+IFNγ for 24 hours. Sex associated genes were removed, and gene counts from the EC sequencing data were subject to variance stabilisation transformation (VST). The top 50 most variable genes were plotted as a heatmap, with hierarchal clustering on the columns and rows. Coloured bars at the top correspond to diagnosis, sex and joint for fibroblasts, as well as EC donor and sex. Res = resolving, VeRA = very early RA, JRep = joint replacement, F = female, M = male, MCP = metacarpophalangeal.

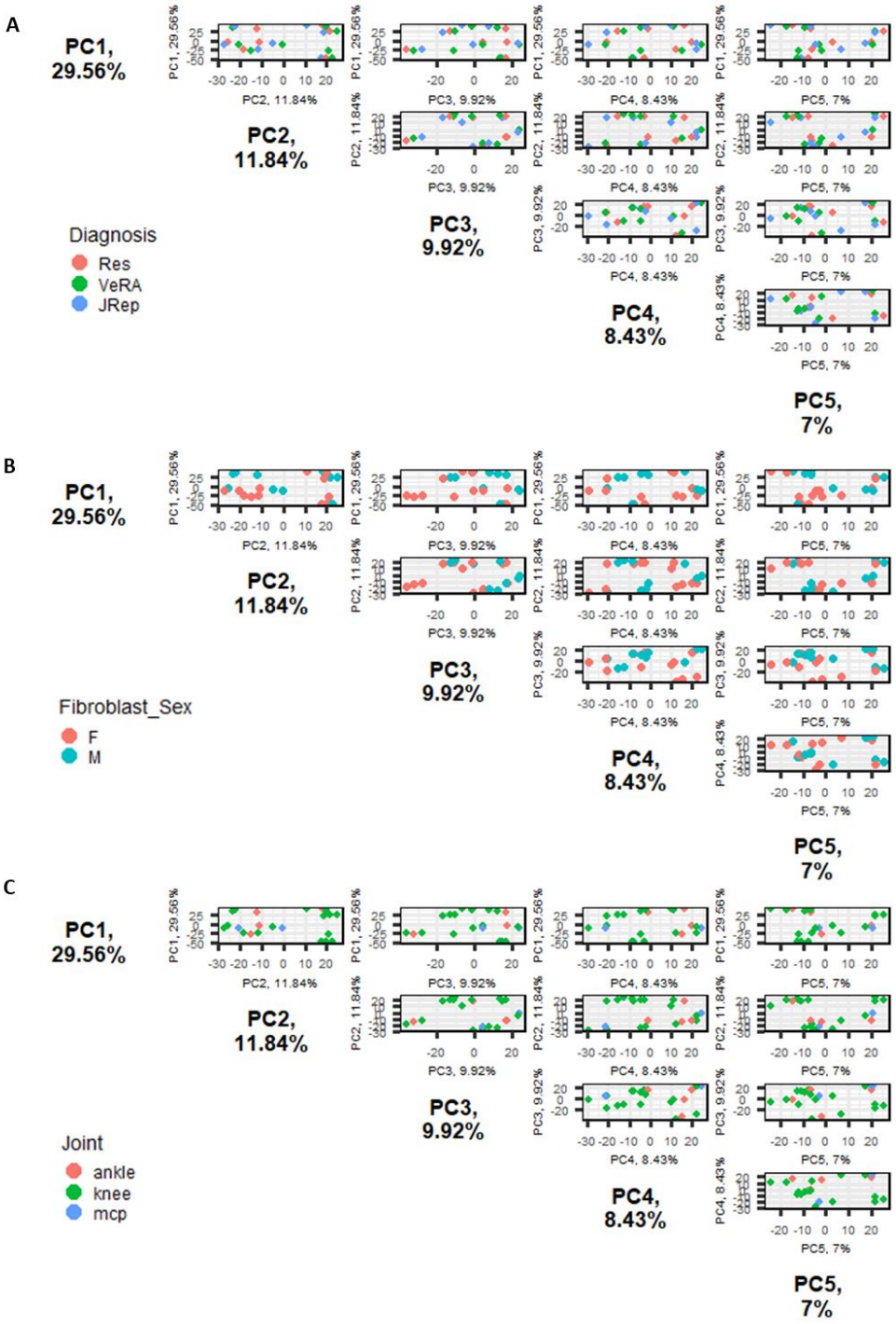

Figure 5.8: Endothelial cells do not cluster according to the diagnosis, sex or joint of the fibroblasts in co-culture. Bulk RNA sequencing was performed on RNA isolated from endothelial cells (ECs) co-cultured with fibroblasts from patients with resolving arthritis (Res), very early rheumatoid arthritis (VeRA) and RA patients undergoing joint replacement (JRep), or left as mono-cultures, and treated with TNF-α+IFNγ for 24 hours. Sex associated genes were removed, and gene counts from the EC sequencing data were subject to variance stabilisation transformation (VST) and principal component analysis (PCA). Pairsplots of the top 5 PCs generated and coloured according to the fibroblast donors

(A) diagnosis, **(B)** sex and **(C)** and joint location of fibroblasts. Res = resolving, VeRA = very early RA, JRep = joint replacement, F = female, M = male, MCP = metacarpophalangeal.

5.2.4.2 Differential gene expression of endothelial cells

Differential gene expression was carried out on the RNAseq data from endothethelial cells. Plots of the gene dispersion estimates looked appropriate, so no prior filtering was carried out (Figure 5.10A). To assess the validity of the results, histograms of the p values were generated to visualise their distribution. Whilst DESeq2 applies independent filtering, this was not applied to the unadjusted p values, therefore genes with lower gene counts were filtered out (cut-off at a normalised count =< 5 in 3 samples or more) for this.

The shape of p-value histogram can give an indication of how the data are behaving and whether the null hypothesis should be accepted, prior to multiple comparison testing (331, 332). Figure 5.9 shows examples of the different shapes that may occur and a brief description of what these may mean is given below. Figure 5.9A shows an anti-conservative distribution, with a large proportion of P values <0.05. In this case the null hypothesis should be rejected as there are a high number of statistically significant differences (coloured blue). Notably, there is also a uniform distribution of P values (coloured pink) across the bottom, which fall under the null hypothesis. This is due to the nature of statistical testing, where there is always a 5% chance of being <0.05, and 10% chance of being <0.1 and so on. As some genes that fit the null hypothesis will also, by chance, have a P value of <0.05 (the pink with P<0.05), false detection rate (FDR) correction is required to remove as many of these falsely significant results as possible (331, 332). On the other hand, a fully uniform distribution (Figure 5.9B) with no peak at <0.05, suggests the null hypothesis should be accepted. At most only a small percentage are not null, and accepting the uncorrected p

values < 0.05 would give a large number of false discoveries (331, 332). Bimodal distribution (Figure 5.9C), has a large number of p values both close to 1 and close to 0 (331, 332). Within RNA-sequencing this is may be caused by low or no gene counts, that when assessed for differential expression are reported as 1 (331, 332). Therefore, filtering out of these genes prior to differential gene expression analysis is required, before applying multiple correction or false detection rates. Finally, there may be a conservative distribution, which suggests the wrong test is being used, for instance the test is for normally distributed data, but the data are non-parametric (Figure 5.9C). In RNA-Seq, it may also be the case that it is uniformly distributed data, combined with low gene counts causing a high number of p values close to 1.

The p value histograms of the DEGs in endothelial cells had a uniform distribution (Figure 5.10B-D) which suggests that there are no or very few significantly different genes and that the null hypothesis should be accepted (331, 332). Volcano plots (Figure 5.10E-G) of the differentially expressed genes (DEGs) that were statistically significant (listed in Table 5.2) support this, with only 11 DEGs comparing “JRep vs Res”, 6 in “VeRA vs Res” and 1 in “VeRA vs JRep”. Plotting of these DEGs as a heatmap (Figure 5.11A) did show clustering of ECs according to Res vs JRep/VeRA, however the heatmap and the counts plots of the genes (Figure 5.11B) indicate these may be caused by outliers, i.e. ECs co-cultured with the RA02 fibroblast.

Pathway analysis with g Profiler of the DEGs that were identified (Figure 5.12) suggests BMP binding could be involved, due to the differential expression of cartilage oligomeric matrix

protein (COMP) and gremlin 2 (GREM2). However, as so few genes were identified these results must be viewed with caution.

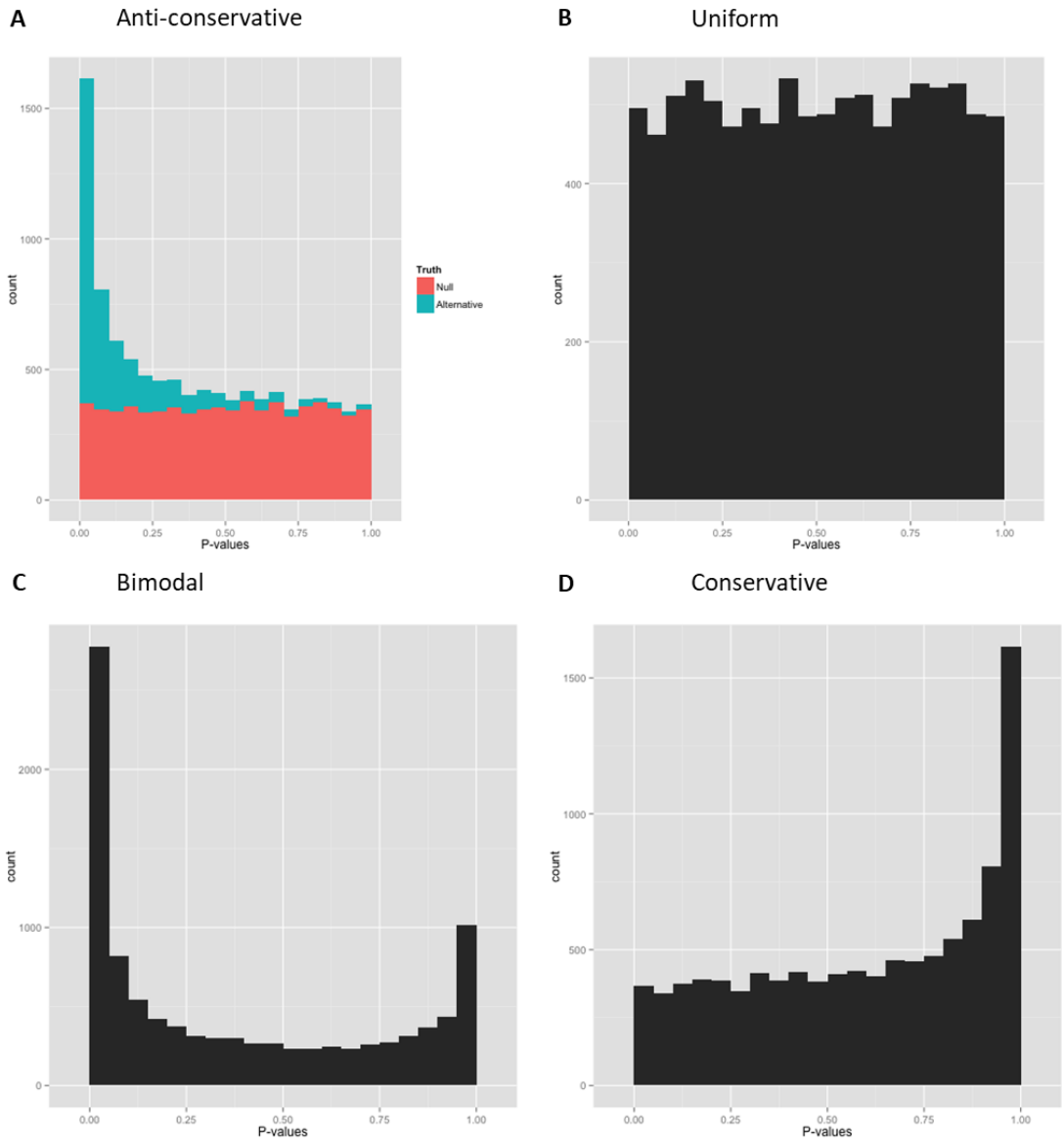

Figure 5.9: Examples of p value histogram distributions. Shape variations of the histograms include: **(A)** Anti-conservative distribution, coloured pink are the null hypotheses and in blue are the alternative hypotheses, **(B)** Uniform distribution, **(C)** Bimodal distribution and **(D)** Conservative distribution. Images taken from (331).

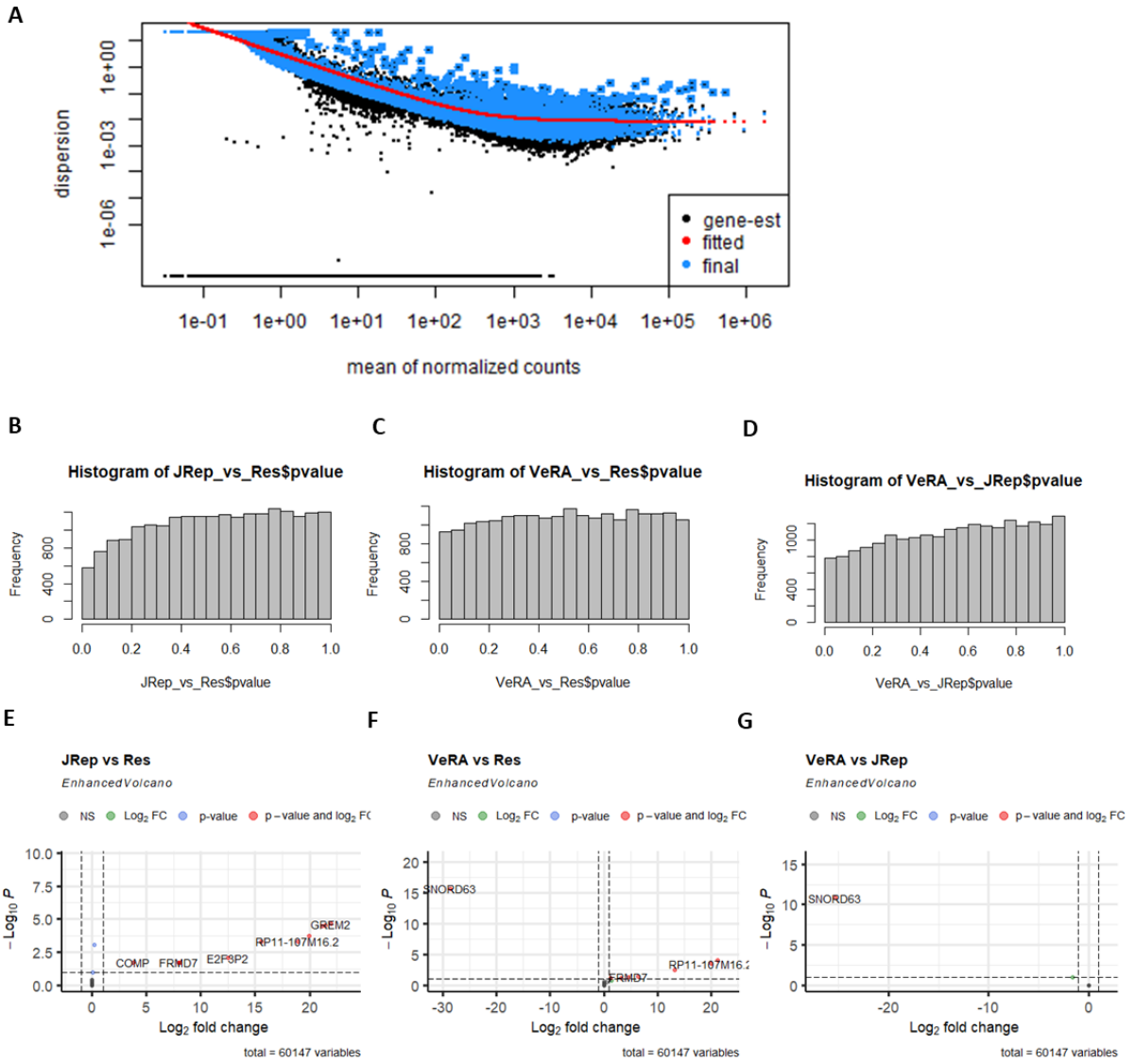

Figure 5.10: There are very few significantly differentially expressed genes between endothelial cells according to diagnosis of fibroblasts in co-culture. Bulk RNA sequencing was performed on RNA isolated from endothelial cells (ECs) co-cultured with fibroblasts from patients with resolving arthritis (Res), very early rheumatoid arthritis (VeRA) and RA patients undergoing joint replacement (JRep), or left as mono-cultures, and treated with TNF-α+IFNγ for 24 hours. Differential gene expression was performed with DEseq2 on the gene counts with sex genes removed and compared according to the diagnosis of fibroblasts in culture with ECs. **(A)** Dispersion estimates from DESeq2 and comparisons of **(B and E)** JRep vs Res, **(C and F)** VeRA vs Res **(D and G)** VeRA vs JRep. **(B-D)** P value histograms, with filtered out genes where there are less than 3 samples with normalized counts greater than or equal to 5. **(E-G)** Volcano plots of the comparisons, on the x axis the "ashr" shrunk Log2foldchange and on the y the –log10 adjusted p value. Significantly different gene expression shown in red.

Table 5.2: List of the significantly differentially expressed genes in endothelial cells with no filtering of genes.

		JRep vs Res			VeRA vs Res			VeRA vs JRep		
Ensemble ID	**Gene name**	**Log2FC**	**Pvalue**	**Padj**	**Log2FC**	**Pvalue**	**Padj**	**Log2FC**	**Pvalue**	**Padj**
ENSG00000105664	COMP	8.26	4.65E-06	0.0186	-	-	-	-	-	-
ENSG00000165694	FRMD7	16.17	5.24E-06	0.0186	15.96	7.12E-06	0.0459	-	-	-
ENSG00000133055	MYBPH	16.37	7.24E-08	0.0005	15.57	3.47E-07	0.0034	-	-	-
ENSG00000248491	AC093772.1	17.04	5.77E-06	0.0186	-	-	-	-	-	-
ENSG00000227158	AC073621.1	17.05	5.60E-06	0.0186	17.15	4.85E-06	0.0375	-	-	-
ENSG00000203435	E2F3P2	17.89	1.83E-06	0.0088	-	-	-	-	-	-
ENSG00000236427	AL589986.2	20.29	6.74E-08	0.0005	20.96	2.31E-08	0.0003	-	-	-
ENSG00000223727	AC034195.1	21.15	1.83E-08	0.0002	21.93	5.02E-09	9.69E-05	-	-	-
ENSG00000181195	PENK	22.31	2.54E-09	3.27E-05	-	-	-	-	-	-
ENSG00000180785	OR51E1	22.59	1.59E-09	3.08E-05	-	-	-	-	-	-
ENSG00000180875	GREM2	23.17	5.74E-10	2.22E-05	-	-	-	-	-	-
ENSG00000206989	SNORD63	-	-	-	-29.30	5.54E-21	2.14E-16	-25.72	4.03E-16	1.56E-11

Log 2FC = Log2 fold change; P value = unadjusted P value; P adj = adjusted P value; Res = resolving arthritis; VeRA = very early rheumatoid arthritis; JRep = RA patients undergoing joint replacement.

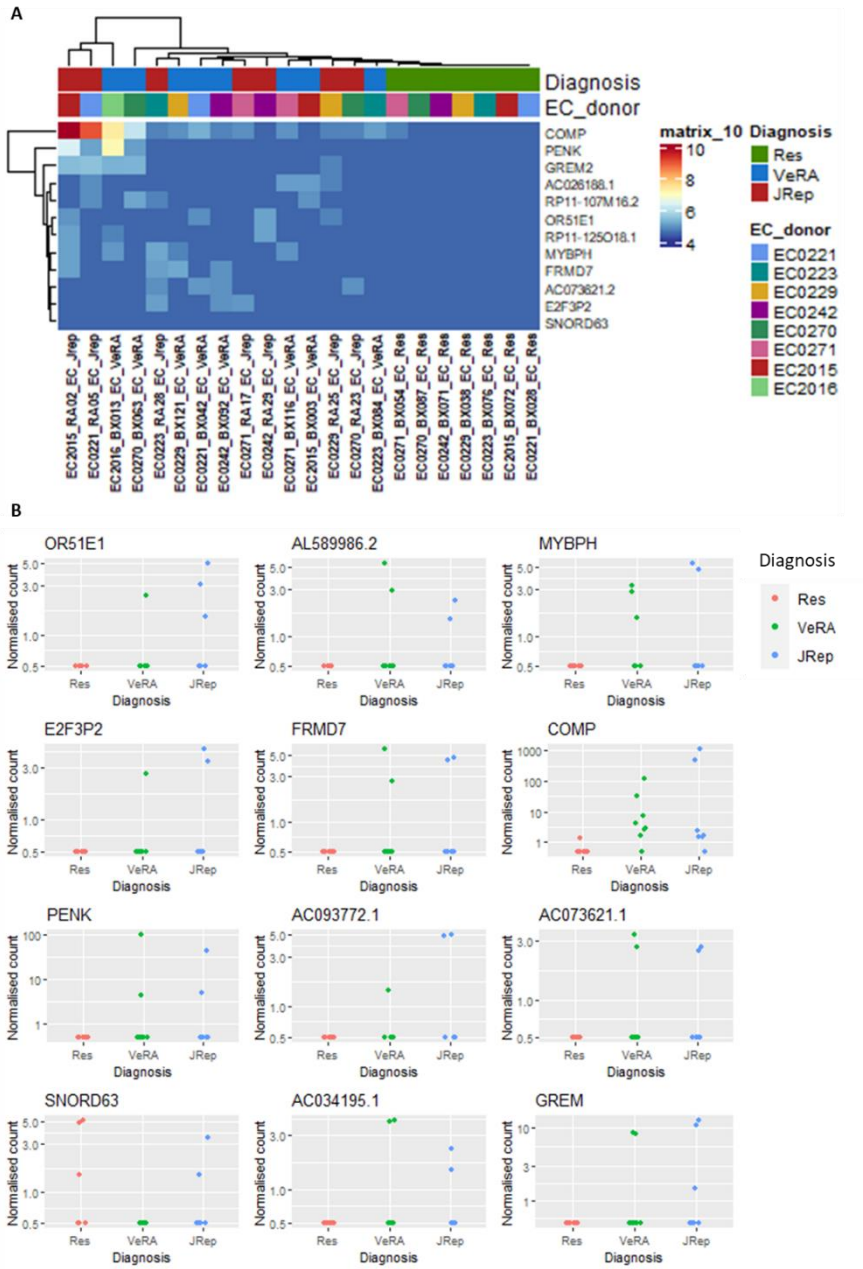

Figure 5.11: Differentially expressed genes between endothelial cells according to diagnosis of fibroblasts in co-culture appear to be largely driven by outliers. Bulk RNA sequencing was performed on RNA isolated from endothelial cells (ECs) co-cultured with fibroblasts from patients with resolving arthritis (Res), very early rheumatoid arthritis (VeRA) and RA patients undergoing joint replacement (JRep), or left as mono-cultures, and treated with TNF-α+IFNγ for 24 hours. Differential gene expression was performed with DEseq2 on the gene counts with sex genes removed of endothelial cells (ECs) to assess differences dependent on the diagnosis of fibroblasts in co-culture. The differentially expressed genes discovered were plotted as **(A)** a heatmap of the variance stabilising transformed counts, with hierarchal clustering on the columns and rows, and the bar coloured at the top according to fibroblast diagnosis and endothelial cell donor, and **(B)** normalised counts plots of the genes, with diagnosis of the x axis and gene counts on the y axis. Coloured according to the diagnosis of fibroblasts in co-culture; Res = resolving (red), VeRA = very early RA (green), JRep = joint replacement (blue).

A

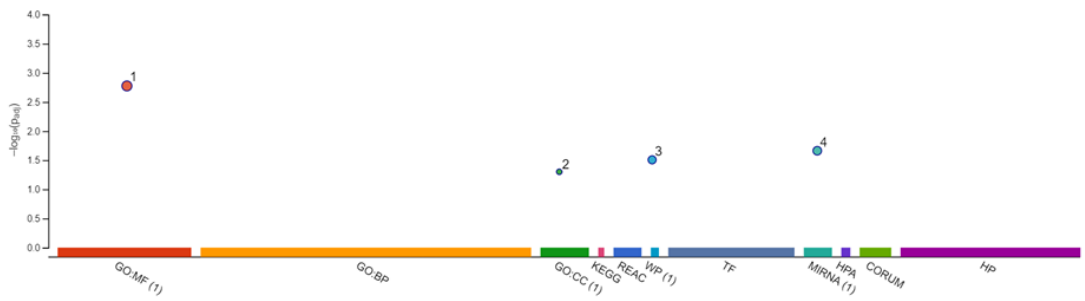

ID	Source	Term ID	Term Name	p_{adj} (query_1)
1	GO:MF	GO:0036122	BMP binding	1.677×10^{-3}
2	GO:CC	GO:0034592	synaptic vesicle lumen	4.994×10^{-2}
3	WP	WP:WP4789	MED and pseudoachondroplasia genes	3.115×10^{-2}
4	MIRNA	MIRNA:hsa-miR...	hsa-miR-4670-5p	2.173×10^{-2}

B

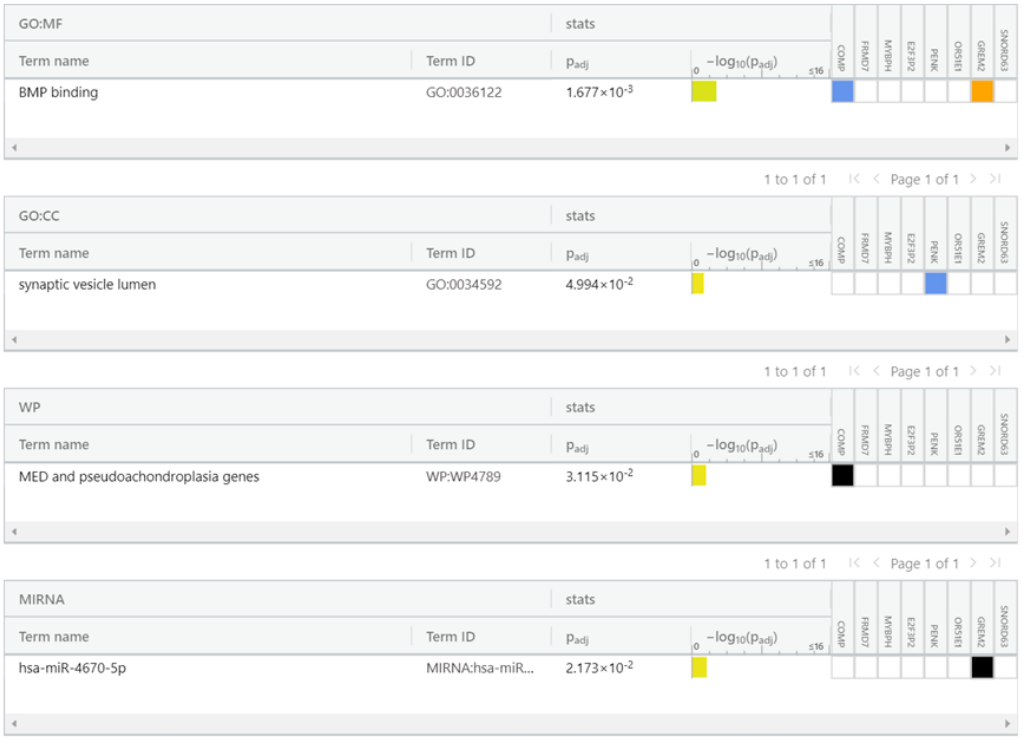

GO:MF

Term name	Term ID	p_{adj}	stats ($-\log_{10}(p_{adj})$, 0 to ≤16)
BMP binding	GO:0036122	1.677×10^{-3}	

1 to 1 of 1 Page 1 of 1

GO:CC

Term name	Term ID	p_{adj}	stats ($-\log_{10}(p_{adj})$, 0 to ≤16)
synaptic vesicle lumen	GO:0034592	4.994×10^{-2}	

1 to 1 of 1 Page 1 of 1

WP

Term name	Term ID	p_{adj}	stats ($-\log_{10}(p_{adj})$, 0 to ≤16)
MED and pseudoachondroplasia genes	WP:WP4789	3.115×10^{-2}	

1 to 1 of 1 Page 1 of 1

MIRNA

Term name	Term ID	p_{adj}	stats ($-\log_{10}(p_{adj})$, 0 to ≤16)
hsa-miR-4670-5p	MIRNA:hsa-miR...	2.173×10^{-2}	

Figure 5.12: Bone morphogenetic protein (BMP) signalling may play role in differences between endothelial cells dependent on co-cultured fibroblasts. Bulk RNA sequencing was performed on RNA isolated from endothelial cells (ECs) co-cultured with fibroblasts from patients with resolving arthritis (Res), very early rheumatoid arthritis (VeRA) and RA patients undergoing joint replacement (JRep) and treated with TNF-α+IFNγ for 24 hours. Differential gene expression was performed with DEseq2 on the gene counts of endothelial cells (ECs) with sex genes removed. The differential expressed genes. **(A)** Overview of results from pathway analysis and **(B)** Genes associated with each pathway from pathway analysis. Colours indicate where evidence for the gene in that pathway was obtained. Black = KEGG, Blue = electronic annotation, Orange = Biological aspect of ancestor. BMP = Bone morphogenetic protein. MED = multiple epiphyseal dysplasia.

5.2.4.3 Batch corrected endothelial cell analysis

Due to the very large effect of EC donor and/or batch (as the samples for each EC donor were prepared at separate times), limma batch correction was applied to the variance stabilizing transformed (VST) data. In the PCA, this removed the clustering according to EC donor (Figure 5.13A), and appeared to allow ECs to cluster, subtly, according to diagnosis (Figure 5.13B). However, counts plots (Figure 5.13B) of the genes contributing to differences identified in the biplot suggest the differences may be attributed to outliers (i.e., EC_RA02_Res at top of PCA, Figure 5.13A and B). Similarly, a heatmap of the top 100 variably expressed genes (Figure 5.14) showed some clustering by diagnosis, in particular of the JRep samples. This appeared to be largely driven by differences in mitochondrial gene expression.

Although the limma batch corrected data showed some potential effects of diagnosis, this batch correction did not change the original counts, therefore differential expression analysis could not be performed. In order to do this, ComBat-Seq batch correction was applied. For this, 3 replicates per batch were needed, therefore EC2016 (which had 1 missing sample, and 1 excluded in the QC) was removed from the analysis. PCA coloured according to batch showed no clustering batch indicating the EC donor/batch effect was removed, Figure 5.15A, and similar to the limma batch corrected samples they separated slightly according to the diagnosis of fibroblasts in culture (Figure 5.15B), with similar genes to the previous batch correction contributing to the principal components (TGFBI, IGFBP5, TNFAIP6 and COL6A). However, similarly to the limma corrected data, counts plots of the batch-corrected genes indicated that the separation may be driven by outliers, Figure 5.15C. Likewise, a heatmap of the top 100 variably expressed genes showed some clustering

according to diagnosis with ECs cultured with fibroblasts from JRep patients on the left (Figure 5.16). Again, this was driven by high mitochondrial gene expression in these JRep samples.

Differential gene expression was performed with DESeq2, and, showed the expected dispersion estimate, Figure 5.17A. The p value histograms (with lowly expressed genes removed) showed a conservative histogram (Figure 5.17B-D), with a large number of null p values. However, despite the higher number of significantly different genes, none had an absolute LogFC > 1, Figure 5.17E-G, suggesting no significantly large differences between treatment groups.

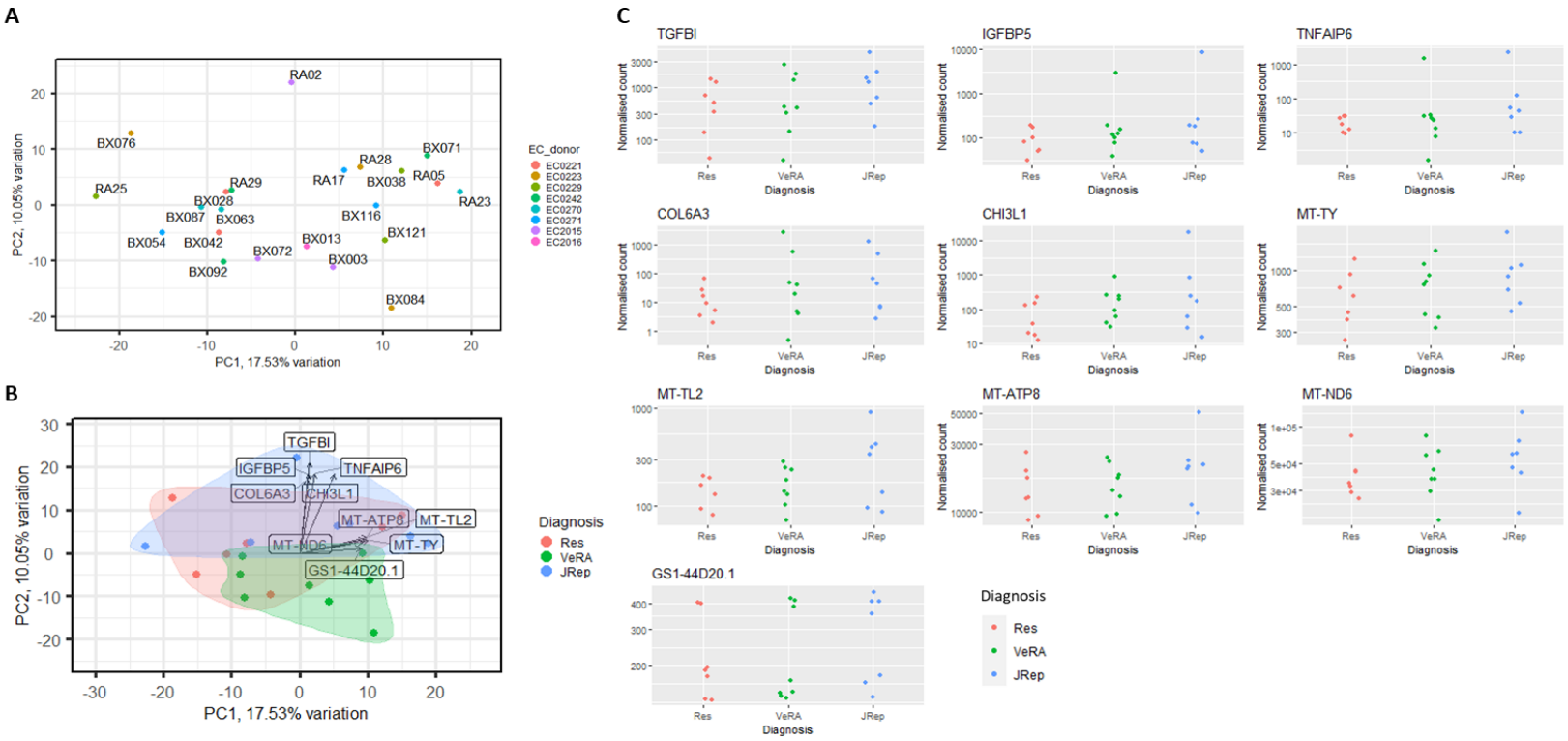

Figure 5.13: Limma batch corrected endothelial cell data showed some clustering according to diagnosis. Bulk RNA sequencing was performed on RNA isolated from endothelial cells (ECs) co-cultured with fibroblasts from patients with resolving arthritis (Res), very early rheumatoid arthritis (VeRA) and RA patients undergoing joint replacement (JRep) and treated with TNF-α+IFNγ for 24 hours. Differential gene expression was performed with DEseq2 on the gene counts of endothelial cells (ECs) with sex genes removed. Limma batch correction was performed on the variance stabilisation transformed (VST) data from the DEseq2 object and principal component analysis (PCA) performed. **(A-B)** PC1 and PC2 were plotted and coloured according to **(A)** EC donor and labelled according to the fibroblast donor in culture and **(B)** diagnosis of fibroblasts in culture, with diagnosis as group encircled and genes contributing to PC loadings shown with arrow. Genes that appeared to contribute to the PC loading were then plotted as **(C)** counts plots. Res = resolving, VeRA = very early RA, JRep = joint replacement. Res = resolving (red), VeRA = very early RA (green), JRep = joint replacement (blue).

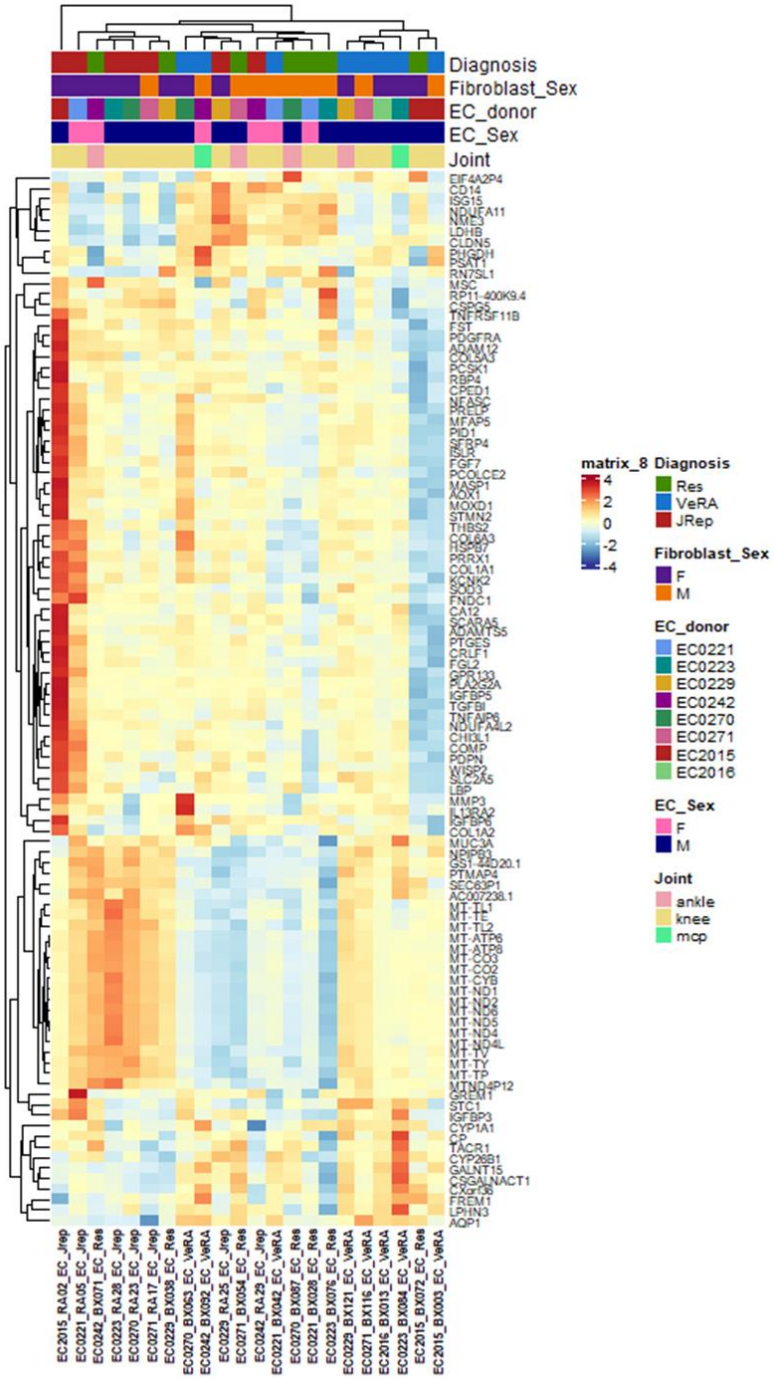

Figure 5.14: Limma corrected endothelial cells do not cluster by donor. Bulk RNA sequencing was performed on RNA isolated from endothelial cells (ECs) co-cultured with fibroblasts from patients with resolving arthritis (Res), very early rheumatoid arthritis (VeRA) and RA patients undergoing joint replacement (JRep) and treated with TNF-α+IFNγ for 24 hours. Gene counts of the ECs, with sex genes removed, was subject to differential expression with DESeq2 and variance stabilisation transformation (VST). Limma batch correction was performed on the VST data from the DEseq2 object and the top 100 most variably expressed genes plotted as a heatmap, with hierarchical clustering on the columns and rows. Coloured bar at the top indicates the sex, and diagnosis of fibroblast donor as well as joint of origin and sex and donor of endothelial cell. Res = resolving, VeRA = very early RA, JRep = joint replacement, F = female, M = male, MCP = metacarpophalangeal.

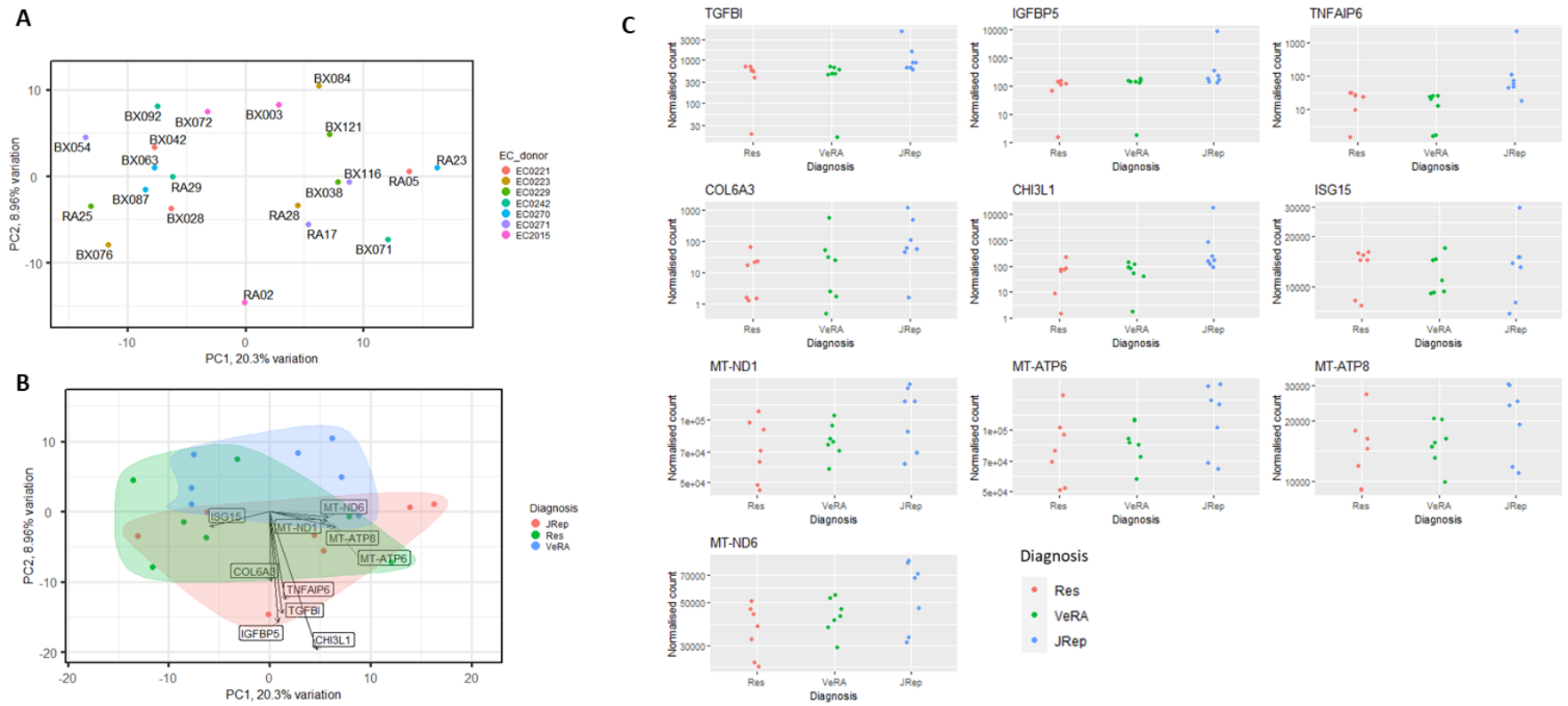

Figure 5.15: ComBat-Seq batch corrected endothelial cell data showed no clustering with donor and some clustering according to diagnosis. Bulk RNA sequencing was performed on RNA isolated from endothelial cells (ECs) donors co-cultured with fibroblasts from patients with resolving arthritis (Res), very early rheumatoid arthritis (VeRA) and RA patients undergoing joint replacement (JRep) and treated with TNF-α+IFNγ for 24 hours. ComBat-Seq batch correction was applied to the gene counts of the ECs, with sex genes removed. Principal component analysis of the variance stabilising transformed (VST) data was performed. **(A-B)** PCs 1 and 2 were plotted and coloured according to **(A)** EC donor and **(B)** diagnosis of fibroblasts in culture, with diagnosis as group encircled and genes contributing to PC loadings shown with arrows. Genes that appeared to contribute to the PC loading were then plotted as **(C)** counts plots, where the x axis is diagnosis and the y axis gene counts. Res = resolving, VeRA = very early RA, JRep = joint replacement.

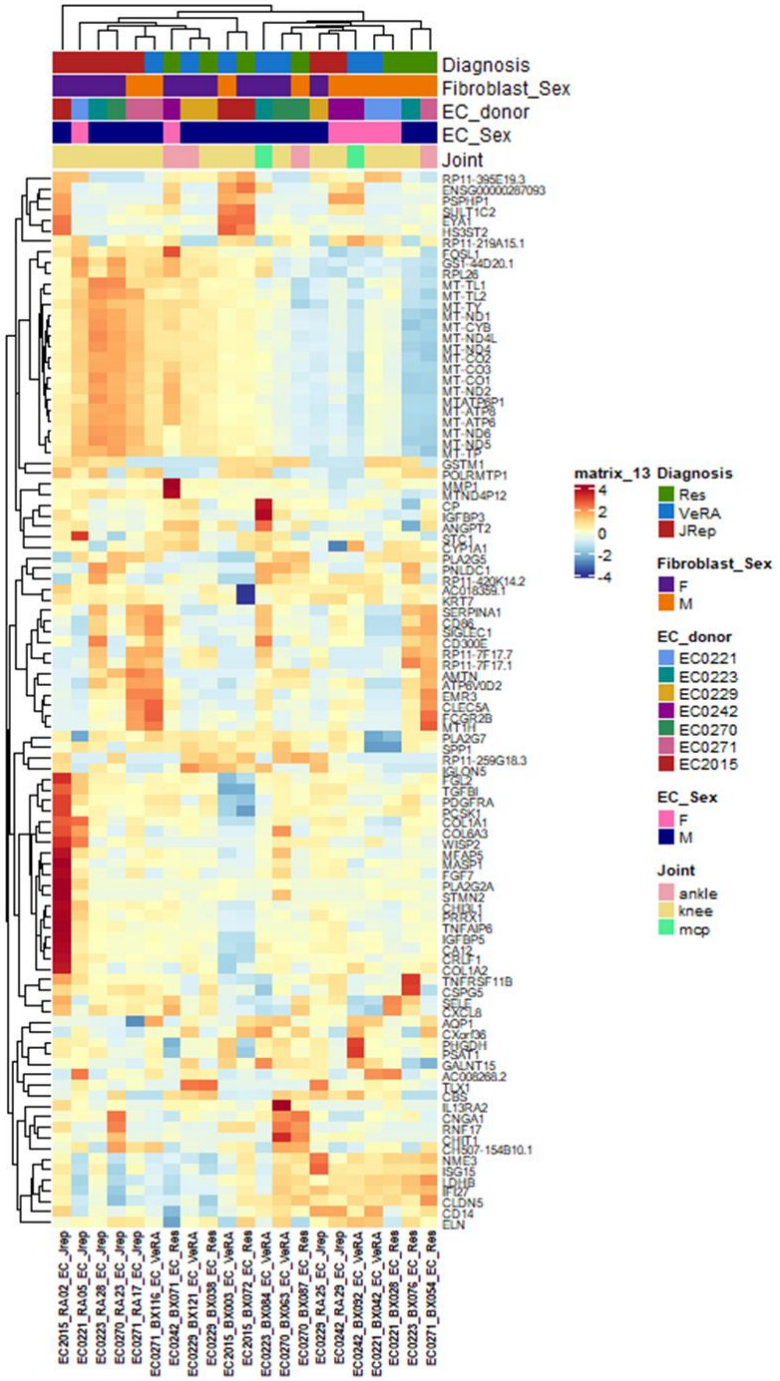

Figure 5.16: ComBat-Seq corrected endothelial cell data showed clustering according diagnosis of fibroblasts in culture. Bulk RNA sequencing was performed on RNA isolated from endothelial cells (ECs) co-cultured with fibroblasts from patients with resolving arthritis (Res), very early rheumatoid arthritis (VeRA) and RA patients undergoing joint replacement (JRep) and treated with TNF-α+IFNγ for 24 hours. ComBat-Seq batch correction was applied to the gene counts of the ECs, with sex genes removed. Variance stabilising transformation (VST) was applied and the top 100 most variably expressed genes plotted as a heatmap, with hierarchical clustering on the columns and rows. Coloured bar at the top indicates the sex, and diagnosis of fibroblast donor as well as joint of origin and sex and donor of endothelial cell. Res = resolving, VeRA = very early RA, JRep = joint replacement, F = female, M = male, MCP = metacarpophalangeal.

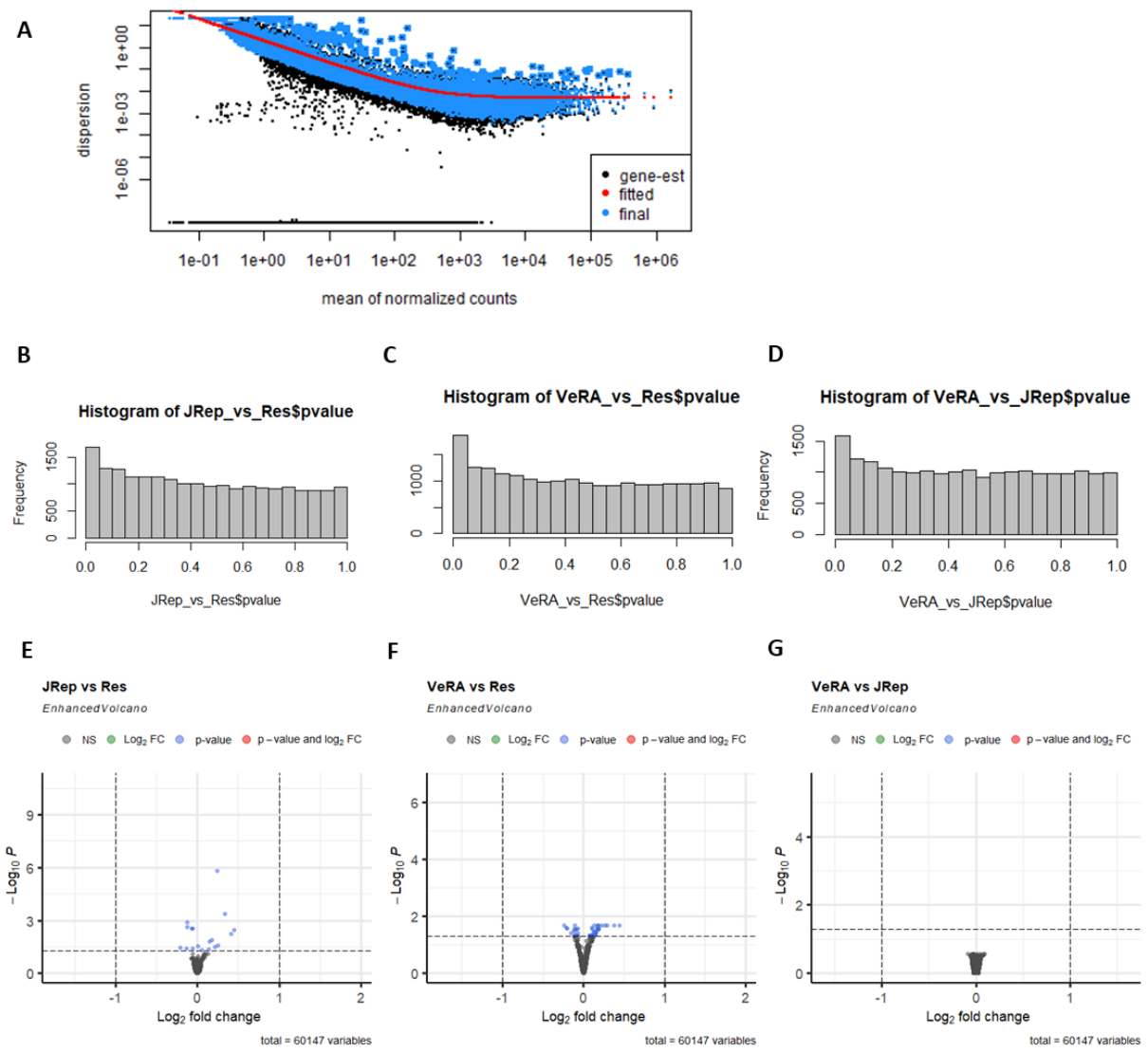

Figure 5.17: ComBat-Seq corrected endothelial cell data had no significantly differentially expressed genes depending on the fibroblasts in culture. Bulk RNA sequencing was performed on RNA isolated from endothelial cells (ECs) co-cultured with fibroblasts from patients with resolving arthritis (Res), very early rheumatoid arthritis (VeRA) and RA patients undergoing joint replacement (JRep) and treated with TNF-α+IFNγ for 24 hours. ComBat-Seq batch correction was applied to the gene counts of the ECs, with sex genes removed and differential gene expression was performed with DEseq2. **(A)** Dispersion estimates from DESeq2 and comparisons of **(B and E)** JRep vs Res, **(C and F)** VeRA vs Res **(D and G)** VeRA vs JRep. **(B-D)** P value histograms, with filtered out genes where there are less than 3 samples with normalized counts greater than or equal to 5. **(E-G)** Volcano plots of the comparisons, on the x axis the "ashr" shrunk Log2foldchange and on the y the –log10 adjusted p value. Significantly different gene expression shown in red.

5.2.5 JRep fibroblasts have differentially expressed genes compared Res and VeRA fibroblasts

5.2.5.1 Exploration of the variably expressed genes in fibroblasts co-cultured with ECs

Co-cultured fibroblasts were also analysed to observe differences according to diagnosis, and to investigate whether any pathways contributing to the differences may complement any changes observed in the endothelial cells or in the functional experiments. Initial biplot (Figure 5.18A), pairsplot (Figure 5.18B) and heatmap of the top 100 variably expressed genes (Figure 5.19) showed partial clustering of fibroblasts according to the diagnosis of the patient donor. In particular, fibroblasts from JRep clustered closely compared to VeRA and Res. Pairsplots coloured by EC donor (Figure 5.20A), sex of patient (Figure 5.20B) or joint (Figure 5.20C) suggest these factors did not strongly contribute to separations observed and so were not built into the DESeq2 model.

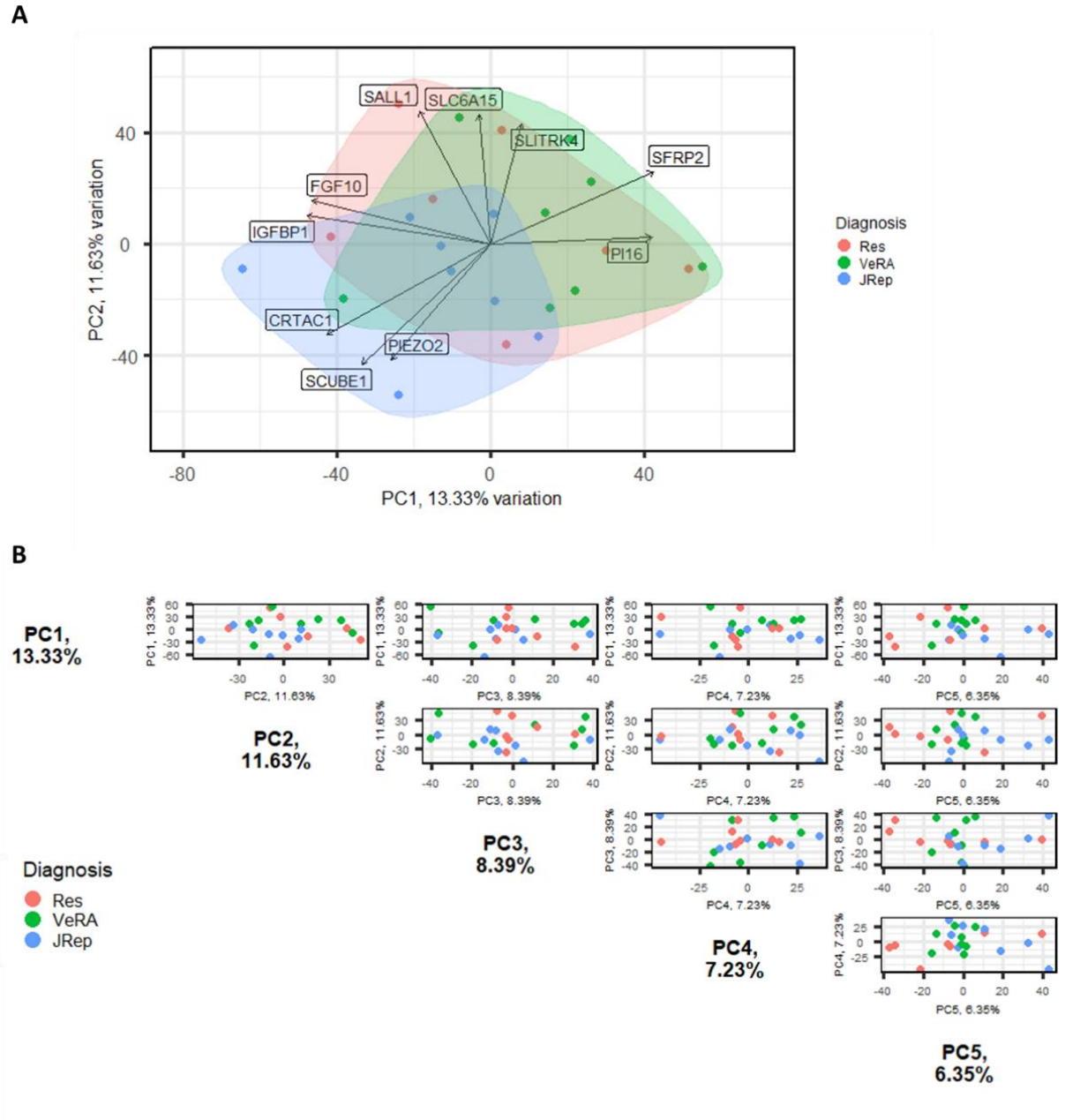

Figure 5.18: Fibroblasts clustered according to diagnosis in principal component analysis. Bulk RNA sequencing was performed on RNA isolated from fibroblasts from patients with resolving arthritis (Res), very early rheumatoid arthritis (VeRA) and RA patients undergoing joint replacement (JRep) in co-culture with endothelial cells (ECs) and treated with TNF-α+IFNγ for 24 hours. Sex genes were removed from the data and the gene counts were subject to variance stabilising transformation (VST) data and principal component analysis (PCA). **(A)** PCs 1 and 2 plotted with genes contributing to PCs shown with arrows. **(B)** Pairsplot of the top 5 PCs. Samples coloured according to the diagnosis of fibroblast donor. Res = resolving, VeRA = very early RA, JRep = joint replacement. Res = resolving, VeRA = very early RA, JRep = joint replacement.

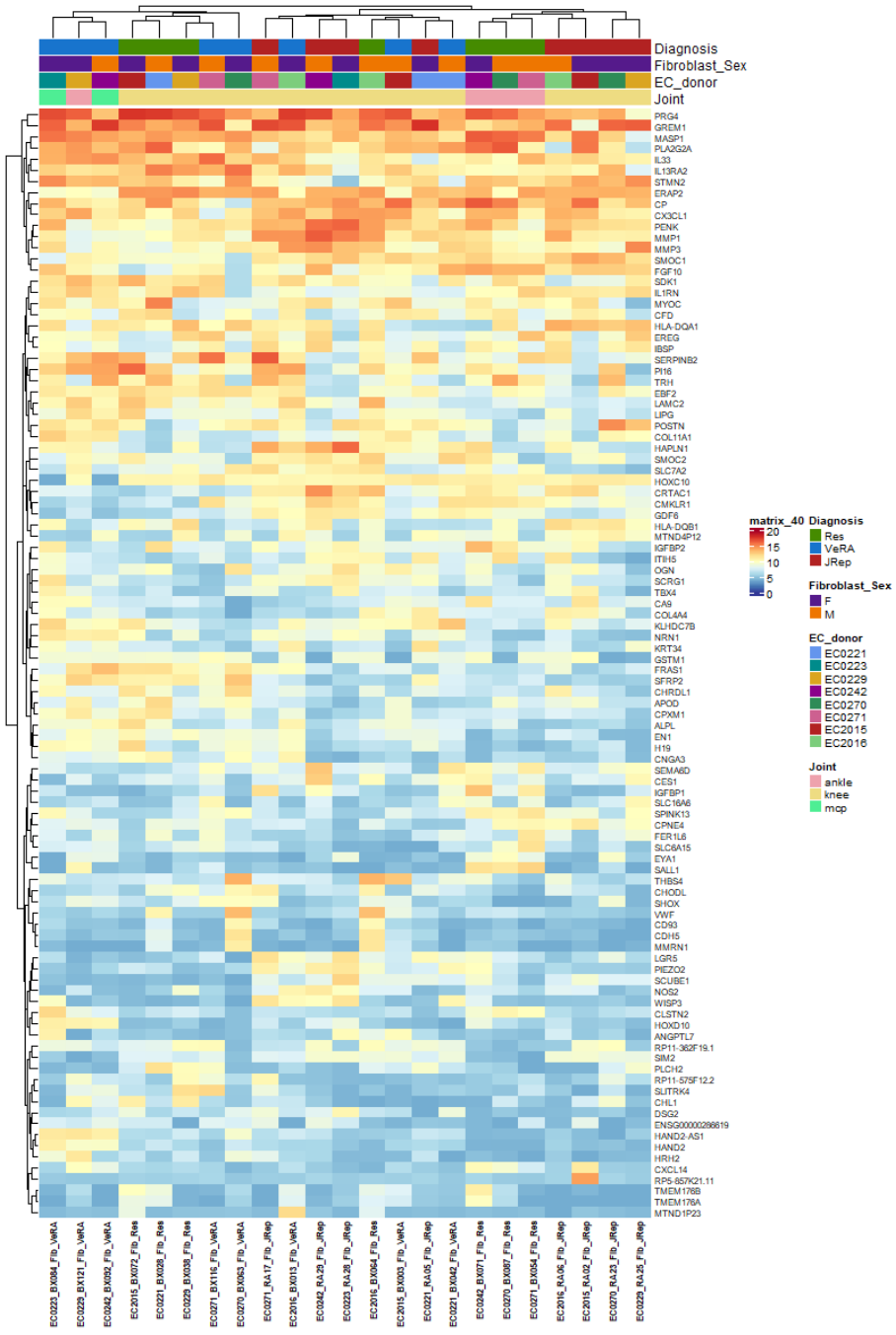

Figure 5.19: Fibroblasts clustered according to diagnosis in heatmap of the top 100 variably expressed genes. Bulk RNA sequencing was performed on RNA isolated from fibroblasts from patients with resolving arthritis (Res), very early rheumatoid arthritis (VeRA) and RA patients undergoing joint replacement (JRep) in co-culture with endothelial cells (ECs) and treated with TNF-α+IFNγ for 24 hours. Sex genes were removed from the data and the gene counts were subject to variance stabilising transformation (VST). The top 100 variably expressed genes were plotted as a heatmap, with clustering in the rows and columns. Coloured bar at the top indicates the sex, and diagnosis of fibroblast donor as well as joint of origin of fibroblasts and sex and donor of endothelial cell. Res = resolving, VeRA = very early RA, JRep = joint replacement, F = female, M = male, MCP = metacarpophalangeal.

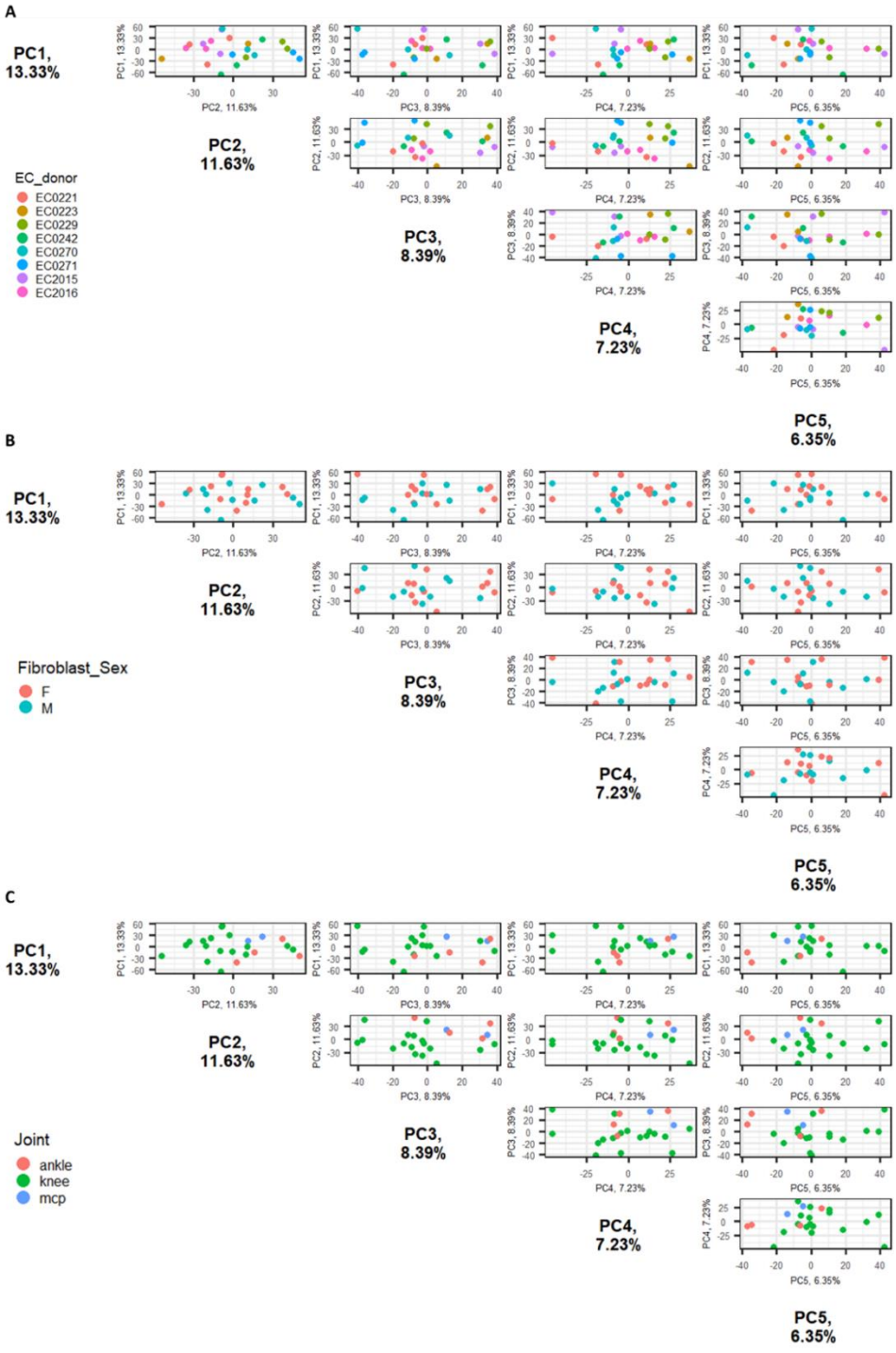

Figure 5.20: Fibroblasts did not cluster according to endothelial cell donor in co-culture, sex of fibroblast donor or joint location. Bulk RNA sequencing was performed on RNA isolated from fibroblasts from patients with resolving arthritis (Res), very early rheumatoid arthritis (VeRA) and RA patients undergoing joint replacement (JRep) in co-culture with endothelial cells (ECs) and treated with TNF-α+IFNγ for 24 hours. Sex genes were removed from the data and the gene counts were subject to variance stabilising transformation (VST) and principal component analysis (PCA). Pairsplots of the top 5 PCs were plotted. Samples coloured according to **(A)** Endothelial cell donor **(B)** Fibroblast sex and **(C)** joint location origin of the fibroblast. Res = resolving, VeRA = very early RA, JRep = joint replacement, F = female, M = male, MCP = metacarpophalangeal

5.2.5.2 Differential gene expression and pathway analysis in fibroblasts co-cultured with ECs

Differential expression analysis was performed in DESeq2 and, similarly to the endothelial data, had expected dispersion estimates (Figure 5.21A). Upon filtering out lowly expressed genes, p-value histograms had a conservative distribution (Figure 5.21 B-D). As shown in the volcano plots (Figure 5.21 G-I), there are more differentially expressed genes comparing JRep and Res (40 DEGs) and JRep and VeRA (28 DEGs) than VeRA and Res (4 DEGs). The significantly differentially expressed genes (Padj < 0.05 and log2FC > 1 or <-1) are given in Table 5.3 for "VeRA vs JRep", Table 5.4 for "VeRA vs Res" and Table 5.5 for "JRep vs Res". Plotting the DEGs of "JRep vs VeRA" and "JRep vs Res" as a heatmap (Figure 5.22 A and B) did reveal some clustering according to diagnosis. Again, clustering was between JRep vs VeRA+Res, and less between VeRA and Res. This suggests a there are transcriptomic differences between JRep and VeRA and JRep and Res fibroblasts, but less so between VeRA and Res.

Pathway analysis was then carried out on the DEGs in "VeRA vs JRep" and "JRep vs Res". KEGG pathway analysis (Figure 5.23) identified similar pathways involved in both comparisons, such as cytokine-cytokine receptor interaction, cell adhesion molecules and ECM-receptor interactions. Similarly, g profiler pathway analysis (Figure 5.24) suggested cell signalling pathways and migration pathways are involved, and in particular the IL-36 signalling pathway for the DEGs of both comparisons. Gene set enrichment analysis of the hallmark pathways identified the enriched pathways for each comparison, given in Table 5.6, Table 5.7 and Table 5.8. Of particular interest was the enrichment of the IL6_JAK_STAT3

pathway, in “JRep vs Res” and “VeRA vs JRep”. The enrichment plot and heatmap of genes from this pathway are shown in Figure 5.25.

Counts plots for the genes of interest identified in the differential expression or pathway analysis are given in Figure 5.26. COMP was chosen due to its differential expression in ECs (Figure 5.26A). It appeared higher in the JRep compared to VeRA and Res samples, although the adjusted p values for differential expression were not significant. IL-36RN and IL-36B (Figure 5.26B-C) were plotted due to being significantly downregulated in JRep compared to VeRA and Res samples. IL-6-JAK-STAT signalling molecules were also plotted due to the involvement of this pathway indicated in the GSEA analysis. In particular, IL-6, SOCS3, SOCS1 and TGF-β1 (Figure 5.26D-G respectively) were plotted due to known involvement of these molecules in the previous co-culture experiments (9). There was slight upregulation of IL-6 and downregulation of SOCS3 in JRep samples, but no large differences were observed for SOCS1 and TGF-β1. TNF (Figure 5.26H) and ACVRL1 (Figure 5.26I) were 2 key differentially regulated molecules indicated in the IL-6-JAK-STAT pathway from the GSEA analysis (Figure 5.25), and appeared down regulated in the JRep samples compared to VeRA and JRep.

In summary, it appears that IL-6-JAK-STAT signalling, as well as IL-36 signalling, in fibroblasts contributes to the separation in JRep compared to Res or VeRA patients. However, there was no clear differential expression between the Res and VeRA fibroblasts.

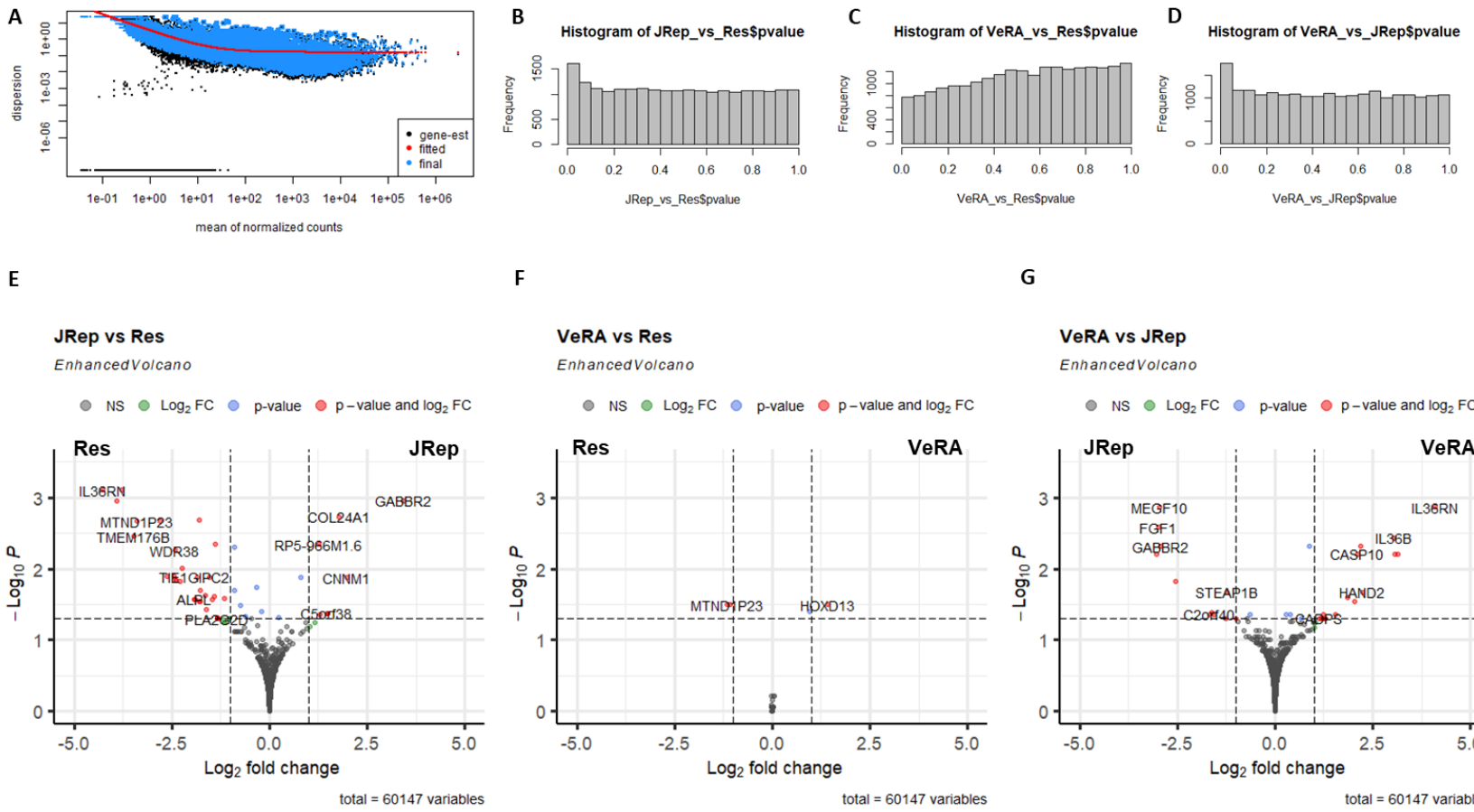

Figure 5.21: Fibroblasts exhibited differential gene expression according to diagnosis. Bulk RNA sequencing was performed on RNA isolated from fibroblasts from patients with resolving arthritis (Res), very early rheumatoid arthritis (VeRA) and RA patients undergoing joint replacement (JRep) in co-culture with endothelial cells (ECs) and treated with TNF-α+IFNγ for 24 hours. Sex genes were removed from the analysis and the gene counts were subject to differential gene expression analysis in DESeq2. **(A)** Dispersion estimates from DESeq2 and comparisons of **(B and E)** JRep vs Res, **(C and F)** VeRA vs Res **(D and G)** VeRA vs JRep. **(B-D)** P value histograms, with filtered out genes where there are less than 3 samples with normalized counts greater than or equal to 5. **(E-G)** Volcano plots of the comparisons, on the x axis the "ashr" shrunk Log2foldchange and on the y the –log10 adjusted p value. Significantly different gene expression shown in red.

Table 5.3: Significant DEGs between VeRA and JRep fibroblasts co-cultured with HUVECs

Ensembl ID	Entrez ID	HGNC symbol	log2FoldChange	Pvalue	Padj
ENSG00000141052	93649	MYOCD	-5.352631253	3.47E-06	0.006231743
ENSG00000101282	343637	RSPO4	-4.514871174	3.56E-05	0.041353557
ENSG00000108602	218	ALDH3A1	-4.128681802	9.13E-06	0.015040275
ENSG00000258545	101928969	RHOXF1-AS1	-3.7510057	4.83E-05	0.043378192
ENSG00000136928	9568	GABBR2	-3.633816226	1.51E-06	0.004839153
ENSG00000113578	2246	FGF1	-3.531307514	3.99E-07	0.002630699
ENSG00000145794	84466	MEGF10	-3.419441911	1.38E-07	0.001362045
ENSG00000119147	84417	ECRG4	-3.203556356	4.39E-05	0.043373802
ENSG00000248491	NA	NA	-2.236240788	6.90E-05	0.049627507
ENSG00000140807	85407	NKD1	-1.671957887	7.28E-05	0.049627507
ENSG00000105889	256227	STEAP1B	-1.514460518	1.51E-05	0.021325501
ENSG00000272143	283481	FGF14-AS2	1.021298727	7.18E-05	0.049627507
ENSG00000205336	9289	ADGRG1	2.145350935	6.65E-05	0.049627507
ENSG00000102760	28984	RGCC	2.223643627	8.06E-05	0.049783671
ENSG00000003400	843	CASP10	2.455143187	3.39E-06	0.006231743
ENSG00000164659	222223	ELAPOR2	2.46807051	1.62E-06	0.004839153
ENSG00000136918	401551	WDR38	2.537233276	1.89E-05	0.024916255
ENSG00000088882	56265	CPXM1	3.072429998	5.23E-05	0.043378192
ENSG00000113296	7060	THBS4	3.430847915	2.30E-05	0.028372493
ENSG00000124440	64344	HIF3A	3.632466761	8.06E-05	0.049783671
ENSG00000158258	64084	CLSTN2	3.703863411	7.61E-05	0.049783671
ENSG00000136696	27177	IL36B	3.723695166	7.42E-07	0.003669065
ENSG00000164107	9464	HAND2	4.359127051	1.51E-05	0.021325501
ENSG00000163618	8618	CADPS	4.685179945	6.48E-05	0.049627507
ENSG00000237125	79804	HAND2-AS1	4.721857595	2.60E-06	0.006231743
ENSG00000164251	2150	F2RL1	4.796944623	3.32E-06	0.006231743
ENSG00000110799	7450	VWF	5.180515621	4.39E-05	0.043373802
ENSG00000136695	26525	IL36RN	5.424338647	8.78E-08	0.001362045

Table 5.4: Significant DEGs between VeRA and Res fibroblasts do-cultured with HUVECs

Ensembl ID	Entrez ID	HGNC symbol	log2FoldChange	Pvalue	Padj
ENSG00000225972	1.01E+08	MTND1P23	-4.058734749	2.37E-06	0.031855257
ENSG00000137441	83888	FGFBP2	-3.254018501	1.76E-06	0.031855257
ENSG00000237125	79804	HAND2-AS1	4.804092616	3.87E-06	0.039036627
ENSG00000128714	3239	HOXD13	8.869858905	2.24E-06	0.031855257

Table 5.5: Significant DEGs between JRep and Res fibroblasts co-cultured with HUVECs

Ensembl ID	Entrez ID	HGNC symbol	log2FoldChange	Pvalue	Padj
ENSG00000106565	28959	TMEM176B	-6.9674124	1.44E-06	0.00352324
ENSG00000103449	6299	SALL1	-6.903948469	5.16E-05	0.032526849
ENSG00000043355	7546	ZIC2	-6.703539554	1.15E-05	0.013373394
ENSG00000066056	7075	TIE1	-5.818337202	9.37E-06	0.012912411
ENSG00000136695	26525	IL36RN	-5.640064828	5.29E-08	0.000789776
ENSG00000110799	7450	VWF	-5.397502858	3.90E-05	0.026869328
ENSG00000146070	7941	PLA2G7	-5.056998411	2.02E-07	0.001114112
ENSG00000147485	137902	PXDNL	-4.622210956	7.16E-08	0.000789776
ENSG00000256513	NA	NA	-4.299752279	4.29E-05	0.028554827
ENSG00000225972	1.01E+08	MTND1P23	-4.261605437	7.77E-07	0.002140976
ENSG00000188859	149297	FAM78B	-3.645363885	6.10E-05	0.037337831
ENSG00000135218	948	CD36	-3.578498064	8.83E-06	0.012912411
ENSG00000162551	249	ALPL	-3.458328754	3.78E-05	0.026869328
ENSG00000088882	56265	CPXM1	-3.407502181	1.46E-05	0.014596666
ENSG00000038945	4481	MSR1	-3.393577207	1.37E-05	0.014376486
ENSG00000165272	360	AQP3	-3.226089951	1.56E-05	0.015005368
ENSG00000163995	84448	ABLIM2	-3.192154462	7.34E-07	0.002140976
ENSG00000136696	27177	IL36B	-3.17837514	4.40E-05	0.028554827
ENSG00000117215	26279	PLA2G2D	-3.156662994	0.000100592	0.049825916
ENSG00000125144	4495	MT1G	-3.142597457	0.000101672	0.049825916
ENSG00000205037	400553	LOC400553	-3.133829409	3.69E-05	0.026869328
ENSG00000136918	401551	WDR38	-2.787885753	3.23E-06	0.005482166
ENSG00000122121	7512	XPNPEP2	-2.694090716	9.20E-05	0.04828295
ENSG00000168079	286133	SCARA5	-2.642534713	6.19E-06	0.009745964
ENSG00000205336	9289	ADGRG1	-2.352346093	2.37E-05	0.020113148
ENSG00000164659	222223	ELAPOR2	-2.226911289	2.90E-05	0.023680696
ENSG00000223458	1.04E+08	LMO7DN-IT1	-1.89898875	5.59E-07	0.00205375
ENSG00000101187	28231	SLCO4A1	-1.881907632	3.14E-05	0.024711005
ENSG00000137960	54810	GIPC2	-1.759677958	1.01E-05	0.013102913
ENSG00000178734	729420	LMO7DN	-1.555151022	3.39E-05	0.025795376
ENSG00000137727	57569	ARHGAP20	-1.479083893	2.14E-06	0.004550928
ENSG00000272143	283481	FGF14-AS2	-1.115188565	2.30E-05	0.020113148
ENSG00000139567	94	ACVRL1	-1.077048938	8.73E-05	0.046937833
ENSG00000243696	NA	NA	1.347493842	2.27E-06	0.004550928
ENSG00000171502	255631	COL24A1	1.87433046	4.19E-07	0.001849127
ENSG00000119946	26507	CNNM1	2.422663719	1.12E-05	0.013373394
ENSG00000235601	1.02E+08	BARX1-DT	3.604328198	7.40E-05	0.041819573
ENSG00000186493	153571	C5orf38	3.883292068	7.37E-05	0.041819573
ENSG00000136928	9568	GABBR2	4.110838505	1.89E-07	0.001114112
ENSG00000101282	343637	RSPO4	4.446795417	7.85E-05	0.043273022

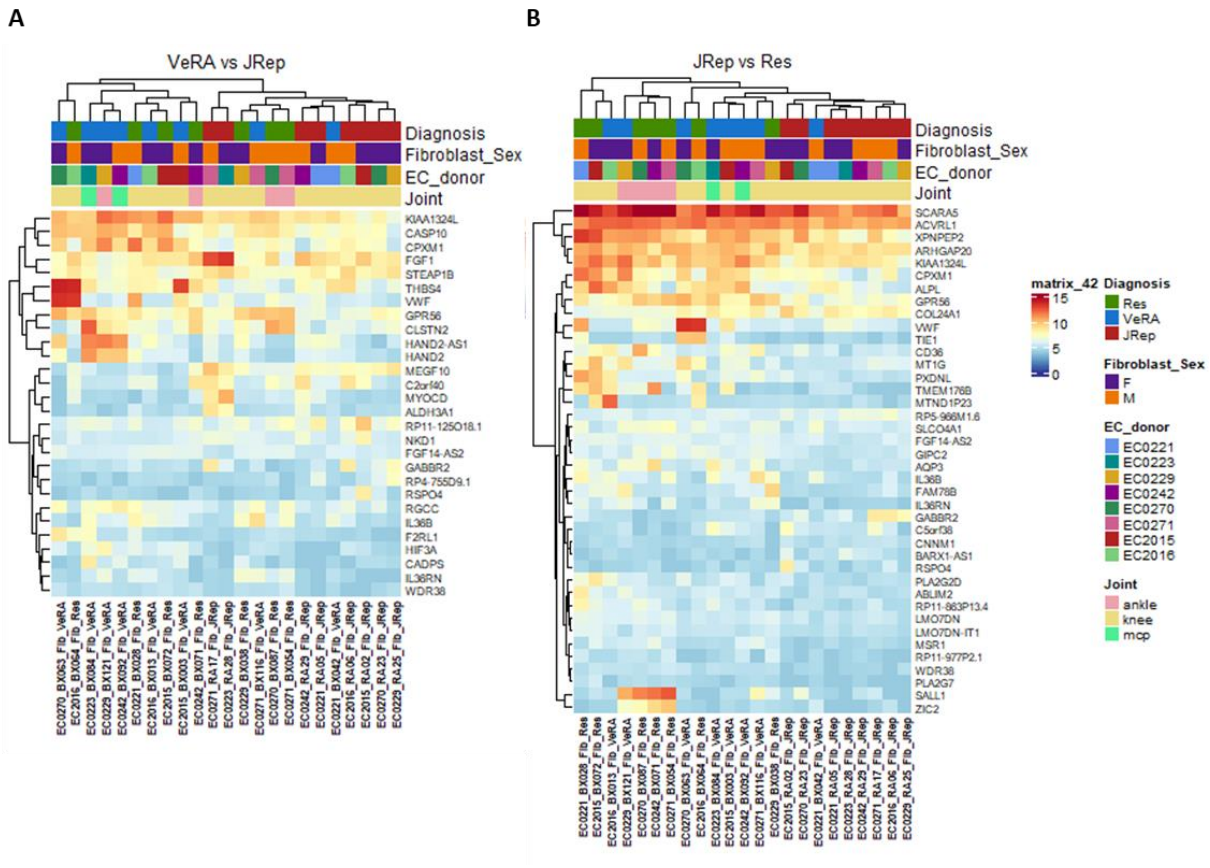

Figure 5.22: Differentially expressed genes in fibroblasts cluster according to diagnosis. Bulk RNA sequencing was performed on RNA isolated from fibroblasts from patients with resolving arthritis (Res), very early rheumatoid arthritis (VeRA) and RA patients undergoing joint replacement (JRep) in co-culture with endothelial cells (ECs) and treated with TNF-α+IFNγ for 24 hours. Sex genes were removed from the analysis and the gene counts were subject to differential gene expression analysis in DESeq2 with filter out genes counts where there are less than 3 samples with normalized counts greater than or equal to 5. Heatmaps of the differentially expressed genes between **(A)** VeRA and JRep and **(B)** JRep and Res with clustering on the columns and rows. Coloured bars at the top correspond to diagnosis and sex of fibroblast patient donors, and joint origin of fibroblasts in culture, as well as the EC donor in culture.

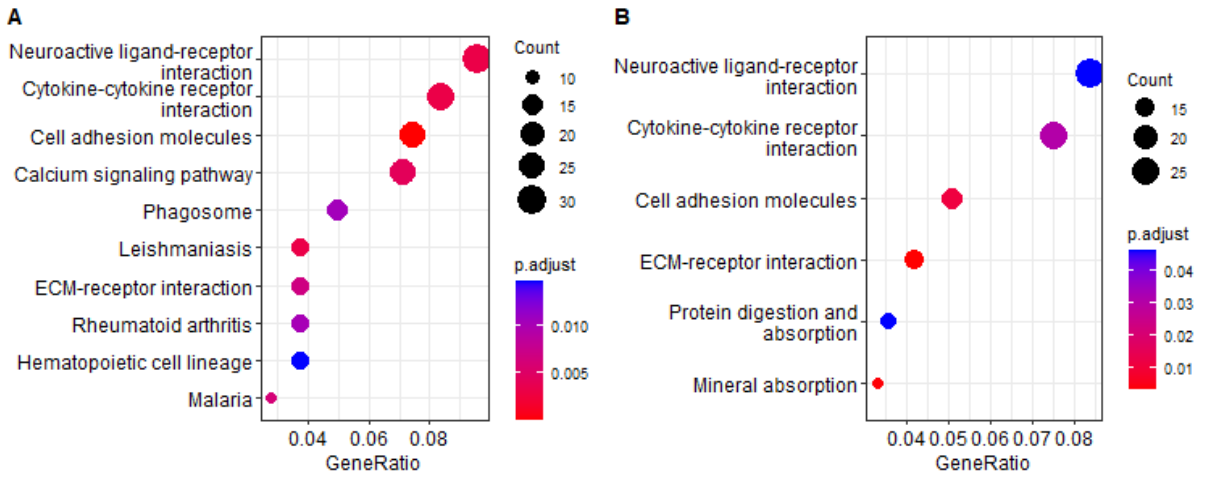

Figure 5.23: Cytokine-cytokine interaction, cell adhesion molecules and ECM-receptor interactions are enriched in fibroblasts. Bulk RNA sequencing was performed on RNA isolated from fibroblasts from patients with resolving arthritis (Res), very early rheumatoid arthritis (VeRA) and RA patients undergoing joint replacement (JRep) in co-culture with endothelial cells (ECs) and treated with TNF-α+IFNγ for 24 hours. Sex genes were removed from the analysis and the gene counts were subject to differential gene expression analysis in DESeq2 with filter out genes counts where there are less than 3 samples with normalized counts greater than or equal to 5. The significantly (Padj < 0.1) differentially expressed genes of **(A)** VeRA vs JRep and **(B)** JRep vs Res, were put through KEGG pathway enrichment analysis and dot plot of the results generated. The y-axis gives pathway name, x-axis the percentage of significant genes of the total genes in the pathway. Dot size indicates the number of genes in the pathway, and colour the adjusted p value (red < purple < blue). Full pathways indicating the upregulated and downregulated genes are shown in appendix Figures for the cell adhesion molecules (Appendix Figure 3, JRep vs Res; Appendix Figure 4, VeRA vs JRep) and cytokine-cytokine receptor interaction pathways (Appendix Figure 5, JRep vs Res; Appendix Figure 6, VeRA vs JRep).

A

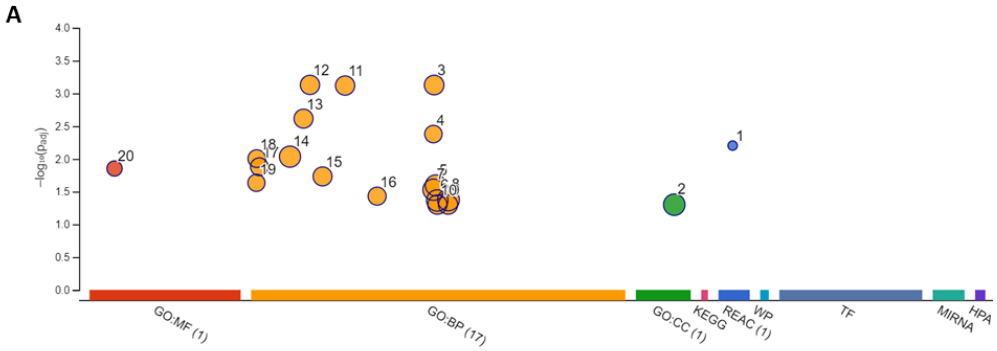

ID	Source	Term ID	Term Name	p_{adj} (query_1)
1	REAC	REAC:R-HSA-90...	Interleukin-36 pathway	6.260×10^{-3}
2	GO:CC	GO:0071944	cell periphery	4.995×10^{-2}
3	GO:BP	GO:0048584	positive regulation of response to stimulus	7.447×10^{-4}
4	GO:BP	GO:0048514	blood vessel morphogenesis	4.285×10^{-3}
5	GO:BP	GO:0048731	system development	2.535×10^{-2}
6	GO:BP	GO:0048856	anatomical structure development	4.312×10^{-2}
7	GO:BP	GO:0048522	positive regulation of cellular process	2.946×10^{-2}
8	GO:BP	GO:0051716	cellular response to stimulus	4.218×10^{-2}
9	GO:BP	GO:0051674	localization of cell	4.991×10^{-2}
10	GO:BP	GO:0048870	cell motility	4.991×10^{-2}
11	GO:BP	GO:0023056	positive regulation of signaling	7.589×10^{-4}
12	GO:BP	GO:0010647	positive regulation of cell communication	7.410×10^{-4}
13	GO:BP	GO:0009967	positive regulation of signal transduction	2.426×10^{-3}
14	GO:BP	GO:0007275	multicellular organism development	9.234×10^{-3}
15	GO:BP	GO:0016477	cell migration	1.85×10^{-2}
16	GO:BP	GO:0035239	tube morphogenesis	3.704×10^{-2}
17	GO:BP	GO:0001944	vasculature development	1.317×10^{-2}
18	GO:BP	GO:0001568	blood vessel development	9.892×10^{-3}
19	GO:BP	GO:0001525	angiogenesis	2.318×10^{-2}
20	GO:MF	GO:0008201	heparin binding	1.401×10^{-2}

B

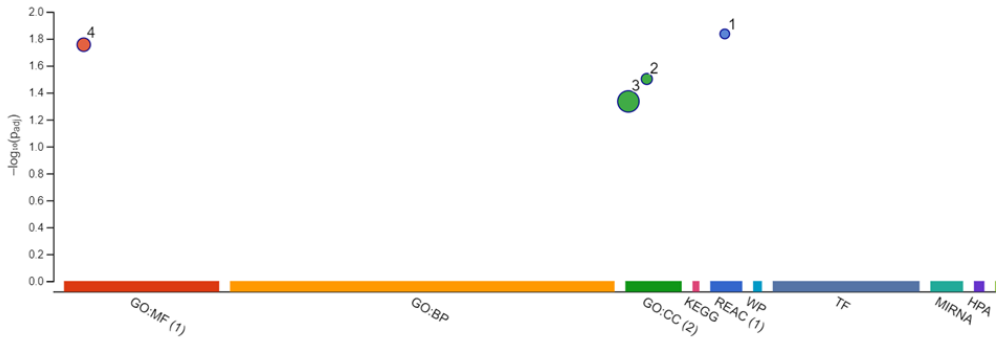

ID	Source	Term ID	Term Name	p_{adj} (query_1)
1	REAC	REAC:R-HSA-90...	Interleukin-36 pathway	1.459×10^{-2}
2	GO:CC	GO:0034362	low-density lipoprotein particle	3.153×10^{-2}
3	GO:CC	GO:0005576	extracellular region	4.629×10^{-2}
4	GO:MF	GO:0005044	scavenger receptor activity	1.74×10^{-2}

Figure 5.24: Pathway analysis with g Profiler showed IL-36 pathway was upregulated. Bulk RNA sequencing was performed on RNA isolated from the fibroblasts of patients with resolving arthritis (Res), very early rheumatoid arthritis (VeRA) and RA patients undergoing joint replacement (JRep) in co-culture with endothelial cells (ECs) and treated with TNF-α+IFNγ for 24 hours. Sex genes were removed from the analysis and the gene counts were subject to differential gene expression analysis in DESeq2 with filtered out genes counts where there are less than 3 samples with normalized counts greater than or equal to 5. The significantly (Padj < 0.05) differentially expressed genes of **(A)** VeRA vs JRep and **(B)** JRep vs Res, were submitted to gProfiler for functional enrichment analysis.

Table 5.6: Significantly enriched pathways (<0.25% FDR) of hallmark pathways comparing "JRep vs Res" fibroblasts

	GS	NES	NOM p-val	FDR q-val
JRep				
1	HALLMARK_G2M_CHECKPOINT	2.84	0	0
2	HALLMARK_E2F_TARGETS	2.74	0	0
3	HALLMARK_MITOTIC_SPINDLE	1.52	0	0.037
Res				
1	HALLMARK_IL6_JAK_STAT3_SIGNALING	-1.73	0	0.023
2	HALLMARK_INFLAMMATORY_RESPONSE	-1.71	0	0.015
3	HALLMARK_HYPOXIA	-1.67	0	0.014
4	HALLMARK_REACTIVE_OXYGEN_SPECIES_PATHWAY	-1.54	0.017	0.061
5	HALLMARK_COAGULATION	-1.47	0.012	0.094
6	HALLMARK_CHOLESTEROL_HOMEOSTASIS	-1.46	0.028	0.091
7	HALLMARK_APICAL_JUNCTION	-1.46	0.005	0.079
8	HALLMARK_COMPLEMENT	-1.44	0.01	0.083
9	HALLMARK_PROTEIN_SECRETION	-1.42	0.029	0.087
10	HALLMARK_ADIPOGENESIS	-1.41	0.013	0.086
11	HALLMARK_APOPTOSIS	-1.39	0.02	0.098
12	HALLMARK_KRAS_SIGNALING_UP	-1.34	0.033	0.146
13	HALLMARK_FATTY_ACID_METABOLISM	-1.33	0.046	0.14
14	HALLMARK_MYOGENESIS	-1.29	0.054	0.181
15	HALLMARK_OXIDATIVE_PHOSPHORYLATION	-1.28	0.058	0.179
16	HALLMARK_HEME_METABOLISM	-1.24	0.067	0.237

Table 5.7: Significantly enriched pathways (<0.25% FDR) of hallmark pathways comparing "VeRA vs JRep" fibroblasts

	GS	NES	NOM p-val	FDR q-val
VeRA				
1	HALLMARK_IL6_JAK_STAT3_SIGNALING	1.7	0.005	0.039
2	HALLMARK_INFLAMMATORY_RESPONSE	1.58	0	0.048
3	HALLMARK_HYPOXIA	1.38	0	0.125
4	HALLMARK_KRAS_SIGNALING_UP	1.36	0.008	0.107
5	HALLMARK_APICAL_SURFACE	1.36	0.068	0.087
6	HALLMARK_TNFA_SIGNALING_VIA_NFKB	1.34	0.02	0.084
7	HALLMARK_ANGIOGENESIS	1.33	0.088	0.081
8	HALLMARK_COAGULATION	1.27	0.029	0.106
9	HALLMARK_EPITHELIAL_MESENCHYMAL_TRANSITION	1.25	0.008	0.108
10	HALLMARK_COMPLEMENT	1.2	0.085	0.142
11	HALLMARK_HEDGEHOG_SIGNALING	1.17	0.219	0.16
12	HALLMARK_SPERMATOGENESIS	1.15	0.154	0.187
13	HALLMARK_CHOLESTEROL_HOMEOSTASIS	1.1	0.247	0.247
JRep				
1	HALLMARK_E2F_TARGETS	-2.3	0	0
2	HALLMARK_G2M_CHECKPOINT	-2.23	0	0
3	HALLMARK_MITOTIC_SPINDLE	-2.04	0	0
4	HALLMARK_INTERFERON_ALPHA_RESPONSE	-1.86	0	0
5	HALLMARK_INTERFERON_GAMMA_RESPONSE	-1.69	0	0.004
6	HALLMARK_ESTROGEN_RESPONSE_LATE	-1.58	0	0.017
7	HALLMARK_TGF_BETA_SIGNALING	-1.46	0.022	0.069
8	HALLMARK_HEME_METABOLISM	-1.34	0.031	0.196

Table 5.8: Significantly enriched pathways (<0.25% FDR) of hallmark pathways comparing "VeRA vs Res" fibroblasts

	GS	*NES*	*NOM p-val*	*FDR q-val*
VeRA				
1	HALLMARK_EPITHELIAL_MESENCHYMAL_TRANSITION	1.45	0	0.118
2	HALLMARK_HEDGEHOG_SIGNALING	1.27	0.114	0.24
3	HALLMARK_ANGIOGENESIS	1.24	0.115	0.191
Res				
1	HALLMARK_INTERFERON_ALPHA_RESPONSE	-2.05	0	0
2	HALLMARK_INTERFERON_GAMMA_RESPONSE	-1.71	0	0.006
3	HALLMARK_REACTIVE_OXYGEN_SPECIES_PATHWAY	-1.68	0.001	0.006
4	HALLMARK_FATTY_ACID_METABOLISM	-1.66	0	0.007
5	HALLMARK_HEME_METABOLISM	-1.65	0	0.007
6	HALLMARK_ADIPOGENESIS	-1.59	0	0.012
7	HALLMARK_OXIDATIVE_PHOSPHORYLATION	-1.53	0	0.023
8	HALLMARK_PEROXISOME	-1.52	0.007	0.025
9	HALLMARK_XENOBIOTIC_METABOLISM	-1.38	0.009	0.108
10	HALLMARK_MYOGENESIS	-1.38	0.008	0.101
11	HALLMARK_MITOTIC_SPINDLE	-1.38	0.006	0.096
12	HALLMARK_PROTEIN_SECRETION	-1.34	0.044	0.128
13	HALLMARK_DNA_REPAIR	-1.33	0.03	0.13
14	HALLMARK_BILE_ACID_METABOLISM	-1.32	0.06	0.139
15	HALLMARK_APOPTOSIS	-1.31	0.041	0.149
16	HALLMARK_ESTROGEN_RESPONSE_LATE	-1.3	0.033	0.157
17	HALLMARK_APICAL_JUNCTION	-1.24	0.055	0.249

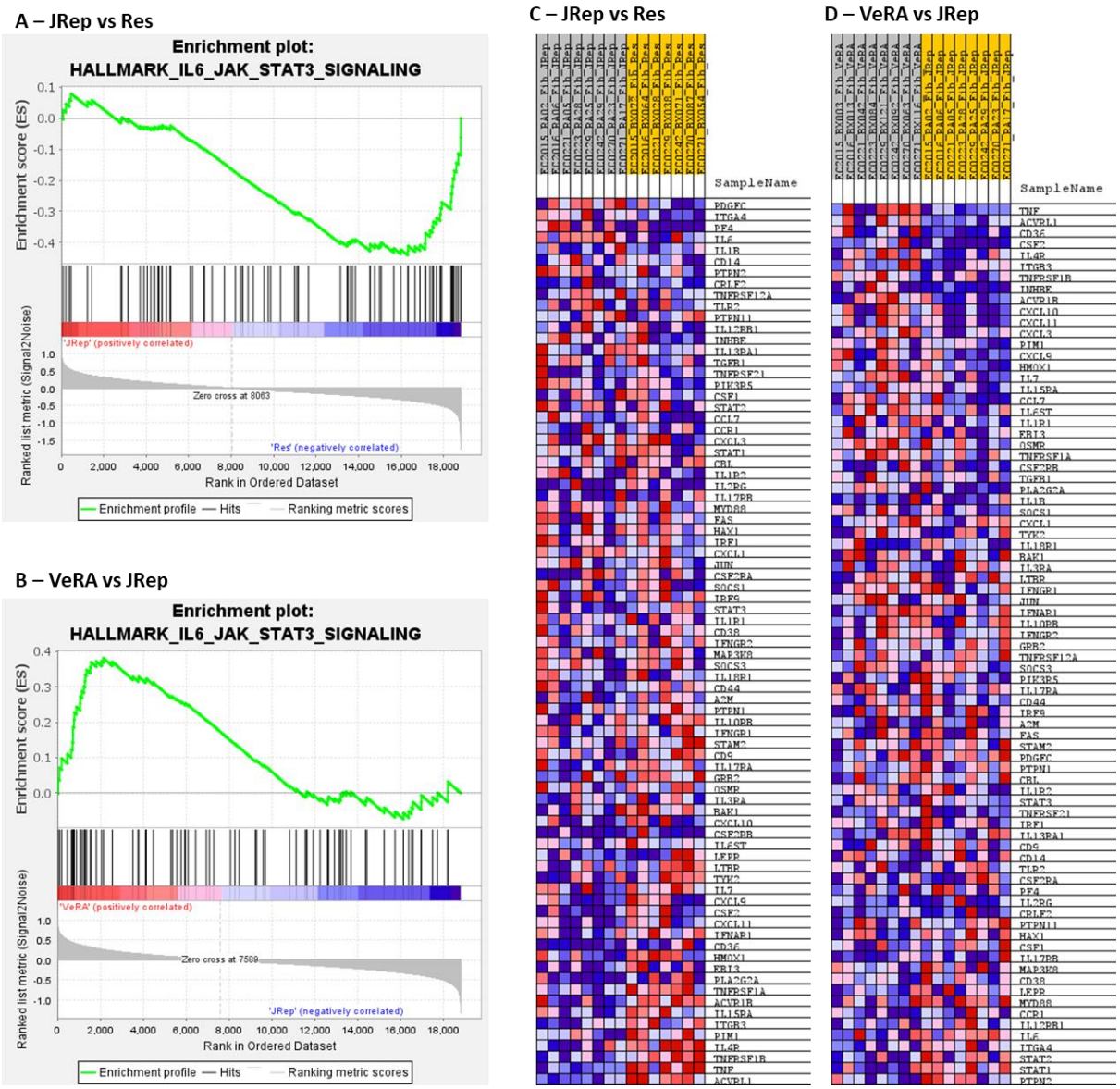

Figure 5.25: Gene set enrichment and heatmap of the IL-6-JAK-STAT3 pathway genes. Bulk RNA sequencing was performed on RNA isolated from the fibroblasts of patients with resolving arthritis (Res), very early rheumatoid arthritis (VeRA) and RA patients undergoing joint replacement (JRep) in co-culture with endothelial cells (ECs) and treated with TNF-α+IFNγ for 24 hours. Sex genes were removed from the analysis and the gene counts were subject to differential gene expression analysis in DESeq2. The gene counts table was submitted for gene set enrichment analysis (GSEA) of the hallmark pathways, and comparisons between **(A, C)** JRep vs Res and **(B, D)** VeRA vs JRep had enrichment in the IL-6-JAK-STAT signalling. **(A-B)** The GSEA and **(C-D)** a heatmap of the genes in the IL-6-JAK-STAT signalling pathway. For **(C)** grey is JRep and yellow is Res**,** in **(D)** grey is VeRA and yellow is JRep.

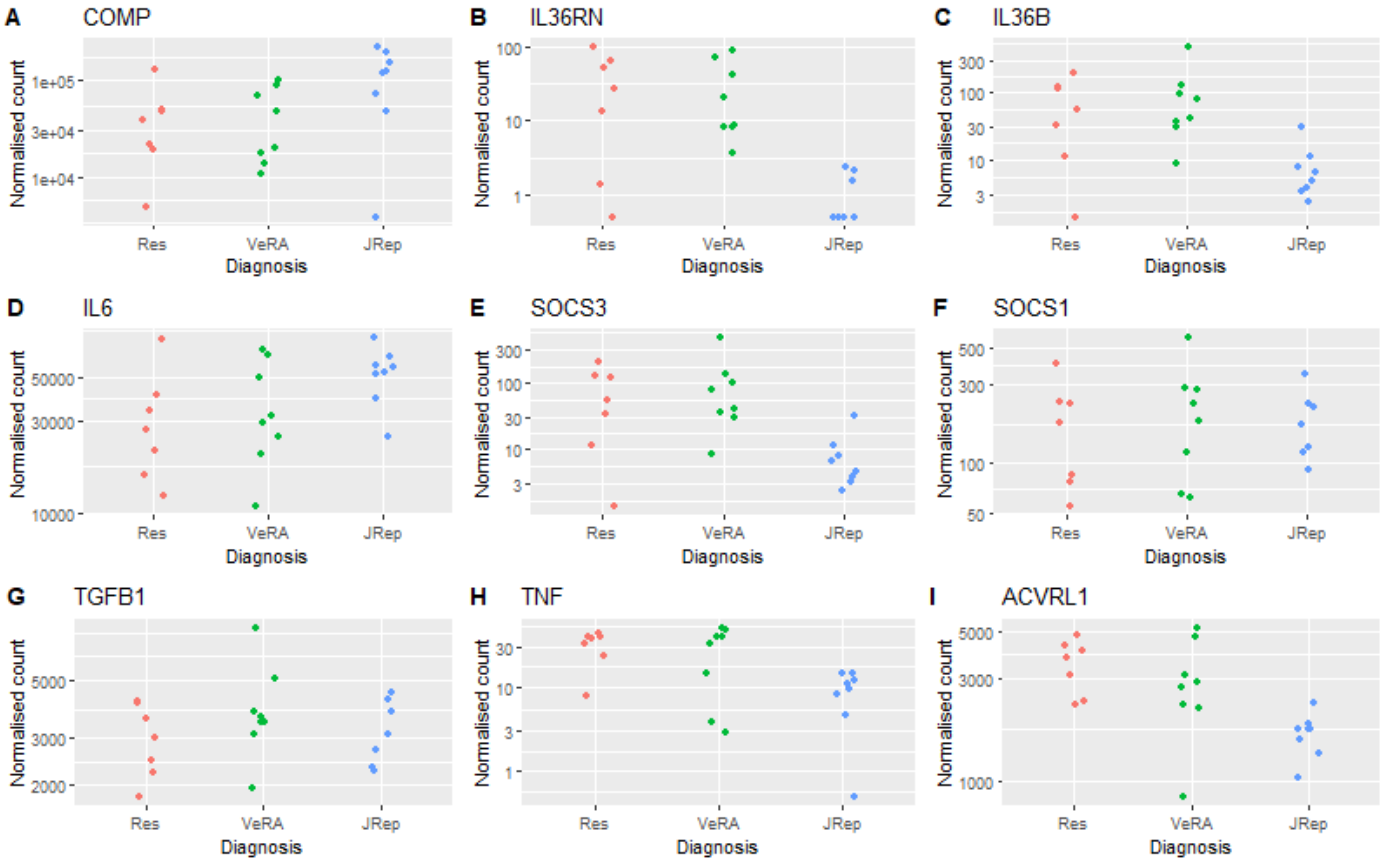

Figure 5.26: Counts plots of the genes of interest in fibroblasts cultured with endothelial cells. Bulk RNA sequencing was performed on RNA isolated from the fibroblasts of patients with resolving arthritis (Res; red), very early rheumatoid arthritis (VeRA; green) and RA patients undergoing joint replacement (JRep; blue) in co-culture with endothelial cells (ECs) and treated with TNF-α+IFNγ for 24 hours. Sex genes were removed from the analysis and the gene counts were subject to differential gene expression analysis in DESeq2. The counts of genes identified as interesting were plotted**.** Interest was determined due to **(A)** expression in co-cultured ECs (COMP; cartilage oligomeric matrix protein), **(B-C)** pathway analysis with gProfiler for IL-36 due to changing **(B)** IL-36RN; interleukin-36 receptor antagonist and **(C)** IL-36B gene expression**,** or **(D-I)** involvement in IL-6 signalling and the JAK-STAT pathway, and counts plots generated for **(D)** IL-6, **(E)** SOCS3 (suppressor of cytokine signalling 3), **(F)** SOCS1, **(G)** TGFB1 (Transforming growth factor beta 1), **(H)** TNF (tumour necrosis factor) and **(I)** ACVRL1 (Activin A Receptor Like Type 1).

5.2.5.3 Mono-cultured fibroblasts have similar gene expression patterns to co-cultured fibroblasts

In order to determine if there were any large differences in the mono-cultured compared to co-cultured fibroblasts, these were directly compared in analysis carried out by Novartis. Differential gene expression for all mono-cultured and co-cultured cells revealed around 1000 significantly differentially expressed genes (Figure 5.27A and B). However, comparing the mono and co cultured cells for each disease group individually yielded few significantly differentially expressed genes (Figure 5.27C-E). Moreover, these differences appeared to be shared across the disease states (Figure 5.27F).

To determine whether similar patterns in differential gene expression were seen in the mono-cultured compared to co-cultured fibroblasts, the same analysis as described above (5.2.5.1 and 5.2.5.2) was performed. Notably, similar levels of differential expression were observed, with a few significant differences in "VeRA vs Res" and larger differences in the "JRep vs Res" and "VeRA vs JRep" pairwise comparisons.

These results suggest that whilst fibroblasts had altered gene expression dependent on co-culture with endothelial cells, there were no disease specific differences and a similar pattern of differential gene expression was observed.

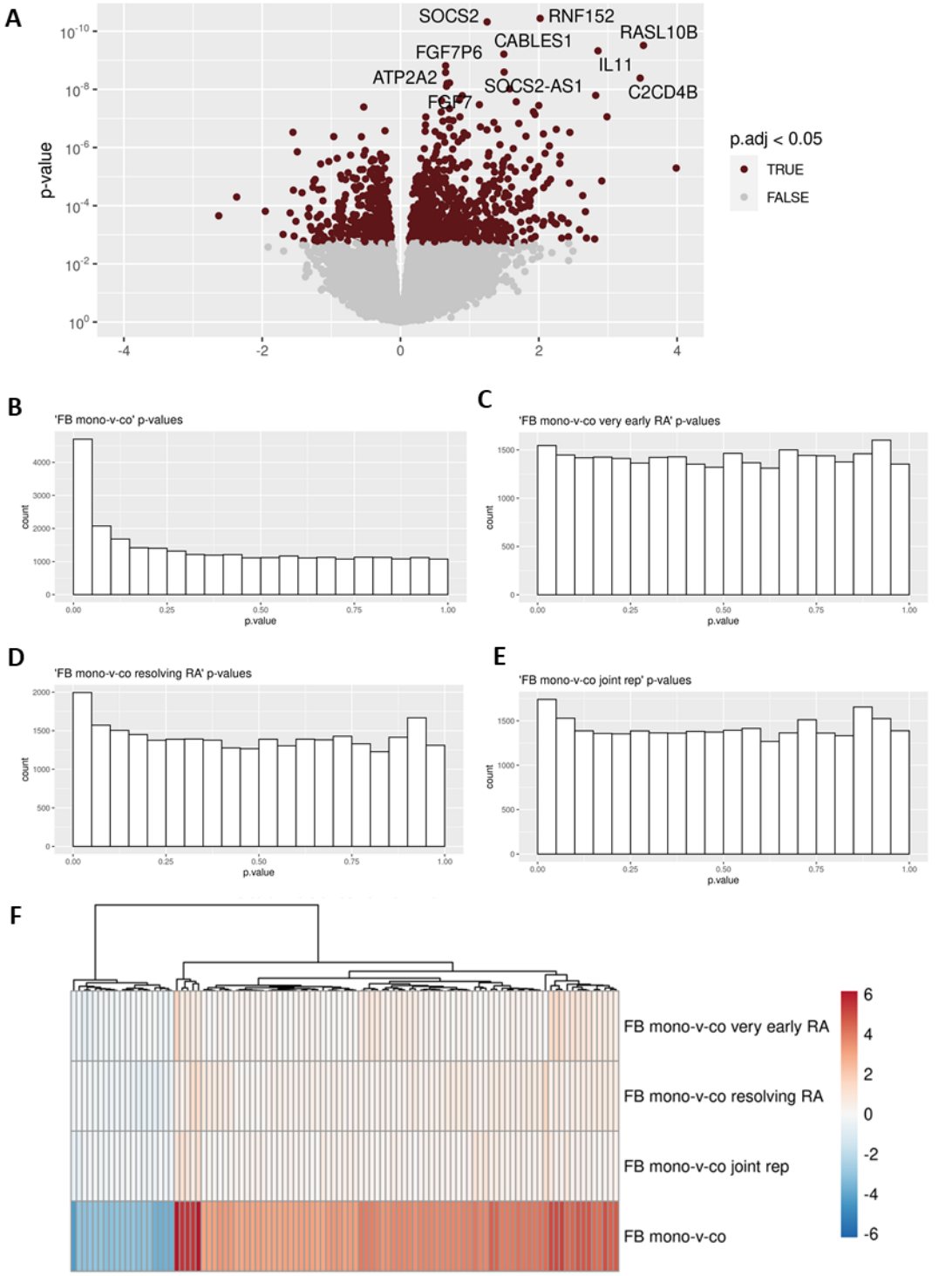

Figure 5.27: Co-cultured compared to mono-cultured cultured fibroblasts have few differentially expressed genes and differences are shared across disease state. RNA sequencing was performed on co-cultured endothelial cells and fibroblasts (and mono-cultured controls) treated with TNF-α+IFNγ for 24 hours. Analysis was carried out by Novartis. **(A)** Volcano plot of the differential expressed genes of all mono-cultured compared to co-cultured fibroblasts. **(B-E)** P value histograms of **(B)** all mono-cultured vs co-cultured fibroblasts, **(C)** Very early rheumatoid arthritis, **(D)** Resolving arthritis, and **(E)** rheumatoid arthritis undergoing joint replacement. **(F)** Heatmap of differential expressed genes according to culture conditions.

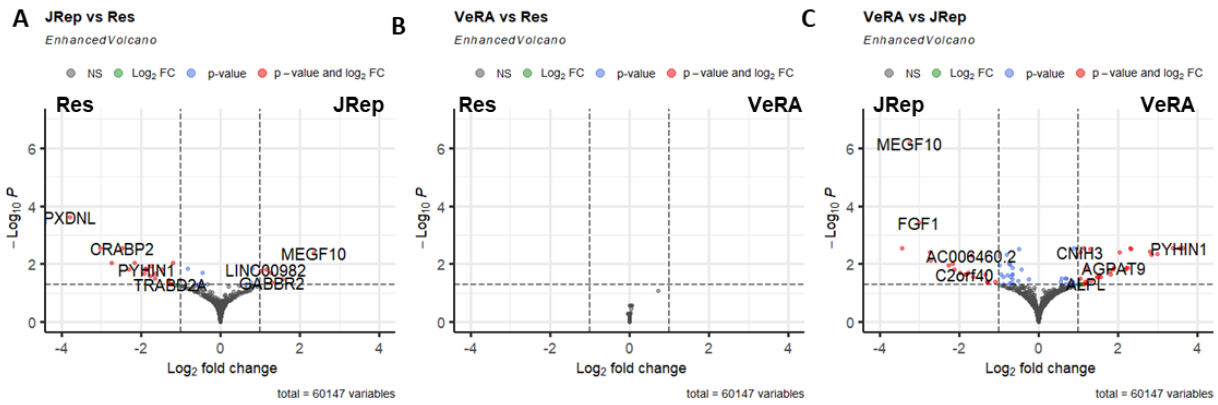

Figure 5.28: Mono-cultured fibroblasts exhibit differential gene expression between those from joint replacement and those from patients with very early rheumatoid arthritis or resolving arthritis. Bulk RNA sequencing was performed on RNA isolated from fibroblasts from patients with resolving arthritis (Res), very early rheumatoid arthritis (VeRA) and RA patients undergoing joint replacement (JRep) in mono-culture and treated with TNF-α+IFNγ for 24 hours. Sex genes were removed from the analysis and the gene counts were subject to differential gene expression analysis in DESeq2. **(A)** Dispersion estimates from DESeq2 and comparisons of **(B and E)** JRep vs Res, **(C and F)** VeRA vs Res **(D and G)** VeRA vs JRep. **(B-D)** P value histograms, with filtered out genes where there are less than 3 samples with normalized counts greater than or equal to 5. **(E-G)** Volcano plots of the comparisons, on the x axis the "ashr" shrunk Log2foldchange and on the y the –log10 adjusted p value. Significantly different gene expression shown in red.

5.3 Results of metabolomic analysis

5.3.1 Sample set-up

Co-culture samples were set up similarly to that described in Section 5.2.1 and shown in Figure 5.1A. In this case, each HUVEC donor was cultured with fibroblasts from patients with established RA (EstRA; >3 month symptom duration, but not receiving treatment), RA undergoing joint replacement (JRep), no inflammation (Norm), resolving arthritis (Res) or very early RA (VeRA). A summary of the patient characteristics are given in Table 5.9 and full details in Appendix Table 4. Supernatants were collected from the co -cultures under both unstimulated and TNF-α/IFN-γ stimulated conditions, and Liquid Chromatography - Mass Spectrometry (LC-MS) performed by Professor Warwick Dunn at the University of Birmingham Phenome Centre.

5.3.2 No differences in metabolites according to diagnosis of fibroblasts in culture

Multivariate, machine learning and univariate methods of analysis were kindly performed by Professor Warwick Dunn (University of Liverpool). Neither multivariate analysis (using all metabolites as predictors e.g., PCA) nor machine learning approaches constructed robust models, so were not further pursued. Univariate analysis using a one-way ANOVA to compare between the diagnoses of fibroblast donors revealed no statistically significant differences with FDR correction. Some were significant without FDR correction and are listed in Appendix Table 5 and for the unstimulated and Appendix Table 6 for the TNF-α-IFN-γ stimulated conditions. However, as multiple testing correction was not applied these must be viewed with caution, as described in Section 5.2.4.2. Of the peaks identified with uncorrected P value < 0.05, 26 known metabolites in the unstimulated and 23 in TNF-α-IFN-γ

conditions were identified. Box and whisker plots of the normalised metabolite concentrations are given in Figure 5.26 and Figure 5.27, which showed relative concentrations were similar across the groups. Often only one diagnosis group showed a difference, and the group that differed was different for each metabolite, with the exception of (20S)-1α, 20, 25- trihydroxyvitamin D3 which was higher in all groups except the VeRA and Res (Figure 5.29 O). There was also frequent variability within each diagnosis group, with some donors within the group having particularly low or high concentrations and so pushing the mean down or up. Pathway enrichment of the metabolites revealed no significantly enriched pathways, and no metabolic pathways or class of metabolites could be identified as statistically important. Therefore, these results suggest there were no significantly different metabolites or metabolite pathways in the supernatants of the fibroblast-EC co-cultures according to the diagnosis of fibroblast donor.

Table 5.9: Summary of patient characteristics of fibroblast donors from fibroblast-endothelial co-cultures used in Mass Spectrometry

	Norm (n=7)	Res (n=7)	VeRA (n=5)	EstRA (n=6)	JRep (n= 4)
Age (years)	41 (39-43)	45 (38-53)	55 (48-60)	54 (46-62)	42 (32-55)
Female, n (%)	3(43)	2(29)	1 (20)	4 (67)	4 (100)
Symptom duration (weeks)	-	5 (5-7)	8 (4-9)	34 (30-49)	910 (624 – 1040)
DAS28, mean (SD)	-	3.9 (±0.4)	4.6 (±1.9)	6 (±1)	5.6 (±1.2)
ESR (mm/hour)	-	15 (5-8)	58 (32-58)	35 (27-49)	50 (33-65)
CRP, mg/L	-	6 (0-12)	38 (0-45)	22 (8-41)	40 (30-50)
RF positive, n (%)	-	0 (0)	2 (40)	2 (33)	4 (100)
CCP positive, n (%)	-	0 (0)	3 (60)	3 (50)	-
SJC28	-	4 (2-5)	4 (1-4)	6 (5-14)	13 (9-15)
TJC28	-	3 (3-5)	3 (1-8)	12 (7-15)	6 (2-10)
VAS	-	36 (33-69)	52 (46-70)	65 (50-74)	66(48-79)
US GS	-	1 (1-1)	2 (0-2)	2 (1-2)	-
US PD	-	1 (0-1)	2 (2-3)	2 (1-2)	-

Median (IQR) shown unless otherwise stated.

DAS28 = Disease Activity Score 28; CCP = cyclic citrullinated peptide, CRP = C-reactive protein; ESR = erythrocyte sedimentation rate; IQR = Interquartile range; JRep = joint replacement; NSAID = non-steroidal anti-inflammatory; RF = Rheumatoid factor; SJC28 = 28 swollen joint counts; TJC28 = 28 tender joint counts; US GS = ultrasound greyscale grade at the biopsied joint; US PD = ultrasound power Doppler grade at the biopsied joint; VAS = visual analogue score; VeRA = Very early rheumatoid arthritis.

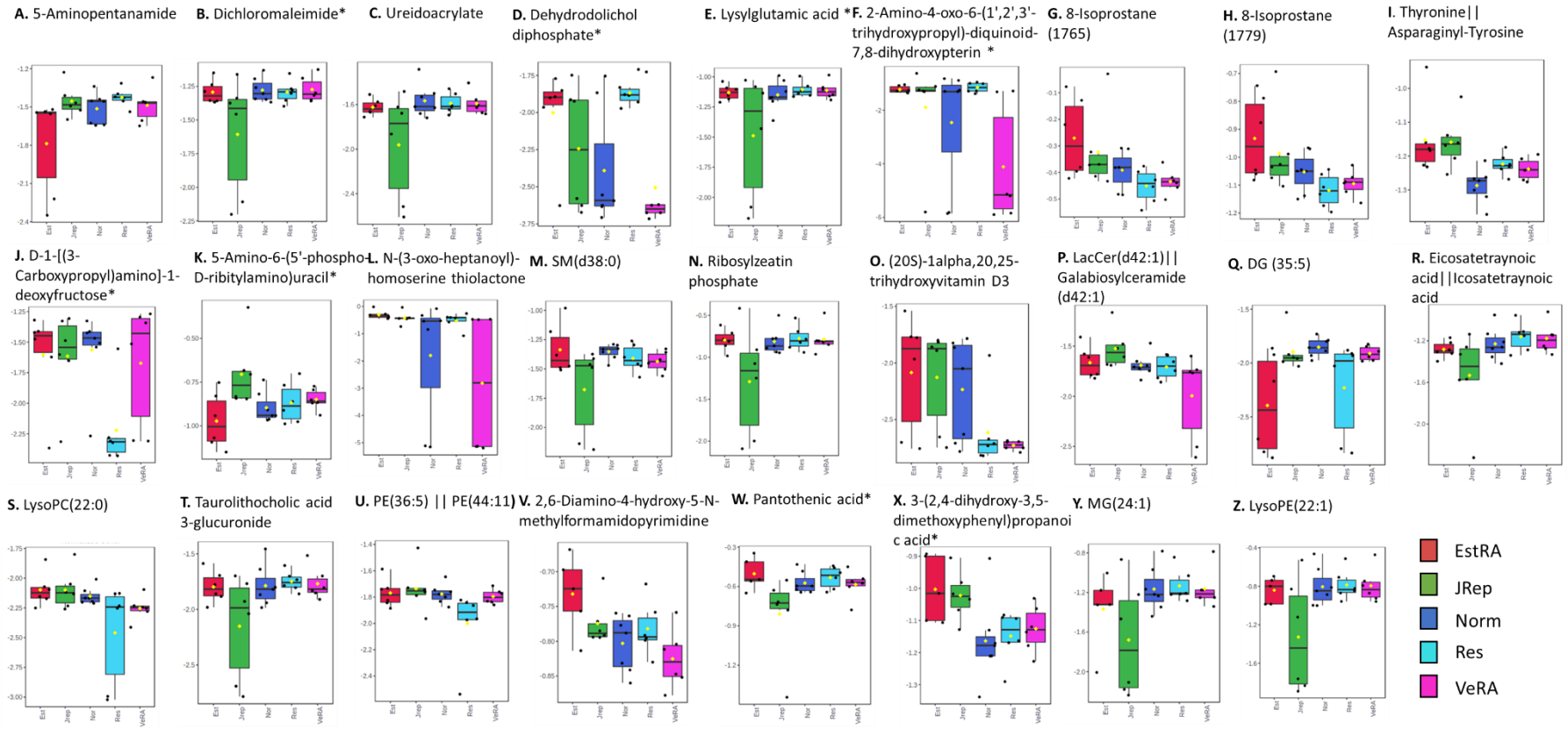

Figure 5.29: Normalised concentrations of metabolites with unadjusted P<0.05 according to fibroblast diagnosis in unstimulated fibroblast-endothelial cell co-cultures. Mass-Spectrometry was performed on supernatants collected from co-cultures, of healthy ECs cultured with fibroblasts from patients with established rheumatoid arthritis (EstRA; red), RA undergoing joint replacement (JRep; green), no inflammation (Nor; dark blue), resolving arthritis (Res; light blue), or very early RA (VeRA; pink). Data were subject to a one-way ANOVA dependent on the diagnosis of the fibroblast donor, and metabolites were identified according to the mass to charge ratio (m/z) and retention time (rt). The normalised concentrations of metabolites with an unadjusted P value < 0.05 are plotted.

*Indicates there are other metabolites it may be according to the rt, and these metabolites are listed in Appendix Table 5.

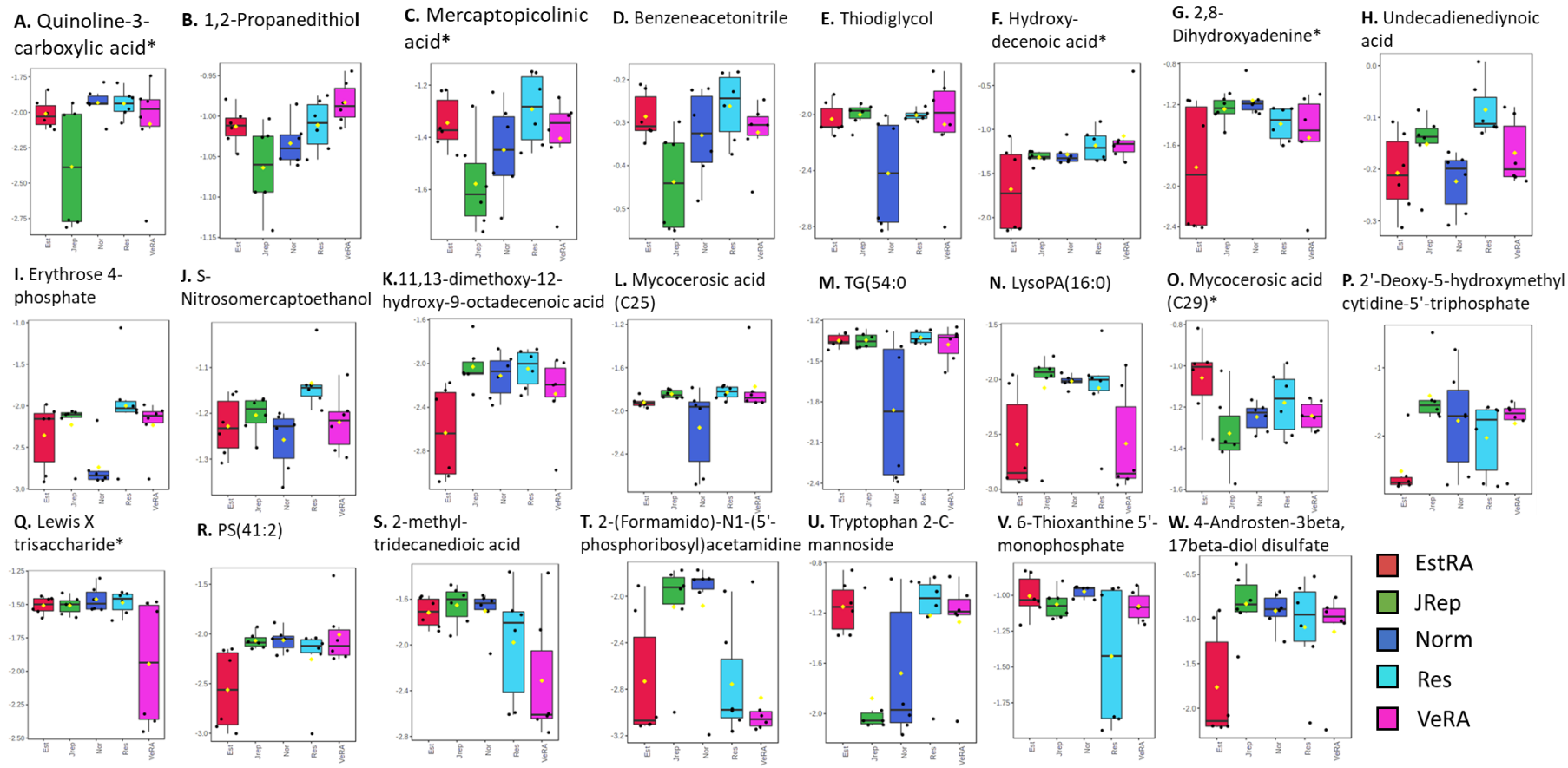

Figure 5.30: Normalised concentrations of metabolites with unadjusted P<0.05 according to fibroblast diagnosis TNF-α-IFNγ stimulated fibroblast-endothelial cell co-cultures. Mass-Spectrometry was performed on supernatants collected from TNF-α-IFN-γ stimulated co-cultures, of healthy ECs cultured with fibroblasts from patients with established rheumatoid arthritis (EstRA; red), RA undergoing joint replacement (JRep; green), no inflammation (Nor; dark blue), resolving arthritis (Res; light blue), or very early RA (VeRA; pink). Data were subject to a one-way ANOVA dependent on the diagnosis of the fibroblast donor, and metabolites were identified according to the mass to charge ratio (m/z) and retention time (rt). The normalised concentrations of metabolites with an unadjusted P value < 0.05 are plotted.
*Indicates there are other metabolites it may be according to the m/z and rt, and these metabolites are listed in Appendix Table 6.

5.4 Discussion

In this chapter we aimed to investigate if there were changes in the endothelial phenotype according to the diagnosis of fibroblasts in co-culture. We anticipated that this could explain previously observed functional differences (9). However, few differences were identified in the transcriptional or secreted metabolome of the endothelial cells depending on the diagnosis of fibroblasts in co-culture. This may be due to large differences in batch and HUVEC donor that masked any subtle changes. Correcting for these revealed some differences, particularly in HUVECs cultured with JRep fibroblasts, which appeared to be separate from VeRA or Res. Likewise, in fibroblasts cultured with HUVECs we observed the JRep samples clustering separately from the other groups. However, few differences were seen between the VeRA and Res samples, thus, the null hypothesis, that there are no transcriptomic changes in ECs dependent on fibroblasts in culture, should be accepted

5.4.1 Alterations in the endothelial cell transcriptome according to fibroblast diagnosis

Differential gene expression analysis of the endothelial cells revealed only 12 differentially expressed genes (DEGs) according to the diagnosis of fibroblasts in culture, and with batch correction no genes were significantly differentially expressed. Interestingly, the 12 DEGs did allow for a separation between the ECs cultured with resolving vs RA (VeRA/JRep), which, under TNF-α-IFNγ stimulated conditions, was where the differences in the functional assays were observed (9). However, assessing the gene counts of these showed that differences were largely driven by only few outliers for most genes, with exception of the cartilage oligomeric matrix protein (COMP) gene. COMP is traditionally considered a signalling molecule produced by fibroblasts (and chondrocytes), but not EC (333-335). The detection of COMP here may be due to: (i) contamination of fibroblasts in the EC prep or (ii) fibroblasts

transferred COMP to EC during co-culture. COMP, in fibroblasts, is known to maintain cartilage integrity through interactions with collagens and fibronectin. In RA, it is an identified autoantigen, inducing arthritis in mice (334) and rat (335) models of inflammatory arthritis. Regarding COMP and ECs, a recent study has shown that it binds to the Piezo-1 channel in ECs and thus regulates blood pressure (333), suggesting a potential role as signalling molecule. Furthermore, recent work using spatial transcriptomics of RA sections has also shown that the COMP+ fibroblast niche associates with the vasculature indicative of potential crosstalk with the endothelium (Reis, 2022, unpublished). However, looking at gene expression of COMP in the fibroblasts, there was no significant difference between groups in adjusted P values and expression only appeared higher in JRep compared to both Res and VeRA.

Pathway analysis of the 12 DEGs suggested an involvement of bone morphogenic protein (BMP) binding, a pathway that has been shown to affect the EC response to hypoxia and inflammatory stimuli (339). BMPs are also members of the transforming growth factor-beta (TGF-β) cytokine family (340), and blockade of TGF-β alongside IL-6 significantly reduced the recruitment of lymphocytes in the stimulated VeRA fibroblast – EC co-cultures (9). However, in this analysis, BMP binding came up due only to the higher expression of COMP and gremlin2 (GREM2) in the VeRA and JRep co-cultures compared to resolving, therefore little can be determined from this.

Due to the large effect of donor and batch, we attempted to correct for these with limma and ComBat-Seq batch correction. However, as the purpose of these tools is to correct solely

for batch effect and we also had true biological variation between the batches this analysis should be viewed with caution. These data indicated that high mitochondrial gene expression in HUVECs cultured with JRep fibroblasts separated them from those cultured with VeRA or Res fibroblasts. High mitochondrial expression has been linked to increased stressed, apoptotic and low-quality cells (345). Therefore, the separation may be due to a difference in sample quality. Importantly, mitochondria are crucial for energy generation, and play roles in cellular metabolism (346, 347). Moreover, alterations in mitochondria and metabolism have been linked to RA pathogenesis (347). Thus, it may be that increased mitochondrial gene expression causes increased energy generation or signalling metabolites in HUVECs cultured with JRep fibroblasts.

Taken together, the results suggest there is either no, or only a very subtle effect of fibroblast diagnosis under TNF-α-IFNγ stimulated conditions. The clustering of ECs according to donor over diagnosis of fibroblasts suggests this is a much stronger contributor to variation than the diagnosis of fibroblasts. This may be due to limitations in study design, discussed further in 5.4.4.

5.4.2 Alterations in the fibroblast transcriptome according to diagnosis

Consistent with previous findings (348), there were very few differentially expressed genes in the VeRA compared to Res fibroblasts, in both co-cultured and mono-cultured conditions. This may in part be due to the high passage of fibroblasts, which, as discussed in 5.4.4.3, causes changes in gene expression when reaching passages 5-6 (349, 350). However, previous microarray analysis was carried out at passage 3 and no difference was observed

(348). Similarly, very few differences were seen in recent bulk-RNA sequencing of entire joint (351), of which fibroblasts are the primary constituent (322) and where cells were not passaged at all. Our results show that in co-culture with ECs, and treated with TNF-α-IFNγ, there appears to be little difference in the fibroblast transcriptome between Res and VeRA fibroblasts. Therefore, these data cannot help determine the differences observed in the functional assays (9).

By contrast, when comparing the JRep fibroblasts with the Res or VeRA fibroblasts there were a larger number of DEGs, many of which were the same in both comparisons, so they are likely to be associated with the JRep phenotype. This was the case for both mono and co-cultured fibroblasts, although there were more and different, differentially expressed genes in co-culture. As JRep samples are taken at late-stage RA from patients undergoing joint replacement surgery, these differences may be caused not only by longer symptom duration, but also by the effect of treatment or differences in initial sample collection (biopsy vs large-scale resection of synovium) or joint location. Previous microarray analysis of mono-cultured fibroblasts identified differential gene expression between VeRA and EstRA fibroblasts (348), which suggests the differences may be at least in part due to symptom duration.

KEGG enrichment analysis for the co-culture comparisons of “JRep vs Res” and “JRep vs VeRA” suggested changes in cytokine-cytokine receptor interactions and cell adhesion molecules were differentially regulated in the JRep fibroblasts compared to both VeRA and Res. Perturbations in these pathways may contribute to the differences observed in

endothelial cell response. However, assessing the genes that brought up these pathways there was no obvious association with ECs.

gProfiler pathway analysis identified IL-36 signalling to be involved, due to the downregulated expression of IL-36β and IL-36RN (the gene encoding the IL-36 receptor antagonist, IL-36Ra) in the JRep samples compared to both VeRA and Res samples. IL-36 is a member of the IL-1 superfamily and there are 4 isoforms, IL-36 -α, -β, -γ and IL-36Ra (352). The first 3 stimulate, whilst IL-36Ra inhibits, IL-36 signalling (352). Intriguingly, both the agonist and antagonists were lower in the JRep compared to VeRA/Res samples, which may be attributed to differences with disease and treatment or due to changing mechanisms of disease. For instance, in collagen-induced arthritis (CIA) and collagen antibody-induced arthritis (CAIA) murine models of inflammatory arthritis, all 4 isoforms were increased, particularly at the peak of inflammation, whilst IL-38 (another IL-36 signalling inhibitor) was elevated during resolution (353). However, in AIA models the only significant differences observed were in IL-36α and IL-36γ (higher during early peak) and IL-36Ra (highest in resolution) (353). These results suggest there are changing roles of IL-36 signalling during disease progression and according to disease mechanisms. As we observe higher expression in JRep samples, it is likely this signalling pathway is involved in the later stages of disease, and/or in patients that are less responsive to current treatments.

Gene set enrichment analysis of the fibroblasts co-cultured with HUVECs suggests that IL-6 and the JAK-STAT pathway significantly contribute to the differences observed, with it being enriched more in VeRA or Res fibroblasts than JRep. Perturbations of this pathway are

perhaps unsurprising due to known involvement of IL-6 in RA (354). Indeed, in the flow-based adhesion assays, blockade of IL-6 with TGF-β appeared to block the inhibitory effect of resolving co-cultures whilst having anti-inflammatory effect in the VeRA co-cultures and no effect in the JRep cultures (9). Furthermore, ECs co-cultured with resolving fibroblasts had higher expression of the IL-6 inhibitor, SOCS3 (9). Although the same difference was not observed in this RNA-sequencing, it does suggest the involvement of IL-6-JAK-STAT signalling.

In conclusion, there are differentially regulated genes and pathways in the JRep compared to Res and VeRA fibroblasts that are co-cultured with HUVECs. The transcriptomic differences described here may partially explain the increase in lymphocyte adhesion observed in HUVECs cultured with JRep compared to VeRA or Res fibroblasts in unstimulated conditions (9). Albeit our data are from TNF-α-IFNγ stimulated samples. Thus, we would need to repeat in unstimulated conditions to determine if the same transcriptomic differences persist.

5.4.3 Mass-Spectrometry of co-culture supernatants

In RA, fibroblasts are known to undergo metabolomic alterations (355). However, we observed no significant difference in the extracellular metabolites according to fibroblast diagnosis. This is similar to other metabolomic (NMR) analysis of fibroblast cell extracts and supernatants (356). They demonstrated that whilst there were changes in the intracellular metabolite concentrations of fibroblasts between VeRA and Res patients, there were few in the supernatant of co-cultures between VeRA and Res (356). However, Seahorse assays of these cells showed that Res, but not VeRA fibroblasts increased glycolysis in response to

TNF-α stimulation (356). As our results are from co-cultured supernatants it suggests, similarly to above, that there were few differences in extracellular metabolites of fibroblasts. Furthermore, it suggests that these did not induce changes to the secreted metabolome of the HUVECs. However, as we did not explore the changes in intracellular metabolites or measure functional outputs of metabolism we do not know if there would be other forms of metabolomic alterations. This may be worth exploring further given the high mitochondrial gene expression in HUVECs cultured with JRep fibroblasts. Although we observed some changes in metabolites, there was no evidence of any particular metabolic pathways or key metabolites being altered that may explain their changing phenotype.

5.4.4 Limitations and study design

5.4.4.1 Batch variation in HUVECs

As described in section 5.2.1, each experiment was set up at a separate time point and with a different HUVEC donor. PCAs showed HUVECs clustered primarily by donor/batch. As little to no batch effect was observed in the fibroblasts, it is likely HUVECs clustered because of genetic differences between donors rather than batch effects in processing. This is further supported by the fact that females and males clustered separately before sex genes were removed, suggesting that the genetic differences drive clustering. However, it may also be that HUVECs were more sensitive to changes in conditions between batches than fibroblasts, given that they are known to act as reporters for the local microenvironment *in vivo* (165). Whilst batch/EC donor was built into the model and two different forms of batch correction were applied, as the effect was not only batch, but also true biological variation these methods may not be ideal or adjusted completely for the variation. Hence, it may be that any subtle differences in the endothelial cells caused by the diagnosis of fibroblast in co-

culture were masked by the large variation between donors, despite modelling or batch correction.

The initial reasoning for running each experiment at a separate time point with a new HUVEC donor was primarily to mimic the initial functional assays as much as possible (9). In the previous study (9), cells were used at P1, because expansion can change HUVEC responsiveness (168). Furthermore, using different HUVEC donors would allow us to know that the effects were observed over a range of donors. However, now it is known that the HUVEC donor has such a large effect, if this experiment were to be repeated it would be important to run it ideally with one donor or at least fewer donors. To do this, it would be best to use a HUVEC donor that had more cells available (i.e., a longer umbilical cord) and in a smaller well format in order to have repeats per HUVEC donor. Likewise, pooling HUVEC donors to increase the number of P1 may have been a better alternative. Otherwise, the HUVECs would need to be passaged, however, passaged cells were not used previously due to the possible change in responsiveness (168). Therefore, passaged HUVECs would need to be tested in the functional assays prior to use.

5.4.4.2 Lack of flow conditions

Another minor difference in this co-culture set up compared to the functional assays is that in the functional experiments the endothelial cells were under flow conditions for 4 minutes, whereas in this set up the cells experienced no flow. However, the effect of shear stress would not be long enough to see differences in the transcriptome or secreted metabolites. Therefore, this is very unlikely to have any impact on the findings obtained here.

5.4.4.3 High passage of fibroblasts

Another limitation to this study was the use of fibroblasts at the relatively high passage of P6. Fibroblast phenotype is, at least partially, maintained in culture (357). Importantly, fibroblasts at this passage were used in the functional assays that demonstrated co-culture of fibroblasts led to alterations in EC recruitment of leukocytes (9, 168). However, studies have also shown that beyond passage 4 the gene expression patterns of synovial fibroblasts are altered with increasing passage, with 7-10% DEGs in passages 5-6 compared to earlier passages (2-4) (349, 350). As all fibroblasts in this experiment were used at the same passage, the confounding effects of passage variability was limited (349). However, it must be noted that the gene expression changes with passage are different between donors (349). Crucially, donors of the same diagnosis had the same functional responses (9), therefore, the differentially expressed genes should have been maintained despite the high passage. Nevertheless, the alterations with passage may have introduced noise in the differential gene expression analysis, and therefore must be considered a limitation when interpreting the results.

5.4.4.4 Assessing fibroblasts as one cell type, not as subsets

Importantly, during this PhD, it was discovered that 2 distinct fibroblast subsets, FAPα+THY1- lining and FAPα+THY1+ sub-lining layer, drive bone destruction or inflammation, respectively (8). Isolating these subsets for use in the co-culture system, would have been interesting and perhaps improved the study design. However, obtaining the numbers required for this bulk-RNA sequencing analysis may not have been possible as the phenotype is not maintained in culture (8). Crucially, following this paper it was discovered that Notch3 signalling emanating

from the vasculature drives the formation of these fibroblast subsets and indeed culturing fibroblasts with endothelial cells in organoids allowed them to maintain this phenotype (141). Thus, using a set-up such as this may have yielded more differences in endothelial phenotype. However, this information was not known until after the samples had been processed. Moreover, as the purpose of this experiment was to explore the differences observed in the functional assays, setting up co-cultures identical to this was appropriate in order to test the hypothesis.

5.4.4.5 Variability in fibroblast donor joint site

One other factor to consider in this analysis was the variability in joint site among the fibroblast donors. Transcriptomic analysis has revealed that non-coding RNAs caused fibroblasts to cluster primarily according to joint site rather than disease in samples RA, OA and normal joints (145). To further confound this, smaller joints are likely to be affected earlier in disease (145). In this analysis, ankle and MCP joint donors were only present in the Res and VeRA patients compared to JRep, which only consisted of knee joints, making it difficult to unpick differences observed in joint site and duration. Some clustering was observed according to joint site in the heatmap of top variable genes, however, as the majority of samples from knee and only a small number from ankle or MCP joint, there was not a high enough n to build this into the model. Moreover, PCAs of the top 5 PCs did not show any clear clustering according joint. Therefore, the effect of joint type was hopefully minimal in this study. However, if this were to be repeated, fibroblasts from the same joint would be used across the comparisons to avoid being a confounder.

5.4.4.6 Functional responses of cells were not confirmed

It is also a possibility that under these co-culture conditions the fibroblast donors and HUVECs did not have the same functional effects as previously observed (9). However, to avoid this, fibroblast donors used in this study were matched to those used in the previous functional assays. Ideally, identical functional assays would have been run alongside those prepared for RNA-seq, however, this was not feasible due to the limited number of HUVECs and fibroblasts available.

5.4.5 Conclusions

Taken together these results suggest there are no large transcriptomic or secreted metabolite differences in ECs depending on the diagnosis of fibroblasts in co-culture. Whilst there were some differentially expressed genes in the ECs according to whether they were cultured with Res compared to RA (JRep or VeRA) fibroblasts, the limited number of differential genes means no pathways could be identified and any interpretations of the results viewed with caution due to the possibility of false positives. Regarding the fibroblasts from these co-cultures, some differences in DEGs and pathways were identified in JRep compared to VeRA and Res. These may, at least partially, account for the increased lymphocyte recruitment observed in HUVECs cultured with JRep as opposed to VeRA and Res fibroblasts (9). However, these changes did not appear to induce transcriptomic differences in the ECs. Furthermore, the functional differences were observed in unstimulated conditions. Therefore, we would need to repeat the experiment without stimuli to see if the same transcriptomic differences in fibroblasts were observed. In conclusion, these data reveal few transcriptomic or extracellular metabolomic changes in ECs dependent on the fibroblasts in culture. Consequently, we cannot use this to unpick the

mechanisms underlying the functional differences observed (9). However, the lack of differences here suggests other cellular changes that we did not measure (e.g., epigenetic, phosphorylation or intracellular metabolic), may instead be responsible for functional observations.

6 The effect of synovial fibroblasts from different stages of rheumatoid arthritis on co-cultured macrophages

6.1 Introduction

Both macrophages and fibroblasts are implicated in the pathogenesis of RA (39). However, the interaction between these two stromal cells is not fully understood. Work by Donlin *et al* has shown that under TNF-α stimulated conditions, co-culture of RA fibroblasts (from patients undergoing joint replacement) with, healthy, M-CSF differentiated, macrophages suppressed TNF-induced induction of interferon (IFN)–β signalling and the expression of IFN-stimulated genes (ISGs) (143). It appeared that TNF-α induced fibroblasts to produce soluble mediators that suppressed the expression of IFN–β via the JAK-STAT signalling pathway (143). Furthermore, transcriptomic analysis showed a third of TNF-regulated genes in macrophages were regulated by co-culture with the fibroblasts (143). However, it is unknown what the effect of fibroblasts from different stages of arthritis may be on the transcriptome of co-cultured macrophages. The aim of this chapter was to identify any transcriptomic differences in the co-cultured macrophages and fibroblasts in order to test the following hypotheses. Firstly, that there would be bidirectional crosstalk between the fibroblasts and macrophages, meaning that i) Fibroblasts would change the transcriptome of the macrophages and ii) Macrophages would change the transcriptome of fibroblasts in co-culture. Furthermore, we hypothesised that the transcriptome of macrophages would differ depending on the outcome group of fibroblasts in co-culture. If so, that these changes support the idea that fibroblast: macrophage interactions play a role in the outcome of disease

6.2 Results

6.2.1 The co-culture set-up

Fibroblasts: macrophage co-cultures were set up similarly to that described by Donlin *et al* (143) and depicted in Figure 6.1. Monocytes were seeded into a 24-well plate and differentiated for 2 days in 10ng/ml M-CSF. Fibroblasts (isolated from patients of the BEACON cohort and described in the paragraph below) were seeded into 24 well porous transwell filters and cultured for 2 days. The cells were then combined and treated with 20ng/ml TNF-α for 16 hours. The experiment was done in 3 batches, each time the same monocyte donor was used. Notably, the macrophage differentiation time is shorter than standard protocols (358), however, in order to replicate the Donlin *et al* protocol (143) as closely as possible the time point of 2 days chosen.

Fibroblasts were isolated from patients with no inflammation (Norm), resolving arthritis (Res), very early RA (VeRA, treatment naïve and <12 weeks symptom duration), established arthritis (EstRA, treatment naïve but >12-week symptom duration), and patients undergoing joint replacement surgery (JRep). A summary of patient characteristics is given in Table 6.1, and full details in Appendix Table 7. Notably, resolving arthritis patients were not positive for CCP or RF and had lower ESR and CRP values than other groups (Table 6.1). Although VAS was higher in Res than VeRA. Similarly, VeRA patients had lower ESR, CRP and VAS than EstRA and JRep patients. Ages were similar across the RA groups, but lower for Norm and Res. Female donors were used throughout.

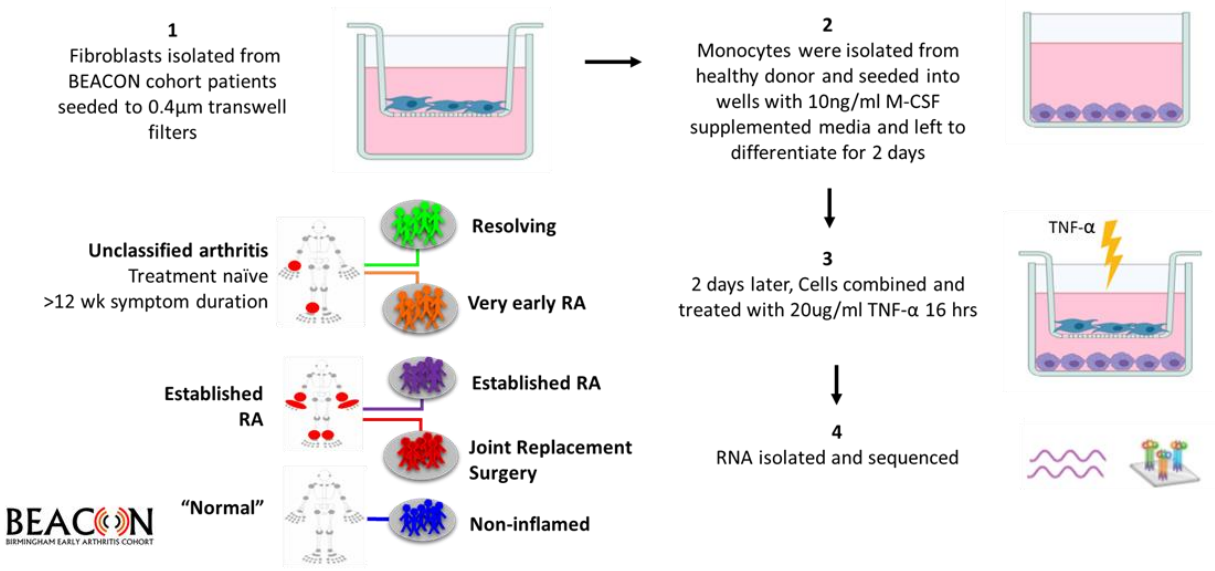

Figure 6.1: Schematic of the co-culture set up fibroblast: macrophage cultures. Fibroblasts from patients in the BEACON cohort were seeded in 0.4µm pore transwell inserts and cultured for 2 days. Monocytes from a healthy donor were seeded in M-CSF supplemented media and left to differentiate for 2 days. After 2 days, the cells were combined and stimulated in 20ng/ml TNF-α supplemented media for 16 hours. Cells were then collected, RNA isolated at stored at -80°C before sequencing.

Table 6.1: Characteristics of patients donating fibroblasts

	Norm (n = 5)	Res (n = 6)	VeRA (n = 7)	EstRA (n = 4)	JRep (n = 6)
Age (years)	41 (41 – 47)	45 (42 – 45)	60 (49 – 65)	59 (48 – 63)	62 (51 – 68)
Female, n (%)	5 (100)	6 (100)	7 (100)	4 (100)	6 (100)
Symptom duration (wks)	-	4 (3 – 6)	5 (4 -10)	41 (27 – 52)	1040 (845 – 1157)
DAS28-ESR, mean (sd)	-	4 (± 2)	5 (± 1)	5 (± 1)	5 (± 2)
ESR (mm/hour)	-	7 (5 – 8)	20 (15 – 38)	30 (10 – 56)	34 (23 – 52)
CRP, mg/L	-	7 (1 -15)	18 (9 – 29)	28 (7 – 55)	44 (27 – 56)
CCP positive, n (%)	-	0 (0)	3 (43)	1 (25)	-
RF positive, n (%)	-	0 (0)	3 (43)	1 (25)	6 (100)
SJC28	-	4 (2 – 7)	3 (2 – 4)	6 (5 – 6)	9 (5 – 15)
TJC28	-	3 (1 – 7)	4 (3 – 8)	7 (7 – 9)	8 (6 – 11)
VAS	-	43 (19 – 51)	35 (31 – 54)	64 (50 – 79)	51 (22 – 79)
US GS	-	2 (1 – 2)	2 (2 – 2)	2 (2 – 2)	-
US PD	-	1 (0 – 2)	1 (0 – 2)	1 (1 – 1)	-
NSAID, n (%)	-	4 (67)	4 (57)	2 (50)	4 (67)

Median (IQR) shown unless otherwise stated.
DAS28 = Disease Activity Score 28; CCP = cyclic citrullinated peptide, CRP = C-reactive protein; ESR = erythrocyte sedimentation rate; IQR = Interquartile range; EstRA = Established rheumatoid arthritis; JRep = joint replacement; NSAID = non-steroidal anti-inflammatory; RF = Rheumatoid factor; Res = Resolving; SJC28 = 28 swollen joint counts; TJC28 = 28 tender joint counts; US GS = ultrasound greyscale grade at the biopsied joint; US PD = ultrasound power Doppler grade at the biopsied joint; VAS = visual analogue score; VeRA = Very early rheumatoid arthritis.

6.2.2 Sample quality control and pre-processing

Cells were collected from the fibroblast: macrophage co-cultures and the RNA integrity numbers (RINs) are given in Appendix Table 8. The majority of samples had a RIN > 6.4, suggesting relatively good quality (239). Although 10 samples had RINs <6.4 these were still included as removal would have decreased the power of the experiment and removal may not be necessary (239). Instead, RIN were considered throughout the analysis (e.g. for outlier assessment).

Once sequenced, samples were trimmed, aligned and counts table generated. Most samples had around 70-80% reads uniquely mapped to the genome with STAR aligner (Figure 6.2A), however, samples 6, 16 and 89 were much lower (40-65%). Generally, unique mapping rates of >80% are considered good, and <50% is suggestive of poor library preparation or data processing (247). In this case, it was likely due to the library preparation and sequencing quality. In the first round of sequencing, the sequencer failed and when the sequencing was repeated, a much lower concentration (0.5ng input) of RNA was used. Library traces from the sequencing indicated samples 6, 16 and 89 were fails, which is confirmed by the high number of unmapped reads in these samples (Figure 6.2A). Consequently, these 3 samples were removed from the analysis. Both 6 (fibroblast) and 16 (macrophage) were EstRA samples and the loss of sample 16 left only 2 macrophages that were cultured with EstRA fibroblasts. Sample 89 was a resolving fibroblast.

To give an overview of the data, initial analysis was carried out on all samples. Principal component analysis (PCA) showed fibroblasts and macrophages clustered separately (Figure

6.3A) as expected. Furthermore, no outliers were identified according to either the PCA or boxplots of the variance stabilised transformed data (Figure 6.3).

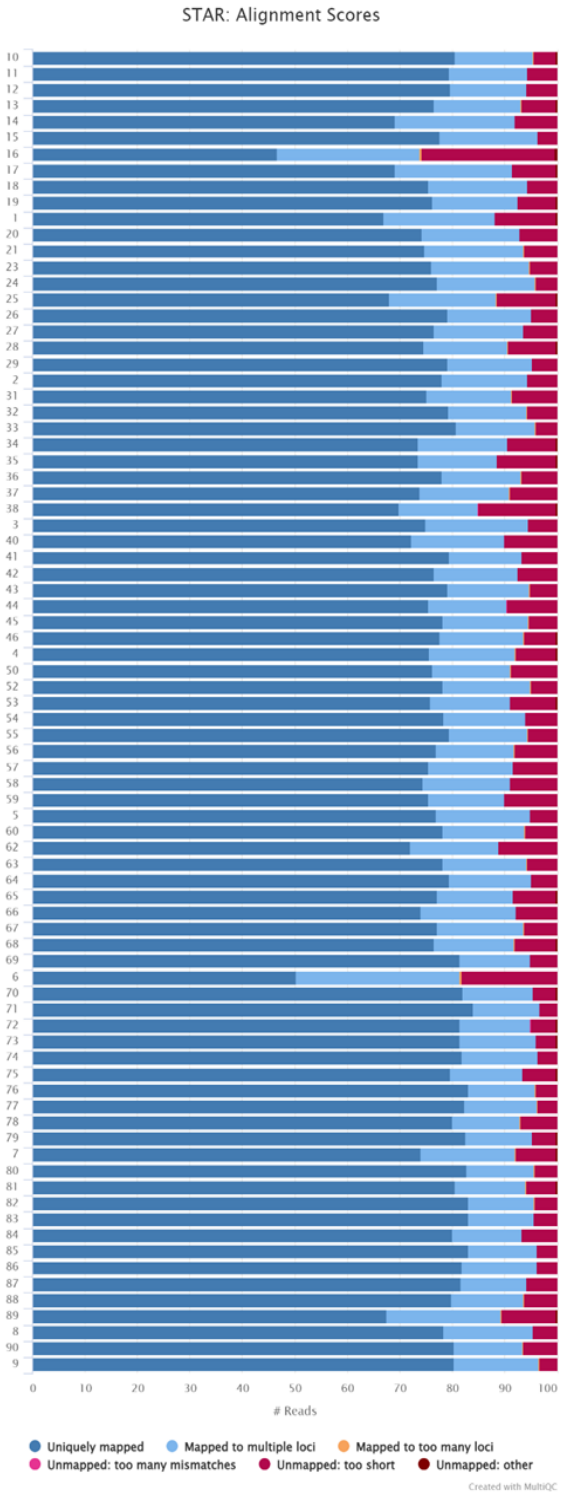

Figure 6.2: Percentage of mapped and assigned reads. Fibroblasts and macrophages were co-cultured and treated with TNF-α for 16 hours. RNA was isolated and bulk RNA sequencing performed. Sequences were trimmed with bbduk and aligned to the GRCh38 human genome with STAR aligner and assigned to features with HTSeq. Plots of mapped reads with STAR aligner were generated with MultiQC. The X axis indicates samples and y axis indicates the percentage of reads and how they are mapped. Uniquely mapped reads are dark blue, reads mapped to multiple loci in light blue and unmapped reads in red.

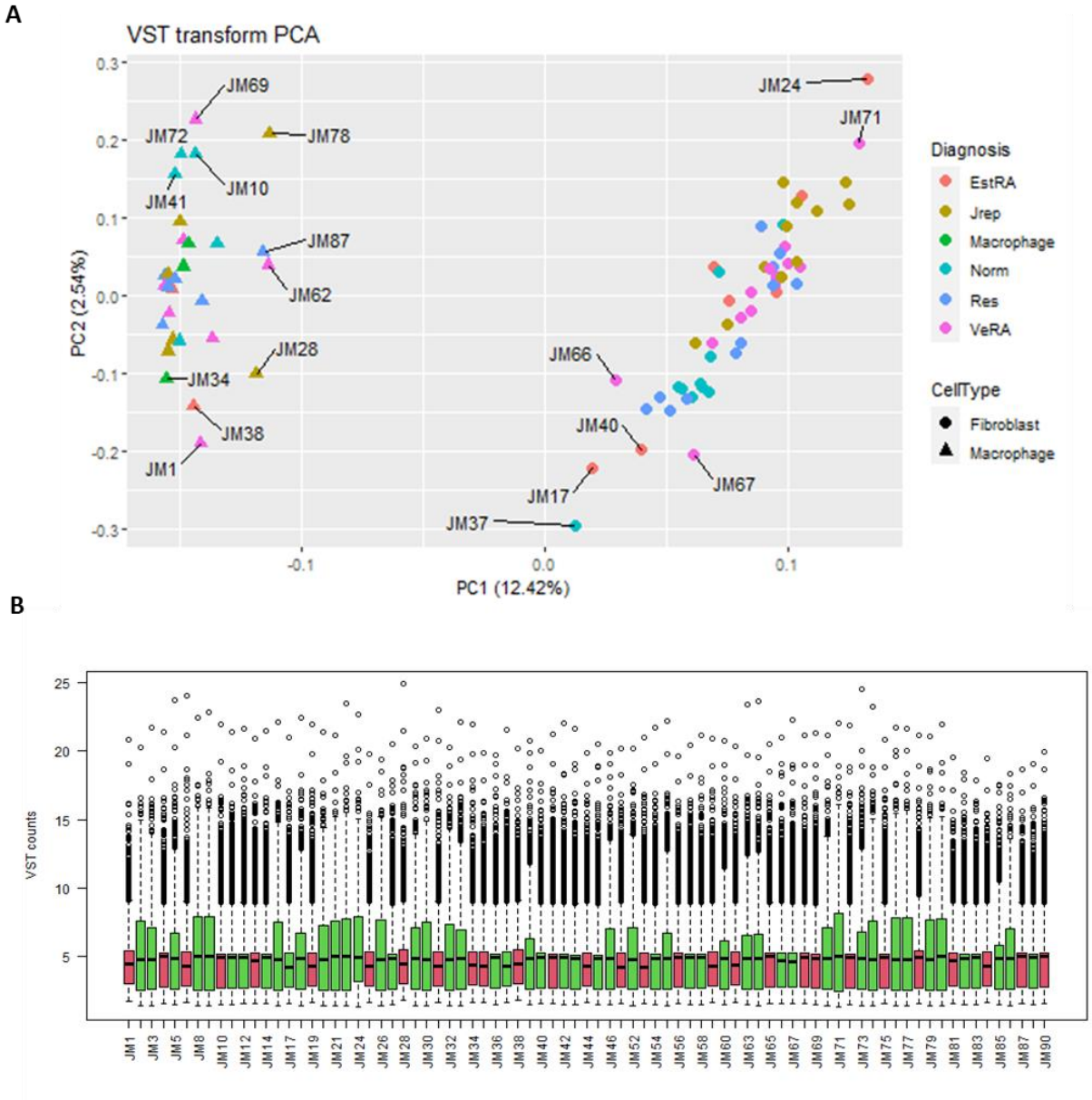

Figure 6.3: Principal component analysis and boxplot of all samples from fibroblast: macrophage co-cultures. Fibroblasts and macrophages were co-cultured and treated with TNF-α for 16 hours. RNA was isolated and bulk RNA sequencing performed. Gene counts from the sequencing data were subject to variance stabilising transformation (VST) and principal components identified. **(A)** Principal Components 1 and 2 were plotted. Samples were coloured according to if they were mono-cultured macrophages (Macrophage; green), or by the diagnosis of fibroblasts in (co-)culture: Norm (Non-inflamed; light blue), Res (Resolving; dark blue), VeRA (very early rheumatoid arthritis; pink), EstRA (established RA; red) and JRep (RA patients undergoing joint replacement; brown). Shape indicates cell type; fibroblast as circle, macrophage as triangle. **(B)** Boxplot of the VST data, coloured according to cell type; fibroblasts in green and macrophages in pink.

6.2.3 Analysis of macrophages from the fibroblast: macrophage co-cultures

6.2.3.1 The most variably expressed genes do not clearly differentiate macrophages according to the diagnosis of fibroblasts in co-culture

To assess which covariates contributed to sample variation, analysis was first performed using the most variable genes. The primary question was to identify differences between the diagnoses of fibroblast donor; therefore, the mono-cultured cells were removed for the analysis. Of note, clustering of the mono-cultured cells was observed in preliminary analysis (Appendix Figure 7). Initial PCAs (Figure 6.4A -D) and heatmap of the top 100 variably expressed genes (Figure 6.5) showed no discernible clustering by diagnosis. Potential, but again not convincing clustering, was observed according to batch and joint location (Figure 6.4C and D). As all patients were female (Table 6.1), and the same macrophage donor used throughout, sex was not considered as a covariate. Correcting for batch effect with limma showed slightly stronger clustering by diagnosis in the PCA and biplot (Figure 6.4E and F) and partially increased clustering by diagnosis in the top 100 variably expressed genes (Figure 6.6). However, count plots and heatmaps of the genes identified from the biplots (Figure 6.7) showed a large amount of variation within the diagnosis groups and no discernible pattern between them. The only exception perhaps being BID (BH3 Interacting Domain Death Agonist), which appeared down regulated in the inflammatory groups (all expect Norm), Figure 6.7G. Notably, the macrophages cultured with EstRA samples also had low expression of multiple genes (i.e. MTMR6, URM1, FUOM, MKNK1, LARP4B, TMEM248, SLC27A1, KLHK5), Figure 6.7.

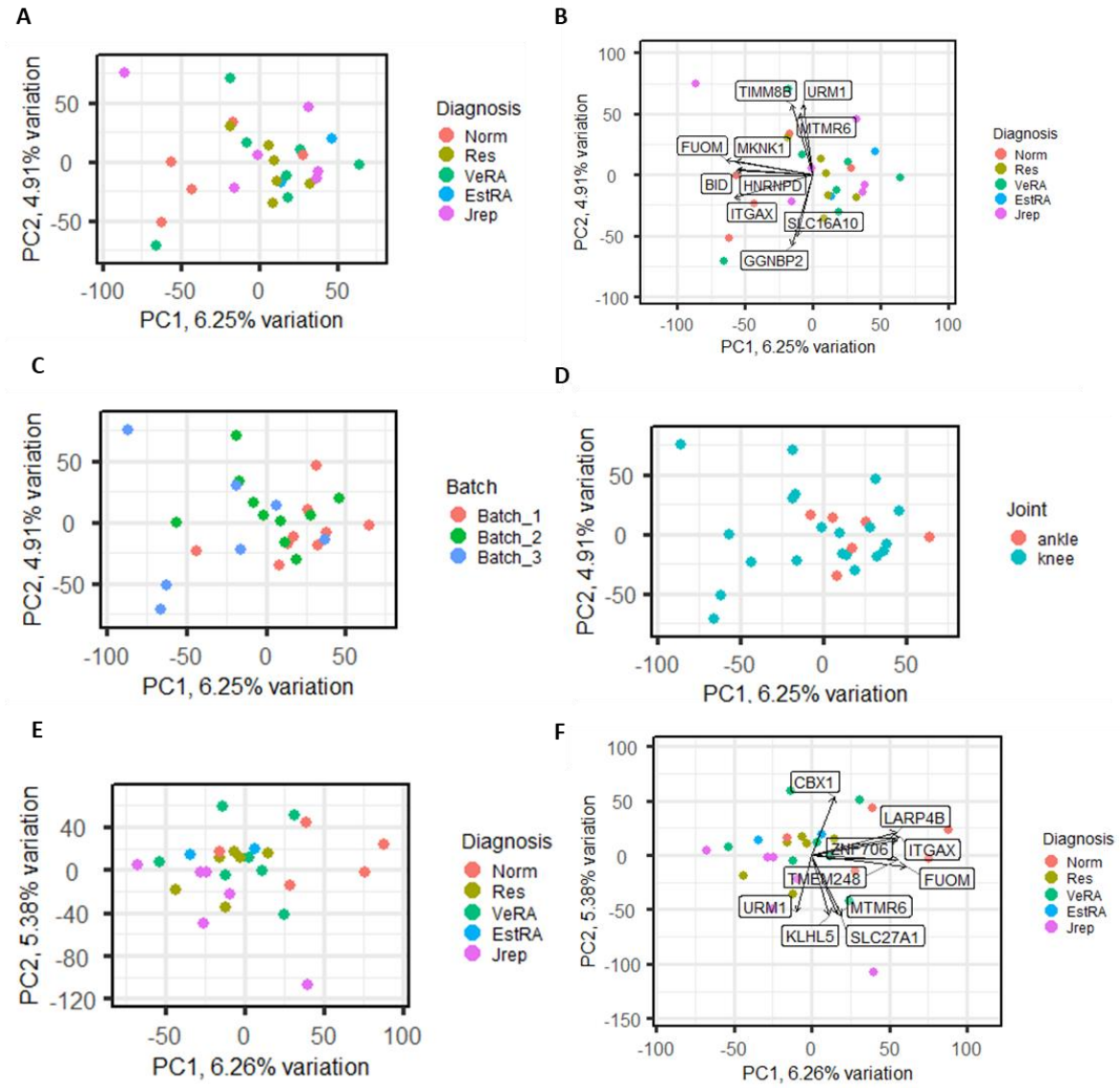

Figure 6.4: Macrophages cluster by batch and joint site. Fibroblasts and macrophages were co-cultured and treated with TNF-α for 16 hours. RNA was isolated and bulk RNA sequencing performed. Gene counts from the macrophage sequencing data were subject to variance stabilising transformation (VST) and in **(E&F)** batch effect was removed before the VST transformation. Principal Components 1 and 2 were plotted and coloured according to **(A, B, E&F)** the diagnosis of fibroblasts in culture, **(C)** the batch, and **(D)** joint site of fibroblasts in co-culture. **(B&F)** also show the genes contributing to PC loadings. Norm = Non-inflamed, Res = resolving, VeRA = very early rheumatoid arthritis, EstRA = established RA, JRep = joint replacement.

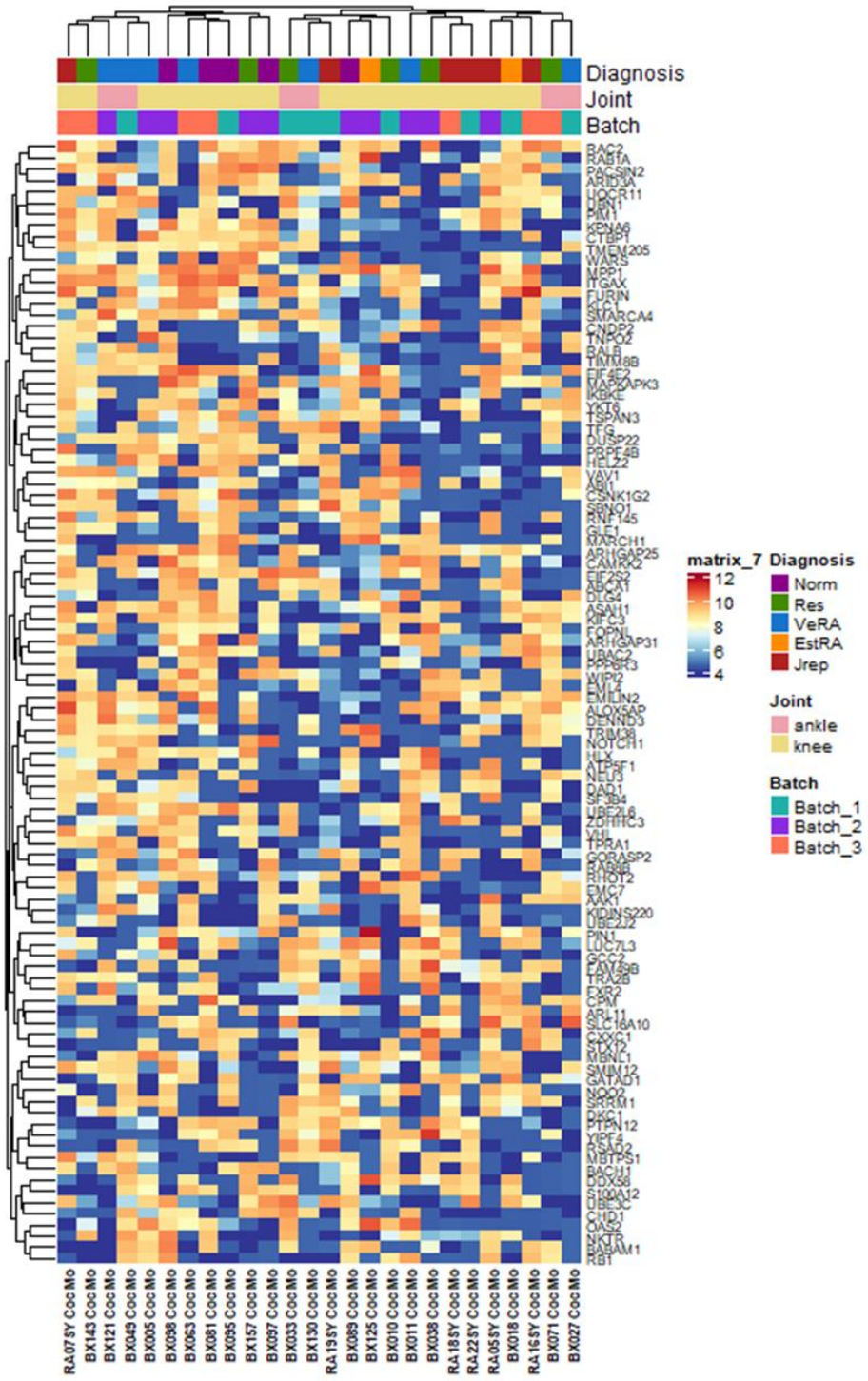

Figure 6.5: Heatmap of the top 100 variably expressed genes in macrophages. Fibroblasts and macrophages were co-cultured and treated with TNF-α for 16 hours. RNA was isolated and bulk RNA sequencing performed. Gene counts from the macrophage sequencing data were subject to variance stabilising transformation (VST). The top 100 variably expressed genes of the VST data were plotted as a heatmap with hierarchical clustering on the columns and rows. Bars at the top show the diagnosis and joint site of the fibroblasts in co-culture, and batch. Norm = Non-inflamed, Res = resolving, VeRA = very early rheumatoid arthritis, EstRA = established RA, JRep = joint replacement.

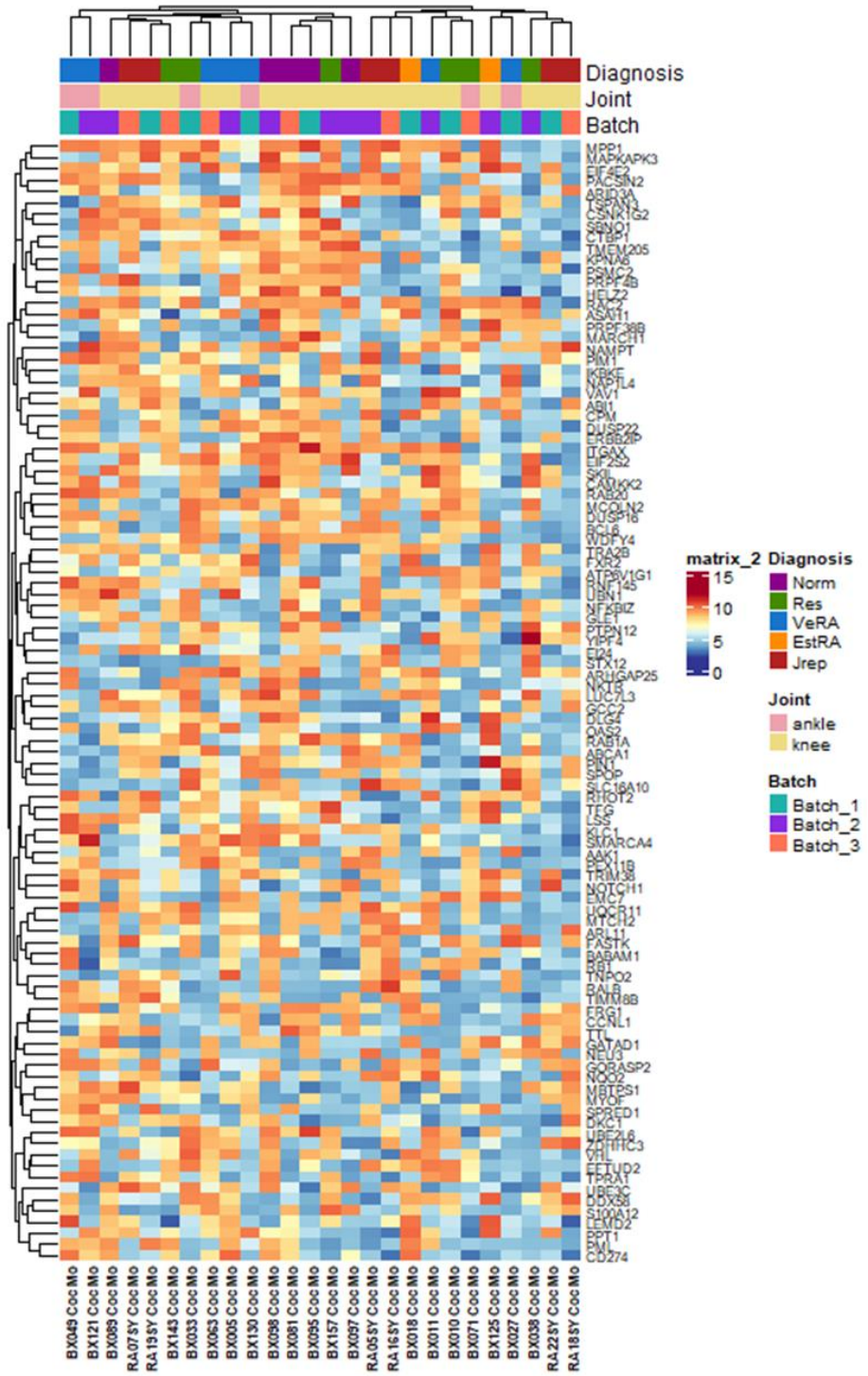

Figure 6.6: Heatmap of 100 most variable genes in macrophages after correcting for batch and joint covariates. Fibroblasts and macrophages were co-cultured and treated with TNF-α for 16 hours. RNA was isolated and bulk RNA sequencing performed. Gene counts from the macrophage sequencing data were corrected according to batch and joint site then subject to variance stabilising transformation (VST). The top 100 variably expressed genes of the VST data were plotted as a heatmap with hierarchical clustering on the columns and rows. Bars at the top show the diagnosis and joint site of the fibroblasts in co-culture, and batch. Norm = Non-inflamed, Res = resolving, VeRA = very early rheumatoid arthritis, EstRA = established RA, JRep = joint replacement.

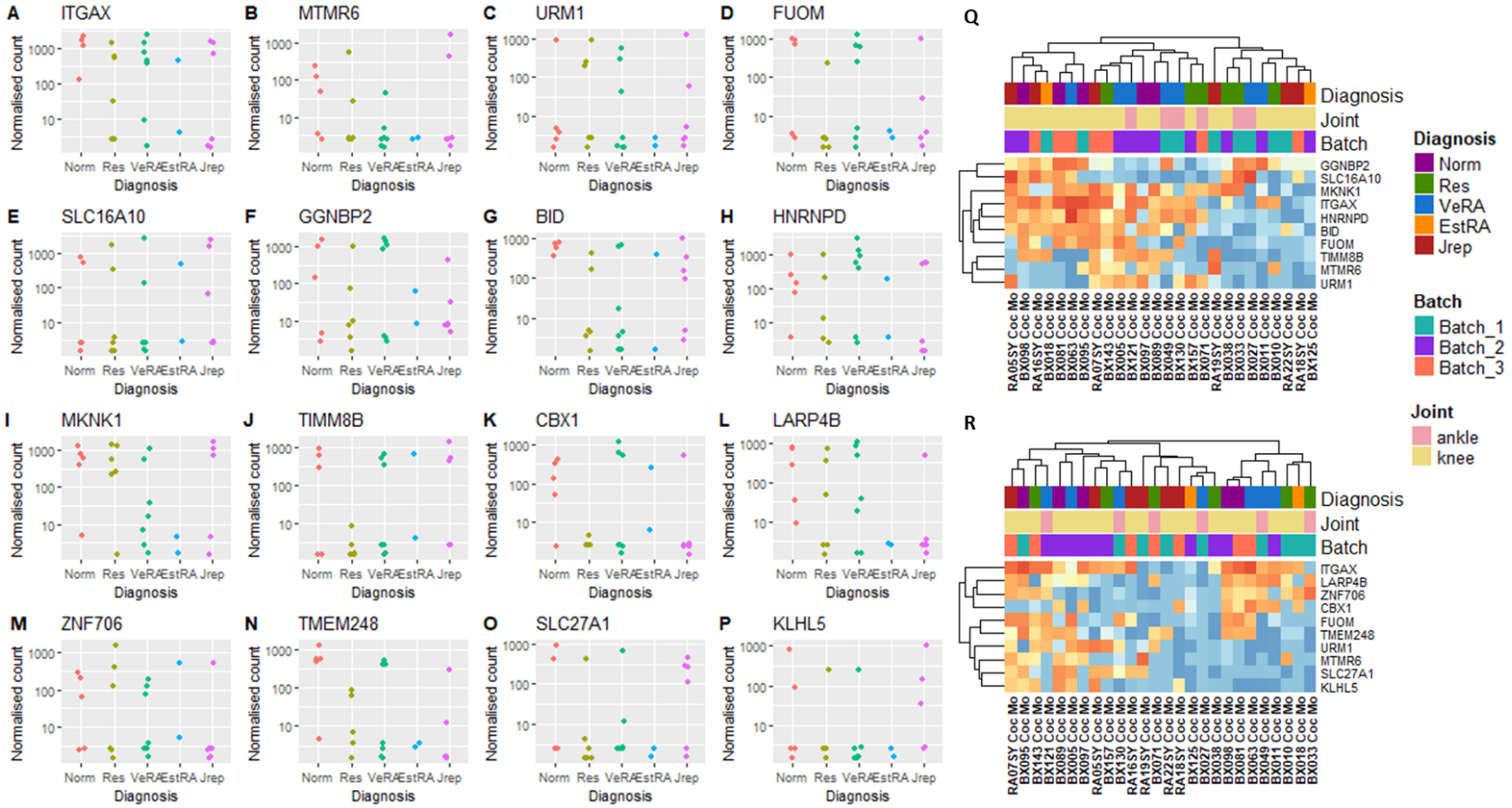

Figure 6.7: No diagnosis specific genes from count plots and heatmap of genes from biplot of macrophage. Fibroblasts and macrophages were co-cultured and treated with TNF-α for 16 hours. RNA was isolated and bulk RNA sequencing performed. Gene counts of the macrophages were subject to variance stabilising transformation and a biplot generated (Figure 6.4A). Batch correction was also performed and biplot generated (Figure 6.4E). Gene counts identified from the biplots were plotted and coloured according to the diagnosis of fibroblast donor: non-inflamed (Norm; red), resolving (Res; yellow), very early rheumatoid arthritis (VeRA; green), established RA (EstRA; blue), joint replacement (JRep; pink). **(A-D)** Genes that appeared in both original and corrected biplots, **(E-J)** the initial biplot only, **(K-P)** Genes from the batch corrected biplot only. Heatmaps were also generated of the genes from the **(Q)** uncorrected and **(R)** batch corrected biplots.

6.2.3.2 Large number of differentially expressed genes identified in macrophages from fibroblast: macrophage co-culture samples according to diagnosis of fibroblast donor

As described above, batch and joint site of the fibroblasts were known covariates within the co-cultured macrophages. Consequently, batch was built into the DESeq2 model, however, joint site was not included into the model due to the lack of sample numbers. The dispersion estimates fitted appropriately (Figure 6.8). Therefore, no further filtering was performed unless to visualise the p value histograms (as described 5.2). Differential expression analysis was performed to determine if there were differences in the macrophage transcriptome according to the outcome groups of fibroblasts in co-culture. This identified ~1000 differentially expressed genes dependent on the diagnosis of fibroblasts in culture of each comparison. A summary of the number of differentially expressed genes (DEGs) for each comparator in given in Table 6.2.

Table 6.2: Number of differentially expressed genes in macrophages between the diagnosis group of fibroblasts in culture, defined as p adj < 0.05 and an absolute log fold change >1.

	VeRA	EstRA	JRep	Norm
Res	1,368	1,035	1,552	1,462
Norm	1,109	1,036	1,317	
JRep	1,171	926		
EstRA	914			

We subsequently focused on 5 key comparisons of interest i) VeRA vs Res, ii) VeRA vs Norm, iii) VeRA vs EstRA, iv) VeRA vs JRep and v) Norm vs Res. The p-value histograms gave an anti-conservative shape (Figure 6.9) for all comparisons, when genes with less than 3 samples with normalized counts greater than or equal to 10 were filtered out. Volcano plots (Figure 6.10) and heatmaps (Figure 6.11) highlight the number differential expressed genes for each comparison. Lists of the 100 most significant DEGs for each comparison are given in Appendix Table 9 - Appendix Table 13.

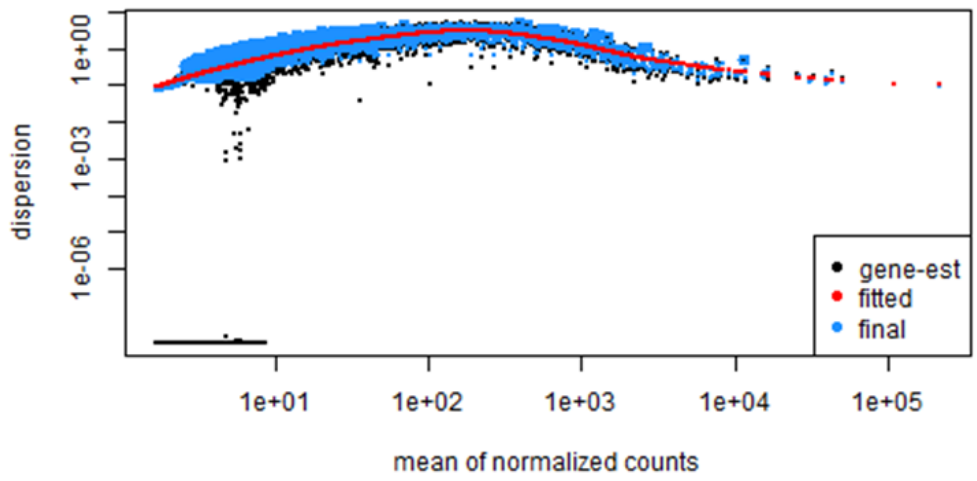

Figure 6.8: Dispersion estimates fit the data well. Fibroblasts and macrophages were co-cultured and treated with TNF-α for 16 hours. RNA was isolated and bulk RNA sequencing performed. Gene counts from the macrophage sequencing data were normalised in DESeq2 and the dispersion estimates plotted.

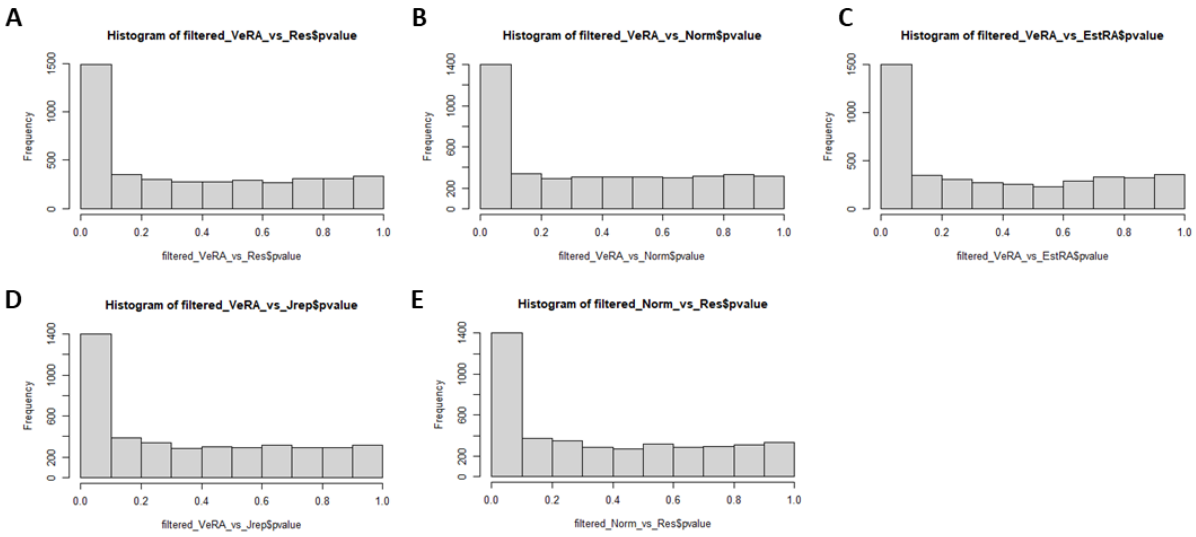

Figure 6.9: P-value histograms have an anti-conservative shape. Fibroblasts and macrophages were co-cultured and treated with TNF-α for 16 hours. RNA was isolated and bulk RNA sequencing performed. For the macrophage gene counts, genes where there are less than 3 samples with normalized counts greater than or equal to 10 were filtered out. Differential expression analysis performed and p value histograms produced for **(A)** Very early rheumatoid arthritis (VeRA) vs Resolving (Res), **(B)** VeRA vs Non-inflamed (Norm), **(C)** VeRA vs Established RA (EstRA), **(D)** VeRA vs RA patients undergoing joint replacement (JRep) and **(E)** Norm vs Res.

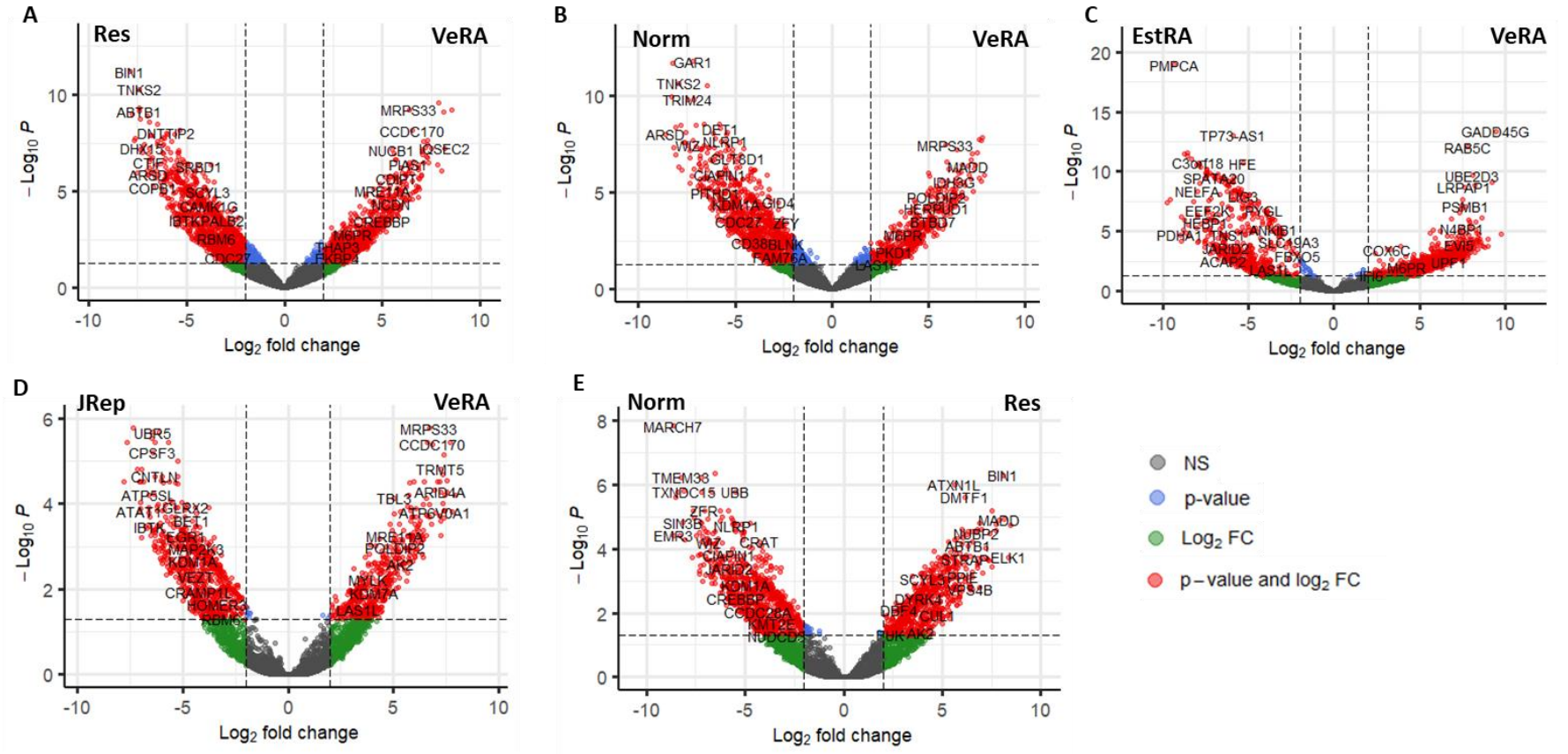

Figure 6.10: Volcano plots indicate a large number of differentially expressed genes for each comparison of interest in macrophages co-cultured with fibroblasts. Fibroblasts and macrophages were co-cultured and treated with TNF-α for 16 hours. RNA was isolated and bulk RNA sequencing performed. Differential expression analysis was performed using DESeq2 on the macrophage gene counts for **(A)** Very early rheumatoid arthritis (VeRA) vs Resolving (Res), **(B)** VeRA vs Non-inflamed (Norm), **(C)** VeRA vs Established RA (EstRA), **(D)** VeRA vs RA patients undergoing joint replacement (JRep) and **(E)** Norm vs Res. Log2 fold change and p values shown in volcano plots.

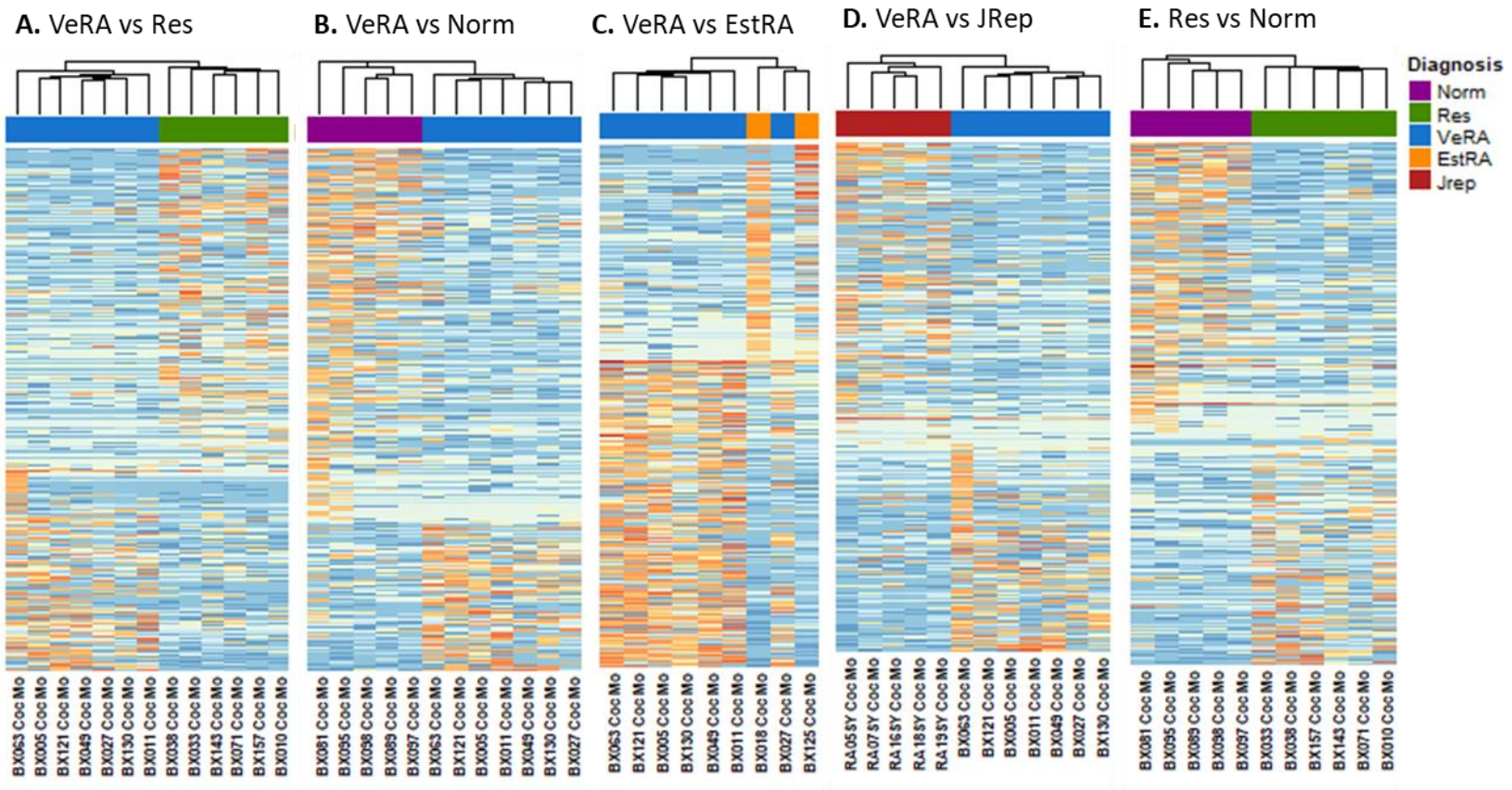

Figure 6.11: Heatmaps indicate a large number of differentially expressed genes between but also within groups for each comparison of interest in macrophages co-cultured with fibroblasts. Fibroblasts and macrophages were co-cultured and treated with TNF-α for 16 hours. RNA was isolated and bulk RNA sequencing performed. Differential expression analysis was performed using DESeq2 on the macrophage gene counts for **(A)** Very early rheumatoid arthritis (VeRA) vs Resolving (Res), **(B)** VeRA vs Non-inflamed (Norm), **(C)** VeRA vs Established RA (EstRA), **(D)** VeRA vs RA patients undergoing joint replacement (JRep) and **(E)** Norm vs Res. Differentially expressed genes were then ordered according to Log2 fold change and heatmap generated.

6.2.3.3 Gene set enrichment analysis indicates IL-6-JAK-STAT3, TNF-α via NF-κB, and IFNγ signalling contribute to the separation of macrophages co-cultured with fibroblasts according to the diagnosis of fibroblast donor

To identify which process and pathways may differ between the groups, gene set enrichment was the performed using the DESeq2 normalised gene counts and hallmark gene sets from the Molecular signature database (MSigDB). Since the EstRA group had only 2 samples, the VeRA vs EstRA comparison could not be carried out, but gene expression of all groups (including EstRA) was evaluated when looking at the genes of interest identified the pathway analysis. GSEA identified no significantly enriched pathways when comparing VeRA to Res, Norm or JRep according to the FDR corrected q-values (where <0.25 was deemed significant), but some were significant according to the nominal p value of <0.05 (Figure 6.12A-C). Notably, 3 pathways were significantly enriched according to FDR q-value in the "Norm vs Res" comparison; "IL6_JAK_STAT3_SIGNALLIING", "TNFA_SIGNALLING_VIA_NFkB", "INTERFERON_GAMMA_RESPONSE" (Figure 6.12D). Interestingly, these were also enriched according to the nominal p value in at least one other comparison. However, as demonstrated in the heatmaps and count plots of genes from these pathways (Figure 6.13 - Figure 6.15), gene expression was highly variable within each group. Therefore, we focused on the least variable genes within each pathway.

Genes identified in the enriched the IL6-JAK-STAT3 signalling pathway

The JAK-STAT signalling pathway (Figure 6.13) was positively enriched for both "VeRA vs Res" and "Norm vs Res", suggesting a potential negative enrichment associated with the Res samples. Notably, PTPN1 (Protein Tyrosine Phosphatase Non-Receptor Type 1) and MAP3K8 (Mitogen-activated protein kinase 8) were two of the top enriched genes in both "VeRA vs Res" and "Norm vs Res", although there was variation in expression within these groups.

Despite this, both had an adjusted p value <0.05 for both comparisons according to the DE analysis, except for PTPN1 in "VeRA vs Res" (Table 6.3). TNFSFR1A (Tumour necrosis factor receptor 1) and IRF9 (Interferon Regulatory Factor 9) had much lower expression in the Norm and Res compared to RA samples. Whilst the DE of these genes appeared to enhance enrichment in the IL-6 pathway, neither was significantly differentially expressed in the DESeq2 analysis (Table 6.3). This may be due to an outlier in the VeRA group (BX027), which had low expression of both genes compared to other VeRA samples. To see if this was the case, we repeated DE analysis without BX027, and both had a higher log fold change and lower p values (TNFRSF1A; LF = 2.506671, Padj = 0.03955147 and IRF9 FC = 3.619844, Padj = 0.0508643). CXCL1 had significantly lower expression in Res compared to Norm (Table 6.3), and was expressed lower in the RA samples compared to Norm.

Genes identified in the enriched TNF-α signalling via NFκB signalling pathway

"TNFA_SIGNALLING_VIA_NFkB" was negatively enriched in "VeRA vs Norm" and positively enriched in "Norm vs Res", suggesting a positive enrichment in the Norm group (Figure 6.14). MAP2K3 was amongst the top genes for both, although it was only significantly DE in the "VeRA vs Norm" comparison. Interestingly, except for one outlier (BX063) MAP2K3 was lower in VeRA compared to all other groups. For "VeRA vs Norm", a number of genes were enriched and all significantly DE according to p value and all expect CEBPD and SOD2, according to the adjusted P value (Table 6.4). Of these genes, SOD2 and IRS2 were of interest as these were higher in the Norm compared to all other groups (Figure 6.14C). Regarding "Norm vs Res", there was a large amount of variability and only EHD1, TRAF1 and NFE2L2 were significantly differentially expressed (Table 6.4).

Genes identified in the enriched IFN-γ response pathway

Interestingly, the "INTERFERON_GAMMA_RESPONSE" was negatively enriched in "VeRA vs Norm", but positively enriched in "Norm vs Res", suggesting an overall positive enrichment for the Norm group (Figure 6.15). It was also positively enriched in "VeRA vs JRep". Similarly, to the "IL6-JAK-STAT" signalling, PTPN1 was again amongst the top genes for both "VeRA vs Norm" and "Res vs Norm", although neither had an adjusted p value <0.05. For "VeRA vs Norm", only SP110 was DE according to adjust, and interestingly SOD2 (also in TNF-α signalling via NFκB) came up. In "VeRA vs JRep", STAT1 was the top gene, though not significantly DE, but again this may be due to one outlier (BX027) which was lower compared to other VeRA samples. Intriguingly, STAT1 was lower in both the JRep and Norm compared to all other samples. Regarding, "Res vs Norm", only HIF1A and SAMD9L, had an adjusted p value < 0.05 (Table 6.5) and even these had a lot of variability within each group.

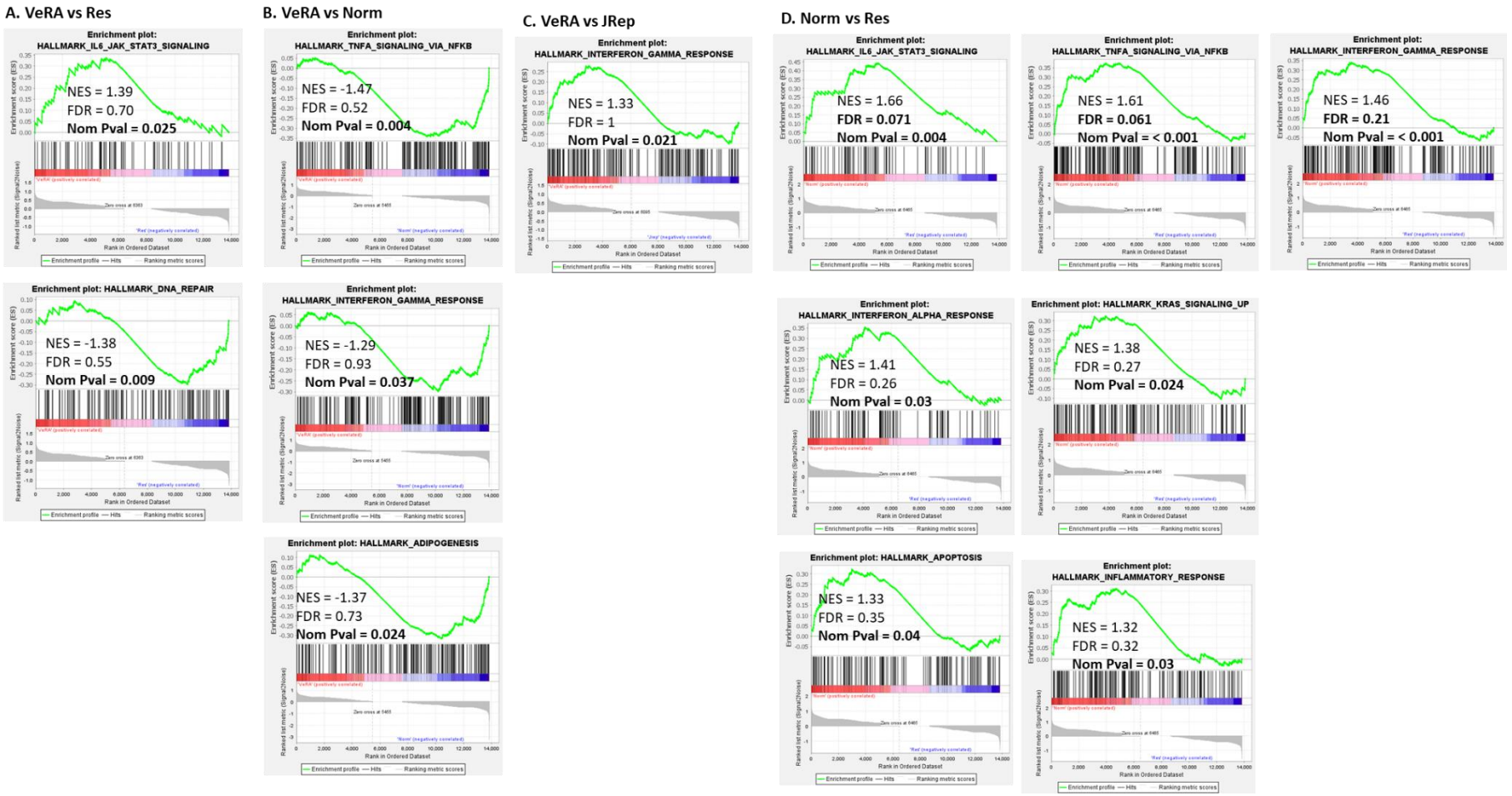

Figure 6.12: Gene set enrichment analysis of macrophage comparisons. Fibroblasts and macrophages were co-cultured and treated with TNF-α for 16 hours. RNA was isolated and bulk RNA sequencing performed. The gene counts table was submitted for gene set enrichment analysis (GSEA) of the hallmark pathways, for comparisons of **(A)** Very early rheumatoid arthritis (VeRA) vs Resolving (Res), **(B)** VeRA vs Non-inflamed (Norm), **(C)** VeRA vs RA patients undergoing joint replacement (JRep) and **(D)** Norm vs Res. Nominal p values <0.05 and FDR p values <0.25 are regarded as significant and shown in bold.

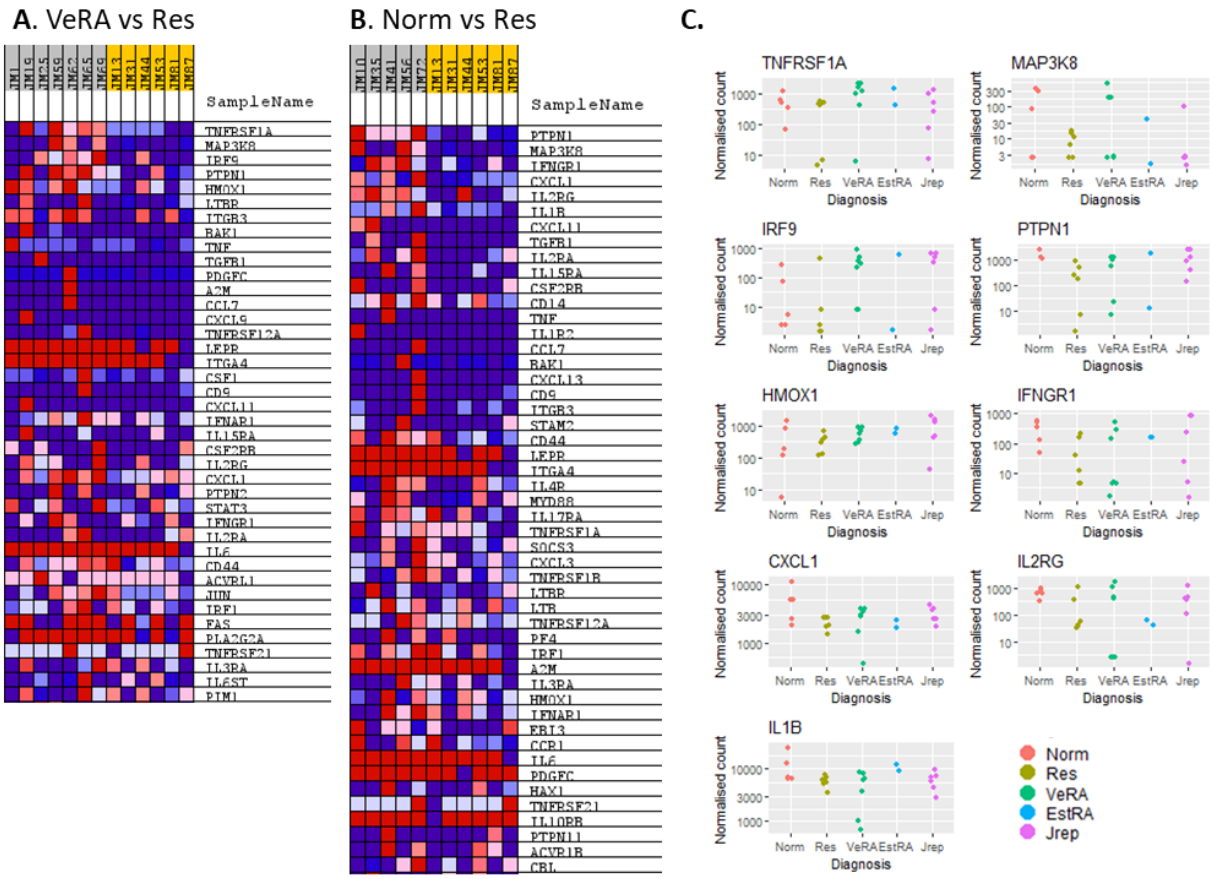

Figure 6.13: Heatmap and gene count plots of the genes from the enriched IL6-JAK-STAT3 pathway gene set. Fibroblasts and macrophages were co-cultured and treated with TNF-α for 16 hours. RNA was isolated and bulk RNA sequencing performed. The DESeq2 normalised gene counts table was submitted for gene set enrichment analysis (GSEA) of the hallmark pathways and IL-6-JAK-STAT pathway deemed significantly enriched and heatmap of the enriched genes was generated for **(A)** VeRA (grey) vs Res (yellow) **(B)** Norm (grey) vs Res (yellow). **(C)** Gene count plots of the top highly enriched genes were plotted.

Table 6.3: DESeq2 results from the top 6 genes in the IL-6_JAK_STAT signalling pathway of macrophages

HGNC symbol	Log2 FoldChange	P value	P adj	Entrez	Ensembl ID
VeRA vs Res					
TNFRSF1A	1.968731	0.051322	0.170975	7132	ENSG00000067182
MAP3K8	3.742511	0.004369	0.025663	1326	ENSG00000107968
IRF9	2.6288	0.058766	0.190553	10379	ENSG00000213928
PTPN1	1.361045	0.188433	0.464095	5770	ENSG00000196396
HMOX1	1.04836	0.20357	0.490134	3162	ENSG00000100292
LTBR	3.60686	0.015951	0.068541	4055	ENSG00000111321
Res vs Norm					
PTPN1	-2.56707	0.023244	0.09156	5770	ENSG00000107968
MAP3K8	-4.22698	0.003152	0.018923	1326	ENSG00000107968
IFNGR1	-1.53228	0.270779	0.599342	3459	ENSG00000027697
CXCL1	-1.21606	0.007023	0.035884	2919	ENSG00000163739
IL2RG	-1.57428	0.218075	0.516873	3561	ENSG00000147168
IL1B	-0.72933	0.110623	0.313881	3553	ENSG00000125538

Norm = Non-inflamed, Res = resolving, VeRA = Very early rheumatoid arthritis.

Genes in both comparisons shown in red.

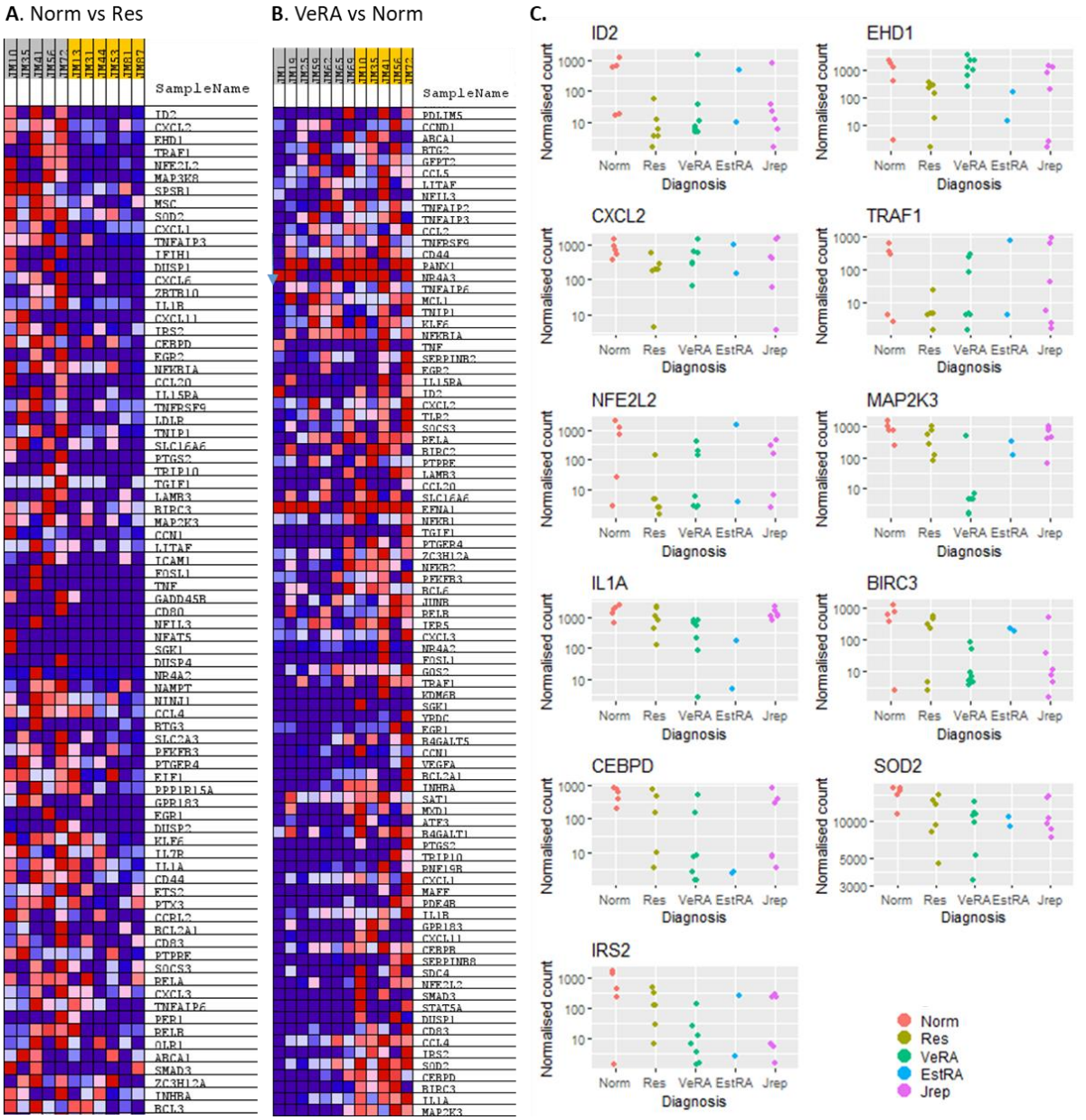

Figure 6.14: Heatmap and gene counts of the genes from the enriched TNF-A signalling pathway gene set. Fibroblasts and macrophages were co-cultured and treated with TNF-α for 16 hours. RNA was isolated and bulk RNA sequencing performed. The gene counts table was submitted for gene set enrichment analysis (GSEA) of the hallmark pathways and IFN-γ response pathway deemed significantly enriched and heatmap of the enriched genes generated for **(A)** Norm (grey) vs Res (yellow) and **(B)** VeRA (grey) vs Norm (yellow). **(C)** Gene count plots for the top highly enriched genes.

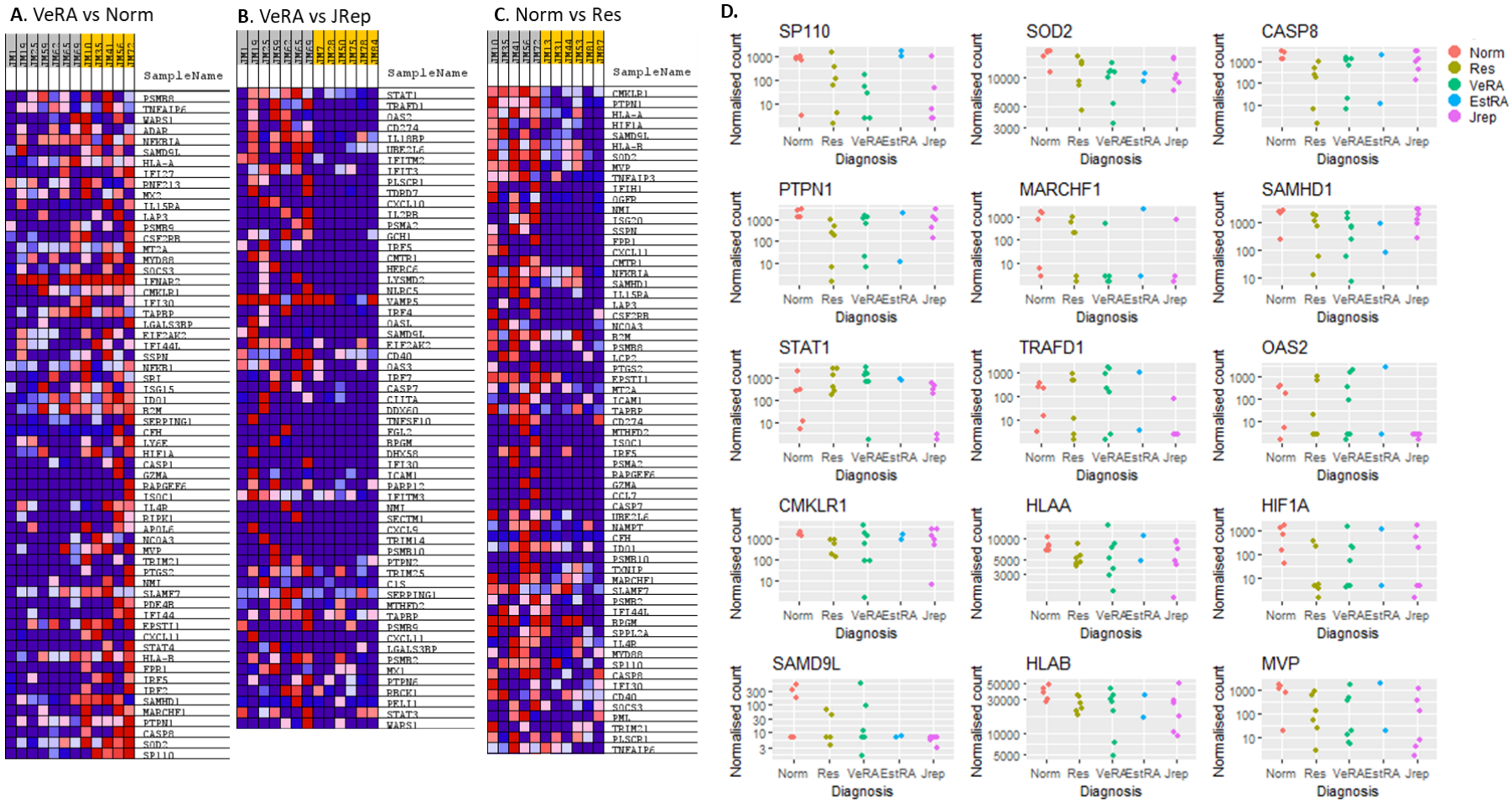

Figure 6.15: Heatmap and gene counts of the genes from the enriched IFN-γ response pathway gene set. Fibroblasts and macrophages were co-cultured and treated with TNF-α for 16 hours. RNA was isolated and bulk RNA sequencing performed. The gene counts table was submitted for gene set enrichment analysis (GSEA) of the hallmark pathways and IFN-γ response pathway deemed significantly enriched and heatmap of the enriched genes was generated for **(A)** VeRA (grey) vs Norm (yellow) **(B)** VeRA (grey) vs JRep (yellow) and **(C)** Norm (grey) vs Res (yellow). **(D)** The top highly enriched genes were plotted as gene counts.

Table 6.4: DESeq2 results from the top 6 genes in the TNF-α via NFκB signalling pathway of macrophages

HGNC symbol	Log2 FoldChange	P value	P adj	Entrez	Ensembl ID
VeRA vs Norm					
MAP2K3	-5.45563	6.59E-07	5.16E-05	5606	ENSG00000034152
IL1A	-1.9878	0.019947	0.098002	3552	ENSG00000115008
BIRC3	-5.12107	6.09E-05	0.001196	330	ENSG00000023445
CEBPD	-2.78957	0.048076	0.194151	1052	ENSG00000221869
SOD2	-0.7814	0.021669	0.104558	6648	ENSG00000112096
IRS2	-4.76459	0.000211	0.003076	8660	ENSG00000185950
Res vs Norm					
ID2	-5.676929654	NA	NA	3398	ENSG00000115738
CXCL2	-1.707532419	0.087384174	0.26126045	2920	ENSG00000081041
EHD1	-2.756117662	0.023430086	0.092016101	10938	ENSG00000110047
TRAF1	-4.675598683	0.001858005	0.012540603	7185	ENSG00000056558
NFE2L2	-6.61495041	2.23E-05	0.000576859	4780	ENSG00000116044
MAP2K3	-1.104658531	0.32874264	0.685363796	5606	ENSG00000034152

Norm = Non-inflamed, Res = resolving, VeRA = Very early rheumatoid arthritis.
Genes in both comparisons shown in red.

Table 6.5: DESeq2 results from the top 6 genes in the IFNγ response pathway of macrophages

HGNC symbol	Log2 FoldChange	P value	P adj	Entrez	Ensembl ID
VeRA vs Norm					
SP110	-5.15686	0.000266	0.003664	3431	ENSG00000135899
SOD2	-0.7814	0.021669	0.104558	6648	ENSG00000112096
CASP8	-4.19606	NA	NA	841	ENSG00000064012
PTPN1	-1.20603	0.268327	0.691187	5770	ENSG00000196396
MARCHF1	-6.08705	NA	NA	55016	ENSG00000145416
SAMHD1	-1.38539	0.153607	0.467765	25939	ENSG00000101347
VeRA vs JRep					
STAT1	1.770162	0.110686	0.357111	6772	ENSG00000115415
TRAFD1	6.684358	2.75E-06	0.000203	10906	ENSG00000135148
OAS2	7.437822	1.56E-06	0.000142	4939	ENSG00000111335
CD274	7.923102	4.2E-07	6.26E-05	29126	ENSG00000120217
IL18BP	1.024791	0.452092	0.868588	10068	ENSG00000137496
UBE2L6	3.340748	0.028079	0.124255	9246	ENSG00000156587
Res vs Norm					
CMKLR1	-1.28024	0.181351	0.455241	1240	ENSG00000174600
PTPN1	-2.56707	0.023244	0.091564	5770	ENSG00000196396
HLA-A	-0.44528	0.284833	0.619314	3105	ENSG00000206503
HIF1A	-4.33464	0.004645	0.025835	3091	ENSG00000100644
SAMD9L	-3.13388	0.009107	0.043941	219285	ENSG00000177409
HLA-B	-0.40528	0.287277	0.62322	3106	ENSG00000234745

JRep = Rheumatoid arthritis patients undergoing joint replacement, Norm = Non-inflamed, Res = resolving, VeRA = Very early RA.
Genes in both comparisons shown in red.

6.2.3.4 No significant differential expression of IFN-β signalling, or other previously described, molecules of interest

Previous findings identified dysregulation of the IFN-β pathway macrophage-JRep fibroblast co-cultures (134, 143). However, this pathway was not present in the hallmark gene sets form the MSigDB dataset. Therefore, to examine if any genes in this pathway were altered, a heatmap of IFN-α/β genes was generated (Appendix Figure 8), but no discernible pattern between the groups was observed. Likewise, we generated counts plots of genes of interest from other studies (133, 134, 143), but no large differences were observed (Appendix Figure 9). The only exceptions were higher MerTK expression in some Norm and Res samples compared to the RA groups (JRep, VeRA and EstRA) and higher CD11b expression in Res and VeRA compared to all other groups. However, expression of CD11b and MerTK was low across all groups limiting possible interpretation.

6.2.3.5 Ingenuity pathway analysis revealed upstream microRNAs and transcription factors may be driving the separation between groups

Ingenuity pathway analysis (IPA) was performed using the log2 fold change and adjusted p values from the DE analysis of the co-cultured macrophages, in order to identify differential pathways and processes (Figure 6.16). For "VeRA vs Res" (Figure 6.16A), mir-17 was activated triggering the inhibition of the transcription factor E2F1 and ultimately inhibition of excision repair.

For "VeRA vs Norm" (Figure 6.16B) there was suggested inhibition of SH3TC2 (SH3 Domain And Tetratricopeptide Repeats 2), RPTOP, HBEGF, development of hematopoietic progenitor cells, ruffling and differentiation of tumour cell lines, whilst there was upregulation of KRAS (Kirsten rat sarcoma virus), GFL1 (growth factor independent 1 transcriptional repressor) and growth failure.

For "VeRA vs JRep" (Figure 6.16C) activation of ZC3H12A (zinc finger CCCH-type containing 12A) causes inhibition of microRNA and links to the inhibition of transcription regulators Esrra (estrogen related receptor, alpha) and HNF4A.

For "Res vs Norm" (Figure 6.16D) there was inhibition of transformation of embryonic lines, transport of D-glucose, hypoxia signalling in the cardiovascular systems, transcription [linked to activation of JARID2 (jumonji and AT-rich interaction domain containing 2)], proliferation of embryonic cell lines and NOX1 (NADPH oxidase 1), and transport of molecule and neoplasia of cells.

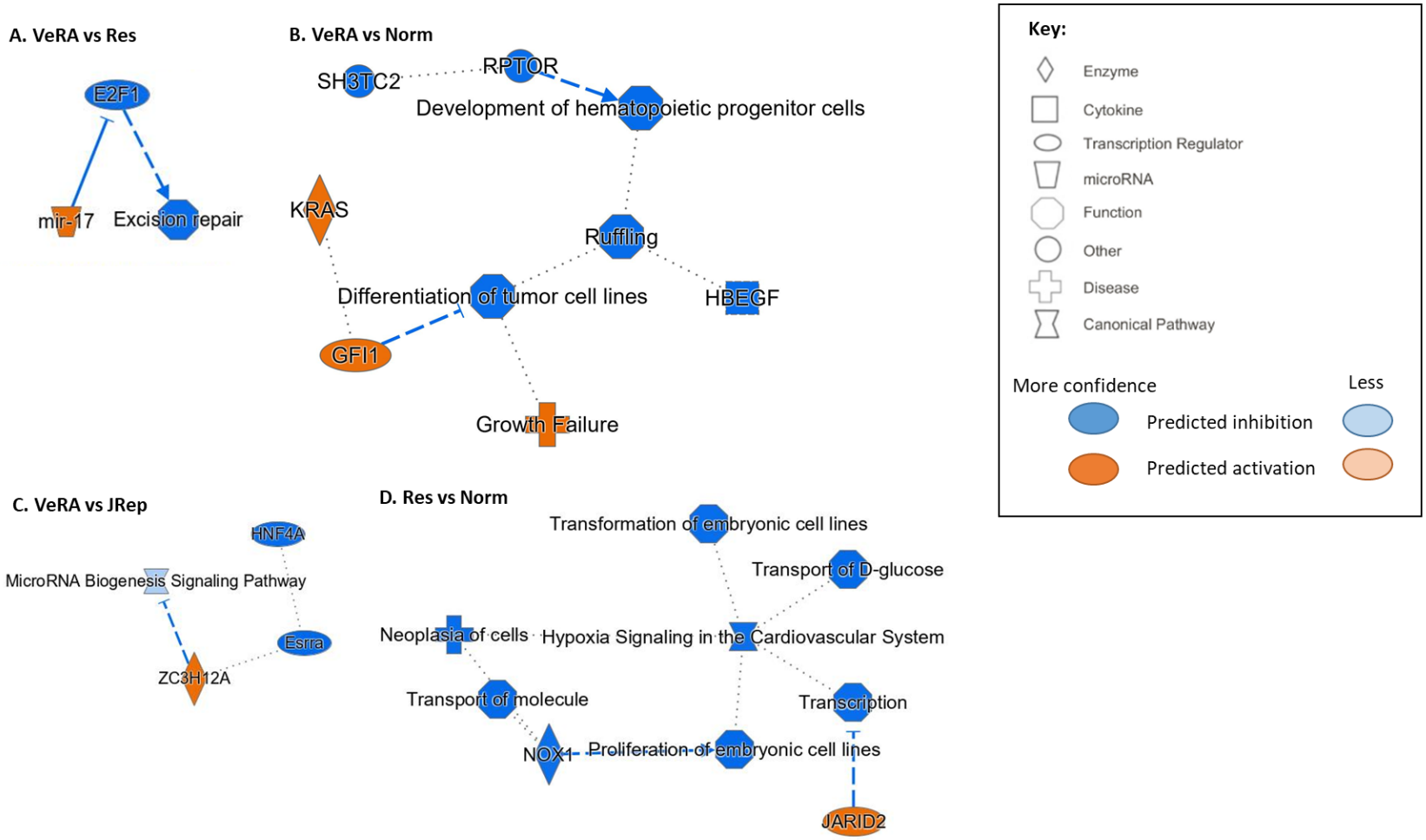

Figure 6.16: Graphical summaries of major biological themes associated with differential expression in macrophages. Log2 Fold Change and adjusted p values from the differential gene expression analysis of macrophages was subjected to ingenuity pathway analysis (IPA). Graphical summaries from IPA core analysis were generated for comparisons of; **(A)** Very early rheumatoid arthritis (VeRA) vs Resolving (Res), **(B)** VeRA vs Non-inflamed (Norm), and **(D)** Norm vs Res.

6.2.3.6 Focusing analysis on macrophages cultured with very early rheumatoid arthritis, non-inflamed and resolving arthritis fibroblasts revealed enhanced separation between groups

Due to the limited number of samples (n=2) for the EstRA and the confounding factors of treatment and disease duration in the JRep cohort, analysis was then focused on the VeRA, Res and Norm groups. This also addressed the question of what changes occur in the earliest, initial stages of disease - a rare opportunity, possible using BEACON cohort. To explore these groups, analysis of the most variably expressed genes was carried out (Figure 6.17). An initial PCA showed a large batch effect (Figure 6.17A) and no clustering by diagnosis (Figure 6.17B). However, correcting for batch effect (Figure 6.17C) revealed clustering of macrophages according the diagnosis of fibroblast in co-culture (VeRA, Norm or Res). A heatmap of the top 100 variably expressed genes (Figure 6.17D) showed clustering according to diagnosis, in particular the 4 macrophage samples co-cultured with the VeRA fibroblasts clustered separately from the others potentially revealing a difference associated with chronic inflammation/disease.

To explore the genes responsible for this separation, differential expression analysis and likelihood ratio test were performed to compare expression across all three groups. A 3D volcano plot (Figure 6.18) revealed the largest number of genes were specific to the Norm group > Res > VeRA. In terms of genes shared across the groups, Norm and Res shared the most, with some shared between Norm and VeRA, but very few genes were shared between VeRA and Res.

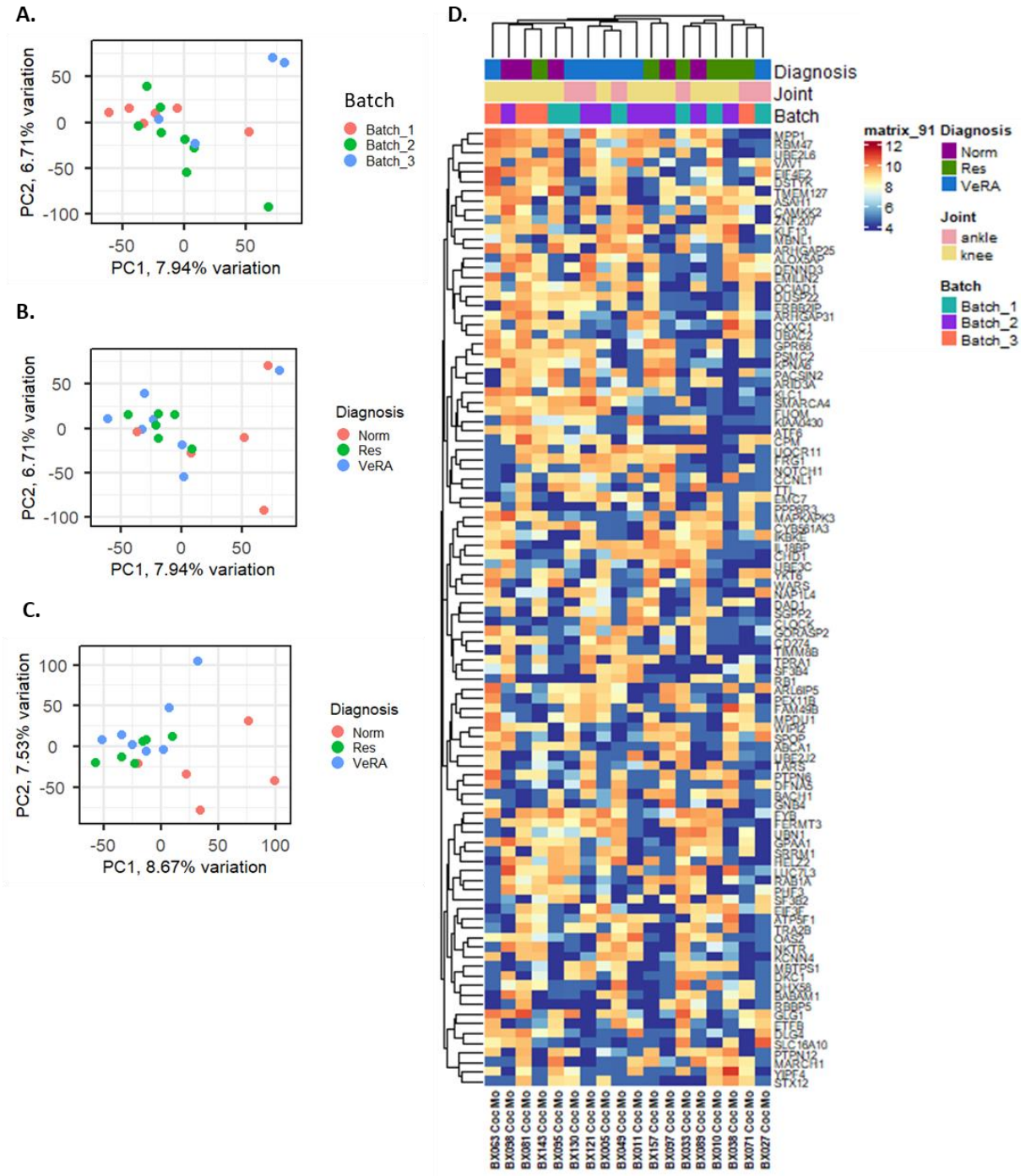

Figure 6.17: Macrophages cluster according to the diagnosis (very early RA, non-inflamed or resolving) of fibroblasts in co-culture. Fibroblasts and macrophages were co-cultured and treated with TNF-α for 16 hours. RNA was isolated and bulk RNA sequencing performed. Gene counts from the macrophage sequencing data were subject to variance stabilising transformation (VST). **(A - C)** Principal component analysis (PCA) was carried out and PCs 1 and 2 were plotted and coloured according to **(A)** Batch or **(B & C)** diagnosis of fibroblast in co-culture. For **(C)** batch correction using limma was applied prior to PCA. **(D)** The top 100 variably expressed genes of the VST data were plotted as a heatmap with hierarchical clustering on the columns and rows. Bars at the top show the diagnosis and joint site of the fibroblasts in co-culture, and batch. Norm = Non-inflamed, Res = resolving, VeRA = very early rheumatoid arthritis.

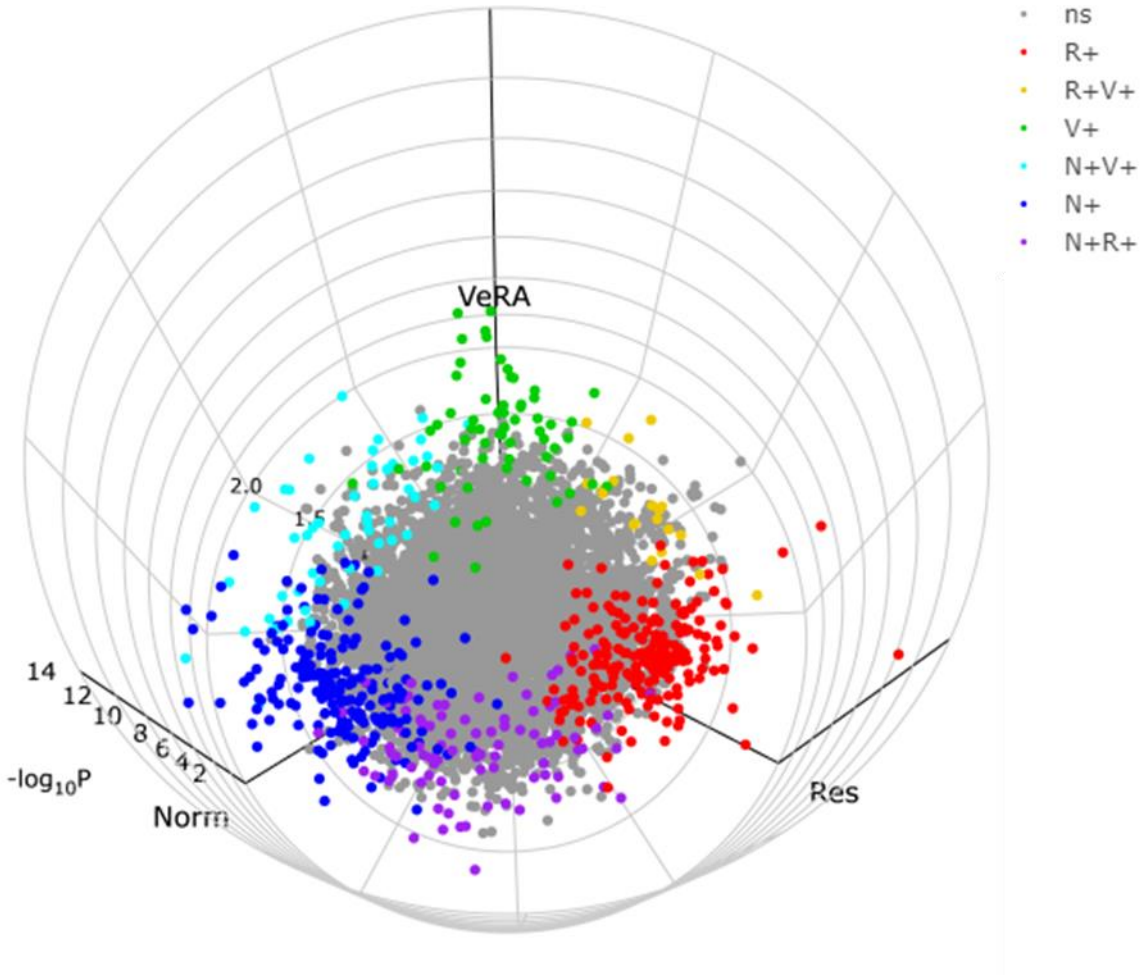

Figure 6.18: 3D volcano plot of macrophages cultured with VeRA, Norm and JRep fibroblasts. Fibroblasts and macrophages were co-cultured and treated with TNF-α for 16 hours. RNA was isolated and bulk RNA sequencing performed. Differential expression analysis was performed using DESeq2 on macrophages cultures with fibroblasts from very early rheumatoid arthritis (VeRA; V), resolving (Res; R) and non-inflame (Norm; N) patients. A likelihood ratio test was performed according to the diagnosis of fibroblast and 3D volcano plot generated with deseq_polar. Colours indicate upregulation in either only one group: VeRA (green), Res (red) and Norm (blue) or two groups combined; VeRA+Res (yellow), Res+Norm (purple) and Norm + VeRA (cyan). An interactive version of this plot is available: http://rpubs.com/Julia857/952283.

6.2.4 Analysis of fibroblasts from fibroblast: macrophage co-culture samples

Previous reports have shown that co-culture with macrophages was required for fibroblasts to degrade cartilage (144). Therefore, we wanted to explore changes between fibroblast diagnoses when in co-culture with macrophages. Furthermore, to see if the changes in the fibroblast transcriptome complimented any transcriptomic changes observed in the macrophages.

6.2.4.1 Exploration of the most variable genes revealed separation in fibroblasts according to diagnosis, particularly JRep compared to other groups,

Initial analysis of all fibroblast together showed some clustering by diagnosis (Appendix Figure 10). However, we wanted to investigate the changes in co-culture, thus analysis was performed on mono and co-cultured cells separately. The PCA (Figure 6.19A) and biplot (Figure 6.19B) showed no clear clustering by diagnosis (Figure 6.19A and B). Similarly, to the macrophages, there was separation between the Norm and JRep samples, with the exception of one JRep sample (RA18SY) which clustered close to the Norm group. Fibroblasts also clustered by batch in PCs1 and 2 (Figure 6.19C) and slightly by joint in PCs 2 and 3 (Figure 6.19D). Correcting for batch effect revealed stronger clustering by diagnosis, in particular JRep separated from other groups (Figure 6.19E and F). A heatmap of the genes identified in the biplots (Figure 6.20) demonstrated batch effects in the initial PCA (Figure 6.20A) and in batch corrected data, clustering of the JRep samples, where again RA18SY was an outlier (Figure 6.20B). Of the genes from the biplot, it appeared that IGF1R, C19orf25 (chromosome 19 open reading frame 25), CNPPD1 (cyclin Pas1/PHO80 domain containing 1), CTHRC1 (collagen triple helix repeat containing 1) and RESTAT (retinol saturase) were higher in the JRep samples compared to the other groups (Figure 6.20B). Despite this, heatmaps of

the top 100 variably expressed genes both for the uncorrected (Figure 6.21) and batch corrected (Figure 6.22) counts showed no definite clusters according to diagnosis.

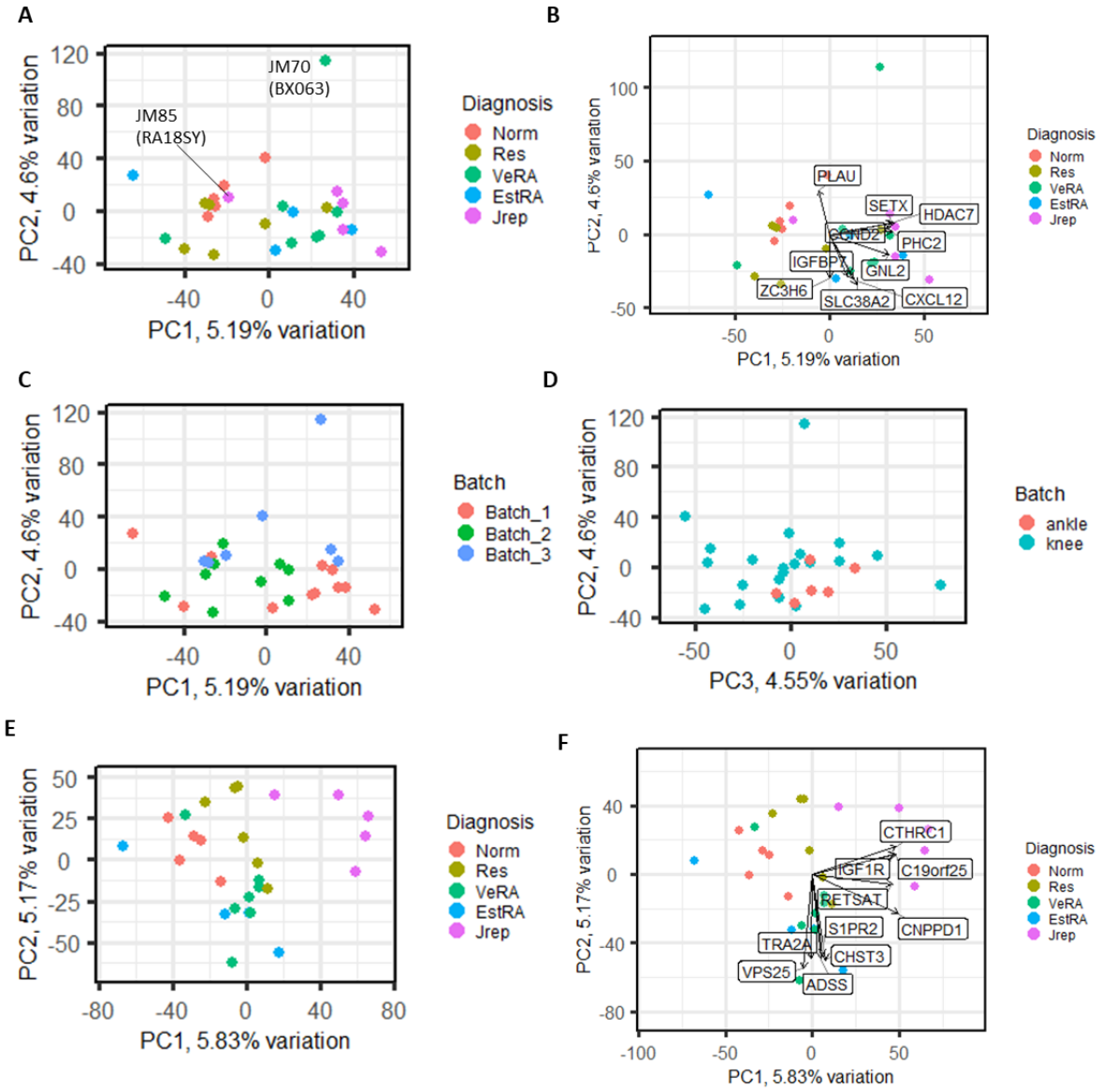

Figure 6.19: Fibroblasts cluster according to fibroblast diagnosis, batch and joint site. Fibroblasts and macrophages were co-cultured and treated with TNF-α for 16 hours. RNA was isolated and bulk RNA sequencing performed. Gene counts from the fibroblasts that were co-cultured, were subject to variance stabilising transformation (VST) and for **(E&F)** batch effect removed before VST transformation. Principal Components were plotted and coloured according to **(A, B, E&F)** the diagnosis of fibroblasts in culture **(C)** the batch, and **(D)** joint site of fibroblasts in co-culture. **(B&F)** also show the genes contributing to PC loadings. In **(A)** outliers are labelled. Norm = Non-inflamed, Res = resolving, VeRA = very early RA, EstRA = established RA, JRep = joint replacement.

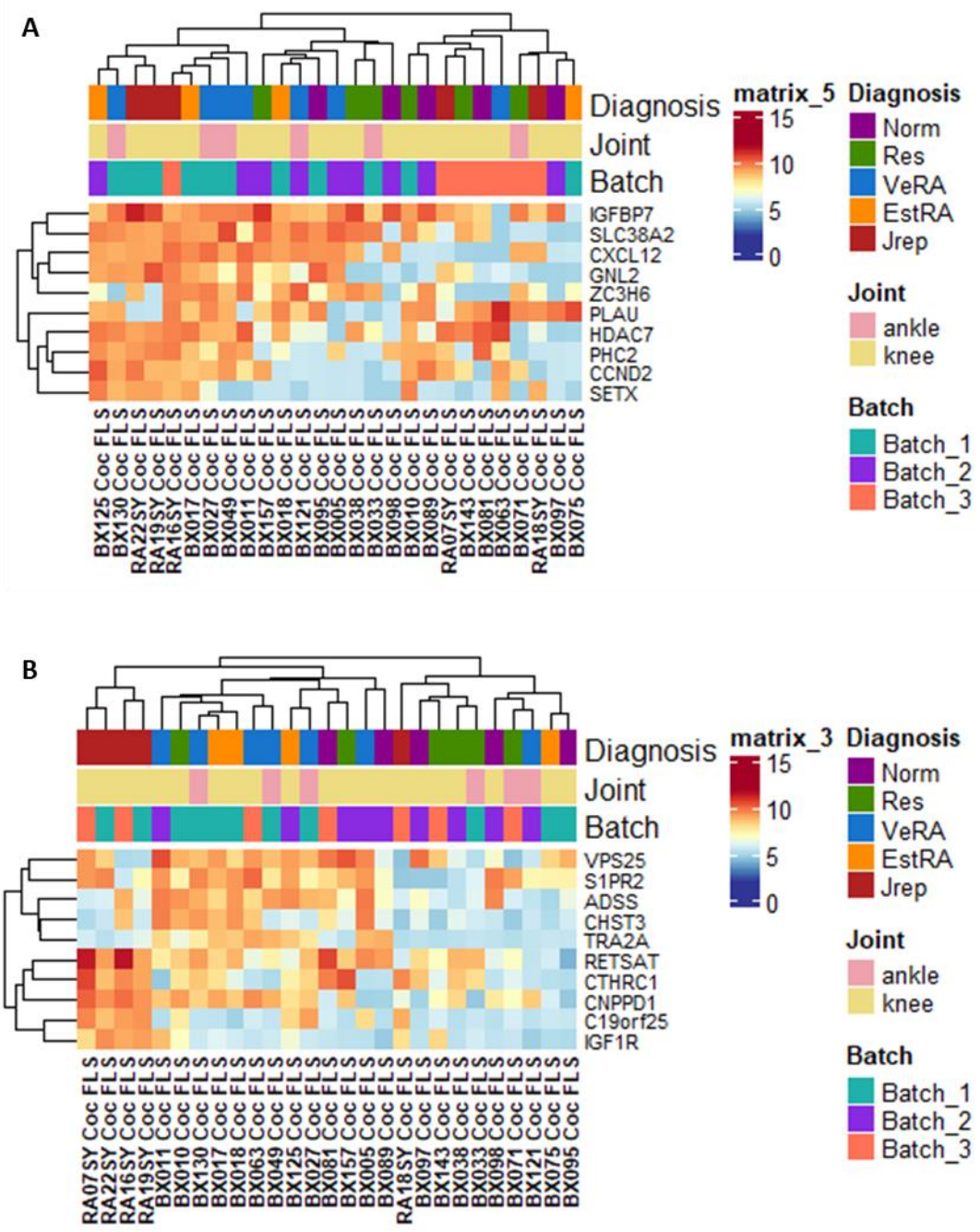

Figure 6.20: Gene count plots of genes that contribute to PC loadings. Fibroblasts and macrophages were co-cultured and treated with TNF-α for 16 hours. RNA was isolated and bulk RNA sequencing performed. Gene counts of the fibroblasts, were subject to PCA, with and without batch effect removal and bioplots generated Figure 6.19. Heatmaps of the genes from these biplots were generated from **(A)** genes in the initial biplot and **(B)** the batch corrected biplot. Norm = Non-inflamed, Res = resolving, VeRA = very early RA, EstRA = established RA, JRep = joint replacement.

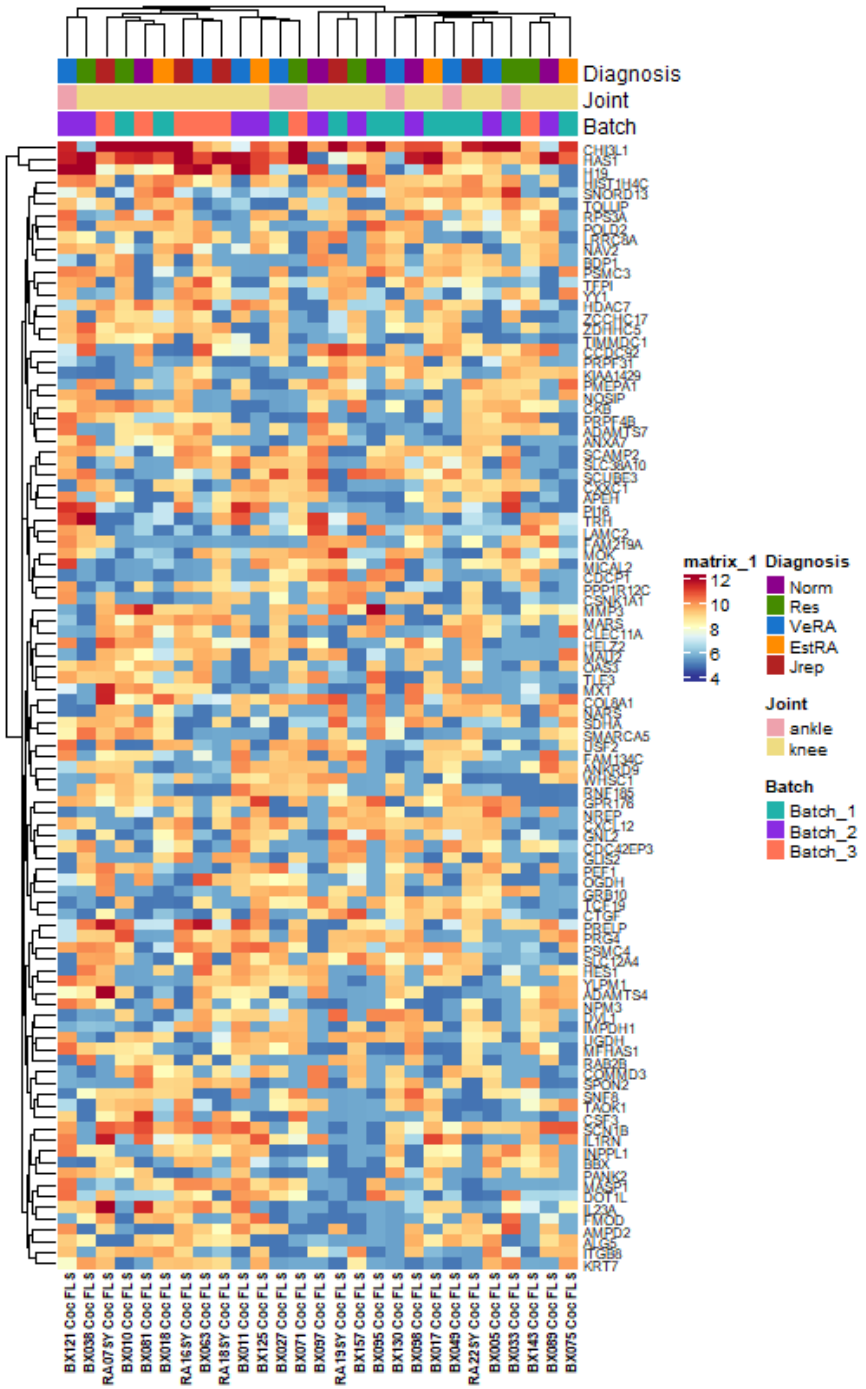

Figure 6.21: Heatmap of the top 100 variably expressed genes in fibroblasts that were co-cultured with macrophages. Fibroblasts and macrophages were co-cultured and treated with TNF-α for 16 hours. RNA was isolated and bulk RNA sequencing performed. Gene counts from the fibroblasts co-cultured with macrophages were subject to variance stabilising transformation (VST). The top 100 variably expressed genes of the VST data were plotted as a heatmap with hierarchical clustering on the columns and rows. Bars at the top show the diagnosis and joint site of the fibroblasts in co-culture, and batch. Norm = Non-inflamed, Res = resolving, VeRA = very early RA, EstRA = established RA, JRep = joint replacement.

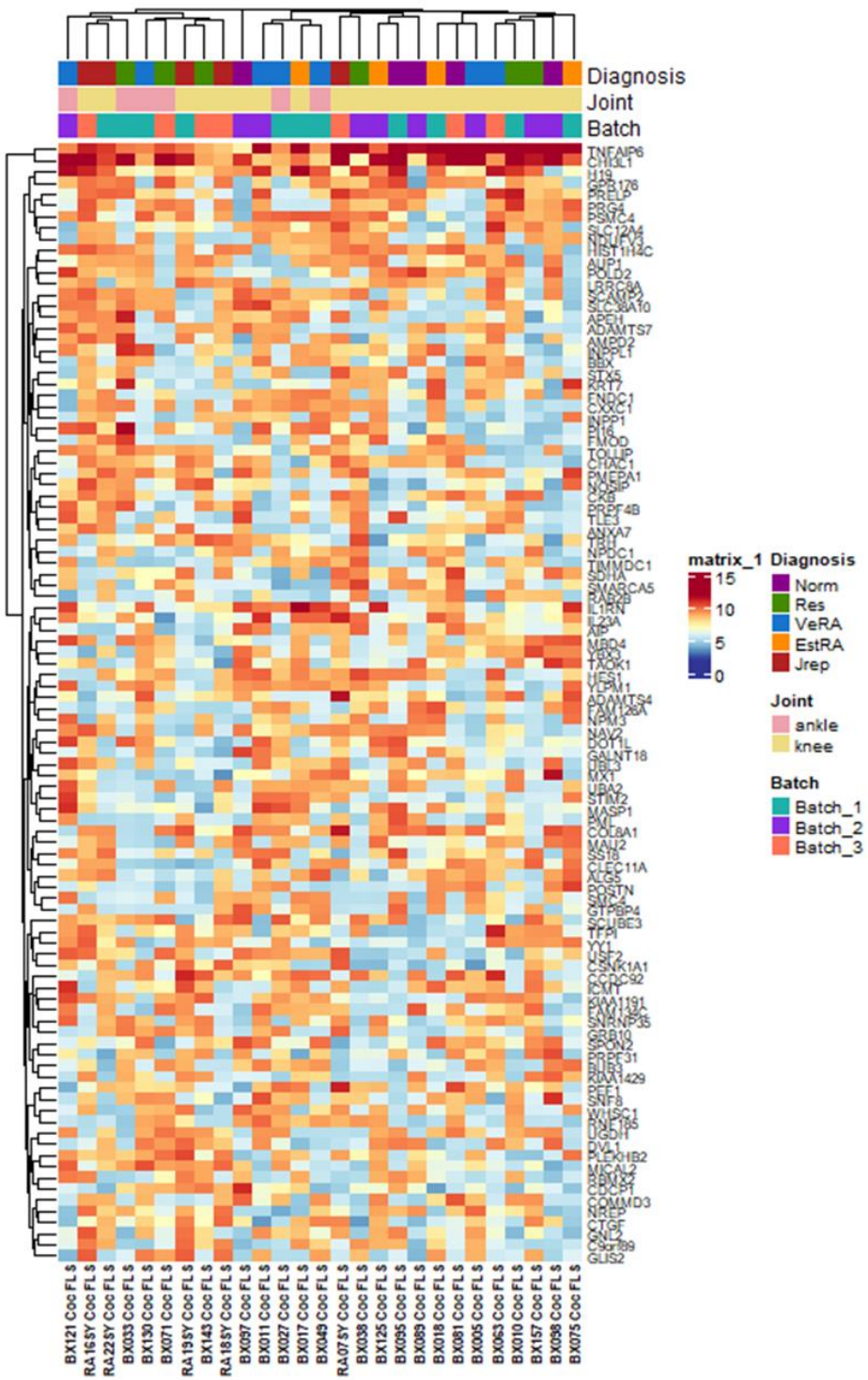

Figure 6.22: Heatmap of the top 100 variably expressed genes in macrophage co-cultured fibroblasts after correcting for batch effects. Fibroblasts and macrophages were co-cultured and treated with TNF-α for 16 hours. RNA was isolated and bulk RNA sequencing performed. Gene counts from the fibroblasts co-cultured with macrophages were subject to variance stabilising transformation (VST). The top 100 variably expressed genes of the VST data were plotted as a heatmap with hierarchical clustering on the columns and rows. Bars at the top show the diagnosis and joint site of the fibroblasts in co-culture, and batch. Norm = Non-inflamed, Res = resolving, VeRA = very early RA, EstRA = established RA, JRep = joint replacement.

6.2.4.2 Large number of differentially expressed genes of the fibroblasts co-cultured with macrophages, according to the diagnosis of fibroblast donor

Similarly, to the macrophage analysis, batch, but not joint site, was added as a covariate in the DESeq2 model, due to the lack of n in joint site. We again focused on the same 5 comparisons as in 6.2.3, but the number of differentially expressed genes for all possible comparisons is reported in Table 6.6. The dispersion estimates fitted appropriately (Figure 6.23) and, once the lower expressed genes were filtered out, had anti-conservative distribution of the p-values (Figure 6.24). The volcano plots (Figure 6.25) and heatmaps (Figure 6.26) highlight the large number of significantly differentially expressed genes. Lists of the top 100 differentially expressed genes are given in Appendix Table 14 - Appendix Table 18.

Table 6.6: Number of differentially expressed genes in fibroblasts co-cultured with macrophages the diagnosis group of fibroblasts, defined as p adj < 0.05 and an absolute log fold change >1.

	VeRA	EstRA	JRep	Norm
Res	1,195	1,133	1,146	1,420
Norm	1,195	1,146	1,280	
JRep	1,087	1,117		
EstRA	952			

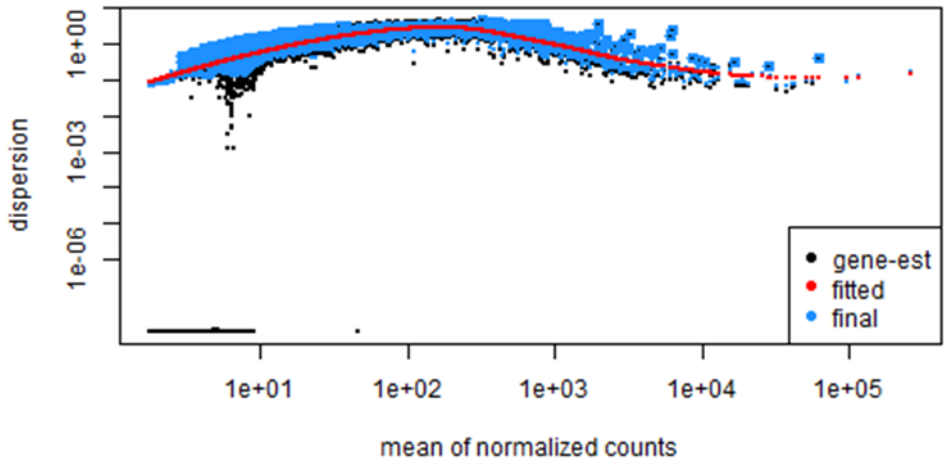

Figure 6.23: Dispersion estimates of fibroblasts co-cultured with macrophages. Fibroblasts and macrophages were co-cultured and treated with TNF-α for 16 hours. RNA was isolated and bulk RNA sequencing performed. Gene counts from the sequencing data of the fibroblasts co-cultured with macrophages were normalised in DESeq2 and the dispersion estimates plotted.

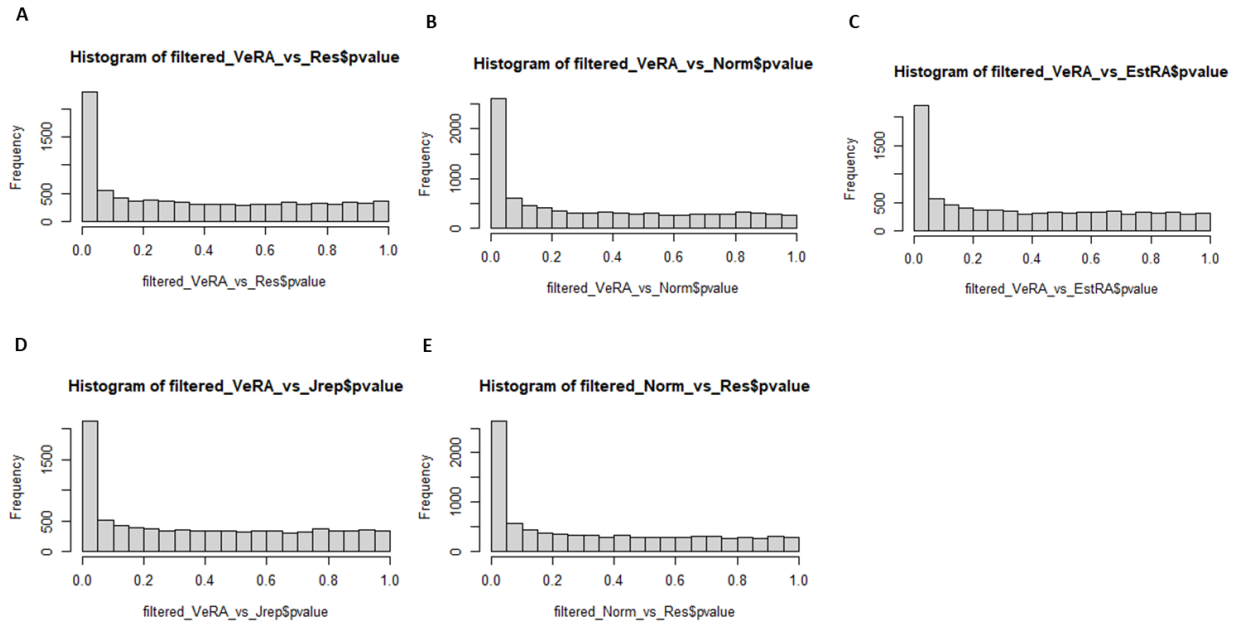

Figure 6.24: P value histograms of fibroblasts co-cultured with macrophages give an anti-conservative shape. Fibroblasts and macrophages were co-cultured and treated with TNF-α for 16 hours. RNA was isolated and bulk RNA sequencing performed. For the co-cultured fibroblast gene counts, genes where there are less than 3 samples with normalized counts greater than or equal to 10 were filtered out. Differential expression analysis performed and p value histograms produced for **(A)** VeRA vs Res, **(B)** VeRA vs Norm, **(C)** VeRA vs EstRA, **(D)** VeRA vs JRep and **(E)** Norm vs Res

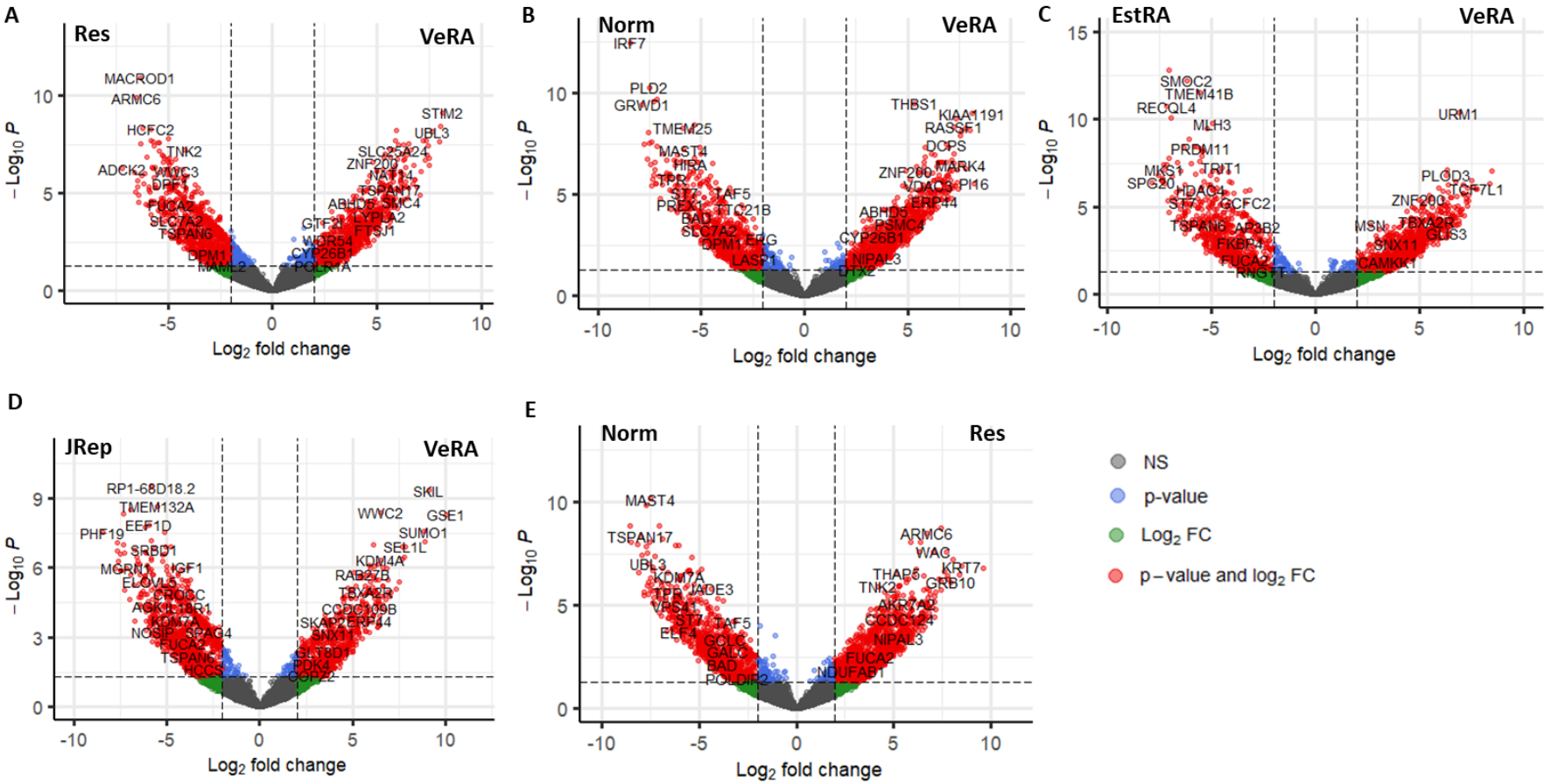

Figure 6.25: Volcano plots indicate a large number of differentially expressed genes for each comparison of interest in fibroblasts co-cultured with macrophages. Fibroblasts and macrophages were co-cultured and treated with TNF-α for 16 hours. RNA was isolated and bulk RNA sequencing performed. Differential expression analysis was performed using DESeq2 on the gene counts of fibroblasts in co-culture with macrophages for **(A)** VeRA vs Res, **(B)** VeRA vs Norm, **(C)** VeRA vs EstRA, **(D)** VeRA vs JRep and **(E)** Norm vs Res**.**

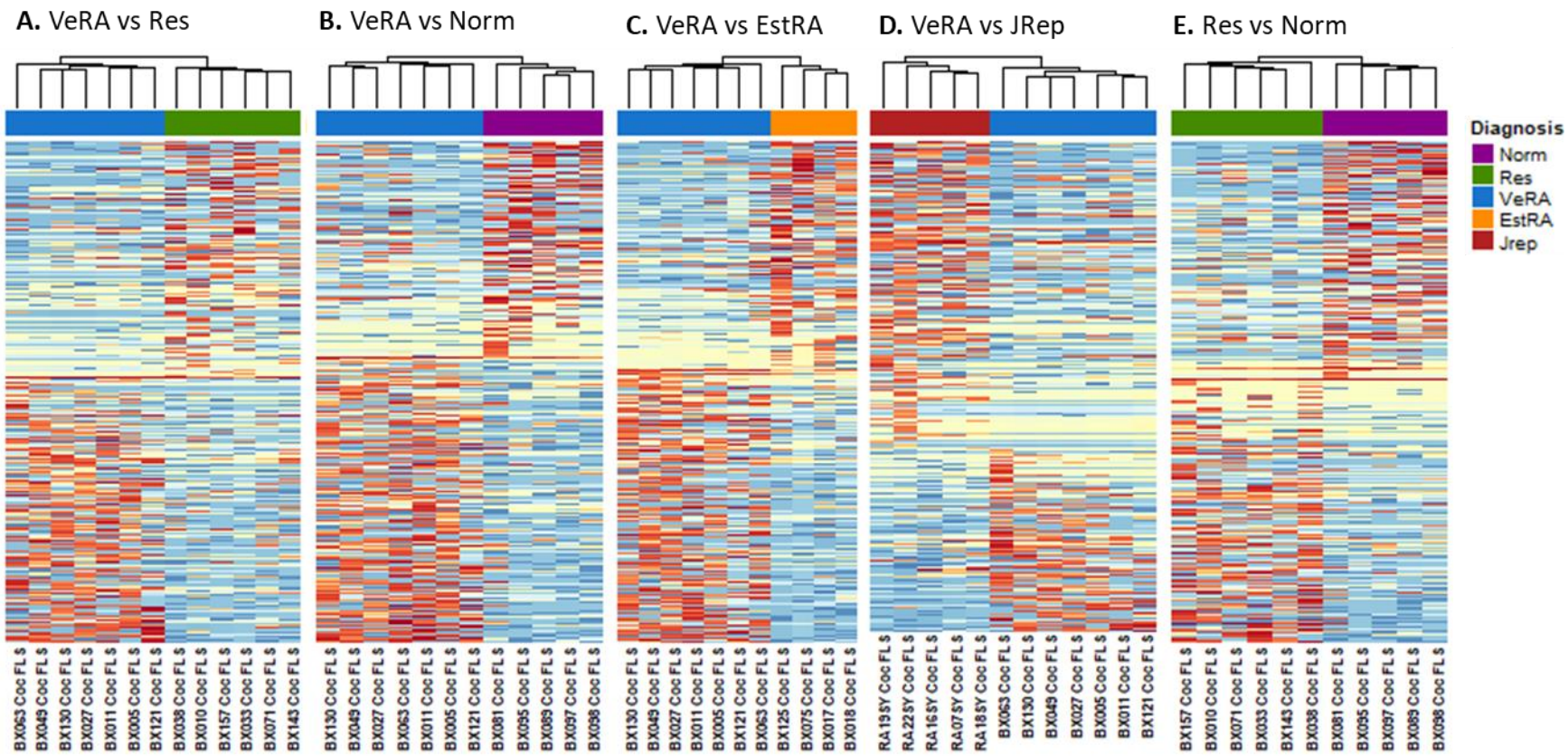

Figure 6.26: Heatmaps indicate a large number of differentially expressed genes between but also within groups for each comparison of interest in macrophages co-cultured with fibroblasts. Fibroblasts and macrophages were co-cultured and treated with TNF-α for 16 hours. RNA was isolated and bulk RNA sequencing performed. Differential expression analysis was performed using DESeq2 on the fibroblast gene counts for **(A)** Very early rheumatoid arthritis (VeRA) vs Resolving (Res), **(B)** VeRA vs Non-inflamed (Norm), **(C)** VeRA vs Established RA (EstRA), **(D)** VeRA vs RA patients undergoing joint replacement (JRep) and **(E)** Norm vs Res. Differentially expressed genes were then ordered according to Log2 fold change and heatmap generated.

6.2.4.3 Gene set enrichment analysis revealed IFN-α, TNF-α, TGF-β and G2M checkpoint signalling were involved in the separation of co-cultured fibroblast according to the diagnosis of fibroblast donor

Gene set enrichment analysis was then performed based on the hallmark gene sets from MSigDB. Similar to the macrophage analysis, few gene sets were enriched according to the FDR p value, with the exception of the IFN-α response in "VeRA vs Norm" and TGF-β signalling in "VeRA vs JRep". However, some pathways were significantly enriched according to the nominal p value (Figure 6.27). Of these pathways, it appeared that VeRA was positively enriched for TGF-β signalling compared to both Norm and JRep, and IFN-α signalling in positively enriched Norm compared to VeRA and Res. On the other hand, TNF-α signalling was negatively enriched for Res compared to VeRA and Norm. The G2M checkpoint was enriched for VeRA compared to EstRA and Res, and also enriched in Norm compared to Res. Similarly to the macrophages, the heatmaps and count plots of genes from these pathways demonstrated there was a large amount variability within each group (Figure 6.28 - Figure 6.31). Some of the least variable genes and differences seen were in TGF-β signalling pathway (Figure 6.29C) where XIAP (X-linked inhibitor of apoptosis protein), SMAD3 (SMAD family member 3), THBS1 (Thrombospondin 1) and SKIL (SKI Like Proto-Oncogene) were lower in Norm, Res and JRep SF compared to the VeRA and EstRA SF. In the IFN-α signalling pathway IRF7 and CSF1 (colony stimulating factor 1) were higher in the Norm (non-inflamed) than other inflamed groups.

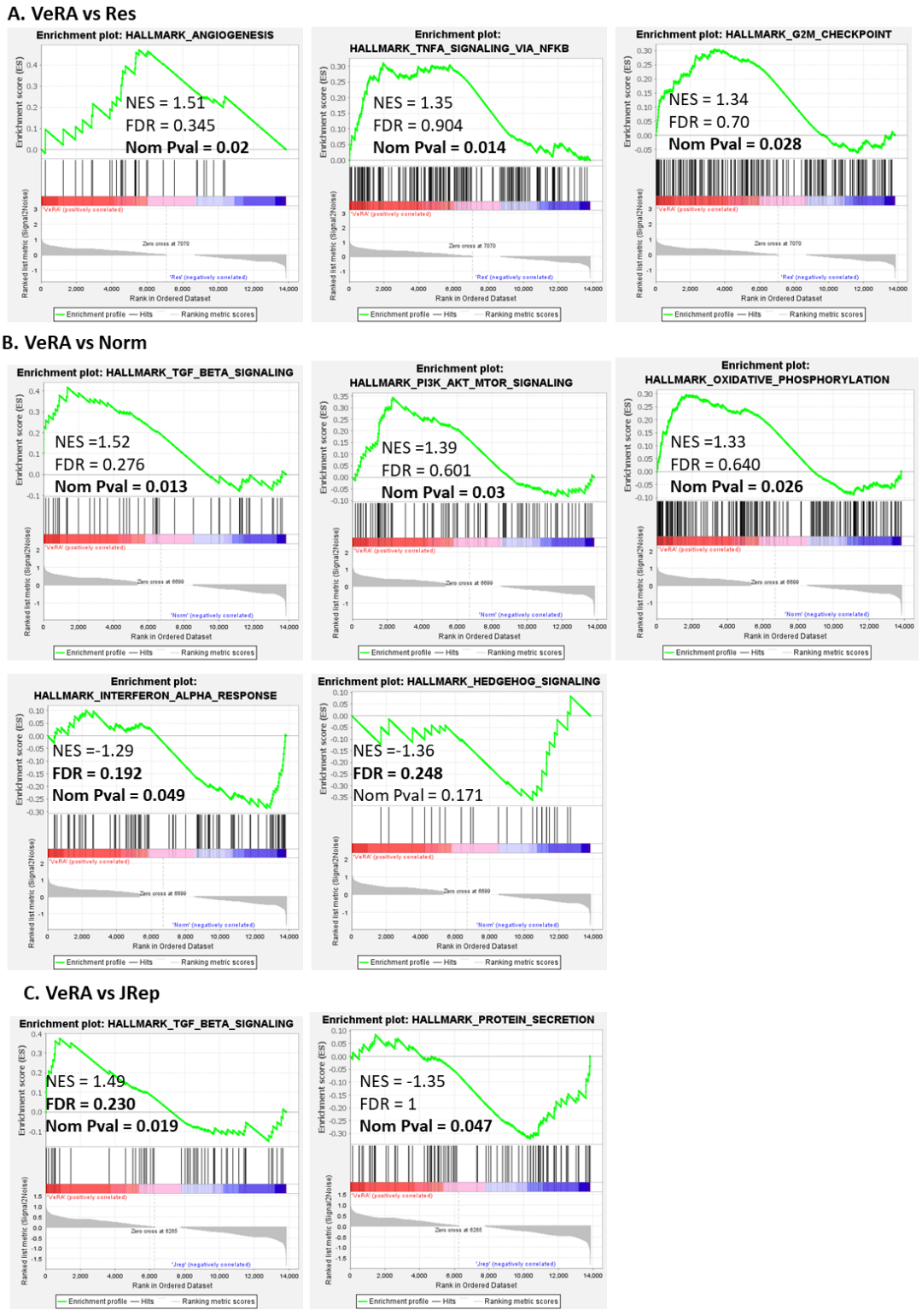

Figure 6.27: Gene set enrichment analysis of fibroblasts from fibroblast: macrophage co-cultures. Fibroblasts and macrophages were co-cultured and treated with TNF-α for 16 hours. RNA was isolated and bulk RNA sequencing performed. The DESEq2 normalised gene counts table of the fibroblasts co-cultured with macrophages was submitted for gene set enrichment analysis (GSEA) of the hallmark pathways, for comparisons of **(A)** VeRA vs Res, **(B)** VeRA vs Norm, **(C)** VeRA vs EstRA and **(D)** VeRA vs EstRA and **(E)** Norm vs Res. **(D)** and **(E)** shown on next page.

D. VeRA vs EstRA

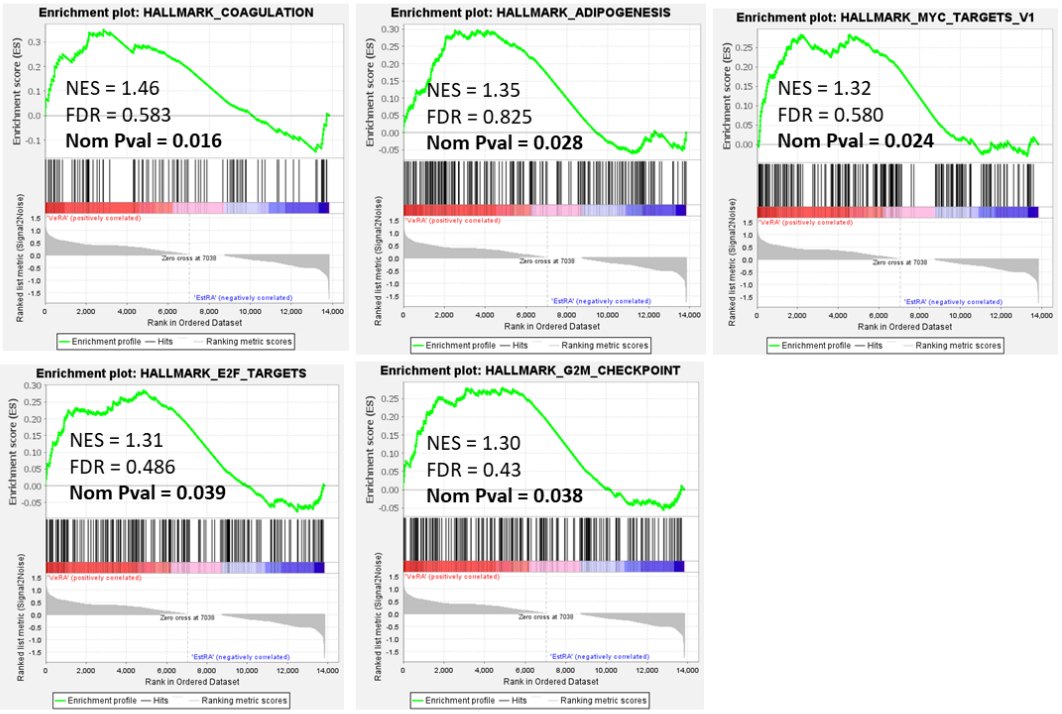

E. Norm vs Res

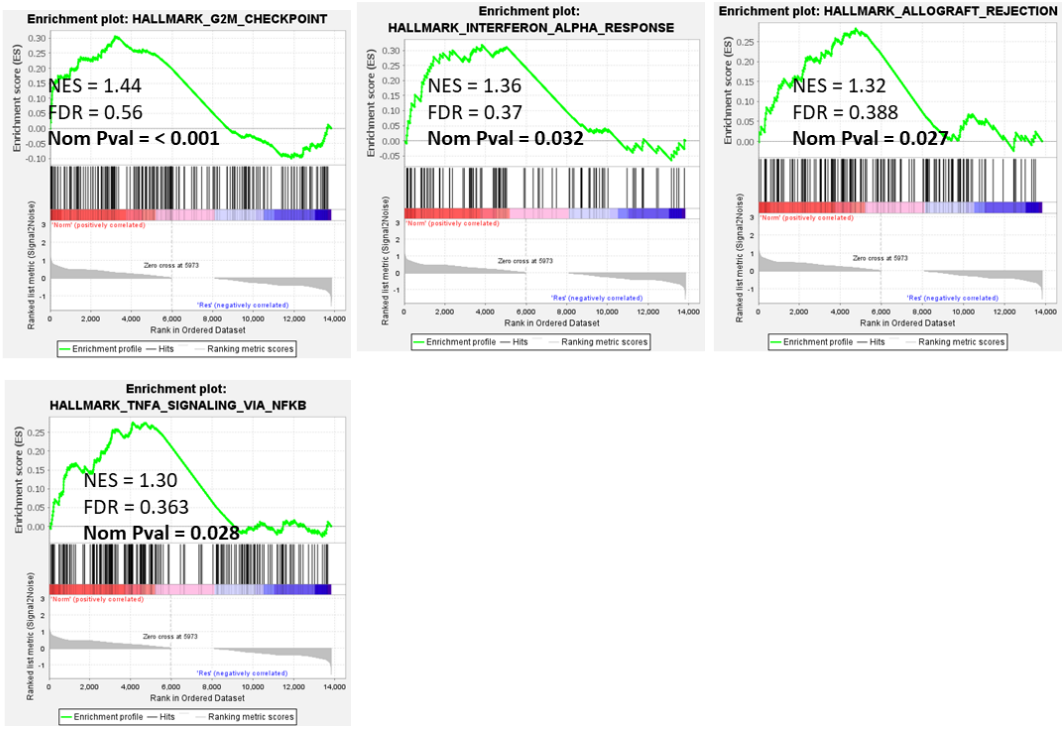

Figure 6.27 continued.

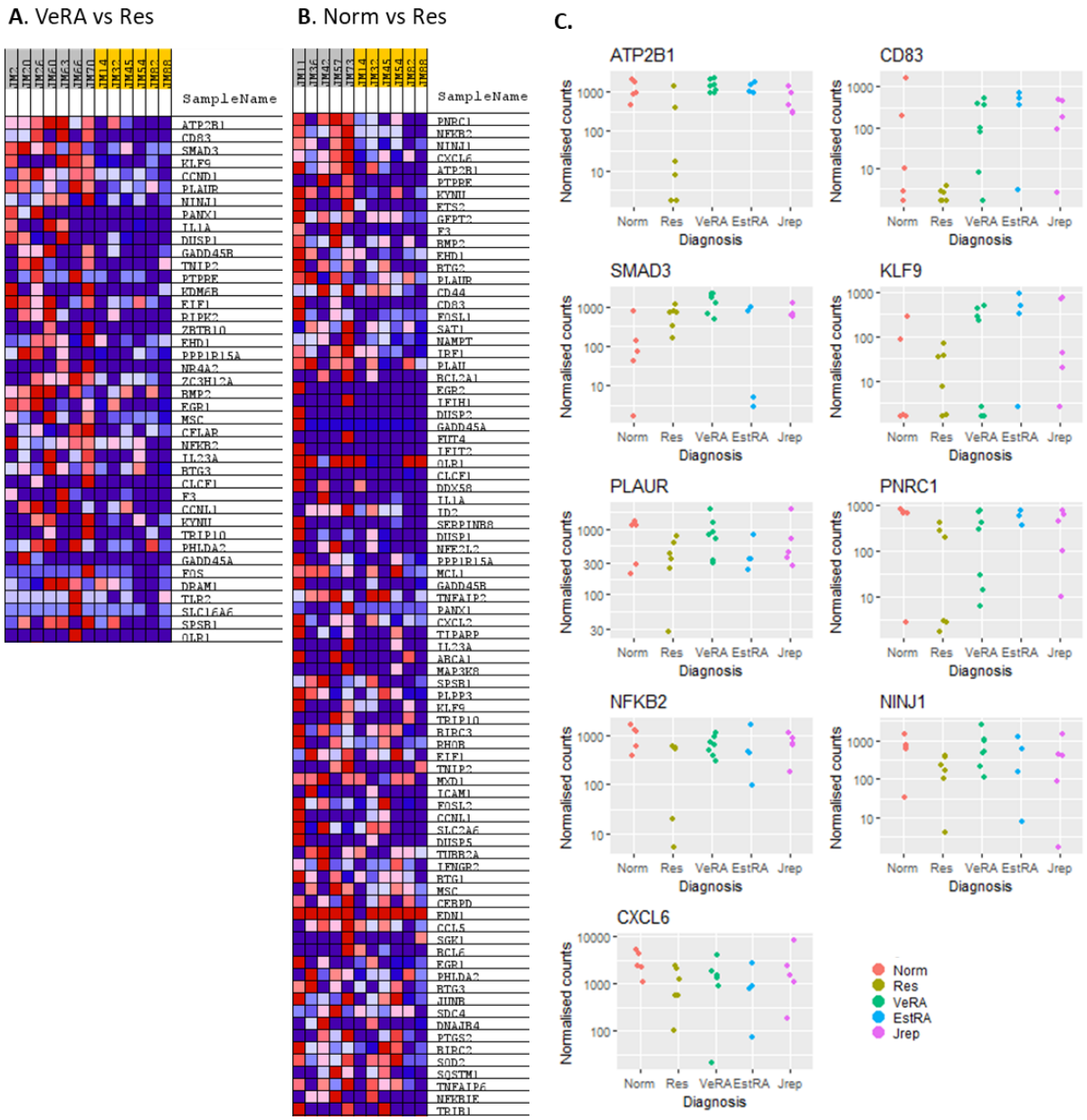

Figure 6.28: Heatmap of and count plots of genes in the enriched TNF-α signalling via NF-κB pathway for fibroblasts. Fibroblasts and macrophages were co-cultured and treated with TNF-α for 16 hours. RNA was isolated and bulk RNA sequencing performed. The gene counts table of fibroblasts was submitted for gene set enrichment analysis (GSEA) of the hallmark pathways and TNF-α signalling via NF-κB pathway deemed significantly enriched and heatmap of the enriched genes generated for **(A)** VeRA (grey) vs Res (yellow) and **(B)** Norm (grey) vs Res (yellow).

Table 6.7: Top genes from TNF-α signalling via NF-κB pathway in fibroblasts

HGNC symbol	Log2 FoldChange	P value	P adj	Entrez	Ensembl ID
VeRA vs Res					
ATP2B1	2.515749865	0.005724823	0.041701092	490	ENSG00000070961
CD83	6.772317205	3.91E-07	5.89E-05	9308	ENSG00000112149
SMAD3	0.949938808	0.301582185	0.680790957	4088	ENSG00000166949
KLF9	5.050751237	0.000189009	0.00340383	687	ENSG00000119138
CCND1	0.926098073	0.294580657	0.672688806	595	ENSG00000110092
PLAUR	1.346622997	0.044100197	0.184468452	5329	ENSG00000011422
NINJ1	1.861691615	0.062250503	0.237673121	4814	ENSG00000131669
Res vs Norm					
PNRC1	-2.222212118	0.075006841	0.245301602	10957	ENSG00000146278
NFKB2	-1.47229751	0.080121118	0.256972183	4791	ENSG00000077150
NINJ1	-1.646330903	0.132006617	0.36824327	4814	ENSG00000131669
CXCL6	-1.371084909	0.085939217	0.270471687	6372	ENSG00000124875
ATP2B1	-2.29675827	0.021196092	0.097313134	490	ENSG00000070961
PTPRE	-6.096640219	NA	NA	5791	ENSG00000132334

Norm = Non-inflamed, Res = resolving, VeRA = Very early rheumatoid arthritis.
Genes occurring in both comparisons in red.

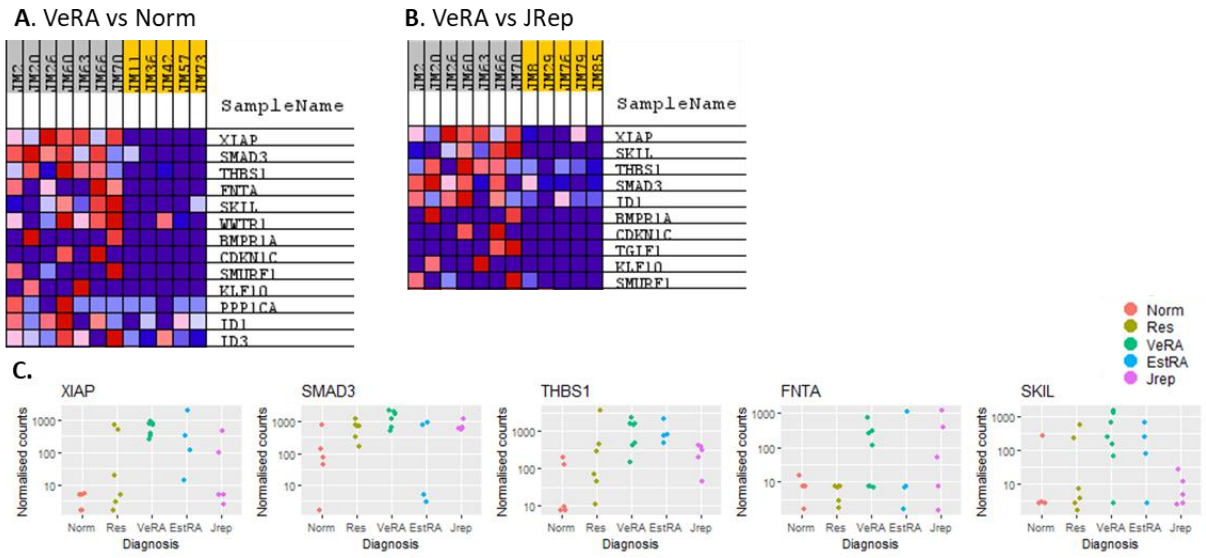

Figure 6.29: Heatmap of and count plots of genes in the enriched TGF-β signalling pathway for fibroblasts. Fibroblasts and macrophages were co-cultured and treated with TNF-α for 16 hours. RNA was isolated and bulk RNA sequencing performed. The gene counts table of fibroblasts was submitted for gene set enrichment analysis (GSEA) of the hallmark pathways and TGF-β signalling pathway deemed significantly enriched and heatmap of the enriched genes generated for **(A)** VeRA (grey) vs Norm (yellow) and **(B)** VeRA (grey) vs JRep (yellow).

Table 6.8: Top genes from the TGF-β signalling pathway in fibroblasts

HGNC symbol	Log2 FoldChange	P value	P adj	Entrez	Ensembl ID
VeRA vs Norm					
XIAP	7.5574328	1.25E-08	5.78E-06	331	ENSG00000101966
SMAD3	2.866064869	0.003088765	0.0249973	4088	ENSG00000166949
THBS1	5.309606942	3.33E-10	4.83E-07	7057	ENSG00000137801
FNTA	4.898240111	0.000319127	0.005000088	2339	ENSG00000168522
SKIL	6.113647364	7.30E-06	0.00033244	6498	ENSG00000136603
WWTR1	2.177867045	0.087235959	0.298300525	25937	ENSG00000018408
VeRA vs JRep					
XIAP	2.271471912	0.09682894	0.43191824	331	ENSG00000101966
SKIL	9.095126463	4.75E-10	2.45E-06	6498	ENSG00000136603
THBS1	0.828750802	0.355439147	0.889588646	7057	ENSG00000137801
SMAD3	0.782725565	0.451365862	0.981358353	4088	ENSG00000166949
ID1	2.502816418	0.061451986	0.317933817	3397	ENSG00000125968
BMPR1A	4.124242	NA	NA	657	ENSG00000107779

JRep = joint replacement, Norm = Non-inflamed, VeRA = Very early rheumatoid arthritis.
Genes occurring in both comparisons in red.

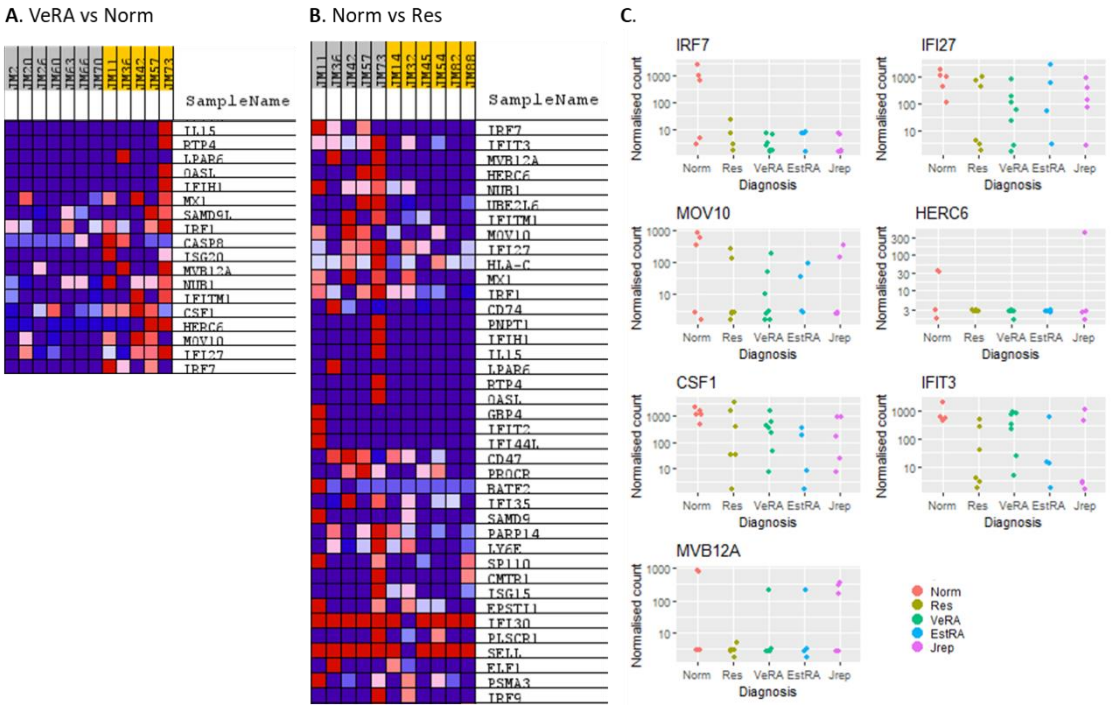

Figure 6.30: Genes enriched in the IFN-a signalling pathways gene set. Fibroblasts and macrophages were co-cultured and treated with TNF-α for 16 hours. RNA was isolated and bulk RNA sequencing performed. The gene counts table of fibroblasts was submitted for gene set enrichment analysis (GSEA) of the hallmark pathways and the IFN-α signalling pathway deemed significantly enriched and heatmap of the enriched genes generated for **(A)** VeRA (grey) vs Norm (yellow) and **(B)** Norm (grey) vs Res (yellow). **(C)** The top highly enriched genes were then plotted as gene counts.

Table 6.9: Top genes from the IFN-α signalling pathway in fibroblasts

HGNC symbol	Log2 FoldChange	P value	P adj	Entrez	Ensembl ID
VeRA vs Norm					
IRF7	-8.42771	3.29E-13	2.58E-09	3665	ENSG00000185507
IFI27	-2.86286	0.035124	0.154241	3429	ENSG00000165949
MOV10	-3.03856	0.040336	0.168978	4343	ENSG00000155363
HERC6	-2.1363	NA	NA	55008	ENSG00000138642
CSF1	-1.18118	0.311771	0.693671	1435	ENSG00000184371
NUB1	-1.3688	0.236579	0.588412	51667	ENSG00000013374
Res vs Norm					
IRF7	-7.068127515	1.43E-09	3.02E-06	3665	ENSG00000185507
IFIT3	-2.236373695	0.123515575	0.351421453	3437	ENSG00000119917
MVB12A	-7.479339318	1.70E-06	0.000177462	93343	ENSG00000141971
HERC6	-2.271237592	NA	NA	55008	ENSG00000138642
NUB1	-3.528396365	0.00343322	0.025041584	51667	ENSG00000013374
UBE2L6	-4.135236987	0.003216105	0.023734449	9246	ENSG00000156587

Norm = Non-inflamed, Res = resolving, VeRA = Very early rheumatoid arthritis.
Genes occurring in both comparisons in red.

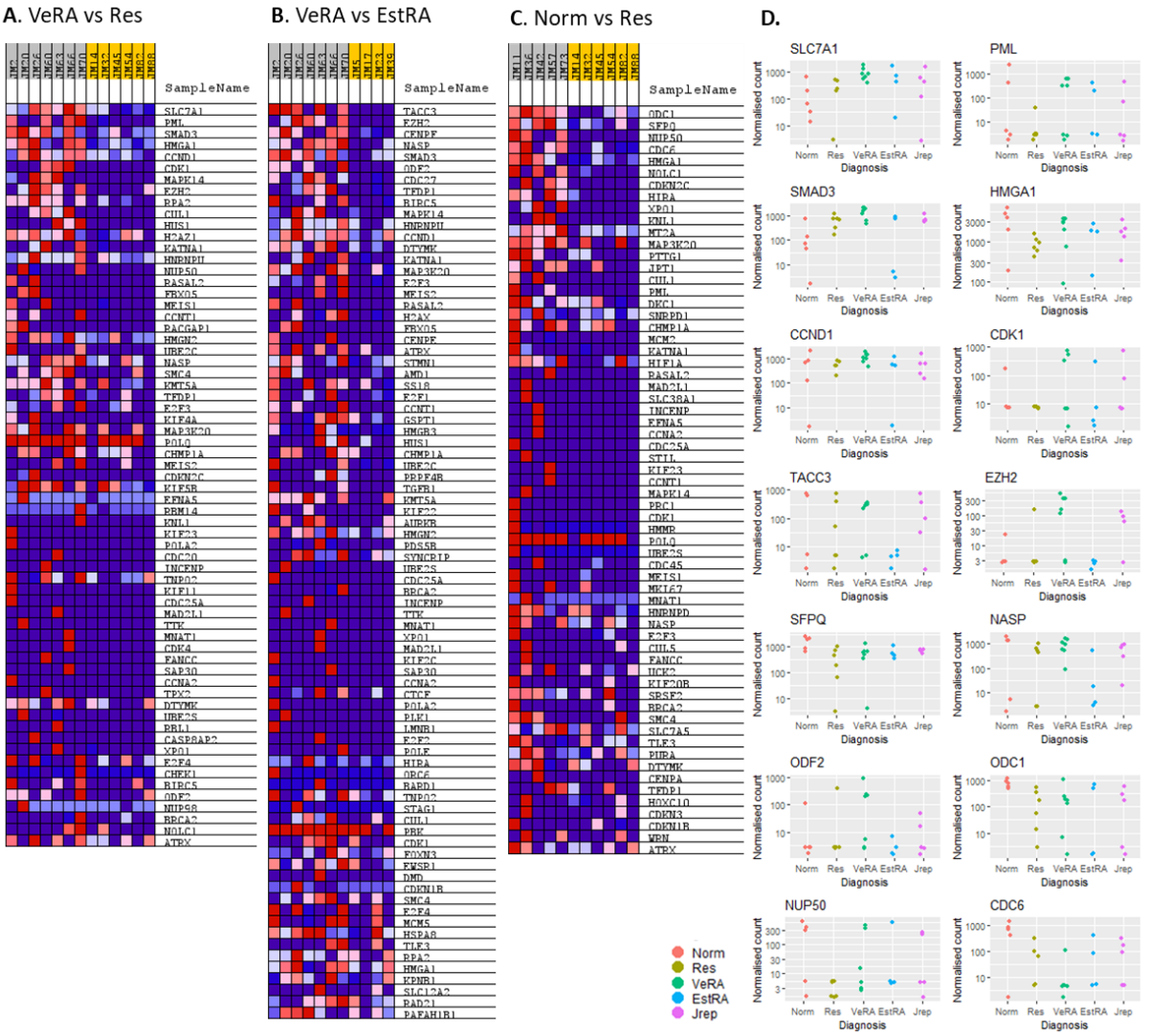

Figure 6.31: Genes enriched in the G2M signalling pathway gene set. Fibroblasts and macrophages were co-cultured and treated with TNF-α for 16 hours. RNA was isolated and bulk RNA sequencing performed. The gene counts table of fibroblasts was submitted for gene set enrichment analysis (GSEA) of the hallmark pathways and G2M signalling pathway deemed significantly enriched and heatmap of the enriched genes generated for **(A)** VeRA (grey) vs Norm (yellow), **(B)** VeRA (grey) vs Res (yellow) and **(C)** VeRA (grey) and Res (yellow). **(D)** The top highly enriched genes were then plotted as gene counts.

Table 6.10: Top 9 genes from G2M signalling pathway in fibroblasts

HGNC symbol	Log2 FoldChange	P value	P adj	Entrez	Ensembl ID
VeRA vs Res					
SLC7A1	1.738377	0.068975	0.255281	6541	ENSG00000139514
PML	6.316707	2.09E-05	0.000808	5371	ENSG00000140464
SMAD3	0.949939	0.301582	0.680791	4088	ENSG00000166949
HMGA1	1.320482	0.046345	0.191012	3159	ENSG00000137309
CCND1	0.926098	0.294581	0.672689	595	ENSG00000110092
CDK1	4.044598	0.001382	0.014371	983	ENSG00000170312
MAPK14	5.838892	5.19E-05	0.0014	1432	ENSG00000112062
EZH2	4.732874	3.53E-05	0.001095	2146	ENSG00000106462
RPA2	2.682936	0.030653	0.140651	6118	ENSG00000117748
VeRA vs EstRA					
TACC3	5.533183457	0.00024636	0.005059719	10460	ENSG00000013810
EZH2	6.498538903	2.86E-06	0.000283126	2146	ENSG00000106462
CENPF	4.545334546	NA	NA	1063	ENSG00000117724
NASP	3.027715043	0.023348597	0.145928731	4678	ENSG00000132780
SMAD3	1.757511092	0.092536435	0.384044492	4088	ENSG00000166949
ODF2L	-3.653031187	0.006744829	0.056487106	57489	ENSG00000122417
CDC27	4.314612003	0.003303018	0.03326781	996	ENSG00000004897
TFDP1	3.219368994	0.031844937	0.182467581	7027	ENSG00000198176
Res vs Norm					
ODC1	-1.986394336	0.150114721	0.403544857	4953	ENSG00000115758
SFPQ	-1.87002543	0.035783039	0.141816696	6421	ENSG00000116560
NUP50	-7.017578794	NA	NA	10762	ENSG00000093000
CDC6	-2.871298317	0.037983014	0.149075089	990	ENSG00000094804
HMGA1	-1.734319702	0.016829352	0.081639409	3159	ENSG00000137309
NOLC1	-5.939213825	NA	NA	9221	ENSG00000166197
CDKN2C	-8.18949196	1.14E-08	7.05E-06	1031	ENSG00000123080
HIRA	-4.078754224	0.000234775	0.003754557	7290	ENSG00000100084
XPO1	-4.988630595	3.83E-05	0.001175535	7514	ENSG00000082898

JRep = Joint replacement, Norm = Non-inflamed, Res = resolving, VeRA = Very early rheumatoid arthritis. Genes occurring in more than one comparison in red.

6.2.4.4 Ingenuity analysis identified differentially regulated pathways in fibroblasts for “VeRA vs Norm” and “Res vs Norm”

Ingenuity pathway analysis of the “Res vs Norm” and “VeRA vs Norm” was also performed using the log2 fold change and adjusted p values from the differential expression of fibroblasts co-cultured with macrophages (Figure 6.32). Multiple pathways were implicated in “Res vs Norm” (Figure 6.32A), and of particular interest was the downregulation of PTEN (Phosphatase and TENsin homolog deleted on chromosome 10) signalling. Whilst for “VeRA vs Norm” there was predicted activation of PNPT1 (Polyribonucleotide Nucleotidyltransferase 1) and inhibition of IFNL1 (Interferon Lambda 1).

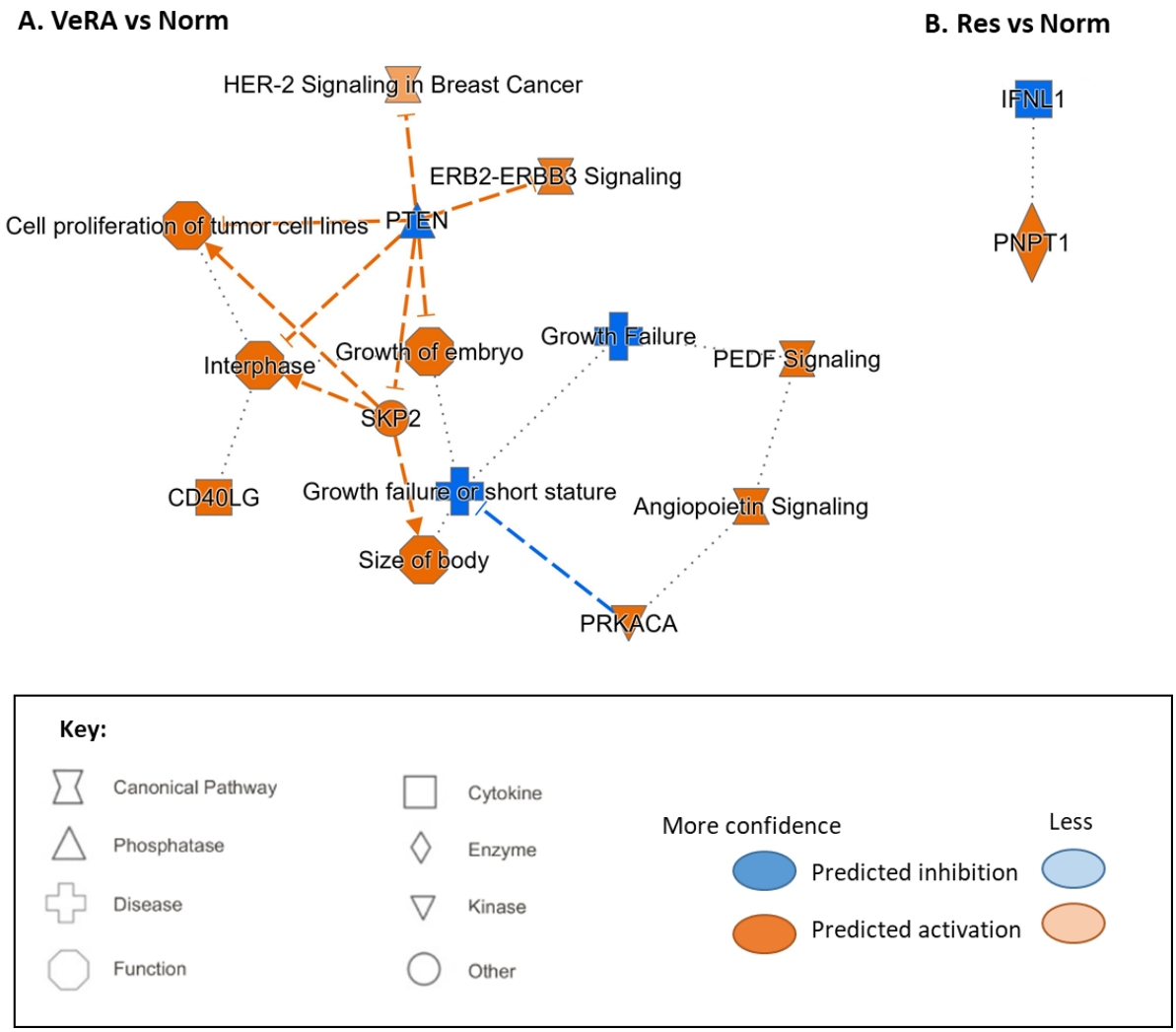

Figure 6.32: Graphical summary from ingenuity pathway analysis of fibroblasts co-cultured with macrophages. Log2 Fold Change and adjusted p values from the differential gene expression analysis of fibroblasts co-cultured with macrophages was subjected to ingenuity pathway analysis (IPA). Graphical summaries from IPA core analysis were generated for comparisons of; **(A)** VeRA vs Norm and **(B)** Res vs Norm.

6.2.4.5 Mono-cultured fibroblasts also have a large number of differentially expressed genes according to the diagnosis of fibroblast donor, but the majority of these are not the same as those in co-culture

When examining the data associated with the fibroblasts cultured alone, we observed a large number of DEGs according to the diagnosis Table 6.11), similar to that seen following co-culture. However, there was a limited number of overlapping DEGs seen in co- or mono-culture analysis for each comparison of interest (e.g. “VeRA vs Res”). Shown in Figure 6.33, the majority of DEGs were unique to either the co- or mono- cultured conditions. This indicates that upon co-culture with macrophages the genes that are differentially expressed in the fibroblasts between diagnosis groups are altered. PCA analysis of the mono-cultured fibroblasts further supported this demonstrating a separation of the JRep and Norm groups (Figure 6.34A and B), with more distinct separation according to diagnosis batch correction (Figure 6.34C and D). Importantly, the genes contributing to this separation, identified from the biplot (Figure 6.34D), were different from those of fibroblasts co-cultured with macrophages (Figure 6.19). Furthermore, a heatmap of the genes in the batch corrected biplots showed a separation of the JRep mono-cultured samples (Figure 6.34E), whilst a similar analysis using the co-cultured data showed no particular clustering according to diagnosis (Figure 6.34F).

Table 6.11: Number of differentially expressed genes in mono-cultured fibroblasts according to the diagnosis group of fibroblast, defined as p adj < 0.05 and an absolute log fold change >1.

	VeRA	EstRA	JRep	Norm
Res	1,503	1,257	1,485	1,642
Norm	1,330	1,146	1,288	
JRep	1,266	1,142		
EstRA	1,084			

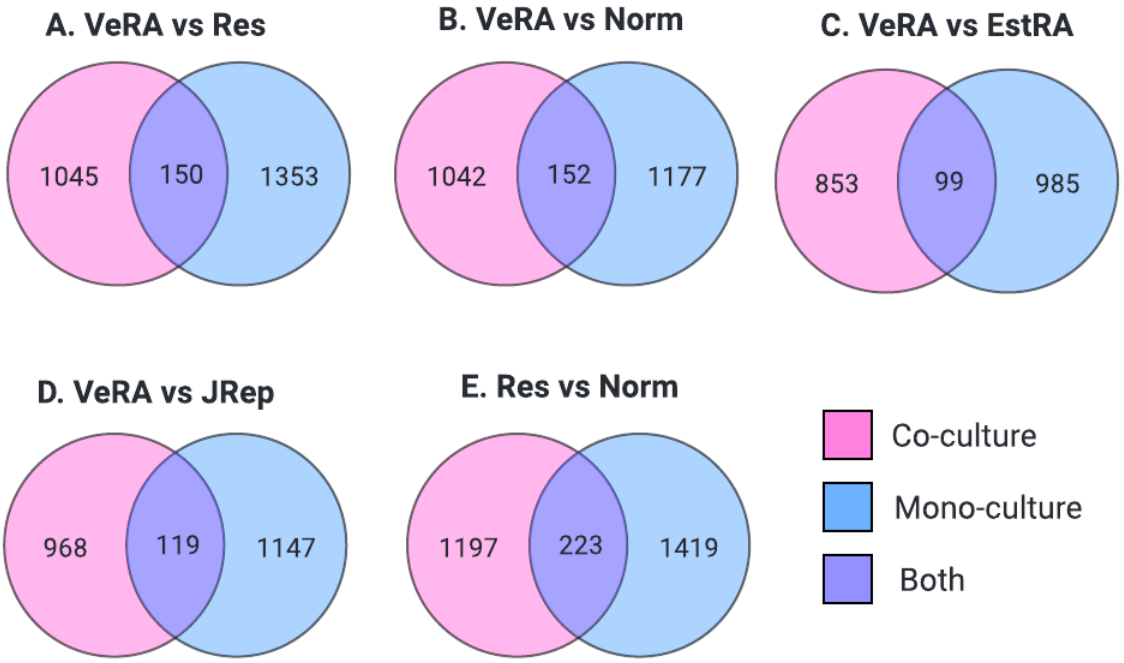

Figure 6.33: Venn diagrams of the number of differentially expressed genes in co-cultured and mono-cultured fibroblasts. Fibroblasts were mono-cultured or co-cultured with macrophages and treated with TNF-α for 16 hours. RNA was isolated and bulk RNA sequencing performed. Differential gene expression was performed on the mono- and co-cultured fibroblasts separately according to the diagnosis of fibroblasts. The differentially expressed genes for the co- (pink) and mono-(blue) cultures were then compared and the number overlapping (purple) or unique to culture conditions is indicated. This was done for the comparisons of **(A)** Very early rheumatoid arthritis vs resolving (VeRA vs Res), **(B)** VeRA vs Norm (Non-inflamed), **(C)** VeRA vs EstRA (established RA), **(D)** VeRA vs JRep (RA patients undergoing joint replacement) and **(E)** Res vs Norm.

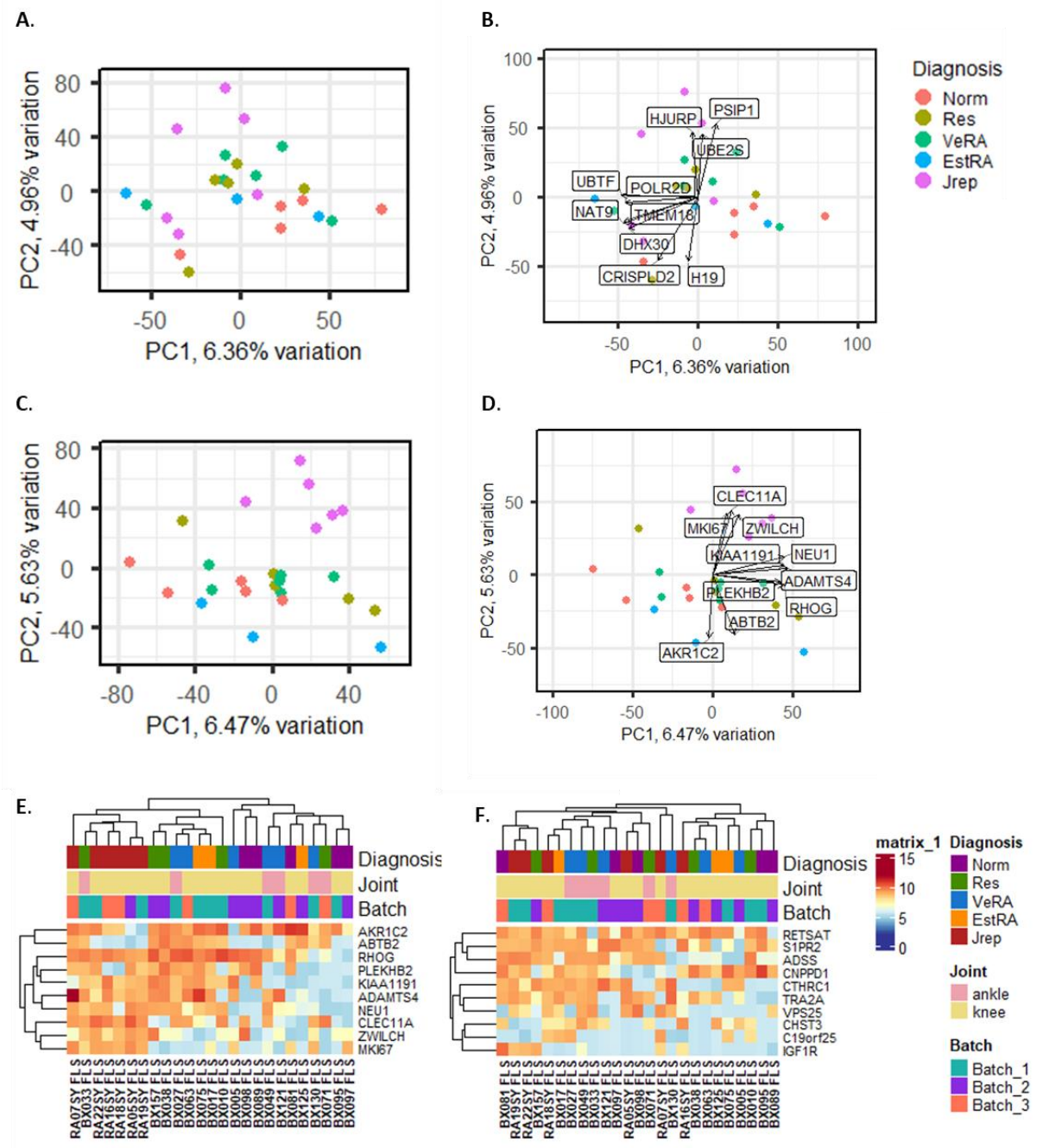

Figure 6.34: Mono-cultured fibroblasts cluster by diagnosis, but separation driven by different genes than the fibroblasts cultured with macrophages. Fibroblasts were cultured with and without macrophages and treated with TNF-α for 16 hours. RNA was isolated and bulk RNA sequencing performed. Gene counts of the mono-cultured fibroblasts, were subject to variance stabilising transformation (VST) and for **(C&D)** batch effect removed before VST transformation. **(A-D)** Principal Components were plotted and coloured according to the diagnosis of fibroblast donor. **(E)** A heatmap of the genes form the batch biplot (E) and the batch corrected biplot of co-cultured fibroblasts (Figure 6.19F) were generated. Norm = Non-inflamed, Res = resolving, VeRA = very early RA, EstRA = established RA, JRep = joint replacement.

6.3 Discussion

Previous studies have demonstrated bi-directional cross-talk between fibroblasts and macrophages (133, 134, 142-144, 214). Here, we show that co-culture of fibroblasts with macrophages alters the transcriptome of both cell types, indicative of fibroblast: macrophage crosstalk. Furthermore, this cross-talk is different depending on the disease state of the fibroblasts co-culture. However, heterogeneity within groups, small sample numbers and lack of validation of genes identified means definitive conclusions are not possible. Therefore, it is impossible to determine if these changes support the idea of fibroblast: macrophage interactions playing a role in the outcome of disease.

6.3.1 Variably expressed gene analysis

Initial PCAs and heatmaps of the top variably expressed genes showed little clustering by diagnosis, suggesting that factors other than fibroblasts diagnosis (e.g., fibroblast joint site and batch) contribute to the differences. Despite this, in PCAs of both the batch corrected co-cultured macrophages and for mono and co-cultured fibroblasts, separation between JRep and Norm groups was observed. Nevertheless, no distinct separation was seen between the VeRA, EstRA and Res samples. The similarities in clustering of macrophages and fibroblast indicate that the fibroblasts are exerting differential effects on the macrophages according to their diagnosis.

Importantly, the JRep fibroblasts were distinct from all other samples both in co and mono-culture. Within the co-cultured JRep fibroblasts this was driven by high expression of IGF1R, C19orf25, CNPPD1, CTHRC1 and RESTAT. All these genes are known to play a role in RA (160, 359, and 360). For example, IGF-1R signalling contributes to IL-6 production and T cell

mediated inflammation in RA (361). CTHRC1 has been implicated in enhanced migratory behaviour and pannus formation (160, 359). Likewise, RETSAT encodes retinol saturase, and retinoic acid signalling is essential for bone and cartilage development (360). Furthermore, associations with RETSAT have already been observed in OA (362) and ankylosing spondylitis (363). Taken together this suggests that fibroblasts in the latter stages of disease aid in bone damage and erosion. Notably, we do not observe these same genes driving separation in the mono-cultured fibroblasts. This is in accordance with previous data (134, 144) which demonstrated that signals from macrophages are required for cartilage degradation by fibroblasts.

The clustering of JRep samples may also be because of both disease duration and treatment in the JRep compared to the other samples. Similarly, the Norm group may have clustered separately as they were the only non-inflamed samples compared to all other groups. On the other hand, the resolving, VeRA and EstRA samples clustered almost together, for the macrophages and fibroblasts. This may be partly attributed to the similar lengths of symptom duration. Whilst EstRA patients had >12-week symptom duration, all patients still had symptom duration of ≤1year, which may still be considered relatively early RA (364). Thus, at these early stages, the impact of fibroblast communicating with macrophages is more subtle. Supporting this idea further, the VeRA vs EstRA comparison had the lowest number of differentially expressed genes than all other comparisons.

Table 6.12: Summary of key findings from the pathway analysis

	Macrophages	Fibroblasts
VeRA vs Res		
GSEA pathways and the top genes	**IL-6_JAK_STAT:** TNFSF1A and IRF9 higher in VeRA than Res **DNA_REPAIR**	**TNFA_VIA_NFkB_SIG**: ATP2B1, CD83 and SMAD3 higher in VeRA than Res **G2M_CHECKPOINT:** SLC17A1, SMAD3, HMGA1, CCND1 higher in VeRA than Res **ANGIOGENESIS**
IPA	> mir-17 < E2F1 and excision repair	N/A
VeRA vs Norm		
GSEA pathways and the top genes	**TNFA_VIA_NFkB**: MAP2K3, IL1A, BIRC3, CEBPD and SOD2 higher in Norm than VeRA **IFN-γ RESPONSE**: SP110, SOD2, CASP8, PTPN1 higher in Norm than VeRA **ADIPOGENESIS**	**IFN-α_RESPONSE*:** IRF7, IFI27, MOV10 and CSF-1 higher in Norm than VeRA **TGF_β_SIG:** XIAP, SMAD3, THBS1, FNTA lower in Norm than VeRA **PI2K_AKT_MTOR_SIG, OXIDATIVE_PHOSPHORYLATION, HEDGEHOG_SIG**
IPA	> KRAS, GF11, growth failure < HBEGF, ruffling, RPTOR, SH3TC2	< PTEN, growth failure > PEDF signalling, SKP2, PRKACA
VeRA vs EstRA		
GSEA pathways and the top genes	N/A	**G2M_CHECKPOINT:** TACC3, EZH2 and NASP higher in VeRA than EstRA **COAGULATION, ADIPOGENESIS, MYC_TARGETS, E2F_TARGETS**
IPA	< TREX1 > IRF7, IFNR2, BAK1, IL-33, PRL, cell movement/migration and leukocyte function	N/A
VeRA vs JRep		
GSEA pathways and the top genes	**IFN-γ RESPONSE**: STAT1 higher in VeRA than JRep	**TGF_β_SIG*:** XIAP, SKIL, SMAD3 and THBS1 higher in VeRA than JRep **PROTEIN_SECRETION**
IPA	> ZC3H12A < HNF4A, Essra microRNA biogenesis signalling pathway	N/A
Res vs Norm		
GSEA pathways and the top genes	**IL-6_JAK_STAT*:** PTPN1, MAP3K8, IFNGR1, CXCL1, IL2RG and IL1B higher in Norm than Res **TNFA_VIA_NFkB*:** CXCL2, EHD1, higher in Norm than Res **IFN-γ RESPONSE*:** CMKLR1, HLAA, HLAB, PTPN1, HIF1A, SAMD9L higher in Norm than Res **KRAS, IFN-α, APOPTOSIS, INFLAMMATORY RESPONSE**	**G2M_CHECKPOINT:** ODC1, CDC6 and NUP50 higher in Norm than Res **IFN-α:** IRF7 and ITIF3 higher in Norm than Res **TNFA_VIA_NFkB_SIG:** PNRC1, NFKB2, NINJ1 and CXCL6 higher in Norm than Res **ALLOGRAFT_REGECTION**
IPA	> JARID2 < NOX1, transcription, hypoxia signalling	< IFNL1 > PNPT1

*The GSEA pathways significant according both FDR corrected P values and nominal p value

< = downregulated, > = upregulated.

6.3.2 Pathway analysis

The key findings from the pathway analyses are given in Table 6.12. In spite of some pathways appearing as significantly enriched in the gene set enrichment analysis, the heatmaps and counts plots of genes from these sets show a large amount of variation. Similarly, due to the sensitivity of ingenuity pathway analysis combined with the low sample numbers in this analysis, little can be ascertained from this analysis with high confidence. Consequently, results from these will only be discussed in brief, and only where the genes important in these pathways were also found to be significantly differentially expressed.

6.3.2.1 Macrophages

VeRA vs Res

Firstly, we wanted to examine the difference between a resolving signature and that in early RA. GSEA indicated that IL-6_JAK_STAT3_SIGNALLING was positively enriched in "VeRA vs Res". However, except for MAP3K8, no genes relevant to this pathway were significantly differentially expressed. Furthermore, MAP3K8 was much higher in the VeRA, but only in 3 out of 7 samples. The relevance of this gene is discussed in more depth in "Res vs Norm". Notably, expression of TNFRSF1A and IRF9 was consistently higher in the macrophages cultured with VeRA rather than Res fibroblasts. With a higher number of samples, these may be significantly different, as the current unadjusted p values are 0.051 and 0.058, respectively.

VeRA vs Norm

GSEA showed positive enrichment of the TNF_VIA_NFkB_SIGNALLING and the IFN-γ_RESPONSE pathways of the "VeRA vs Norm" comparison. Notably, higher expression of SOD2 in Norm than VeRA was important in both pathways. This difference was also significant according to the p value (0.021), albeit not the adjusted p value (0.105).

Furthermore, it was highly expressed in Norm compared to all other groups indicating low expression may be associated with an inflammatory signature. SOD2 is an antioxidant enzyme, located in the mitochondria where it removes the free radicals generated by the electron transport chain (372). Contrastingly to our findings, recent scRNA-seq indicated SOD2 was higher in RA macrophages compared to healthy controls (133). The difference may be attributed to the fact that our experiment was *in vitro*, and using macrophages differentiated for a short period of time, as opposed to tissue resident macrophages found *in vivo*.

VeRA vs JRep

GSEA gave positive enrichment of the "IFN-Y-RESPONSE" in macrophages co-cultured with "VeRA vs JRep" fibroblasts. The top gene identified here was STAT1, although interestingly this was lower in both macrophages cultured with JRep and Norm fibroblasts compared to the other groups (and maybe slightly higher in VeRA and EstRA compared to Res). However, these changes were not statistically significant according to the DESeq2 analysis. Donlin *et al* found upon co-culture with JRep RA SF macrophages decreased expression of STAT1. However, our findings suggest that this decrease may only be observed in the later stages of RA, not in the very early stages of RA or inflammation (as the Res group was also increased).

Norm vs Res

GSEA of macrophages cultured with VeRA compared to Res SF had the highest number of enriched pathways; IL-6_JAK_STAT3, TNFA_VIA_NFkB and IFN-γ_RESPONSE signalling pathways were all positively enriched in "Norm vs Res" comparison. Notably, significantly lower expression of PTPN1 in the Res compared to Norm, was important in the enrichment of both the IL-6_JAK_STAT3 and the IFN-γ_RESPONSE. *In vitro* and *in vivo* silencing of PTPN1 (aka PTP1B) in human and mouse caused a loss of viability and increased the pro-

inflammatory effects of macrophages (386). This suggests PTPN1 expression in macrophages has an anti-inflammatory effect.

Within the IL-6_JAK_STAT3 pathway, MAP3K8 was higher in the Norm (and all other groups) compared to the Res. This suggests perhaps that a low MAP3K8 expression in macrophages aids in resolution. MAP3K8 is activated downstream of the TNF-α and TLR signalling (387), furthermore KO experiments have identified that MAP3K8 is essential for IL-1β production (388). This may explain the lower (albeit not significantly different) expression of IL-1β in Res compared to Norm and other samples. Thus, it may be that fibroblasts exert a pro-resolving phenotype by limiting macrophage IL-1β production.

The lower expression of EHD1 in the Res compared to Norm, was a key contributor to the TNF-α signalling pathway. This was significant (0.02) in the p-value, with an unadjusted p-value of <0.1. Notably, EHD1 was also higher in the VeRA samples, and low and variable in the EstRA and JRep groups. EHD1 is a positive regulator of CSF-1R abundance as demonstrated in EHD1 KO macrophages which had significantly lower cell surface and total levels of CSF1R (389). CSF1R controls the growth and differentiation of macrophages (390) and *in vitro* CSF-1 signalling via CSF1R stimulates the macrophages into the M2 like phenotype (391). Consequently, this low expression of EHD1 observed in the macrophages cultured with Res fibroblasts, suggests that maybe in resolving inflammation fibroblasts lower macrophage response to CSF-1, but this is not seen in RA suggesting the prolonged inflammation is regulated in a different manner.

6.3.2.2 Fibroblasts

Similarly, to the macrophages, GSEA of the fibroblast analysis revealed few significantly enriched pathways according to the FDR corrected values. Of particular interest, however, was the TGF-β signalling and IFN-α response across multiple comparators.

Regarding the TGF-β signalling pathway, amongst the top genes were SMAD3, THBS1, XIAP and SKIL that had lower expression in the Norm (and Res) fibroblasts compared to the VeRA (and EstRA) fibroblasts. This upregulation is consistent with previous findings that the TGF-β pathway was upregulated in RA SF compared to OA SF (394). Furthermore, TGF-β/Smad signalling is known to promote the migration, invasion, and proliferation of SF (395, 396). SMAD3 is an essential part of the TGFβ signalling cascade; upon activation of the TGF-β receptor, Smad3 (and Smad2) becomes phosphorylated, binds Smad4, enters the nucleus and exerts its downstream effects (396). SKIL encodes SNON, a SMAD transcriptional corepressor which antagonises the TGF-β signalling pathway (397). Likewise, THBS1 protein expression is known to activate the latent form of TGF-β (398). Increased expression of these molecules was previously observed in RA SF either compared to OA (394) or control SF (396). XIAP is a gene regulated by the TGF-β pathway, hence the same differential expression pattern. Furthermore, previous studies have also shown expression was higher active compared to inactive RA tissue (399) and that the micro-RNA that targets XIAP (miR-431-5P) is downregulated in RA SF (400). XIAP is an inhibitor of apoptosis, and is often found upregulated in cancers where it promotes survival and invasiveness (401). This is consistent with RA SF having a more aggressive phenotype, as TGF-β/Smad signalling promotes the migration, invasion and proliferation of SF (395, 396).

TGF-β signalling molecules were lower in the JRep compared to the VeRA (and EstRA) groups. This may be because the JRep fibroblasts are from late-stage RA, where the patient has received treatment, which may alter the TGF-β signalling pathway and the way in which fibroblasts exert their pathogenic effects. Notably as well, although there was no enrichment in the TGF-β signalling in "Norm vs Res" fibroblasts, SMAD3 was higher the Res compared to Norm fibroblasts, and enough so to be in top genes for the enriched pathways; G2M_SIGNALLING pathway. However, its expression and the expression of other TGF-β signalling molecules, was still lower in Res compared to VeRA and EstRA. This suggests that resolving fibroblasts may decreased TGF-β signalling compared to untreated RA, but it is not low as observed in a non-inflamed environment.

In the IFN-α response, IRF7 and CSF1 were the top genes consistently higher in the Norm compared to VeRA fibroblasts. IRF7 is a regulatory protein of the IFN pathway (404). Interestingly, using the K/BxN mouse model of arthritis, IRF7 knockout (KO) mice showed increased disease severity coupled with decreased IFNβ expression (404). Furthermore, *in vitro* poly (I-C) stimulation of IRF7 KO SF, increased pro-inflammatory gene expression, but had no effect on IFNβ expression (404). On the other hand, in IRF7 KO macrophages there was significantly less IFNβ induction (404). Coupled with the data shown in this chapter (that high IRF7 expression is observed only in the Norm fibroblasts), perhaps a lack of IRF7 signalling from fibroblasts to macrophages in arthritis results in the pathogenic effects in macrophages by preventing IFN- β signalling. This is also in line with the work of Donlin *et al* where JRep RA fibroblasts damped IFN-β signalling in co-cultured macrophages (404). Notably as well, CSF1 (M-CSF), was higher in Norm, and some Res fibroblasts, then the VeRA,

EstRA and JRep. CSF-1 is used *in vitro* to differentiate macrophages into the anti-inflammatory (M2) phenotype (405). Furthermore, fibroblast production of CSF1 has been demonstrated both *in vivo* and *in vitro* to support the growth and survival of macrophages (391). Thus, perhaps the down regulation of CSF-1 in VeRA fibroblasts shifts the macrophage population from an anti-inflammatory to pro-inflammatory state.

6.3.3 Limitations

Small number of samples in each patient group and heterogeneity within the patients reduces the power of the study and limits the interpretations that can be made. One of the major causes of variability was the joint site of fibroblast donors. Here, ankle samples were only present in the VeRA and Res groups. Therefore, differences in these groups compared to others may have been caused by joint site (406), rather than disease stage. If repeating this experiment the same joint, or at least the same proportion of different joints would be used in each group to limit heterogeneity.

Whilst the batch needed to be corrected in the analysis, the effect on the overall findings was minimal due to the experimental design. Two more significant limitations were the use of a single monocyte donor and the duration of differentiation. Repeating this RNA-Seq experiment with multiple donors in each batch would determine if these findings are replicated across donors. However, this would add more heterogeneity to an already variable dataset, therefore n would need to be increased. To mirror the Donlin study (143) macrophages differentiation was performed over 2 days rather than the week used by the majority of other studies investigating macrophages (358). Consequently, we do not know if

the effects observed here are due to fibroblasts having an effect on monocyte, macrophage or partially differentiated macrophages. Therefore, repeating this experiment with a longer differentiation time is required.

Due to the limited number of cells in culture, there was a relatively low concentration and amount of RNA available for sequencing. This problem was exacerbated by the fact that the sequencer failed on the first round of sequencing and had to be repeated with an even lower amount of RNA. The low input meant that genes with low expression were not picked up in any samples, meaning differential expression of all genes could not be determined and when investigating genes of interest, some expression levels could not be assessed. Furthermore, it may be that genes appeared expressed in some samples, but not in others, only due to limited starting amounts of RNA, as opposed to there being no expression.

6.3.4 Conclusions

Taken together these results indicate that fibroblast: macrophage crosstalk changes dependent on the disease state of the fibroblasts. Notably, there were alterations in genes related to inflammation, in particular IFN and TNF-α signalling (e.g., IRF9, TNFRSF1A and STAT1). We also demonstrated bidirectional crosstalk (i.e., macrophage to fibroblast communication). This suggested that RA fibroblasts co-cultured with macrophages express genes characteristic of a more migratory and invasive phenotype (i.e. via TGFβ signalling in the VeRA/EstRA and CTHRC1 and RETSAT expression in JRep). Consistent with the findings in macrophages, IFN-α signalling (e.g. IRF7 and CSF1 expression) was also dysregulated in the fibroblasts. In conclusion, the data presented here suggests fibroblast: macrophage crosstalk changes during disease progression. However, due to limited n and sample variability we

were unable to draw definitive conclusions, and our findings require validation at both the gene and protein level. Nonetheless, it does suggest that further investigations into how these cell types interact may yield interesting results and provide novel avenues of research.

7 General Discussion

7.1 Summary of Findings

In this thesis we aimed to explore the pathogenic mechanisms underlying three autoimmune rheumatic diseases; PMR, GCA and RA. In the rarer and less well understood diseases of PMR and GCA, we were amongst the first to utilise metabolomics to determine how disease alters the circulating metabolome, and, in PMR, the changes that occur following GC treatment and in relation to patient symptoms. Within the more complex and harder to treat, RA, we focused on the role of stromal cells within the joint. Initially, by mining publicly available data and using multiplex imaging, we investigated how the endothelial phenotype changes with disease pathotype and duration. Building on this we examined if fibroblasts from different stages of RA (Res, VeRA and JRep) can alter the phenotype of healthy endothelial cells (HUVECs). Finally, we also explored the effect of these fibroblasts on the transcriptome of the other major constituent of the joint, macrophages. The main findings from this study are as follows:

- Metabolomic changes occur with PMR and GCA that do not normalise with glucocorticoid treatment
- Disease activity in PMR (inflammation, pain and stiffness) was associated with 3-hydroxybutyrate and acetoacetate
- A distinct metabolic signature, including low glutamine, was associated with fatigue in PMR patients

- Endothelial cells have a heterogeneous expression pattern of functionally important molecules, altered dependent by pathotype and frequently increase with disease duration
- HUVECs do not display large transcriptomic or secreted metabolomic differences according to the diagnosis of fibroblasts in co-culture
- Macrophages exhibit transcriptomic changes dependent on the diagnosis of fibroblast donor in co-culture, with alterations in IFN and TNF-α signalling
- JRep fibroblasts have a different transcriptome compared to VeRA and Res, but which genes are differentially change upon culture with either macrophages or HUVECs

7.2 Significance of Findings

In the field of RA, metabolomics has been used extensively and identified biomarkers of disease activity (80, 407-409) and treatment response (410-413). However, in PMR and GCA no papers have yet been published on metabolomic correlations with disease or treatment. From our data, we identified multiple metabolites which change with disease. Notably, many of these (i.e., ketone bodies, glycerol, lactate and pyruvate) have also been identified as dysregulated in other inflammatory diseases, including RA (80, 86). This suggests they may be associated with hallmarks of inflammation, as opposed to a disease specific response. It also highlights the overlap in systemic changes that occur within ARDs. We observed that whilst GCs alter the serum metabolome in PMR patients, it does not return to that observed in controls. This is perhaps unsurprising given the plethora of effects GCs have (414), and indeed a large number of serum metabolites were altered in healthy males after only a

short-term, low-dose use of GCs (262). Arguably one of the most interesting findings was the association of low glutamine with high fatigue in PMR patients both before and after treatment. In particular given that low glutamine has also been observed in other diseases including those typically associated with fatigue (i.e. cancer and chronic fatigue syndrome) (291-293). Although in RA no perturbations were found in glutamine concentrations in relation to fatigue (82), it is hypothesised that alterations in glutamatergic responses contribute to fatigue in rheumatic disorders (415). This highlights the need for our results to be replicated, but also that low glutamine may be predicative of fatigue in multiple disorders and an avenue worth investigating further.

In RA, we found that EC molecule expression changed according to disease pathotype and duration. Interestingly, we observed that E selectin and senescence molecule expression was associated with myeloid and lymphoid pathotypes, whilst the opposite was true of VAP1, and CD248 or Notch signalling molecules. However, we do not know whether these altered levels of expression are a cause or consequence of the phenotype. Considering the function of E selectin in mediating leukocyte adhesion and rolling, and that senescent ECs have sustained cytokine production (326, 327) it is likely these contribute to the increased lymphocyte infiltration observed in the lymphoid pathotypes. On the other hand, why VAP1, CD248 and Notch signalling molecules are higher in the fibroid pathotype is less well understood based on their known functions. It may well be that these are more highly expressed as a consequence, rather than cause of the fibroid pathotype. Importantly, it has already been demonstrated that patient response to treatment may be different depending on the pathotype (118). The lymphoid pathotype patients had the highest disease activity

and were most likely to require biologics, whilst patients with a primarily fibroid pathotype were less likely to respond the anti-TNF-α (118). Therefore, as our understanding of these pathotypes increases and patient stratification becomes more common, it is important to understand the differences in these pathotypes and how they may best be treated. Whilst we were limited in n when comparing the VeRA, Res and JRep samples there did not appear any large differences between the VeRA and Res groups which would aid in differentiating RA patients in the early stages of disease, or acting as early treatment targets. However, we did observe that the adhesion molecules, p53 and MMRN2 were higher in the JRep patients. This suggests these molecules contribute to the progression of disease, either via increasing lymphocyte recruitment or via angiogenesis. Considering that these are patients who will have previously failed treatments before requiring a replacement joint, it may be that these molecules identified as being upregulated could be treatment targets in patients who do not initially respond to treatment.

Despite the observed differences in the EC phenotype described above, there was little alteration in the HUVEC transcriptome or secreted metabolites dependent on diagnosis of fibroblasts in co-culture. This was surprising given that the previous functional studies demonstrated that, in stimulated conditions, co-culture with Res fibroblasts ECs limited lymphocyte recruitment, but VeRA and JRep fibroblasts were unable to induce this immunoprotective effect (9). Furthermore, this did not align with the already observed transcriptional changes; high expression of SOCS3 in ECs cultured with Res fibroblasts (9). Notably, there were limitations to this study, which may have masked subtle differences (discussed in 5.4.4). However, from the results in this study we must accept the null

hypothesis that there are no (or very few) transcriptional or secreted metabolite changes in ECs dependent on the diagnosis of fibroblast in co-cultures. The previously observed functional differences could be explained by epigenetic or phosphorylation changes. In particular the differential effects of IL-6 and TGF-β inhibition, combined with changes in SOCS3 expression from the previous study (9), suggests that alterations in JAK/STAT signalling (which are regulated by phosphorylation (416)).

In contrast to the EC-fibroblast co-cultures, macrophages had a large number of differentially expressed genes dependent on the diagnosis of fibroblast in culture. However, due to low n and the heterogeneity of the data it was difficult to discern a clear patterns of expressed and few pathways were significantly enriched. In spite of this, we did notice dysregulation of some key genes (e.g. IRF9, STAT1 and TNFRSF1A) which suggest IFN and TNF-α signalling are altered in macrophages depending on the disease of fibroblasts in co-culture. These results are in accordance with those of Donlin *et al* (143), but go on to show that fibroblasts have different effects on macrophages depending on their disease state.

In the mono and co-cultured fibroblasts from both the EC-fibroblast and macrophage-fibroblast dataset we observed the JRep fibroblasts clustered separately from the other groups. This may be due to a combination of factors, including disease duration, effects of treatment and indeed, the way in which the samples are collected (joint replacement as opposed to biopsy). Interestingly, upon co-culture with the macrophages we observed different differentially expressed genes in the JRep group. This is accordance with previous findings that showed macrophages were required for OA or RA fibroblasts to degrade

cartilage (144). Similarly, we saw in co-culture and increase in pro-migratory and bone destructive genes (e.g. CTHRC1 and RETSAT) in JRep fibroblasts. Notably, fibroblasts from the macrophage-fibroblast dataset, both in co- and mono- culture, had DEGs between all groups, including VeRA and Res. This is in contrast to findings in the EC-fibroblast data and previous results of mono-cultured fibroblasts and bulk RNA-sequencing of the joint (348, 351). This discrepancy may be due to differences in sequencing, culture conditions and the limited n in the macrophage dataset, but highlights that these data should be viewed with caution.

Although PMR and GCA occur at separate locations from RA, many of the same cell types (ECs, macrophages and fibroblasts) are known to play a role in pathogenesis (49). Indeed, growing evidence suggests these cells do contribute to the pathogenesis of these diseases (49). Whilst in this thesis we have not explored the role of stromal cells in PMR and GCA, it may be that similar alterations to those described in RA are occurring.

7.3 Limitations

Due to difficulties in obtaining patient samples, throughout this thesis we were limited by a small sample size. This problem was exacerbated further given the heterogeneity within the population (e.g., age, sex etc.) and in the diseases (e.g. ACPA+/-, pathotypes etc.). Likewise, the number was limited further still when looking at subsets of patients (e.g., PMR patients with fatigue).

All the work in this thesis was carried out as screening experiments to identify novel differences between groups of interest. Whilst these were useful in identifying potential

biomarkers and targets, without validation we cannot be confident of our observations. Consequently, we are severely limited in the conclusions that can be drawn from this data.

Notably, a large amount of analysis in this thesis is form transcriptomic data (the bulk RNA sequencing, and co-culture work). Whilst this does indicate there may be changes in protein expression, this must be confirmed at the protein level.

In assessing the endothelial phenotype we were limited by access to tissue, and the relatively small number of ECs in the joint compared to other stromal cells (i.e. fibroblasts). Therefore I was unable to isolate a sufficient number of ECs from patient samples. As the PEAC dataset was from bulk-RNA sequencing, we could only be sure that changes in expression equated to altered endothelial phenotype for molecules selectively expressed by ECs. On the other hand, the CellDIVE work did not have this limitation, changes were being examined on protein level and visualisation allowed us to confirm EC levels of expression. However, as we lacked markers of the different vessels and immune cells, although we observe selective expression we cannot confirm or hypothesise why this may be.

Within both co-culture experiments we used fibroblasts from a range of joint sites. This is problematic as transcriptomic data, in particular non-coding RNAs, caused fibroblasts to cluster by joint site rather than disease in fibroblast isolated from the RA, OA and normal joint (145). Smaller joints are also more likely to be affected earlier in disease (145) and in our data ankle or MCP joint donors were only present in the Res and VeRA groups (all other

donors from the knee). Unfortunately, due to limited numbers we were unable to correct for this in either form of analysis.

Regarding the EC-fibroblast data specifically, we were limited by the large effect observed by a combined donor and batch effect. Whilst we attempted to batch correct for this, we did not observe any true improvement in differential gene expression. Furthermore, this is not an ideal form of correction as there would be true biological variation, amongst differences due to batch. Whilst batch effects were observed in the macrophage dataset, the effect was limited as the same donor was used throughout and accounting for batch variation in the model should be adequate. However, the macrophage dataset was limited due to using only partially differentiated macrophages, which would have somewhere between a monocyte and macrophage phenotype. Therefore, when assessing these results, we do not know if these changes would also be observed *in vivo* in macrophages, or could this is more an effect of fibroblasts on monocytes, or specifically, monocytes part way through differentiation?

All of the co-culture work was carried out in a simple *in vitro* co-culture model of diseased fibroblasts and healthy cells. Whilst this is useful as a reductionist approach to assess the effects of one pathogenic cell type and another cell type it is not an accurate recapitulation of what occurs in the joint. Crucially, we used healthy ECs and macrophages. However, we know that both of these cell types, demonstrated here and by others (133, 134, 141), have their own pathogenic, or (depending on subtype) resolving effects, on surrounding stromal cells. Therefore, we do not know the effects of diseased fibroblasts on diseased cells. Vice versa, we do not know the effect of diseased macrophages or EC on the diseased fibroblasts.

Importantly, we observed that even upon co-culture with healthy cells the transcriptome of fibroblasts changed greatly, and crucially, co-culture with macrophages revealed unique differences between groups in the fibroblasts (e.g., changes in migratory and invasive genes). Thus, using macrophages and ECs isolated from patients would greatly improve this model, although there may be difficulties in acquiring the number of cells required for this. Likewise, all three cell types exist as subsets within the joint (8, 133, 134, and 141), thus co-cultures with these may help to truly unpick the pathogenic mechanisms of RA.

The 2D culturing and passaging cells prior to co-culture is another limitation to this model. It has been demonstrated that the fibroblast transcriptome changes with passage (349, 350) and importantly fibroblasts lose their lining and sublining identities entirely by the second passage (141). However, this can be overcome by culturing the fibroblasts with endothelial cells in a 3D organoid model (141). Likewise, the HUVECs in this model form tubules, more consistent to how they would be observed in tissue as opposed to a 2D monolayer (141). Moreover, this model would also overcome to the potential limitation of obtaining the required cell numbers from the subsets of cells within the joint. Building on this as model, and incorporating all three cell types, and using, if feasible, cells isolated from the joint would prove to be a much truer model of the *in vivo* joint.

Markedly, however, all *in vitro* models have their limitations. As highlighted by the metabolomics work, inflammation has systemic effects in the body, and *in vitro* models are unable to recapitulate this. Therefore, any findings from these data would need final confirmation within *in vivo* models.

7.4 Future work

Whilst the studies in this thesis found a number of molecules which may be differentially regulated in the diseases of PMR, GCA and RA, further work is required in order to validate these findings and in investigate the differences further.

- Validate the metabolite changes in a separate cohort of PMR and GCA patients
- Investigate the metabolome changes that occur in fatigue in PMR (and other rheumatic diseases) and incorporating factors such as weight gain and muscle mass into the study to identify if these can also associate with fatigue
- Providing low glutamine in patients reporting high fatigue is validated
    - Explore whether glutamine supplementation is an effective treatment of fatigue in PMR patients
    - Examine the cellular basis of why low serum glutamine concentrations occurs in patients suffering from; identify if this is a cause of effect of fatigue
- Confirm if the altered expression of molecules observed in the bulk RNA-Seq equates to changes in endothelial expression via deconvolution, analysis of single cell data, or, if possible, on isolated endothelial cells and staining of tissue sections
- Examine via phosphokinase arrays or ATAC sequencing if there are changes in phosphorylation or epigenetics of ECs depending on the fibroblasts in co-culture, ensuring the use of the same or pooled EC donor(s) in initial experiments
- Validate the DEGs from the macrophage work at both the gene (e.g., qPCR) and protein level

- Build on the findings here in more complex, 3D organoid model to explore the effects of fibroblasts from different disease stages, and using the identified fibroblast and macrophage subsets

7.5 Conclusions

In conclusion, in this thesis we explored the metabolomic alterations in PMR and GCA patients' serum, and in RA we investigated changes that occur in stromal cells with disease. We observed that the circulating metabolome is altered in patients with PMR and GCA. Furthermore, markers of inflammation (CRP, pain and stiffness) were associated with ketone bodies, but fatigue was not. However, particular metabolites did associate with fatigue, in particular low glutamine before and after treatment. In RA, we observed changes in the expression pattern of functionally important molecules according to disease pathotype and increased expression with disease duration (higher in JRep than VeRA or Res). However, co-culture of HUVECs with Res, VeRA or JRep fibroblasts revealed few changes in the transcriptome or secreted metabolites. In contrast to this, culture of macrophages with these (and non-inflamed) fibroblasts revealed a large number of transcriptomic differences. In both the ECs and macrophage data we observed that the transcriptome of the JRep fibroblasts was different from other groups. Furthermore, co-culture with another cell type induced different transcriptional differences. Thus, we have identified a number of differentially regulated molecules in GCA, PMR and RA, however, as all of these were performed as exploratory analyses, validation of these findings is required.

8 References

1. Hedar AM, Stradner MH, Roessler A, Goswami N. Autoimmune Rheumatic Diseases and Vascular Function: The Concept of Autoimmune Atherosclerosis. J Clin Med. 2021;10(19).
2. Angum F, Khan T, Kaler J, Siddiqui L, Hussain A. The Prevalence of Autoimmune Disorders in Women: A Narrative Review. Cureus. 2020;12(5):e8094.
3. Ebel AV, O'Dell JR. Clinical Features, Diagnosis, and Treatment of Rheumatoid Arthritis. Physician Assistant Clinics. 2021;6(1):41-60.
4. González-Gay MA, Matteson EL, Castañeda S. Polymyalgia rheumatica. The Lancet. 2017;390(10103):1700-12.
5. Ciofalo A, Gulotta G, Iannella G, Pasquariello B, Manno A, Angeletti D, et al. Giant Cell Arteritis (GCA): Pathogenesis, Clinical Aspects and Treatment Approaches. Curr Rheumatol Rev. 2019;15(4):259-68.
6. Burmester GR, Pope JE. Novel treatment strategies in rheumatoid arthritis. The Lancet. 2017;389(10086):2338-48.
7. Huber LC, Distler O, Tarner I, Gay RE, Gay S, Pap T. Synovial fibroblasts: key players in rheumatoid arthritis. Rheumatology. 2006;45(6):669-75.
8. Croft AP, Campos J, Jansen K, Turner JD, Marshall J, Attar M, et al. Distinct fibroblast subsets drive inflammation and damage in arthritis. Nature. 2019;570(7760):246-51.
9. Filer A, Ward LSC, Kemble S, Davies CS, Munir H, Rogers R, et al. Identification of a transitional fibroblast function in very early rheumatoid arthritis. Annals of the Rheumatic Diseases. 2017;76(12):2105.
10. Buckley CD, McGettrick HM. Leukocyte trafficking between stromal compartments: lessons from rheumatoid arthritis. Nature Reviews Rheumatology. 2018;14(8):476-87.
11. Zhang J, Alcaide P, Liu L, Sun J, He A, Luscinskas FW, et al. Regulation of endothelial cell adhesion molecule expression by mast cells, macrophages, and neutrophils. PloS one. 2011;6(1):e14525-e.
12. Hunt BJ, Jurd KM. Endothelial cell activation. A central pathophysiological process. BMJ (Clinical research ed). 1998;316(7141):1328-9.
13. Nourshargh S, Alon R. Leukocyte Migration into Inflamed Tissues. Immunity. 2014;41(5):694-707.
14. Vestweber D. How leukocytes cross the vascular endothelium. Nature Reviews Immunology. 2015;15(11):692-704.
15. Neurath MF. Resolution of inflammation: from basic concepts to clinical application. Seminars in Immunopathology. 2019;41(6):627-31.
16. Serhan CN, Savill J. Resolution of inflammation: the beginning programs the end. Nature Immunology. 2005;6(12):1191-7.
17. Sugimoto MA, Sousa LP, Pinho V, Perretti M, Teixeira MM. Resolution of Inflammation: What Controls Its Onset? Front Immunol. 2016;7:160-.
18. Manning JE, Lewis JW, Marsh LJ, McGettrick HM. Insights Into Leukocyte Trafficking in Inflammatory Arthritis - Imaging the Joint. Front Cell Dev Biol. 2021;9:635102.
19. Richard-Eaglin A, Smallheer BA. Immunosuppressive/Autoimmune Disorders. Nurs Clin North Am. 2018;53(3):319-34.
20. Goldblatt F, O'Neill SG. Clinical aspects of autoimmune rheumatic diseases. Lancet. 2013;382(9894):797-808.
21. Alarcón GS, Williams GV, Singer JZ, Steen VD, Clegg DO, Paulus HE, et al. Early undifferentiated connective tissue disease. I. Early clinical manifestation in a large cohort of patients with undifferentiated connective tissue diseases compared with cohorts of well established connective tissue disease. J Rheumatol. 1991;18(9):1332-9.

22. Deane KD, El-Gabalawy H. Pathogenesis and prevention of rheumatic disease: focus on preclinical RA and SLE. Nature Reviews Rheumatology. 2014;10(4):212-28.
23. Weyand CM, Hunder NN, Hicok KC, Hunder GG, Goronzy JJ. HLA-DRB1 alleles in polymyalgia rheumatica, giant cell arteritis, and rheumatoid arthritis. Arthritis Rheum. 1994;37(4):514-20.
24. Jakobsson K, Jacobsson L, Warrington K, Matteson EL, Liang K, Melander O, et al. Body mass index and the risk of giant cell arteritis—results from a prospective study. Rheumatology. 2014;54(3):433-40.
25. Deane KD, Demoruelle MK, Kelmenson LB, Kuhn KA, Norris JM, Holers VM. Genetic and environmental risk factors for rheumatoid arthritis. Best Pract Res Clin Rheumatol. 2017;31(1):3-18.
26. Choy E. Understanding the dynamics: pathways involved in the pathogenesis of rheumatoid arthritis. Rheumatology. 2012;51(suppl_5):v3-v11.
27. Chang K, Yang SM, Kim SH, Han KH, Park SJ, Shin JI. Smoking and rheumatoid arthritis. International journal of molecular sciences. 2014;15(12):22279-95.
28. Espinoza JL, Ai S, Matsumura I. New Insights on the Pathogenesis of Takayasu Arteritis: Revisiting the Microbial Theory. Pathogens. 2018;7(3):73.
29. Camellino D, Giusti A, Girasole G, Bianchi G, Dejaco C. Pathogenesis, Diagnosis and Management of Polymyalgia Rheumatica. Drugs & Aging. 2019;36(11):1015-26.
30. Mikuls TR, Payne JB, Yu F, Thiele GM, Reynolds RJ, Cannon GW, et al. Periodontitis and Porphyromonas gingivalis in patients with rheumatoid arthritis. Arthritis Rheumatol. 2014;66(5):1090-100.
31. Schieir O, Tosevski C, Glazier RH, Hogg-Johnson S, Badley EM. Incident myocardial infarction associated with major types of arthritis in the general population: a systematic review and meta-analysis. Ann Rheum Dis. 2017;76(8):1396-404.
32. Baillet A, Gossec L, Carmona L, Wit Md, van Eijk-Hustings Y, Bertheussen H, et al. Points to consider for reporting, screening for and preventing selected comorbidities in chronic inflammatory rheumatic diseases in daily practice: a EULAR initiative. Annals of the Rheumatic Diseases. 2016;75(6):965.
33. Gibofsky A. Epidemiology, pathophysiology, and diagnosis of rheumatoid arthritis: A Synopsis. Am J Manag Care. 2014;20(7 Suppl):S128-35.
34. Taylor PC, Alten R, Gomez-Reino JJ, Caporali R, Bertin P, Sullivan E, et al. Clinical characteristics and patient-reported outcomes in patients with inadequately controlled rheumatoid arthritis despite ongoing treatment. RMD Open. 2018;4(1):e000615.
35. Fischer BD, Adeyemo A, O'Leary ME, Bottaro A. Animal models of rheumatoid pain: experimental systems and insights. Arthritis Research & Therapy. 2017;19(1):146.
36. Terrades-Garcia N, Cid MC. Pathogenesis of giant-cell arteritis: how targeted therapies are influencing our understanding of the mechanisms involved. Rheumatology. 2018;57(suppl_2):ii51-ii62.
37. Bartikoski BJ, De Oliveira MS, Do Espírito Santo RC, Dos Santos LP, Dos Santos NG, Xavier RM. A Review of Metabolomic Profiling in Rheumatoid Arthritis: Bringing New Insights in Disease Pathogenesis, Treatment and Comorbidities. Metabolites. 2022;12(5).
38. Xu L, Chang C, Jiang P, Wei K, Zhang R, Jin Y, et al. Metabolomics in rheumatoid arthritis: Advances and review. Front Immunol. 2022;13:961708.
39. Dakin SG, Coles M, Sherlock JP, Powrie F, Carr AJ, Buckley CD. Pathogenic stromal cells as therapeutic targets in joint inflammation. Nature Reviews Rheumatology. 2018;14(12):714-26.
40. Crowson CS, Matteson EL, Myasoedova E, Michet CJ, Ernste FC, Warrington KJ, et al. The lifetime risk of adult-onset rheumatoid arthritis and other inflammatory autoimmune rheumatic diseases. Arthritis Rheum. 2011;63(3):633-9.
41. Weyand CM, Goronzy JJ. Clinical practice. Giant-cell arteritis and polymyalgia rheumatica. N Engl J Med. 2014;371(1):50-7.

42. Mackie SL, Pease CT, Fukuba E, Harris E, Emery P, Hodgson R, et al. Whole-body MRI of patients with polymyalgia rheumatica identifies a distinct subset with complete patient-reported response to glucocorticoids. Annals of the Rheumatic Diseases. 2015;74(12):2188.
43. Marzo-Ortega H, Rhodes LA, Tan AL, Tanner SF, Conaghan PG, Hensor EM, et al. Evidence for a different anatomic basis for joint disease localization in polymyalgia rheumatica in comparison with rheumatoid arthritis. Arthritis Rheum. 2007;56(10):3496-501.
44. Mackie SL, Hensor EM, Haugeberg G, Bhakta B, Pease CT. Can the prognosis of polymyalgia rheumatica be predicted at disease onset? Results from a 5-year prospective study. Rheumatology (Oxford). 2010;49(4):716-22.
45. Hutchings A, Hollywood J, Lamping DL, Pease CT, Chakravarty K, Silverman B, et al. Clinical outcomes, quality of life, and diagnostic uncertainty in the first year of polymyalgia rheumatica. Arthritis Care & Research. 2007;57(5):803-9.
46. Salvarani C, Macchioni PL, Tartoni PL, Rossi F, Baricchi R, Castri C, et al. Polymyalgia rheumatica and giant cell arteritis: a 5-year epidemiologic and clinical study in Reggio Emilia, Italy. Clin Exp Rheumatol. 1987;5(3):205-15.
47. Pipitone N, Salvarani C. Update on polymyalgia rheumatica. European Journal of Internal Medicine. 2013;24(7):583-9.
48. Luqmani R. Large vessel vasculitides: update for the cardiologist. Curr Opin Cardiol. 2012;27(6):578-84.
49. Weyand CM, Goronzy JJ. Immune mechanisms in medium and large-vessel vasculitis. Nature Reviews Rheumatology. 2013;9(12):731-40.
50. Jennette JC, Falk RJ, Bacon PA, Basu N, Cid MC, Ferrario F, et al. 2012 Revised International Chapel Hill Consensus Conference Nomenclature of Vasculitides. Arthritis & Rheumatism. 2013;65(1):1-11.
51. Low C, Conway R. Current advances in the treatment of giant cell arteritis: the role of biologics. Ther Adv Musculoskelet Dis. 2019;11:1759720X19827222-1759720X.
52. Crow RW, Katz BJ, Warner JEA, Alder SC, Zhang K, Schulman S, et al. Giant cell arteritis and mortality. J Gerontol A Biol Sci Med Sci. 2009;64(3):365-9.
53. Ponte C, Rodrigues AF, O'Neill L, Luqmani RA. Giant cell arteritis: Current treatment and management. World J Clin Cases. 2015;3(6):484-94.
54. Hellmich B, Agueda A, Monti S, Buttgereit F, de Boysson H, Brouwer E, et al. 2018 Update of the EULAR recommendations for the management of large vessel vasculitis. Annals of the Rheumatic Diseases. 2020;79(1):19-30.
55. Dejaco C, Singh YP, Perel P, Hutchings A, Camellino D, Mackie S, et al. 2015 Recommendations for the management of polymyalgia rheumatica: a European League Against Rheumatism/American College of Rheumatology collaborative initiative. Annals of the Rheumatic Diseases. 2015;74(10):1799-807.
56. Da Silva JA, Jacobs JW, Kirwan JR, Boers M, Saag KG, Inês LB, et al. Safety of low dose glucocorticoid treatment in rheumatoid arthritis: published evidence and prospective trial data. Ann Rheum Dis. 2006;65(3):285-93.
57. Proven A, Gabriel SE, Orces C, O'Fallon WM, Hunder GG. Glucocorticoid therapy in giant cell arteritis: Duration and adverse outcomes. Arthritis Care & Research. 2003;49(5):703-8.
58. Meliconi R, Pulsatelli L, Uguccioni M, Salvarani C, Macchioni P, Melchiorri C, et al. Leukocyte infiltration in synovial tissue from the shoulder of patients with polymyalgia rheumatica. Quantitative analysis and influence of corticosteroid treatment. Arthritis & Rheumatism. 1996;39(7):1199-207.
59. Owen CE, Liew DFL, Buchanan RRC. Musculotendinous Inflammation: The Defining Pathology of Polymyalgia Rheumatica? The Journal of Rheumatology. 2019;46(12):1552-5.
60. Liddle J, Bartlam R, Mallen CD, Mackie SL, Prior JA, Helliwell T, et al. What is the impact of giant cell arteritis on patients' lives? A UK qualitative study. BMJ Open. 2017;7(8):e017073.

61. Harky A, Fok M, Balmforth D, Bashir M. Pathogenesis of large vessel vasculitis: Implications for disease classification and future therapies. Vasc Med. 2019;24(1):79-88.
62. Al-Mousawi AZ, Gurney SP, Lorenzi AR, Pohl U, Dayan M, Mollan SP. Reviewing the Pathophysiology Behind the Advances in the Management of Giant Cell Arteritis. Ophthalmology and Therapy. 2019;8(2):177-93.
63. Partington RJ, Muller S, Helliwell T, Mallen CD, Abdul Sultan A. Incidence, prevalence and treatment burden of polymyalgia rheumatica in the UK over two decades: a population-based study. Annals of the Rheumatic Diseases. 2018;77(12):1750.
64. Salvarani C, Crowson CS, O'Fallon WM, Hunder GG, Gabriel SE. Reappraisal of the epidemiology of giant cell arteritis in Olmsted County, Minnesota, over a fifty-year period. Arthritis Care & Research. 2004;51(2):264-8.
65. Mohan SV, Liao YJ, Kim JW, Goronzy JJ, Weyand CM. Giant cell arteritis: immune and vascular aging as disease risk factors. Arthritis research & therapy. 2011;13(4):231-.
66. Mackie SL. Polymyalgia rheumatica: pathogenesis and management. Clin Med (Lond). 2013;13(4):398-400.
67. Dejaco C, Duftner C, Buttgereit F, Matteson EL, Dasgupta B. The spectrum of giant cell arteritis and polymyalgia rheumatica: revisiting the concept of the disease. Rheumatology. 2016;56(4):506-15.
68. González-Gay MA, Amoli MM, Garcia-Porrua C, Ollier WER. Genetic markers of disease susceptibility and severity in giant cell arteritis and polymyalgia rheumatica. Seminars in Arthritis and Rheumatism. 2003;33(1):38-48.
69. Mackie SL, Taylor JC, Haroon-Rashid L, Martin S, Dasgupta B, Gough A, et al. Association of HLA-DRB1 amino acid residues with giant cell arteritis: genetic association study, meta-analysis and geo-epidemiological investigation. Arthritis Res Ther. 2015;17(1):195.
70. Salvarani C, Gabriel SE, O'Fallon WM, Hunder GG. The incidence of giant cell arteritis in Olmsted County, Minnesota: apparent fluctuations in a cyclic pattern. Ann Intern Med. 1995;123(3):192-4.
71. Watanabe R, Goronzy JJ, Berry G, Liao YJ, Weyand CM. Giant Cell Arteritis: From Pathogenesis to Therapeutic Management. Current Treatment Options in Rheumatology. 2016;2(2):126-37.
72. Barone F, Nayar S, Buckley C. The role of non-hematopoietic stromal cells in the persistence of inflammation. Front Immunol. 2013;3.
73. Piggott K, Deng J, Warrington K, Younge B, Kubo JT, Desai M, et al. Blocking the NOTCH pathway inhibits vascular inflammation in large-vessel vasculitis. Circulation. 2011;123(3):309-18.
74. Guggino G, Ferrante A, Macaluso F, Triolo G, Ciccia F. Pathogenesis of polymyalgia rheumatica. Reumatismo. 2018;70(1):10-7.
75. Ma-Krupa W, Jeon M-S, Spoerl S, Tedder TF, Goronzy JJ, Weyand CM. Activation of arterial wall dendritic cells and breakdown of self-tolerance in giant cell arteritis. J Exp Med. 2004;199(2):173-83.
76. Kingston A, Comas-Herrera A, Jagger C. Forecasting the care needs of the older population in England over the next 20 years: estimates from the Population Ageing and Care Simulation (PACSim) modelling study. Lancet Public Health. 2018;3(9):e447-e55.
77. Mosley JD, Witte JS, Larkin EK, Bastarache L, Shaffer CM, Karnes JH, et al. Identifying genetically driven clinical phenotypes using linear mixed models. Nat Commun. 2016;7:11433.
78. Carmona FD, Vaglio A, Mackie SL, Hernández-Rodríguez J, Monach PA, Castañeda S, et al. A Genome-wide Association Study Identifies Risk Alleles in Plasminogen and P4HA2 Associated with Giant Cell Arteritis. Am J Hum Genet. 2017;100(1):64-74.
79. Clish CB. Metabolomics: an emerging but powerful tool for precision medicine. Cold Spring Harb Mol Case Stud. 2015;1(1):a000588-a.

80. Young SP, Kapoor SR, Viant MR, Byrne JJ, Filer A, Buckley CD, et al. The impact of inflammation on metabolomic profiles in patients with arthritis. Arthritis Rheum. 2013;65(8):2015-23.
81. Sasaki C, Hiraishi T, Oku T, Okuma K, Suzumura K, Hashimoto M, et al. Metabolomic approach to the exploration of biomarkers associated with disease activity in rheumatoid arthritis. PLOS ONE. 2019;14(7):e0219400.
82. Surowiec I, Gjesdal CG, Jonsson G, Norheim KB, Lundstedt T, Trygg J, et al. Metabolomics study of fatigue in patients with rheumatoid arthritis naïve to biological treatment. Rheumatology International. 2016;36(5):703-11.
83. Jain A, Kumar D, Guleria A, Misra DP, Zanwar A, Chaurasia S, et al. NMR-Based Serum Metabolomics of Patients with Takayasu Arteritis: Relationship with Disease Activity. J Proteome Res. 2018;17(9):3317-24.
84. Guleria A, Misra DP, Rawat A, Dubey D, Khetrapal CL, Bacon P, et al. NMR-Based Serum Metabolomics Discriminates Takayasu Arteritis from Healthy Individuals: A Proof-of-Principle Study. Journal of Proteome Research. 2015;14(8):3372-81.
85. Al-Ani B, Fitzpatrick M, Al-Nuaimi H, Coughlan AM, Hickey FB, Pusey CD, et al. Changes in urinary metabolomic profile during relapsing renal vasculitis. Sci Rep. 2016;6:38074.
86. Cedola F, Coras R, Sanchez-Lopez E, Mateo L, Pedersen A, Brandy-Garcia A, et al., editors. Choline Metabolite Is Associated with Inflammation in Arthritis in the Elderly. Arthritis Rheumatology; 2019.
87. Prior JA, Muller S, Helliwell T, Hider SL, Barraclough K, Dasgupta B, et al. The association of pain and stiffness with fatigue in incident polymyalgia rheumatica: baseline results from the polymyalgia rheumatica cohort study. Prim Health Care Res Dev. 2019;20:e46.
88. Cimmino MA, Parodi M, Montecucco C, Caporali R. The correct prednisone starting dose in polymyalgia rheumatica is related to body weight but not to disease severity. BMC Musculoskelet Disord. 2011;12(1):94-.
89. Gabriel SE, Sunku J, Salvarani C, O'Fallon WM, Hunder GG. Adverse outcomes of antiinflammatory therapy among patients with polymyalgia rheumatica. Arthritis & Rheumatism. 1997;40(10):1873-8.
90. Moghadam-Kia S, Werth VP. Prevention and treatment of systemic glucocorticoid side effects. Int J Dermatol. 2010;49(3):239-48.
91. Malkawi AK, Alzoubi KH, Jacob M, Matic G, Ali A, Al Faraj A, et al. Metabolomics Based Profiling of Dexamethasone Side Effects in Rats. Frontiers in Pharmacology. 2018;9(46).
92. Radhakutty A, Mangelsdorf BL, Drake SM, Rowland A, Smith MD, Mangoni AA, et al. Opposing effects of rheumatoid arthritis and low dose prednisolone on arginine metabolomics. Atherosclerosis. 2017;266:190-5.
93. Kapoor SR. Metabolomics of Inflammatory Arthritis: The University of Birmingham; 2014.
94. Burgess K, Rankin N, Weidt S. Chapter 10 - Metabolomics. In: Padmanabhan S, editor. Handbook of Pharmacogenomics and Stratified Medicine. San Diego: Academic Press; 2014. p. 181-205.
95. Zhang A, Sun H, Yan G, Wang P, Wang X. Metabolomics for Biomarker Discovery: Moving to the Clinic. BioMed Research International. 2015;2015:354671.
96. Goodacre R, Vaidyanathan S, Dunn WB, Harrigan GG, Kell DB. Metabolomics by numbers: acquiring and understanding global metabolite data. Trends in Biotechnology. 2004;22(5):245-52.
97. Morrison B, Scotland CJ, Fleck A. The determination of plasma glucose in a diabetic clinic. Clinica Chimica Acta. 1972;39(2):301-6.
98. Chatham JC, Blackband SJ. Nuclear Magnetic Resonance Spectroscopy and Imaging in Animal Research. ILAR Journal. 2001;42(3):189-208.
99. Nicholson JK, Lindon JC. Metabonomics. Nature. 2008;455(7216):1054-6.

100. Emwas A-HM. The Strengths and Weaknesses of NMR Spectroscopy and Mass Spectrometry with Particular Focus on Metabolomics Research. In: Bjerrum JT, editor. Metabonomics: Methods and Protocols. New York, NY: Springer New York; 2015. p. 161-93.
101. Emwas A-H, Roy R, McKay RT, Tenori L, Saccenti E, Gowda GAN, et al. NMR Spectroscopy for Metabolomics Research. Metabolites. 2019;9(7):123.
102. Broadhurst D, Goodacre R, Reinke SN, Kuligowski J, Wilson ID, Lewis MR, et al. Guidelines and considerations for the use of system suitability and quality control samples in mass spectrometry assays applied in untargeted clinical metabolomic studies. Metabolomics. 2018;14(6):72.
103. Rasch EK, Hirsch R, Paulose-Ram R, Hochberg MC. Prevalence of rheumatoid arthritis in persons 60 years of age and older in the United States: effect of different methods of case classification. Arthritis Rheum. 2003;48(4):917-26.
104. Gerosa M, De Angelis V, Riboldi P, Meroni PL. Rheumatoid arthritis: a female challenge. Womens Health (Lond). 2008;4(2):195-201.
105. Strand V, Kimberly R, Isaacs JD. Biologic therapies in rheumatology: lessons learned, future directions. Nat Rev Drug Discov. 2007;6(1):75-92.
106. Smith MD. The normal synovium. Open Rheumatol J. 2011;5:100-6.
107. Cosway E, Anderson G, Garside P, Prendergast C. The thymus and rheumatology: should we care? Curr Opin Rheumatol. 2016;28(2):189-95.
108. Köhler BM, Günther J, Kaudewitz D, Lorenz H-M. Current Therapeutic Options in the Treatment of Rheumatoid Arthritis. J Clin Med. 2019;8(7):938.
109. Smolen JS, Landewé RBM, Bijlsma JWJ, Burmester GR, Dougados M, Kerschbaumer A, et al. EULAR recommendations for the management of rheumatoid arthritis with synthetic and biological disease-modifying antirheumatic drugs: 2019 update. Annals of the Rheumatic Diseases. 2020;79(6):685-99.
110. Felson DT, Anderson JJ, Boers M, Bombardier C, Furst D, Goldsmith C, et al. American college of rheumatology preliminary definition of improvement in rheumatoid arthritis. Arthritis & Rheumatism. 1995;38(6):727-35.
111. Russell MD, Bukhari M, Galloway J. The price of good health care. Rheumatology. 2018;58(6):931-2.
112. Manasson J, Blank RB, Scher JU. The microbiome in rheumatology: Where are we and where should we go? Annals of the Rheumatic Diseases. 2020;79(6):727-33.
113. Xu H, Zhao H, Fan D, Liu M, Cao J, Xia Y, et al. Interactions between Gut Microbiota and Immunomodulatory Cells in Rheumatoid Arthritis. Mediators Inflamm. 2020;2020:1430605-.
114. Scher JU, Joshua V, Artacho A, Abdollahi-Roodsaz S, Öckinger J, Kullberg S, et al. The lung microbiota in early rheumatoid arthritis and autoimmunity. Microbiome. 2016;4(1):60-.
115. Zhang X, Zhang D, Jia H, Feng Q, Wang D, Liang D, et al. The oral and gut microbiomes are perturbed in rheumatoid arthritis and partly normalized after treatment. Nat Med. 2015;21(8):895-905.
116. Blair JPM, Bay-Jensen AC, Tang MH, Frederiksen P, Bager C, Karsdal M, et al. Identification of heterogenous treatment response trajectories to anti-IL6 receptor treatment in rheumatoid arthritis. Sci Rep. 2020;10(1):13975.
117. Nerviani A, Di Cicco M, Mahto A, Lliso-Ribera G, Rivellese F, Thorborn G, et al. A Pauci-Immune Synovial Pathotype Predicts Inadequate Response to TNFα-Blockade in Rheumatoid Arthritis Patients. Front Immunol. 2020;11(845).
118. Humby F, Lewis M, Ramamoorthi N, Hackney JA, Barnes MR, Bombardieri M, et al. Synovial cellular and molecular signatures stratify clinical response to csDMARD therapy and predict radiographic progression in early rheumatoid arthritis patients. Annals of the Rheumatic Diseases. 2019;78(6):761-72.
119. Song YW, Kang EH. Autoantibodies in rheumatoid arthritis: rheumatoid factors and anticitrullinated protein antibodies. QJM. 2010;103(3):139-46.

120. Arend WP, Firestein GS. Pre-rheumatoid arthritis: predisposition and transition to clinical synovitis. Nature Reviews Rheumatology. 2012;8(10):573-86.
121. Vander Cruyssen B, Hoffman IE, Peene I, Union A, Mielants H, Meheus L, et al. Prediction models for rheumatoid arthritis during diagnostic investigation: evaluation of combinations of rheumatoid factor, anti-citrullinated protein/peptide antibodies and the human leucocyte antigen-shared epitope. Ann Rheum Dis. 2007;66(3):364-9.
122. Nielsen SF, Bojesen SE, Schnohr P, Nordestgaard BG. Elevated rheumatoid factor and long term risk of rheumatoid arthritis: a prospective cohort study. BMJ : British Medical Journal. 2012;345:e5244.
123. Guo Q, Wang Y, Xu D, Nossent J, Pavlos NJ, Xu J. Rheumatoid arthritis: pathological mechanisms and modern pharmacologic therapies. Bone Research. 2018;6(1):15.
124. van Venrooij WJ, Pruijn GJM. How citrullination invaded rheumatoid arthritis research. Arthritis Research & Therapy. 2014;16(1):103.
125. György B, Tóth E, Tarcsa E, Falus A, Buzás EI. Citrullination: A posttranslational modification in health and disease. The International Journal of Biochemistry & Cell Biology. 2006;38(10):1662-77.
126. Padyukov L, Seielstad M, Ong RT, Ding B, Rönnelid J, Seddighzadeh M, et al. A genome-wide association study suggests contrasting associations in ACPA-positive versus ACPA-negative rheumatoid arthritis. Ann Rheum Dis. 2011;70(2):259-65.
127. Malmström V, Catrina AI, Klareskog L. The immunopathogenesis of seropositive rheumatoid arthritis: from triggering to targeting. Nature Reviews Immunology. 2017;17(1):60-75.
128. Ingegnoli F, Castelli R, Gualtierotti R. Rheumatoid factors: clinical applications. Dis Markers. 2013;35(6):727-34.
129. Pitzalis C, Kelly S, Humby F. New learnings on the pathophysiology of RA from synovial biopsies. Curr Opin Rheumatol. 2013;25(3).
130. Ouboussad L, Burska AN, Melville A, Buch MH. Synovial Tissue Heterogeneity in Rheumatoid Arthritis and Changes With Biologic and Targeted Synthetic Therapies to Inform Stratified Therapy. Frontiers in Medicine. 2019;6(45).
131. Lewis MJ, Barnes MR, Blighe K, Goldmann K, Rana S, Hackney JA, et al. Molecular Portraits of Early Rheumatoid Arthritis Identify Clinical and Treatment Response Phenotypes. Cell Reports. 2019;28(9):2455-70.e5.
132. Noort AR, van Zoest KPM, van Baarsen LG, Maracle CX, Helder B, Papazian N, et al. Tertiary Lymphoid Structures in Rheumatoid Arthritis: NF-κB–Inducing Kinase–Positive Endothelial Cells as Central Players. Am J Pathol. 2015;185(7):1935-43.
133. Alivernini S, MacDonald L, Elmesmari A, Finlay S, Tolusso B, Gigante MR, et al. Distinct synovial tissue macrophage subsets regulate inflammation and remission in rheumatoid arthritis. Nat Med. 2020;26(8):1295-306.
134. Kuo D, Ding J, Cohn IS, Zhang F, Wei K, Rao DA, et al. HBEGF(+) macrophages in rheumatoid arthritis induce fibroblast invasiveness. Sci Transl Med. 2019;11(491):eaau8587.
135. Smolen JS, Aletaha D, Koeller M, Weisman MH, Emery P. New therapies for treatment of rheumatoid arthritis. The Lancet. 2007;370(9602):1861-74.
136. Salmi M, Rajala P, Jalkanen S. Homing of mucosal leukocytes to joints. Distinct endothelial ligands in synovium mediate leukocyte-subtype specific adhesion. The Journal of Clinical Investigation. 1997;99(9):2165-72.
137. Kzhyshkowska J, Gratchev A, Goerdt S. Stabilin-1, a homeostatic scavenger receptor with multiple functions. J Cell Mol Med. 2006;10(3):635-49.
138. Szekanecz Z, Haines GK, Lin TR, Harlow LA, Goerdt S, Rayan G, et al. Differential Distribution of Intercellular Adhesion Molecules (ICAM–1, ICAM–2, and ICAM–3) and THE MS–1 Antigen in Normal and Diseased Human Synovia. Arthritis & Rheumatism. 1994;37(2):221-31.
139. Ager A. High Endothelial Venules and Other Blood Vessels: Critical Regulators of Lymphoid Organ Development and Function. Front Immunol. 2017;8:45-.

140. Cañete JD, Santiago B, Cantaert T, Sanmartí R, Palacin A, Celis R, et al. Ectopic lymphoid neogenesis in psoriatic arthritis. Ann Rheum Dis. 2007;66(6):720-6.
141. Wei K, Korsunsky I, Marshall JL, Gao A, Watts GFM, Major T, et al. Notch signalling drives synovial fibroblast identity and arthritis pathology. Nature. 2020;582(7811):259-64.
142. Steinhauser ML, Kunkel SL, Hogaboam CM, Evanoff H, Strieter RM, Lukacs NW. Macrophage/fibroblast coculture induces macrophage inflammatory protein-1alpha production mediated by intercellular adhesion molecule-1 and oxygen radicals. J Leukoc Biol. 1998;64(5):636-41.
143. Donlin LT, Jayatilleke A, Giannopoulou EG, Kalliolias GD, Ivashkiv LB. Modulation of TNF-Induced Macrophage Polarization by Synovial Fibroblasts. The Journal of Immunology. 2014;193(5):2373.
144. Scott BB, Weisbrot LM, Greenwood JD, Bogoch ER, Paige CJ, Keystone EC. Rheumatoid arthritis synovial fibroblast and U937 macrophage/monocyte cell line interaction in cartilage degradation. Arthritis & Rheumatism. 1997;40(3):490-8.
145. Ospelt C, Gay S, Klein K. Epigenetics in the pathogenesis of RA. Semin Immunopathol. 2017;39(4):409-19.
146. Buckley CD. Why does chronic inflammation persist: An unexpected role for fibroblasts. Immunol Lett. 2011;138(1):12-4.
147. Turner JD, Filer A. The role of the synovial fibroblast in rheumatoid arthritis pathogenesis. Curr Opin Rheumatol. 2015;27(2):175-82.
148. Crowley T, O'Neil JD, Adams H, Thomas AM, Filer A, Buckley CD, et al. Priming in response to pro-inflammatory cytokines is a feature of adult synovial but not dermal fibroblasts. Arthritis Res Ther. 2017;19(1):35.
149. Buckley CD, Pilling D, Lord JM, Akbar AN, Scheel-Toellner D, Salmon M. Fibroblasts regulate the switch from acute resolving to chronic persistent inflammation. Trends Immunol. 2001;22(4):199-204.
150. Pap T, Meinecke I, Müller-Ladner U, Gay S. Are fibroblasts involved in joint destruction? Ann Rheum Dis. 2005;64 Suppl 4(Suppl 4):iv52-4.
151. Ospelt C, Gay S. The role of resident synovial cells in destructive arthritis. Best Pract Res Clin Rheumatol. 2008;22(2):239-52.
152. Castor CW, Dorstewitz EL. Abnormalities of connective tissue cells cultured from patients with rheumatoid arthritis. I. Relative unresponsiveness of rheumatoid synovial cells to hydrocortisone. J Lab Clin Med. 1966;68(2):300-13.
153. Rosengren S, Boyle DL, Firestein GS. Acquisition, culture, and phenotyping of synovial fibroblasts. Methods Mol Med. 2007;135:365-75.
154. Karouzakis E, Raza K, Kolling C, Buckley CD, Gay S, Filer A, et al. Analysis of early changes in DNA methylation in synovial fibroblasts of RA patients before diagnosis. Sci Rep. 2018;8(1):7370.
155. Doody KM, Bottini N, Firestein GS. Epigenetic alterations in rheumatoid arthritis fibroblast-like synoviocytes. Epigenomics. 2017;9(4):479-92.
156. Sohn C, Lee A, Qiao Y, Loupasakis K, Ivashkiv LB, Kalliolias GD. Prolonged tumor necrosis factor α primes fibroblast-like synoviocytes in a gene-specific manner by altering chromatin. Arthritis Rheumatol. 2015;67(1):86-95.
157. Bottini N, Firestein GS. Duality of fibroblast-like synoviocytes in RA: passive responders and imprinted aggressors. Nature Reviews Rheumatology. 2013;9(1):24-33.
158. Lefèvre S, Knedla A, Tennie C, Kampmann A, Wunrau C, Dinser R, et al. Synovial fibroblasts spread rheumatoid arthritis to unaffected joints. Nat Med. 2009;15(12):1414-20.
159. Croft AP, Naylor AJ, Marshall JL, Hardie DL, Zimmermann B, Turner J, et al. Rheumatoid synovial fibroblasts differentiate into distinct subsets in the presence of cytokines and cartilage. Arthritis Res Ther. 2016;18(1):270.

160. Mizoguchi F, Slowikowski K, Wei K, Marshall JL, Rao DA, Chang SK, et al. Functionally distinct disease-associated fibroblast subsets in rheumatoid arthritis. Nature Communications. 2018;9(1):789.
161. Stephenson W, Donlin LT, Butler A, Rozo C, Bracken B, Rashidfarrokhi A, et al. Single-cell RNA-seq of rheumatoid arthritis synovial tissue using low-cost microfluidic instrumentation. Nature Communications. 2018;9(1):791.
162. Micheroli R, Elhai M, Edalat S, Frank-Bertoncelj M, Bürki K, Ciurea A, et al. Role of synovial fibroblast subsets across synovial pathotypes in rheumatoid arthritis: a deconvolution analysis. RMD Open. 2022;8(1):e001949.
163. Pober JS, Sessa WC. Evolving functions of endothelial cells in inflammation. Nature Reviews Immunology. 2007;7(10):803-15.
164. Krüger-Genge A, Blocki A, Franke R-P, Jung F. Vascular Endothelial Cell Biology: An Update. International journal of molecular sciences. 2019;20(18):4411.
165. Chi J-T, Chang HY, Haraldsen G, Jahnsen FL, Troyanskaya OG, Chang DS, et al. Endothelial cell diversity revealed by global expression profiling. Proceedings of the National Academy of Sciences. 2003;100(19):10623-8.
166. Kalucka J, de Rooij LPMH, Goveia J, Rohlenova K, Dumas SJ, Meta E, et al. Single-Cell Transcriptome Atlas of Murine Endothelial Cells. Cell. 2020;180(4):764-79.e20.
167. Parsonage G, Filer AD, Haworth O, Nash GB, Rainger GE, Salmon M, et al. A stromal address code defined by fibroblasts. Trends Immunol. 2005;26(3):150-6.
168. McGettrick HM, Smith E, Filer A, Kissane S, Salmon M, Buckley CD, et al. Fibroblasts from different sites may promote or inhibit recruitment of flowing lymphocytes by endothelial cells. Eur J Immunol. 2009;39(1):113-25.
169. Munir H, Ward LSC, Sheriff L, Kemble S, Nayar S, Barone F, et al. Adipogenic Differentiation of Mesenchymal Stem Cells Alters Their Immunomodulatory Properties in a Tissue-Specific Manner. STEM CELLS. 2017;35(6):1636-46.
170. Al-Soudi A, Kaaij MH, Tas SW. Endothelial cells: From innocent bystanders to active participants in immune responses. Autoimmunity Reviews. 2017;16(9):951-62.
171. Middleton J, Americh L, Gayon R, Julien D, Aguilar L, Amalric F, et al. Endothelial cell phenotypes in the rheumatoid synovium: activated, angiogenic, apoptotic and leaky. Arthritis Res Ther. 2004;6(2):60-72.
172. Tong B, Yu J, Wang T, Dou Y, Wu X, Kong L, et al. Sinomenine suppresses collagen-induced arthritis by reciprocal modulation of regulatory T cells and Th17 cells in gut-associated lymphoid tissues. Mol Immunol. 2015;65(1):94-103.
173. Yue M, Xia Y, Shi C, Guan C, Li Y, Liu R, et al. Berberine ameliorates collagen-induced arthritis in rats by suppressing Th17 cell responses via inducing cortistatin in the gut. Febs j. 2017;284(17):2786-801.
174. Naskar D, Teng F, Felix KM, Bradley CP, Wu HJ. Synthetic Retinoid AM80 Ameliorates Lung and Arthritic Autoimmune Responses by Inhibiting T Follicular Helper and Th17 Cell Responses. J Immunol. 2017;198(5):1855-64.
175. Abbot SE, Whish WJ, Jennison C, Blake DR, Stevens CR. Tumour necrosis factor alpha stimulated rheumatoid synovial microvascular endothelial cells exhibit increased shear rate dependent leucocyte adhesion in vitro. Annals of the rheumatic diseases. 1999;58(9):573-81.
176. Paleolog EM, Hunt M, Elliott MJ, Feldmann M, Maini RN, Woody JN. Deactivation of vascular endothelium by monoclonal anti-tumor necrosis factor alpha antibody in rheumatoid arthritis. Arthritis Rheum. 1996;39(7):1082-91.
177. Kavanaugh AF, Davis LS, Nichols LA, Norris SH, Rothlein R, Scharschmidt LA, et al. Treatment of refractory rheumatoid arthritis with a monoclonal antibody to intercellular adhesion molecule 1. Arthritis Rheum. 1994;37(7):992-9.

178. Schulze-Koops H, Lipsky PE, Kavanaugh AF, Davis LS. Elevated Th1- or Th0-like cytokine mRNA in peripheral circulation of patients with rheumatoid arthritis. Modulation by treatment with anti-ICAM-1 correlates with clinical benefit. J Immunol. 1995;155(10):5029-37.
179. Issekutz AC, Mu JY, Liu G, Melrose J, Berg EL. E-selectin, but not P-selectin, is required for development of adjuvant-induced arthritis in the rat. Arthritis Rheum. 2001;44(6):1428-37.
180. Deyab G, Hokstad I, Whist JE, Smastuen MC, Agewall S, Lyberg T, et al. Methotrexate and anti-tumor necrosis factor treatment improves endothelial function in patients with inflammatory arthritis. Arthritis Research & Therapy. 2017;19(1):232.
181. Carter RA, Campbell IK, O'Donnel KL, Wicks IP. Vascular cell adhesion molecule-1 (VCAM-1) blockade in collagen-induced arthritis reduces joint involvement and alters B cell trafficking. Clin Exp Immunol. 2002;128(1):44-51.
182. Mulherin DM, Veale DJ, Belch JJF, Bresnihan B, Fitzgerald O. Adhesion molecule in untreated inflammatory arthritis. QJM: An International Journal of Medicine. 1996;89(3):195-204.
183. Gardner L, Wilson C, Patterson AM, Bresnihan B, FitzGerald O, Stone MA, et al. Temporal expression pattern of Duffy antigen in rheumatoid arthritis: up-regulation in early disease. Arthritis Rheum. 2006;54(6):2022-6.
184. Smith E, McGettrick HM, Stone MA, Shaw JS, Middleton J, Nash GB, et al. Duffy antigen receptor for chemokines and CXCL5 are essential for the recruitment of neutrophils in a multicellular model of rheumatoid arthritis synovium. Arthritis Rheum. 2008;58(7):1968-73.
185. Lally F, Smith E, Filer A, Stone MA, Shaw JS, Nash GB, et al. A novel mechanism of neutrophil recruitment in a coculture model of the rheumatoid synovium. Arthritis & Rheumatism. 2005;52(11):3460-9.
186. Rainger GE, Stone P, Morland CM, Nash GB. A novel system for investigating the ability of smooth muscle cells and fibroblasts to regulate adhesion of flowing leukocytes to endothelial cells. Journal of Immunological Methods. 2001;255(1):73-82.
187. Lavin Y, Mortha A, Rahman A, Merad M. Regulation of macrophage development and function in peripheral tissues. Nature Reviews Immunology. 2015;15(12):731-44.
188. Watanabe S, Alexander M, Misharin AV, Budinger GRS. The role of macrophages in the resolution of inflammation. The Journal of Clinical Investigation. 2019;129(7):2619-28.
189. Collison J. Origins of synovial macrophages revealed. Nature Reviews Rheumatology. 2019;15(8):451-.
190. Tu J, Hong W, Guo Y, Zhang P, Fang Y, Wang X, et al. Ontogeny of Synovial Macrophages and the Roles of Synovial Macrophages From Different Origins in Arthritis. Front Immunol. 2019;10:1146.
191. Mu X, Li Y, Fan G-C. Tissue-Resident Macrophages in the Control of Infection and Resolution of Inflammation. Shock. 2021;55(1):14-23.
192. Mills CD, Kincaid K, Alt JM, Heilman MJ, Hill AM. M-1/M-2 Macrophages and the Th1/Th2 Paradigm. The Journal of Immunology. 2000;164(12):6166-73.
193. Martinez FO, Gordon S. The M1 and M2 paradigm of macrophage activation: time for reassessment. F1000Prime Rep. 2014;6:13.
194. Mantovani A, Sica A, Sozzani S, Allavena P, Vecchi A, Locati M. The chemokine system in diverse forms of macrophage activation and polarization. Trends Immunol. 2004;25(12):677-86.
195. Viola A, Munari F, Sánchez-Rodríguez R, Scolaro T, Castegna A. The Metabolic Signature of Macrophage Responses. Front Immunol. 2019;10:1462.
196. Bolego C, Cignarella A, Staels B, Chinetti-Gbaguidi G. Macrophage Function and Polarization in Cardiovascular Disease. Arteriosclerosis, Thrombosis, and Vascular Biology. 2013;33(6):1127-34.
197. Saqib U, Sarkar S, Suk K, Mohammad O, Baig MS, Savai R. Phytochemicals as modulators of M1-M2 macrophages in inflammation. Oncotarget. 2018;9(25):17937-50.
198. He C, Carter AB. The Metabolic Prospective and Redox Regulation of Macrophage Polarization. J Clin Cell Immunol. 2015;6(6).

199. Clayton S. A novel microRNA signalling pathway in macrophages linking glucocorticoids and cellular metabolism: University of Birmingham; 2020.
200. Udalova IA, Mantovani A, Feldmann M. Macrophage heterogeneity in the context of rheumatoid arthritis. Nature Reviews Rheumatology. 2016;12(8):472-85.
201. Kennedy A, Fearon U, Veale DJ, Godson C. Macrophages in synovial inflammation. Front Immunol. 2011;2:52-.
202. Herenius MM, Thurlings RM, Wijbrandts CA, Bennink RJ, Dohmen SE, Voermans C, et al. Monocyte migration to the synovium in rheumatoid arthritis patients treated with adalimumab. Ann Rheum Dis. 2011;70(6):1160-2.
203. Haringman JJ, Gerlag DM, Zwinderman AH, Smeets TJM, Kraan MC, Baeten D, et al. Synovial tissue macrophages: a sensitive biomarker for response to treatment in patients with rheumatoid arthritis. Annals of the rheumatic diseases. 2005;64(6):834-8.
204. Gautier EL, Shay T, Miller J, Greter M, Jakubzick C, Ivanov S, et al. Gene-expression profiles and transcriptional regulatory pathways that underlie the identity and diversity of mouse tissue macrophages. Nature Immunology. 2012;13(11):1118-28.
205. Peters KM, Koberg K, Rosendahl T, Klosterhalfen B, Straub A, Zwadlo-Klarwasser G. Macrophage reactions in septic arthritis. Arch Orthop Trauma Surg. 1996;115(6):347-50.
206. Cauli A, Yanni G, Panayi GS. Interleukin-1, interleukin-1 receptor antagonist and macrophage populations in rheumatoid arthritis synovial membrane. Br J Rheumatol. 1997;36(9):935-40.
207. Kurowska-Stolarska M, Alivernini S. Synovial tissue macrophages: friend or foe? RMD open. 2017;3(2):e000527-e.
208. De Rycke L, Baeten D, Foell D, Kruithof E, Veys EM, Roth J, et al. Differential expression and response to anti-TNFα treatment of infiltrating versus resident tissue macrophage subsets in autoimmune arthritis. The Journal of Pathology. 2005;206(1):17-27.
209. Vogl T, Eisenblätter M, Völler T, Zenker S, Hermann S, van Lent P, et al. Alarmin S100A8/S100A9 as a biomarker for molecular imaging of local inflammatory activity. Nature Communications. 2014;5(1):4593.
210. Herenius MMJ, Thurlings RM, Wijbrandts CA, Bennink RJ, Dohmen SE, Voermans C, et al. Monocyte migration to the synovium in rheumatoid arthritis patients treated with adalimumab. Annals of the Rheumatic Diseases. 2011;70(6):1160-2.
211. Weiss M, Byrne AJ, Blazek K, Saliba DG, Pease JE, Perocheau D, et al. IRF5 controls both acute and chronic inflammation. Proc Natl Acad Sci U S A. 2015;112(35):11001-6.
212. Misharin Alexander V, Cuda Carla M, Saber R, Turner Jason D, Gierut Angelica K, Haines GK, III, et al. Nonclassical Ly6C[−] Monocytes Drive the Development of Inflammatory Arthritis in Mice. Cell Reports. 2014;9(2):591-604.
213. Thurlings RM, Wijbrandts CA, Bennink RJ, Dohmen SE, Voermans C, Wouters D, et al. Monocyte Scintigraphy in Rheumatoid Arthritis: The Dynamics of Monocyte Migration in Immune-Mediated Inflammatory Disease. PLOS ONE. 2009;4(11):e7865.
214. Turner JD. Characterising bidirectional interactions between synovial fibroblasts and myeloid cells. Birmingham: University of Birmingham; 2017.
215. Duraiyan J, Govindarajan R, Kaliyappan K, Palanisamy M. Applications of immunohistochemistry. J Pharm Bioallied Sci. 2012;4(Suppl 2):S307-S9.
216. StageBio. IHC or IF: Which is Best for My Study? 2018 [Available from: https://www.stagebio.com/blog/ihc-or-if-which-is-best-for-my-study.
217. Corwin A, McDonough E, Surrette C, Dumpuri P, Sood A, Ginty FM. Abstract 1448: Cell DIVE™: A robust and standardized platform for multiplexed whole slide imaging and single cell analysis. Cancer Research. 2020;80(16 Supplement):1448-.
218. Kukurba KR, Montgomery SB. RNA Sequencing and Analysis. Cold Spring Harb Protoc. 2015;2015(11):951-69.

219. Chen G, Ning B, Shi T. Single-Cell RNA-Seq Technologies and Related Computational Data Analysis. Frontiers in Genetics. 2019;10(317).
220. Vogelzang NJ, Breitbart W, Cella D, Curt GA, Groopman JE, Horning SJ, et al. Patient, caregiver, and oncologist perceptions of cancer-related fatigue: results of a tripart assessment survey. The Fatigue Coalition. Semin Hematol. 1997;34(3 Suppl 2):4-12.
221. Luqmani R, Lee E, Singh S, Gillett M, Schmidt WA, Bradburn M, et al. The Role of Ultrasound Compared to Biopsy of Temporal Arteries in the Diagnosis and Treatment of Giant Cell Arteritis (TABUL): a diagnostic accuracy and cost-effectiveness study. Health Technol Assess. 2016;20(90):1-238.
222. Tiziani S, Emwas A-H, Lodi A, Ludwig C, Bunce CM, Viant MR, et al. Optimized metabolite extraction from blood serum for 1H nuclear magnetic resonance spectroscopy. Analytical Biochemistry. 2008;377(1):16-23.
223. Ludwig C, Günther UL. MetaboLab--advanced NMR data processing and analysis for metabolomics. BMC Bioinformatics. 2011;12:366-.
224. Xi Y, Rocke DM. Baseline Correction for NMR Spectroscopic Metabolomics Data Analysis. BMC Bioinformatics. 2008;9(1):324.
225. Dieterle F, Ross A, Schlotterbeck G, Senn H. Probabilistic quotient normalization as robust method to account for dilution of complex biological mixtures. Application in 1H NMR metabonomics. Anal Chem. 2006;78(13):4281-90.
226. Weljie AM, Newton J, Mercier P, Carlson E, Slupsky CM. Targeted Profiling: Quantitative Analysis of 1H NMR Metabolomics Data. Analytical Chemistry. 2006;78(13):4430-42.
227. Wu Z, Li D, Meng J, Wang H. Introduction to SIMCA-P and Its Application. In: Esposito Vinzi V, Chin WW, Henseler J, Wang H, editors. Handbook of Partial Least Squares: Concepts, Methods and Applications. Berlin, Heidelberg: Springer Berlin Heidelberg; 2010. p. 757-74.
228. Chong J, Soufan O, Li C, Caraus I, Li S, Bourque G, et al. MetaboAnalyst 4.0: towards more transparent and integrative metabolomics analysis. Nucleic Acids Research. 2018;46(W1):W486-W94.
229. Chong J, Wishart DS, Xia J. Using MetaboAnalyst 4.0 for Comprehensive and Integrative Metabolomics Data Analysis. Current Protocols in Bioinformatics. 2019;68(1):e86.
230. Kidd ME, Shumaker DK, Ridge KM. The role of vimentin intermediate filaments in the progression of lung cancer. Am J Respir Cell Mol Biol. 2014;50(1):1-6.
231. Gerdes MJ, Sevinsky CJ, Sood A, Adak S, Bello MO, Bordwell A, et al. Highly multiplexed single-cell analysis of formalin-fixed, paraffin-embedded cancer tissue. Proc Natl Acad Sci U S A. 2013;110(29):11982-7.
232. Bankhead P, Loughrey MB, Fernández JA, Dombrowski Y, McArt DG, Dunne PD, et al. QuPath: Open source software for digital pathology image analysis. Sci Rep. 2017;7(1):16878.
233. Munir H, Rainger GE, Nash GB, McGettrick H. Analyzing the effects of stromal cells on the recruitment of leukocytes from flow. J Vis Exp. 2015(95):e52480.
234. Cooke BM, Usami S, Perry I, Nash GB. A simplified method for culture of endothelial cells and analysis of adhesion of blood cells under conditions of flow. Microvasc Res. 1993;45(1):33-45.
235. Jaffe EA, Nachman RL, Becker CG, Minick CR. Culture of human endothelial cells derived from umbilical veins. Identification by morphologic and immunologic criteria. J Clin Invest. 1973;52(11):2745-56.
236. Desjardins P, Conklin D. NanoDrop microvolume quantitation of nucleic acids. J Vis Exp. 2010(45).
237. Clayton SA, Daley KK, MacDonald L, Fernandez-Vizarra E, Bottegoni G, O'Neil JD, et al. Inflammation causes remodeling of mitochondrial cytochrome c oxidase mediated by the bifunctional gene C15orf48. Sci Adv. 2021;7(50):eabl5182.

238. Schroeder A, Mueller O, Stocker S, Salowsky R, Leiber M, Gassmann M, et al. The RIN: an RNA integrity number for assigning integrity values to RNA measurements. BMC Molecular Biology. 2006;7(1):3.
239. Gallego Romero I, Pai AA, Tung J, Gilad Y. RNA-seq: impact of RNA degradation on transcript quantification. BMC Biology. 2014;12(1):42.
240. Team R. RStudio: Integrated Development Environment for R. R studio, PBC, Boston, MA URL http://wwwrstudiocom/. 2021.
241. Wickham H, Averick M, Bryan J, Chang W, McGowan L, François R, et al. Welcome to the Tidyverse. Journal of Open Source Software. 2019;4:1686.
242. FastQC. 2015.
243. Ewels P, Magnusson M, Lundin S, Käller M. MultiQC: summarize analysis results for multiple tools and samples in a single report. Bioinformatics. 2016;32(19):3047-8.
244. BBDuk. [Available from: https://jgi.doe.gov/data-and-tools/software-tools/bbtools/bb-tools-user-guide/). .
245. Dobin A, Davis CA, Schlesinger F, Drenkow J, Zaleski C, Jha S, et al. STAR: ultrafast universal RNA-seq aligner. Bioinformatics. 2013;29(1):15-21.
246. Cunningham F, Allen JE, Allen J, Alvarez-Jarreta J, Amode M R, Armean Irina M, et al. Ensembl 2022. Nucleic Acids Research. 2022;50(D1):D988-D95.
247. Dobin A, Gingeras TR. Mapping RNA-seq Reads with STAR. Current protocols in bioinformatics. 2015;51:11.4.1-.4.9.
248. Liao Y, Smyth GK, Shi W. featureCounts: an efficient general purpose program for assigning sequence reads to genomic features. Bioinformatics. 2013;30(7):923-30.
249. Putri GH, Anders S, Pyl PT, Pimanda JE, Zanini F. Analysing high-throughput sequencing data in Python with HTSeq 2.0. Bioinformatics. 2022;38(10):2943-5.
250. R Core Team. R: A language and environment for statistical computing. Vienna, Austria: R Foundation for Statistical Computing; 2021.
251. Love MI, Huber W, Anders S. Moderated estimation of fold change and dispersion for RNA-seq data with DESeq2. Genome Biology. 2014;15(12):550.
252. Tibshirani R. Variance Stabilization and the Bootstrap. Biometrika. 1988;75(3):433-44.
253. Anders S, Huber W. Differential expression analysis for sequence count data. Genome Biology. 2010;11(10):R106.
254. Huber W, von Heydebreck A, Sueltmann H, Poustka A, Vingron M. Parameter estimation for the calibration and variance stabilization of microarray data. Stat Appl Genet Mol Biol. 2003;2:Article3.
255. Blighe K, Lun A. PCAtools: PCAtools: Everything Principal Components Analysis. R package version 2.4.0. ed2021.
256. Gu Z, Eils R, Schlesner M. Complex heatmaps reveal patterns and correlations in multidimensional genomic data. Bioinformatics. 2016;32(18):2847-9.
257. Stephens M. False discovery rates: a new deal. Biostatistics. 2016;18(2):275-94.
258. Kevin Blighe SRaML. EnhancedVolcano: Publication-ready volcano plots with enhanced colouring and labeling 2021 [R package version 1.12.0]. Available from: https://github.com/kevinblighe/EnhancedVolcano.
259. Krämer A, Green J, Pollard J, Jr, Tugendreich S. Causal analysis approaches in Ingenuity Pathway Analysis. Bioinformatics. 2013;30(4):523-30.
260. Dunn WB, Broadhurst D, Brown M, Baker PN, Redman CW, Kenny LC, et al. Metabolic profiling of serum using Ultra Performance Liquid Chromatography and the LTQ-Orbitrap mass spectrometry system. J Chromatogr B Analyt Technol Biomed Life Sci. 2008;871(2):288-98.
261. Sumner LW, Amberg A, Barrett D, Beale MH, Beger R, Daykin CA, et al. Proposed minimum reporting standards for chemical analysis Chemical Analysis Working Group (CAWG) Metabolomics Standards Initiative (MSI). Metabolomics. 2007;3(3):211-21.

262. Bordag N, Klie S, Jürchott K, Vierheller J, Schiewe H, Albrecht V, et al. Glucocorticoid (dexamethasone)-induced metabolome changes in healthy males suggest prediction of response and side effects. Sci Rep. 2015;5(1):15954.
263. Sproston NR, Ashworth JJ. Role of C-Reactive Protein at Sites of Inflammation and Infection. Front Immunol. 2018;9:754-.
264. Fazaa A, Boussaa H, Ouenniche K, Miladi S, Sellami M, Souabni L, et al. OPTIMAL ASSESSMENT OF FATIGUE IN RHEUMATOID ARTHRITIS: VISUAL ANALOG SCALE VERSUS FUNCTIONAL ASSESSMENT OF CHRONIC ILLNESS THERAPY – FATIGUE. Annals of the Rheumatic Diseases. 2021;80(Suppl 1):1113-4.
265. Vignoli A, Santini G, Tenori L, Macagno F, Macis G, Mores N, et al. A NMR-based metabolomics approach to the assessment of inhaled pharmacotherapy in patients with COPD. European Respiratory Journal. 2019;54(suppl 63):OA3585.
266. Rittig N, Bach E, Thomsen HH, Pedersen SB, Nielsen TS, Jørgensen JO, et al. Regulation of Lipolysis and Adipose Tissue Signaling during Acute Endotoxin-Induced Inflammation: A Human Randomized Crossover Trial. PloS one. 2016;11(9):e0162167-e.
267. Bird HA, Esselinckx W, Dixon AS, Mowat AG, Wood PH. An evaluation of criteria for polymyalgia rheumatica. Ann Rheum Dis. 1979;38(5):434-9.
268. Youm Y-H, Nguyen KY, Grant RW, Goldberg EL, Bodogai M, Kim D, et al. The ketone metabolite β-hydroxybutyrate blocks NLRP3 inflammasome–mediated inflammatory disease. Nature Medicine. 2015;21(3):263-9.
269. Serrano A, Carmona FD, Castañeda S, Solans R, Hernández-Rodríguez J, Cid MC, et al. Evidence of association of the NLRP1 gene with giant cell arteritis. Annals of the Rheumatic Diseases. 2013;72(4):628.
270. Guo C, Fu R, Wang S, Huang Y, Li X, Zhou M, et al. NLRP3 inflammasome activation contributes to the pathogenesis of rheumatoid arthritis. Clin Exp Immunol. 2018;194(2):231-43.
271. Matteson EL, Maradit-Kremers H, Cimmino MA, Schmidt WA, Schirmer M, Salvarani C, et al. Patient-reported outcomes in polymyalgia rheumatica. J Rheumatol. 2012;39(4):795-803.
272. Ahmed A, Saeed F, Arshad MU, Afzaal M, Imran A, Ali SW, et al. Impact of intermittent fasting on human health: an extended review of metabolic cascades. International Journal of Food Properties. 2018;21(1):2700-13.
273. Chariot P, Chevalier X, Yerroum M, Drogou I, Authier FJ, Gherardi R. Impaired redox status and cytochrome coxidase deficiency in patients with polymyalgia rheumatica. Annals of the Rheumatic Diseases. 2001;60(11):1016.
274. Haas R, Smith J, Rocher-Ros V, Nadkarni S, Montero-Melendez T, D'Acquisto F, et al. Lactate Regulates Metabolic and Pro-inflammatory Circuits in Control of T Cell Migration and Effector Functions. PLoS Biol. 2015;13(7):e1002202.
275. van Raalte DH, Brands M, van der Zijl NJ, Muskiet MH, Pouwels PJW, Ackermans MT, et al. Low-dose glucocorticoid treatment affects multiple aspects of intermediary metabolism in healthy humans: a randomised controlled trial. Diabetologia. 2011;54(8):2103-12.
276. Geer EB, Islam J, Buettner C. Mechanisms of glucocorticoid-induced insulin resistance: focus on adipose tissue function and lipid metabolism. Endocrinol Metab Clin North Am. 2014;43(1):75-102.
277. Berhane F, Fite A, Daboul N, Al-Janabi W, Msallaty Z, Caruso M, et al. Plasma Lactate Levels Increase during Hyperinsulinemic Euglycemic Clamp and Oral Glucose Tolerance Test. Journal of Diabetes Research. 2015;2015:102054.
278. Juraschek SP, Shantha GPS, Chu AY, Miller ER, III, Guallar E, Hoogeveen RC, et al. Lactate and Risk of Incident Diabetes in a Case-Cohort of the Atherosclerosis Risk in Communities (ARIC) Study. PLOS ONE. 2013;8(1):e55113.

279. Doar JWH, Wynn V, Cramp DG. Blood pyruvate and plasma glucose levels during oral and intravenous glucose tolerance tests in obese and non-obese women. Metabolism. 1968;17(8):690-701.
280. Hodson L, Humphreys SM, Karpe F, Frayn KN. Metabolic signatures of human adipose tissue hypoxia in obesity. Diabetes. 2013;62(5):1417-25.
281. Connaughton S, Chowdhury F, Attia RR, Song S, Zhang Y, Elam MB, et al. Regulation of pyruvate dehydrogenase kinase isoform 4 (PDK4) gene expression by glucocorticoids and insulin. Mol Cell Endocrinol. 2010;315(1-2):159-67.
282. Serrano MA, Curi R, Parry-Billings M, Williams JF, Newsholme EA. Effects of glucocorticoids on lymphocyte metabolism. Am J Physiol. 1993;264(1 Pt 1):E24-8.
283. Kreiner F, Galbo H. Elevated muscle interstitial levels of pain-inducing substances in symptomatic muscles in patients with polymyalgia rheumatica. PAIN. 2011;152(5):1127-32.
284. Ratter JM, Rooijackers HMM, Hooiveld GJ, Hijmans AGM, de Galan BE, Tack CJ, et al. In vitro and in vivo Effects of Lactate on Metabolism and Cytokine Production of Human Primary PBMCs and Monocytes. Front Immunol. 2018;9(2564).
285. Dorokhov YL, Shindyapina AV, Sheshukova EV, Komarova TV. Metabolic Methanol: Molecular Pathways and Physiological Roles. Physiological Reviews. 2015;95(2):603-44.
286. Tong Z, Han C, Luo W, Wang X, Li H, Luo H, et al. Accumulated hippocampal formaldehyde induces age-dependent memory decline. Age (Dordr). 2013;35(3):583-96.
287. Lacourt TE, Vichaya EG, Chiu GS, Dantzer R, Heijnen CJ. The High Costs of Low-Grade Inflammation: Persistent Fatigue as a Consequence of Reduced Cellular-Energy Availability and Non-adaptive Energy Expenditure. Front Behav Neurosci. 2018;12:78-.
288. Louati K, Berenbaum F. Fatigue in chronic inflammation - a link to pain pathways. Arthritis research & therapy. 2015;17:254-.
289. Omdal R. SP0059 CNS Effects of Inflammation: The Brain and Fatigue. Annals of the Rheumatic Diseases. 2015;74(Suppl 2):16-.
290. Cruzat V, Macedo Rogero M, Noel Keane K, Curi R, Newsholme P. Glutamine: Metabolism and Immune Function, Supplementation and Clinical Translation. Nutrients. 2018;10(11):1564.
291. Jiang J, Srivastava S, Zhang J. Starve Cancer Cells of Glutamine: Break the Spell or Make a Hungry Monster? Cancers (Basel). 2019;11(6):804.
292. Kim M-H, Kim H. The Roles of Glutamine in the Intestine and Its Implication in Intestinal Diseases. International journal of molecular sciences. 2017;18(5):1051.
293. Armstrong CW, McGregor NR, Sheedy JR, Buttfield I, Butt HL, Gooley PR. NMR metabolic profiling of serum identifies amino acid disturbances in chronic fatigue syndrome. Clinica Chimica Acta. 2012;413(19):1525-31.
294. Wagenmakers AJ. Amino acid metabolism, muscular fatigue and muscle wasting. Speculations on adaptations at high altitude. Int J Sports Med. 1992;13 Suppl 1:S110-3.
295. Kermani TA, Warrington KJ. Polymyalgia rheumatica. The Lancet. 2013;381(9860):63-72.
296. Schakman O, Gilson H, Kalista S, Thissen JP. Mechanisms of Muscle Atrophy Induced by Glucocorticoids. Hormone Research in Paediatrics. 2009;72(suppl 1)(Suppl. 1):36-41.
297. Dollet L, Kuefner M, Caria E, Rizo-Roca D, Pendergrast L, Abdelmoez AM, et al. Glutamine Regulates Skeletal Muscle Immunometabolism in Type 2 Diabetes. Diabetes. 2022;71(4):624-36.
298. Coqueiro AY, Raizel R, Bonvini A, Hypólito T, Godois AdM, Pereira JRR, et al. Effects of Glutamine and Alanine Supplementation on Central Fatigue Markers in Rats Submitted to Resistance Training. Nutrients. 2018;10(2):119.
299. van Beijnum JR, Rousch M, Castermans K, van der Linden E, Griffioen AW. Isolation of endothelial cells from fresh tissues. Nature Protocols. 2008;3(6):1085-91.
300. Goncharov NV, Popova PI, Avdonin PP, Kudryavtsev IV, Serebryakova MK, Korf EA, et al. Markers of Endothelial Cells in Normal and Pathological Conditions. Biochemistry (Moscow), Supplement Series A: Membrane and Cell Biology. 2020;14(3):167-83.

301. Jackson DG. The Lymphatics Revisited: New Perspectives from the Hyaluronan Receptor LYVE-1. Trends in Cardiovascular Medicine. 2003;13(1):1-7.
302. Salmi M, Jalkanen S. Vascular Adhesion Protein-1: A Cell Surface Amine Oxidase in Translation. Antioxid Redox Signal. 2019;30(3):314-32.
303. Tohka S, Laukkanen M-L, Jalkanen S, Salmi M. Vascular adhesion protein 1 (VAP-1) functions as a molecular brake during granulocyte rolling and mediates recruitment in vivo. The FASEB Journal. 2001;15(2):373-82.
304. Salmi M, Kalimo K, Jalkanen S. Induction and function of vascular adhesion protein-1 at sites of inflammation. Journal of Experimental Medicine. 1993;178(6):2255-60.
305. Weston CJ, Shepherd EL, Claridge LC, Rantakari P, Curbishley SM, Tomlinson JW, et al. Vascular adhesion protein-1 promotes liver inflammation and drives hepatic fibrosis. The Journal of Clinical Investigation. 2015;125(2):501-20.
306. Trivedi PJ, Tickle J, Vesterhus MN, Eddowes PJ, Bruns T, Vainio J, et al. Vascular adhesion protein-1 is elevated in primary sclerosing cholangitis, is predictive of clinical outcome and facilitates recruitment of gut-tropic lymphocytes to liver in a substrate-dependent manner. Gut. 2018;67(6):1135-45.
307. Kong D-H, Kim YK, Kim MR, Jang JH, Lee S. Emerging Roles of Vascular Cell Adhesion Molecule-1 (VCAM-1) in Immunological Disorders and Cancer. International journal of molecular sciences. 2018;19(4):1057.
308. Ley K, Laudanna C, Cybulsky MI, Nourshargh S. Getting to the site of inflammation: the leukocyte adhesion cascade updated. Nature Reviews Immunology. 2007;7(9):678-89.
309. Koch AE, Burrows JC, Haines GK, Carlos TM, Harlan JM, Leibovich SJ. Immunolocalization of endothelial and leukocyte adhesion molecules in human rheumatoid and osteoarthritic synovial tissues. Lab Invest. 1991;64(3):313-20.
310. Weinstein AM, Storkus WJ. Biosynthesis and Functional Significance of Peripheral Node Addressin in Cancer-Associated TLO. Front Immunol. 2016;7(301).
311. Bugatti S, Caporali R, Manzo A, Vitolo B, Pitzalis C, Montecucco C. Involvement of subchondral bone marrow in rheumatoid arthritis: Lymphoid neogenesis and in situ relationship to subchondral bone marrow osteoclast recruitment. Arthritis & Rheumatism. 2005;52(11):3448-59.
312. Vousden KH, Lane DP. p53 in health and disease. Nature Reviews Molecular Cell Biology. 2007;8(4):275-83.
313. Tak PP, Smeets TJ, Boyle DL, Kraan MC, Shi Y, Zhuang S, et al. p53 overexpression in synovial tissue from patients with early and longstanding rheumatoid arthritis compared with patients with reactive arthritis and osteoarthritis. Arthritis Rheum. 1999;42(5):948-53.
314. Robinson J, Whitworth K, Jinks E, Nagy Z, Bicknell R, Lee SP. An evaluation of the tumour endothelial marker CLEC14A as a therapeutic target in solid tumours. The Journal of Pathology: Clinical Research. 2020;6(4):308-19.
315. Khan KA, Naylor AJ, Khan A, Noy PJ, Mambretti M, Lodhia P, et al. Multimerin-2 is a ligand for group 14 family C-type lectins CLEC14A, CD93 and CD248 spanning the endothelial pericyte interface. Oncogene. 2017;36(44):6097-108.
316. Maia M, de Vriese A, Janssens T, Moons M, van Landuyt K, Tavernier J, et al. CD248 and its cytoplasmic domain: a therapeutic target for arthritis. Arthritis Rheum. 2010;62(12):3595-606.
317. Abcam. Direct vs indirect immunofluorescence [Available from: https://www.abcam.com/secondary-antibodies/direct-vs-indirect-immunofluorescence.
318. Al-Kofahi Y, Sevinsky C, Santamaria-Pang A, Ginty F, Sood A, Li Q, editors. Multi-channel algorithm for segmentation of tumor blood vessels using multiplexed image data. 2016 IEEE 13th International Symposium on Biomedical Imaging (ISBI); 2016 13-16 April 2016.
319. Milstone DS, O'Donnell PE, Stavrakis G, Mortensen RM, Davis VM. E-selectin Expression and Stimulation by Inflammatory Mediators are Developmentally Regulated during Embryogenesis. Laboratory Investigation. 2000;80(6):943-54.

320. Lalor PF, Edwards S, McNab G, Salmi M, Jalkanen S, Adams DH. Vascular adhesion protein-1 mediates adhesion and transmigration of lymphocytes on human hepatic endothelial cells. J Immunol. 2002;169(2):983-92.
321. Danielli M, Thomas RC, Quinn LM, Tan BK. Vascular adhesion protein-1 (VAP-1) in vascular inflammatory diseases. Vasa.0(0):null.
322. Marsh L-J, Kemble S, Reis Nisa P, Singh R, Croft AP. Fibroblast pathology in inflammatory joint disease. Immunological Reviews. 2021;302(1):163-83.
323. Dennis G, Holweg CTJ, Kummerfeld SK, Choy DF, Setiadi AF, Hackney JA, et al. Synovial phenotypes in rheumatoid arthritis correlate with response to biologic therapeutics. Arthritis Research & Therapy. 2014;16(2):R90.
324. Elshabrawy HA, Chen Z, Volin MV, Ravella S, Virupannavar S, Shahrara S. The pathogenic role of angiogenesis in rheumatoid arthritis. Angiogenesis. 2015;18(4):433-48.
325. Xiu M, Wang Y, Li B, Wang X, Xiao F, Chen S, et al. The Role of Notch3 Signaling in Cancer Stemness and Chemoresistance: Molecular Mechanisms and Targeting Strategies. Frontiers in Molecular Biosciences. 2021;8.
326. Khan SY, Awad EM, Oszwald A, Mayr M, Yin X, Waltenberger B, et al. Premature senescence of endothelial cells upon chronic exposure to TNFα can be prevented by N-acetyl cysteine and plumericin. Sci Rep. 2017;7:39501.
327. Kandhaya-Pillai R, Miro-Mur F, Alijotas-Reig J, Tchkonia T, Kirkland JL, Schwartz S. TNFα-senescence initiates a STAT-dependent positive feedback loop, leading to a sustained interferon signature, DNA damage, and cytokine secretion. Aging (Albany NY). 2017;9(11):2411-35.
328. Del Rey MJ, Valín Á, Usategui A, Ergueta S, Martín E, Municio C, et al. Senescent synovial fibroblasts accumulate prematurely in rheumatoid arthritis tissues and display an enhanced inflammatory phenotype. Immunity & Ageing. 2019;16(1):29.
329. Rème T, Travaglio A, Gueydon E, Adla L, Jorgensen C, Sany J. Mutations of the p53 tumour suppressor gene in erosive rheumatoid synovial tissue. Clin Exp Immunol. 1998;111(2):353-8.
330. Zhao J, Guo S, Schrodi SJ, He D. Molecular and Cellular Heterogeneity in Rheumatoid Arthritis: Mechanisms and Clinical Implications. Front Immunol. 2021;12:790122.
331. Robinson D. How to interpret a p-value histogram 2014 [Available from: http://varianceexplained.org/statistics/interpreting-pvalue-histogram/.
332. Breheny P, Stromberg A, Lambert J. p-Value Histograms: Inference and Diagnostics. High Throughput. 2018;7(3):23.
333. Wang H, Yuan Z, Wang B, Li B, Lv H, He J, et al. COMP (Cartilage Oligomeric Matrix Protein), a Novel PIEZO1 Regulator That Controls Blood Pressure. Hypertension. 2022;79(3):549-61.
334. Zhao Y, Urbonaviciute V, Xu B, Cai W, Sener Z, Ge C, et al. Cartilage Oligomeric Matrix Protein Induced Arthritis—A New Model for Rheumatoid Arthritis in the C57BL/6 Mouse. Front Immunol. 2021;12.
335. Carlsén S, Hansson AS, Olsson H, Heinegård D, Holmdahl R. Cartilage oligomeric matrix protein (COMP)-induced arthritis in rats. Clin Exp Immunol. 1998;114(3):477-84.
336. Hussein DA, El Bakry SA, Morshedy NA, Ibrahim SE, Sakr HM, Abo-Shady RA. Role of cartilage oligomeric matrix protein (COMP) as a prognostic biomarker in follow-up of early rheumatoid arthritis patients: Correlation to musculoskeletal ultrasonographic findings. The Egyptian Rheumatologist. 2018;40(4):221-6.
337. Cui J, Zhang J. Cartilage Oligomeric Matrix Protein, Diseases, and Therapeutic Opportunities. Int J Mol Sci. 2022;23(16).
338. Wang S, Wang B, Shi Y, Möller T, Stegmeyer RI, Strilic B, et al. Mechanosensation by endothelial PIEZO1 is required for leukocyte diapedesis. Blood. 2022;140(3):171-83.
339. Dyer LA, Pi X, Patterson C. The role of BMPs in endothelial cell function and dysfunction. Trends Endocrinol Metab. 2014;25(9):472-80.

340. Hiepen C, Mendez PL, Knaus P. It Takes Two to Tango: Endothelial TGFβ/BMP Signaling Crosstalk with Mechanobiology. Cells. 2020;9(9).
341. Sanders LN, Schoenhard JA, Saleh MA, Mukherjee A, Ryzhov S, McMaster WG, Jr., et al. BMP Antagonist Gremlin 2 Limits Inflammation After Myocardial Infarction. Circ Res. 2016;119(3):434-49.
342. Ween MP, Oehler MK, Ricciardelli C. Transforming growth Factor-Beta-Induced Protein (TGFBI)/(βig-H3): a matrix protein with dual functions in ovarian cancer. Int J Mol Sci. 2012;13(8):10461-77.
343. Liu M, Iosef C, Rao S, Domingo-Gonzalez R, Fu S, Snider P, et al. Transforming Growth Factor-induced Protein Promotes NF-κB-mediated Angiogenesis during Postnatal Lung Development. Am J Respir Cell Mol Biol. 2021;64(3):318-30.
344. Bayliss MT, Howat SLT, Dudhia J, Murphy JM, Barry FP, Edwards JCW, et al. Up-regulation and differential expression of the hyaluronan-binding protein TSG-6 in cartilage and synovium in rheumatoid arthritis and osteoarthritis. Osteoarthritis and Cartilage. 2001;9(1):42-8.
345. Osorio D, Cai JJ. Systematic determination of the mitochondrial proportion in human and mice tissues for single-cell RNA-sequencing data quality control. Bioinformatics. 2020;37(7):963-7.
346. Taanman J-W. The mitochondrial genome: structure, transcription, translation and replication. Biochimica et Biophysica Acta (BBA) - Bioenergetics. 1999;1410(2):103-23.
347. Clayton SA, MacDonald L, Kurowska-Stolarska M, Clark AR. Mitochondria as Key Players in the Pathogenesis and Treatment of Rheumatoid Arthritis. Front Immunol. 2021;12:673916.
348. Perez MJJ. Functional and transcriptional characterisation of synovial fibroblasts in early inflammatory arthritis and established rheumatoid arthritis [PhD]. University of Birmingham: University of Birmingham; 2014.
349. Neumann E, Riepl B, Knedla A, Lefèvre S, Tarner IH, Grifka J, et al. Cell culture and passaging alters gene expression pattern and proliferation rate in rheumatoid arthritis synovial fibroblasts. Arthritis Research & Therapy. 2010;12(3):R83.
350. Zimmermann T, Kunisch E, Pfeiffer R, Hirth A, Stahl H-D, Sack U, et al. Isolation and characterization of rheumatoid arthritis synovial fibroblasts from primary culture — primary culture cells markedly differ from fourth-passage cells. Arthritis Research & Therapy. 2000;3(1):72.
351. Carr H. Transcriptional and histological characterisation of the synovium in early inflammatory arthritis [PhD]. University of Birmingham: University of Birmingham; 2022.
352. Elias M, Zhao S, Le HT, Wang J, Neurath MF, Neufert C, et al. IL-36 in chronic inflammation and fibrosis - bridging the gap? J Clin Invest. 2021;131(2).
353. Boutet MA, Bart G, Penhoat M, Amiaud J, Brulin B, Charrier C, et al. Distinct expression of interleukin (IL)-36α, β and γ, their antagonist IL-36Ra and IL-38 in psoriasis, rheumatoid arthritis and Crohn's disease. Clin Exp Immunol. 2016;184(2):159-73.
354. Yoshida Y, Tanaka T. Interleukin 6 and rheumatoid arthritis. Biomed Res Int. 2014;2014:698313.
355. Falconer J, Murphy AN, Young SP, Clark AR, Tiziani S, Guma M, et al. Review: Synovial Cell Metabolism and Chronic Inflammation in Rheumatoid Arthritis. Arthritis Rheumatol. 2018;70(7):984-99.
356. Falconer J, Pucino V, Clayton SA, Marshall JL, Raizada S, Adams H, et al. Spontaneously Resolving Joint Inflammation Is Characterised by Metabolic Agility of Fibroblast-Like Synoviocytes. Front Immunol. 2021;12.
357. Chang HY, Chi J-T, Dudoit S, Bondre C, Rijn Mvd, Botstein D, et al. Diversity, topographic differentiation, and positional memory in human fibroblasts. Proceedings of the National Academy of Sciences. 2002;99(20):12877-82.
358. Jin X, Kruth HS. Culture of Macrophage Colony-stimulating Factor Differentiated Human Monocyte-derived Macrophages. J Vis Exp. 2016(112).

359. Shekhani MT, Forde TS, Adilbayeva A, Ramez M, Myngbay A, Bexeitov Y, et al. Collagen triple helix repeat containing 1 is a new promigratory marker of arthritic pannus. Arthritis Res Ther. 2016;18:171.
360. Hatzikotoulas K, Roposch A, Wainwright A, Theologis T, Clarke NMP, Dwyer JSM, et al. Genome-wide association study of developmental dysplasia of the hip identifies an association with GDF5. Communications Biology. 2018;1(1):56.
361. Erlandsson MC, Töyrä Silfverswärd S, Nadali M, Turkkila M, Svensson MND, Jonsson I-M, et al. IGF-1R signalling contributes to IL-6 production and T cell dependent inflammation in rheumatoid arthritis. Biochimica et Biophysica Acta (BBA) - Molecular Basis of Disease. 2017;1863(9):2158-70.
362. Wilkinson JM, Zeggini E. The Genetic Epidemiology of Joint Shape and the Development of Osteoarthritis. Calcif Tissue Int. 2021;109(3):257-76.
363. Feng R, Lu M, Liu L, Xu K, Xu P. Transcriptome-Wide Association Studies and Integration Analysis of mRNA Expression Profiles Identify Candidate Genes and Pathways Associated With Ankylosing Spondylitis. Front Immunol. 2022;13:814303.
364. Heidari B. Rheumatoid Arthritis: Early diagnosis and treatment outcomes. Caspian J Intern Med. 2011;2(1):161-70.
365. Egusquiaguirre SP, Yeh JE, Walker SR, Liu S, Frank DA. The STAT3 Target Gene TNFRSF1A Modulates the NF-κB Pathway in Breast Cancer Cells. Neoplasia. 2018;20(5):489-98.
366. Parameswaran N, Patial S. Tumor necrosis factor-α signaling in macrophages. Crit Rev Eukaryot Gene Expr. 2010;20(2):87-103.
367. Dieudé P, Goossens M, Cornélis F, Michou L, Bardin T, Tchernitchko DO. The TNFRSF1A R92Q mutation is frequent in rheumatoid arthritis but shows no evidence for association or linkage with the disease. Ann Rheum Dis. 2007;66(8):1113-5.
368. Gordon RA, Grigoriev G, Lee A, Kalliolias GD, Ivashkiv LB. The interferon signature and STAT1 expression in rheumatoid arthritis synovial fluid macrophages are induced by tumor necrosis factor α and counter-regulated by the synovial fluid microenvironment. Arthritis Rheum. 2012;64(10):3119-28.
369. Platanias LC. Mechanisms of type-I- and type-II-interferon-mediated signalling. Nature Reviews Immunology. 2005;5(5):375-86.
370. Liu P, Zhang X, Li Z, Wei L, Peng Q, Liu C, et al. A significant role of transcription factors E2F in inflammation and tumorigenesis of nasopharyngeal carcinoma. Biochemical and Biophysical Research Communications. 2020;524(4):816-24.
371. Saeki N, Inoue K, Ideta-Otsuka M, Watamori K, Mizuki S, Takenaka K, et al. Epigenetic regulator UHRF1 orchestrates proinflammatory gene expression in rheumatoid arthritis in a suppressive manner. The Journal of Clinical Investigation. 2022;132(11).
372. Song JQ, Jiang LY, Fu CP, Wu X, Liu ZL, Xie L, et al. Heterozygous SOD2 deletion deteriorated chronic intermittent hypoxia-induced lung inflammation and vascular remodeling through mtROS-NLRP3 signaling pathway. Acta Pharmacol Sin. 2020;41(9):1197-207.
373. Ganini D, Santos JH, Bonini MG, Mason RP. Switch of Mitochondrial Superoxide Dismutase into a Prooxidant Peroxidase in Manganese-Deficient Cells and Mice. Cell Chemical Biology. 2018;25(4):413-25.e6.
374. Condon ND, Stow JL, Wall AA. Automated Analysis of Cell Surface Ruffling: Ruffle Quantification Macro. Bio Protoc. 2020;10(2):e3494.
375. Umar S, Palasiewicz K, Volin MV, Zanotti B, Al-Awqati M, Sweiss N, et al. IRAK4 inhibitor mitigates joint inflammation by rebalancing metabolism malfunction in RA macrophages and fibroblasts. Life Sciences. 2021;287:120114.
376. Chen MS, Lo YH, Chen X, Williams CS, Donnelly JM, Criss ZK, 2nd, et al. Growth Factor-Independent 1 Is a Tumor Suppressor Gene in Colorectal Cancer. Mol Cancer Res. 2019;17(3):697-708.

377. Möröy T, Khandanpour C. Role of GFI1 in Epigenetic Regulation of MDS and AML Pathogenesis: Mechanisms and Therapeutic Implications. Frontiers in Oncology. 2019;9.
378. Fang Q, Li T, Chen P, Wu Y, Wang T, Mo L, et al. Comparative Analysis on Abnormal Methylome of Differentially Expressed Genes and Disease Pathways in the Immune Cells of RA and SLE. Front Immunol. 2021;12.
379. Hamarsheh Sa, Groß O, Brummer T, Zeiser R. Immune modulatory effects of oncogenic KRAS in cancer. Nature Communications. 2020;11(1):5439.
380. Xing W, Xiao Y, Lu X, Zhu H, He X, Huang W, et al. GFI1 downregulation promotes inflammation-linked metastasis of colorectal cancer. Cell Death & Differentiation. 2017;24(5):929-43.
381. Pilz A, Ramsauer K, Heidari H, Leitges M, Kovarik P, Decker T. Phosphorylation of the Stat1 transactivating domain is required for the response to type I interferons. EMBO Rep. 2003;4(4):368-73.
382. Kim GD, Das R, Rao X, Zhong J, Deiuliis JA, Ramirez-Bergeron DL, et al. CITED2 Restrains Proinflammatory Macrophage Activation and Response. Mol Cell Biol. 2018;38(5).
383. Yang T, Poenisch M, Khanal R, Hu Q, Dai Z, Li R, et al. Therapeutic HNF4A mRNA attenuates liver fibrosis in a preclinical model. Journal of Hepatology. 2021;75(6):1420-33.
384. Yuk JM, Kim TS, Kim SY, Lee HM, Han J, Dufour CR, et al. Orphan Nuclear Receptor ERRα Controls Macrophage Metabolic Signaling and A20 Expression to Negatively Regulate TLR-Induced Inflammation. Immunity. 2015;43(1):80-91.
385. Liu B, Huang J, Ashraf A, Rahaman O, Lou J, Wang L, et al. The RNase MCPIP3 promotes skin inflammation by orchestrating myeloid cytokine response. Nature Communications. 2021;12(1):4105.
386. Través PG, Pardo V, Pimentel-Santillana M, González-Rodríguez Á, Mojena M, Rico D, et al. Pivotal role of protein tyrosine phosphatase 1B (PTP1B) in the macrophage response to pro-inflammatory and anti-inflammatory challenge. Cell Death Dis. 2014;5(3):e1125.
387. Xu D, Matsumoto ML, McKenzie BS, Zarrin AA. TPL2 kinase action and control of inflammation. Pharmacological Research. 2018;129:188-93.
388. Mielke LA, Elkins KL, Wei L, Starr R, Tsichlis PN, O'Shea JJ, et al. Tumor Progression Locus 2 (Map3k8) Is Critical for Host Defense against Listeria monocytogenes and IL-1β Production. The Journal of Immunology. 2009;183(12):7984-93.
389. Cypher LR, Bielecki TA, Adepegba O, Huang L, An W, Iseka F, et al. CSF-1 receptor signalling is governed by pre-requisite EHD1 mediated receptor display on the macrophage cell surface. Cell Signal. 2016;28(9):1325-35.
390. Sehgal A, Donaldson DS, Pridans C, Sauter KA, Hume DA, Mabbott NA. The role of CSF1R-dependent macrophages in control of the intestinal stem-cell niche. Nature Communications. 2018;9(1):1272.
391. Zhou X, Franklin RA, Adler M, Carter TS, Condiff E, Adams TS, et al. Microenvironmental Sensing by Fibroblasts Controls Macrophage Population Size. bioRxiv. 2022:2022.01.18.476683.
392. Matsumoto M, Liu J, Iwata K, Ibi M, Asaoka N, Zhang X, et al. NOX1/NADPH oxidase is involved in the LPS-induced exacerbation of collagen-induced arthritis. Journal of Pharmacological Sciences. 2021;146(2):88-97.
393. Celik H, Koh WK, Kramer AC, Ostrander EL, Mallaney C, Fisher DAC, et al. JARID2 Functions as a Tumor Suppressor in Myeloid Neoplasms by Repressing Self-Renewal in Hematopoietic Progenitor Cells. Cancer Cell. 2018;34(5):741-56.e8.
394. Pohlers D, Beyer A, Koczan D, Wilhelm T, Thiesen H-J, Kinne RW. Constitutive upregulation of the transforming growth factor-β pathway in rheumatoid arthritis synovial fibroblasts. Arthritis Research & Therapy. 2007;9(3):R59.
395. Zhu D, Zhao J, Lou A, Huang Q, OuYang Q, Zhu J, et al. Transforming growth factor β1 promotes fibroblast-like synoviocytes migration and invasion via TGF-β1/Smad signaling in rheumatoid arthritis. Molecular and Cellular Biochemistry. 2019;459(1):141-50.

396. Wang S, Wang S, Li H, Zhu L, Wang Y. Inhibition of the TGF-β/Smads signaling pathway attenuates pulmonary fibrosis and induces anti-proliferative effect on synovial fibroblasts in rheumatoid arthritis. Int J Clin Exp Pathol. 2019;12(5):1835-45.
397. Tecalco-Cruz AC, Sosa-Garrocho M, Vázquez-Victorio G, Ortiz-García L, Domínguez-Hüttinger E, Macías-Silva M. Transforming Growth Factor-β/SMAD Target Gene SKIL Is Negatively Regulated by the Transcriptional Cofactor Complex SNON-SMAD4*. Journal of Biological Chemistry. 2012;287(32):26764-76.
398. Murphy-Ullrich JE, Suto MJ. Thrombospondin-1 regulation of latent TGF-β activation: A therapeutic target for fibrotic disease. Matrix Biol. 2018;68-69:28-43.
399. Dharmapatni AA, Smith MD, Findlay DM, Holding CA, Evdokiou A, Ahern MJ, et al. Elevated expression of caspase-3 inhibitors, survivin and xIAP correlates with low levels of apoptosis in active rheumatoid synovium. Arthritis Research & Therapy. 2009;11(1):R13.
400. Wang Y, Zhang K, Yuan X, Xu N, Zhao S, Hou L, et al. miR-431-5p regulates cell proliferation and apoptosis in fibroblast-like synoviocytes in rheumatoid arthritis by targeting XIAP. Arthritis Res Ther. 2020;22(1):231.
401. Van Themsche C, Chaudhry P, Leblanc V, Parent S, Asselin E. XIAP gene expression and function is regulated by autocrine and paracrine TGF-beta signaling. Mol Cancer. 2010;9:216.
402. Lee Y-R, Chen M, Pandolfi PP. The functions and regulation of the PTEN tumour suppressor: new modes and prospects. Nature Reviews Molecular Cell Biology. 2018;19(9):547-62.
403. Pap T, Franz JK, Hummel KM, Jeisy E, Gay R, Gay S. Activation of synovial fibroblasts in rheumatoid arthritis: lack of Expression of the tumour suppressor PTEN at sites of invasive growth and destruction. Arthritis Res. 2000;2(1):59-64.
404. Sweeney SE, Corr M, Kimbler TB. Role of interferon regulatory factor 7 in serum-transfer arthritis: regulation of interferon-β production. Arthritis Rheum. 2012;64(4):1046-56.
405. Orecchioni M, Ghosheh Y, Pramod AB, Ley K. Macrophage Polarization: Different Gene Signatures in M1(LPS+) vs. Classically and M2(LPS–) vs. Alternatively Activated Macrophages. Front Immunol. 2019;10.
406. Frank-Bertoncelj M, Trenkmann M, Klein K, Karouzakis E, Rehrauer H, Bratus A, et al. Epigenetically-driven anatomical diversity of synovial fibroblasts guides joint-specific fibroblast functions. Nat Commun. 2017;8:14852.
407. Hur B, Gupta VK, Huang H, Wright KA, Warrington KJ, Taneja V, et al. Plasma metabolomic profiling in patients with rheumatoid arthritis identifies biochemical features predictive of quantitative disease activity. Arthritis Research & Therapy. 2021;23(1):164.
408. Li J, Che N, Xu L, Zhang Q, Wang Q, Tan W, et al. LC-MS-based serum metabolomics reveals a distinctive signature in patients with rheumatoid arthritis. Clin Rheumatol. 2018;37(6):1493-502.
409. Cuppen BVJ, Fu J, van Wietmarschen HA, Harms AC, Koval S, Marijnissen ACA, et al. Exploring the Inflammatory Metabolomic Profile to Predict Response to TNF-α Inhibitors in Rheumatoid Arthritis. PLOS ONE. 2016;11(9):e0163087.
410. Teitsma XM, Yang W, Jacobs JWG, Pethö-Schramm A, Borm MEA, Harms AC, et al. Baseline metabolic profiles of early rheumatoid arthritis patients achieving sustained drug-free remission after initiating treat-to-target tocilizumab, methotrexate, or the combination: insights from systems biology. Arthritis Res Ther. 2018;20(1):230.
411. Hambardzumyan K, Bolce RJ, Wallman JK, van Vollenhoven RF, Saevarsdottir S. Serum Biomarkers for Prediction of Response to Methotrexate Monotherapy in Early Rheumatoid Arthritis: Results from the SWEFOT Trial. J Rheumatol. 2019;46(6):555-63.
412. Tasaki S, Suzuki K, Kassai Y, Takeshita M, Murota A, Kondo Y, et al. Multi-omics monitoring of drug response in rheumatoid arthritis in pursuit of molecular remission. Nature Communications. 2018;9(1):2755.

413. Kapoor SR, Filer A, Fitzpatrick MA, Fisher BA, Taylor PC, Buckley CD, et al. Metabolic profiling predicts response to anti-tumor necrosis factor alpha therapy in patients with rheumatoid arthritis. Arthritis Rheum. 2013;65(6):1448-56.
414. Timmermans S, Souffriau J, Libert C. A General Introduction to Glucocorticoid Biology. Front Immunol. 2019;10:1545.
415. Korte SM, Straub RH. Fatigue in inflammatory rheumatic disorders: pathophysiological mechanisms. Rheumatology. 2019;58(Supplement_5):v35-v50.
416. Croker BA, Kiu H, Nicholson SE. SOCS regulation of the JAK/STAT signalling pathway. Semin Cell Dev Biol. 2008;19(4):414-22.

9 Appendix

Appendix Table 1: Patient characteristics of final patients used in CellDIVE analysis

	Outcome	Joint	CCP+/-	RHF +/-	Age	Sex	Disease duration (wks)	DAS28	ESR (mm/hr)	CRP (mg/L)	Global VAS	SJC28	TJC28	US PD worst	US GS worst	NSAID	Medication
BX064	Res	Knee	-	-	35	M	1	1.6	2	9	6	3	1	2	1	N	
BX178	Res	Ankle	-	-	37	M	13	3.2	37	18	45	0	0	1	0	N	
BX202	Res	Knee	-	-	55	F	11	4.3	14	4	69	3	3	2	1	N	
BX290	Res	Knee	+	-	60	m	1	3.1	22	21	7	1	1	1	0	N	
BX115	VeRA	knee	+	+	51	M	8	6.7	61	97	75	10	11	2	3	N	
BX194	VeRA	Knee	-	-	76	F	6	7.0	39	39	50	20	19	1	0	Y	
BX248	VeRA	Wrist	-	+	59	F	3	5.2	10	36	49	11	12	3	3	N	
JRP118	Jrep	L Knee	-	NA	66	M	1040	-	3	2	-	-	-	-	-	Y	MTX
JRP122	Jrep	R Knee	NA	NA	60	M	Unknown	-	NA	1	-	-	-	-	-	N	MTX, salazopyrine, Golimumab/simponi and pred when needed
JRP130	Jrep	R Knee	-	NA	67	F	728	-	NA	NA	-	-	-	-	-	N	MTX, SSA/salazopyrine
JRP132	Jrep	R Knee	+	NA	68	F	1560	-	NA	4	-	-	-	-	-	Y	NA
JRP136	Jrep	L Elbow	-	NA	56	F	1872	-	34	NA	-	-	-	-	-	N	Prednisolone
JRP139	Jrep	L Knee	-	-	67	M	364	-	18	20	-	-	-	-	-	N	Pred, Tocilizumab(stopped 2 wk prior to surgery)
JRP099	Jrep	L Knee	+	+	31	F	1092	-	11	10	-	-	-	-	-	N	Pred and Naproxen

DAS28 = Disease Activity Score 28; CCP = cyclic citrullinated peptide, CRP = C-reactive protein; DMARD = Disease modifying anti-rheumatic drug; ESR = erythrocyte sedimentation rate; JRep = joint replacement; MTX = Methotrexate; NSAID = Non-steroidal anti-inflammatory; Pred = prednisolone; RF = Rheumatoid factor; SSA = Sulfasalazine; SJC28 = 28 swollen joint counts; TJC28 = 28 tender joint counts; US GS = ultrasound greyscale grade at the biopsied joint; US PD = ultrasound power Doppler grade at the biopsied joint; VAS = visual analogue score; VeRA = Very early rheumatoid arthritis.

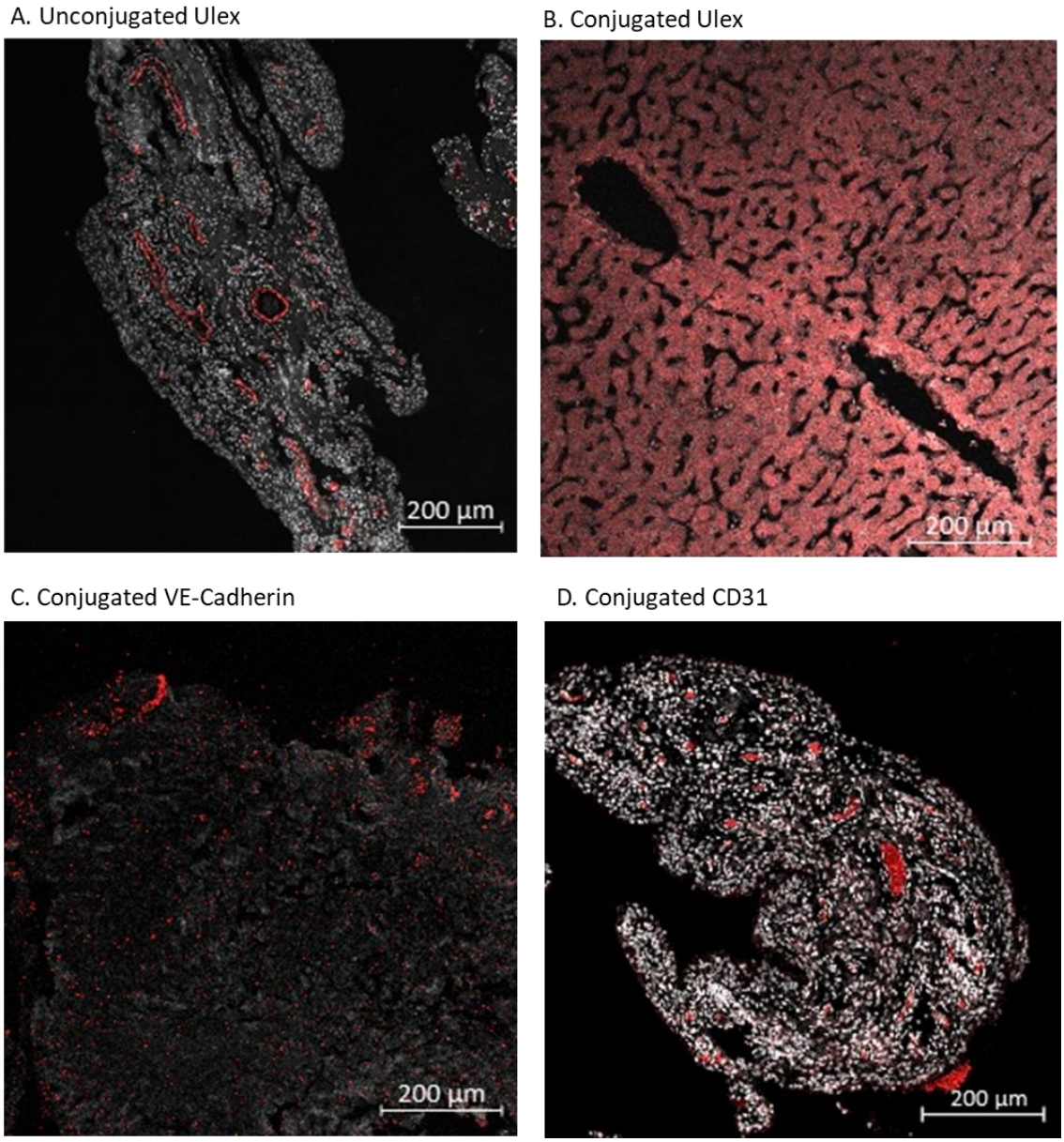

Appendix Figure 1: Markers not used from endothelium antibody validation. Formalin fixed paraffin embedded (FFPE) sections were used from were used from RA joint replacement synovial tissue Sections were deparaffinised, rehydrated and antigen retrieval was performed. Sections were then stained with antibody against **(A)** Ulex, **(B)** AF555 conjugated Ulex, **(C)** AF647 conjugated VE-Cadherin and **(D)** AF488 conjugated CD31.

Appendix Table 2: Patient characteristics of fibroblast donors from the fibroblast-endothelial cell co-cultures used for RNA-sequencing

ID	Group	Site	Age	Sex	CCP +/-	RHF +/-	Disease Duration (wks)	DAS28 Baseline	ESR (mm /hr)	CRP (mg/L)	Global VAS	SJC28	TJC28	US PD worst	US GS worst	NSAID (Y/N)	DMARD
RA02	JRep	Knee	52	F	NA	+	1040	4.4	70	46	16	2	2	NA	NA	N	MTX
RA05	JRep	Knee	62	F	NA	+	1040	6.8	63	62	95	11	9	NA	NA	N	NA
RA06	JRep	Knee	60	M	NA	+	1560	6.4	54	75	65	9	11	NA	NA	Y	SSA
RA28	JRep	Knee	41	F	NA	-	1040	3.3	20	26	64	1	0	NA	NA	N	Gold
RA25	JRep	Knee	53	F	NA	+	1560	NA	NA	NA	65	8	11	NA	NA	N	HCQ + Pred 10mg
RA29	JRep	Knee	67	F	+	+	364	6.6	57	66	75	13	9	NA	NA	N	ETANERCEPT + MTX + Pred 7.5mg
RA23	JRep	Knee	58	F	NA	+	572	6.7	23	32	97	17	13	NA	NA	N	MTX
RA17	JRep	Knee	77	M	NA	+	1144	4.0	16	9	25	7	3	NA	NA	Y	SSA + MTX
BX072	Res	Knee	32	M	-	-	10	3.6	15	0	36	1	3	0	1	N	
BX064	Res	Knee	35	M	-	-	1	1.6	2	9	6	3	1	1	2	N	
BX028	Res	Knee	74	M	-	-	5	4.8	45	13	55	23	0	0	1	Y	
BX076	Res	Knee	28	M	-	-	6	4.5	18	8	99	1	2	1	2	Y	
BX038	Res	Knee	45	F	-	-	1	4.0	4	0	83	5	5	1	1	N	
BX071	Res	Ankle	41	F	-	-	4	1.7	5	9	10	2	0	0	2	Y	
BX087	Res	Ankle	27	M	-	-	4	3.8	37	28	3	2	2	0	1	Y	
BX054	Res	Ankle	55	M	-	-	6	3.5	2	6	91	5	4	1	2	Y	
BX003	VeRA	Knee	50	M	+	+	4	5.7	31	26	28	11	13	1	3	N	
BX013	VeRA	Knee	45	F	-	-	10	3.8	24	12	12	3	3	0	2	Y	
BX042	VeRA	Knee	55	M	+	-	4	3.5	58	45	9	4	0	0	2	N	
BX084	VeRA	MCP	49	M	+	+	6	6.8	25	18	87	12	17	3	3	Y	
BX121	VeRA	Ankle	60	F	+	+	11	4.3	32	45	46	1	3	2	2	N	
BX092	VeRA	MCP	48	M	+	+	4	6.0	63	38	51	9	8	2	3	Y	
BX063	VeRA	Knee	74	F	+	-	9	4.4	20	32	62	3	3	2	3	N	
BX116	VeRA	Knee	63	M	-	-	8	2.3	2	0	70	1	1	2	3	Y	

DAS28 = Disease Activity Score 28; CCP = cyclic citrullinated peptide, CRP = C-reactive protein; DMARD = Disease modifying anti-rheumatic drug; ESR = erythrocyte sedimentation rate; HCQ = Hydroxychloroquine; JRep = joint replacement; MTX = Methotrexate; NSAID = Non-steroidal anti-inflammatory; Pred = prednisolone; RF = Rheumatoid factor; SSA = Sulfasalazine; SJC28 = 28 swollen joint counts; TJC28 = 28 tender joint counts; US GS = ultrasound greyscale grade at the biopsied joint; US PD = ultrasound power Doppler grade at the biopsied joint; VAS = visual analogue score; VeRA = Very early rheumatoid arthritis.

Appendix Table 3: Quality control of RNA form fibroblast: EC co-cultures

Sample #	Sample name	260/280	260/230	RIN	Concentration (ng/ul)
1	EC2015_RA02_Fib_JRep	1.97	0.83	9.9	44.74
2	EC2015_BX072_Fib_Res	2.08	1.09	9.7	277.18
3	EC2015_BX003_Fib_VeRA	2.06	1.85	9.5	152.34
4	EC2015_RA02_EC_Jrep	1.98	1.56	9.7	60.50
5	EC2015_BX072_EC_Res	2.00	1.59	9.8	76.24
6	EC2015_BX003_EC_VeRA	2.06	1.15	9.6	69.56
7	RA02_mono_Fib_JRep	1.46	2.05	9.5	59.25
8	BX072_mono_Fib_Res	1.88	2.09	9.6	111.28
9	BX003_mono_Fib_VerRA	1.42	2.08	9.4	201.05
10	EC2015_mono_EC_	0.78	2.05	9.4	47.22
11	EC2016_mono_EC_	2.06	0.35	10	47.97
12	EC2016_BX064_EC_Res	2.01	0.81	9.9	156.76
13	EC2016_BX064_Fib_Res	2.04	1.17	9.6	30.44
14	EC2016_BX013_EC_VeRA	2.08	1.85	9.7	187.56
15	EC2016_BX013_Fib_VeRA	2.05	1.75	9.5	135.78
16	EC2016_RA06_EC_Jrep	Missing sample			
17	EC2016_RA06_Fib_JRep	2.10	0.18	9.5	55.80
18	BX064_mono_Fib_Res	2.06	0.69	9.5	73.27
19	BX013_mono_Fib_VerRA	2.10	0.12	9.8	18.78
20	RA06_mono_Fib_JRep	2.05	1.20	9.3	11.16
21	EC0221_mono_EC_	2.05	1.88	9.8	77.08
22	EC0221_BX028_EC_Res	2.04	1.00	9.8	68.12
23	EC0221_BX028_Fib_Res	2.08	1.85	9.7	141.66
24	EC0221_BX042_EC_VeRA	2.05	0.98	9.9	64.96
25	EC0221_BX042_Fib_VeRA	2.09	0.85	9.3	183.37
26	EC0221_RA05_EC_Jrep	2.04	1.32	9.8	58.71
27	EC0221_RA05_Fib_JRep	2.05	1.35	9.9	119.71
28	BX028_mono_Fib_Res	2.08	1.91	9.6	224.56
29	BX042_mono_Fib_VerRA	2.08	1.85	9.3	273.39
30	RA05_mono_Fib_JRep	2.08	1.99	9.6	63.33
31	EC0223_mono_EC_	2.06	1.02	9.9	68.87
32	EC0223_BX076_EC_Res	2.09	0.58	9.9	111.70
33	EC0223_BX076_Fib_Res	2.04	0.68	9.5	34.71
34	EC0223_BX084_EC_VeRA	2.09	0.52	9.3	99.56
35	EC0223_BX084_Fib_VeRA	2.08	1.62	9.5	553.38
36	EC0223_RA28_EC_Jrep	1.86	0.08	10	3.54
37	EC0223_RA28_Fib_JRep	2.07	1.41	9.5	97.57
38	BX076_mono_Fib_Res	2.05	0.17	10	11.21
39	BX084_mono_Fib_VerRA	2.11	2.11	9.3	668.78
40	RA28_mono_Fib_JRep	2.06	1.37	10	54.78
41	EC0229_mono_EC_	2.08	1.86	9.8	64.55
42	EC0229_BX038_EC_Res	2.06	1.42	9.7	75.46
43	EC0229_BX038_Fib_Res	2.09	1.45	9.6	108.54
44	EC0229_BX121_EC_VeRA	2.09	0.41	10	125.10
45	EC0229_BX121_Fib_VeRA	2.11	0.46	9.6	116.90

46	EC0229_RA25_EC_Jrep	2.06	1.71	9.6	118.70
47	EC0229_RA25_Fib_JRep	2.11	0.28	9.7	123.21
48	BX038_mono_Fib_Res	2.13	0.15	9.7	51.54
49	BX121_mono_Fib_VerRA	2.07	0.47	9.6	83.60
50	RA25_mono_Fib_JRep	2.10	0.68	9.4	252.91
51	EC0242_mono_EC_	2.07	1.37	9.8	155.30
52	EC0242_BX071_EC_Res	2.01	1.07	9.6	30.09
53	EC0242_BX071_Fib_Res	2.09	1.29	9.3	232.79
54	EC0242_BX092_EC_VeRA	2.03	0.68	9.7	64.57
55	EC0242_BX092_Fib_VeRA	2.02	2.87	9.6	78.04
56	EC0242_RA29_EC_Jrep	2.00	1.40	9.7	73.25
57	EC0242_RA29_Fib_JRep	2.04	0.90	9.4	76.35
58	BX071_mono_Fib_Res	2.05	0.75	9.4	97.89
59	BX092_mono_Fib_VerRA	2.10	0.44	9.4	128.87
60	RA29_mono_Fib_JRep	2.03	0.37	9.2	33.66
61	EC0270_mono_EC_	2.04	1.48	9.8	54.35
62	EC0270_BX087_EC_Res	2.08	1.41	9.9	105.08
63	EC0270_BX087_Fib_Res	2.05	1.60	9.6	80.74
64	EC0270_BX063_EC_VeRA	2.03	1.67	8.9	38.81
65	EC0270_BX063_Fib_VeRA	2.06	1.16	9.9	50.71
66	EC0270_RA23_EC_Jrep	2.08	0.33	10	55.31
67	EC0270_RA23_Fib_JRep	2.07	1.79	9.5	65.30
68	BX087_mono_Fib_Res	2.08	1.73	10	108.68
69	BX063_mono_Fib_VerRA	2.07	1.02	10	93.68
70	RA23_mono_Fib_JRep	2.03	1.88	10	50.95
71	EC0271_mono_EC_	2.12	0.28	9.6	80.2
72	EC0271_BX054_EC_Res	2.00	1.61	9.8	59.6
73	EC0271_BX054_Fib_Res	2.03	1.18	9.5	45.8
74	EC0271_BX116_EC_VeRA	2.06	0.56	9.9	46
75	EC0271_BX116_Fib_VeRA	1.98	0.27	9.8	18.2
76	EC0271_RA17_EC_Jrep	1.99	1.64	9.7	44.8
77	EC0271_RA17_Fib_JRep	1.90	0.71	9.2	18.9
78	BX054_mono_Fib_Res	2.09	0.22	9.2	36.2
79	BX116_mono_Fib_VerRA	1.09	0.26	9.4	30.2
80	RA17_mono_Fib_JRep	1.99	0.68	9.5	17.6

EC = endothelial cell, JRep = joint replacement, Fib = fibroblast, VeRA = very early rheumatoid arthritis.

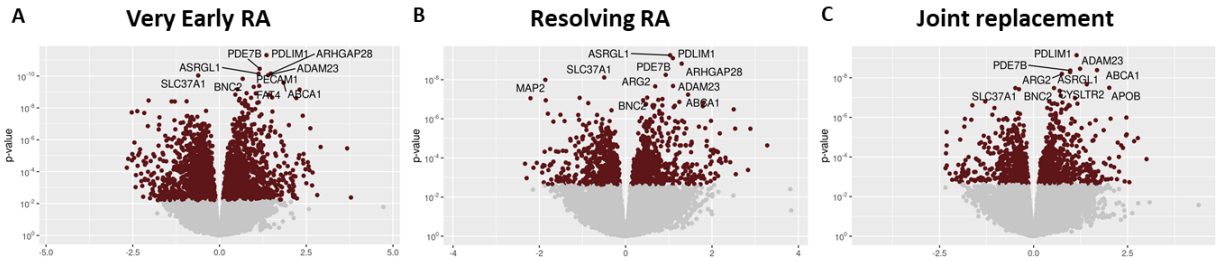

Appendix Figure 2: Volcano plots of differentially expressed genes between mono-cultured and co-cultured endothelial cells. RNA sequencing was performed on co-cultured endothelial cells and fibroblasts (and mono-cultured controls) treated with TNF-α+IFNγ for 24 hours. Analysis was carried out by Novartis. Volcano plots of differentially expressed genes between mono-cultured endothelial cells and those co-cultured with fibroblasts from patients with **(A)** Resolving arthritis, **(B)** Very early rheumatoid arthritis and **(C)** rheumatoid arthritis undergoing joint replacement.

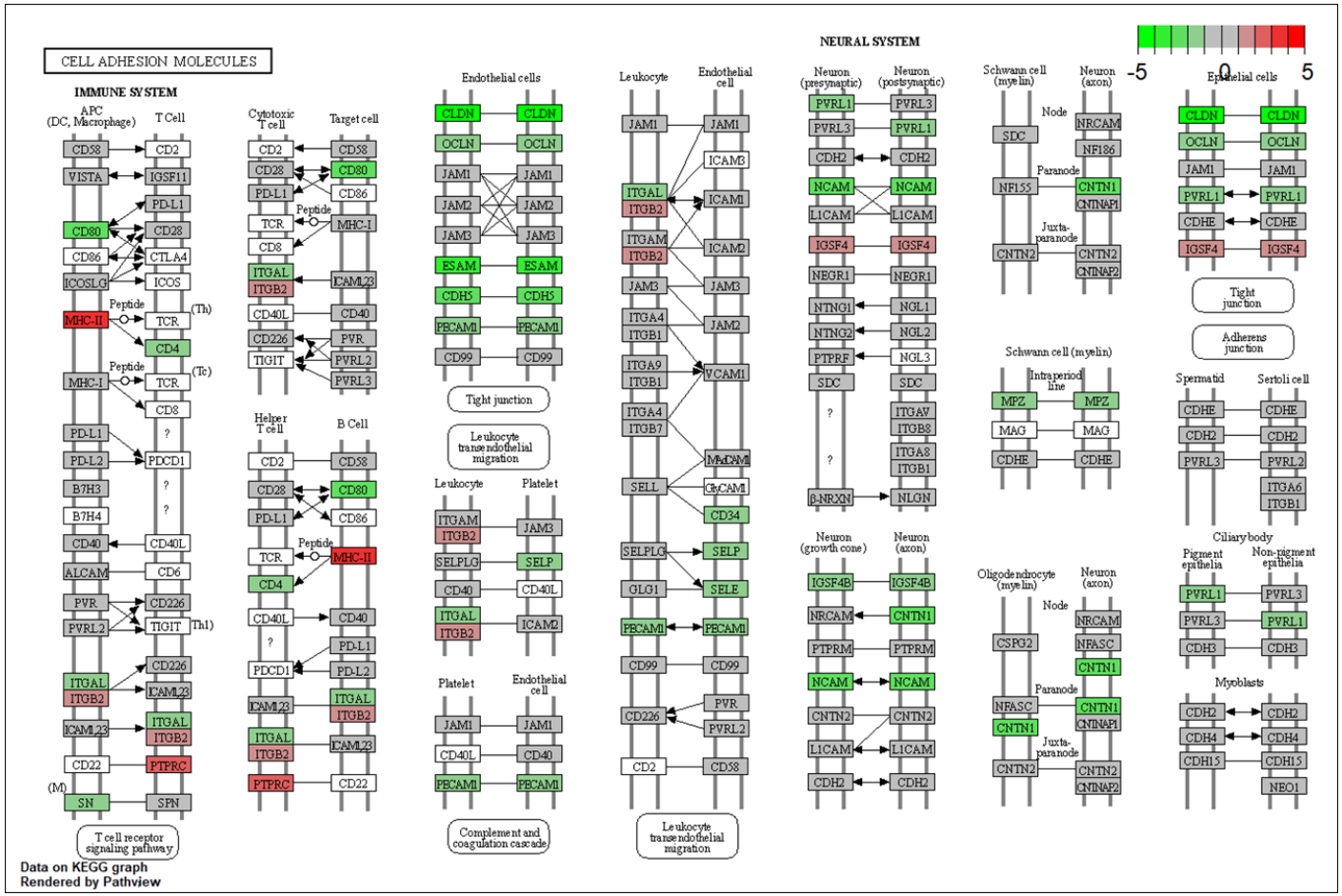

Appendix Figure 3: Genes involved in the KEGG pathway of cell adhesion molecules from differential gene expression analysis of JRep vs Res fibroblasts. Bulk RNA sequencing was performed on RNA isolated from fibroblasts from patients with resolving arthritis (Res), very early rheumatoid arthritis (VeRA) and RA patients undergoing joint replacement (JRep) in co-culture with endothelial cells (ECs) and treated with TNF-α+IFNγ for 24 hours. Sex genes were removed from the analysis and the gene counts were subject to differential gene expression analysis in DESeq2. The significantly (Padj < 0.1) differentially expressed genes of JRep vs Res, were put through KEGG pathway enrichment analysis and the cell adhesion pathway deemed significant. Genes up (green) and down (red) -regulated in in this pathway in JRep vs Res are shown.

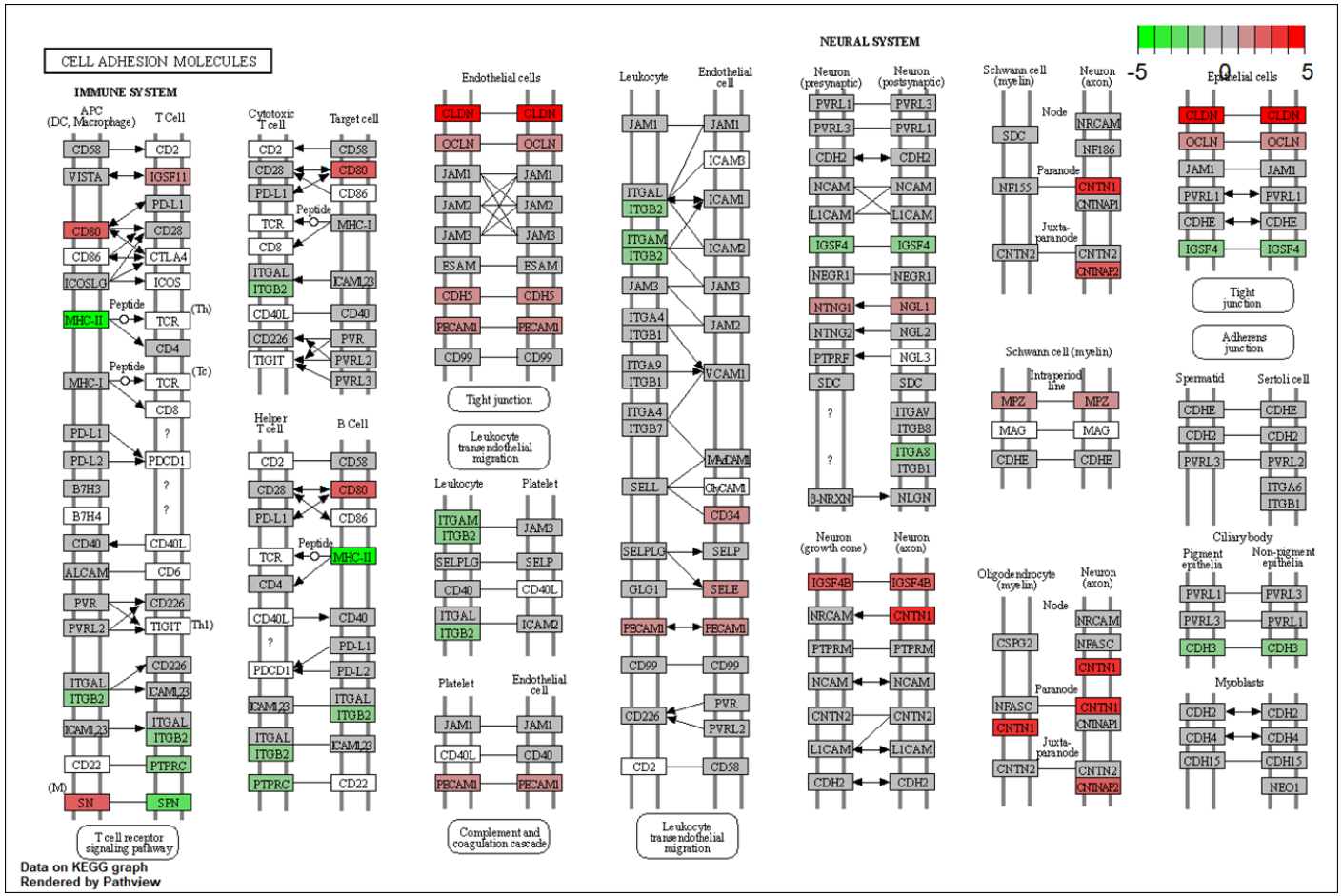

Appendix Figure 4: Genes involved in the KEGG pathway of cell adhesion molecules from differential gene expression analysis expression analysis of VeRA vs JRep fibroblasts. Bulk RNA sequencing was performed on RNA isolated from fibroblasts from patients with resolving arthritis (Res), very early rheumatoid arthritis (VeRA) and RA patients undergoing joint replacement (JRep) in co-culture with endothelial cells (ECs) and treated with TNF-α+IFNγ for 24 hours. Sex genes were removed from the analysis and the gene counts were subject to differential gene expression analysis in DESeq2. The significantly (Padj < 0.1) differentially expressed genes of VeRA vs JRep, were put through KEGG pathway enrichment analysis and the cell adhesion pathway deemed significant. Genes up (green) and down (red) -regulated in in this pathway in VeRA vs JRep are shown.

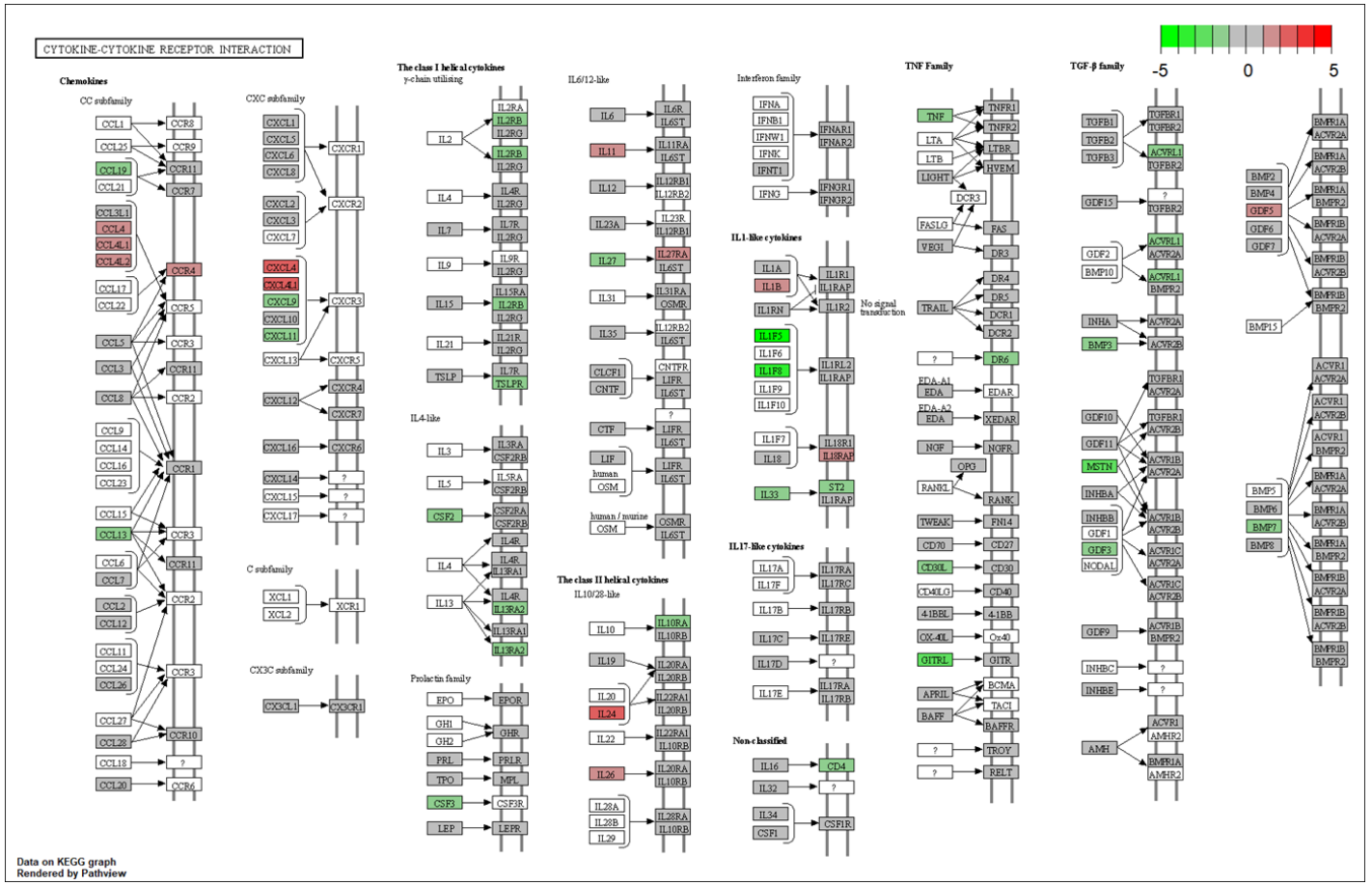

Appendix Figure 5: Genes involved in the KEGG pathway of cytokine-cytokine receptor interactions from differential gene expression analysis expression analysis of JRep vs Res fibroblasts. Bulk RNA sequencing was performed on RNA isolated from fibroblasts from patients with resolving arthritis (Res), very early rheumatoid arthritis (VeRA) and RA patients undergoing joint replacement (JRep) in co-culture with endothelial cells (ECs) and treated with TNF-α+IFNγ for 24 hours. Sex genes were removed from the analysis and the gene counts were subject to differential gene expression analysis in DESeq2. The significantly (Padj < 0.1) differentially expressed genes of JRep vs Res, were put through KEGG pathway enrichment analysis and the cytokine-cytokine receptor interaction pathways was deemed significant. Genes up (green) and down (red) -regulated in in this pathway in JRep vs Res are shown.

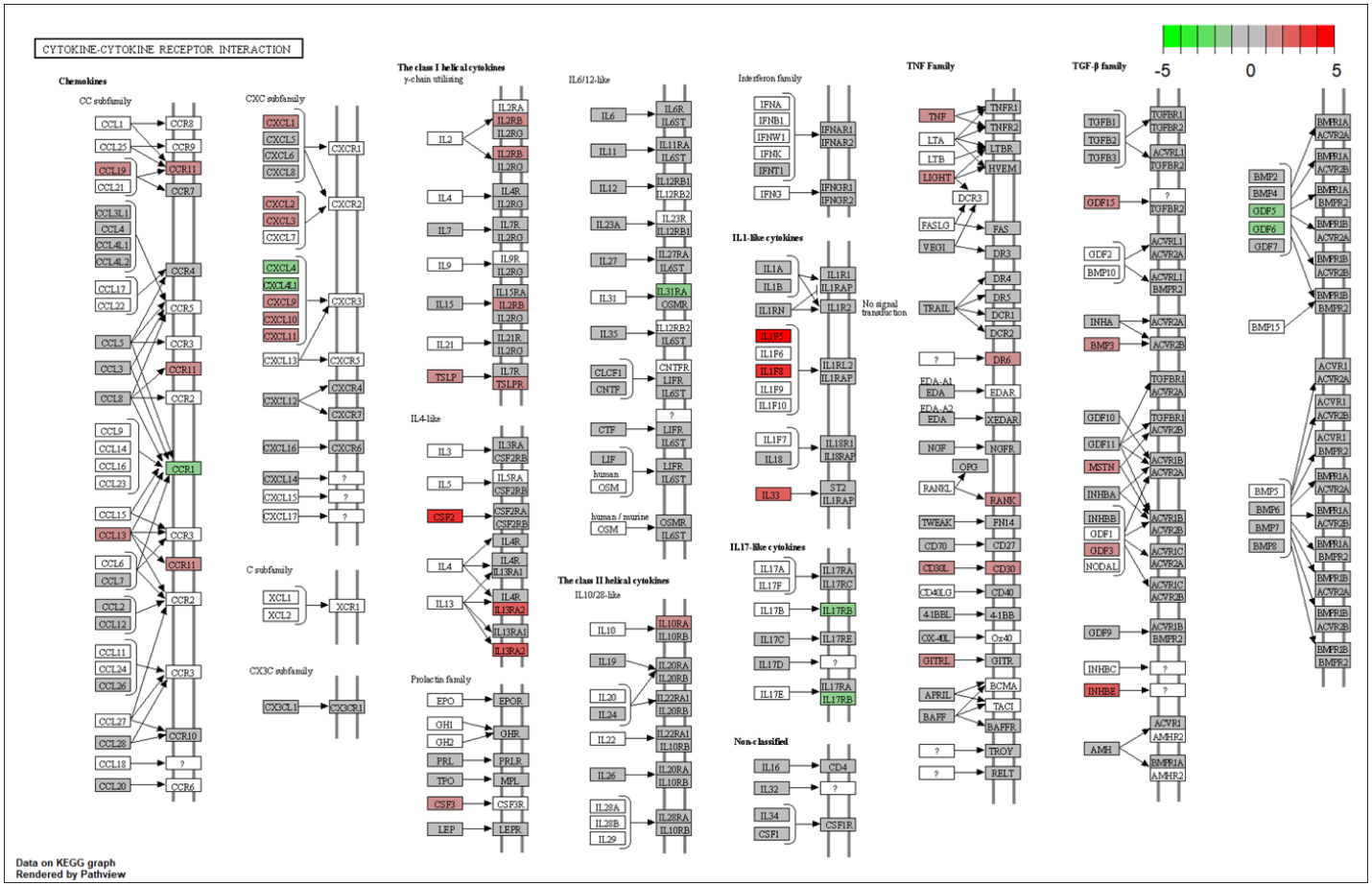

Appendix Figure 6: Genes involved in the KEGG pathway of cytokine-cytokine receptor interactions from differential gene expression analysis expression analysis of VeRA vs JRep fibroblasts. Bulk RNA sequencing was performed on RNA isolated from fibroblasts from patients with resolving arthritis (Res), very early rheumatoid arthritis (VeRA) and RA patients undergoing joint replacement (JRep) in co-culture with endothelial cells (ECs) and treated with TNF-α+IFNγ for 24 hours. Sex genes were removed from the analysis and the gene counts were subject to differential gene expression analysis in DESeq2. The significantly (Padj < 0.1) differentially expressed genes of VeRA vs JRep, were put through KEGG pathway enrichment analysis and the cytokine-cytokine receptor interaction pathways was deemed significant. Genes up (green) and down (red) -regulated in in this pathway in VeRA vs JRep are shown.

Appendix Table 4: Patient characteristics of fibroblast donors from the fibroblast-endothelial cell co-cultures used for Mass-Spectrometry

ID	Group	Site	Age	Sex	CCP +/-	RHF +/-	Disease Duration (wks)	DAS28 Baseline	ESR (mm/hr)	CRP (mg/L)	Global VAS	SJC28	TJC28	US PD worst	US GS worst	NSAID (Y/N)	DMARD
BX016	EstRA	Knee	46	M	+	+	150	6.7	34	7	75	16	13	1	2	Y	
BX017	EstRA	Knee	61	F	-	-	30	4.9	8	9	45	6	15	1	1	N	
BX032	EstRA	Ankle	46	F	+	-	30	5.2	24	34	47	4	10	2	2	Y	
BX075	EstRA	Knee	22	F	-	-	52	6.4	81	79	89	6	6	2	3	Y	
BX077	EstRA	Knee	72	M	-	-	38	7.4	53	43	70	16	21	3	2	Y	
BX117	EstRA	Knee	63	F	+	+	26	5.2	35	0	60	3	6	2	1	Y	
RA02	JRep	Knee	52	F	NA	+	1040	4.4	70	46	16	2	2	na		N	MTX
RA05	JRep	Knee	62	F	NA	+	1040	6.8	63	62	95	11	9	na		N	
RA12	JRep	Hip	32	F	NA	+	156	4.8	21	21	74	14	1	na		Y	Gold
RA16	JRep	Knee	30	F	NA	+	780	6.5	37	33	58	19	12	na		Y	Azathioprine
BX070	Norm	Knee	44	M	-	-											
BX085	Norm	Knee	38	M	-	-											
BX088	Norm	Knee	34	M	-	-											
BX095	Norm	Knee	47	F	-	-											
BX098	Norm	Knee	41	F	-	-											
BX089	Norm	Knee	41	F	-	-											
BX099	Norm	Knee	42	M	-	-											
BX030	Res	Knee	72	M	-	-	8	3.6	5	0	34	4	7	1	1	N	
BX038	Res	Knee	45	F	-	-	1	4.0	4	0	83	5	5	1	1	N	
BX072	Res	Knee	32	M	-	-	10	3.6	15	0	36	1	3	0	1	N	
BX087	Res	Ankle	27	M	-	-	4	3.8	37	28	3	2	2	0	1	Y	
BX054	Res	Ankle	55	M	-	-	6	3.5	2	6	91	5	4	1	2	Y	
BX028	Res	Knee	74	M	-	-	5	4.8	45	13	55	23	0	0	1	Y	
BX027	Res	Ankle	44	F	-	-	5	3.8	18	10	32	2	3	1	1	Y	
BX031	VeRA	Knee	43	M	-	-	9	6.9	58	0	76	4	19	0	1	Y	
BX042	VeRA	Knee	55	M	+	-	4	3.5	58	45	9	4	0	0	2	N	
BX092	VeRA	MCP	48	M	+	+	4	6.0	63	38	51	9	8	2	3	Y	
BX116	VeRA	Knee	63	M	-	-	8	2.3	2	0	70	1	1	2	3	Y	
BX121	VeRA	Ankle	60	F	+	+	11	4.3	32	45	46	1	3	2	2	N	

DAS28 = Disease Activity Score 28; CCP = cyclic citrullinated peptide, CRP = C-reactive protein; DMARD = Disease modifying anti-rheumatic drug; ESR = erythrocyte sedimentation rate; JRep = joint replacement; MTX = Methotrexate; NSAID = Non-steroidal anti-inflammatory; RF = Rheumatoid factor; SJC28 = 28 swollen joint counts; TJC28 = 28 tender joint counts; US GS = ultrasound greyscale grade at the biopsied joint; US PD = ultrasound power Doppler grade at the biopsied joint; VAS = visual analogue score; VeRA = Very early rheumatoid arthritis.

Appendix Table 5: Metabolites with unadjusted p value<0.05 dependent on fibroblast diagnosis in unstimulated fibroblast-endothelial cell co-cultures

Idx	Ion mode	P value	P adj	mz	rt	Potential metabolite
257	Positive	0.029059	0.99957	139.0836	322.3700	5-Aminopentanamide
765	Positive	0.039247	0.99957	200.9828	501.0687	Dichloromaleimide||1-Methyl-4-nitroimidazole||5-Amino-4-imidazole carboxylate||8-Hydroxypurine||Purine||3,4-Dihydroxybutyric acid||2,4-Dihydroxybutanoic acid||4-Deoxyerythronic acid||4-Deoxythreonic acid
1041	Negative	0.015849	0.99996	250.0540	322.3470	2,6-Diamino-4-hydroxy-5-N-methylformamidopyrimidine
1069	Positive	0.031984	0.99957	233.0089	501.1756	Ureidoacrylate||Dopachrome o-semiquinone||O-Ureidohomoserine
1281	Negative	0.036061	0.99996	278.1247	55.5692	Pantothenic acid||Hydroxypropionylcarnitine
1439	Positive	0.018563	0.99957	268.6490	498.0685	Dehydrodolichol diphosphate||Geranylfarnesyl diphosphate
1537	Positive	0.045485	0.99957	277.1627	499.0102	Lysylglutamic acid||gamma-Glutamyllysine
1549	Negative	0.021079	0.99996	309.0582	277.6397	3-(2,4-dihydroxy-3,5-dimethoxyphenyl)propanoic acid||4-hydroxy-5-(2,4,5-trihydroxyphenyl)pentanoic acid||4-hydroxy-5-(3,4,5-trihydroxyphenyl)pentanoic acid||Elenaic acid||Genipinic acid
1688	Positive	0.034883	0.99957	291.1178	359.3972	2-Amino-4-oxo-6-(1',2',3'-trihydroxypropyl)-diquinoid-7,8-dihydroxypterin||N-Succinyl-L,L-2,6-diaminopimelate
1765	Positive	0.029587	0.99957	298.3458	482.5840	8-Isoprostane
1779	Positive	0.026574	0.99957	299.3492	482.6202	8-Isoprostane
1986	Positive	0.005892	0.99957	319.1006	31.5977	Thyronine||Asparaginyl-Tyrosine
2124	Positive	0.03238	0.99957	333.1040	53.8292	D-1-[(3-Carboxypropyl)amino]-1-deoxyfructose||(1,3-diphenylpropoxy)sulfonic acid
2462	Positive	0.026316	0.99957	374.1071	63.6888	5-Amino-6-(5'-phospho-D-ribitylamino)uracil||N-Acetyl-4-O-acetylneuraminic acid||N-Acetyl-7-O-acetylneuraminic acid||N-Acetyl-9-O-acetylneuraminic acid||N-acetyl-O-acetylneuraminate
2500	Positive	0.03981	0.99957	379.0683	333.5256	N-(3-oxo-heptanoyl)-homoserine thiolactone
2664	Positive	0.047724	0.99957	400.3100	501.1576	SM(d38:0)
3077	Negative	0.046773	0.99996	525.3401	509.5876	MG(24:1)
3110	Positive	0.034851	0.99957	455.1117	317.4431	Ribosylzeatin phosphate
3117	Positive	0.02639	0.99957	455.3121	422.2196	(20S)-1alpha,20,25-trihydroxyvitamin D3||(22R)-1alpha,22,25-trihydroxy-20-epivitamin D3||(23R)-1alpha,23,25-trihydroxyvitamin D3||(23S)-1alpha,23,25-trihydroxyvitamin D3||(23S)-23,24,25-trihydroxyvitamin D3||(23S,25R)-23,25,26-trihydroxyvitamin D3||(24S)-1alpha,24,25-trihydroxyvitamin D3
3414	Negative	0.018552	0.99996	594.3792	525.6310	LysoPE(22:1)||LysoPC(20:1)
3469	Positive	0.028354	0.99957	506.8587	802.2511	LacCer(d42:1)||Galabiosylceramide (d42:1)
3994	Positive	0.011999	0.99957	603.4994	567.4080	DG(35:5)
4068	Positive	0.046906	0.99957	615.3456	520.5834	Eicosatetraynoic acid||Icosatetraynoic acid
4178	Positive	0.038623	0.99957	637.3847	529.8383	LysoPC(22:0)
4367	Positive	0.041402	0.99957	682.3251	521.2142	Taurolithocholic acid 3-glucuronide
5166	Positive	0.045494	0.99957	837.5533	479.8315	PE(36:5)||PE(44:11)
1808	Negative	0.020152	0.99996	339.0027	279.6771	Not identified
2490	Negative	0.042676	0.99996	431.0381	334.8413	Not identified

3027	Negative	0.038855	0.99996	515.0513	45.2347	Not identified
3245	Negative	0.015321	0.99996	557.3236	500.6956	Not identified
3598	Negative	0.036812	0.99996	637.0684	325.2343	Not identified
3951	Negative	0.030119	0.99996	738.2779	498.2187	Not identified
4214	Negative	0.035128	0.99996	842.3215	521.1923	Not identified
267	Positive	0.018537	0.99957	140.9398	111.8121	Not identified
442	Positive	0.016109	0.99957	162.9067	827.1647	Not identified
1209	Positive	0.045925	0.99957	247.9465	804.0321	Not identified
1686	Positive	0.034963	0.99957	290.9902	62.6079	Not identified
1741	Positive	0.023639	0.99957	296.1986	527.0798	Not identified
3484	Positive	0.046299	0.99957	508.8683	550.0843	Not identified

Idx = peak number, m/z = mass to charge ratio, P adj = Benjamini-Hochberg adjusted P value, rt = retention time.

Appendix Table 6: Metabolites with unadjusted p value<0.05 dependent on fibroblast diagnosis in TNF-α-IFNγ stimulated fibroblast-endothelial cell co-cultures

Idx	Ion mode	P value	FDR	mz	rt	Potential metabolite
52	Positive	0.039193	0.99973	108.0445	15.15254	Quinoline-3-carboxylic acid||Octatriynoic acid||Quinaldic acid||Quinoline-4-carboxylic acid||p-Benzoquinone imine
163	Positive	0.006941	0.99973	126.0411	322.0003	1,2-Propanedithiol||1,3-Propanedithiol
261	Positive	0.045001	0.99973	140.0488	240.5182	Mercaptopicolinic acid||Mercaptonicotinic acid
311	Positive	0.023034	0.99973	146.0606	241.1317	Benzeneacetonitrile||Indole||Indole-3-carboxaldehyde
625	Positive	0.046399	0.99973	184.9694	110.2384	Thiodiglycol
840	Positive	0.020482	0.99973	209.1149	343.7178	Hydroxy-decenoic acid||oxo-decanoic acid||2-Methylbutyl 3-hydroxy-2-methylidenebutanoate
1035	Positive	0.046677	0.99973	229.9742	62.99867	2,8-Dihydroxyadenine||8-Hydroxyguanine
1106	Positive	0.010567	0.99973	236.9974	43.89946	Undecadienediynoic acid
1119	Positive	0.048779	0.99973	238.9719	822.206	Erythrose 4-phosphate||N-Carbamoyl-L-aspartate||Ureidosuccinic acid||1,4-Dithiothreitol
1260	Positive	0.021048	0.99973	252.9714	43.90134	S-Nitrosomercaptoethanol||Glycerolphosphate||Phosphohydroxypyruvic acid
1600	Negative	0.021306	0.99996	315.1349	298.6424	2-methyl-tridecanedioic acid||3-methyl-tridecanedioic acid||4-methyl-tridecanedioic acid||Diethyl decanedioate||Tetradecanedioic acid
1953	Negative	0.021363	0.99996	358.0655	355.6946	2-(Formamido)-N1-(5'-phosphoribosyl)acetamidine||5'-Phosphoribosyl-N-formylglycinamidine
2012	Negative	0.023703	0.99996	365.1359	239.5351	Tryptophan 2-C-mannoside
2381	Negative	0.02572	0.99996	414.989	47.90017	6-Thioxanthine 5'-monophosphate
2646	Positive	0.008234	0.99973	398.2383	478.8176	11,13-dimethoxy-12-hydroxy-9-octadecenoic acid||13,14-Dihydro PGF-1a||9,10-dimethoxy-13-hydroxy-11-octadecenoic acid||9,12-dimethoxy-13-hydroxy-10-octadecenoic acid||9,13-dihydroxy-10-ethoxy-11-octadecenoic acid||9,13-dihydroxy-12-ethoxy-10-octadecenoic acid
2916	Negative	0.026774	0.99996	495.1381	298.2869	4-Androsten-3beta,17beta-diol disulfate
2984	Positive	0.046459	0.99973	440.339	542.9996	Mycocerosic acid (C25)||Mycosanoic acid (C25)||Pentacosanoic acid||Tetracosahexaenoylethanolamide||(23S)-methylcholic acid||Homocholic acid||3-hydroxyoctadecatrienoylcarnitine
3108	Positive	0.003585	0.99973	454.9362	42.94509	TG(54:0)
3405	Positive	0.029883	0.99973	495.2035	32.47888	LysoPA(16:0)||Phytyl diphosphate||LysoPE(15:0)
3443	Positive	0.044105	0.99973	501.3748	515.0393	Mycocerosic acid (C29)||Nonacosanoic acid||nonacosanoic acid
3563	Positive	0.025273	0.99973	520.9837	66.10352	2'-Deoxy-5-hydroxymethylcytidine-5'-triphosphate
3917	Positive	0.004832	0.99973	588.162	529.6173	Lewis X trisaccharide||O-6-deoxy-a-L-galactopyranosyl-(1->2)-O-b-D-galactopyranosyl-(1->3)-2-(acetylamino)-2-deoxy-D-Galactose
5467	Positive	0.017717	0.99973	925.6048	479.263	PS(41:2)
458	Negative	0.032369	0.99996	181.9772	817.27	Not identified
1053	Negative	0.042187	0.99996	251.1475	448.5085	Not identified
1098	Negative	0.030644	0.99996	257.1204	321.9388	Not identified
1113	Negative	0.041209	0.99996	258.9164	881.8535	Not identified
1184	Negative	0.013531	0.99996	266.8522	855.3003	Not identified
1512	Negative	0.005873	0.99996	304.9425	106.731	Not identified
1564	Negative	0.021057	0.99996	310.9316	802.2753	Not identified
1696	Negative	0.002664	0.99996	326.1347	203.9685	Not identified
1736	Negative	0.035903	0.99996	329.8389	837.4416	Not identified
1761	Negative	0.030013	0.99996	333.0409	240.3986	Not identified
2382	Negative	0.017858	0.99996	415.0952	298.1255	Not identified
3468	Negative	0.049628	0.99996	606.9954	34.01315	Not identified

3803	Negative	0.029658	0.99996	690.8426	807.1173	Not identified
3809	Negative	0.004227	0.99996	692.7248	37.19548	Not identified
4045	Negative	0.038808	0.99996	770.7978	810.5217	Not identified
4110	Negative	0.002222	0.99996	799.1584	322.8288	Not identified
4300	Negative	0.023406	0.99996	882.3021	240.4885	Not identified
213	Positive	0.03071	0.99973	133.9596	884.0594	Not identified
279	Positive	0.001439	0.99973	142.1224	15.2544	Not identified
556	Positive	0.013197	0.99973	176.1006	32.75524	Not identified
679	Positive	0.023983	0.99973	192.0439	322.6614	Not identified
1113	Positive	0.023129	0.99973	238.0006	43.66881	Not identified
1174	Positive	0.035264	0.99973	244.8744	38.55471	Not identified
1306	Positive	0.039446	0.99973	257.3024	460.1303	Not identified
1511	Positive	0.037857	0.99973	274.8817	38.3238	Not identified
2540	Positive	0.020584	0.99973	383.3115	525.284	Not identified
2714	Positive	0.032794	0.99973	407.2768	478.8857	Not identified
3134	Positive	0.035462	0.99973	457.3493	514.9974	Not identified
3428	Positive	0.0349	0.99973	499.1592	298.1199	Not identified
4674	Positive	0.048527	0.99973	731.1759	333.5776	Not identified

Idx = peak number, m/z = mass to charge ratio, P adj = Benjamini-Hochberg adjusted P value, rt = retention time.

Appendix Table 7: Patient characteristics of fibroblast donors used in the fibroblast: macrophage co-cultures for RNA-sequencing

Sample Name	Diagnosis	Joint	Age	CCP +/-	RHF +/-	Disease duration (wks)	DAS28 baseline ESR	ESR	CRP	Global VAS	SJC28	TJC28	US PD worst	GS worse	NSAID therapy	DMARD
BX005	VeRA	Knee	70	N	N	5	6.04	68	26	96	5	4	1	2	Y	
BX010	Res	Knee	40	N	N	4	3.85	5	0	36	7	7	1	1	Y	
BX011	VeRA	Knee	49	N	N	2	4.70	12	8	35	8	9	0	2	N	
BX017	EstRA	Knee	61	N	N	30	4.94	8	9	45	6	15	1	1	N	
BX018	EstRA	Knee	69	N	N	52	4.63	11	0	52	7	7	1	2	N	
BX027	VeRA	Ankle	44	N	N	5	3.84	18	10	32	2	3	1	1	Y	
BX033	Res	Ankle	81	N	N	7	6.73	60	52	50	11	16	2	2	Y	
BX038	Res	Knee	45	N	N	1	4.01	4	0	83	5	5	1	1	N	
BX049	VeRA	Ankle	48	P	P	3	3.87	10	0	29	3	6	0	2	Y	
BX063	VeRA	Knee	74	P	N	9	4.42	20	32	62	3	3	2	3	N	
BX071	Res	Ankle	41	N	N	4	1.66	5	9	10	2	0	0	2	Y	
BX075	EstRA	Knee	22	N	N	52	6.38	81	79	89	6	6	2	3	Y	
BX081	Norm	Knee	59	N	N											
BX089	Norm	Knee	38	N	N											
BX095	Norm	Knee	47	N	N											
BX097	Norm	Knee	41	N	N											
BX098	Norm	Knee	41	N	N											
BX121	VeRA	Ankle	60	P	P	11	4.32	32	45	46	1	3	2	2	N	
BX125	EstRA	Knee	56	p	p	16	5.52	48	47	75	1	7	1	2	Y	
BX130	VeRA	Ankle	61	N	p	15	5.42	43	18	24	1	15	0	1	Y	
BX143	Res	Knee	45	N	N	17	3.01	8	4	51	1	1	0	3	Y	
BX157	Res	Knee	45	N	N	2	2.59	8	17	13	2	1	2	2	N	
RA05SY	Jrep	Knee	62	NA	P	1040	6.84	63	62	95	11	9	NA	NA	N	MTX
RA07SY	Jrep	Knee	71	NA	P	52	7.23	31	54	86	16	20	NA	NA	N	Pred + Azathioprine
RA16SY	Jrep	Knee	30	NA	P	780	6.50	37	33	58	19	12	NA	NA	Y	Pred + Etanercapt
RA18SY	Jrep	Knee	62	NA	P	1040	4.11	8	8	44	4	7	NA	NA	Y	Etanercept
RA19SY	Jrep	Knee	47	NA	P	1196	3.80	57	na	9	1	1	NA	NA	Y	Adalimumab
RA22SY	Jrep	Knee	70	NA	P	1560	4.42	20	na	15	7	6	NA	NA	Y	

DAS28 = Disease Activity Score 28; CCP = cyclic citrullinated peptide, CRP = C-reactive protein; DMARD = Disease modifying anti-rheumatic drug; ESR = erythrocyte sedimentation rate; JRep = joint replacement; MTX = Methotrexate; NSAID = Non-steroidal anti-inflammatory; Pred = prednisolone; RF = Rheumatoid factor; SJC28 = 28 swollen joint counts; TJC28 = 28 tender joint counts; US GS = ultrasound greyscale grade at the biopsied joint; US PD = ultrasound power Doppler grade at the biopsied joint; VAS = visual analogue score; VeRA = Very early rheumatoid arthritis

Appendix Table 8: RIN scores and concentrations of macrophage-fibroblast co-culture samples

Sample #	Sample Name	Batch	Diagnosis	Concentration (ng/ul)	RIN
1	BX027 Coc Mϕ	1	VeRA	1.354110887	7.2
2	BX027 Coc FLS	1	VeRA	3.682787698	9.4
3	BX027 FLS	1	VeRA	2.876089577	9.2
4	BX018 Coc Mϕ	1	EstRA	1.385489344	8.2
5	BX018 Coc FLS	1	EstRA	2.353527089	8.5
6	BX018 FLS	1	EstRA	3.079926009	8.3
7	RA22SY Coc Mϕ	1	Jrep	1.302966474	7.1
8	RA22SY Coc FLS	1	Jrep	3.004815372	9.2
9	RA22SY FLS	1	Jrep	3.510823872	9.1
10	BX095 Coc Mϕ	1	Norm	1.553747053	8.1
11	BX095 Coc FLS	1	Norm	1.943630555	7.9
12	BX095 FLS	1	Norm	3.651162166	8.5
13	BX033 Coc Mϕ	1	Res	1.579936946	5.7
14	BX033 Coc FLS	1	Res	3.50687068	8.4
15	BX033 FLS	1	Res	2.764906069	8.9
16	BX075 Coc Mϕ	1	EstRA	1.367699983	5.4
17	BX075 Coc FLS	1	EstRA	2.981590373	8.4
18	BX075 FLS	1	EstRA	2.971954469	9.2
19	BX049 Coc Mϕ	1	VeRA	1.357817004	7.6
20	BX049 Coc FLS	1	VeRA	3.167143294	2.2
21	BX049 FLS	1	VeRA	2.508936926	8.8
22	BX017 Coc Mϕ	1	EstRA	1.354852111	5.1
23	BX017 Coc FLS	1	EstRA	4.07489487	8.9
24	BX017 FLS	1	EstRA	NOT THERE	
25	BX130 Coc Mϕ	1	VeRA	1.360781898	4.6
26	BX130 Coc FLS	1	VeRA	2.111147041	8.9
27	BX130 FLS	1	VeRA	1.761289602	9
28	RA19SY Coc Mϕ	1	Jrep	1.280729772	9.2
29	RA19SY Coc FLS	1	Jrep	1.95054864	7.3
30	RA19SY FLS	1	Jrep	7.404470328	8.8
31	BX010 Coc Mϕ	1	Res	1.324956101	4.4
32	BX010 Coc FLS	1	Res	3.198768825	8.5
33	BX010 FLS	1	Res	2.576388254	8.8
34	B1 HD4 macrophages only	1		1.406737748	8
35	BX097 Coc Mϕ	2	Norm	1.597726308	8.2
36	BX097 Coc FLS	2	Norm	3.007039042	9.5
37	BX097 FLS	2	Norm	1.58290184	7.5
38	BX125 Coc Mϕ	2	EstRA	1.904098641	5.5
39	BX125 Coc FLS	2	EstRA	MIXED	
40	BX125 FLS	2	EstRA	MIXED	
41	BX098 Coc Mϕ	2	Norm	1.609832956	6.1
42	BX098 Coc FLS	2	Norm	1.846036143	7.4
43	BX098 FLS	2	Norm	1.938689066	1.8
44	BX157 Coc Mϕ	2	Res	1.508532427	9
45	BX157 Coc FLS	2	Res	3.685505517	9

46	BX157 FLS	2	Res	2.921304204	8.4
47	Not Used				
48	Not Used				
49	Not Used				
50	RA05SY Coc Mϕ	2	Jrep	1.319520463	6.5
51	RA05SY Coc FLS	2	Jrep	2.271745442	
52	RA05SY FLS	2	Jrep	2.360692248	9.3
53	BX038 Coc Mϕ	2	Res	1.411432163	6.8
54	BX038 Coc FLS	2	Res	2.427402353	83
55	BX038 FLS	2	Res	2.383423099	8.7
56	BX089 Coc Mϕ	2	Norm	1.519403703	7.9
57	BX089 Coc FLS	2	Norm	3.256090101	9.2
58	BX089 FLS	2	Norm	2.700666709	9.2
59	BX011 Coc Mϕ	2	VeRA	1.507791203	8.4
60	BX011 Coc FLS	2	VeRA	2.586518307	9.2
61	BX011 FLS	2	VeRA	NOT THERE	
62	BX005 Coc Mϕ	2	VeRA	1.306178442	9.2
63	BX005 Coc FLS	2	VeRA	2.053084542	8.2
64	BX005 FLS	2	VeRA	1.906569386	9.3
65	BX121 Coc Mϕ	2	VeRA	1.37362977	9
66	BX121 Coc FLS	2	VeRA	1.707427369	9.3
67	BX121 FLS	2	VeRA	1.627375243	9.3
68	B2 HD4 macrophages only	2		1.33434493	2.9
69	BX063 Coc Mϕ	3	VeRA	2.239378687	7.9
70	BX063 Coc FLS	3	VeRA	15.18089196	9.4
71	BX063 FLS	3	VeRA	8.414016582	9.5
72	BX081 Coc Mϕ	3	Norm	1.711133486	7.6
73	BX081 Coc FLS	3	Norm	3.64967972	9.1
74	BX081 FLS	3	Norm	6.476458646	9.1
75	RA16SY Coc Mϕ	3	Jrep	1.866543323	7.3
76	RA16SY Coc FLS	3	Jrep	5.112360538	8.9
77	RA16SY FLS	3	Jrep	3.469809511	8.8
78	RA07SY Coc Mϕ	3	Jrep	1.710145188	8
79	RA07SY Coc FLS	3	Jrep	4.916677564	9
80	RA07SY FLS	3	Jrep	4.109732369	8.9
81	BX071 Coc Mϕ	3	Res	1.882603163	7.9
82	BX071 Coc FLS	3	Res	3.185426804	8.8
83	BX071 FLS	3	Res	4.029433169	9.5
84	RA18SY Coc Mϕ	3	Jrep	1.766972314	4.7
85	RA18SY Coc FLS	3	Jrep	6.449280455	9.5
86	RA18SY FLS	3	Jrep	4.321969332	9.3
87	BX143 Coc Mϕ	3	Res	2.902773619	9.5
88	BX143 Coc FLS	3	Res	2.51140767	9.6
89	BX143 FLS	3	Res	3.596805785	9.6
90	B3 HD4 macrophages only	3		2.731056868	9

CoC = Co-culture, EstRA = Established rheumatoid arthritis, FLS = fibroblast like synoviocytes, HD = Healthy donor, JRep = joint replacement, Fib = fibroblast, Mϕ = macrophage, Res = Resolving, VeRA = Very early Rheumatoid Arthritis.

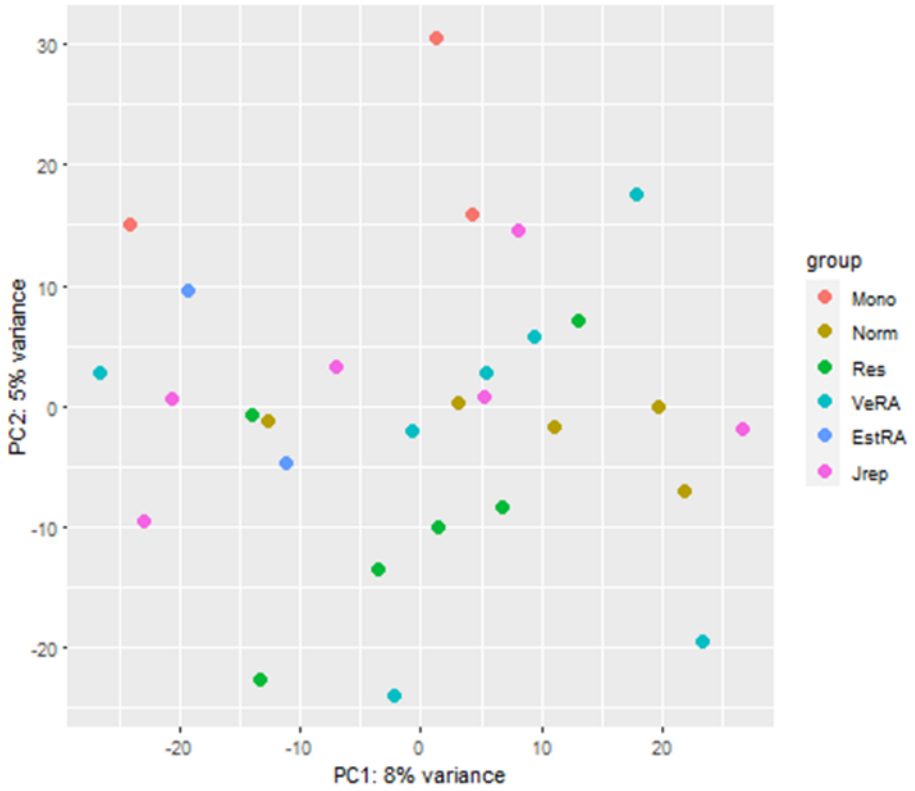

Appendix Figure 7: Mono-cultured macrophages cluster separately from co-cultured macrophages. Fibroblasts and macrophages were co-cultured and treated with TNF-α for 16 hours. RNA was isolated and bulk RNA sequencing performed. Gene counts from the macrophages sequencing data were subject to variance stabilising transformation (VST) and principal components identified and PCs 1 and 2 plotted. Samples were coloured according to whether they were in mono-culture (red), or the diagnosis of fibroblasts in culture; Norm (Non-inflamed; brown), Res (Resolving; green), VeRA (very early rheumatoid arthritis; light blue), EstRA (established RA; dark blue) and Jrep (RA patients undergoing joint replacement; pink).

Appendix Table 9: The 100 most significantly differentially expressed genes in macrophages cultured with VeRA compared to Res fibroblasts

Ensembl ID	Entrez	HGNC symbol	Log2FC	pvalue	padj
ENSG00000136717	274	BIN1	-7.8851	6.30E-12	4.06E-08
ENSG00000139597	90634	N4BP2L1	-7.78039	9.72E-10	6.96E-07
ENSG00000102054	5931	RBBP7	-7.63804	2.22E-08	5.73E-06
ENSG00000153066	51061	TXNDC11	-7.60104	1.82E-08	5.11E-06
ENSG00000164124	55314	TMEM144	-7.41142	4.82E-10	6.46E-07
ENSG00000114626	80325	ABTB1	-7.40319	7.11E-10	6.54E-07
ENSG00000107854	80351	TNKS2	-7.39607	5.50E-11	1.77E-07
ENSG00000138069	5861	RAB1A	-7.34335	1.93E-09	1.13E-06
ENSG00000167186	10229	COQ7	-7.33785	6.55E-08	1.03E-05
ENSG00000130414	4705	NDUFA10	-7.25397	1.05E-07	1.35E-05
ENSG00000109606	1665	DHX15	-7.22931	5.99E-08	1.03E-05
ENSG00000136875	9128	PRPF4	-7.12676	3.99E-08	7.78E-06
ENSG00000136758	10730	YME1L1	-6.96788	1.33E-09	8.59E-07
ENSG00000125375	27109	DMAC2L	-6.94948	1.10E-07	1.36E-05
ENSG00000119596	56252	YLPM1	-6.90279	2.65E-09	1.42E-06
ENSG00000160584	23387	SIK3	-6.89436	6.43E-08	1.03E-05
ENSG00000134030	9811	CTIF	-6.88566	3.07E-07	2.88E-05
ENSG00000061936	6433	SFSWAP	-6.88258	6.35E-07	4.54E-05
ENSG00000132604	7014	TERF2	-6.84571	2.07E-07	2.22E-05
ENSG00000145936	3779	KCNMB1	-6.81415	1.34E-08	4.31E-06
ENSG00000095906	10101	NUBP2	-6.8032	1.30E-08	4.31E-06
ENSG00000118263	8609	KLF7	-6.74093	1.77E-07	1.98E-05
ENSG00000118058	4297	KMT2A	-6.53836	4.30E-07	3.44E-05
ENSG00000100395	83746	L3MBTL2	-6.52624	8.24E-07	5.59E-05
ENSG00000125089	54436	SH3TC1	-6.48906	2.53E-08	5.81E-06
ENSG00000156504	159090	PABIR2	-6.48377	3.28E-09	1.63E-06
ENSG00000139613	6601	SMARCC2	-6.45449	3.96E-08	7.78E-06
ENSG00000126903	8273	SLC10A3	-6.29974	3.59E-07	3.12E-05
ENSG00000111052	8825	LIN7A	-6.24188	2.01E-08	5.39E-06
ENSG00000165861	53349	ZFYVE1	-6.23775	9.69E-08	1.35E-05
ENSG00000162396	25973	PARS2	-6.19737	4.12E-08	7.80E-06
ENSG00000113597	80006	TRAPPC13	-6.17671	1.70E-08	5.11E-06
ENSG00000139718	23067	SETD1B	-6.17103	1.14E-07	1.39E-05
ENSG00000164611	9232	PTTG1	-6.1453	3.90E-08	7.78E-06
ENSG00000166503	50810	HDGFL3	-6.13196	2.83E-07	2.74E-05
ENSG00000159496	266747	RGL4	-6.08878	1.81E-08	5.11E-06
ENSG00000156265	56911	MAP3K7CL	-6.04744	5.60E-07	4.14E-05
ENSG00000146083	22838	RNF44	-6.04339	1.99E-07	2.18E-05
ENSG00000067334	30836	DNTTIP2	-5.99015	9.88E-09	3.98E-06
ENSG00000103995	22995	CEP152	-5.94211	1.13E-08	4.03E-06
ENSG00000120798	7181	NR2C1	-5.93402	6.19E-08	1.03E-05
ENSG00000119912	3416	IDE	-5.81676	9.84E-08	1.35E-05
ENSG00000167615	114823	LENG8	-5.8122	2.32E-07	2.37E-05
ENSG00000225973	1.02E+08	PIGBOS1	-5.77578	2.67E-08	5.93E-06
ENSG00000131013	85313	PPIL4	-5.69619	6.59E-07	4.67E-05
ENSG00000009830	29954	POMT2	-5.62055	4.99E-07	3.82E-05
ENSG00000102531	22862	FNDC3A	-5.61073	1.08E-08	4.03E-06
ENSG00000110046	23130	ATG2A	-5.49713	7.85E-07	5.44E-05
ENSG00000128563	79706	PRKRIP1	-5.49704	2.69E-07	2.67E-05
ENSG00000118197	83479	DDX59	-5.46055	1.03E-07	1.35E-05
ENSG00000136933	10244	RABEPK	-5.45582	8.51E-07	5.65E-05
ENSG00000228923	NA	NA	-5.40959	1.01E-07	1.35E-05
ENSG00000123353	29095	ORMDL2	-5.4056	7.95E-08	1.16E-05
ENSG00000172006	115196	ZNF554	-5.38671	1.67E-07	1.92E-05
ENSG00000172939	9943	OXSR1	-5.35957	3.18E-07	2.88E-05
ENSG00000166165	1152	CKB	-5.34412	5.53E-07	4.14E-05
ENSG00000135164	9988	DMTF1	-5.33453	6.77E-09	3.11E-06
ENSG00000077420	54518	APBB1IP	-5.23746	7.76E-07	5.44E-05
ENSG00000120509	51248	PDZD11	-5.1777	2.37E-07	2.39E-05
ENSG00000074582	617	BCS1L	-5.12005	2.85E-07	2.74E-05
ENSG00000157693	203197	TMEM268	-5.08653	4.11E-07	3.44E-05
ENSG00000170779	55038	CDCA4	-5.08511	8.42E-07	5.65E-05
ENSG00000172005	4118	MAL	-4.9388	4.73E-07	3.72E-05

ENSG00000151092	55768	NGLY1	-4.91694	3.66E-07	3.14E-05
ENSG00000236914	1.08E+08	LINC01852	-4.64162	8.83E-07	5.69E-05
ENSG00000068784	55133	SRBD1	-4.38129	4.94E-07	3.82E-05
ENSG00000224470	342371	ATXN1L	-3.74655	4.32E-07	3.44E-05
ENSG00000104805	4924	NUCB1	5.477135	7.17E-08	1.07E-05
ENSG00000128585	4289	MKLN1	5.598769	1.08E-07	1.36E-05
ENSG00000169738	51181	DCXR	5.646877	2.18E-07	2.31E-05
ENSG00000108561	708	C1QBP	5.673199	2.28E-07	2.37E-05
ENSG00000099795	4713	NDUFB7	5.962349	6.29E-07	4.54E-05
ENSG00000033800	8554	PIAS1	6.294458	4.01E-07	3.40E-05
ENSG00000112996	10884	MRPS30	6.36903	8.68E-07	5.65E-05
ENSG00000090263	51650	MRPS33	6.37353	6.02E-10	6.46E-07
ENSG00000267534	9294	S1PR2	6.383808	3.50E-07	3.09E-05
ENSG00000063245	29924	EPN1	6.474246	5.54E-07	4.14E-05
ENSG00000120262	80129	CCDC170	6.517984	7.32E-09	3.15E-06
ENSG00000163964	54965	PIGX	6.579689	3.12E-07	2.88E-05
ENSG00000166135	55662	HIF1AN	6.81792	4.28E-07	3.44E-05
ENSG00000131966	55860	ACTR10	6.836106	6.15E-07	4.51E-05
ENSG00000156711	5603	MAPK13	6.849492	8.02E-07	5.50E-05
ENSG00000158669	137964	GPAT4	7.020599	6.80E-08	1.04E-05
ENSG00000110719	10312	TCIRG1	7.025043	9.14E-08	1.31E-05
ENSG00000162517	553115	PEF1	7.045337	1.30E-07	1.55E-05
ENSG00000137074	54840	APTX	7.084549	3.16E-07	2.88E-05
ENSG00000155097	528	ATP6V1C1	7.101694	2.51E-08	5.81E-06
ENSG00000144840	285282	RABL3	7.1873	5.14E-08	9.46E-06
ENSG00000107130	23413	NCS1	7.248309	1.54E-07	1.80E-05
ENSG00000184787	7327	UBE2G2	7.289443	3.56E-08	7.64E-06
ENSG00000132549	157680	VPS13B	7.291966	2.36E-08	5.81E-06
ENSG00000106780	1955	MEGF9	7.318265	1.78E-07	1.98E-05
ENSG00000148803	282969	FUOM	7.357138	3.49E-07	3.09E-05
ENSG00000109111	6830	SUPT6H	7.483164	6.23E-08	1.03E-05
ENSG00000158435	55571	CNOT11	7.799437	4.33E-07	3.44E-05
ENSG00000126214	3831	KLC1	7.840758	2.79E-10	5.99E-07
ENSG00000144674	2803	GOLGA4	8.004183	8.62E-07	5.65E-05
ENSG00000100811	7528	YY1	8.104132	8.35E-10	6.73E-07
ENSG00000124313	23096	IQSEC2	8.14844	5.78E-08	1.03E-05
ENSG00000115806	26003	GORASP2	8.558023	5.91E-10	6.46E-07

Appendix Table 10: The 100 most significantly differentially expressed genes in macrophages cultured with VeRA compared to Norm fibroblasts

Ensembl ID	Entrez	HGNC symbol	Log2FC	pvalue	padj
ENSG00000006756	414	ARSD	-8.6073	9.86E-09	3.69E-06
ENSG00000138069	5861	RAB1A	-8.26573	1.15E-10	1.55E-07
ENSG00000136536	64844	MARCHF7	-8.22876	2.04E-12	6.86E-09
ENSG00000105618	26121	PRPF31	-8.20939	5.04E-08	9.08E-06
ENSG00000163939	55193	PBRM1	-8.07859	1.07E-07	1.35E-05
ENSG00000101654	8731	RNMT	-8.07763	4.17E-09	2.34E-06
ENSG00000105821	27000	DNAJC2	-7.91199	4.79E-07	4.03E-05
ENSG00000107854	80351	TNKS2	-7.9009	2.26E-11	5.08E-08
ENSG00000138757	9908	G3BP2	-7.83489	3.38E-09	2.07E-06
ENSG00000164543	9263	STK17A	-7.78857	7.14E-07	5.23E-05
ENSG00000132604	7014	TERF2	-7.6784	2.56E-08	6.38E-06
ENSG00000076108	11176	BAZ2A	-7.59845	2.76E-08	6.65E-06
ENSG00000160446	84885	ZDHHC12	-7.56539	7.65E-09	3.68E-06
ENSG00000122779	8805	TRIM24	-7.45273	1.61E-10	1.55E-07
ENSG00000011451	58525	WIZ	-7.43034	3.74E-08	7.97E-06
ENSG00000124214	6780	STAU1	-7.33231	1.61E-07	1.8E-05
ENSG00000198585	131870	NUDT16	-7.32225	6.6E-08	9.88E-06
ENSG00000082996	11342	RNF13	-7.19348	2.03E-08	5.96E-06
ENSG00000109534	54433	GAR1	-7.18711	1.76E-12	6.86E-09
ENSG00000136141	23143	LRCH1	-7.11996	1.58E-10	1.55E-07
ENSG00000163602	23429	RYBP	-7.11328	6.4E-07	5.11E-05
ENSG00000155008	139322	APOOL	-7.03886	4.02E-08	8.21E-06
ENSG00000133250	84330	ZNF414	-7.03241	3.2E-09	2.07E-06
ENSG00000105404	10567	RABAC1	-6.87009	3.48E-07	3.26E-05

ENSG00000103490	29108	PYCARD	-6.86722	3.25E-07	3.09E-05
ENSG00000115084	80255	SLC35F5	-6.81708	1.73E-07	1.89E-05
ENSG00000055147	10827	FAM114A2	-6.81491	5.4E-08	9.1E-06
ENSG00000133030	23164	MPRIP	-6.81089	6.8E-07	5.23E-05
ENSG00000071205	79658	ARHGAP10	-6.79427	1.31E-07	1.54E-05
ENSG00000116221	51253	MRPL37	-6.78792	6.42E-08	9.83E-06
ENSG00000111276	1027	CDKN1B	-6.7528	4.63E-07	3.95E-05
ENSG00000116001	7072	TIA1	-6.72169	5.26E-08	9.08E-06
ENSG00000103707	123263	MTFMT	-6.60604	3.01E-09	2.07E-06
ENSG00000139718	23067	SETD1B	-6.60501	3.78E-08	7.97E-06
ENSG00000117868	57488	ESYT2	-6.57293	2.86E-07	2.75E-05
ENSG00000103024	4832	NME3	-6.49884	4.21E-07	3.78E-05
ENSG00000114770	10057	ABCC5	-6.45135	9.25E-08	1.27E-05
ENSG00000160932	4061	LY6E	-6.44868	7.03E-07	5.23E-05
ENSG00000137441	83888	FGFBP2	-6.44554	3.1E-11	5.22E-08
ENSG00000056097	51663	ZFR	-6.37769	4.59E-08	8.9E-06
ENSG00000163785	6259	RYK	-6.37037	4.66E-08	8.9E-06
ENSG00000146872	11011	TLK2	-6.28541	2.02E-07	2.15E-05
ENSG00000105486	3978	LIG1	-6.18248	2.22E-07	2.23E-05
ENSG00000188994	23036	ZNF292	-6.13645	9.33E-09	3.69E-06
ENSG00000170473	84305	PYM1	-6.10275	2.04E-07	2.15E-05
ENSG00000181045	284129	SLC26A11	-6.08139	4.76E-08	8.9E-06
ENSG00000158941	57805	CCAR2	-6.05702	1.72E-08	5.54E-06
ENSG00000133243	55643	BTBD2	-6.02523	1.31E-07	1.54E-05
ENSG00000127152	64919	BCL11B	-5.93707	1.08E-06	7.38E-05
ENSG00000079739	5236	PGM1	-5.92926	9.64E-08	1.3E-05
ENSG00000166788	113174	SAAL1	-5.8069	3.03E-09	2.07E-06
ENSG00000140543	55070	DET1	-5.78491	5.1E-09	2.64E-06
ENSG00000162961	84661	DPY30	-5.76629	8.75E-08	1.25E-05
ENSG00000133935	11161	ERG28	-5.72815	1.42E-07	1.63E-05
ENSG00000108433	9570	GOSR2	-5.70612	2.31E-08	6.22E-06
ENSG00000155545	166968	MIER3	-5.57644	7.22E-07	5.23E-05
ENSG00000080822	56650	CLDND1	-5.56225	1.14E-06	7.71E-05
ENSG00000164751	5828	PEX2	-5.5141	7.14E-08	1.05E-05
ENSG00000091592	22861	NLRP1	-5.4886	2.22E-08	6.22E-06
ENSG00000111801	10384	BTN3A3	-5.48271	4.55E-07	3.95E-05
ENSG00000034152	5606	MAP2K3	-5.45563	6.59E-07	5.16E-05
ENSG00000101868	5422	POLA1	-5.43328	9.47E-09	3.69E-06
ENSG00000161956	26168	SENP3	-5.39857	3.6E-08	7.97E-06
ENSG00000199990	56664	VTRNA1-1	-5.39286	8.26E-09	3.69E-06
ENSG00000272933	NA	NA	-5.34868	6.37E-08	9.83E-06
ENSG00000145780	56929	FEM1C	-5.34104	2.15E-07	2.19E-05
ENSG00000151292	1456	CSNK1G3	-5.30113	1.24E-07	1.52E-05
ENSG00000127337	8089	YEATS4	-5.14639	1.01E-07	1.31E-05
ENSG00000131697	261734	NPHP4	-5.14485	1.36E-07	1.58E-05
ENSG00000269967	NA	NA	-5.12592	5.86E-08	9.61E-06
ENSG00000113360	29102	DROSHA	-4.95128	2.53E-07	2.51E-05
ENSG00000272379	NA	NA	-4.91801	5.28E-07	4.39E-05
ENSG00000016864	55830	GLT8D1	-4.85298	1.74E-07	1.89E-05
ENSG00000170315	7314	UBB	-4.79249	2.52E-08	6.38E-06
ENSG00000284735	NA	NA	-4.7539	4.57E-07	3.95E-05
ENSG00000186951	5465	PPARA	-4.74108	1.08E-07	1.35E-05
ENSG00000185158	114659	LRRC37B	-4.57653	5.17E-08	9.08E-06
ENSG00000085415	81929	SEH1L	-4.20993	9.14E-07	6.41E-05
ENSG00000153485	26175	TMEM251	-4.18635	6.19E-07	5.03E-05
ENSG00000101928	56180	MOSPD1	-4.10406	7.85E-07	5.63E-05
ENSG00000240143	NA	NA	-4.05376	7.14E-07	5.23E-05
ENSG00000205643	150383	CDPF1	-3.97198	6.94E-07	5.23E-05
ENSG00000183751	10607	TBL3	4.986027	1.03E-06	7.1E-05
ENSG00000090263	51650	MRPS33	5.91706	3.4E-08	7.89E-06
ENSG00000169738	51181	DCXR	5.938028	2.73E-07	2.66E-05
ENSG00000198231	11325	DDX42	6.06635	6.45E-07	5.11E-05
ENSG00000129534	55320	MIS18BP1	6.427639	7.22E-07	5.23E-05
ENSG00000120262	80129	CCDC170	6.468058	5.99E-08	9.61E-06
ENSG00000147601	7013	TERF1	6.562211	9.87E-07	6.85E-05
ENSG00000115828	25797	QPCT	6.665471	8.92E-07	6.32E-05
ENSG00000126814	57570	TRMT5	6.736303	3.53E-07	3.26E-05
ENSG00000110514	8567	MADD	7.054608	4.38E-07	3.88E-05

ENSG00000178605	8225	GTPBP6	7.219879	2.08E-07	2.16E-05
ENSG00000132205	84034	EMILIN2	7.273325	1.01E-07	1.31E-05
ENSG00000137074	54840	APTX	7.35472	6.11E-07	5.02E-05
ENSG00000166135	55662	HIF1AN	7.410296	3.93E-07	3.58E-05
ENSG00000144840	285282	RABL3	7.516968	9.21E-08	1.27E-05
ENSG00000129315	904	CCNT1	7.631929	1.73E-08	5.54E-06
ENSG00000141699	162427	RETREG3	7.740922	2.04E-08	5.96E-06
ENSG00000100811	7528	YY1	7.804486	1.39E-08	4.92E-06

Appendix Table 11: The 100 most significantly differentially expressed genes in macrophages cultured with VeRA compared to EstRA fibroblasts

Ensembl ID	Entrez	HGNC symbol	Log2FC	pvalue	padj
ENSG00000109270	8649	LAMTOR3	-9.71113	3.95E-08	3.03E-06
ENSG00000138069	5861	RAB1A	-9.57993	2.07E-08	1.74E-06
ENSG00000165688	23203	PMPCA	-9.30672	1.26E-19	7.91E-16
ENSG00000164821	1669	DEFA4	-8.71779	3.39E-12	3.56E-09
ENSG00000164024	23173	METAP1	-8.58119	2.74E-12	3.44E-09
ENSG00000152133	253635	GPATCH11	-8.53865	4.97E-12	4.46E-09
ENSG00000155530	136332	LRGUK	-8.31291	8.55E-12	6.72E-09
ENSG00000139610	1990	CELA1	-8.21583	3.31E-08	2.57E-06
ENSG00000135245	29923	HILPDA	-8.01591	3.05E-11	1.60E-08
ENSG00000185049	7469	NELFA	-7.97548	4.48E-09	5.12E-07
ENSG00000088543	51161	C3orf18	-7.91797	1.88E-11	1.31E-08
ENSG00000143801	5664	PSEN2	-7.8722	1.02E-09	1.53E-07
ENSG00000130368	4142	MAS1	-7.81426	2.42E-11	1.38E-08
ENSG00000113456	5810	RAD1	-7.77347	4.57E-11	2.21E-08
ENSG00000160318	125875	CLDND2	-7.51801	3.62E-10	7.35E-08
ENSG00000162929	84542	SANBR	-7.47519	1.40E-10	4.87E-08
ENSG00000127824	7277	TUBA4A	-7.45744	6.86E-11	2.88E-08
ENSG00000188107	346007	EYS	-7.45724	1.06E-10	4.15E-08
ENSG00000141337	22901	ARSG	-7.45454	1.55E-10	4.94E-08
ENSG00000125434	399512	SLC25A35	-7.43852	2.52E-10	6.33E-08
ENSG00000105289	27134	TJP3	-7.41192	5.95E-11	2.67E-08
ENSG00000103319	29904	EEF2K	-7.38823	1.56E-07	9.94E-06
ENSG00000161179	150223	YDJC	-7.37674	1.57E-10	4.94E-08
ENSG00000234616	8629	JRK	-7.30428	2.54E-08	2.07E-06
ENSG00000166823	55897	MESP1	-7.2567	1.38E-10	4.87E-08
ENSG00000123595	9367	RAB9A	-7.1965	1.84E-08	1.60E-06
ENSG00000113555	51294	PCDH12	-7.05096	2.17E-10	5.76E-08
ENSG00000106809	4969	OGN	-6.96522	2.20E-10	5.76E-08
ENSG00000122550	55975	KLHL7	-6.93637	3.33E-10	7.03E-08
ENSG00000006282	64847	SPATA20	-6.92631	3.36E-10	7.03E-08
ENSG00000122435	54482	TRMT13	-6.76636	1.66E-10	4.98E-08
ENSG00000145390	54532	USP53	-6.6954	5.00E-10	9.25E-08
ENSG00000018510	8540	AGPS	-6.64452	7.57E-09	7.56E-07
ENSG00000070718	10947	AP3M2	-6.62676	3.32E-10	7.03E-08
ENSG00000271926	NA	NA	-6.53412	6.70E-10	1.11E-07
ENSG00000153487	3621	ING1	-6.5225	4.88E-08	3.65E-06
ENSG00000155729	130535	KCTD18	-6.51767	3.90E-10	7.67E-08
ENSG00000114790	26084	ARHGEF26	-6.49878	3.00E-10	7.03E-08
ENSG00000165113	80318	GKAP1	-6.34855	8.92E-10	1.37E-07
ENSG00000164162	10393	ANAPC10	-6.28867	4.72E-10	9.00E-08
ENSG00000256894	NA	NA	-6.22947	4.38E-09	5.10E-07
ENSG00000129680	79649	MAP7D3	-6.21333	1.50E-09	2.05E-07
ENSG00000122335	84947	SERAC1	-6.20521	1.16E-09	1.70E-07
ENSG00000107537	5264	PHYH	-6.1968	1.34E-09	1.87E-07
ENSG00000081189	4208	MEF2C	-6.18127	6.12E-10	1.07E-07
ENSG00000115902	6509	SLC1A4	-6.17246	7.91E-08	5.53E-06
ENSG00000163795	130557	ZNF513	-6.1136	1.63E-09	2.18E-07
ENSG00000170921	26115	TANC2	-6.03073	1.30E-08	1.17E-06
ENSG00000173818	284131	ENDOV	-6.00123	1.39E-07	8.94E-06

ENSG00000226360	1E+08	RPL10AP6	-5.9928	1.16E-07	7.63E-06
ENSG00000246366	286190	LACTB2-AS1	-5.94386	4.75E-09	5.24E-07
ENSG00000213347	83463	MXD3	-5.94383	5.52E-10	9.92E-08
ENSG00000227372	57212	TP73-AS1	-5.91483	8.95E-14	1.88E-10
ENSG00000092208	8487	GEMIN2	-5.90152	8.18E-10	1.28E-07
ENSG00000152926	51351	ZNF117	-5.89737	5.91E-09	6.19E-07
ENSG00000286153	NA	NA	-5.88748	6.44E-10	1.09E-07
ENSG00000182919	28970	C11orf54	-5.8616	1.95E-08	1.68E-06
ENSG00000106009	221927	BRAT1	-5.83888	3.06E-10	7.03E-08
ENSG00000171861	55178	MRM3	-5.82204	2.12E-08	1.75E-06
ENSG00000277610	1.02E+08	RNVU1-4	-5.81666	3.97E-09	4.72E-07
ENSG00000288066	NA	NA	-5.81627	3.41E-09	4.21E-07
ENSG00000122386	7755	ZNF205	-5.78389	3.98E-09	4.72E-07
ENSG00000133624	79970	ZNF767P	-5.63568	9.56E-09	9.10E-07
ENSG00000163002	129401	NUP35	-5.61511	4.93E-09	5.35E-07
ENSG00000166333	3611	ILK	-5.57657	2.31E-09	2.97E-07
ENSG00000142945	11004	KIF2C	-5.56733	5.05E-09	5.38E-07
ENSG00000226608	NA	NA	-5.56081	6.26E-09	6.45E-07
ENSG00000008516	64386	MMP25	-5.46312	2.73E-08	2.20E-06
ENSG00000085382	57531	HACE1	-5.45882	4.62E-09	5.19E-07
ENSG00000145247	132299	OCIAD2	-5.45085	8.68E-09	8.53E-07
ENSG00000151883	79668	PARP8	-5.43541	3.23E-09	4.06E-07
ENSG00000103248	64779	MTHFSD	-5.35432	1.16E-07	7.63E-06
ENSG00000240418	729679	RPS2P51	-5.34776	7.07E-09	7.17E-07
ENSG00000076003	4175	MCM6	-5.33878	6.43E-08	4.65E-06
ENSG00000164284	134266	GRPEL2	-5.313	9.57E-08	6.47E-06
ENSG00000010704	3077	HFE	-5.27729	2.09E-11	1.31E-08
ENSG00000125945	80818	ZNF436	-5.27679	3.27E-08	2.57E-06
ENSG00000005156	3980	LIG3	-5.27476	1.10E-08	1.00E-06
ENSG00000165792	64745	METTL17	-5.16686	1.44E-08	1.27E-06
ENSG00000168016	9881	TRANK1	-5.14126	5.93E-08	4.39E-06
ENSG00000103932	26015	RPAP1	-5.09535	1.01E-08	9.52E-07
ENSG00000177463	7182	NR2C2	-5.01479	8.67E-08	5.92E-06
ENSG00000046653	2824	GPM6B	-4.96026	8.90E-09	8.61E-07
ENSG00000222057	1.06E+08	RNU4-62P	-4.94983	1.05E-08	9.68E-07
ENSG00000101695	54941	RNF125	-4.90486	1.33E-07	8.63E-06
ENSG00000207468	641451	SNORA19	-4.87821	3.02E-08	2.40E-06
ENSG00000267197	NA	NA	-4.84452	6.40E-08	4.65E-06
ENSG00000173198	10800	CYSLTR1	-4.80024	4.13E-08	3.13E-06
ENSG00000275004	140883	ZNF280B	-4.51329	8.58E-08	5.92E-06
ENSG00000100504	5836	PYGL	-4.03968	1.74E-07	1.09E-05
ENSG00000204389	3303	HSPA1A	7.429993	1.14E-07	7.59E-06
ENSG00000136830	64855	NIBAN2	7.44326	7.26E-08	5.18E-06
ENSG00000158710	8407	TAGLN2	7.532783	2.03E-08	1.72E-06
ENSG00000163956	4043	LRPAP1	7.606318	1.93E-09	2.53E-07
ENSG00000008018	5689	PSMB1	7.711855	7.92E-08	5.53E-06
ENSG00000108774	5878	RAB5C	7.795825	8.63E-13	1.36E-09
ENSG00000109332	7323	UBE2D3	8.082077	2.04E-10	5.76E-08
ENSG00000147065	4478	MSN	8.246235	1.30E-09	1.86E-07
ENSG00000173193	54625	PARP14	9.248736	7.80E-10	1.26E-07
ENSG00000130222	10912	GADD45G	9.480442	4.20E-14	1.32E-10

Appendix Table 12: The 100 most significantly differentially expressed genes in macrophages cultured with VeRA compared to JRep fibroblasts

Ensembl ID	Entrez	HGNC symbol	Log2FC	pvalue	padj
ENSG00000148334	80142	PTGES2	-7.79746	1.46E-07	3.03E-05
ENSG00000160584	23387	SIK3	-7.67462	5.13E-09	3.75E-06
ENSG00000135334	55122	AKIRIN2	-7.36754	3.74E-10	1.69E-06
ENSG00000125384	5732	PTGER2	-7.16792	4.02E-08	1.52E-05
ENSG00000136875	9128	PRPF4	-7.07034	1.39E-07	3E-05
ENSG00000137343	79969	ATAT1	-7.06989	1.79E-06	0.000152

ENSG00000119899	26503	SLC17A5	-7.01836	1.2E-07	3E-05
ENSG00000083223	79670	TUT7	-7.00709	1.36E-06	0.000132
ENSG00000102054	5931	RBBP7	-7.00644	7.13E-07	9.27E-05
ENSG00000082996	11342	RNF13	-6.95402	4.01E-08	1.52E-05
ENSG00000241837	539	ATP5PO	-6.84813	1.34E-07	3E-05
ENSG00000165801	55701	ARHGEF40	-6.64137	1.94E-06	0.000158
ENSG00000105341	55101	DMAC2	-6.61149	4.02E-07	6.17E-05
ENSG00000127084	89846	FGD3	-6.59605	1.23E-06	0.000124
ENSG00000158796	9191	DEDD	-6.57773	2.67E-06	0.0002
ENSG00000137185	7746	ZSCAN9	-6.48215	2.27E-09	2.93E-06
ENSG00000104517	51366	UBR5	-6.4377	1.16E-09	2.11E-06
ENSG00000119203	51692	CPSF3	-6.40716	1.16E-08	6.24E-06
ENSG00000144231	5433	POLR2D	-6.35673	3.68E-07	5.92E-05
ENSG00000134982	324	APC	-6.34495	5.5E-09	3.75E-06
ENSG00000044459	54875	CNTLN	-6.30515	6.62E-08	2.24E-05
ENSG00000153179	283349	RASSF3	-6.24826	1.04E-06	0.000115
ENSG00000109046	26118	WSB1	-6.21559	1.57E-06	0.000142
ENSG00000161551	84765	ZNF577	-6.16825	8.95E-07	0.000103
ENSG00000147475	11160	ERLIN2	-6.15047	1.31E-09	2.11E-06
ENSG00000167850	10871	CD300C	-6.06904	4.34E-06	0.00028
ENSG00000096063	6732	SRPK1	-6.03477	1.04E-07	2.9E-05
ENSG00000147437	2796	GNRH1	-5.98595	1.67E-06	0.000145
ENSG00000169084	207063	DHRSX	-5.97402	7.48E-08	2.29E-05
ENSG00000147894	203228	C9orf72	-5.94544	1.76E-07	3.23E-05
ENSG00000131759	5914	RARA	-5.89881	1.41E-06	0.000134
ENSG00000186566	23131	GPATCH8	-5.84354	8.74E-07	0.000102
ENSG00000198961	9867	PJA2	-5.80941	2.78E-06	0.000204
ENSG00000235859	NA	NA	-5.72259	3.89E-06	0.000256
ENSG00000138772	306	ANXA3	-5.7076	4.98E-09	3.75E-06
ENSG00000197070	92714	ARRDC1	-5.65278	1.23E-07	3E-05
ENSG00000168297	54899	PXK	-5.57323	5.91E-07	8.1E-05
ENSG00000082515	29093	MRPL22	-5.53619	2.95E-06	0.000204
ENSG00000160294	8888	MCM3AP	-5.48088	7.15E-07	9.27E-05
ENSG00000112659	23113	CUL9	-5.36265	1.2E-06	0.000123
ENSG00000175727	22877	MLXIP	-5.35842	2.93E-06	0.000204
ENSG00000213516	494115	RBMXL1	-5.32707	1.68E-07	3.21E-05
ENSG00000176124	10301	DLEU1	-5.258	1.94E-07	3.47E-05
ENSG00000226328	1.01E+08	NUP50-DT	-5.24911	2.15E-08	9.88E-06
ENSG00000064115	51768	TM7SF3	-5.24652	7.19E-08	2.29E-05
ENSG00000103479	5934	RBL2	-5.24554	1.2E-06	0.000123
ENSG00000188404	6402	SELL	-5.03411	7.2E-07	9.27E-05
ENSG00000104321	8989	TRPA1	-4.90253	2.95E-06	0.000204
ENSG00000123836	5208	PFKFB2	-4.87388	1.47E-06	0.000137
ENSG00000023572	51022	GLRX2	-4.83923	1.14E-06	0.000122
ENSG00000078747	83737	ITCH	-4.81783	8.36E-07	0.000101
ENSG00000105829	10282	BET1	-4.55315	3.73E-06	0.000253
ENSG00000198841	112970	KTI12	-4.42763	1.27E-06	0.000126
ENSG00000168062	116071	BATF2	-4.38128	2.1E-06	0.000167
ENSG00000171155	29071	C1GALT1C1	-3.76038	1.19E-06	0.000123
ENSG00000133812	81846	SBF2	5.031436	2.08E-06	0.000167
ENSG00000183751	10607	TBL3	5.034265	5.29E-07	7.41E-05
ENSG00000168575	6575	SLC20A2	5.334066	1.89E-06	0.000158
ENSG00000132612	27183	VPS4A	5.655151	1.01E-06	0.000114
ENSG00000169738	51181	DCXR	5.715839	4.28E-07	6.26E-05
ENSG00000128585	4289	MKLN1	5.785976	1.7E-07	3.21E-05
ENSG00000164168	55751	TMEM184C	5.826313	3.97E-06	0.000258
ENSG00000105738	23094	SIPA1L3	5.826398	1.12E-06	0.000122
ENSG00000126870	55112	DYNC2I1	5.842839	1.62E-06	0.000145
ENSG00000129534	55320	MIS18BP1	5.869655	2.95E-06	0.000204
ENSG00000104765	665	BNIP3L	5.90984	2.84E-06	0.000204
ENSG00000108561	708	C1QBP	5.963684	1.55E-07	3.12E-05
ENSG00000185721	4733	DRG1	6.053384	2.66E-06	0.0002
ENSG00000215908	84809	CROCCP2	6.088945	1.38E-06	0.000133
ENSG00000151500	29087	THYN1	6.257856	3.78E-06	0.000254
ENSG00000133835	3295	HSD17B4	6.41619	8.24E-07	0.000101
ENSG00000173726	9804	TOMM20	6.452697	1.33E-07	3E-05
ENSG00000115524	23451	SF3B1	6.533834	5.22E-07	7.41E-05
ENSG00000164258	4724	NDUFS4	6.576424	2.33E-06	0.000183

ENSG00000107130	23413	NCS1	6.58751	2.52E-06	0.000193
ENSG00000141380	6760	SS18	6.588085	5.4E-09	3.75E-06
ENSG00000135148	10906	TRAFD1	6.684358	2.75E-06	0.000203
ENSG00000090263	51650	MRPS33	6.692121	5.24E-10	1.69E-06
ENSG00000107862	8729	GBF1	6.695282	8.49E-07	0.000101
ENSG00000120262	80129	CCDC170	6.871085	6.89E-09	4.03E-06
ENSG00000163964	54965	PIGX	6.946007	2.68E-07	4.67E-05
ENSG00000033627	535	ATP6V0A1	6.98469	1.92E-06	0.000158
ENSG00000132549	157680	VPS13B	7.076781	1.4E-07	3E-05
ENSG00000067208	7813	EVI5	7.178179	1.35E-07	3E-05
ENSG00000133597	90956	ADCK2	7.212833	2.45E-06	0.00019
ENSG00000032219	5926	ARID4A	7.244282	3.16E-07	5.29E-05
ENSG00000113712	1452	CSNK1A1	7.255366	3.86E-06	0.000256
ENSG00000126814	57570	TRMT5	7.266942	3.68E-08	1.52E-05
ENSG00000136630	3142	HLX	7.340942	5.64E-08	2.02E-05
ENSG00000187837	3006	H1-2	7.356315	7.89E-07	9.97E-05
ENSG00000131148	10328	EMC8	7.384168	3.13E-06	0.000214
ENSG00000115904	6654	SOS1	7.403721	1.66E-06	0.000145
ENSG00000132823	51526	OSER1	7.414625	1.48E-08	7.33E-06
ENSG00000111335	4939	OAS2	7.437822	1.56E-06	0.000142
ENSG00000144711	9922	IQSEC1	7.451344	3.9E-07	6.13E-05
ENSG00000132274	10346	TRIM22	7.530364	1.01E-07	2.9E-05
ENSG00000153140	1070	CETN3	7.548145	3.2E-07	5.29E-05
ENSG00000129315	904	CCNT1	7.700005	5.82E-09	3.75E-06
ENSG00000158716	54935	DUSP23	7.776083	1.74E-06	0.00015
ENSG00000120217	29126	CD274	7.923102	4.2E-07	6.26E-05

Appendix Table 13: The 100 most significantly differentially expressed genes in macrophages cultured wih Res compared to Norm fibroblasts

Ensembl ID	Entrez	HGNC symbol	Log2FC	pvalue	padj
ENSG00000131355	84658	ADGRE3	-8.64016	3.42E-07	3.84E-05
ENSG00000136536	64844	MARCHF7	-8.62108	2.26E-12	1.53E-08
ENSG00000140740	7385	UQCRC2	-8.51983	4.72E-09	2.47E-06
ENSG00000158669	137964	GPAT4	-8.40784	2.71E-09	1.67E-06
ENSG00000123096	8082	SSPN	-8.30514	3.68E-07	3.97E-05
ENSG00000109133	55161	TMEM33	-8.27218	3.52E-10	5.93E-07
ENSG00000127511	23309	SIN3B	-8.17231	6.30E-08	1.51E-05
ENSG00000113621	79770	TXNDC15	-8.10262	1.70E-09	1.63E-06
ENSG00000135506	10956	OS9	-8.05678	5.67E-07	5.33E-05
ENSG00000130311	79016	DDA1	-7.61127	1.78E-08	6.66E-06
ENSG00000139629	11226	GALNT6	-7.56415	3.47E-08	1.11E-05
ENSG00000148356	90678	LRSAM1	-7.45398	3.71E-07	3.97E-05
ENSG00000115459	84173	ELMOD3	-7.31554	2.32E-07	3.07E-05
ENSG00000118971	894	CCND2	-7.26015	6.06E-08	1.51E-05
ENSG00000161980	51728	POLR3K	-7.22898	6.59E-07	6.00E-05
ENSG00000136141	23143	LRCH1	-7.22576	4.68E-10	6.31E-07
ENSG00000122779	8805	TRIM24	-7.21414	2.33E-09	1.67E-06
ENSG00000126214	3831	KLC1	-7.19582	7.83E-08	1.60E-05
ENSG00000111276	1027	CDKN1B	-7.14044	3.90E-07	4.10E-05
ENSG00000140474	25989	ULK3	-7.1181	1.32E-07	2.28E-05
ENSG00000056097	51663	ZFR	-7.02847	1.52E-08	6.38E-06
ENSG00000110719	10312	TCIRG1	-7.0066	8.59E-07	7.06E-05
ENSG00000110851	11108	PRDM4	-6.98577	2.10E-07	2.96E-05
ENSG00000067955	865	CBFB	-6.93965	7.68E-07	6.46E-05
ENSG00000176087	113829	SLC35A4	-6.92545	5.01E-07	4.96E-05
ENSG00000128789	56984	PSMG2	-6.91443	4.87E-07	4.89E-05
ENSG00000105122	64926	RASAL3	-6.90021	4.06E-08	1.20E-05
ENSG00000160446	84885	ZDHHC12	-6.88341	2.53E-07	3.18E-05
ENSG00000011451	58525	WIZ	-6.85126	7.17E-07	6.28E-05
ENSG00000074356	55421	NCBP3	-6.78029	7.77E-07	6.46E-05
ENSG00000197061	8364	H4C3	-6.76258	1.66E-06	0.000119
ENSG00000164751	5828	PEX2	-6.67494	2.20E-09	1.67E-06
ENSG00000108651	55813	UTP6	-6.61213	2.79E-07	3.36E-05
ENSG00000103024	4832	NME3	-6.55338	8.80E-07	7.14E-05
ENSG00000137441	83888	FGFBP2	-6.5242	1.36E-10	4.60E-07

ENSG00000105486	3978	LIG1	-6.52144	2.14E-07	2.96E-05
ENSG00000157837	121665	SPPL3	-6.50977	9.02E-07	7.23E-05
ENSG00000155008	139322	APOOL	-6.47713	7.38E-07	6.37E-05
ENSG00000113282	9685	CLINT1	-6.45332	1.28E-06	9.65E-05
ENSG00000106948	80709	AKNA	-6.40985	2.00E-06	0.000137
ENSG00000187164	57698	SHTN1	-6.39196	5.16E-07	5.03E-05
ENSG00000188994	23036	ZNF292	-6.28152	1.70E-08	6.66E-06
ENSG00000103707	123263	MTFMT	-6.25035	5.47E-08	1.42E-05
ENSG00000069974	5873	RAB27A	-6.17882	7.65E-07	6.46E-05
ENSG00000145780	56929	FEM1C	-6.1715	2.91E-08	1.03E-05
ENSG00000166788	113174	SAAL1	-5.82604	1.42E-08	6.37E-06
ENSG00000140543	55070	DET1	-5.69703	3.31E-08	1.11E-05
ENSG00000108433	9570	GOSR2	-5.65193	9.09E-08	1.70E-05
ENSG00000127337	8089	YEATS4	-5.64264	4.84E-08	1.31E-05
ENSG00000133243	55643	BTBD2	-5.63849	1.39E-06	0.000102
ENSG00000131697	261734	NPHP4	-5.60746	7.76E-08	1.60E-05
ENSG00000161956	26168	SENP3	-5.54924	6.68E-08	1.55E-05
ENSG00000167130	57171	DOLPP1	-5.47956	1.62E-07	2.54E-05
ENSG00000170315	7314	UBB	-5.45388	2.73E-09	1.67E-06
ENSG00000151292	1456	CSNK1G3	-5.45352	2.14E-07	2.96E-05
ENSG00000091592	22861	NLRP1	-5.42847	1.06E-07	1.88E-05
ENSG00000199990	56664	VTRNA1-1	-5.18294	9.09E-08	1.70E-05
ENSG00000109534	54433	GAR1	-5.14099	2.55E-07	3.18E-05
ENSG00000113360	29102	DROSHA	-5.13379	3.55E-07	3.93E-05
ENSG00000272933	NA	NA	-5.12682	5.69E-07	5.33E-05
ENSG00000269967	NA	NA	-5.06786	2.40E-07	3.11E-05
ENSG00000101868	5422	POLA1	-5.04014	2.24E-07	3.02E-05
ENSG00000284735	NA	NA	-4.7731	1.14E-06	8.74E-05
ENSG00000185158	114659	LRRC37B	-4.73037	7.04E-08	1.58E-05
ENSG00000016864	55830	GLT8D1	-4.63084	1.30E-06	9.65E-05
ENSG00000095321	1384	CRAT	-4.25649	6.48E-07	5.98E-05
ENSG00000240143	NA	NA	-4.15968	1.05E-06	8.10E-05
ENSG00000101928	56180	MOSPD1	-4.13188	1.70E-06	0.000121
ENSG00000068784	55133	SRBD1	4.601584	1.76E-06	0.000123
ENSG00000102531	22862	FNDC3A	5.340969	6.76E-07	6.02E-05
ENSG00000130748	54958	TMEM160	5.414088	1.82E-06	0.000126
ENSG00000228923	NA	NA	5.609354	5.41E-07	5.21E-05
ENSG00000224470	342371	ATXN1L	5.623549	9.13E-10	1.02E-06
ENSG00000180198	1104	RCC1	5.633241	1.45E-06	0.000105
ENSG00000166165	1152	CKB	5.696366	2.20E-06	0.000148
ENSG00000172006	115196	ZNF554	5.736218	4.79E-07	4.89E-05
ENSG00000162396	25973	PARS2	5.888286	2.04E-06	0.000139
ENSG00000103995	22995	CEP152	6.003753	1.61E-07	2.54E-05
ENSG00000111052	8825	LIN7A	6.008707	9.24E-07	7.32E-05
ENSG00000170779	55038	CDCA4	6.034166	2.95E-07	3.43E-05
ENSG00000156504	159090	PABIR2	6.050524	4.34E-07	4.50E-05
ENSG00000135164	9988	DMTF1	6.16258	4.77E-09	2.47E-06
ENSG00000120798	7181	NR2C1	6.237742	3.24E-07	3.70E-05
ENSG00000114626	80325	ABTB1	6.293339	1.02E-06	8.02E-05
ENSG00000113597	80006	TRAPPC13	6.296571	1.92E-07	2.87E-05
ENSG00000165861	53349	ZFYVE1	6.50642	6.80E-07	6.02E-05
ENSG00000136933	10244	RABEPK	6.527581	2.15E-07	2.96E-05
ENSG00000095906	10101	NUBP2	6.750942	2.64E-07	3.24E-05
ENSG00000125089	54436	SH3TC1	6.781235	1.54E-07	2.53E-05
ENSG00000119596	56252	YLPM1	6.89416	7.38E-08	1.60E-05
ENSG00000145936	3779	KCNMB1	6.977433	1.45E-07	2.45E-05
ENSG00000167186	10229	COQ7	7.188853	1.30E-06	9.65E-05
ENSG00000136875	9128	PRPF4	7.390408	2.95E-07	3.43E-05
ENSG00000164124	55314	TMEM144	7.509647	1.34E-08	6.37E-06
ENSG00000146676	5814	PURB	7.714406	1.75E-07	2.68E-05
ENSG00000115935	7456	WIPF1	7.728039	9.00E-08	1.70E-05
ENSG00000110514	8567	MADD	7.900487	4.47E-08	1.25E-05
ENSG00000136717	274	BIN1	8.072885	2.31E-10	5.19E-07
ENSG00000140320	22893	BAHD1	8.151285	4.10E-08	1.20E-05
ENSG00000142185	7226	TRPM2	8.489176	9.91E-08	1.80E-05

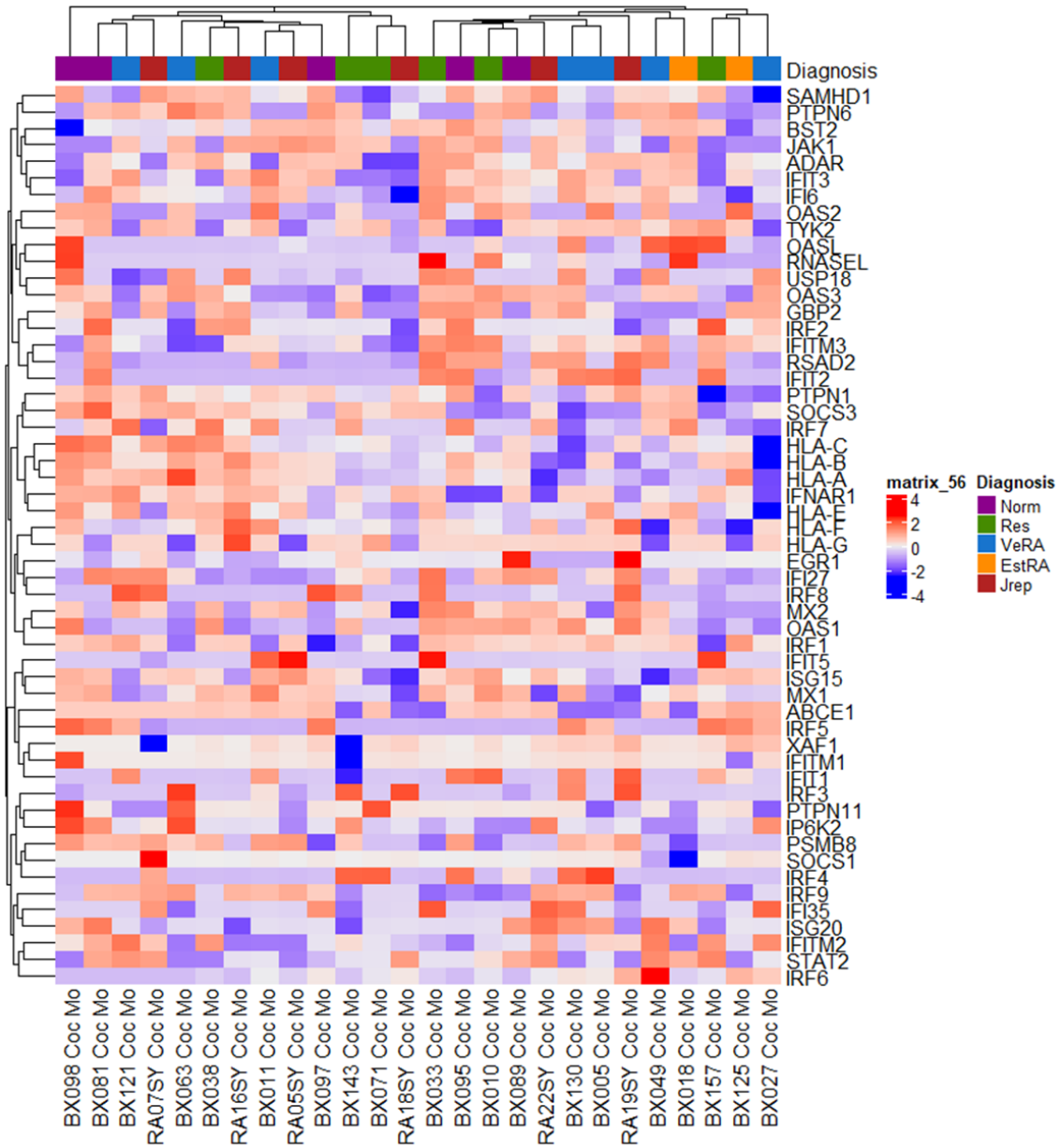

Appendix Figure 8: IFN-α/β signalling pathway genes. Fibroblasts and macrophages were co-cultured and treated with TNF-α for 16 hours. RNA was isolated and bulk RNA sequencing performed. Gene counts from the macrophage sequencing data were subject to variance stabilising transformation (VST) and genes known to be involved in the IFN-α/β signalling pathways shown as a heatmap. Coloured bar at the top indicates the diagnosis of fibroblast donor. Norm = non-inflamed, Res = resolving, VeRA = very early RA, EstRA = established RA, JRep = joint replacement.

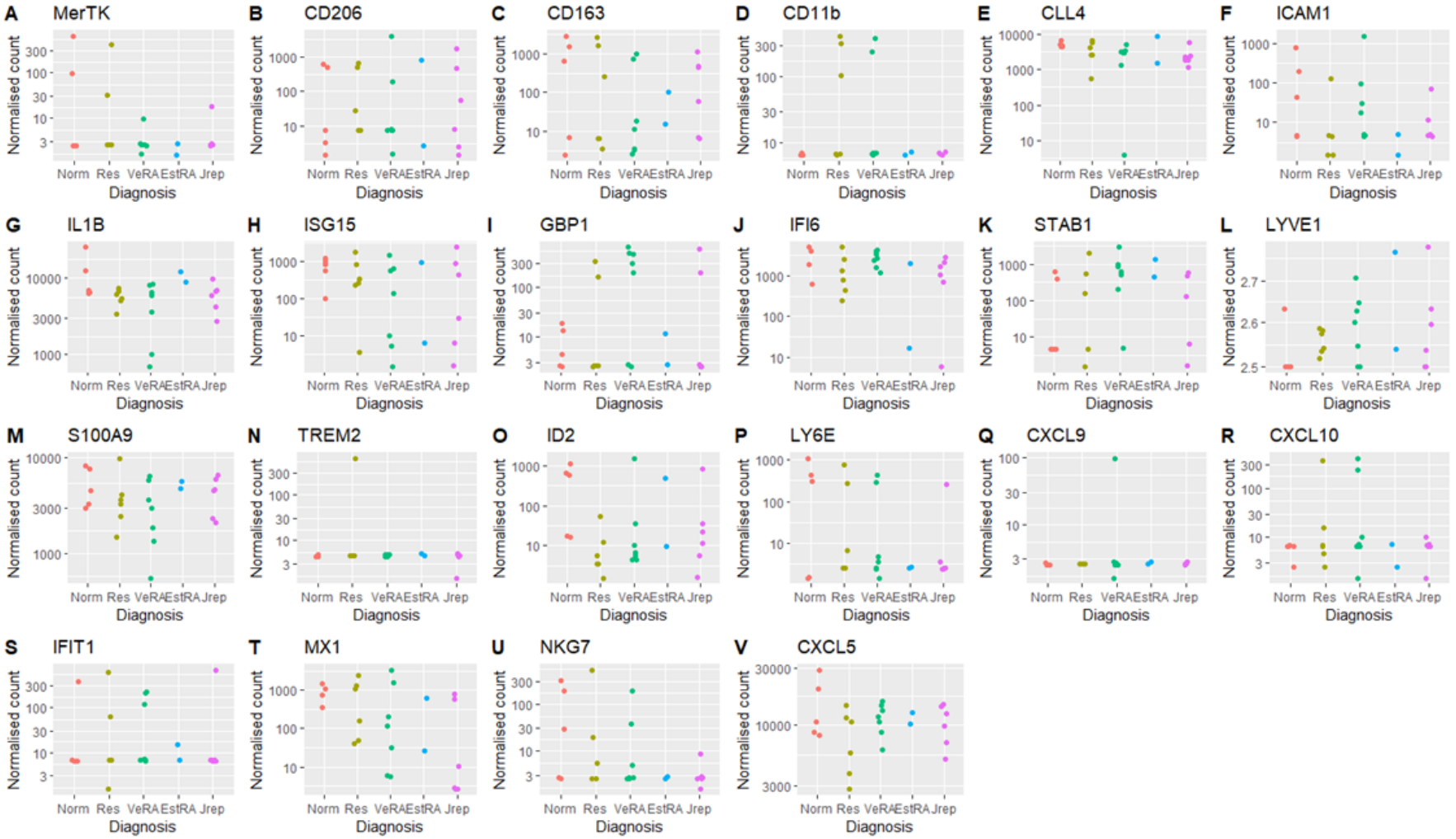

Appendix Figure 9: Counts plots of potential genes of interest. Fibroblasts and macrophages were co-cultured and treated with TNF-α for 16 hours. RNA was isolated and bulk RNA sequencing performed. To assess the effect of fibroblast diagnosis on known macrophage genes of interest, counts plots were plotted for **(A-P)** genes from (133) and **(Q-V)** genes from (143).

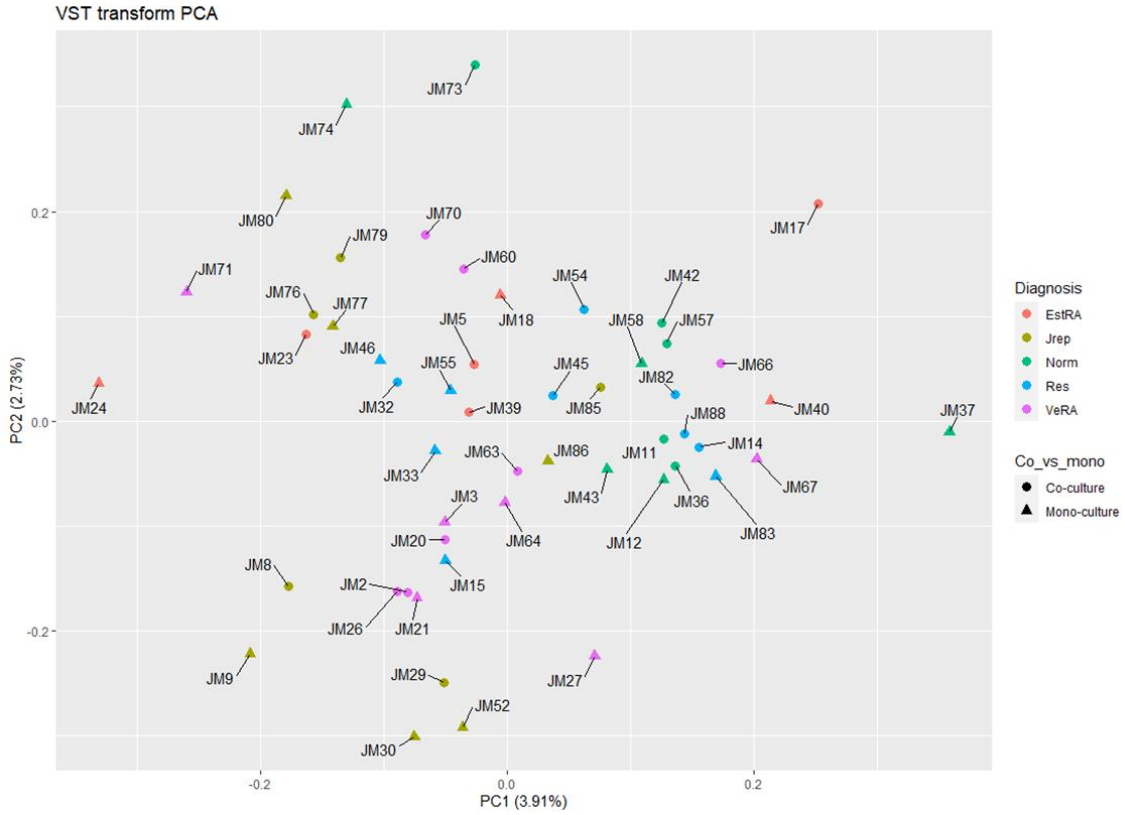

Appendix Figure 10: PCA of all fibroblasts. Fibroblasts and macrophages were co-cultured and treated with TNF-α for 16 hours. RNA was isolated and bulk RNA sequencing performed. Gene counts from the fibroblasts in mono-culture and that were co-cultured with macrophages, were subject to variance stabilising transformation (VST) and principal component analysis performed.

Appendix Table 14: The 100 most significantly differentially expressed genes of VeRA compared to Res fibroblasts that were co-cultured with macrophages

Ensembl ID	Entrez	HGNC symbol	Log2FC	pvalue	padj
ENSG00000133597	90956	ADCK2	-7.191911886	5.71E-07	7.49E-05
ENSG00000197894	128	ADH5	-6.608631133	8.82E-07	9.45E-05
ENSG00000105676	93436	ARMC6	-6.532962971	1.34E-10	5.47E-07
ENSG00000133315	28992	MACROD1	-6.297780406	1.22E-11	9.96E-08
ENSG00000132017	90379	DCAF15	-6.293142463	2.87E-08	1.30E-05
ENSG00000102858	23295	MGRN1	-6.267661644	1.27E-06	0.000117795
ENSG00000156172	157657	CFAP418	-6.222601319	4.87E-09	7.09E-06
ENSG00000157837	121665	SPPL3	-6.100083532	1.01E-06	0.000105101
ENSG00000165355	254170	FBXO33	-6.035288008	1.41E-07	3.11E-05
ENSG00000111727	29915	HCFC2	-5.845043954	5.25E-09	7.09E-06
ENSG00000122778	57670	KIAA1549	-5.813824527	2.01E-08	1.29E-05
ENSG00000165935	341346	SMCO2	-5.782225097	4.69E-07	6.82E-05
ENSG00000126003	5326	PLAGL2	-5.749710428	5.44E-07	7.26E-05
ENSG00000155666	79831	KDM8	-5.729050595	2.40E-08	1.30E-05
ENSG00000122376	54537	SHLD2	-5.686752659	1.54E-06	0.000133668
ENSG00000148384	56623	INPP5E	-5.664372296	3.92E-08	1.39E-05
ENSG00000130005	2593	GAMT	-5.613533142	4.92E-07	6.91E-05
ENSG00000152642	23171	GPD1L	-5.487992154	2.57E-08	1.30E-05
ENSG00000140459	1583	CYP11A1	-5.451891995	6.93E-08	1.94E-05
ENSG00000144559	132001	TAMM41	-5.442821864	2.73E-08	1.30E-05
ENSG00000113971	27031	NPHP3	-5.440397411	8.78E-07	9.45E-05
ENSG00000139629	11226	GALNT6	-5.304229323	1.07E-07	2.72E-05
ENSG00000158941	57805	CCAR2	-5.225358715	1.20E-07	2.79E-05
ENSG00000160602	284086	NEK8	-5.209840008	2.68E-07	4.34E-05
ENSG00000213757	643932	RPS3AP20	-5.163688509	6.04E-07	7.68E-05
ENSG00000185115	56160	NSMCE3	-5.160190194	1.52E-07	3.25E-05
ENSG00000124641	9477	MED20	-5.054375455	1.79E-07	3.33E-05
ENSG00000074935	51175	TUBE1	-5.049487569	1.11E-06	0.000111346
ENSG00000130592	4046	LSP1	-5.043953935	6.20E-07	7.68E-05
ENSG00000176182	339344	MYPOP	-5.012262254	1.61E-08	1.29E-05
ENSG00000154511	388650	DIPK1A	-4.990319751	2.61E-07	4.33E-05
ENSG00000133937	145258	GSC	-4.95891522	3.41E-07	5.34E-05
ENSG00000275630	NA	NA	-4.95827117	1.66E-07	3.33E-05
ENSG00000121152	23397	NCAPH	-4.951653255	6.23E-07	7.68E-05
ENSG00000171408	27115	PDE7B	-4.92505902	1.15E-06	0.000111346
ENSG00000114378	3373	HYAL1	-4.831801627	2.53E-07	4.29E-05
ENSG00000167842	79003	MIS12	-4.809122446	1.63E-06	0.000138483
ENSG00000182389	785	CACNB4	-4.685772656	1.37E-06	0.000123487
ENSG00000234380	100506385	LINC01426	-4.651726908	1.81E-07	3.33E-05
ENSG00000078487	55063	ZCWPW1	-4.616123227	1.68E-06	0.000139901
ENSG00000047644	55841	WWC3	-4.597498867	7.32E-07	8.46E-05
ENSG00000132821	128434	VSTM2L	-4.576008667	5.35E-07	7.26E-05
ENSG00000100162	79019	CENPM	-4.343100995	1.68E-06	0.000139901
ENSG00000175643	116028	RMI2	-4.306897341	6.17E-07	7.68E-05
ENSG00000213676	1388	ATF6B	-4.271673158	2.05E-06	0.000167173
ENSG00000061938	10188	TNK2	-4.214651065	6.15E-08	1.92E-05
ENSG00000196177	36	ACADSB	-4.189156447	1.24E-06	0.000116758
ENSG00000143248	8490	RGS5	-4.115908098	1.48E-06	0.000130195
ENSG00000120262	80129	CCDC170	4.640872359	1.25E-06	0.000116758
ENSG00000010539	7752	ZNF200	4.820287196	2.72E-07	4.34E-05
ENSG00000118707	60436	TGIF2	4.988500093	7.59E-07	8.58E-05
ENSG00000151718	80014	WWC2	5.018809464	6.82E-07	8.05E-05
ENSG00000184752	55967	NDUFA12	5.24765258	1.49E-06	0.000130195
ENSG00000115274	83444	INO80B	5.276990406	6.40E-07	7.78E-05
ENSG00000128654	10651	MTX2	5.356496217	1.60E-07	3.33E-05
ENSG00000126858	55288	RHOT1	5.378365163	1.03E-07	2.69E-05
ENSG00000165533	123016	TTC8	5.556113715	9.10E-07	9.62E-05
ENSG00000123124	11059	WWP1	5.625232724	1.37E-07	3.10E-05
ENSG00000127125	79717	PPCS	5.631524511	6.20E-08	1.92E-05
ENSG00000058729	55781	RIOK2	5.6640794	6.77E-07	8.05E-05
ENSG00000167130	57171	DOLPP1	5.673664427	1.59E-06	0.000136507
ENSG00000105723	2931	GSK3A	5.692976824	1.23E-06	0.000116758
ENSG00000090971	57106	NAT14	5.713086148	1.08E-06	0.00011032

ENSG00000085491	29957	SLC25A24	5.78162859	6.37E-08	1.92E-05
ENSG00000107771	54462	CCSER2	5.799568553	1.32E-06	0.000120682
ENSG00000185900	84197	POMK	5.8225867	1.13E-06	0.000111346
ENSG00000183688	359845	RFLNB	5.823163343	5.08E-07	7.01E-05
ENSG00000164548	29896	TRA2A	5.827917095	1.03E-06	0.000106316
ENSG00000169857	57099	AVEN	5.89199309	3.98E-07	5.89E-05
ENSG00000163249	151195	CCNYL1	5.90649304	1.98E-08	1.29E-05
ENSG00000172456	55277	FGGY	5.930650992	6.10E-09	7.09E-06
ENSG00000066135	9682	KDM4A	5.966804266	1.73E-07	3.33E-05
ENSG00000111271	80724	ACAD10	6.023497969	3.37E-08	1.31E-05
ENSG00000180817	5464	PPA1	6.109419561	7.38E-07	8.46E-05
ENSG00000121064	59342	SCPEP1	6.12143059	8.63E-07	9.45E-05
ENSG00000196365	9361	LONP1	6.174791626	1.49E-06	0.000130195
ENSG00000141580	56270	WDR45B	6.198227189	9.89E-08	2.68E-05
ENSG00000160062	653121	ZBTB8A	6.253245826	1.99E-07	3.53E-05
ENSG00000123810	80776	B9D2	6.267534657	3.30E-08	1.31E-05
ENSG00000137038	90871	DMAC1	6.271671528	1.15E-06	0.000111346
ENSG00000130935	25926	NOL11	6.340239378	1.84E-07	3.33E-05
ENSG00000164125	51313	GASK1B	6.387521587	4.91E-07	6.91E-05
ENSG00000153015	10283	CWC27	6.403962952	6.60E-08	1.92E-05
ENSG00000186577	221491	SMIM29	6.442726802	1.13E-07	2.72E-05
ENSG00000102038	6594	SMARCA1	6.511614686	3.04E-08	1.30E-05
ENSG00000130958	11046	SLC35D2	6.601277303	6.45E-08	1.92E-05
ENSG00000112149	9308	CD83	6.772317205	3.91E-07	5.89E-05
ENSG00000257267	10778	ZNF271P	6.82960372	2.04E-06	0.000167173
ENSG00000119185	9270	ITGB1BP1	7.123010133	7.89E-07	8.80E-05
ENSG00000140262	6938	TCF12	7.199255983	2.06E-08	1.29E-05
ENSG00000136689	3557	IL1RN	7.320250777	2.09E-07	3.61E-05
ENSG00000160131	203547	VMA21	7.355912736	1.97E-08	1.29E-05
ENSG00000166133	27079	RPUSD2	7.397307492	1.14E-07	2.72E-05
ENSG00000113456	5810	RAD1	7.45565695	3.93E-08	1.39E-05
ENSG00000106853	22949	PTGR1	7.507095589	3.54E-07	5.43E-05
ENSG00000139718	23067	SETD1B	7.527629267	1.68E-07	3.33E-05
ENSG00000122042	5412	UBL3	7.648557218	7.17E-09	7.29E-06
ENSG00000127241	5648	MASP1	8.011487351	2.46E-08	1.30E-05
ENSG00000198015	28977	MRPL42	8.060810747	3.95E-09	7.09E-06
ENSG00000109689	57620	STIM2	8.148214414	7.51E-10	2.04E-06

Appendix Table 15: The 100 most significantly differentially expressed genes of VeRA compared to Norm fibroblasts that were co-cultured with macrophages

Ensembl ID	Entrez	HGNC symbol	Log2FC	pvalue	padj
ENSG00000185507	3665	IRF7	-8.42771	3.29E-13	2.58E-09
ENSG00000105447	83743	GRWD1	-7.879	3.70E-10	4.83E-07
ENSG00000127948	5447	POR	-7.77448	3.54E-08	1.32E-05
ENSG00000148362	286257	PAXX	-7.61552	1.72E-07	3.84E-05
ENSG00000213523	10011	SRA1	-7.55679	8.46E-09	4.14E-06
ENSG00000117697	25936	NSL1	-7.5191	3.01E-08	1.24E-05
ENSG00000129219	5338	PLD2	-7.49242	5.26E-11	2.06E-07
ENSG00000170619	28991	COMMD5	-7.44846	3.30E-07	4.79E-05
ENSG00000166135	55662	HIF1AN	-7.39493	2.64E-08	1.15E-05
ENSG00000149476	26007	TKFC	-7.33077	1.89E-06	0.000146
ENSG00000160551	57551	TAOK1	-7.29393	1.16E-06	0.00011
ENSG00000131381	64145	RBSN	-7.27074	2.72E-10	4.83E-07
ENSG00000166532	57494	RIMKLB	-7.24746	6.28E-07	7.93E-05
ENSG00000119403	26147	PHF19	-7.23573	2.65E-07	4.32E-05
ENSG00000106012	23288	IQCE	-7.15021	2.15E-10	4.83E-07
ENSG00000157837	121665	SPPL3	-7.14094	4.03E-08	1.44E-05
ENSG00000144895	83939	EIF2A	-7.01303	1.19E-06	0.000111
ENSG00000122126	4952	OCRL	-6.84683	1.68E-06	0.000142
ENSG00000197555	26037	SIPA1L1	-6.81837	1.04E-07	2.72E-05
ENSG00000136933	10244	RABEPK	-6.69864	1.06E-06	0.000106
ENSG00000143889	92906	HNRNPLL	-6.69539	2.01E-07	4.32E-05
ENSG00000145476	285440	CYP4V2	-6.67111	1.89E-06	0.000146
ENSG00000125898	83541	FAM110A	-6.6568	8.92E-07	9.54E-05
ENSG00000269958	NA	NA	-6.57826	1.26E-06	0.000111

ENSG00000128915	79664	ICE2	-6.52086	1.06E-06	0.000106
ENSG00000173950	152002	XXYLT1	-6.51289	1.02E-06	0.000105
ENSG00000047410	7175	TPR	-6.41839	1.79E-06	0.000146
ENSG00000133195	201266	SLC39A11	-6.33632	2.09E-07	4.32E-05
ENSG00000167315	10449	ACAA2	-6.24647	3.82E-07	5.34E-05
ENSG00000186174	283149	BCL9L	-6.18926	2.44E-07	4.32E-05
ENSG00000166261	7753	ZNF202	-6.17695	1.11E-07	2.72E-05
ENSG00000132000	79883	PODNL1	-6.12222	1.19E-06	0.000111
ENSG00000179958	79077	DCTPP1	-6.12157	1.60E-06	0.000136
ENSG00000159079	56683	CFAP298	-5.94818	2.40E-07	4.32E-05
ENSG00000149582	84866	TMEM25	-5.9157	5.14E-09	3.42E-06
ENSG00000069020	375449	MAST4	-5.85246	6.27E-08	1.89E-05
ENSG00000147121	55634	KRBOX4	-5.7075	2.72E-07	4.32E-05
ENSG00000196367	8295	TRRAP	-5.66947	1.87E-06	0.000146
ENSG00000073111	4171	MCM2	-5.65295	1.50E-06	0.00013
ENSG00000138663	51138	COPS4	-5.58467	1.10E-06	0.000108
ENSG00000158050	1844	DUSP2	-5.54581	7.86E-07	8.93E-05
ENSG00000100084	7290	HIRA	-5.4969	3.18E-07	4.70E-05
ENSG00000260025	NA	NA	-5.47868	7.30E-09	4.08E-06
ENSG00000128578	57464	STRIP2	-5.39621	6.85E-07	8.52E-05
ENSG00000165097	221656	KDM1B	-5.38803	8.58E-07	9.33E-05
ENSG00000179862	163732	CITED4	-5.34661	3.69E-09	3.21E-06
ENSG00000078403	8028	MLLT10	-5.32477	1.70E-07	3.84E-05
ENSG00000166432	84460	ZMAT1	-5.20952	1.60E-06	0.000136
ENSG00000100979	5360	PLTP	-5.18676	2.52E-07	4.32E-05
ENSG00000165895	143872	ARHGAP42	-5.15487	2.48E-07	4.32E-05
ENSG00000075089	64431	ACTR6	-5.0973	1.26E-06	0.000111
ENSG00000174485	10260	DENND4A	-5.0639	4.97E-08	1.56E-05
ENSG00000168067	5871	MAP4K2	-5.04218	7.98E-07	8.93E-05
ENSG00000133731	3612	IMPA1	-5.0288	9.46E-08	2.72E-05
ENSG00000164758	90390	MED30	-4.7083	1.90E-06	0.000146
ENSG00000101442	79913	ACTR5	-4.57031	1.24E-06	0.000111
ENSG00000102221	9767	JADE3	-4.45487	3.10E-07	4.67E-05
ENSG00000010539	7752	ZNF200	4.922004	7.08E-07	8.55E-05
ENSG00000118707	60436	TGIF2	5.111653	1.90E-06	0.000146
ENSG00000137801	7057	THBS1	5.309607	3.33E-10	4.83E-07
ENSG00000126858	55288	RHOT1	5.455915	4.01E-07	5.51E-05
ENSG00000123124	11059	WWP1	5.543745	8.40E-07	9.26E-05
ENSG00000115274	83444	INO80B	5.557115	7.66E-07	8.93E-05
ENSG00000123810	80776	B9D2	5.779671	7.91E-07	8.93E-05
ENSG00000131747	7153	TOP2A	5.800039	4.14E-07	5.59E-05
ENSG00000085491	29957	SLC25A24	5.824433	2.69E-07	4.32E-05
ENSG00000163249	151195	CCNYL1	5.846335	1.37E-07	3.25E-05
ENSG00000172456	55277	FGGY	5.8611	4.93E-08	1.56E-05
ENSG00000165533	123016	TTC8	5.938332	9.67E-07	0.000101
ENSG00000111271	80724	ACAD10	6.167193	1.05E-07	2.72E-05
ENSG00000105723	2931	GSK3A	6.233611	9.01E-07	9.54E-05
ENSG00000130779	6249	CLIP1	6.316908	1.10E-07	2.72E-05
ENSG00000185900	84197	POMK	6.406637	4.49E-07	5.96E-05
ENSG00000164125	51313	GASK1B	6.414414	1.84E-06	0.000146
ENSG00000153015	10283	CWC27	6.470916	2.61E-07	4.32E-05
ENSG00000136485	10238	DCAF7	6.501328	1.06E-06	0.000106
ENSG00000160062	653121	ZBTB8A	6.586981	2.62E-07	4.32E-05
ENSG00000130958	11046	SLC35D2	6.62902	2.76E-07	4.32E-05
ENSG00000107771	54462	CCSER2	6.718923	2.63E-07	4.32E-05
ENSG00000108848	51747	LUC7L3	6.890355	2.49E-07	4.32E-05
ENSG00000110063	28960	DCPS	6.899573	3.41E-08	1.32E-05
ENSG00000129460	25983	NGDN	6.899673	1.24E-06	0.000111
ENSG00000149639	140710	SOGA1	6.952779	1.12E-06	0.000109
ENSG00000102125	6901	TAFAZZIN	6.978547	1.25E-06	0.000111
ENSG00000182872	8241	RBM10	7.010175	4.91E-08	1.56E-05
ENSG00000164576	79685	SAP30L	7.023948	7.20E-07	8.55E-05
ENSG00000153130	60592	SCOC	7.129301	7.19E-07	8.55E-05
ENSG00000160131	203547	VMA21	7.142339	2.05E-07	4.32E-05
ENSG00000074071	65993	MRPS34	7.239165	2.90E-07	4.46E-05
ENSG00000068028	11186	RASSF1	7.248571	4.78E-09	3.42E-06
ENSG00000140262	6938	TCF12	7.262524	9.87E-08	2.72E-05
ENSG00000095787	51322	WAC	7.362122	1.90E-09	1.86E-06

ENSG00000158186	22808	MRAS	7.421464	5.91E-07	7.59E-05
ENSG00000101966	331	XIAP	7.557433	1.25E-08	5.78E-06
ENSG00000007047	57787	MARK4	7.590883	3.49E-07	4.97E-05
ENSG00000162496	9249	DHRS3	7.621731	8.07E-09	4.14E-06
ENSG00000122257	5930	RBBP6	7.800384	5.23E-09	3.42E-06
ENSG00000112759	2030	SLC29A1	7.815983	5.33E-07	6.96E-05
ENSG00000109689	57620	STIM2	8.018675	7.10E-09	4.08E-06
ENSG00000122203	57179	KIAA1191	8.147586	1.03E-09	1.15E-06

Appendix Table 16: The 100 most significantly differentially expressed genes of VeRA compared to EstRA fibroblasts that were co-cultured with macrophages

Ensembl ID	Entrez	HGNC symbol	Log2FC	pvalue	padj
ENSG00000133104	23111	SPART	-7.88117	3.84E-07	7.17E-05
ENSG00000113318	4437	MSH3	-7.56538	1.47E-07	3.64E-05
ENSG00000187239	23048	FNBP1	-7.37523	3.1E-07	6.54E-05
ENSG00000108582	1362	CPD	-7.32982	2.32E-07	5.27E-05
ENSG00000132199	55556	ENOSF1	-7.32522	3.69E-07	7.12E-05
ENSG00000119720	55051	NRDE2	-7.30925	3.62E-08	1.45E-05
ENSG00000130363	83861	RSPH3	-7.25216	4.71E-07	8.42E-05
ENSG00000011143	54903	MKS1	-7.23696	7.38E-08	2.48E-05
ENSG00000141337	22901	ARSG	-7.16501	3.81E-08	1.45E-05
ENSG00000160957	9401	RECQL4	-7.13659	1.88E-11	3.95E-08
ENSG00000149269	5058	PAK1	-7.10577	4.65E-06	0.000384
ENSG00000129534	55320	MIS18BP1	-7.04716	1.54E-13	1.3E-09
ENSG00000116266	6814	STXBP3	-7.025	1.63E-08	8.06E-06
ENSG00000140320	22893	BAHD1	-6.92937	8.06E-11	1.13E-07
ENSG00000010165	51603	METTL13	-6.87561	2.97E-06	0.000287
ENSG00000148019	84131	CEP78	-6.86223	1.77E-07	4.13E-05
ENSG00000143889	92906	HNRNPLL	-6.6912	1.42E-06	0.000165
ENSG00000196290	60491	NIF3L1	-6.66213	3.37E-06	0.000308
ENSG00000164818	54919	DNAAF5	-6.64157	2.77E-08	1.22E-05
ENSG00000142784	23038	WDTC1	-6.53854	1.16E-06	0.000147
ENSG00000103707	123263	MTFMT	-6.45333	8.72E-08	2.53E-05
ENSG00000129295	23639	DNAAF11	-6.33374	4.19E-09	2.93E-06
ENSG00000152520	255967	PAN3	-6.28401	5.51E-07	8.9E-05
ENSG00000153094	10018	BCL2L11	-6.24879	4.55E-06	0.000384
ENSG00000112562	64094	SMOC2	-6.19183	5.96E-13	2.5E-09
ENSG00000161513	2232	FDXR	-6.13514	1.99E-06	0.000211
ENSG00000141040	57336	ZNF287	-6.08766	1.42E-09	1.32E-06
ENSG00000136490	80774	LIMD2	-6.08271	3.09E-06	0.000291
ENSG00000104133	80208	SPG11	-5.94413	3.56E-08	1.45E-05
ENSG00000140374	2108	ETFA	-5.89514	1.29E-06	0.000157
ENSG00000132964	1024	CDK8	-5.80923	3.36E-09	2.82E-06
ENSG00000144395	284992	CCDC150	-5.77241	1.44E-07	3.64E-05
ENSG00000163481	64320	RNF25	-5.72177	3.82E-09	2.92E-06
ENSG00000269821	10984	KCNQ1OT1	-5.65127	3.2E-06	0.000299
ENSG00000138614	81556	INTS14	-5.54364	2.71E-08	1.22E-05
ENSG00000166471	440026	TMEM41B	-5.53913	3E-12	8.41E-09
ENSG00000019485	56981	PRDM11	-5.51635	4.61E-09	2.98E-06
ENSG00000068024	9759	HDAC4	-5.4986	9.66E-07	0.000131
ENSG00000280332	NA	NA	-5.46695	6.11E-09	3.66E-06
ENSG00000157306	NA	NA	-5.4634	7.44E-07	0.000112
ENSG00000154874	284047	CCDC144B	-5.46258	8.39E-08	2.53E-05
ENSG00000118513	4602	MYB	-5.44687	1.32E-08	6.94E-06
ENSG00000137878	145781	GCOM1	-5.40107	6.54E-09	3.66E-06
ENSG00000143536	49860	CRNN	-5.37557	3.42E-07	6.94E-05
ENSG00000037474	54888	NSUN2	-5.28507	3.84E-06	0.000329
ENSG00000137492	5612	THAP12	-5.18425	3.37E-10	3.54E-07
ENSG00000123407	3228	HOXC12	-5.14367	5.75E-07	9.12E-05
ENSG00000108590	51003	MED31	-5.13739	2.61E-06	0.000265
ENSG00000159714	29800	ZDHHC1	-5.06558	5.3E-07	8.9E-05
ENSG00000163535	151246	SGO2	-5.06112	6.92E-07	0.000108
ENSG00000123739	81579	PLA2G12A	-5.04178	1.65E-07	3.95E-05
ENSG00000103932	26015	RPAP1	-4.95952	8.32E-08	2.53E-05
ENSG00000119684	27030	MLH3	-4.9559	1.76E-10	2.12E-07

ENSG00000145246	57205	ATP10D	-4.94299	1.06E-06	0.000142
ENSG00000256087	9668	ZNF432	-4.90861	1.16E-06	0.000147
ENSG00000196312	84278	MFSD14C	-4.84722	3.84E-06	0.000329
ENSG00000159788	6002	RGS12	-4.81858	2.67E-06	0.000267
ENSG00000163209	6707	SPRR3	-4.78599	1.28E-06	0.000157
ENSG00000253802	1.13E+08	SIRLNT	-4.74627	8.69E-07	0.000125
ENSG00000109654	23321	TRIM2	-4.72483	2.75E-07	6.08E-05
ENSG00000234683	NA	NA	-4.71739	3.39E-06	0.000308
ENSG00000109762	83891	SNX25	-4.65659	1.02E-07	2.86E-05
ENSG00000043514	54802	TRIT1	-4.47033	5.69E-08	2.08E-05
ENSG00000141642	55520	ELAC1	-4.41303	3.03E-06	0.000289
ENSG00000104613	55174	INTS10	-4.39442	1.36E-06	0.000161
ENSG00000260428	642658	SCX	-4.30723	1.52E-06	0.000173
ENSG00000197323	51592	TRIM33	-4.25246	1.63E-06	0.00018
ENSG00000221886	63920	ZBED8	-4.15513	1.09E-07	2.95E-05
ENSG00000200913	94161	SNORD46	-4.11741	3.47E-07	6.94E-05
ENSG00000196405	51466	EVL	-4.00215	4.1E-07	7.48E-05
ENSG00000249115	23354	HAUS5	-3.91106	1.7E-06	0.000186
ENSG00000272841	NA	NA	-3.37683	1.31E-06	0.000158
ENSG00000167981	146434	ZNF597	-3.16079	1.08E-06	0.000142
ENSG00000010539	7752	ZNF200	4.977058	3.68E-06	0.000322
ENSG00000126858	55288	RHOT1	5.499635	2.16E-06	0.000227
ENSG00000085491	29957	SLC25A24	5.644799	3.56E-06	0.000314
ENSG00000163249	151195	CCNYL1	5.928332	8.85E-07	0.000125
ENSG00000123124	11059	WWP1	6.1193	1.18E-06	0.000149
ENSG00000103647	10391	CORO2B	6.146117	3.56E-06	0.000314
ENSG00000106397	8985	PLOD3	6.31647	1.47E-07	3.64E-05
ENSG00000151718	80014	WWC2	6.358191	7.3E-08	2.48E-05
ENSG00000111271	80724	ACAD10	6.37479	5.45E-07	8.9E-05
ENSG00000123810	80776	B9D2	6.394799	1.44E-06	0.000166
ENSG00000106462	2146	EZH2	6.498539	2.86E-06	0.000283
ENSG00000092470	79968	WDR76	6.555135	2.93E-06	0.000286
ENSG00000110063	28960	DCPS	6.764717	3.73E-07	7.12E-05
ENSG00000121064	59342	SCPEP1	6.802862	2.5E-06	0.000256
ENSG00000167118	81605	URM1	6.918285	4.32E-11	7.25E-08
ENSG00000144118	5899	RALB	7.112218	1.57E-06	0.000176
ENSG00000141759	10907	TXNL4A	7.134918	5.19E-07	8.9E-05
ENSG00000151148	89910	UBE3B	7.137739	1.97E-06	0.000211
ENSG00000140406	59274	TLNRD1	7.251132	3.41E-06	0.000308
ENSG00000132294	23167	EFR3A	7.300431	8.12E-07	0.00012
ENSG00000100519	5706	PSMC6	7.367325	2.2E-06	0.000228
ENSG00000140262	6938	TCF12	7.524587	3.12E-07	6.54E-05
ENSG00000169375	25942	SIN3A	7.556275	7.37E-07	0.000112
ENSG00000162923	80232	WDR26	7.731241	9.26E-07	0.000127
ENSG00000152284	83439	TCF7L1	7.776178	8.92E-07	0.000125
ENSG00000121898	119587	CPXM2	8.373322	5.01E-07	8.77E-05
ENSG00000136270	9238	TBRG4	8.503583	8.49E-08	2.53E-05

Appendix Table 17: The 100 most significantly differentially expressed genes of VeRA compared to JRep fibroblasts that were co-cultured with macrophages

Ensembl ID	Entrez	HGNC symbol	Log2FC	pvalue	padj
ENSG00000119403	26147	PHF19	-8.462509296	3.02E-08	2.60E-05
ENSG00000106477	95681	CEP41	-7.790021399	1.09E-06	0.000207617
ENSG00000158321	26053	AUTS2	-7.686558275	1.96E-07	8.37E-05
ENSG00000197635	1803	DPP4	-7.663741464	8.29E-08	5.70E-05
ENSG00000120616	80314	EPC1	-7.615120205	5.11E-07	0.000140643
ENSG00000133104	23111	SPART	-7.501450696	1.30E-06	0.000227062
ENSG00000111653	51147	ING4	-7.500519996	2.62E-07	9.36E-05
ENSG00000152409	133746	JMY	-7.4337944	1.32E-06	0.000227062
ENSG00000186566	23131	GPATCH8	-7.342003309	1.00E-07	6.32E-05
ENSG00000139437	84260	TCHP	-7.330786797	4.74E-09	7.66E-06
ENSG00000110871	84274	COQ5	-7.267769201	2.30E-07	8.78E-05

ENSG00000102858	23295	MGRN1	-7.148748624	1.02E-06	0.000204528
ENSG00000111605	11052	CPSF6	-6.946433495	1.89E-06	0.000295362
ENSG00000108786	3292	HSD17B1	-6.922759758	3.23E-09	7.66E-06
ENSG00000144063	7851	MALL	-6.751042975	1.73E-07	7.76E-05
ENSG00000179958	79077	DCTPP1	-6.645731743	1.25E-06	0.000222387
ENSG00000065491	55633	TBC1D22B	-6.609118177	3.59E-07	0.000117016
ENSG00000112305	60682	SMAP1	-6.606644297	7.28E-07	0.000178521
ENSG00000173418	51126	NAA20	-6.582494134	5.38E-07	0.000142048
ENSG00000150977	196383	RILPL2	-6.479903745	4.75E-06	0.000494962
ENSG00000148677	27063	ANKRD1	-6.446224081	2.08E-06	0.000295362
ENSG00000162086	7627	ZNF75A	-6.440854538	6.81E-07	0.000171629
ENSG00000110427	25758	KIAA1549L	-6.244604409	3.77E-06	0.000417379
ENSG00000163827	79442	LRRC2	-6.21881059	3.04E-06	0.000377692
ENSG00000166881	23306	NEMP1	-6.194845236	2.03E-07	8.37E-05
ENSG00000120314	54853	WDR55	-6.163406117	2.83E-06	0.000355156
ENSG00000118507	9465	AKAP7	-6.155878372	1.79E-08	2.05E-05
ENSG00000103657	8925	HERC1	-6.15497302	2.30E-06	0.000307632
ENSG00000105176	8725	URI1	-6.15311482	2.10E-06	0.000295362
ENSG00000108591	1819	DRG2	-6.126419869	2.27E-07	8.78E-05
ENSG00000157456	9133	CCNB2	-6.04998341	8.18E-07	0.000191524
ENSG00000100522	64841	GNPNAT1	-5.988538628	9.70E-07	0.000203982
ENSG00000104529	1936	EEF1D	-5.929039529	1.42E-08	1.83E-05
ENSG00000138834	23162	MAPK8IP3	-5.915310634	1.40E-06	0.000232732
ENSG00000012660	60481	ELOVL5	-5.887506549	3.86E-06	0.000418272
ENSG00000151388	81792	ADAMTS12	-5.862041635	3.93E-07	0.000122739
ENSG00000123575	139231	FAM199X	-5.8368458	6.86E-08	5.44E-05
ENSG00000251194	NA	NA	-5.826741597	3.34E-10	2.45E-06
ENSG00000141956	63977	PRDM15	-5.823479264	1.15E-06	0.000212442
ENSG00000136052	84102	SLC41A2	-5.817539358	4.85E-07	0.000138932
ENSG00000111666	56994	CHPT1	-5.791256961	2.03E-06	0.000295362
ENSG00000130758	4294	MAP3K10	-5.736075831	1.96E-06	0.000295362
ENSG00000068784	55133	SRBD1	-5.671757158	1.55E-07	7.25E-05
ENSG00000006118	54972	TMEM132A	-5.518424307	2.26E-09	7.66E-06
ENSG00000112293	2822	GPLD1	-5.356161876	3.50E-06	0.000404807
ENSG00000242086	727956	SDHAP2	-5.226709309	5.19E-07	0.000140643
ENSG00000164687	2171	FABP5	-5.224347021	2.86E-07	9.81E-05
ENSG00000155868	9443	MED7	-5.145238675	2.97E-08	2.60E-05
ENSG00000119906	55719	SLF2	-5.114566603	2.63E-07	9.36E-05
ENSG00000181031	9501	RPH3AL	-5.048448382	1.22E-07	6.32E-05
ENSG00000149262	92105	INTS4	-5.028257704	1.37E-06	0.000231667
ENSG00000233521	105372978	LINC01638	-5.017911322	8.50E-07	0.000194705
ENSG00000148225	114987	WDR31	-4.883235721	2.04E-06	0.000295362
ENSG00000143768	7044	LEFTY2	-4.874634593	3.82E-06	0.000418272
ENSG00000250251	353511	PKD1P6	-4.769548632	1.29E-07	6.32E-05
ENSG00000070718	10947	AP3M2	-4.715231018	2.74E-06	0.000352687
ENSG00000121417	10520	ZNF211	-4.704401599	1.12E-06	0.000210242
ENSG00000171169	203245	NAIF1	-4.697653349	3.62E-06	0.000410494
ENSG00000034533	28990	ASTE1	-4.642963137	4.41E-06	0.000463547
ENSG00000196411	2050	EPHB4	-4.612400585	9.63E-07	0.000203982
ENSG00000156970	701	BUB1B	-4.390969177	2.08E-06	0.000295362
ENSG00000109466	11275	KLHL2	-4.384194199	1.84E-06	0.000295362
ENSG00000236296	441046	GUSBP5	-4.221657076	1.19E-06	0.000215958
ENSG00000273972	NA	NA	-4.176637756	3.37E-06	0.000394161
ENSG00000251151	100874365	HOXC-AS3	-4.01344776	3.61E-06	0.000410494

ENSG00000237686	101929705	SCIRT	-3.924067716	3.69E-06	0.000413735
ENSG00000257702	151534	LBX2-AS1	-3.864015703	4.85E-06	0.000499627
ENSG00000017427	3479	IGF1	-3.862481733	9.29E-07	0.000203735
ENSG00000198521	7594	ZNF43	-3.76194579	3.36E-06	0.000394161
ENSG00000077458	143684	FAM76B	5.071109389	1.56E-06	0.000254542
ENSG00000128654	10651	MTX2	5.41178261	2.18E-06	0.000298618
ENSG00000126858	55288	RHOT1	5.430911228	2.59E-06	0.000342357
ENSG00000127125	79717	PPCS	5.520396041	2.65E-06	0.000346299
ENSG00000041353	5874	RAB27B	5.58109293	1.90E-06	0.000295362
ENSG00000123124	11059	WWP1	5.821145863	2.12E-06	0.000295362
ENSG00000111271	80724	ACAD10	5.917712862	1.94E-06	0.000295362
ENSG00000163249	151195	CCNYL1	5.923522041	7.91E-07	0.000189519
ENSG00000131747	7153	TOP2A	5.950314962	1.06E-06	0.000206752
ENSG00000058729	55781	RIOK2	5.960159139	4.23E-06	0.000448918
ENSG00000123810	80776	B9D2	6.107226813	2.20E-06	0.000298618
ENSG00000155158	158219	TTC39B	6.111882104	2.81E-06	0.000355156
ENSG00000172456	55277	FGGY	6.150381924	1.05E-07	6.32E-05
ENSG00000162894	9214	FCMR	6.179409096	8.87E-07	0.000198825
ENSG00000153015	10283	CWC27	6.257610622	3.25E-06	0.000393614
ENSG00000116750	51377	UCHL5	6.344076694	6.83E-07	0.000171629
ENSG00000115183	85461	TANC1	6.379675721	3.15E-06	0.000386376
ENSG00000151718	80014	WWC2	6.501097437	4.14E-09	7.66E-06
ENSG00000066135	9682	KDM4A	6.503931797	4.52E-07	0.000132955
ENSG00000145777	85480	TSLP	6.614194551	9.95E-07	0.000204528
ENSG00000197579	10210	TOPORS	6.862528886	1.03E-06	0.000204528
ENSG00000151148	89910	UBE3B	6.914593105	3.35E-06	0.000394161
ENSG00000153885	79047	KCTD15	7.507552889	3.93E-06	0.000421861
ENSG00000086589	55696	RBM22	7.669988641	4.25E-07	0.000128819
ENSG00000147224	5631	PRPS1	7.673423325	1.25E-07	6.32E-05
ENSG00000135899	3431	SP110	7.784254528	3.63E-07	0.000117016
ENSG00000071537	6400	SEL1L	7.820326452	1.24E-07	6.32E-05
ENSG00000116030	7341	SUMO1	8.841174932	2.76E-08	2.60E-05
ENSG00000110514	8567	MADD	8.887746045	7.51E-08	5.53E-05
ENSG00000136603	6498	SKIL	9.095126463	4.75E-10	2.45E-06
ENSG00000131149	23199	GSE1	10.06343381	5.20E-09	7.66E-06

Appendix Table 18: The 100 most significantly differentially expressed genes of Norm compared to Res fibroblasts that were co-cultured with macrophages

Ensembl ID	Entrez	HGNC symbol	Log2FC	pvalue	padj
ENSG00000133704	10526	IPO8	-8.56133	1.51E-09	3.02E-06
ENSG00000198015	28977	MRPL42	-8.49287	8.86E-09	6.31E-06
ENSG00000123080	1031	CDKN2C	-8.18949	1.14E-08	7.05E-06
ENSG00000110328	374378	GALNT18	-8.13588	2.65E-07	5.62E-05
ENSG00000048140	26262	TSPAN17	-7.99846	4.77E-09	5.54E-06
ENSG00000167202	23102	TBC1D2B	-7.93486	3.87E-08	1.5E-05
ENSG00000109686	152503	SH3D19	-7.83102	2.39E-06	0.000213
ENSG00000145214	1609	DGKQ	-7.75173	1.48E-08	7.51E-06
ENSG00000129219	5338	PLD2	-7.72492	1.46E-10	5.93E-07
ENSG00000166135	55662	HIF1AN	-7.68234	3.07E-08	1.25E-05
ENSG00000129691	9070	ASH2L	-7.64459	1.18E-06	0.000141
ENSG00000122042	5412	UBL3	-7.64347	9.48E-08	3.09E-05
ENSG00000147408	55790	CSGALNACT1	-7.61242	7.78E-07	0.000106
ENSG00000110628	5002	SLC22A18	-7.59806	2.88E-06	0.000239
ENSG00000105447	83743	GRWD1	-7.57304	9.3E-09	6.31E-06
ENSG00000137812	57082	KNL1	-7.5215	4.64E-07	7.87E-05
ENSG00000069020	375449	MAST4	-7.49263	7.06E-11	5.75E-07

ENSG00000141971	93343	MVB12A	-7.47934	1.7E-06	0.000177
ENSG00000162144	220002	CYB561A3	-7.43168	9.33E-07	0.000121
ENSG00000119326	8727	CTNNAL1	-7.41311	2.03E-07	5.01E-05
ENSG00000164904	501	ALDH7A1	-7.39992	1.49E-07	4.45E-05
ENSG00000121022	10987	COPS5	-7.39615	1.94E-06	0.000186
ENSG00000133313	55748	CNDP2	-7.28428	4.47E-08	1.64E-05
ENSG00000112149	9308	CD83	-7.2512	5.74E-07	8.65E-05
ENSG00000162804	25992	SNED1	-7.17926	1.8E-06	0.00018
ENSG00000148297	6837	MED22	-7.10806	2.35E-06	0.000213
ENSG00000124126	57580	PREX1	-7.09337	3.02E-06	0.000246
ENSG00000185507	3665	IRF7	-7.06813	1.43E-09	3.02E-06
ENSG00000173546	1464	CSPG4	-6.93546	7.38E-07	0.000105
ENSG00000117620	23443	SLC35A3	-6.9336	1.05E-06	0.000134
ENSG00000106299	8976	WASL	-6.91786	1.63E-07	4.58E-05
ENSG00000106012	23288	IQCE	-6.89175	6.28E-09	6.31E-06
ENSG00000143333	6004	RGS16	-6.81021	1.52E-06	0.000165
ENSG00000163597	1.01E+08	SNHG16	-6.69336	2.33E-06	0.000213
ENSG00000133195	201266	SLC39A11	-6.62375	2.68E-07	5.62E-05
ENSG00000143889	92906	HNRNPLL	-6.60322	9.18E-07	0.000121
ENSG00000047410	7175	TPR	-6.59698	2.41E-06	0.000213
ENSG00000178752	151176	ERFE	-6.44636	1.29E-06	0.000143
ENSG00000186577	221491	SMIM29	-6.24595	2.35E-06	0.000213
ENSG00000168067	5871	MAP4K2	-6.24417	1.3E-08	7.05E-06
ENSG00000140350	8125	ANP32A	-6.14542	1.27E-06	0.000143
ENSG00000149582	84866	TMEM25	-6.053	1.3E-08	7.05E-06
ENSG00000159079	56683	CFAP298	-6.03879	5.44E-07	8.46E-05
ENSG00000006459	80853	KDM7A	-6.02717	3.94E-07	6.82E-05
ENSG00000166261	7753	ZNF202	-6.02107	6.23E-07	9.22E-05
ENSG00000189266	55629	PNRC2	-5.97536	2.97E-06	0.000244
ENSG00000131381	64145	RBSN	-5.91972	3.88E-07	6.82E-05
ENSG00000158050	1844	DUSP2	-5.71466	1.36E-06	0.00015
ENSG00000163655	8833	GMPS	-5.63071	2.29E-07	5.22E-05
ENSG00000147121	55634	KRBOX4	-5.62786	1.14E-06	0.000139
ENSG00000078403	8028	MLLT10	-5.55755	1.97E-07	5.01E-05
ENSG00000100979	5360	PLTP	-5.52227	2.12E-07	5.09E-05
ENSG00000165895	143872	ARHGAP42	-5.41429	2.8E-07	5.69E-05
ENSG00000174485	10260	DENND4A	-5.37308	4.64E-08	1.64E-05
ENSG00000128578	57464	STRIP2	-5.31561	2.68E-06	0.000227
ENSG00000076650	55094	GPATCH1	-5.2648	9.4E-07	0.000121
ENSG00000133731	3612	IMPA1	-5.07206	2.69E-07	5.62E-05
ENSG00000164758	90390	MED30	-4.92569	2.49E-06	0.000214
ENSG00000179862	163732	CITED4	-4.87142	1.79E-07	4.71E-05
ENSG00000153310	51571	CYRIB	-4.75837	1.84E-06	0.00018
ENSG00000260025	NA	NA	-4.72456	1.26E-06	0.000143
ENSG00000102221	9767	JADE3	-4.35679	1.57E-06	0.000168
ENSG00000061938	10188	TNK2	4.198624	1.24E-06	0.000143
ENSG00000175643	116028	RMI2	4.533452	2.19E-06	0.000208
ENSG00000114378	3373	HYAL1	4.990501	1.83E-06	0.00018
ENSG00000177683	168451	THAP5	5.143737	2.87E-07	5.69E-05
ENSG00000139629	11226	GALNT6	5.231797	2.47E-06	0.000214
ENSG00000124641	9477	MED20	5.24233	1.23E-06	0.000143
ENSG00000144559	132001	TAMM41	5.271785	1.13E-06	0.000139
ENSG00000152642	23171	GPD1L	5.338535	1.1E-06	0.000138
ENSG00000140459	1583	CYP11A1	5.645169	5.42E-07	8.46E-05
ENSG00000155666	79831	KDM8	5.662539	7.56E-07	0.000106
ENSG00000122778	57670	KIAA1549	5.751269	5.23E-07	8.46E-05
ENSG00000133315	28992	MACROD1	5.899564	8.37E-09	6.31E-06
ENSG00000165355	254170	FBXO33	5.945008	2.45E-06	0.000214
ENSG00000131747	7153	TOP2A	6.026814	3.88E-07	6.82E-05
ENSG00000156172	157657	CFAP418	6.17255	1.73E-07	4.69E-05
ENSG00000111727	29915	HCFC2	6.304665	2.65E-08	1.13E-05
ENSG00000117298	1889	ECE1	6.36536	9.01E-09	6.31E-06
ENSG00000116171	6342	SCP2	6.525029	1.89E-06	0.000183
ENSG00000068028	11186	RASSF1	6.569166	3.63E-07	6.82E-05
ENSG00000105676	93436	ARMC6	6.690873	3.33E-09	4.51E-06
ENSG00000198931	353	APRT	6.695875	1.61E-06	0.000171
ENSG00000132535	1742	DLG4	6.844679	1.81E-06	0.00018
ENSG00000149091	8525	DGKZ	6.87763	2.87E-06	0.000239

ENSG00000095787	51322	WAC	7.074063	2.62E-08	1.13E-05
ENSG00000116747	6738	RO60	7.188003	2.26E-06	0.000212
ENSG00000163933	91869	RFT1	7.304498	5.15E-07	8.46E-05
ENSG00000164877	79778	MICALL2	7.41859	1.8E-06	0.00018
ENSG00000130779	6249	CLIP1	7.423746	1.85E-09	3.02E-06
ENSG00000124659	6903	TBCC	7.435751	6.69E-07	9.73E-05
ENSG00000115760	57448	BIRC6	7.627512	2.31E-07	5.22E-05
ENSG00000122203	57179	KIAA1191	7.692982	2.59E-08	1.13E-05
ENSG00000115661	8576	STK16	7.781418	5.51E-07	8.46E-05
ENSG00000165775	65991	FUNDC2	7.790179	3.91E-07	6.82E-05
ENSG00000106070	2887	GRB10	7.946668	7.68E-07	0.000106
ENSG00000153130	60592	SCOC	8.060798	5.93E-08	2.01E-05
ENSG00000131374	9779	TBC1D5	8.36462	3.52E-07	6.82E-05
ENSG00000135480	3855	KRT7	8.520257	1.32E-07	4.15E-05
ENSG00000164530	221476	PI16	9.597168	1.53E-07	4.45E-05